THIRD EUROPEAN CONFERENCE

ON

CONTROLLED FUSION AND PLASMA PHYSICS

SYMPOSIUM ON BEAM-PLASMA INTERACTIONS

UTRECHT

The Netherlands

23—27 June 1969

WOLTERS – NOORDHOFF PUBLISHING

Contributions to the

"THIRD EUROPEAN CONFERENCE ON CONTROLLED FUSION AND PLASMA PHYSICS"

and the

"SYMPOSIUM ON BEAM-PLASMA INTERACTIONS"

Utrecht, The Netherlands, 23-27 June 1969

This book will be made available free of charge to all participants of the Conference. Further copies can be ordered from the publishers at U.S.$ 5.25. Cash price during the Conference U.S.$ 4.00.

WOLTERS-NOORDHOFF PUBLISHING - GRONINGEN
The Netherlands

CONTENTS

PREFACE

This book contains the papers to be presented at the "Third European Conference on Controlled Fusion and Plasma Physics" and the "Symposium on Beam-Plasma Interactions", which will take place in Utrecht, The Netherlands, from 23 till 27 June 1969. The Conference is the third in a series of which the previous two took place in Munich, 1965, and in Stockholm, 1967. The first Symposium on Beam-Plasma Interactions has been held in Prague, 1967.

The papers have been selected for presentation by the Paper Selecting and Programma Committee. The authors are responsible for the contents of their contributions (received 15 April 1969). No editorial work has been done by the Organizing Committee. The papers have been arranged in groups of related subjects. For some papers only the abstracts (received 1 February 1969) have been printed since the full text was not available in time. The papers marked "substituted paper" were received after the deadline for submission had passed, apparently as substitutions for papers accepted by the Paper Selecting and Programme Committee. The Organizing Committee has fitted these, together with one post-deadline paper, into the programme. The papers numbered 30, 31, 61, 62, 90, 91, 116, and 117 have been withdrawn.

We wish to thank the authors for their co-operation.

The Organizing Committee,

Utrecht, 15 April, 1969.

Organizing Committee

C.M. Braams, L.Th.M. Ornstein,	co-chairmen
R.F. de Vries,	general secretary
J.H. Zurburg,	manager, Congress bureau Jaarbeurs
Miss T. Spaans,	assistant-manager, Congress bureau Jaarbeurs
J. Rem,	secretary, Paper Selecting and Programme Committee

H.J. Hopman
F.P. Küpper
A.J. Postma
Mrs. H. Toft-Betke

Paper Selecting and Programme Committee

D. Eckhartt, Garching, W. Germany
R.S. Pease, Culham, United Kingdom
M. Trocheris, Fontenay-aux-Roses, France
M.P.H. Weenink, Jutphaas, The Netherlands

Sponsoring Organizations and Industries

Ministerie van Onderwijs en Wetenschappen (Ministry of Education and Sciences), The Hague
Euratom, Brussels
International Atomic Energy Agency, Vienna
Gemeentebestuur van Utrecht (Municipality of Utrecht), Utrecht
Rijksuniversiteit, Utrecht
F.O.M. Stichting voor Fundamenteel Onderzoek der Materie (Foundation for Fundamental Research on Matter), Utrecht
N.V. Philips' Gloeilampenfabrieken, Eindhoven
Rank Xerox (Nederland) N.V., Amsterdam
Smit Nijmegen Electrotechnische Fabrieken N.V., Nijmegen

A SURVEY OF STELLARATOR PROBLEMS

G. von Gierke

Institut für Plasmaphysik

Garching, West Germany

On the Confinement Properties of the Low-Shear Stellarator WIIb

D. Eckhartt, G. von Gierke, G. Grieger, W. Ohlendorf
Institut für Plasmaphysik GmbH, Garching near Munich, Federal Republic of Germany

The confinement of low-ß plasmas in a stellarator magnetic field has been studied in the Wendelstein W IIb stellarator as a continuation of our previous work. This machine is d.c. operated, has a purely circular shape with major diameter of 1 m, avoids interruptions of the helical windings that generate an $\ell = 2$ helical field, and possesses five-fold rotational symmetry. The magnetic confining field has practically no shear but a small average magnetic well, 3-5% in depth. Barium plasma was produced by contact ionization on a radiation heated tantalum sphere located on or near the magnetic axis. Measurements of the steady state density distribution were performed for various values of the magnetic field, the angle of rotational transform and the magnitude of the input ion flux. The particle density was determined by Langmuir probes, resonance fluorescence of the Ba-ions and by microwave phase shift measurements. It has been previously reported [1] that the confinement time of this barium plasma showed rather close agreement with the predictions of the Pfirsch-Schlüter model. However, deviations from this model have been observed (1) for low values of the angle of rotational transform $\iota = \frac{L}{2\pi}$, and (2) for distinct and narrow ranges of L which seem to be connected with the fact whether or not the magnetic lines of force are closed upon themselves after a not too large number of revolutions around the machine.

As for (1), the value of the rotational transform must exceed a certain threshold value in order that the density builds up. As long as this threshold is not surpassed, the steady state density is far below the number calculated from the Pfirsch-Schlüter model. However, once the threshold is surpassed, a hysteresis is observed such that upon reducing the rotational transform below the threshold, the density still follows the theoretically predicted value. New experiments have been performed to study this effect. A tentative explanation considers the influence of collisions and the connection with either the method of plasma production or the mechanism of plasma confinement in the stellarator magnetic field. Residual deviations from the predicted n vs ϵ curves might find their explanation when estimating the effect of ion inertia and considering that the balancing mass flow in a stellarator cannot exceed the velocity of sound.

(2) Considering the appearance of deep minima of the mean particle life time for distinct values of ϵ, the condition of closure of the magnetic lines of force can be satisfied with a high degree of accuracy for an appreciable part of the plasma cross section simultaneously because of the particular construction of the helical windings (low shear). The occurrence of these minima in the confinement time has been studied in more detail making use of improved stabilization of the generator currents which produce the magnetic field components. Profiles of particle density and mean particle life times have been measured for either group of cases, good and bad confinement.

In view of the apparent plasma stability in this low shear stellarator (density fluctuations less than one percent) the question arises to what extent the shallow magnetic well might contribute to stability, for example, by suppressing resistive interchange modes. To study this question a new machine is under construction which has the same physical dimensions but will be equipped with a set of four helical conductors that allow to vary the depth of the magnetic well as well as the amount of shear in the magnetic confining field. A numerical programme has been started to investigate field configurations which result from varying the signs and magnitudes of the currents through these helical windings and from locally changing the pitch angles of these conductors. Results of the numerical calculations will be given and the merits of the various configurations discussed.

This work was performed under the terms of the agreement between the Institut für Plasmaphysik GmbH, Munich-Garching, and Euratom to conduct joint research in the field of plasma physics.

[1] E. Berkl, D. Eckhartt, G. von Gierke, G. Grieger, E. Hinnov, K.U. von Hagenow, W. Ohlendorf
"Confinement of Contact-Ionized Barium Plasma in the Wendelstein Stellarator W II"
Plasma Physics and Controlled Nuclear Fusion Research 1, 513 (1969) IAEA Wien

A Numerical Model For Low-ß Magnetohydrodynamics In A Torus.

B.J. Green and K.U. von Hagenow
Institut für Plasmaphysik GmbH, 8046 Garching b. München

Numerical solutions of the usual low beta one fluid equations including finite resistivity in axially symmetric configurations are presented. In contrast to similar work being done in Princeton[1] a direct time integration of the equations is attempted. The numerical difficulty due to the generally small acceleration term is overcome by using an implicit scheme which furthermore eliminates the necessity to adapt the coordinate system to the magnetic surfaces. As a first application an idealized stellarator model with a source in the center has been employed, so it is able to reach a stationary state.
As the model allows for a potential difference to be applied between source and outer wall effects of an induced plasma rotation on the confinement may be studied. Results include generally satisfactory agreement with earlier calculations[2] on a simpler model using the Pfirsch-Schlüter formula for classical diffusion in a torus. Deviations occur mainly where the velocity along the field lines becomes comparable to the velocity of sound and near the outer wall.

1) N.K. Winsor, J.L. Johnson, J.M. Dawson
Princeton Report MATT-602, 1968.

2) G. v. Gierke, G. Grieger, K.U. v. Hagenow
Garching Report IPP 2/70 (1968)

This work was performed under the terms of the agreement on association between the Institut für Plasmaphysik and Euratom.

CONFINEMENT OF PHOTOELECTRONS IN A STELLARATOR

J. Hugill, A. Gibson and G. W. Reid,
U.K.A.E.A., Culham Laboratory, Culham,
Nr. Abingdon, Berkshire, England.

INTRODUCTION

The object of the experiments to be described is to measure the fraction, $\mathcal{E}$, of electrons with an isotropic velocity distribution which escapes from a stellarator; the so-called loss region in velocity space; and to compare this with theoretical estimates based on calculation of particle orbits[1]. The electron density is so low that no co-operative or plasma effects occur.

The stellarator used in the experiments is the CLASP apparatus, described elsewhere[2]. Previous measurements (3, 4) have shown that the stellarator is an almost perfect trap for particles not in the loss region of velocity space. Here we investigate in more detail the magnitude of the loss region and its variation with position and with gyroradius.

ELECTRON PRODUCTION

Electrons are produced photoelectrically, by irradiating a tungsten wire 0.5 mm diameter with x-rays from a copper anode x-ray set, operated at 20 kV and 20 mA. The total photoelectron current is approximately 2×10^{-13}A.

The photoelectron emission can be divided into two nearly equal groups: high energy primary photoelectrons, and low energy electrons liberated by these as they escape from the wire. Table I shows the main features of the energy spectrum.

The velocity distribution of photoelectrons emitted at each point on the wire is a cosine distribution about the local normal, giving a resultant which is almost isotropic. However, in a magnetic field, electrons whose velocity along the field,

TABLE I

Energy range	Fraction of total flux	Group
0 - 2.5eV	0.20	Low energy electrons
2.5 - 10 eV	0.20	
10 - 30 eV	0.08	
30 - 800eV	< 0.005	high energy electrons
3 - 13keV	> 0.370	
13 - 20keV	< 0.047	

$v_{\parallel}$, is small return to near their starting point after one gyro-orbit and are likely to be reabsorbed by the wire. This has two effects - the photoelectron current is reduced and the velocity distribution becomes anisotropic. Numerical calculations of this effect show that there results a distribution like that in Fig. 1. By comparing the calculated reduction in current with that measured, the fraction of low and high energy electrons escaping from the wire, and by inference their velocity distribution can be estimated.

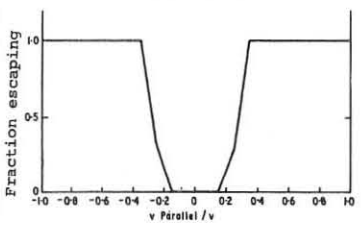

Final distribution

Fig. 1

METHOD OF MEASURING $\mathcal{E}$

The photoelectron current is measured with a vibrating reed electrometer. With maximum field strength the output time constant is adjusted to 0.2s. The noise level at the output is then 4×10^{-15}A, or 2% of the total current. Lower fields can be maintained for longer, and the electrometer time constant increased to 1s, giving improved signal to noise ratio.

The wire is mounted in a vertical sliding seal, so it can be placed a distance z above the horizontal median plane, variable from -20 mm to +58 mm.

Three current readings are taken as follows:-

J_c = current with no fields on.

J_1 = current with fields on, but with a stainless steel wiper probe placed across the magnetic surfaces so that no electrons can return to the wire. The ratio J_1/J_o can be used to estimate the fraction of particles escaping the wire and their velocity distribution as discussed above.

J_2 = current with wiper withdrawn. Trapped electrons now return to the wire after about 100 transits. J_2 is therefore less than J_1 and the difference is a direct measure of the trapped particle current.

RESULTS AND DISCUSSION

The experiments are done in two ways. The first, designed to measure $\mathcal{E}$ for the high energy electrons, uses field strengths of around 1000G with the wire almost parallel to the field. The fraction of low energy electrons escaping the wire is then small and, neglecting secondary emission and anisotropy, $\mathcal{E} \approx J_2/J_1$.

Comparison with calculated values of $\mathcal{E}$ is shown in Fig.2, for different values of S/r_L, where S is the ℓ-winding radius and r_L the Larmor radius. Agreement is quite good. At these values of S/r_L all the localised and blocked (1) particles and some passing particles escape.

For the low energy electrons $\mathcal{E}$ is measured separately, by reducing the field strength to about 200 Gauss, when all the high energy electrons escape. (Determined both by calculation and extrapolation from experiments at higher field strength). $J_1 - J_2$ now gives the low energy electron confined current only. Fig. 3 shows the variation of $\mathcal{E}$ with z for two different values of major radius. In this case a vertical field 0.012%

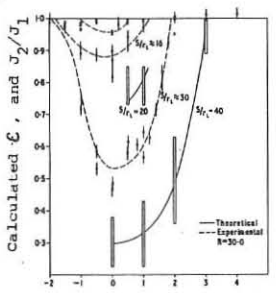

Position of wire, z (cm)

Fig. 2

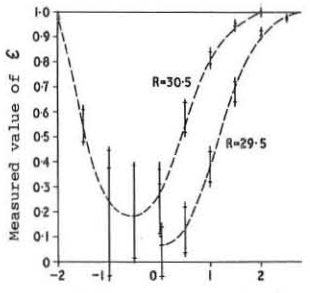

Position of wire, z (cm)

Fig. 3

of the main field was applied, so as to make the configuration a mean antiwell. When this field is removed no confinement is observed, but this behaviour is not predicted by computation until the vertical field is reversed. The discrepancy is not yet explained. For the low energy electrons S/r_L is about 300 so that in the interior of the trap only the localised particles are expected to escape; and this is consistent with the measured loss when the vertical field is adjusted for optimum confinement.

CONCLUSIONS

Measurements of the loss of a nearly isotropic distribution of electrons from a stellarator are in good agreement with that expected on the basis of particle orbit calculations.

ACKNOWLEDGEMENTS

The authors wish to thank R.S. Pease for suggesting the experiment; M.R. Barnes, B.C. Sanders and J.R. Watkins for running the machine; K. Axon, W.C. Core, M. Ellis and C. Wilson for data analysis and computation; and D.W. Mason and M. Larkin for assistance in design and analysis of the magnetic analyser.

1. Gibson, A., and Taylor, J.B., Phys. Fluids 10 12 2653 (1967)
2. Sanders, B.C., Rowe, R.A., and Varley, G.L., 5th Symposium on Fusion Technology, Oxford (July 1968).
3. Gibson, A., Hugill, J., Reid, G.W. and Sanders, B.C., 'Plasma Physics & Controlled Nuclear Fusion Research' 1 465 IAEA, Vienna (1969).
4. Gibson, A. et al Phys. Rev. Letts. 21 1052 (1968).

THE PROPERTIES OF A PLASMA INJECTED INTO A HIGH SHEAR STELLARATOR

by

D. J. Lees, R A.E. Bolton, C.R.J. Hoffman*, S.S Medley*, P. Reynolds and B. M. White

U.K.A.E.A., Culham Laboratory, Abingdon, Berks, England

(i) Introduction

Experimental work by Gibson[1] has shown that single charged particles not in the loss cone can be contained in a stellarator trap for a number of transits adequate for thermonuclear purposes. The PROTO-CLEO stellarator was designed as a small scale experiment to investigate some of the remaining problems of this configuration, namely the confinement in a stellarator of a low-β plasma injected into the trap and the scaling laws governing this confinement. The apparatus has already been described[2] but Table I lists, for convenience, the main experimental parameters. In this paper we describe further results on containment particularly on the scaling of containment time with magnetic field.

Table I
Parameters of PROTO-CLEO ℓ=3 Stellarator Experiment

Trap	
Major radius R (true toroid)	40 cm
Helical winding mean radius s	9 cm
Separatrix radius (to apex of trefoil) r_m	5 cm
Number of field periods on torus	7
Current at B_o = 3 kG: Helical winding I_ℓ	15 kA
Toroidal winding I_o	20 kA
Computed rotational transform at separatrix ι	224°
Mean shear length $L_s = 2\pi R/\iota$	75 cm
Mean shear parameter $\theta = r_m/L_s$	1/15
Useful time duration of magnetic fields	~10 msec
Plasma	
Density	10^{10}-10^{11} cm^{-3}
Electron temperature	~ 5 eV
Ion Energy	~10 eV

(ii) Plasma production and diagnostics

Plasma is produced and injected either by the quasi-D.C. injector using hydrogen-occluded titanium electrodes[2], or by a conventional two electrode button gun. Two versions of the latter have been made, injecting either along the magnetic field or across it, at a point just outside the separatrix. Time resolved ion density and electron temperature measurements are made using a swept double probe.

The average plasma density is measured with a 16 mm wavelength version of the microwave interferometer developed by Hotston and Seidl[3]. The general arrangement of the machine and the disposition of diagnostic ports are shown in Figure 1.

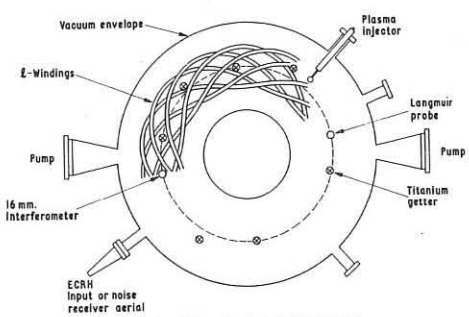

Fig.1 Schematic view of PROTO-CLEO stellarator showing diagnostic positions.

Figure 1

A 1-2 kW pulse, lasting 1 msec, of microwave power at the electron cyclotron resonance has been used to heat the injected plasma. It normally produces a pump-out effect during the pulse, when the plasma density rapidly decays by an order of magnitude. Under some injection conditions the density increases during ECRH, suggesting that the injector is a source of neutral gas. We have avoided containment measurements made under these conditions, choosing results obtained only when the ECRH indicates that plasma properties are not dominated by neutrals. Under these circumstances we interpret the density decay time τ as giving the value of the particle containment time.

(iii) Scaling of containment time with confining field

Density decay times up to about 5 milliseconds have been measured. It is found that containment depends on the magnitude of confining field B and, less strongly, on the electron temperature. The dependence of τ on B is shown in Figure 2.

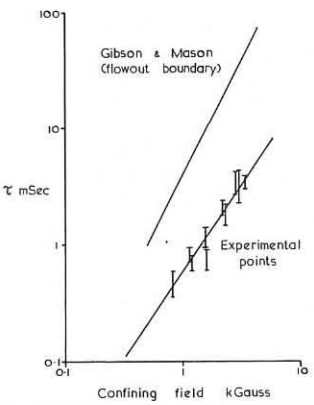

Fig.2 Density decay time as a function of confining field compared with results of a numerical computation by Gibson and Mason[5]. Plasma density $2 \cdot 10^{10}$ cm^{-3}.

Figure 2

The spread in experimental results is partly due to the variation with electron temperature between 2-5 eV: in general, the higher temperature corresponds to the shorter containment time. The wide spread of results is also possibly due to the shot to shot variation of the neutral back-ground density. Since the decay is only approximately exponential, values of τ and T_e measured at the same instant of time have been used.

The normalized quantity τ/τ_B given by the above results increases with B: the highest value measured is 15-20. (τ_B is the Bohm containment time).

(iv) Discussion

It has already been suggested that the level of fluctuations is too small to account for the plasma loss[2]. It is therefore important to compare the containment measurements with predictions of theory of equilibrium in toroidal traps. Gibson and Mason[4] have computed the diffusion co-efficient expected in a cylindrical system when localised and blocked particles are expected to make an important contribution. In this work the effect of an ambipolar electric field on particle orbits has been ignored. More refined theory, however[5,6] produces the same diffusion rates for any given class of particle as the ones used by Gibson and Mason. Figure 2 shows, in addition to the experimental results, the containment times given by this computation on the assumption that at the plasma boundary (the separatrix) plasma flows to the walls at sonic speed. It is seen that the actual containment times are an order of magnitude too small, although the scaling with magnetic field is approximately correct.

(v) Conclusions

We have shown that for a low-β plasma injected into a medium high shear stellarator, it is possible to obtain containment times ~15 times the Bohm value. The scaling of τ with B is as $\tau \propto B^n$ where $1.5 < n < 2$.

(vi) Acknowledgements

The authors gratefully acknowledge the experimental help given by Messrs. P. A. Shatford and D.R.A. Webb: we are also grateful to Dr. A. Gibson for access to his diffusion programme. Finally we thank Dr. R. J. Bickerton for his advice and encouragement throughout.

References

1. Gibson, A., Hugill, J., Reid, G.W., Rowe, R.A., and Sanders, B.C., Novosibirsk Conference Paper CN-24/D-1.
2. Adlam J. H. et al, Novosibirsk Conference Paper CN-24/D-8.
3. Hotston, E.S., and Seidl, M., J. Sci. Inst. 42, (1965) 225.
4. Gibson, A., and Mason, D.W., Plasma Physics 11 (1969) 121
5. Galeev, A.A., and Sagdeev, R.Z., Sov.Phys.J.E.T.P. 26 (1968)
6. Stringer, T. E., Phys. Rev. Lett. in press.

* National Research Council of Canada, Post-Doctorate Fellow

ON A POSSIBLE MECHANISM OF A PLASMA DIFFUSION IN L-I STELLARATOR

M.S.BEREZHETSKY, S.E.GREBENTSHIKOV, L.M.KOVRIZHNIKH, I.A.KOSSY, I.S.SBITNIKOVA, I.S.SHPIGEL

LEBEDEV INSTITUTE ACADEMY OF SCIENCE. MOSCOW, USSR

An abnormally high plasma diffusion rate observed in the experiments in closed systems attracts close attention of scientists in the last years. The mechanism of a plasma loss from the traps has not been clarified. The measurements of turbulent plasma flow at L-I stellarator, caused by fluctuations, did not make it possible to relate it to the observed values of confinement time [I]. It has been noted recently that the presence of blocked and localized particles in a toroidal stellarator [2], the trajectories of which have an essential difference from magnetic surfaces, may lead to a substantial increase in a collision diffusion. The theoretical analysis of this problem is given in paper [3,4]. In this report the first attempt is made to make a comparison of L-I experiments with a diffusion theory for such systems.

The density of the diffusion flow of the j-type particles (ions and electrons) is given by

$$\Gamma_j = -\frac{15}{4}\sqrt{\frac{n\varepsilon I_n(nkr_0)}{2}}\left(\frac{r_0}{R}\right)^2 \frac{\nu_j N_j T_j^2}{\left(\frac{e_j r_0}{c}\right)^2 \nu_j^2 H^2 + e_j^2 E^2 + \left(\frac{k_n T_j}{r_0}\right)^2}\left[\frac{\partial k_n N_j T_j}{\partial r_0} - \frac{e_j E}{T_j}\right] \quad (I)$$

where N_j is the density; e_j is the charge of the particles; ν_j is the sum of particle collision frequences of the given kind with other particles and between themselves; $\varepsilon = \frac{H_1}{H_0}$ is a ratio of the fundamental harmonic of a helical field to a longitudinal; $k = \frac{2\pi}{L}$ is a wave number of a helical winding having a L pitch; r_0 is an average radius of the magnetic surface; R is the large radius of a torus; n is a multipolarity of the system (in L-I n=2); T_j is a temperature; $\lambda_n = \max\left(\frac{r_0}{R}, n\varepsilon^2 \frac{\partial}{\partial r_0} I_n(nkr_0)\right)$ is the value characterizing nonuniformity of the magnetic field.

As seen from (I), the diffusion flows have a complicated dependence on the temperatures, collision frequencies and an intensity of the magnetic field. The radial electrical field $E = E(\nu_j, T_j, H)$ is an equilibrium field and is caused by ambipolarity of the diffusion. Its value and sign are determined on the basis of $\Gamma_e = \Gamma_i$.

To make comparisons with the theory it is necessary to know experimental values of electron and ion temperatures, density as well as their gradients. The measurements of density distribution and electron temperature were made with probes. Ion temperature was determined with multigrid probes.

The Fig. I shows in relative units the curves of density and temperature distribution of particles, measured with an emitting probe. It can be seen from Fig.I that the charge of the plasma is negative.

The value of the radial electrical field is equal to several volts per cm.

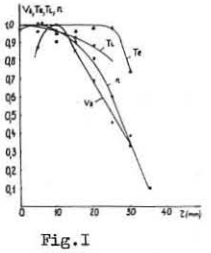

Fig.I

The study of electrical fields have shown [I] that the relaxation time of the plasma potential is commensurable with that of a quasiequilibrium density distribution (~100 μsec). The potential undergoes relatively weak change during the plasma lifetime, and the dependence of electrical fields on the parameters of the stellarator field (H and ε) is similar to the dependence of plasma lifetime on these quantities. All this suggests that the observed electrical fields are equilibrium ones.

The study of the injected plasma parameters has revealed that ion temperature has a substantial dependence on the value of the magnetic field, into which an injection is made, while electron temperature practically does not change. The relation of ion temperature to the magnetic field intensity is shown in Fig.2. The existance of this dependence may be related both to the effect of magnetic field on the operating conditions of the injector, mounted inside the trap chamber, and to the variation of trapping conditions of plasma during injection.

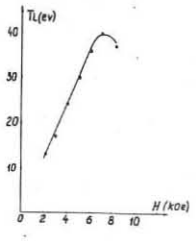

Fig.2

For purpose of comparison of the experimental data with the theoretical conclusions the calculations were made of an equilibrium electrical field and the plasma lifetime for the plasma parameters that are close to the experimental data. The calculations were made for electron temperature of 2-12 ev and for ion temperatures of 9-36 ev; the plasma density was assumed to be $N_e = N_i = 10^{10}$ cm^{-3}; the density of neutrals - $N_0 = 10^{11}$ cm^{-3}; magnetic field H=2-10 koe.

The calculation results are shown in Fig.3, the solid curves represent theoretical dependence of the radial electrical field on the magnetic field intensity for the electron temperature T_e=6 ev and for a number of values of ion temperatures. It can be seen from Fig.3 that an equilibrium electrical field increases with the rise of the magnetic field. The dots in Fig.3, represent the results of various series of measurements of the radial electrical field, made during a lengthy time period. The dotted curve stands for theoretical relation of an electrical field to a magnetic field, the variation of an ion temperature observed in the experiment is taken into account. It can be seen from the comparison of the curves in Fig.3 that the measured electrical fields have the same sign and approximately the same absolute value as the calculated ones. The character of variation of electrical fields with the variation of magnetic fields is also in agreement with the theory.

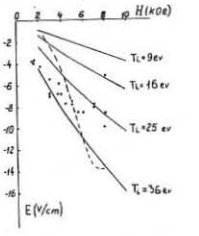

Fig.3

The calculation of the confinement time corresponding to Fig.3 shows that $\tau \sim H^{3/2}$. The value of the calculated confinement time at H=5 koe is equal ~15 msec, that exceeds approximately by an order the actually observed lifetime of a plasma. According to the theory the confinement time has a weak dependence on ion temperature in the discussed density and temperature interval. At the same time there should be a strong dependence of the lifetime on an electron temperature ($\tau \sim T_e^{-2,2}$). On the one hand, this relation facilitates verification of the theory, while, on the other hand, it requires a high accuracy of the absolute values of an electron temperature in an experiment.

The data given in this paper show that this theory evidently provides a correct value for equilibrium electrical fields. Nevertheless, there is a marked difference in the experimentally observed and the calculated confinement times, which, however, is not so great as to neglect the collision diffusion as a possible mechanism of plasma losses. At present we have no explanation for this discrepancy. Only some contemplations can be made. First, the theory was developed for an idealized toroidal stellarator. In real conditions there may exist perturbations of magnetic surfaces, magnetic islands which can bring about a marked rise in a diffusion flow. Second, it can not be excluded, that some mechanism exists leading to the same rate of ion and electron leakage from the trap, making a substantial contribution into a diffusion flow, which does not determine the plasma potential. The equilibrium electrical field in this case will be defined be the above mentioned collision diffusion.

REFERENCES

I. M.S.Berzhetsky et al. "Plasma Physics and Contr. Nuclear Fusion Research" (IAEA), Vienna, 1969, vol.I, 529.
2. A.Gibson, J.B.Taylor. Phys.Fl., 10, 2683 (1967).
3. A.A.Galeev, R.S.Sagdeev, JETP 53, 359 (1967).
4. L.M.Kovrizhnikh, JETP, 56, b 3 (1969).

INVESTIGATION OF HIGH SHEAR MAGNETIC STRUCTURE IN THE "URAGAN" STELLARATOR

V.F. Alexin, O.V. Biryukov, A.V. Georgievsky, Yu.I.Grot, A.G.Diky, V.E.Ziser, L.Kh.Kitaevsky, D.P.Pogojev, Yu.F.Sergeev, V.A.Souprunenko, and V.T.Tolok.

Physical-Technical Institute of Academy of Sciences of Ukr.SSR, Kharkov, USSR.

The investigation of the stellarator-racetrack "Uragan" magnetic field structure with l=3 helical field was carried out by means of electron beams at single [1,2] and multiple [3]electron passes around the system (Fig.1).

The influence of a current value as well as "circularizer" and helical winding position on the magnetic field surface configuration has been found. The mean radius of the outer closed-line surface r_o at given $\mathcal{E}$ value* will be less than r_o calculated value (Fig.2) according to single-round measurement results. This can be explained by uncomplete"circularizing" of magnetic line surfaces [4]. The measured angles i_o** complied with the calculated ones. It made possible the estimation of "shear" value S** upon the exact formulae of the work [5].

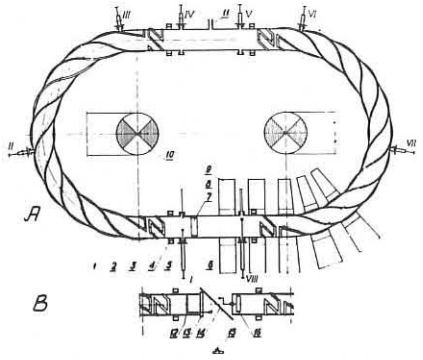

Fig.1. The schematic diagram of multi-round (A) and single-round (B) magnetic measurements in the machine.

1 - vacuum chamber, 2 - helical winding, 3 -"circularizer", 4 - compensating coil, 5 - point-focused electron gun, 6 - local probes (I-VIII), 7 - pick-up electrode, 8 - neon injection system, 9 - longitudinal magnetic field coil, 10 - ohmic heating transformer for plasma, 11 - pumping tube, 12 - luminescent screen, 13 - transparent scale, 14 - mirror, 15 - camera, 16 - rotating electron gun.

The parameters of magnetic line surfaces obtained as a result of multi-round measurements will differ from "single-round" magnetic line surface parameters: at given value $\mathcal{E}$ the last closed-line surface radius r_o would be somewhat less as compared with multi-round measurements. The oval shape of the surfaces will increase as i_o decreases - this applies to inner surfaces at given $\mathcal{E}$ value and to surfaces having the same r_o values, while $\mathcal{E}$ decreases. The surfaces with big r_o and i_o values are displaced inside by ~5 mm, what can be explained by the toroidal shape of the magnetic system; the surfaces having smaller i_o's are shifted more to the outside from the torus centre.

The difference given can be explained by the existence of uncompensated transverse component $H_1/H_o = 1\cdot10^{-3}$ [4,6] and by the possible small, ~3', distortion of winding planes both of the helical one and that of the longitudinal field[7], or by the relative 2÷3 mm shift of listed above windings in the horizontal plane.

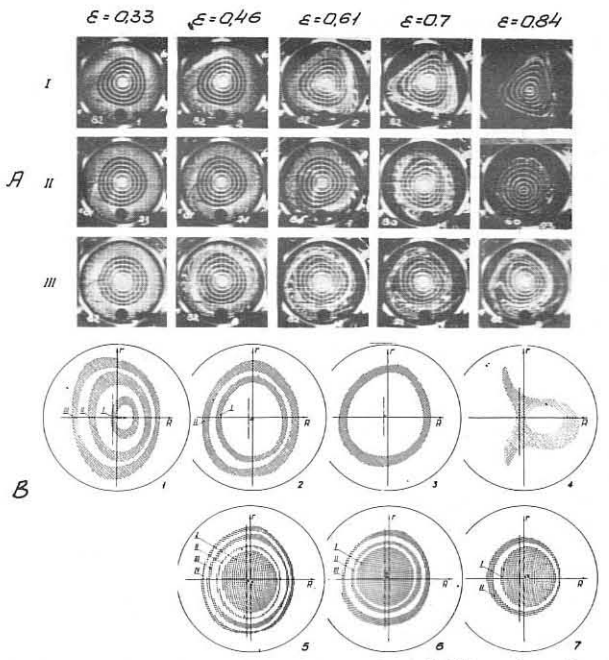

Fig.2. The shape of "magnetic line surfaces":(A) - at various $\mathcal{E}$ values after electron passing in regions with the circularizer and helical winding (I), the circularizer,helical winding and circularizer (II), and the whole machine (III); and (B) - the cross-section of magnetic surfaces (I-IV) built by means of the local probe at a fixed gun position (1-4) and according to pick-up electrode signals at gun position changes (5-7) with $\mathcal{E}$=0.46(1), 0.61(2,5), 0.7(3,6,7) and 1.02(4); (7) differs from (6) by existence of additional $H_1/H_o=1\cdot10^{-3}$, x - being the magnetic surface centre.

As a result (Fig.3), the measured maximum value will be $i_o \approx 230^o$ on the radius $r_o \approx 60$ mm at $\mathcal{E} \approx 0.65$ which complies with the "shear" value of $S_o \approx 0.09$.

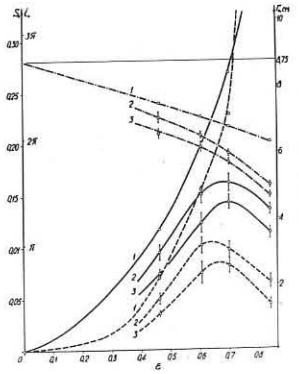

Fig.3. Magnetic surface parameters r_o(dash lines), i_o(solid lines), and S_o(broken lines) versus $\mathcal{E}$ according to results of (1) calculations, single-round (2) and multi-round (3) measurements.

REFERENCES

1. B.P.Illenko, V.G.Zikov, Zhurn.Tekhn.Fiz. 31 (1961).
2. B.I.Gavrilov, F.V.Karmanov, G.P.Maximov, Atomnaya Energia, 18 (1964) 273.
3. M.S.Berejezky, S.E.Grebenshchikov, A.P.Popryadukhin, I.S.Shpiegel, Zhurn.Tekhn.Fiz. 35 (1965) 2167.
4. J.F.Sheffield, Matt-Q-24. Annual report (1/1-31/XII-1966). Princeton Plasma Physics Laboratory, USA.
5. A.M.Morozov, L.S.Solovyev, Plasma Theory Problems, v.2, p.3, Atomizdat (1963).
6. A.Gibson, Phys.Fluids 10 (1967) 1553.
7. C.Gourdon, D.Marty, E.K.Maschke, J.P.Dumont. Third Conference on Plasma Physics and Controlled Nuclear Fusion Research, Novosibirsk, U.S.S.R.(1968).Report CN-24/F-2.

*$\mathcal{E}=h_3/H_o$, where h_3 is the fundamental third harmonic of the helical magnetic field, H_o - the longitudinal magnetic field strength.

**$S_o = \frac{di_o}{dr}\frac{r_o^2}{L_o}$, where i_o is the angle of rotation transformations of magnetic field lines along the machine length.

substituted paper

Confinement of a Potassium Plasma in the Garching Octopole W V

F. Rau, Institut für Plasmaphysik GmbH, Garching near Munich, Federal Republic of Germany

Introduction

Previous experiments with a Cs plasma and a moderate magnetic field in the Octopole W V [1-3] yielded an appreciable increase in peak density when an azimuthal magnetic field (typically of 65 G) was superimposed on the purely meriodional multipole configuration. This feature was discussed [2, 3] as part of a qualitative loss model, especially in the case of a collisionless plasma with a non-Maxwellian ion distribution and large ion Larmor radii. Using a K plasma and furthermore enlarging the magnetic field as compared to the above mentioned Cs experiments, within about 20% we find the same peak densities in both cases, with and without the azimuthal magnetic field applied [3]. This leads to the conclusion that large Larmor radii effects as regarded dominant in the case of a Cs plasma at low magnetic fields are no longer of such relevance [3].

Therefore, in the present paper, some details of the confinement of a potassium plasma in the Octopole are studied. Effects of the supports of the current rings inside the vacuum tank are considered to be of importance. Consequently, it appears useful to investigate the purely meridional magnetic field configuration because of its simpler structure without translational transform or shear.

Experiments and Discussion

The apparatus as well as the plasma source and the diagnostics are described elsewhere [2, 3]. Fig. 1 shows the magnetic field plot. In the present investigation we use higher magnetic fields than those stated in the references. At the midplane of the device about 12 Larmor radii ϱ_i of a 0.2 eV potassium ion are between the boundary field line of a flute-stable confinement, ψ_c, and the main separatrix. The maximum magnetic field of the main separatrix is B_o=5.2 kG. The experiments are done in the stationary state. Axial and radial density profiles are shown in fig. 2. Three single Langmuir probes are used and cross-calibrated during several runs. The data are normalized to an ion input flux of $\Phi = 3.4 \cdot 10^{15} s^{-1}$. The profiles are taken at different azimuthal positions φ=60, 120 and 180° with respect to the plasma source. At φ=120° they reveal somewhat lower peak densities than at the other positions. The profiles are rather flat-topped and show close to the minor separatrices a moderate dip. As compared to the profiles of a Cs plasma at lower magnetic field we find steeper gradients which tend to vanish outside the critical field line ψ_c. There fluctuations are observed the amplitude of which is indicated by the dashed vertical lines. The fluctuations seem to be present inside of ψ_c at a distance comparable to $2\varrho_i$, the Larmor diameter of a 0.2 eV potassium ion. This feature as well as further details of the fluctuations remain to be studied in the future; especially their relevance with respect to plasma losses.

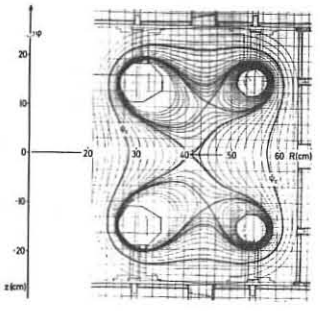

Fig. 1 Magnetic field plot

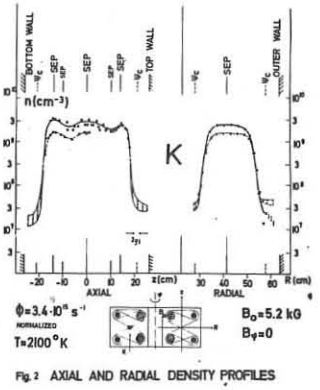

Fig. 2 AXIAL AND RADIAL DENSITY PROFILES
PROBES AT φ = 60° 180° 120°

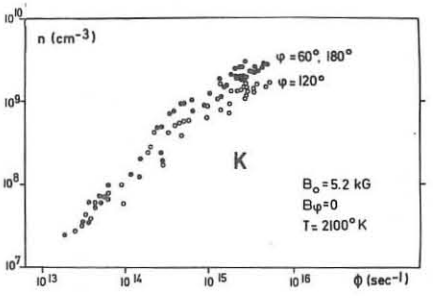

Fig.3 DENSITY VS ION INPUT FLUX

Measuring at the main separatrix at a position near the upper outer ring we find the density to be slightly lower than at the center of the device. Whether this is due to a possible discrepancy of the different probes used has not yet been proved.

The experimental confinement time τ can be evaluated from the relation of peak density n vs ion input flux Φ (fig. 3). The dots correspond to the data found at φ = 60 and 180° and, at generally slightly lower density, the open circles to those at φ = 120°. At a typical density of $n = 10^9$ cm^{-3} we find an experimental confinement time τ = 0.24 s. In the low density region $n \sim \Phi$ is obtained approximately. The experimental points seem to rise slower than that relation at densities higher than $n \approx 0.7 \cdot 10^9$ cm^{-3}. There τ is larger than τ_{eq}, the electron-ion equipartition time; τ tends to decrease slightly with increasing density.

Diffusion mechanisms according to FICK's law with the BOHM or the resistive diffusion coefficient yield confinement times much too low (7 ms) or too high (45 s, at $n = 10^9$ cm^{-3}, respectively. With the use of the profiles measured close to the rings the confinement time corresponding to direct loss of particles at the ring supports results in τ_{s1} = 0.5 - 0.8 s. The lower (higher) value corresponds to one (two) Larmor radii added on either side to the width of the support. Secondary support losses according to a confinement time τ_{s2} can be caused by an azimuthal density gradient. The losses are towards the rings or the outer walls, depending on the direction of the meridional magnetic field and the azimuthal density gradient. In a simple model only the ratio of density measured at φ = 120 and 180°(60°) enters [4]. It yields values of τ_{s2} = 0.6 to 0.04 s.

Conclusion

The calculated confinement time τ_{s1} due to direct loss at the supports is found, on the average, higher by about a factor of three than the observed confinement time. From the observation of reduced density at the azimuth where the supports are situated we conclude that support losses of the secondary type should be present. Up to now, however, no definite experimental value seems to have been obtained. Measuring the flux of particles towards the outer walls at positions close to the azimuth of the supports and also reversing the polarity of the magnetic field should give more information about those additional particle losses. Far beyond the limits of consideration are losses according to BOHM or resistive diffusion, as stated previously.

References

[1] Eckhartt, D. et.al., Proceedings of the Culham Conf. 1965, Vol.II, 718

[2] Erickson, C.W., et.al., Proc.Int.Conf.on Controlled Fusion and Plasma Physics, Novosibirsk, Vol.I, 339 (1968)

[3] Rau, F., Colloquium on Closed Configurations, Rottach-Egern 1969

[4] Rau, F., IPP-Report 2/78 (1969)

This work is part of the joint program between IPP and Euratom.

PLASMA CONTAINMENT IN THE CLIMAX TOROIDAL QUADRUPOLE

by

T. K. Allen, A. N. Dellis, J. H. P. C. Megaw, R. Prentice
D. A Reynolds, and B. A. Ward

U.K.A.E.A. Culham Laboratory, Abingdon, Berkshire, England

CLIMAX[1] is a toroidal quadrupole apparatus with induced currents of up to 800 kA in two concentric coplanar solid copper rings, each positioned in the vertical plane by three slender supports. The major diameters of the rings are 130 and 190 cm. The computed field configuration, with no toroidal field applied is shown in Figure 1, the flux function ψ being a measure of the flux between a given surface and the separatrix($\psi = 0$). The quantity $\oint dl/B$ is a minimum at $\psi = 3$, the critical surface.

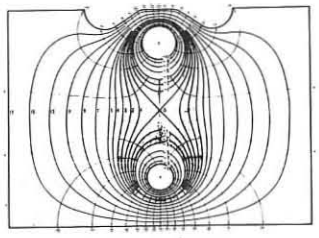

Figure 1

A hydrogen plasma, $T_i \approx 50$ eV, is injected across the quadrupole field from $\psi = 6$, using a conical theta pinch gun and a screened solenoid guide field[2]. For the work reported here injection occurs as the quadrupole field is slowly decaying (by 25% in 10 ms).

Small Langmuir probes are used to measure the electron density n and temperature T_e. Similar probes incorporating series resistors measure the average and fluctuating components of the plasma floating potential. After a filling phase lasting about 100μs the peak plasma density in the trap can reach 10^{12}cm^{-3}. The density variation with ψ, as measured for a ring current of 270 kA (quadrupole capacitor bank voltage Q = 6.8 kV) is shown in Figure 2. Assuming that T_i = 50 eV, an ordinate of 100 arbitrary units is calculated as $n = 1.0 \times 10^{11}$cm^{-3}.

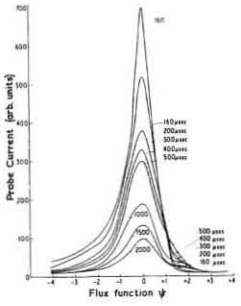

Figure 2

The decay of saturation ion current to a probe at $\psi = 0$, expressed as a time varying exponential time constant τ, is plotted in Figure 3 for several values of the voltage Q. It is clear that changing the magnitude of Q has little effect on τ. Additional experiments show that τ does not depend significantly on density.

The direct loss to the ring supports has been found by measuring the positive ion saturation current to a biased 'dummy' support. The total number of ions in the trap is compiled from the density profiles (n = const. along a line of force). These two measurements are combined to calculate the value of τ for plasma density decay corresponding to this direct support loss and this is shown in Figure 3. A theoretical estimate of the Bohm decay time[3] based on the measured time variation of electron temperature is also plotted.

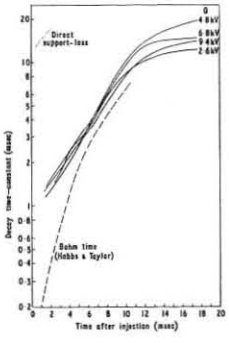

Figure 3

A 8.6 mm microwave interferometer designed to measure less than 1° phase shift[4] is used to monitor the line integral of plasma density along the mid plane between the rings. The decay time constant for this quantity is longer than the value of τ in Figure 3, measured with a probe at $\psi = 0$, and is typically about 2 ms in the first 2 ms after injection. This difference is due to the change in density profile with time (cf. Figure 2).

A toroidal magnetic field B_θ up to 200 G produces no marked change in the plasma confinement time. It does, however, markedly change the ψ dependence of floating potential. Figure 4 shows the potential profile as measured at different times both with and without B_θ. The solid curves were measured at $\theta = 90°$ from the injection point: the dashed curves were measured on the opposite side of the toroidal tank from injection, at $\theta = 207°$. Most of the change in potential distribution is accomplished by the application of only about 10G toroidal field, in either direction. The change is particularly marked for early times at $\theta = 207°$.

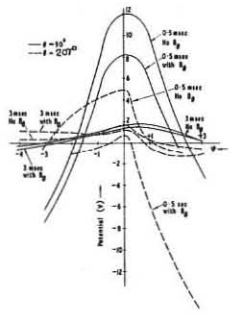

Figure 4

The change in potential profile with toroidal position implies the existence of a local E_θ field which could cause radial E x B particle drift. Preliminary measurements have shown E_θ fields of the order of 0.1 V/cm. In measuring the variation of potential in the θ direction, it is found that an obstacle (the dummy support) immersed in the plasma causes a potential step of a form similar to that previously reported in the Wisconsin octupole work[5]. This potential step is observed all along the magnetic lines of force which pass through the region of the obstacle and its polarity reverses on crossing the separatrix. The direction of E x B particle drift produced at the obstacle is away from the separatrix: this drift is probably the dominant loss mechanism.

Fluctuations in the floating potential are observed with a frequency spectrum peaked around 20 kHz. The amplitude of the fluctuations is small for $\psi < 1$. Figure 5 shows the peak amplitude as a function of time for $\psi = +1$ and $+2$. The measured electron temperature, expressed in electron volts, is plotted for comparison. For the first 150 μs after injection, the fluctuations are well correlated around a line of force (length ≈ 100 cm), but, after this, the correlation distance decreases to less than 10 cm.

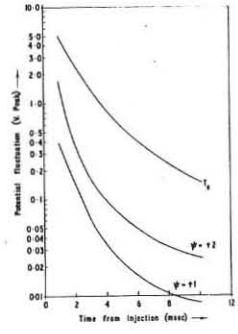

Figure 5

References

1. Phillpott, J., Allen, T.K., Harries, K., Hunt, R., and James, T.E., 5th Symposium on Fusion Technology, Oxford July, 1968. Paper 3.
2. Allen, T.K., Cox, A.J., Spalding, I.J., I.A.E.A. Conf. on Plasma Physics and Controlled Nuclear Fusion, Sept. 1965. Paper CN-21/31.
3. Hobbs, G.D. and Taylor, J.B., Plasma Physics 10, 207 (1968)
4. Hotston, E.S. and Seidl, M., J.Sci.Instrum. 42, 225 (1965)
5. Forsen, H., et al, I.A.E.A. Conf. on Plasma Physics and Controlled Nuclear Fusion Research, Novosibirsk, Paper CN-24/C1 (1968).

EXPERIMENTAL STUDY OF LOW FREQUENCY INSTABILITIES IN A LINEAR QUADRUPOLE

M. BERNARD, J. P. BUSSAC, G. BRIFFOD, R. FRANK, M. GREGOIRE & J. WEISSE

CENTRE d'ETUDES NUCLEAIRES DE SACLAY

Service d'Ionique Générale

Département de Physique du Plasma et de la Fusion Contrôlée
B.P. n° 2 - 91 - Gif-sur-Yvette (France)

In order to investigate the effects of $\oint \frac{dl}{B}$ upon low frequency oscillations and particles losses we used a linear quadrupole device PUMA. Preliminary results of this investigation are presented in this paper.

Description of the experimental device. -

The magnetic configuration is generated as in LM 1 device /1/ by two parallel rods each of them carrying a steady current up to 25 kA. As the distance between the two rods can easily be varied even during operation of the plasma source, the extension of the magnetic well and the values of $\oint \frac{dl}{B}$ are, in our case, experimental parameters. In fig. (1) we give numerical values of $\oint \frac{dl}{B}$ as a function of the distance r to the rods, for three positions of the rods.

A steady state hydrogen plasma is produced by a crossed fields discharge. The two plane electrodes : hot cathode and anode are parallel to the rods. Neutral pressure is about 5.10^{-4} mm Hg and the ion density coming out from the ionization region is around 10^{10} p/cm^3 (measured by Langmuir probe). Another essential feature of our experiment is the possibility to vary the density gradient position with respect to magnetic field lines by varying the source position. This can easily be done even when the plasma source is in operation. Thus we can shift the density gradient from a stable to an unstable region as it can be seen on photographs n° 2 and n° 3.

Experimental studies. -

1. Magnetic configuration. We first try to obtain an experimental determination of the location of the separatrix. We do this by using a small electron gun moving above one rod and directed horizontally towards the second rod were a probe is placed. When the electron gun is moved upward no electrons reach the probe unless the electron gun is not far from the separatrix. At this position a current can be measured at the probe due to the B=0 region. The probe position corresponding to the maximum value of the probe current gives the separatrix position - fig. 4. These measurements agree very well with theoretical calculations of the separatrix location. Consequently it was reasonable to determine ψ_c directly from the calculated magnetic properties of the rods.

2. Fluctuations. Experimentally we have investigated how the density profile $n_o(r)$ and the characteristics of the fluctuations change as a function of $\oint \frac{dl}{B}$. For all experimental configurations that were tried, the fluctuations were found to be related to the density gradient. Our measurements indicate that the ratio $\frac{\tilde{n}}{n_o}$ is always minimum near the point $\nabla n = 0$ - fig. 5. When the density maximum is shifted from the stable to the unstable region, the average level of the fluctuations increases rapidly as can be seen in fig. 5. The fluctuations are measured by Langmuir probes in the region where the curvature is concave. The measured auto-correlation function $C(\tau)$ indicates that a wide band of noise is present rather than discrete modes - fig. 6. It is important to note that for similar plasma parameters, the absolute value of the density fluctuation $\frac{\tilde{n}}{n_o}$ is an order of magnitude less in these magnetic configuration than the value in a straight magnetic field /2/.

In order to identify the fluctuations and to determine the effect of the distance between the rods, detailed cross correlation measurements $C(\tau, \lambda)$ have been started.

References. -

/1/ S. YOSHIKAWA & al. - CN 24 - C7 - Novosibirsk 1968

/2/ M. BERNARD & al. -CN 24 - E 10 - Novosibirsk 1968

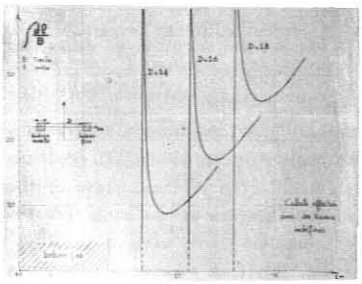

Fig. 1 - Values of $\oint \frac{dl}{B}$ for three positions of the rods.

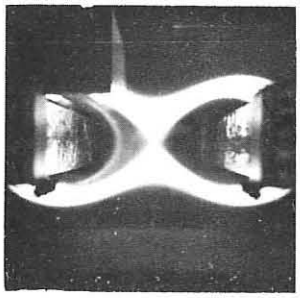

Fig. 2

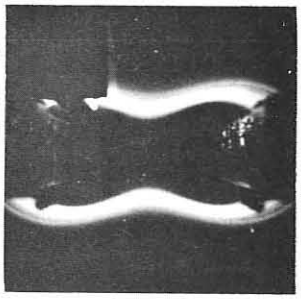

Fig. 3

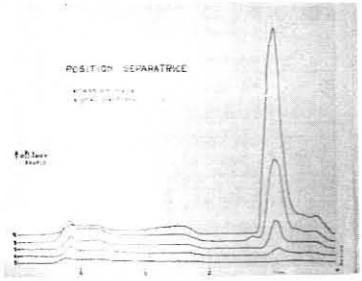

Fig. 4 - Location of the separatrix by measuring the electronic density profile for several positions of the electron gun.

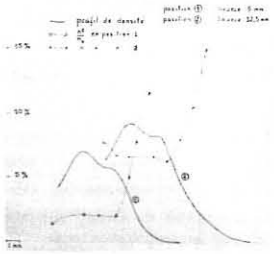

Fig. 5 - Profiles of particle density and $\frac{\tilde{n}}{n_o}$ for two positions of the discharge.

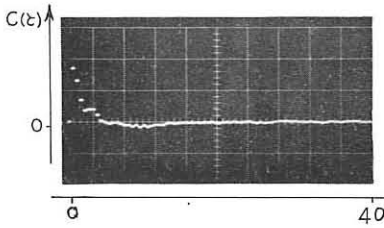

Fig. 6 - Auto-correlation function C(τ)

LOSS OF A QUIESCENT PLASMA BY CONVECTION

by
W. L. Harries
Plasma Physics Laboratory
Princeton University
Princeton, New Jersey, USA

An important question that arises in the confinement of plasmas by magnetic fields is whether nonclassical plasma losses would be reduced if fluctuations were eliminated. The purpose of this paper is to investigate this question experimentally in a multipole configuration.

The experiments were in linear quadrupole (Fig. 1a) with ohmically-heated and electron cyclotron resonance heated plasmas. The measurements were mainly in helium afterglows with $10^{12} > n_e > 10^{10}$ cm^{-3}, 10 eV > $T_e > 0.5$ eV, $T_i < 1$ eV, mean free paths ≈ 100 cm and the distance along a magnetic line between regions of favorable and unfavorable curvature ≈ 20 cm. Outside ψ_c (the flux line where $\partial/\partial\psi(\oint d\ell/B) = 0$) the fluctuation level $\delta n/n \approx 50\%$, where n is the plasma density measured by a probe, and δn is the peak-to-peak fluctuation. At Q inside ψ_c, $\delta n/n \approx 20\%$ but at P and C, $\delta n/n < 1\%$.[1] Collectors external to the plasma showed the losses were mainly radial (> 80%) with end losses of about 15%.[2] Probes at P, Q, and C showed the loss rates were approximately equal with a loss time $\tau \approx 1$ msec $\approx 10\ \tau_B$ where τ_B is the Bohm time. A particle at C could travel to Q where there were fluctuations, on the same flux line, but the flux line through P was entirely in a quiescent region. The diffusion coefficient calculated from the fluctuations at P, $D_f \approx 10^{-3} D_B$ where D_B is the Bohm diffusion coefficient, and too small to explain the loss. Particles at P were not lost to the conductor, as collectors on the conductor (Fig. 1a) recorded less than 1% of the total loss. The density showed a maximum at ψ_s so such particles must have traveled in a direction opposite to that given by $-D_f \nabla n$. Thus we are led to consider processes which do not depend on diffusion caused by fluctuations.

Plasma "structure" or variation of parameters as a function of z the axial position has been measured: (1) particle collectors at D (Fig. 1a) in a line parallel to z showed variations in plasma flux loss as a function of z of order 50%.[2] (2) two pairs of microwave horns displaced axially by 10 cm showed that the plasma density varied with z as well as time.[3] (3) probe measurements described below showed variations in I_s the ion saturation current and V_f the floating potential with z.

A probe whose tip could move radially and axially was used to map the plane AB (Fig. 1a). Lines of equal I_s and V_f (dotted) at a given time t_s when the ohmic heating current was turned off, are shown (Fig. 1b). The structure was very reproducible, showing spatial variations ≈ 50% (about 200 pulses were used), and died away in the afterglow in about a millisecond. The electron temperature T_e measured with a single probe was constant to within an accuracy of 20% at any given time over the plane AB, so the I_s lines approximately represent density contours. To get the plasma potential $V_p = V_f + 4.5\ kT_e$ any error in T_e is multiplied by 4.5. Assuming T_e = constant, then V_f differs from V_p by a constant and the equipotentials represent the plasma flow lines from E/B velocities (Fig. 1b). The lines form closed paths suggesting convective cells. Similar patterns were obtained correcting with the measured values of T_e except they were displaced by about 8 cm in the z direction. Thus, the potential contours should be taken as qualitative rather than quantitative observations. Measurements along field lines showed n_e and T_e to be constant within experimental error, so the patterns should follow the closed lines around the machine.

As the periodicity of I_s and V_f approximated the coil spacing, another coil 120 cm long and of 2.5 cm spacing was used, and probe measurements made over a range $-100 < z < +100$ cm, $-0.8 < r < 4.1$ cm. On energizing turns 3 and 4, 10 and 11, etc. with the same periodicity as before, patterns similar to Fig. 1b were recorded. Using all the turns, the 20 cm periodicity disappeared and the 120 cm period of the coil appeared, showing a vortex of order 100 cm length (Fig. 2). The E/B velocities were calculated assuming T_e constant, and correcting for T_e made the values about twice as high.

As the E/B velocities were uncertain, an independent method of measuring particle flux directly was tried for a 100 cm vortex. Two plates 2 mm × 2 mm were mounted back-to-back in the z plane, and moved over z and r. An estimate of the drift velocity in the z direction could be made from the difference in ion saturation currents. The drift velocity patterns were similar to the E/B velocity patterns and on reversing the current in the conductors, both reversed together. The magnitudes of the velocities estimated with the plates were 4 times or more times lower than those estimated from the potentials.

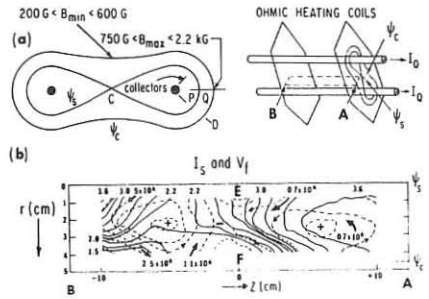

Fig. 1. (a) Linear quadrupole arrangement. (b) Curves of equal I_s (in mA) and V_f (dotted) for plane AB, showing E/B velocities; helium, I_o = 15 kA, $t = t_s$.

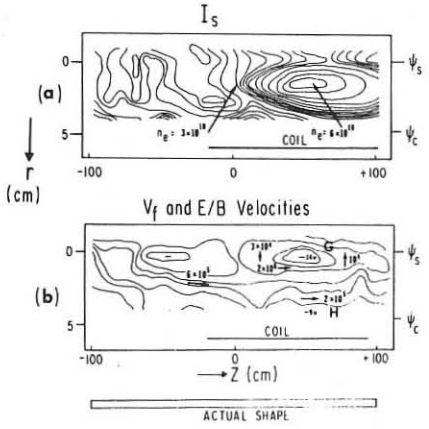

Fig. 2. Result with coil 2.5 cm spacing; I_o = -45 kA, $t = t_s$ + 220 μsec.

For both coils the plasma containment time was about 1 msec. Although the drift velocities and flow lines were not known accurately, the values suggested that particles could move from the quiescent region near ψ_s to the vicinity of ψ_c in less than a containment time. In Fig. 1b the time from region E to F ≈ 10 μsec, implying that most particles would return again to E without being lost. Whilst near F, where turbulence was observed, there could be a finite probability that the particles were lost outwards from the plasma. In Fig. 2b the time from G to H was of order but less than 1 msec. Hence we suggest that loss from the quiescent region was a two-step process of convection plus another process, probably diffusion, in the outer region of the plasma. For the quiescent region neither process by itself would be sufficient to cause the loss. The overall containment time was probably determined by the process in the outside region. If so, the elimination of temporal fluctuations may not necessarily provide good confinement in the stable region of the plasma.

The author wishes to acknowledge helpful discussions with S. Yoshikawa, R. W. Palladino, and H. P. Furth.

This work was performed under the auspices of the U. S. Atomic Energy Commission, Contract AT(30-1)-1238.

1. S. Yoshikawa and D. Meade, Phys. Fluids 10, 2649 (1967).
2. R. W. Palladino and S. Yoshikawa, Phys. Fluids 11, 1820 (1968).
3. W. L. Harries, S. Yoshikawa, and R. W. Palladino, Princeton Plasma Physics Laboratory MATT-592 (1968) (submitted to Physics of Fluids).

EXPERIMENTS ON PLASMA CONTAINMENT IN THE PRINCETON SPHERATOR

by

R. Freeman, M. Okabayashi, H. Pacher, M. Sadowski,+

S. von Goeler, and S. Yoshikawa

Plasma Physics Laboratory, Princeton University,

Princeton, New Jersey, USA

The supported spherator experiment [1] was carried out in order to determine:

(i) whether plasma is stable against low frequency instabilities--answer: yes, the fluctuation level as seen by a Langmuir probe could be made smaller than 1%

(ii) whether plasma confinement times are limited to values smaller than the Bohm time, τ_B,--no, the measured ratio τ/τ_B fell in the range 1 to 20

(iii) whether particles are lost across the magnetic field--yes, measurements with flux detectors indicated the presence of a radial plasma loss.

In a relatively short period (the experiment started on January 31, 1968), the above questions were answered, and we have added questions about causes of particle loss other than fluctuation. In doing so we have introduced the possibility of loss due to quasi-static convection. The spherator system has very strong stability properties, such as high shear, short connection length, and minimum average B. In the experiments so far performed, the center ring is supported by 6 supports of 1-mm diameter. Thus, strictly speaking, while the magnetic field is azimuthally symmetric the plasma is not.

The initial experiments were performed with a ring current of ~ 30 kA. The ring size we used up to now is 26 inches in diameter, and the ring is housed in a vacuum vessel 5 feet in diameter. The typical magnetic field strength was ~ 1 kilogauss. The plasma is made chiefly by electron resonance heating, but ohmic heating and a plasma gun were also used. The number of Larmor radii between the pressure maximum and the limiter is 20 or more for protons at 1 eV, in the afterglow where the main measurements were taken. Electron temperatures were measured by single Langmuir pulses and ranged from 1 eV (later in the afterglow) to 5 eV (earlier in the afterglow).

We used hydrogen, deuterium, helium, neon, argon, krypton, and xenon gases to make comparisons. The calculated loss times to the support were typically 8 msec for protons. The plasma density was varied between 10^{10} and 10^{12}/cc. The confinement times ranged from 1 msec to 30 msec. The ionization degree ranged from 1% to 50%.

Typical density profiles with time as parameter are shown in Fig. 1, along with oscilloscope pictures of ion saturation currents vs time. We note that density profiles (precisely speaking, ion saturation current profiles) go to zero near the limiting surfaces, as expected, and that the density decays with time. Oscilloscope traces show no noticeable oscillations under standard conditions, but if the toroidal field strength is halved (equivalent to reducing shear by a factor of ~ 2), the oscillation is evident (see A' in Fig. 1). Thus we conclude that the oscillations can be suppressed by increasing stability properties.

The next question is about the confinement times. We know that the measurement of confinement times is meaningful only if the ionization can be accurately estimated. For the measurement of confinement times we need afterglows where the electron temperature is very small, and the excitation light of neutrals is very small. The latter indicates that runaway elecrons, if any, are not producing appreciable ionization. Thus, the observed decay times of the density, measured from the microwave interferometer, were considered as the confinement times. The confinement times, plotted vs the reciprocal of $v_i \propto \sqrt{M/M_H T_e(eV)}$, are shown in Fig. 2. All data points are for a discharge in which the electron temperature, T_e was over 1 eV. In this plot the magnetic field was kept approximately constant. The theoretical times for the loss of plasmas to supports are proportional to $\sqrt{M/M_H T_e}$, as shown in the graph. The observed confinement times are somewhat less than the theoretical times. We also note that, for shorter confinement times, the confinement times are closer to the thecretical times, but for the whole range the confinement times are, on the average, approximately half the theoretical support loss times. The calculated Bohm time at T_e = 1 eV is, however, independent of the horizontal axis and is 1.5 msec. Hence we conclude that our confinement times do not appear to obey the Bohm law and that τ/τ_B can reach as high as 18 at T_e = 1 eV. Also, we can conclude from Fig. 2 that even if we restrict ourselves to hydrogen, τ/τ_B can become 4 to 7 for T_e higher than 1 eV.

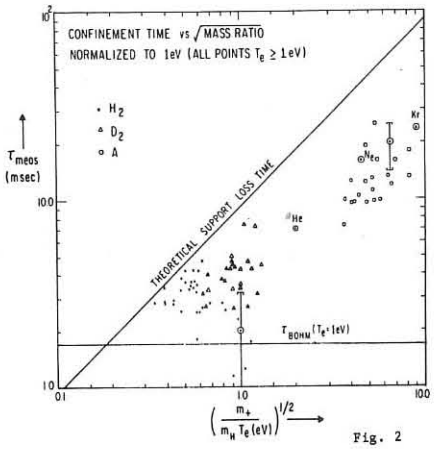

Fig. 2

The third question is where the plasma is lost. We have means to detect the plasma flux to limiter, supports, and surfaces of the poloidal field coil. The result is that approximately half of the total plasma particles are lost across the magnetic field, in reasonable agreement with the results of confinement time measurements. There is some finite probability that this cross-field loss is brought about by the perturbing electric field created by supports, the effective cross section of the supports being increased by a factor of ~ 2 above the geometric cross section.

This finite cross-field loss is present even when the fluctuation amplitude in the range of 1 kc/sec to 1 Mc/sec is suppressed such that $\Delta n/n < 1\%$, where Δn is the peak-to-peak amplitude variation of density n. Thus we are forced to look into nonfluctuational causes of the particle loss. Experiments on that subject are being continued.

This work was performed under the auspices of the U. S. Atomic Energy Commission, Contract AT(30-1)-1238.

+ On leave from Institute of Nuclear Research, Warsaw, Poland.

1 S. Yoshikawa, M. Barrault, W. Harries, D. Meade, R. Palladino, and S. von Goeler, Linear Multipole and Spherator Experiments, MATT-620 (1968); also paper CN-24/C-7, Proceedings of the Third Conference on Plasma Physics and Controlled Nuclear Fusion Research, Novosibirsk, USSR, August 1-7, 1968.

STABILIZATION DUE TO SHEAR AS TORODIAL FIELD IS INCREASED BY TWO-FOLD

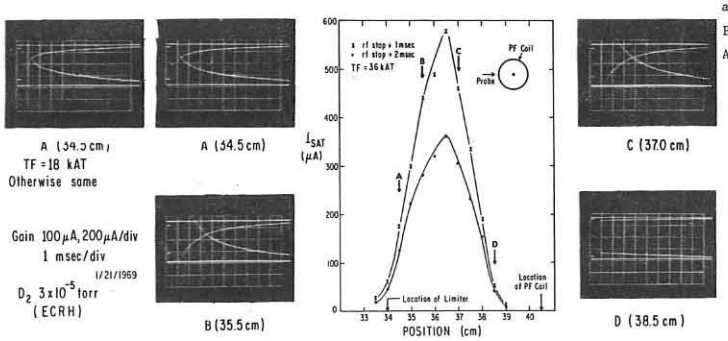

Fig. 1

STABILISATION OF ION CYCLOTRON INSTABILITIES BY ELECTRON HEATING AND FLUTE INSTABILITY BY FEEDBACK IN MAGNETIC WELL/MIRROR GEOMETRIES

by

M.J. Church, V.A. Chuyanov*, E.G. Murphy,
M. Petravic, D.R. Sweetman, E. Thompson

U.K.A.E.A. Culham Laboratory, Abingdon, Berks., England.
*On leave from the Kurchatov Institute, USSR

Introduction

In the PHOENIX II experiment a plasma of density $10^8 - 10^{10}$ cm^{-3} is produced by passing a 20 keV neutral atom beam across the 10-20 kgauss magnetic field of a simple mirror trap. By the addition of a quadrupole cusp field the trap may be converted to a minimum B geometry. The first part of this paper describes the attempts to understand and stabilise the ion gyrofrequency instabilities in the minimum B configuration and the second part describes the feedback stabilisation of the flute instability in the simple mirror configuration.

1. Stabilisation of Ion Cyclotron Instabilities in Well Geometry

Previous work has established that in minimum B geometry the density is limited to $2\text{-}5 \times 10^9$ cm^{-3} by a microinstability at the harmonics of the ion gyrofrequency. As the density is raised the instability moves to successively higher harmonics, the third harmonic being dominant at the highest density achievable. The instability bursts cause a considerable spreading of the ion energy distribution and electrons are expelled resulting in a plasma potential fluctuation between 100 volts and 1000 volts.

The instability has been identified as a finite geometry version of a mode that depends on the loss cone distribution of the ions[1]. Recent detailed measurements of the mode structure confirm this identification. The first harmonic instability, which has maximum intensity at a density of 3.6×10^8 cm^{-3} has a perturbed potential 180° out of phase at the ends ($\lambda_{\parallel} \approx 2L$, where L is the length of the plasma). The second harmonic emission which has a maximum intensity at a density of 1.2×10^9 cm^{-3} has a similar mode structure at densities below this but at higher densities switches to a mode which is in phase at the ends and 180° out of phase at the centre ($\lambda_{\parallel} \approx L$).

In addition, however, a new mode at the fundamental of the ion gyrofrequency has been observed at densities above those achieved in previously reported work ($> 3 \times 10^9$ cm^{-3}). This mode is in phase along the length of the plasma ($k_{\parallel} \approx 0$) and is more continuous in time than the other modes.

Simple infinite geometry theory suggests that the modes with $k_{\parallel} \neq 0$ should be quenched by Landau damping if T_e is raised above about 70 ℓ^2 eV, where ℓ is the harmonic number[2]. The following sections describe two attempts to suppress this instability by increasing the energy of the electrons. In addition these experiments throw some light on the mechanism for loss of the hot ions.

Microwave heating experiment

The perpendicular energy of the electrons has been raised using microwave heating at the electron gyrofrequency. A previous paper[1] described the suppression of the instability at the second and third harmonics of the ion gyrofrequency during microwave heating and the substitution of a strong instability at the fundamental which resulted in a reduced, but substantial, plasma loss rate.

Recently the average perpendicular energy of the electrons has been determined by measuring the emission at their gyrofrequency and has been shown to increase from some tens of eV in the unheated plasma to some keV in the heated plasma.

The wavelength of the instability modes in the direction parallel to the field lines has also been determined and the strong instability at the fundamental gyrofrequency shown to alternate between a mode out of phase at the ends ($\lambda_{\parallel} \approx 2L$) and a higher mode ($\lambda_{\parallel} \approx L$). This instability is intermittent in nature and is superimposed on the more continuous $k_{\parallel} \approx 0$ which is only slightly reduced during microwave heating.

The plasma potential remains low during the microwave heating period (40-400 volts) but the spreading of the ion energy distribution is similar to that observed in the unheated plasma.

Transit-time heating experiments

In other recent experiments attempts have been made to heat the electrons using electric fields oscillating at 80 Mc/s ($\approx 5\ \omega_{ci}$) parallel to the field lines. It has been shown experimentally that the average perpendicular energy of the electrons (measured by microwave emission at the gyrofrequency) is little changed during this 'heating' but that electrons are expelled from the ends and the plasma potential is raised to 1 kV or more.

The instability at the first three harmonics of the ion gyrofrequency is completely quenched by the application of this oscillating field and the energy spread of the ions is substantially reduced. The loss of plasma is, however, essentially unchanged. Some stimulated emission is observed near the applied frequency but the loss of plasma appears to be better correlated with the rise of plasma potential than with this emission.

Discussion

The microwave heating experiments demonstrate that the instability with $k_{\parallel} \neq 0$ is profoundly affected by the changes in the electron energy. It is clear, however, from the order in which the harmonics disappear as the microwave power is raised and the appearance of the strong instability at the fundamental, that a simple interpretation in terms of Landau damping due to a high electron "temperature" is not possible and the complexity of the electron energy distribution function must be taken into account.

The $k_{\parallel} \approx 0$ instability observed at the highest densities has not yet been positively identified. The modified negative mass instability and the drift loss cone instability are possible contenders.

The influence of the plasma potential demonstrated by the transit time heating experiments is probably due to its effect on the bounce frequency of the electrons which decides the damping of long wavelength modes. Rises in plasma potential may be an important stabilising effect during normal instability bursts.

The results also throw some light on the ion loss mechanism under normal conditions. In the microwave heated plasma where the plasma potential is low there is some evidence from direct loss measurements and from the energy spread that losses are mainly by scattering in velocity space. In the transit time heating experiments the loss is correlated with the rise of plasma potential and the energy spread is lower. Under normal conditions it is likely that both mechanisms are operating.

2. Feedback Stabilisation of Flute Instability in Simple Mirror Geometry

As was shown by experiments reported at the 1968 Novosibirsk Conference[3] flute instabilities can be suppressed by a feedback system in a simple mirror field, at least at low plasma densities ($\approx 10^7$ cm^{-3}). In view of the potential importance of this method the verification of this result at higher densities presents considerable interest.

Preliminary experiments using a one electrode feedback system, were carried out on PHOENIX II working as a simple mirror machine. An electrostatic probe detected the electric field fluctuations in the plasma, which were amplified by a factor of about 10^3, and fed back to the control electrode through a delay line.

Without feedback, in a simple mirror field, an m = 1 flute instability was observed; this limited the plasma density to about 3×10^8 cm^{-3}.

As in the case of OGRA II[3], switching on the feedback system led to substantial increase of density, a decrease in the amplitude and frequency of the low frequency oscillations, and to a change of their azimuthal mode.

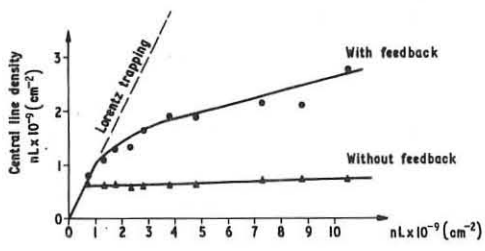

The figure shows the relationship between the plasma line density and the line density expected from the product of the injection current and the charge exchange lifetime for stabilised and unstabilised plasmas. The dashed curve shows the expected density if charge exchange were the only loss mechanism. It can be seen that, with feedback stabilisation, the losses caused by the flute instability (deviation from the dashed line) are very much reduced. However, there are still residual losses and these are connected with low frequency oscillations with frequency about 50 kHz (compared with 130 kHz for the flute) and with azimuthal mode m = 2. These are not stabilised by a feedback system using a single electrode.

It has been shown that feedback stabilisation of the flute instability can be effective at densities of 10^9 cm^{-3}, two orders of magnitude higher than in previous experiments[3]. Also densities reached in a simple mirror were approximately the same as those achieved in PHOENIX II operating as a magnetic well.

References

1. J.G. Cordey et al., Novosibirsk Conf. Paper CN-24/H-5 (1968).
2. C.O. Beasley and J.G. Cordey, Plasma Physics 10, 411 (1968).
3. V.V. Arsenin, V.A. Zhiltsov, V.A. Chuyanov. Novosibirsk Conf. Paper CN-24/J-13 (1968).

ELECTRON TEMPERATURE MEASUREMENTS IN MTSE II

M.H. Hughes, J.W. Hill, and B.D. Cooper,
Culham Laboratory, Abingdon, Berkshire,
England

1. INTRODUCTION

This paper discusses the use of neutral beam techniques[1] for the measurement of electron temperature, T_e, in the regime $n \geq 10^{13}$ cm^{-3} and $T_e \leq 50$eV, where other established techniques may be difficult or unsuitable. The experiments were carried out on MTSE II[2], a magnetic well filled by gun injection. The trapped plasma in this machine has a mean ion energy of 2 keV and a density of $\sim 10^{13}$ cm^{-3}. Previous results[2] have shown that the loss of energetic ions from the trap is consistent with classical ion-electron scattering if it is postulated that T_e is limited to 20-30eV by thermal conduction.

2. PRINCIPLE OF MEASUREMENT

A beam of monoenergetic neutral atoms is directed across the confining magnetic field so that when an atom is ionised the resulting ion is removed from the beam. The resulting beam attenuation ratio, α, can be written as

$$\alpha = \exp -\left\{ -\left[\frac{\langle \sigma_{ion} V_e \rangle}{V_B} + \sigma_{cx} \right] \int n d\ell \right\} \text{ if } V_e \gg V_B \gg V_i,$$

$$\text{or } \alpha = \exp \left\{ -\left[\frac{\langle \sigma_{ion} V_e \rangle}{V_B} + \frac{\langle \sigma_{cx} V_i \rangle}{V_B} \right] \int n d\ell \right\} \text{ if } V_e \gg V_i \gg V_B,$$

where V_e, V_i and V_B are the velocities of the electrons, protons and beam atoms respectively, n is the plasma density and σ_{cx}, σ_{ion} are the cross-sections for charge exchange and electron impact ionisation.

If $V_B \gg V_i$ the attenuation of the neutral beam is independent of V_i and both $\int n d\ell$ and T_e can be determined by simultaneously probing the plasma with two species of neutral atoms. In practice it is usually necessary to use He^o or H^o in order to make the beam velocity exceed the ion velocity which in turn entails $\int n d\ell \geq 2 \times 10^{15}$ cm^{-2} so that adequate attenuation is obtained. If $V_B \ll V_i$ the attenuation is a function of V_i and the ion energy distribution must be known before $\int n d\ell$ and Te can be determined.

For probing the MTSE II plasma, where $\int n d\ell \approx 5 \times 10^{13}$cm^{-2}, atomic hydrogen was chosen together with one of the rare gases Ar, Kr or Xe whose cross-sections are well established[3,4,5] and are sufficiently large to ensure adequate attenuation. The method of filling MTSE II produces a plasma having a very narrow ion energy distribution. The ratio V_i/V_B was therefore known and the contribution of charge exchange to the attenuation of the rare gas could be evaluated.

3. APPARATUS

A 5keV beam of neutral atoms was produced by charge exchange neutralisation of ions accelerated from an R.F. ion source. Neutralisation of the ion beam on background gas occurred in a short distance from the accelerating electrode of the ion source so that a separate charge exchange cell was unnecessary. Beams comprising a rare gas and atomic hydrogen were produced by mixing the gases in the R.F. source. The two species of atoms in the beam were time-of-flight resolved by pulsing the accelerating electrode. The beam was detected by a simple secondary emission detector which gave an emission current of a few microamperes. Statistical fluctuations in the detected current were negligible.

4. RESULTS AND DISCUSSION

Results obtained from MTSE II show that the attenuation of the rare gas beams 100μs or more after injection is too small to be consistent with the attenuation of the H^o beam. This result is consistent with the hypothesis that the trapped plasma is surrounded by "cold" ions. In this cold plasma charge exchange ionisation of the rare gas atoms will be negligible if the ion energy << 100eV. On the other hand the H^o beam measures the total $\int n d\ell$ including both classes of ions. If T_e is assumed to be zero, the relative attenuation of the rare gas and H^o beams indicate that $\int n d\ell$ in the hot plasma is $\sim 2 \times 10^{13}$ cm^{-2} and in the cold component is $\sim 4 \times 10^{13}$ cm^{-2}; if T_e is 100eV these numbers become $\sim 1 \times 10^{13}$ cm^{-2} and 5×10^{13} cm^{-2} respectively. In principle T_e could be determined by comparing the attenuation of two rare gases but, unfortunately, the relative attenuation of Ar, Kr and Xe is almost independent of T_e. The occurrence of cold ions in the central chamber of MTSE II therefore precludes the determination of T_e.

As a first attempt to modify the cold plasma, which is believed to originate from the gun, a titanium gettering surface was deposited in the drift section. This had no significant effect either on the neutral beam result or on the containment of energetic ions as indicated by the fast neutral emission[6] from the plasma. When the entire machine was gettered the containment time of energetic ions was increased considerably; for example, the duration of 4keV neutral emission was increased from 400μsec to 1.7 msec. suggesting an increase in T_e. An increase in T_e of possibly 10eV or more is, in fact, indicated by an increased absolute attentuation of the rare gas beam in the gettered case. The magnitude of this temperature change cannot, however, be estimated with any certainty since the relative attentuation of the rare gas and H^o beam still shows the presence of cold ions in the trap.

REFERENCES

1. Kozlov, O.V., Rodin, A.M., Rusanov, V.D., Skoblo, Yu. A., Chernetskii, A.V., Collection of Articles on Plasma Diagnostics. Edited by B.P. Konstantinov, U.S. Atomic Energy Commission Translation, page 185, 1963.
2. Francis, G., Hill, J.W., McNamara, B., and Mason, D.W., III Conf. on Plasma Physics and Fusion Research, Novosibirsk, 1968.
3. Stedeford, J.B.H., and Hasted, J.B., Proc. Roy. Soc. (London), A227, 466, 1955.
4. Koopman, D.W., Phys. Rev., 154, 79, 1967.
5. Rapp, D., and Englander-Golden, P., J. Chem. Phys., 43, 1464, 1965.
6. Mason, D.W. and Schofield, J.M.S., Culham Report CLM-R49, 1966.

INSTABILITIES AND CYCLOTRON WAVE EXCITATION IN A HOT ELECTRON PLASMA.

J.Jacquinot, S.Kawasaki, C.Leloup, J.P.Poffé, M.de Pretis
J.Ripault and F.Waelbroeck
ASSOCIATION EURATOM-CEA
Département de la Physique du Plasma et de la Fusion Contrôlée
Centre d'Etudes Nucléaires
Boîte Postale n° 6 · **92 Fontenay-aux-Roses** (France)

I.INTRODUCTION - In this paper we report new measurements on a velocity space instability which has often been observed in mirror confined hot electron plasmas [1]. The results are compared with theoretical expectation derived from linear electrostatic (ES) and electromagnetic (EM) theories. We also study the amplification and damping of an externally induced cyclotron wave during its propagation along the axis of the hot electron plasma.

II. EXPERIMENTAL PROCEDURE - The apparatus, the methods of determining the plasma parameters and general behavior of the plasma have already been described [1]. Using plasma gun injection and a pulse-heating technique a hot electron plasma is obtained together with a cold component in a simple magnetic mirror bottle of 1.7 mirror ratio. Between the mirrors, located 1.6 meters apart, the field B_o is uniform (±1%) over .8 meters (usually $B_o \approx 1.5$kG). Simultaneous measurements were obtained of the cold plasma density (n_c), the average energy of cold electrons (T_e) and hot electrons (T_h), the diamagnetism ($r_p^2 n_h T_{\perp h}$) and the anisotropy ($\theta = T_{\perp h}/T_{\parallel h}$) of the hot electron plasma. By changing the density of the injected plasma, n_c (cm^{-3}) could be varied between 5×10^{10} and 5×10^{13}. The other parameters would then be : $5\times10^{9} \leq n_h(cm^{-3}) \leq 7\times10^{10}$; $10 \leq T_h(keV) \leq 20$; $6 \leq \theta \leq 15$. The plasma radius in the midplane is $r_p \approx 2.5$cm.

III. THE VELOCITY SPACE INSTABILITY - For low plasma densities ($n_c < 10^{11}$, $n_h < 10^{10}$ cm^{-3}) the hot plasma is confined for several milliseconds. Above these values, anomalous losses associated with two types of instabilities may occur in bursts. The first one corresponds to a flute-like motion of the plasma column towards the walls [1]. The second one corresponds to a powerful microwave radiation and causes scattering of electrons into the loss cone. This paper is concerned with the second type of instability. In ref.[1] it was reported that: i the wave frequency is between 0.6 and 0.8 ν_{co} (ν_{co} is the electron cyclotron frequency in the center of the trap); ii the wave can propagate along the axis in the cold plasma existing outside the mirrors but is completely absorbed when it reaches a region where the cyclotron frequency equals the wave frequency; iii finally a circular wave guide placed along the axis receives an EM wave which is strongly right-hand polarized.

New measurements have recently been performed, namely : the signal from an antenna located on the axis outside the mirrors has been directly displayed on a 3.5 GHz oscilloscope. In the whole range of density where the instability occurs, only a small frequency shift downwards is observed for higher densities (fig.1). The 1 μs radiation burst previously detected by crystal rectifiers appears to be composed, in some cases, of shorter bursts lasting 10 ns and separated by 10 to 20 ns. At the same point, outside the mirrors, phase shift measurements between the microwave signals collected by two antennae give a parallel wavelength of 3.8 cm for $n_c \approx 5.10^{11}$ cm^{-3} (local $B = 1.38B_o$).

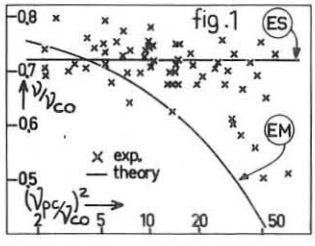

IV.COMPARISON WITH LINEAR THEORIES OF INSTABILITY IN AN ANISOTROPIC PLASMA - We assume that the equilibrium distribution function of the hot electrons is $f = (\pi^{3/2}\alpha_{\perp h}^2\alpha_{\parallel h})^{-1}\exp\left[-\left(v_\perp/\alpha_{\perp h}\right)^2+\left(v_\parallel/\alpha_{\parallel h}\right)^2\right]$ where $\alpha_{\perp h}^2 = 2kT_{\perp h}/m_e$ and $\alpha_{\parallel h}^2 = 2kT_{\parallel h}/m_e$. Taking into account an additional cold isotropic plasma, the dispersion relation for right hand polarized waves propagating along the magnetic field is [2] equation (1) :

$$0 = \omega^2 - K_\parallel^2 c^2 + \omega_{Ph}^2\left\{Z(\phi_h)\,\omega/K\alpha_{\parallel h}+(\theta-1)\left[1+\phi_h Z(\phi_h)\right]\right\}+\omega_{pc}^2 Z(\phi_c)\,\omega/K\alpha_{\parallel c}$$

where Z is the plasma dispersion function and $\phi = (\omega - |\omega_c|)/K\alpha_\parallel$. On the other hand, in the case of a longitudinal ES wave, assuming that the cold plasma has a zero temperature, the dispersion relation is found to be equation (2) :

$$0 = 1+\frac{2\omega_{ph}^2}{K^2\alpha_{\perp h}^2}\,\theta\exp-\lambda\sum_{n=-\infty}^{+\infty}\left[1-\frac{\omega-n|\omega_c|}{K_\parallel\alpha_{\parallel h}}\frac{\theta-1}{\theta}\,Z(\phi_n)\right]I_n(\lambda)+\frac{\omega_{pc}^2(K_\parallel^2\omega_c^2-K^2\omega^2)}{K^2\omega^2(\omega^2-\omega_c^2)}$$

where $\phi_n = (n|\omega_c|-\omega)/K_\parallel\alpha_\parallel$, $\lambda = K_\perp^2\alpha_\perp^2/2\omega_c^2$, I_n are the modified Bessel functions of the first kind and $\omega_p/2\pi$ is the plasma frequency.

Both equations 1 and 2 have been solved numerically for $\omega < \omega_c$. In both cases unstable modes can only be found if $\omega < \omega_c(\theta-1)/\theta$. The EM modes are very weak unless $\alpha_{\parallel h}^2\left[\theta^2(\theta-1)\left(\omega_{ph}^2+\omega_{pc}^2\right)/\omega_c^2+(\theta-1)^2\right]/c^2 > 1$. The ES modes are unstable only when $\omega > 0.5\,\omega_c$ and above a critical density which corresponds to $\omega_p \approx 0.65\,\omega_c$ in our case. Maximum growth rates and frequency spectra have been calculated for different values of ω_{ph}, ω_{pc}, θ and $\alpha_{\perp h}$ corresponding to the experimental conditions. Frequency spectra predicted by both theories are often very similar except for high densities. In this case the EM theory predicts smaller unstable frequencies (fig.2). The maximum growth rate of ES modes depends on λ (fig.3) and reaches its maximum value for $\lambda \approx 0,25$.

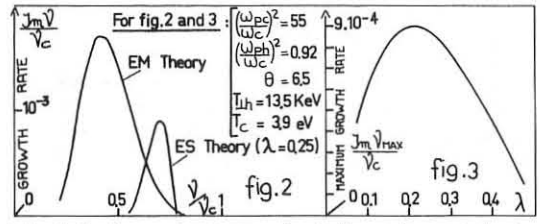

In fig.1, the frequencies corresponding to the maximum growth rates are compared with the measured frequencies. It appears that both theories are compatible with the measurements. Moreover the growth rates for EM and ES waves are found to be equal within a factor 2 ($I_m\nu/\nu_c \approx 5.10^{-3}$). Nevertheless the parallel wave length and the polarization measurements are in better agreement with the EM theory which predicts a wavelength of 3.5 cm at the measuring point. The ES theory gives 2.8cm assuming that $K_\perp$ remains constant during the propagation.

V.AMPLIFICATION AND DAMPING OF AN EXTERNALLY INDUCED CYCLOTRON WAVE - Using a small dipole antenna outside one mirror as a source, a right hand polarized cyclotron wave is excited and received outside the other mirror by a circular wave guide. The radiation is then analyzed with a turnstyle junction and the average parallel wave length in the plasma could be determined with an interferometer. A strongly polarized right hand wave could be received only when the wave frequency was such that $\nu_p < \nu < \nu_c$ everywhere in the plasma. For these values a resonance and a cutoff are observed. The measured wave length agrees with the Appleton Hartree dispersion equation if we assume that $\lambda_\perp = 14$ cm.

The microwave power transmitted through the plasma could be very different when the hot electron plasma was present. The ratio of the power transmitted after and before heating depends on ν/ν_{co}. Experimentally a limiting frequency ν_M is found (fig.4) separating two domains of amplification and damping . If the anisotropy of the plasma is increased by introducing an obstacle inside the mirror, ν_M becomes greater.When the obstacle is removed, the anisotropy can be measured and ν_M is found to be in close agreement with the EM marginal frequency, $\nu_M = \nu_{co}(\theta-1)/\theta$. Although the dependance of the amplification versus ν/ν_{co} is in agreement with the EM theory, the maximum amplification is much smaller than expected. It corresponds to Im $K = 1.2\ 10^{-2} cm^{-1}$ instead of 5.10^{-2}. The discrepancy may result from the assumption made in the theory ($K_\perp = 0$ and infinite geometry).

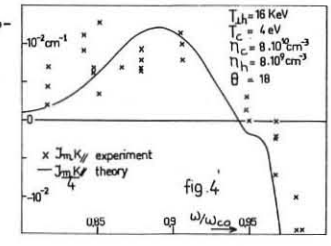

REFERENCES

[1] J.JACQUINOT et al. - Proceedings Conf.Novosibirsk (1968) I.A.E.A. (to be published)

[2] J.E.SCHARER and A.W.TRIVELPIECE Phys.Fluids, vol.10,p.591 (1967)

CONFINEMENT OF PLASMA IN TORNADO TRAPS

by

G.M.Vorobiev, G.A.Galechyan, B.P.Peregood

A.F.Ioffe Physical-Technical Institute, Academy of Sciences of the USSR, Leningrad, K-21, USSR.

In previous investigations[1-3] field distribution, field structure, and electron behaviour in Tornado-II traps were studied. The traps are realized by the use of two spherical spirals with identic or contrary winding and two rectilinear conductors connecting spirals ends (fig.1). Current directions in spiral conductors are opposite. The field distribution measurements[1] and calculations[2] showed that the central part of trap with weak field was surrounded with magnetic barrier. Detail numerical calculations of the magnetic field lines[2] gave possibility to establish the presence inside the trap a region without escaping magnetic lines. The boundary of the region is approximately the spherical surface situated between spirals. In experiments on electron confinement it was established that traps were able to confine charged particles during long time: the time of confinement was 10^4–10^5 times more then time of flight and was limited by diffusion. Furthermore it was found a critical value of disturbance at which the life time rapidly reduced to time of flight. Topological stability of the field appeared to be high.

Simultaneously plasma behaviour in traps was studied. Results of the work are subject of the report.

Traps. Tornado II traps with contrary winding of turns were used. Spherical spirals are produced from copper bars and have 9 turns. Plasma behaviour was investigated in two traps: the smaller one had the diameter of the greatest turn of outer spiral 200 mm (diameter of bar – 8 mm), the bigger – 300 mm (bar – 10 mm). The trap was situated inside the porcelain vacuum chamber, initial pressure was not higher than 10^{-6} torr. The working gas was hydrogen at the pressure P=5 10^{-5} – 10^{-3} torr. The maximum field in the magnetic barrier region was 4.5 koe, the duration of confining field existence $\frac{T}{2}$ = 3 msec (fig.2).

Diagnostics. The density and temporal dependence were measured by the use of interferometrical microwave method : in the range 910^{12} – 510^{11} cm^{-3} (λ = 10,8 mm). Electron temperature was inferred from plasma conductivity by using double electrical probes and from relative intensity of $H\alpha$, $H\beta$, $H\gamma$ and $H\delta$ spectral lines.

Method of plasma production and its parameters. Plasma was produced by means of Σ-discharge inside trap along its axis. To this end a special electrode was introduced slightly inside the trap, while the conductor of the inner spiral was used as the second electrode. The discharge current was 35 ka the duration of active period – 200 μsec. The discharge was finished approximately at the moment of confining field maximum (fig. 2a). Plasma density at the end of discharge was 10^{14} cm^{-3} and weakly depended on initial pressure. All methods of electron temperature determination gave approximately the same value 3 ev.

Fig. I

Plasma behaviour. As it was established by means of photoregistration, plasma occupied the central region of the trap and lived there as a spherical formation with a clear rather rigid and even boundary. In the range of initial pressures 5 10^{-5} – 10^{-3} torr plasma e-foling time did not depend on P_0, the increasing P_0 above 5 10^{-5} torr the time increased. Naturally all experiments were made at $P_0 < 5\ 10^{-3}$ torr. The rations of intensities of four spectral lines (fig.2d) were practically constant during plasma life-time. Thus one can conclude that electron temperature during decay changes slightly. The measurement of plasma density was began after stopping microwave cut off /n = 9 10^{12} cm^{-3} for λ = 10,8 mm/and could be continued till n = 5 10^{11} cm^{-3} (fig.2b). According the curves $\ln n = f(t)$ (fig.2c) produced at different values of confining field H the dependences of life time τ versus H were determined. For both traps in which the confinement was investigated the dependence appeared to be square law. Fig.3 is for 300 mm trap: lines are τ = = F(H), points – experiment. At the increasing of the trap diameter from 200 mm to 300 mm and equal conditions plasma life time increased approximately in 2 times. The dependence of plasma life time on the value of field disturbance was invesfigated. The disturbance was introduced as well as in [3] by means of distortion current equality in spiral conductors. Unexpected and unexplained till now is the fact that plasma life time had maximum at m = = $\frac{I_{out}}{I_{in}} \neq 1$ (fig.4). Maximum value of decay constant Imsec (for 300 mm trap) for m = 0,6. It is not excepted that this is connected with realization imperfection of confining field. Apparently the nearest to ideal ones are realized in used traps at unequal currents in spirals.

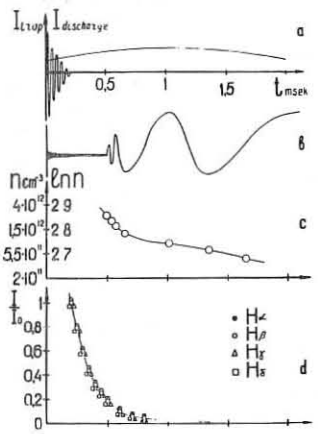

Fig. 2

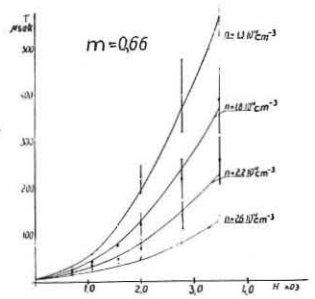

Fig. 3

Plasma oscillations. On the probe currents oscillograms and spectral lines intensities oscillations are not seen. Intensive oscillations appeared in dereasing ratio till the value m less than 0,4. In increasing m above 0,8, oscillations also appeared but with comparatively small intensity

So written above experiments on plasma in Tornado II traps gave rather high plasma life time, absence of lar large scale instabilities and square law dependence of plasma life time from the value of confining field.

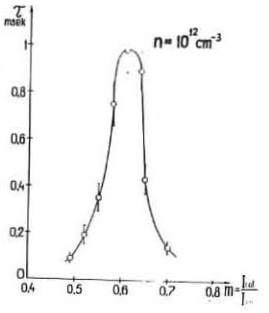

Fig. 4

REFERENCES

1. K.B.Abramova, G.A.Galechyan, B.P.Peregood. Journ. Techn. Fis. XXXVI, 1426, 1966.
2. A.N.Kozyrev, B.P.Peregood. Magnetic field structure of Tornado II traps. Preprint Phys. Techn. Institute, 1969.
3. A.N.Kozyrev, B.P.Peregood, L.V.Khabarin. II Europ. Conf. Fus. 1967.

THE MAGNETIC FIELD STRUCTURE IN "TORNADO 2" TRAP

by
A.N.Kozyrev and B.P.Peregood
Ioffe Physical-Technical Institute Academy of Sciences USSR
Leningrad K-21 , USSR .

The magnetic field in "Tornado2" trap was investigated by means of computer.

1. The model and computing method.

The system of linear conductors, consisting of two spirals with constant and equal angular pitches and straight conductors, connecting the ends of the spirals (Fig.1), was chosen as a model of "Tornado 2" trap. These spirals are located on the surfaces of two spheres with the same centre so that if the radius intersects one spiral it intersects another one too. The straight conductors are located on the diameter which connects the "poles" of the trap.

The system of spherical co-ordinates η, ϑ, φ was chosen for description of the system (Fig.1). OO′ is the symmetry axis.

The equations for the spirals and filaments are.

$\vartheta = \alpha\varphi$; $\eta = \eta_1$ - for the inner spiral,

$\vartheta = \alpha\varphi$; $\eta = \eta_2$ - for the outer spiral,

$\eta_1 \le \eta \le \eta_2$; $\vartheta = \pi/2$; $\varphi = 0$

$\eta_1 \le \eta \le \eta_2$; $\vartheta = -\pi/2$; $\varphi = 0$ } for the filaments .

Here $\alpha = \frac{1}{2n}$, where n-is the number of windings.

The mathematical expression for the components of magnetic field intensity are too complicated to be given here.

The magnetic field lines were traced step by step by numerical integration of the well-known system of differential equations.

$$\frac{d\eta}{H_\eta} = \frac{\eta\, d\vartheta}{H\vartheta} = \frac{\eta \cos\vartheta\, d\varphi}{H\varphi} = \frac{ds}{H}$$

using the Runge-Kutta scheme . Here H-is the magnetic field intensity and ds - the differential of the arc length.

The accuracy has been checked by reintegrating with the step two times smaller and by comparing the results. The mistakes in positions of the ends of magnetic field lines were $\sim 5\times10^{-4}$.

2. The computing results .

The results of computations of magnetic field intensity along the different directions indicate that in the trap exists a region with relatively small intensity of the field and a magnetic barrier around it.

The purpose of this stage of the investigation of magnetic field lines in "Tornado 2" trap consists in receiving the main idea about the behaviour of relatively short intercepts of magnetic lines trajectories. In Fig.2 are represented the projections of magnetic field lines on the co-ordinate plane $\varphi = 0, \pi$ for the trap with n=14. One can see from this figure that the magnetic field lines can be divided into three groups.

One group consists of field lines which, going out from the central region into the interval between spirals, return into the central region again.

The second group consists of the field lines which enter the trap from outside penetrate into the interval between spirals and leave the trap again.

Every line belonging to the 1 and 2 groups receives an angular shift $\Delta\varphi$ after going around the conductors. When the field line goes around the whole system the number of conductors which are enveloped must be changed per unit in every interval $0 < \varphi < \pi$ and $\pi < \varphi < 2\pi$. Such "jumps" really exist inthe system.

The lines belonging to the third group generate a layer between the first and the second group of lines. In contrast to the lines considered above the part of the third group of lines which remain in the trap after making some number of turns around the filament keeps turn around the conductor moving along the spiral to the opposite pole and there penatrates in the interval between two spirals again. The transition from the inner spiral to the outer one is forbidden because of existence a point on the filament where the component of the field along the filament vanishes .

Thus the intercepts of the lines form two spatial separated classes: the class of lines remaining in the trap and the class of escaping lines .

To receive the answer on the question is this system closed or not the lines going out of the central region were traced. After making some numbers of turns around the spiral conductors these lines remain in the trap . This result is in disagreement with the result developed by R.J.Bickerton (1), who observed the lines leaving the trap after one turn. We have an oppinion that this disagreement is a consequence of the breaking of the "reflecting current" principle(2) in the system of currents used in (1). But this question requires more detail investigations.

The field lines belonging to the first group after going around the whole system return nearly to the point from where they have started. Therefore there is a reason to determine the value $\int\frac{d\ell}{B}$ for the different lines intersecting the equatorial plane on the different distances from the center (Fig.3). The value of $\int\frac{d\ell}{B}$ was computed for one turn around the conductors and since the value of the angular shift $\Delta\varphi$ was known it was possible to recalculate $\int\frac{d\ell}{B}$ for the turn around the whole system. Fig.3 shows that "Tornado 2" possesses the average minimum "B" and that the lowest value $\int\frac{d\ell}{B}$ belongs to the lines located near the intermediate layer, that is near the sphere with the radius $\eta = 1.1$. This sphere divides the field lines into two classes mentioned above.

Thus one can draw a conclusion that "Tornado 2" possesses minimum "B" , averege minimum "B" and that unless the flux connected with the escaping lines is equal to zero, it is small enough .

References:

(1) R.J.Bickerton, L.Lonamon Nucl.Fus. 8, 121 , 1968 .

(2) K.B.Abramova, G.A.Galechan , B.P.Peregood
Gurnal Tehnichescoy Physiki XXXVI , 1426 ,1966 .

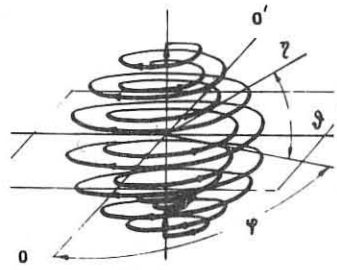

Fig.1

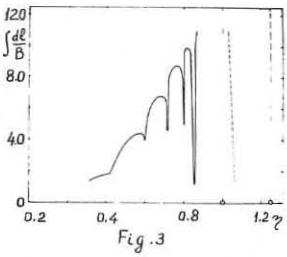

Fig.3

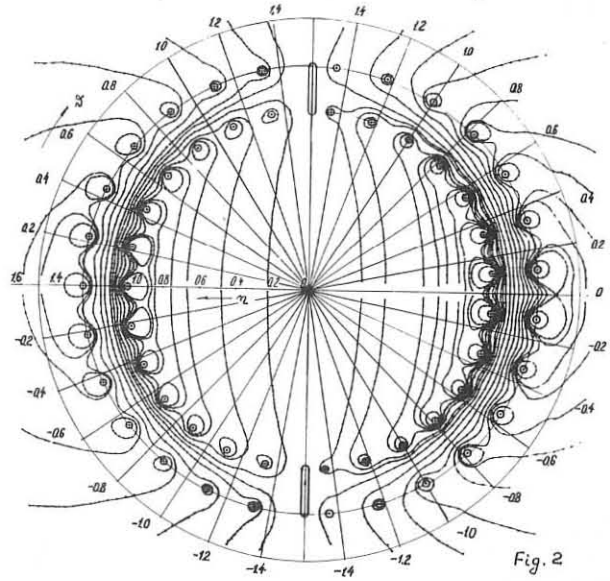
Fig. 2

---

substituted paper.

ALPHA PARTICLE HEATING AND ENERGY BALANCE IN A MIRROR REACTOR

by

L.G. Kuo-Petravic, M. Petravic and C.J.H. Watson

U.K.A.E.A., Culham Laboratory, Abingdon, Berks., England.

There is a growing awareness that a fusion reactor employing mirror confinement has significant technological advantages over a toroidal reactor. Its principal shortcoming is the uncomfortably small value of Q, the ratio of the thermonuclear power generated to the injected power. For a 50%-50% D-T mixture, this is given by $Q = \frac{1}{4}\, n\tau\, (\overline{\sigma v})_{DT}\, E_N/E_o$, where n is the plasma density, τ its lifetime, $(\overline{\sigma v})_{DT}$ the mean reaction rate, E_N the energy release resulting from a thermonuclear reaction (taken in this paper to be 22.4 MeV), and E_o the ion + electron injection energy. The basic difficulty in evaluating Q lies in the calculation of $n\tau$, which is usually obtained by solving the Fokker-Planck equation of Rosenbluth, McDonald and Judd[1] or the equivalent equation of Landau[2]. The weak points in the derivation of this equation, and in its reduction to the form used in earlier computations, have been reviewed by McNamara and Watson[3]. The most questionable points appear to be the assumptions: (i) that in evaluating the Fokker-Planck coefficients, the energy dependent cut-off for the Coulomb interaction can be replaced by some mean value; (ii) that the equation is separable, using spherical polar coordinates in velocity space; (iii) that the number of distinguishable charged species can be taken as one or two only, ignoring the effect of the thermonuclear α-particles. A partial justification of assumption (ii) is to be found in the work of Roberts and Carr[4], Bing and Roberts[5] and BenDaniel and Allis[6], who, however, considered only a single species. Their results were used by Post[7] to derive an expression for the maximum attainable Q, $Q_{max} = 11 \log_{10} R$, where R is the mirror ratio.

Doubts about the accuracy of Post's expression for Q were raised by Fowler and Rankin[8] in 1965, who improved the $n\tau$ calculations, considering two interacting charged species (electrons and deuterons) and simulating the role of the electrostatic potential by introducing an 'effective' mirror ratio $R_{eff} = R(1 + \frac{e\phi}{E})^{-1}$. The equations which they used in their computations were of the form:

$$-\frac{\partial}{\partial E}(Vf) + \frac{\partial^2}{\partial E^2}(Df) - \frac{1}{\tau(E)} f + I\,\delta(E - E_o) = 0$$

with separate equations for each species, the coupling between the equations being via the friction and diffusion coefficients, V and D, and the particle lifetime $\tau(E)$, which all depend on the two distribution functions $f_{\pm}(E)$; for ions

$$\tau_+^{-1}(E) = \frac{2\gamma}{\sqrt{2m_+}}\frac{\Lambda}{4E}\left\{\frac{1}{\sqrt{E}}\int_0^E dE'\left(1 - \frac{1}{3}\frac{E'}{E}\right) f_+(E') + \frac{2}{3}\int_E^\infty \frac{dE'}{\sqrt{E'}} f_+(E')\right.$$

$$\left. + \frac{1}{\sqrt{E}}\int_0^{\frac{m_-}{m_+}E} dE'\left(1 - \frac{1}{3}\frac{m_+}{m_-}\frac{E'}{E}\right) f_-(E') + \frac{2}{3}\sqrt{\frac{m_-}{m_+}}\int_{\frac{m_-}{m_+}E}^\infty \frac{dE'}{\sqrt{E'}} f_-(E')\right\}$$

where $\gamma = 2\pi e^4 \ln D$ is the Coulomb logarithm and $\Lambda = (\log_{10} R_{eff})^{-1}$.

Fowler and Rankin found that, for R = 3, the plasma potential reduces $n\tau$ by a factor of two, and the cooling of the ions by electrons leads to a further factor of two reduction, resulting in $Q_{max} = 3 \log_{10} R$. They also found that the optimum injection energy was 260 keV (as compared with Post's 140 keV) and (by replacing the electrons in their programme by α-particles) they inferred that trapped 3.5 MeV α-particles, products of fusion reactions, increased Q by only 10%.

Our interest in the problem was aroused by the observation of Rose[9] that α-particle heating would be dominant if the $n\tau$ value were close to that of Post. Since several methods of increasing $n\tau$ have already been proposed (e.g. Kelley[10], Watson[11]), we have sought to understand the consequences of varying $n\tau$. Our procedure has been to take the Fowler-Rankin computer programme, which they kindly made available to us, and modify it by including a third species (α-particles or tritons). Changes in $n\tau$ were simulated by arbitrarily varying the mirror ratio R. Our results are summarised below.

The effect of the plasma potential is found to be small; for R = 3 the $n\tau$ value is reduced by a factor of 1.5 and at R = 10 by less than 1.2, provided that self-consistent potentials and distribution functions are used. Its effect on ions has therefore been ignored in calculations involving α's, by setting $\phi_D = 0$.

The cooling of ions by electrons is much more important, and it accounts for a reduction in $n\tau$ by factors of 3 and 3.6 at R = 3 and R = 10 respectively. The <u>total</u> transfer of energy from ions to electrons increases with R or $n\tau$ (although the <u>rate</u> decreases), and this is responsible for the substantial deviation from $n\tau \sim \log_{10} R$ as shown by the dashed line in Fig.3. This effect arises because τ is less than the ion-electron energy equipartition time, and it shows that almost any method for increasing $n\tau$ will become progressively less effective as $n\tau$ increases.

We find Q-values even lower than Fowler and Rankin. For R = 3 our value, corrected for the separability assumption, is $Q_o = 0.9$ as compared with their $Q_o = 1.5$. At R = 10 we find $Q_o = 1.5$, attained with an average reaction rate $(\overline{\sigma v})_{DT} = 9.8 \times 10^{-16}$. The discrepancy is entirely attributable to our use of different nuclear cross-section.

The effect of heating by α-particles turns out to be predicted with reasonable accuracy by supposing that the whole of the available α-particle energy is given to the ions and that the ion injection energy is correspondingly reduced. The $n\tau$ then stays constant, whereas Q is improved by the ratio $E_o/(E_o - \frac{1}{2}\, b \times 3.5\ \text{MeV})$, where b is the fractional burn-up. Equivalently one can write $Q_\alpha = Q_o/(1 - Q_o/6.4)$ where Q_o is the value obtained if the α's are allowed to escape and Q_α is the value when they are retained.

In our calculations the injection energy was kept constant and equal to 100 keV. It was found (see Fig.1) that the α-particles gave most of their energy to the electrons, but the proportion given to the ions increased with R. Both transfers have the effect of increasing $n\tau$: by heating the electrons, their interaction with the ions is reduced and the extra energy acquired by the ions increases their lifetime as $T_i^{3/2}$. The α-particles give up more than 90% of their energy before leaving the system, as can be seen from their energy distribution function shown in Fig.2, together with the corresponding deuteron and electron distribution functions. Typically the alphas leave with less than 200 keV, whereas their average energy in the plasma is about 1 MeV.

The improvement in Q which results from containing the α-particles is shown in Fig.3 and Fig.4, where Q_α, as defined above, is plotted against Q_o. At R = 10 for deuterons injected at 100 keV, $Q_o = 1.5$ and $Q_\alpha = 1.9$. By increasing the injection energy to 150 keV and replacing the deuterons by a deuterium tritium mixture in the $n\tau$ calculation, Q_o can be increased to 1.9 and Q_α to 2.5. Clearly, at these $n\tau$ values, α-particle heating plays a rather modest role. However, as Fig.4 shows, small improvements in $n\tau$ can lead to disproportionate improvements in Q_α, and a number of assumptions in the present $n\tau$ calculation err on the side of pessimism. For example, plasma injection perpendicular to the field lines (which violates assumption (ii) above) would increase $n\tau$, and it seems probable that the RMJ Fokker-Planck equation overestimates the ion-electron friction coefficient, since in evaluating the Coulomb logarithm it is assumed that thermal ions and electrons interact, whereas in fact only those electrons with $v_e \leq v_i$ interact strongly, so the effective $\ln D$ should be considerably smaller for this term. We conclude that if these or other effects could improve the basic $n\tau$ of a mirror machine by a factor of two, with a corresponding increase in Q_o to 4, this would suffice to give a useful energy balance with $Q_\alpha > 10$.

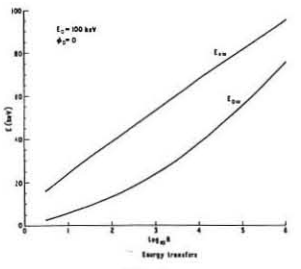

Fig.1

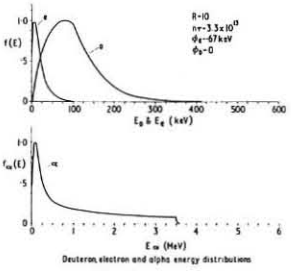

Fig.2

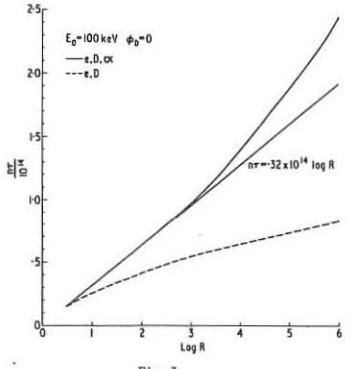

Fig.3

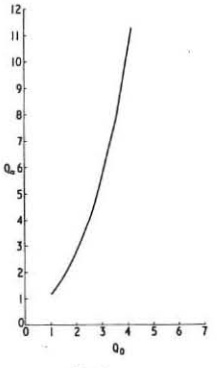

Fig.4

References

1. Rosenbluth, M.N., Mac Donald, W.M., Judd, D.C., Phys. Rev. 107, 1 (1957).
2. Landau, L.D., Zh.E.T.F., 7, 203 (1937).
3. McNamara, B., Watson, C.J.H., CLM-R 94.
4. Roberts, J.E., Carr, M.L., UCRL-5651-T (1960).
5. Bing, G.F., Roberts, J.E., Phys. Fluids, 4, 1039 (1961).
6. BenDaniel, D.J., Allis, W.P., Plasma Phys. 4, 31, 79 (1962).
7. Post, R.F., Nuclear Fusion, Suppl. Pt.1, 99 (1962).
8. Fowler, T.K., Rankin, M., Plasma Phys., 8, 121 (1966).
9. Rose, D.J., ORNL-TM-2204.
10. Kelley, G.G., Plasma Phys., 9, 503 (1967).
11. Watson, C.J.H., Proc. Int. Coll. Int. RF Flds, Saclay (1968) (CLM-P 164).

Microinstabilities in Finite Mirror Plasmas

C.O. Beasley, Jr. and W.M. Farr
Oak Ridge National Laboratory, Oak Ridge, Tenn.
Hubert Grawe
Institut für Plasmaphysik, Garching bei München

The theory of microinstabilities in an infinite, uniform plasma has been examined by many authors, resulting in the prediction that convectively and absolutely unstable modes exist in both anisotropic and loss-cone plasmas. While the perpendicular wavelength of the fastes-growing convective and absolute modes is on the order of the ion gyroradius, in most cases, the wavelength along the magnetic field is many tens of gyroradii, or the same order of magnitude as the length of mirror machines. For these plasmas, the wave-packet concept and the WKB treatment, which demand that the wavelength be much less than the plasma length, are not really valid.

In our theory, we concentrate on the non-uniformity and finite-length effects along the applied magnetic field ($\vec{B} = \hat{z}\, B_z$). Perpendicular to that field, we assume the plasma to be infinite and uniform. The presence of a mirror magnetic field results in three effects : a bouncing of the plasma particles between the mirrors with a frequency ω_b, a density gradient along the field lines, and a variation of the gyrofrequency along the magnetic field. From the bounce contribution, we should expect to see resonance effects near $n\omega_b$ not present in infinite plasmas. The density gradient should provide a set of turning points for finite-wavelength, infinite-plasma modes, or for flute-like modes, prescribe a standing wave solution which may or may not admit the class of infinite modes. The effect of the spread in gyrofrequencies provides local gyrofrequency resonances at various points along the magnetic field as well as a detuning of sharply resonant infinite-plasma eigenmodes.

In our initial model, we ignore the variation in magnetic field by representing the mirror field in terms of a fictitious potential

$$\Phi(z) = \frac{m_\ell}{2}\,\omega_{b\ell}^2\, z^2 \qquad (\ell : \text{particle species})$$

This model permits an examination of important inhomogeneity effects on flute-like modes. The density gradient is a result of the equilibrium distribution F being a function of the constants of motion. We propose F to be a separable distribution of the form

$$F(v_\perp, v_z, z) = g(v_\perp)\, h(v_z, z)$$

$$g = \frac{1}{\alpha_\perp^2 \pi\, j!}\left(\frac{v_\perp}{\alpha_\perp}\right)^{2j} \exp\left(-\frac{v_\perp^2}{\alpha_\perp^2}\right) \;;\quad h = \frac{1}{\alpha_\parallel \pi^{1/2}} \exp\left(-\frac{v_z^2}{\alpha_\parallel^2} - \frac{\omega_b^2 z^2}{\alpha_\parallel^2}\right)$$

where the integer parameter j prescribes the width of $g(v_\perp)$. As $j \to \infty$, $g(v_\perp) \to \frac{1}{2\pi v_\perp}\,\delta(v_\perp - v_m)$, where $v_m = \alpha_\perp j^{1/2}$ is the peak perpendicular velocity.

Since the plasma is homogeneous in the direction perpendicular to the z-axis, the electrostatic perturbed potential may be assumed to be of the form

$$\psi = \hat{\psi}(z) \exp\{i(k_x x - \omega t)\}$$

And the perturbed distribution, a function of cylindrical coordinates in velocity space, $v_\perp$, φ, v_z, is of the form

$$f = f(v_\perp, \varphi, v_z, z) \exp[i(k_x x - \omega t)]$$

Then the linearized Vlasov equation is

$$\frac{\partial f}{\partial \varphi} + \frac{1}{m\Omega}\frac{d\Phi}{dz}\frac{\partial f}{\partial v_z} - \frac{v_z}{\Omega}\frac{\partial f}{\partial z} + \frac{i(\omega - k_x v_\perp \cos\varphi)}{\Omega} f \qquad (1)$$

$$= -\frac{q}{m\Omega}\left(i k_x \cos\varphi\, \hat{\psi}\frac{\partial F}{\partial v_\perp} - \frac{d\hat{\psi}}{dz}\frac{\partial F}{\partial v_z}\right) \qquad (\Omega : \text{the gyrofrequency})$$

One can explicitly calculate the perturbed density

$$g(z) = \int_{-\infty}^{+\infty} dv_z \int_0^\infty v_\perp dv_\perp \int_0^{2\pi} d\varphi\, f(v_\perp, \varphi, v_z, z) \qquad (2)$$

and the solution to Poisson's equation

$$k_x^2 \hat{\psi} - \frac{d^2\hat{\psi}}{dz^2} = 4\pi \sum_\ell q_\ell\, g_\ell(z) \qquad (3)$$

may be obtained numerically by iteration of an integral equation solved by computer.

Just as in the case of a homogeneous plasma, the integrations of f over φ and $v_\perp$ yield a sum over the cyclotron harmonics $n\Omega$. After doing these integrations, we obtain a differential equation for $\beta_n(v_z, z)$:

$$\left\{ i\left(\frac{\omega}{\Omega} - n\right) + \frac{\omega_b^2}{\Omega^2} z \frac{\partial}{\partial v_z} - \frac{v_z}{\Omega}\frac{\partial}{\partial z} \right\} \beta_n(v_z, z) \qquad (4)$$

$$= \frac{2q}{m\alpha_\parallel^2}\, h(v_z, z)\left(i n T D_n \hat{\psi}(z) + \frac{v_z}{\Omega} C_n \frac{d\hat{\psi}(z)}{dz}\right)$$

where

$$g(z) \equiv \sum_{n=-\infty}^{\infty} \int_{-\infty}^{+\infty} dv_z\, \beta_n(v_z, z) \qquad (5)$$

$$T \equiv \frac{\alpha_\perp^2}{\alpha_\parallel^2} \quad ; \quad C_n \equiv 2\pi \int_0^{+\infty} v_\perp dv_\perp\, J_n\left(\frac{k_x v_\perp}{\Omega}\right) g(v_\perp)$$

$$D_n \equiv -\pi\alpha_\perp^2 \int_0^\infty v_\perp dv_\perp\, J_n\left(\frac{k_x v_\perp}{\Omega}\right) \frac{1}{v_\perp}\frac{dg(v_\perp)}{dv_\perp}$$

We may take advantage of the fact that $\hat{\psi}$ and $\frac{d\hat{\psi}}{dz}$ vanish at some distance large compared with the plasma length to write $\hat{\psi}$ in terms of Fourier components

$$\hat{\psi}(z) = \sum_{\mu=-\infty}^{\infty} \varphi_\mu \exp\left(i\mu \frac{z}{L}\right)$$

We specify $L = \omega_b/\alpha_\parallel$, this being the e-folding half-length of the plasma. Then it is convenient to make $\hat{\psi}$ periodic with period $2\pi L$. The Fourier decomposition allows us to write

$$g(z) \equiv \frac{2q}{m\alpha_\parallel^2} Q(z) = -\frac{2q}{m\alpha_\parallel^2} \sum_{n,\mu,\nu=-\infty}^{\infty} \frac{n\Omega T D_n + \nu\omega_b C_n}{n\Omega - \omega + \nu\omega_b}\, \gamma_{\mu\nu}^{(z)} \varphi_\mu \qquad (6)$$

where the form factors

$$\gamma_{\mu\nu}^{(z)} \equiv \frac{\exp(-\hat{z}^2)}{\pi^{1/2}} \int_{-\infty}^{+\infty} d\hat{v}\, e^{-\hat{v}^2} J_\nu(\mu\sqrt{\hat{v}^2 + \hat{z}^2})\, \frac{(\hat{v} + i\hat{z})^\nu}{(\hat{v}^2 + \hat{z}^2)^{\nu/2}} \;;\quad \hat{z} \equiv \frac{z}{L} \qquad (7)$$

are independent of plasma species.

For even solutions of Poisson's equation which include flute-like modes we impose the following boundary conditions

$$\hat{\psi}(0) = 1 \;;\quad \hat{\psi}'(0) = 0 \;;\quad \hat{\psi}(\pi L) = 0$$

These conditions yield the equations

$$\frac{\omega_{pi}^2}{\Omega_i^2} = \frac{\frac{k_x^2 \rho_i^2}{2j} T}{k_x L \int_0^\pi e^{-k_x L\hat{z}}\, Q(\hat{z})\, d\hat{z}} \qquad (8)$$

and

$$\hat{\psi}(\hat{z}) = \left(\frac{2j}{k_x^2 \rho_i^2}\right)\left(\frac{k_x L}{T}\right)\left(\frac{\omega_{pi}^2}{\Omega_i^2}\right) \frac{e^{k_x L\hat{z}}}{2} \int_{\hat{z}}^{\pi} d\hat{z}'\, e^{-k_x L\hat{z}'}\, Q(\hat{z}') \qquad (9)$$

$$+ \frac{e^{-k_x L\hat{z}}}{2}\left\{1 + \left(\frac{2j}{k_x^2 \rho_i^2}\right)\left(\frac{k_x L}{T}\right)\left(\frac{\omega_{pi}^2}{\Omega_i^2}\right) \int_0^{\hat{z}} d\hat{z}'\, e^{k_x L\hat{z}'}\, Q(\hat{z}')\right\}$$

where

$$Q \equiv Q_i + Q_e/\Theta \quad ; \quad \Theta \equiv m_e\alpha_e^2 / m_i\alpha_{\parallel i}^2$$

We solve the equations (8) and (9) by inserting a trial $\hat{\psi}$ in (8), then using the resulting eigenvalue to obtain a new eigenfunction from (9). With smoothing techniques, convergence to flute-like modes is good in cases in which they exist.

This research was partly sponsored by the U.S. Atomic Energy Commission under contract with the Union Carbide Corporation and partly performed under the terms of the agreement on association between the Institut für Plasmaphysik and Euratom.

HIGH FREQUENCY ELECTROSTATIC INSTABILITIES IN AN INHOMOGENEOUS PLASMA.

J.P. GIRARD et F. HENNION.

ASSOCIATION EURATOM-CEA
Département de la Physique du Plasma et de la Fusion Contrôlée
Centre d'Etudes Nucléaires
Boite Postale n° 6 · **92 Fontenay-aux-Roses** (France)

The ion cyclotron drift instability with $k_{//}=0$ is studied for the case of different widths of the ion distribution function, magnetic curvature and addition of cold plasma. We show numerically that this instability is sensitive to these three parameters.

The relation dispersion is obtained by usual method for a perturbation exp i(−ωt + ky) and applied to distribution functions of the form :

$$F_{oj} = f_{//j}(v_{//}) \times \frac{1}{\pi \alpha_{\perp j}^2 p!}\left(\frac{v_\perp^2}{\alpha_{\perp j}^2}\right)^p \exp\left(-\frac{v_\perp^2}{\alpha_{\perp j}^2}\right)^2 \cdot \left\{1-\varepsilon_j\left(\alpha + \frac{v_y}{\Omega_j}\right)\right\}$$

We suppose that the plasma is composed of a hot ion part having a loss cone distribution ($p\neq 0$), a cold Maxwellian ion part ($p=0$) and electrons.

The parameters which are used in the text are :

$$\gamma = \frac{T_c}{T_h} = \frac{m_c \alpha_{\perp c}^2}{m_h \alpha_{\perp h}^2} \; ; \; \varepsilon = \frac{1}{n}\frac{dn}{dx}, \Delta = \frac{n_h}{n_h+n_c}, \omega_{pi}^2 = \frac{4\pi q^2 (n_h+n_c)}{m_h}$$

$\rho_h = \alpha_{\perp h}/\Omega_h$, $\Omega_h = qB_o/m_h$ (h = hot ions, c = cold ions)

For all the unstable domains (the domain N is obtained for $\omega \sim N\Omega_h$), we took the wave number k, for which these domains are the largest.

I. INSTABILITY OF A PLASMA WITH ONLY ONE POPULATION ($\Delta = 1$).

a) Homogeneous magnetic field. This case has been studied previously for a Maxwellian plasma ($p=0$) [1] and for a loss cone plasma ($p\neq 0$) [2].

Our stability limits are presented in figure (1) for different values of the width of the distribution function (p different). The analytical results of Post [1] is quite similar to our results for $p = 1$ and small gradients. The analytical results of Fowler [3] are similar to ours for steep gradients but quite different for small gradients. We observe that when the gradient increases, the unstable domains of $k\rho_i$ and ω increase. The calculations of the growth rates show that these instabilities are highly resonant for $p = 0$ and non resonant at all for $p\neq 0$. For $p=0$ the maximum growth rate for $\omega_{pi}/\Omega_i = 8$ is $0{,}1\,\Omega_i$, for $p = 1$ it is $0{,}8\,\Omega_i$ and for $p \to \infty$ (delta function) $1{,}5\,\Omega_i$.

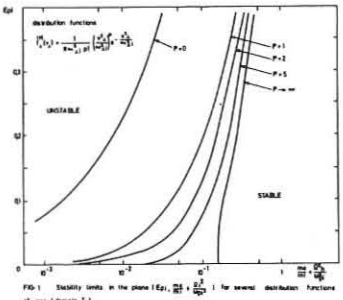

FIG. 1 Stability limits in the plane ($\varepsilon\rho_i$, $\frac{\omega_{pi}^2}{\Omega_i^2}+\frac{k^2}{\Omega_i^2}$) for several distribution functions of ions (domain I).

b) Inhomogeneous magnetic field. If we introduce the curvature of the lines of force R_c, the inhomogeneous electron terme changes and becomes $(\varepsilon - \frac{2}{R_c})\Omega_i/k\omega$. The ion term is only changed in the denominateur but we have shown that the instability was not resonant, so we always have $|\omega - n\Omega_i| \gg k v_{Di}$. Thus for a magnetic well the inhomogeneous electron term is increased and the unstable domains of $k\rho_i$, ω and ω_{pi}/Ω_i are increased. This results confirms these obtained in [4].

II. INSTABILITIES OF A PLASMA WITH TWO ION POPULATIONS ($\Delta\neq 1$).

The other effect which can be interesting to stabilize the plasma is the addition of a cold Maxwellian plasma. We have studied this effect with a well spread hot ions distribution ($p=1$). Two different cases are considered.

a) The masses of the two ion populations are identical. When the temperature T_c of the Maxwellian plasma is small (Fig. 2) a very small proportion of cold plasma considerably modifies the stability limits (solid lines).

Waves with frequency near the ion cyclotron frequency are stabilized by a few per cent of cold plasma but the other frequencies are always unstable in a limited domain of density (dashed lines). When the temperature of the cold plasma increases, the instability domains are reduced (fig. 3). If $\varepsilon\rho_h = 0.1$ the plasma is completely stable for $\Delta < 0{,}9$. If $\varepsilon\rho_h = 0.4$ the instability due mainly to the loss-cone doesn't exist if $\Delta < 0.6$, however the Mikhailovskii type instability persists even for $\Delta = 0$. The growth rates calculations show that these instabilities are not resonant except for $\Delta = 0$. The growth rate is of the order of Ω_i for $\Delta \sim 1$ and decreases with Δ .

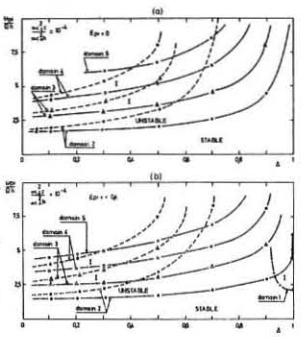

FIG. 2 Stability limits in the plane (ω_{pi}/Ω_h, Δ) for two values of the density gradient.

These results are in agreement with those obtained in [5].

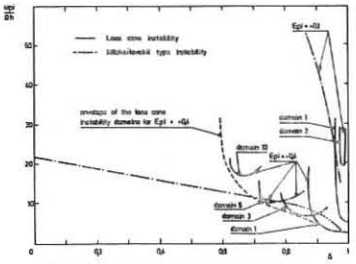

FIG. 3 Stability limits in the plane (ω_{pi}/Ω_h, Δ) for the energy ratio $\gamma = 0$.

b) The masses of the two ion populations are different. In figure (4) the results are shown for two cases : hot hydrogen and cold lithium, hot lithium and cold hydrogen. The stability limits for the density obtained in these cases are lower than for a plasma with only hydrogen ions (cold and hot) and do not vary much with Δ . We also found that when we change the temperature ratio γ from 10^{-4} to 10^{-1} these curves are nearly the same.

III. CONCLUSION.

For a plasma composed of only one ion population we find an important stabilization by spreading the distribution function when the density gradient is small. In that case we also show that the introduction of curvature of lines of force is destabilizing for a magnetic well.

The addition of a maxwellian plasma is destabilizing independantly of the density gradient if the added plasma is very cold. When the ions of hot and cold plasma are of the same type , the effect may be stabilizing if the temperature of the cold plasma is sufficient and its density a few per cent of the hot plasma density. This is not true for different types of ions ; in this case the stabilization seems very difficult.

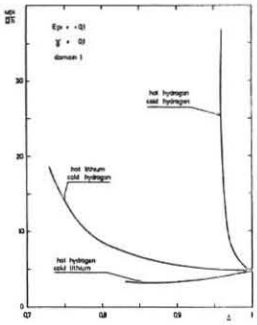

FIG. 4 Stability limits in the plane (ω_{pi}/Ω_h, Δ) when the masses of hot and cold ions are different.

A part of this work has been carried out in collaboration with P. BROSSIER and is published elsewhere [6].

[1] A.B. MIKHAILOVSKII, A.V. TIMOFEEV, Sov. Phys. JETP 17, 626 (1963).
[2] R.F. POST, M.N. ROSENBLUTH, Phys. Fluids 9 , 730 , (1966).
[3] T.K. FOWLER, conference of Gatlinburg, Nov. 1967, 350.
[4] J.G. CORDEY and al. Nuclear Fusion 8 , 153 (1968).
[5] R.F. POST, Conference of Gatlingburg, Nov. 1967 , 309
[6] P. BROSSIER and al. will be published in Plasma Physics.

PLASMA INJECTION AND CONTAINMENT IN A SPHERICAL MULTIPOLE MAGNETIC WELL

by

M. SADOWSKI*

Institute of Nuclear Research

Swierk k. Otwocka, Poland

Containment of plasmas in open-ended minimum-B configurations has been a subject of a number of theoretical and experimental studies because of the magnetohydrodynamic stability of the systems. The major disadvantage of open-ended traps is the rapid loss of particles, mostly through linear loss-gaps [1]. In the search for a minimum-B configuration with no linear loss-gaps, spherical multipole (SM) magnetic traps have been developed [2]. It has been proved that the high-order SM configurations are successful in the elimination of line-cusps [3]. The purpose of this paper is to discuss some questions of the SM geometry, and to present experimental results and some general remarks on the application of SM traps. The topology of SM systems based on regular polyhedrons has been fully described elsewhere [3,4]. Particular interest was paid to a high-order SM system based on the icosahedron geometry. It was shown [3] that such a system constitutes a minimum-B well which has no linear cusps, but it possesses 30 point cusps symmetrically spaced around the effective confinement region. The replacement of wide line-cusp regions by a given number of narrow point cusps should reduce particle losses, but there result some problems. Let us consider plasma injection along the axis of a given point cusp, where the magnetic field has only a radial component B_r. The spherical vacuum chamber is shown in Fig. 1. The field strength rises from zero at $r = 0$ to a maximum at $r = R_{eff}$, corresponding to the apex of the loss cone, and after that it drops to zero and goes to a maximum in the negative direction. If a plasma injector is placed outside the spherical chamber on which the electromagnets are arranged, a plasmoid has to pass the first high-field barrier, and low-field zone, and after that to pierce the actual point cusp of the confinement region. An identical situation occurs at each point cusp of the system; during injection the plasmoids can partially expand within the low-field/zero-field zones. Such effects lower the density and energy of the injected plasmoids, and under certain conditions they can considerably reduce the penetration of plasma into the effective confinement region. These difficulties can be avoided if the injector outlet is placed in the low-field/zero-field zone. The situation is then analogous to the injection through a point cusp of a standard spindle-cusped geometry; no expansion is possible before the plasma has passed the field maximum. Such a geometry can be easy realized and studied experimentally.

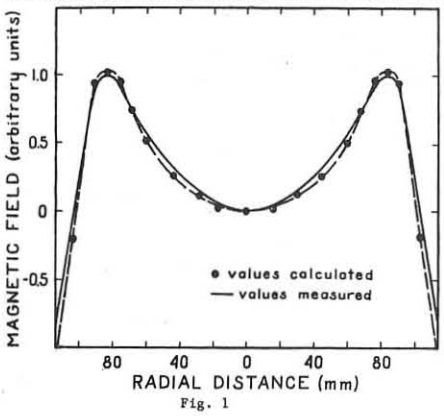

Fig. 1

In the experiments to be described, the SM-type magnetic field was created by 32 pulsed electromagnets of 50 mm o.d. which were symmetrically spaced around a spherical, 23-cm-i.d., vacuum chamber [4]. For comparative studies of cusped geometry, two additional 25 kG coils were placed on opposite sides of the chamber. The electromagnets were powered by four DC generators of 450 kW total-output in 1 second pulses. In most experiments the base pressure was 2×10^{-6} torr, and 0.5 cm^3 of gas at atmospheric pressure was supplied to injectors. Plasma was produced by 6 coaxial guns located symmetrically around the chamber, and energized by 6 sections of an 18 μF, 30 kV condenser bank. Currents in the injectors rose to a peak value of 90 kA in 2.5 μsec and were damped almost critically. Energetic plasmoids, in which the ions had a mean directed energy of about 280 eV [5], were injected radially through loss cones into the central region of the trap, where the directed energy was partially randomized by collisions of plasma streams.

Injection and containment of plasmas in the SM magnetic well have been experimentally compared with those in the spindle-cusped configuration. Measurements were performed under the same experimental conditions except for the confining field-geometry. In the SM-configuration, plasmoids from coaxial guns were injected through 6 point cusps at which the field reached 330 G. In the spindle-cusped geometry, plasma injection was effected by four injectors placed in the ring cusp and two others at the point cusps. The maximum field in the spindle point-cusps amounted to 12,000 G, and in the ring cusp reached 320 G, i.e., was close to the field in the loss-cones of the SM trap. Measurements with Langmuir probes showed that in the two geometries the maximum plasma density within the trap was about 10^{13} cm^{-3}, and the electron temperature reached $5\text{-}8 \times 10^{4}$°K. Rough observations of the total visible radiation of the plasma by means of a high-speed camera showed that the plasma in the SM configuration is confined approximately 3 times longer than in the spindle-cusped geometry. To investigate plasma trapping in the SM configuration, internal magnetic probes have been used, to measure perturbations in the radial component of the field along the symmetry axes of the point cusps. Typical probe signals (3 superimposed traces) obtained with the probe at a radius of 20 mm are shown in Fig. 2. The lower trace shows the discharge currents in the plasma injectors. The persistance of the diamagnetic signals when compared to the trap-filling time provides evidence that plasma trapping and containment do occur. The shape and lifetime of the trapped plasma are of particular interest, but difficult to investigate because of disturbances introduced by the insertion of probes. Therefore, in measurements of plasma containment, only one miniature Langmuir probe has been used [6]. The plasma containment time in the SM trap reached 85 μsec as compared with 30 μsec in the spindle-cusped geometry. Some preliminary experiments were also performed with a hybrid configuration obtained by a superposition of the above SM field and a mirror-type field which amounted to 2500 G in the midplane and had a mirror ratio equal to 4.8. A considerable difference in the trap-filling process has been observed. This effect can be explained by the fact that plasmoids injected from 4 guns placed in the central plane had to overcome the transverse magnetic field. Therefore, no collimation of plasma jets was observed and the trap-filling time was longer. The parameters and lifetime of the trapped plasma were, however, almost the same as in the SM trap with no superimposed field. The reason was probably that the plasma parameters were largely determined by the plasmoids injected through the two point cusps, which did not have to cross the transverse magnetic field. The results of the studies performed so far can be summarized as follows. The high-order SM configurations really avoid linear loss-gaps which occur in the standard minimum-B systems. The experiments were of exploratory nature only, but proved the feasibility of the application of the SM traps for plasma containment. To analyze a mechanism of plasma trapping and confinement in SM configurations, further investigations are needed. The low-field/zero-field lines from inside to outside of the SM traps, discussed above are of importance only in the case when the plasma injectors are localized far from the trap center. Therefore, the injector muzzles should be immersed in the magnetic field to be close to the point cusps of the effective confinement region. It should, however, be noted that the appearance of the low-field/zero-field zones, although outside the trap region, can have some influence on plasma containment. Since the effective confinement region is surrounded by a given number of smaller cusped regions, there is a certain analogy to the picket-fence geometry, but the SM trap has spherical symmetry. It should also be noted that experiments with plasma injection produce complex configurations in which field and plasma are intermixed. Therefore, an alternative approach, involving the compression of a shock-produced plasma by a fast-rising SM field, seems to be of particular interest.

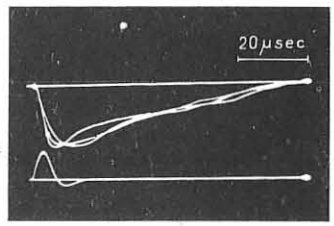

Fig. 2

* Present address: Plasma Physics Laboratory, Princeton University, Princeton, New Jersey.

[1] T. K. Allen, et al., Proc. Culham Conf. 1965, IAEA, Vol. II, p. 427.

[2] M. Sadowski, Phys. Letters 25A, 695 (1967).

[3] M. Sadowski, Phys. Letters 27A, 435 (1968).

[4] M. Sadowski, Nucl. Instrum. Methods (to be published).

[5] K. Sudlitz (unpublished).

[6] M. Sadowski, INR Report No. 914/XVIII/PP (Warsaw, 1968); Phys. Letters 28A, 626 (1969).

Dynamic Control of Line Cusp Loss

by

T. Sato, S. Miyake, Y. Kubota, K. Takayama and K. Husimi
Institute of Plasma Physics, Nagoya University, Nagoya, Japan

. Introduction

A plasma confined in a cusp field is magnetohydrodynamically stable but rapid loss of the plasma from the line cusp due to nonadiabatic particle motions is an essential disadvantage. It is very interesting to reduce such losses with RF field. Earlier works[1] suggested the possibility of trapping plasma inside the magnetic bottle with the electron cyclotron resonance phenomenon. The experiment based on the ion cyclotron resonance in a nonuniform magnetic field was carried out by S. Miyake et al.[2] and they observed accelerated ions near the resonance frequency.

In this paper, we present experimental results on the suppression of particle losses from line cusp with RF electric field near the ion cyclotron frequency.

. Experimental Apparatus

The apparatus used in this experiment is shown in Fig. 1. A steady state helium plasma with a diameter 4 mm produced by the TPD-type source[3] is fed into the simple cusp field along the spindle cusp. The maximum field strength in the line and the spindle cusp regions are B_{ML} = 2450 gauss at 22 cm and B_{MS} = 4350 gauss at 21 cm from the center of the cusp, respectively. The neutral helium pressure in the cusp chamber is 2 ~ x 10^{-6} Torr and the base pressure is about 5 x 10^{-7} Torr. The plasma density at the center of the cusp is varied from 10^{7} to 10^{11} cm^{-3}.

Two kinds of RF electrodes are used. One consists of two ring plates and the other is the sector plates with azimuthal angle of 120°. Their dimensions are 30 cm in inner diameter and 40 cm in outer one. Two plates are faced 6.5 cm apart each other. The back sides of the electrodes is covered with mica plates and on it a little Faraday cup is set to measure the ion flux reaching onto the electrode. The RF power is fed from a 500 watts grounded-grid Hartley oscillator whose frequency can be swept from 0.5 MHz to 1.0 MHz with the constant RF voltage. The "ion eaters" which are negatively biased large plates are set to measure the loss flux to the line and the spindle cusps. Ion energy is analyzed by Faraday cups or a 127° deflection type electrostatic analyzer. The former are composed of three grids and a collector in a shielding case with a hole of 20 mmϕ covered with the mesh of spacing 0.2 mm. While the plasma parameters are measured with cylindrical probes 1 mm in length and 1 mmϕ .

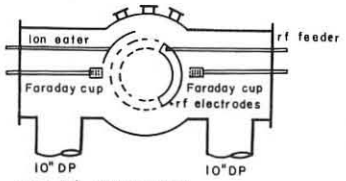

Fig.1 (a) Cusp chamber

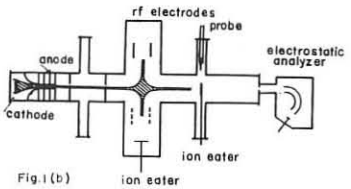

Fig.1(b)

. Experimental Results and Discussions

In the case of sector electrodes the currents to the ion eater against the oscillator frequency with the parameter of the RF electric field are shown in Fig. 2. The current decreases are observed near the ion cyclotron frequency corresponding to the magnetic field strength inside the sector electrodes. Under the resonance condition, the loss from the line cusp is suppressed down to several per cent of that without RF field.

With the use of ring electrodes, the spatial distributions of ion density inside and outside the line cusp are shown in Fig. 3. The ion density outside the cusp decreases resonantly at f = 0.75 MHz as shown in Fig. 3(a), while it increases

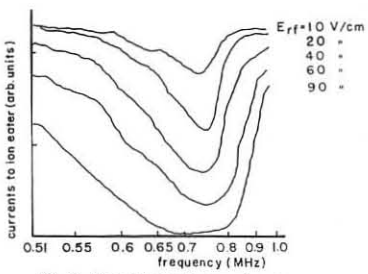

Fig. 2 Line cusp loss in case of sector electrodes

inside the cusp at the same frequency as in Fig. 3(b). The resonant change of the ion density is more dominant at the opposite side of the plasma source. The percentage of the ion flux to the line and the spindle cusps and to the ring electrodes is listed in Table 1 for various RF fields and n = 10^{8} cm^{-3} at the center of the cusp. It is obvious that the most part of the ions reflected from RF region flow out through the spindle cusps.

Fig. 4 shows the typical characteristics of Faraday cup placed outside the line cusp for different frequencies in the

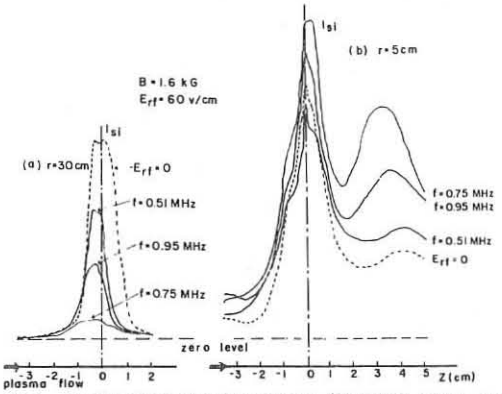

Fig. 3 Spatial distribution of ion density (a) outside of line cusp (b) inside of line cusp.

Table 1. Percentage of ion flux

RF field	0 V/cm	15 V/cm	45 V/cm
to line cusp	63 %	38 %	18 %
to spindle cusps	37 %	54 %	80 %
to RF electrodes	< 1 %	< 1 %	4 %

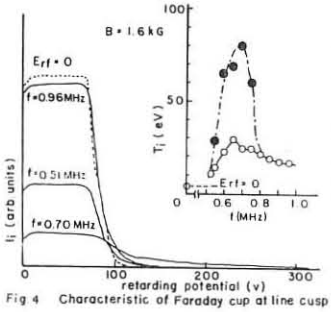

Fig. 4 Characteristic of Faraday cup at line cusp

case of the ring electrodes. When E_{rf} = 0, the characteristics show a Maxwellian distribution of T_i = 4 eV. Under the resonance condition, the flux decreases to 18 % and the high energy tail extends to 300 volts. The tail displays a Maxwellian distribution of T_i = 80 eV. The measurements by a Faraday cup and an electrostatic analyzer in the spindle cusp show that the flux is twice as much as that without RF field and the small fraction of high energy ions flows out.

The authors wish to express their appreciation to Dr. T. Honzawa and Mr. T. Kodama for their measurement by the electrostatic analyzer and to Dr. T. Watanabe for his helpful discussion.

References:

(1) R.Bardet, T.Consoli and R.Geller, C.r.hebd.Seanc.Acad. Sci., Paris 259, 1044 (1963). H. Toyama, M. Okabayashi and H. Ishizuka, Plasma Physics 10, 319 (1968).

(2) S. Miyake, T. Sato and K. Takayama, Phys. Letters 28A, 613 (1969).

(3) K. Takayama, M. Otsuka, Y. Tanaka, K. Ishii and Y. Kubota, Proc. Eighth Intern. Conf. on Phenomena in Ionized Gases, Vienna, 551 (1967).

INJECTION, CONTAINMENT, AND HEATING OF ELECTRONS IN A STUFFED CUSP

by
W. Strijland and H. de Kluiver
Association Euratom-FOM
FOM-Instituut voor Plasma-Fysica
Rijnhuizen, Jutphaas, The Netherlands

The injection of electrons into a cusped geometry has been described earlier (ref. 1). The containment is limited by nonadiabatic losses which may be diminished through improvement of the adiabaticity by an azimuthal field generated by an axial conductor. The components of the field are: $B_r = ar$, $B_z = -2az$, $B_\theta = A/r$, and the total induction is: $B = (a^2r^2 + 4a^2z^2 + A^2/r^2)^{1/2}$. The adiabaticity parameter ε is the ratio between the radius of gyration and a characteristic length, L, related to the field gradient. The latter is defined as: $L = (B^2/S^2)^{1/2}$, where $S^2 = 6a^2 + 2A^2/r^4$, the spur of the tensor gradient of the field, $\nabla\underline{B} = (\partial/\partial r + r^{-1}\partial/\partial\theta + \partial/\partial z)(B_r i_r + B_\theta i_\theta + B_z i_z)$. Hence, $\varepsilon = r_{gyr}S/B = mvS/eB^2$, where r_{gyr} is the local maximum of the radius of gyration, m is the electron mass, and v is the velocity. For the azimuthal field alone, ε is independent of the position, which is taken as some justification for the use of this single constant. The locus of the positions of the maxima of ε along the lines of force is $z^2 = \frac{1}{2}r^2.(3a^2r^4 - A^2)(6a^2r^4 + A^2)^{-1}$, and the maximum itself is given by: $\bar{\varepsilon} = (mv\sqrt{2}/e).(6a^2r^4 + A^2)(3a^2r^4 + A^2)^{-3/2}$.

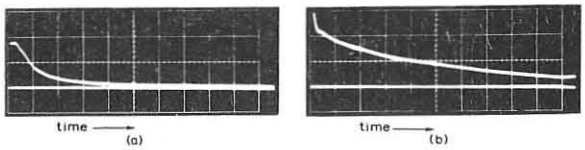

Fig. 1 The two kinds of decay curves; a: without rf-power, 0.5 μs/div; b: 3 W rf-power at 300 MHz; 185 eV electrons, a = 0.14 T/m, A = 0, pressure 2.10^{-5} Torr.

In the experiment the beam is injected through the r-mirror. This is difficult to do symmetrically, because the lines of force converge strongly in the r-z-plane. Often, only a small fraction of the beam is trapped temporarily, and most of the electrons escape after one transit through a "preferred" z-mirror. Electron-cyclotron resonance is used to capture the particles in adiabatic orbits. The rf-power is coupled into the vacuum vessel with an antenna that is inserted through the r-mirror. A comparison between the two modes of operation can be found in Fig. 1. The decay of the collector current starts when the injection beam and the rf-power are cut off within $\frac{1}{2}$ μs and remain so for roughly 20 μs. The phenomenon is both stable and reproducible. The e-folding time of the decay is inversely proportional to the pressure and is for energies higher than 150 eV independent of the energy. Both phenomena are consistent with loss by collisions on the neutrals of the residual gas. At several hundreds of eV the collision frequency is independent of the energy[2]. Approximate agreement is found with an expression for large-angle scattering: $\tau = 2M/n\sigma v$. Here, τ, is the containment time, n, the neutral density, σ, the scattering cross section, and M, the mirror ratio. We have inserted M = 5 and a correction factor of $\frac{1}{2}$ because of collisions that do not take place at the field minimum.

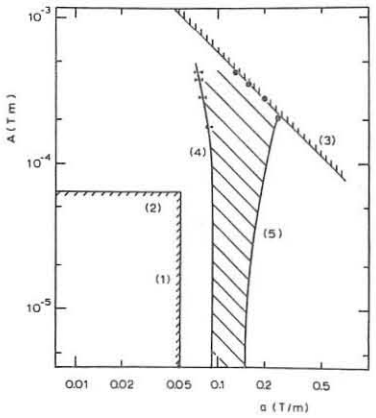

Fig. 2 The allowed region for cyclotron resonance expressed in the field parameters for a fixed frequency of 300 MHz. The upper right-hand and the lower left-hand corner are forbidden, as follows from theory.

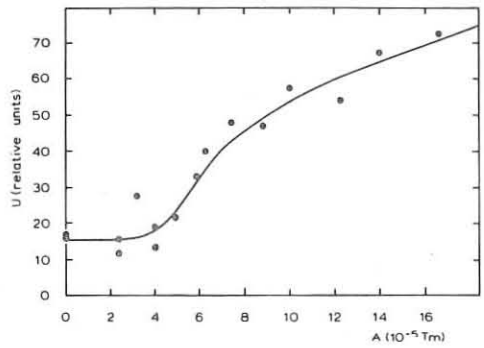

Fig. 3 The initial height U of the longer tail on the inner part of the z-collector increases for higher azimuthal field. Particle energy 185 eV, rf-power 20 W at 300 MHz, cusp field a = 0.14 T/m, background pressure 10^{-5} Torr.

In Fig. 2 we show the constraints on the values of the field parameters for the occurrence of the long containment. For high fields the field minimum becomes too high if $\sqrt{2aA} = 6.10^8(e/m)^2$. Similar constraints give lower theoretical bounds to the separate fields. Experimentally, the long containment has only been seen if the values of the field parameters lie in the rather narrow strip in Fig. 2, which has been shaded.

Integration of the longer tail of the decay yields the increase of the contained population. The containment time depends little on the field parameters. Therefore, the influence of the better adiabaticity has been determined by comparing the decay on two ring collectors in one of the z-mirrors which are concentric with the axis. We take the initial height of the longer tail, U, as a rough measure for the contained populations in the concentric shells. The inner and the outer radii of the collector rings are 7 and $12\frac{1}{2}$, and 13 and $18\frac{1}{2}$ mm, respectively. For the inner ring U increases strongly with the azimuthal field (Fig. 3). For the outer one the increase is much less. In the following table we give the value of $\bar{\varepsilon}$ for the lines of force that strike the inner and the outer edge, respectively, of the inner ring, for several cases. The favourable influence of a small decrease in $\bar{\varepsilon}$ can be clearly seen.

a	A	$\bar{\varepsilon}$ (inner edge)	$\bar{\varepsilon}$ (outer edge)
0.14 T/m	0	0.82	0.40
0	8.5×10^{-5} Tm	0.76	0.76
0.14 T/m	8.5×10^{-5} Tm	0.57	0.35

With a multigrid collector in the r-mirror, only a small increase of the parallel energy of the escaping electrons has been found. The situation is the "strong external effect"-case of ref. 4, where the electron is pulled through the resonance layer that lies astride a toroidal surface of constant induction. The first approximation ignores the changes of the parallel velocity, and also relativistic effects. Then the transverse energy increases in a step accompanied by a rapidly damped oscillation. We may write down the energy gain of an isotropic velocity distribution as: $\Delta W_\perp = eE^2/a\dot{z}_1$, where $\dot{z}_1$ is the initial parallel velocity and E is the electric field strength. In our case this is usually of the order of the initial electron energy, so it is reasonable to suppose that the increase of the parallel velocity in the mirror is not great.

Acknowledgements are due to Ir. D.C. Schram and Mr. B. de Groot for their enthusiastic support.

This work was performed under the association agreement of Euratom and FOM with financial support from ZWO and Euratom.

References:

1. H. de Kluiver et al., Proc. IAEA Conf. on Plasma Physics and Contr. Nucl. Fusion Research, Culham 1965, Vienna, pt. 2 (1966) 177.
2. Landolt-Börnstein, Zahlenwerte u. Funktionen, I, 1., Berlin 1950.
3. B. Lehnert, Dynamics of charged particles, Amsterdam 1964, 181.
4. D.C. Schram et al., paper to this conference.

BEAM-PLASMA INTERACTION STUDIES

A. Bers

Department of Electrical Engineering and Research
Laboratory of Electronics
Massachusetts Institute of Technology,
Cambridge, Massachusetts, U.S.A.

Guggenheim Memorial Foundation Fellow,
now at Université de Paris, Laboratoire de Physique
des Plasma, Faculté des Sciences d'Orsay

CONDITIONS FOR ELECTRON HEATING IN A BEAM PLASMA EXPERIMENT .

by

Franco Bottiglioni.

ASSOCIATION EURATOM-CEA
Département de la Physique du Plasma et de la Fusion Contrôlée
Centre d'Etudes Nucléaires
Boite Postale n° 6 - **92 Fontenay-aux-Roses** (France)

I. INTRODUCTION.

In our beam plasma experiment [4], the production of high energy electrons is connected with an important increase in hf emission, diamagnetism, and in plasma density. It is accompanied by strong fluctuations of these quantities. We present here some experimental results dealing with the transition from the stable (first) to the unstable (second) regime. The electron heating occurs if the cold plasma density exceeds a critical value n_c, given by $0.5\, f_c \leq f_p \leq 0.7\, f_c$, in agreement with results reported in [6], [7], Besides the excitation of strong oscillations, a trapping magnetic configuration seems to be necessary to heat the electrons [1], [4], [8], [9], [10]. In a simple model of electron heating, presented here, the condition for electron trapping is given by a relation between the mirror ratio R and the amplitude of the fluctuating electric fields.

II. EXPERIMENTAL APPARATUS AND RESULTS.

An electron beam ($I_{MAX.} = 1$ A ; $V_{o\,MAX} = 10$ kV; Ø = 1 cm ; Present experiment I = 20 mA ; $V_o = 5$ KV; beam pulsed during 200 ms), is injected in a stainless steel liner pumped by three pumps. Fig.1. The magnetic field has a mirror ratio changeable from 2 to 8 . The maximum field at the mirrors is 0.6 T. At present, a stationary plasma is produced in our external source, independently of the electron beam. The cold plasma density is measured, by a movable Langmuir probe, before switching on the beam. The density ranges from 5.10^{15} to $3.10^{16}\ m^{-3}$, the H_2 gas pressure is about 10^{-5} Torr. A fixed probe checks the possible changes in the density at the transition. X-rays, produced by hot electrons diffusing across the magnetic field, are detected by a scintillation counter. X-rays are emitted in bursts of about 20 µs, with a repetition rate of 100-200 µs, in phase with the hf emission. The oscillations are detected by an electrostatic antenna. When the cold plasma density is gradually increased , for all other parameters fixed, at a critical density n_c , a sudden emission of X-rays, accompanied by a strong hf emission near f_p, give experimental evidence of the transition to the heating regime. In Fig. 2 is plotted n_c versus the square of the magnetic field, in the middle of the magnetic configuration. It can be seen that $0.5\, f_c \leq f_p \leq 0{,}7 f_c$. The frequency spectrum exhibits a very strong line near f_p. A second line, much less intense , is about the hybrid frequency $f_h \simeq \sqrt{f_p^2 + f_c^2}$. Fig. 3. The line corresponding to f_c is not clearly visible . Some other lines may appear near 2 f. The frequency near f_p depends only on the plasma density. This dependence, plotted in Fig. 4, shows that $0.7 f_p \leq f \leq 0.9\, f_p$. When the mirror ratio R is smaller than 3 we don't observe the heating regime.

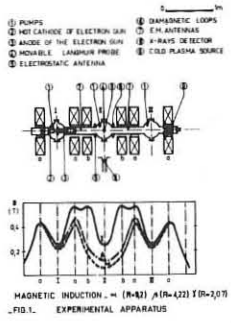

FIG.1. EXPERIMENTAL APPARATUS

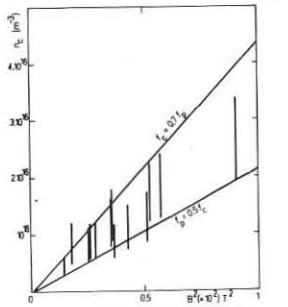

FIG.2. DEPENDANCE OF THE CRITICAL DENSITY n_c ON THE SQUARE OF THE MAGNETIC FIELD STRENGTH

III. DISCUSSION.

The energy gained by the electrons is mostly perpendicular to the magnetic field, therefore we suppose that the electrons are heated by a resonant interaction, at frequency f_c, with a wave propagating across the magnetic field. In the beam-plasma system , two quasi e.s. waves are possible near f_p ($f \simeq f_p \cos\theta$) due to the interaction of the plasma wave of the plasma with the corresponding wave of the beam (growth rate ω_1^*, max at $\theta = 0$) or with the slow cyclotron wave of the beam (growth rate ω_2^*, max at $\theta \simeq 53°$). From our measurements we find $25° \leq \theta \leq 45°$. In our experiment is $\omega_2^*/\omega_1^* \simeq 1/1{,}35\ \frac{\sin\theta}{\sqrt{\cos\theta}} \left(\frac{f_c}{f_{pb}}\right)^{1/6} \left(\frac{f_p}{f_c}\right)^{3/2} \geq 1$, if $f_p \geq 0{,}85 f_c$ for $\theta \simeq 45°$. Therefore we think that the heating of the electrons is connected with the development of the slow cyclotron instability propagating near the direction of its maximum growth rate. After the jump to the unstable regime, the plasma density increases, so ω_2^* becomes quite greater than ω_1^*. Frequencies near f_H can result from the interaction of the plasma cyclotron wave with the plasma wave of the beam (growth rate $\omega_3^* = \omega_2^*$).

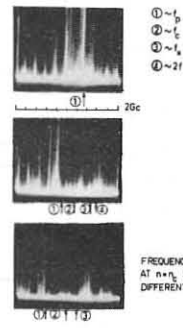

FIG.3.

IV. HEATING OF ELECTRONS.

Because of their great amplitude, the oscillations near f_p are certainly the most effective ones to heat the electrons. At the beginning of the unstable regime, only the beam electrons have a sufficient high velocity to interact with these waves ; nevertheless electrons can gain energy only if they are trapped between the mirrors. For this to happen in a transit time, the electric field of the wave must be $E \geq 4 V_o / L\, (R-1)^{-1/2}$ [5], for a beam with a completely longitudinal energy V_o . Taking the path of interaction L equal to a few wave lengths [2] and R 3 , we find E of the order of a few KV/cm. This field strength is very high, but fields of this magnitude have been measured by [1] [3]. X-rays are emitted in phase with the hf emission, so it seems that electrons are heated and lost at the same time. The averaged growth rate of the electron energy is $\langle \frac{dW}{dt} \rangle = Q \sqrt{W}\ (eV/s)$ with $Q \simeq (e/m)^{1/2} V_o / L\, \delta$

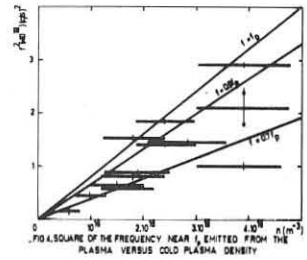

FIG.4. SQUARE OF THE FREQUENCY NEAR f_c EMITTED FROM THE PLASMA VERSUS COLD PLASMA DENSITY

The dependence on the pressure of the electron energy could be explained if $Q \simeq (e/m)^{1/2} V_o / L\, \delta\, P_o/P$ ($p_o = 2.10^{-4}$ Torr). When $p < p_o$ electrons doesn't reach an equilibrium temperature [4] ; then , from the heating time (20 µs) and from the observed electron energy, it is possible to evaluate Q and α . For usual conditions with an intense beam [4], we find $Q \simeq 3.10^{+7} \frac{P_o}{P} \frac{(eV)^{1/2}}{S}$ and $\alpha = 50$. The instability would then be effective to heat only during 1/50 of the hf pulse, but we haven't directly observed this fact.

LIST OF SYMBOLS.

- θ = angle between the wave vector $\bar{K}$ and the magnetic field ;
- f_{pb} = plasma frequency of the beam ;
- α = reduction factor taking into account that instability could be affective only during a fraction of the hf burst.
- δ = distance between the mirrors.

REFERENCES :

[1] I. ALEXEFF et al. 3d AIEA Conf. Novosibirsk 1968, paper CN24/L2.
[2] I. ALEXEFF et al. Phys. Rev. Letters 21, 6, 1968 pg.344.
[3] A.K. BEREZIN et al. Atomaja Energija 18, 1 ,1965 pg 1.
[4] F. BOTTIGLIONI et al. Proc. of 2nd Coll. Int. entre Champs Oscillants et Plasmas Saclay 1968, Vol 1, pg. 289.
[5] J. COUTANT, private communication.
[6] H.J. HOPMAN et al. Plasma Physics , 10 , 12 , 1968 pg 1051.
[7] E.A.KORNILOV et al. Sov. Phys. Tech. Phys. 10 , 8, 1966 pg 1064 and 1069.
[8] A.G. PLAKHOV et al. 3d AIEA Conf. Novosibirsk 1968 , paper CN24/L3.
[9] M.SEIDL et al. IPP CZ-81 Prague, 1967.
[10] L.D. SMULLIN et al. 2nd AIEA Conf. Culham 1965 , Vol II , pg. 815.

INTERACTIONS OF A PLASMA WITH A SPIRALING ELECTRON BEAM*

by

B. R. Kusse and A. Bers**

Department of Electrical Engineering and Research Laboratory of Electronics, Massachusetts Institute of Technology
Cambridge, Massachusetts, U.S.A.

The interactions which can take place between a spiraling electron beam and a plasma have been studied experimentally and the observed wavelengths and frequencies of the waves generated by these interactions agree with theory if finite Larmor radius effects of the plasma are considered. The experimental apparatus used to study the interactions is shown in Figure 1. The electron gun was located in the left hand end of the system. A hollow, cylindrical, axially flowing electron beam was emitted from this gun and passed through a sharp magnetic cusp formed by the coils and the soft iron shield. The magnetic cusp transformed some of the beam's axial energy into rotational energy and formed the hollow, spiraling beam. The beam energy, density and pitch could be controlled independently. To the right of the soft iron shield the magnetic field was uniform and axially directed. The spiraling beam produced the plasma in this uniform field region, inside the conducting screen. The plasma and r.f. fields produced by the beam were studied with probes which could be moved inside this region enclosed by the screen.

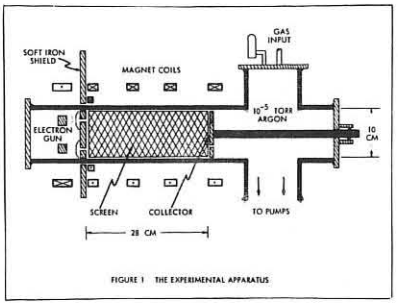

FIGURE 1 THE EXPERIMENTAL APPARATUS

Since the plasma was produced by the beam, increasing the beam density caused an increase in plasma density. At a fixed magnetic field, increasing the plasma density caused oscillations to set in at frequencies shifted above multiples of the electron cyclotron frequency, ω_{ce}. These oscillations were observed on small electric field probes in the region where the spiraling beam produced the plasma. The observed frequency of the oscillations v.s. the magnetic field is shown in Figure 2. At a fixed field, as the plasma density increased, the first oscillation was observed above ω_{ce}. Increasing the plasma density caused a slight increase in the frequency and then a sudden jump to a frequency above $2\omega_{ce}$. A similar jump to a frequency above $3\omega_{ce}$ was observed.

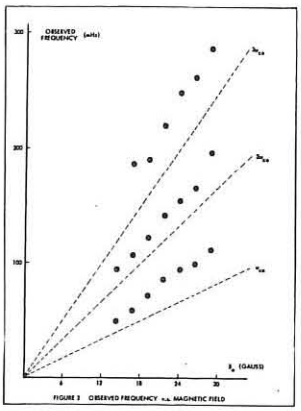

FIGURE 2 OBSERVED FREQUENCY v.s. MAGNETIC FIELD

The axial and azimuthal wavelengths and the frequencies of these oscillations were measured during various operating conditions. These wavelength values were then used to determine the axial and azimuthal wave numbers, β and m and to construct the Doppler frequency, $(m\omega_{ce} + \beta v_{bz})$ where v_{bz} was the axial beam velocity. This frequency was then compared to the observed frequency and the results are shown in Figure 3. These measurements also indicated that these oscillations were in the form of waves propagating in the direction of the beam flow and described by $e^{j(\omega t - m\theta - \beta z)}$. Changing the direction of the field caused a change in the sign of m.

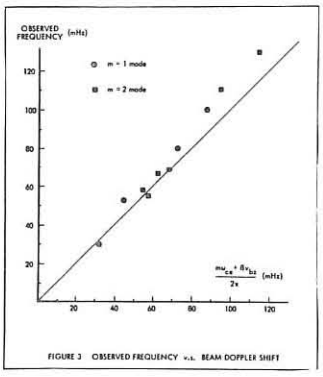

FIGURE 3 OBSERVED FREQUENCY v.s. BEAM DOPPLER SHIFT

This relationship between the observed frequencies and wavelengths implied that the unstable waves might well be explained by the coupling of spiraling beam and plasma waves. The beam supports quasistatic waves such that $\omega \approx m\omega_{ce} + \beta v_{bz}$. An analysis showed that if these beam waves were coupling with quasistatic, cold plasma waves the interaction frequency should be close to the upper hybrid frequency, ω_h where $\omega_h^2 = \omega_{ce}^2 + \omega_p^2$ and ω_p is the plasma frequency. This explanation, however, would require that the observed frequency increase continuously as the plasma density increased. The experimentally observed oscillations did not occur precisely at ω_h, and as mentioned, did not increase continuously with plasma density.

For the plasma of the experiment, the magnetic field was low (10-20 gauss). Finite Larmor radius effects can be neglected if $\lambda \ll 1$ where $\lambda = [pv_t/\omega_{ce}]^2$ and p is the wave number across the magnetic field and v_t is the electron thermal velocity. The plasma of the experiment was characterized by a λ which ranged from 0.1 to 1.0 and consequently finite Larmor radius effects could not be neglected. Including these temperature effects in the analysis resulted in the prediction of different interaction frequencies than were obtained assuming $v_t = 0$. Interaction frequencies occurred at values shifted above multiples of the cyclotron harmonics and increased with increasing ω_p as shown in Figure 4. As can be seen finite λ introduces gaps in the interaction frequencies. Also in Figure 4 are plotted a set of observed frequencies as a function of ω_p. These data points describe a jump from a frequency above ω_{ce} to one above $2\omega_{ce}$, a jump from a m=1 mode to a m=2 mode. The dashed lines in the figure were constructed using plasma parameters measured during the jump. It can be seen that the data points do not follow ω_h, but agree well with the theory which includes finite Larmor radius effects.

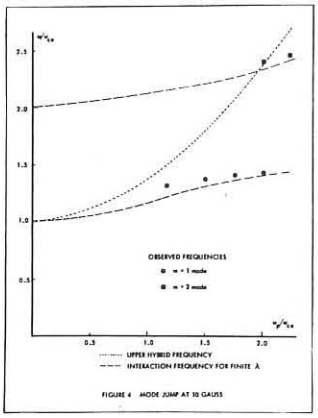

FIGURE 4 MODE JUMP AT 10 GAUSS

* This work was supported in part by the National Science Foundation (Grant GK-10472).

** Guggenheim Memorial Foundation Fellow, now at Université de Paris, Laboratoire de Physique des Plasmas, Faculté des Sciences d'Orsay.

THEORETICAL AND EXPERIMENTAL INVESTIGATION OF WAVE PROPAGATION IN A BEAM-PLASMA SYSTEM

by

A. Bouchoule and M. Weinfeld

Institut d'Electronique Fondamentale, Laboratoire associé au CNRS, Bât.220- Faculté des Sciences - 91 ORSAY (France)

and

S. Bliman

Laboratoire de Physique des Plasmas, ENSEG, Avenue des Martyrs - 38 GRENOBLE (France)

The experimental device, in which independent settings of plasma and electron beam parameters can be made, has been described elsewhere[1].

The 60 cm-long diffused plasma column is confined by a strong magnetic field. Average values of electron density, column radius and magnetic field lie in the domains of 10^8 to some 10^9 cm^{-3}, 2 to 4 mm, 1 to 2,5 kG.

The electron gun, immersed in the magnetic field, gives a quasi monoenergetic beam, coaxial to the plasma column, and having almost the same radius. It gives typically a current of 500 A for an anode voltage of 100 V.

A theoretical simplified model is used for computer calculations : homogeneous, collisionless cold beam-plasma column in vacuum, for which a quantitative treatment has already been performed[2].

Starting from the gun, the system shows a linear behaviour over a length L of about 20 cm ; that is to say, linear amplification of a modulating signal injected in the beam may occur, as it can be seen on fig.1. The figure 2 is a typical dispersion diagram, which shows real and imaginary parts of the longitudinal propagation constant plotted against frequency.

The agreement between theoretical and experimental datas is fairly good, but one remark must be made : we use for computation the mean plasma density, measured with a microwave cavity ; the column radius giving the best fit with experimental results is a little different from the measured one, because of the radial density inhomogeneity of the column.

Beyond the interaction length L, (the smaller as the gain is higher), one can see the saturation, than the decrease of an injected signal. This length does not depend on the signal level over a domain of power of some orders of magnitude (fig.1).

In the region z > L, a strong noise level appears. If the signal is amplitude modulated, the noise becomes also modulated in the same way, at frequencies close to the signal frequency.

The low frequency instabilities of the system lead to a "disintegration" of the signal and to the creation of satellites 30 to 150 kHz apart, the violet satellite being stronger. But this phenomenon, already observed[3], which is equivalent to a damping of the signal itself, can not explain the influence of the weak signal on noise frequencies differing of some MHz (fig.3).

The total noise power increases at first exponentially, then, for a sufficient beam density decreases and becomes stationary. (We have verified that the neutral pressure is low enough to avoid collisional damping). Also, the noise spectrum spreads towards high frequencies : it is a well known effect[4,5,6] which has been connected with deceleration and thermalisation of the beam.

In experimental conditions very different from ours, one has shown the role played by the coupling between unstable modes at $\omega \simeq \omega_p$ and $\omega \simeq \omega_H$[7]. In our conditions, the coupling between modes of same nature are important, as the "Cerenkov instability" happens in a broad frequency range.

This appears clearly when a double-humped noise spectrum exists at the beginning of the system, in the unstable domain of frequency probably in relation with some dimensional effect. We see then the growing of harmonic frequencies and frequency mixing, due to these couplings (fig.4-1). This effect is enhanced by injection of a signal in the above mentioned noise bands the noise spectrum spreads then towards high frequencies (fig. 4-2).

We have so additional damping mechanism for that frequency ; that can lead to modes having high propagation constants, strongly absorbed by the plasma[8], which limits the high frequency spreading of the spectrum. This effect is probably enhanced by radial density inhomogeneity.

An increase of injected signal power leads to the stabilization of the system as it can be seen on figure 4-3. The total output noise power becomes smaller in that case than without injected signal. This effect is the greater as the signal is closer to the maximum gain frequency. It happens also when the signal injected is at a lower frequency, but is less noticeable ; in this case (fig.5), the harmonic frequencies created and amplified by the system reach rapidly a level greater than the level of the fundamental, and can be responsible of the weaker stabilization observed.

Typical spectrum evolution in z is shown on figure 6.

Bibliography

(1). M. Weinfeld, 7th CIPIG, Belgrade 1965.

(2). S. Bliman, A. Bouchoule, JAP 38, 13, 5065, 1967.

(3). Y. Fedorchenko et al, Sov. Phys. Tech. Phys. 10,11,1549, 1966 and 11, 11, 1462, 1962.

(4). H.J. Hopman et al, Plasma Phys. 9, 39, 1967.

(5) H.J. Hopman, W. Ott, PLasma Phys. 10, 315, 1968.

(6). S.M. Levitskii, I.P. Shashurin, JETP 25, 2, 227, 1967.

(7). I.P. Shashurin, JETP 6, 8, 245, 1967.

(8). J.H. Malmberg, C.B. Wharton, Phys. Rev. Lett.13, 6, 184, 1964.

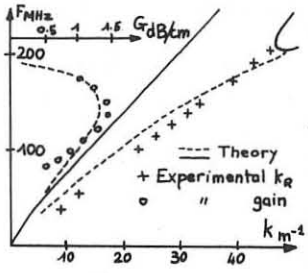

Figure 2

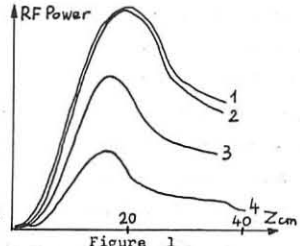

Figure 1
1:Input power 0.015 mW
2: " " 0.15 mW
3: " " 1.5 mW
4: " " 6 mW

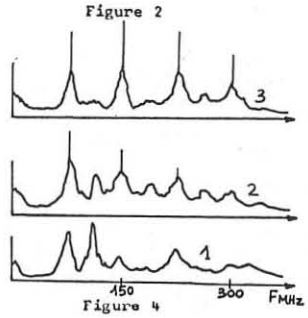

Figure 4

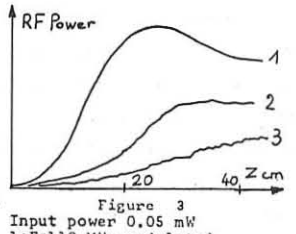

Figure 3
Input power 0.05 mW
1:F=110 MHz modulated
2:Noise at 107 MHz
3:Modulated noise at 107 MHz

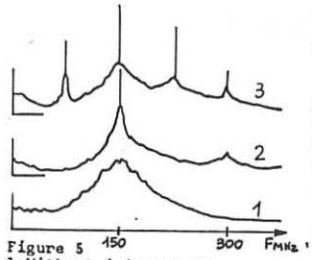

Figure 5
1:Without injected RF
2:Injected RF :105MHz
3:Injected RF : 75MHz

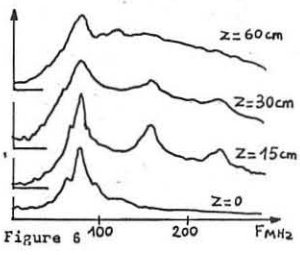

Figure 6

Electron and Ion Heatings in Beam-Plasma Discharge Experiments

K. Yatsui, Y. Yamamoto, K. Saeki and A. Hasegawa

Faculty of Engineering Science, Osaka University, Toyonaka, Osaka, Japan

1. Introduction

Recently, high power electron beam interaction with plasmas has been energetically investigated by many authors.[1] As the most characteristic feature of beam-plasma discharge, a presence of hot electrons exceeding several hundreds of keV is pointed out. No established theory, however, has been found on such an anomalously accelerated mechanism of electrons. From this point of view, the present work is devoted to study the production mechanism of these hot electrons both experimentally and theoretically, and subsequently to heat plasma ions in this beam-plasma system extending the heating principle thus clarified.

2. Description of the Plasma

Figure 1 shows the schematic diagram of the apparatus. Maximum beam energy is ~5 kW (2.5 kV, 2A) under continuous operation. A pressure of $8 \times 10^{-6} \sim 6 \times 10^{-4}$ Torr. of hydrogen is preserved at the interaction region, where almost uniform or mirror magnetic fields (mirror ratio $R_m \lesssim 5.5$) are applied with its intensity B = 30~1800 G. Plasma properties associated with cold electrons are determined by Langmuir probes or X-band microwave interferometer. X-radiation is picked up from a thin mylar window through a collimator, then led to measuring equipments such as G-M counter, survey meter and spectrometer. According to various plasma diagnostics, following features are revealed:[2] (a) Densities of cold- and hot electrons are approximately $n_c \lesssim 10^{12}$ cm^{-3}, and $n_h \lesssim 10^{10}$ cm^{-3}, respectively. (b) Strongly ionized plasmas with the ionization rate ~80 % is obtained in the burnout state. (c) Temperatures of cold- and hot electrons are typically $T_c \simeq 10$ eV and $T_h \lesssim 100$ keV. (d) Containment time of cold- and hot electrons are about $\tau_c \lesssim 400\ \mu$sec and $\tau_h \lesssim 10$ msec. (e) In the preburnout state, ion plasma waves are excited due to coupling with slow cyclotron waves of the beam. (f) Electron hybrid wave interaction with beam slow waves becomes essential in the burnout state.

FIG. 1

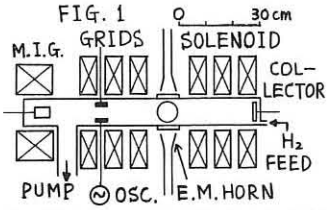

3. Hot Electron Production

Figure 2 shows the hot electron temperature vs. beam accelerating voltage. From Fig. 2, the temperature is found to be conspicuously enhanced with increasing beam voltage. Now, we examine the heating process theoretically from a view point of resonant resistive instability.[3] If we assume that the heating rate of electrons absorbing RF electric field at $\omega \simeq \omega_{ce}$ created by two-stream instability due to cyclotron damping balances the kinetic energy of hot electrons, next relation is obtained

FIG. 2

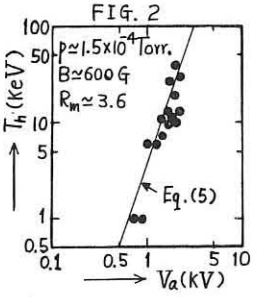

$$\frac{d}{dt}(n_h m v_\perp^2) = \frac{1}{2}\varepsilon_0 \mathrm{Im}\,\varepsilon_h\, \omega_{ce} \langle E^2 \rangle . \tag{1}$$

Here, for anisotropic velocity distribution, $\mathrm{Im}\,\varepsilon_h$ and E may be given by[3,4]

$$\mathrm{Im}\,\varepsilon_h = \sqrt{\frac{\pi}{8}} \cdot \frac{\omega_{ph}^2 v_b^3 k_\perp^2}{\omega_{ce}^4 v_{//}} , \tag{2}$$

$$\langle E \rangle = 2 \frac{m}{e} \omega_{pb} \sqrt{\frac{2\omega_{pb}}{\omega_{pp}}}\, v_b . \tag{3}$$

From Eqs. (1) to (3), perpendicular temperature $T_{h\perp}$ (in eV) is derived as

$$\frac{T_{h\perp}}{V_a} \simeq \sqrt{\frac{\pi \omega_{pp}}{\omega_{pb}}} \cdot \frac{\omega_{pb}^3}{\omega_{ce}\omega_{pp}} \left(\frac{k_\perp}{k}\right)^2 \tau_h . \tag{4}$$

Noting that $\omega_{pb}^2 \propto v_a$, $k \propto 1/v_b$ and $\omega_{pp} \propto \omega_{pb}$, we have

$$T_h \propto v_a^3 . \tag{5}$$

The above slope is plotted in Fig. 2. From this, the data is found to be in an agreement with Eq. (5), and consequently the result seems to give a possible evidence of electron cyclotron heating in this RF discharge.

4. Ion Heating by Modulated Electron Beam

Extending above heating principle, it would be possible to accelerate plasma ions selectively due to ion cyclotron damping of low frequency waves near $\omega \simeq \omega_{ci}$ excited internally by some methods. From this point of view, process of ion heating has been studied by modulated beam.[5,6] Voltage for modulation grids is supplied by a 1 kW cw transmitter with a frequency range f = 0.8~12 Mc/sec. Temperature of plasma ions is measured with a Faraday cup. Typical example is illustrated in Fig. 3, where the rate of increase in ion temperature $\Delta T_i/T_i$ is plotted vs. modulation frequency f_m. In the absence of modulation, ion temperature observed is (8~10) eV. It is found in Fig. 3 that plasma ions are highly accelerated when the modulation frequency coincides with the cyclotron frequency of ions shown by arrows. These results, therefore, may be ascribed to cyclotron heating of plasma ions.

FIG. 3

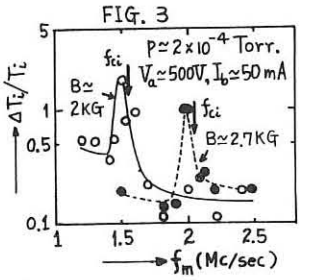

5. Ion Heating by Spiral Electron Beam

It is known that, if axial beam velocity $v_{//}$ is smaller than thermal velocity v_{Te}, low frequency waves are easily excited by the two-stream instability. From these facts, spiral beam-plasma interaction is studied in the view point of ion heating.[7,8] Short pitch, small $v_{//}$-beam has been obtained using a cusp field. Typical results are shown in Fig. 4 (oscillation intensity V_{osc} and frequency vs. B) and Fig. 5 ($v_{//}$ and T_i vs. B). From these results, small $v_{//}$-beam is found to be created at lower fields. Correspondingly, it is clear that low frequency waves near f_{ci} are strongly excited, and that ion temperatures tend to be considerably increased. These data may also indicate a possibility of cyclotron heating in such a system as is similar to electron and ion heatings mentioned previously.

FIG. 4

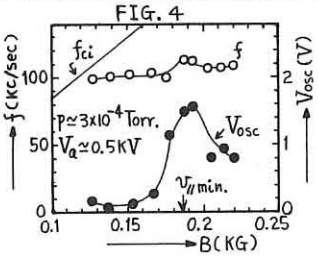

FIG. 5

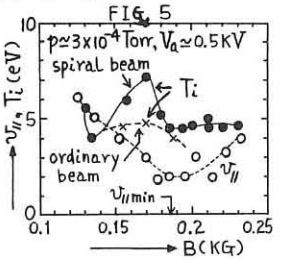

References

1) See, for example, L. D. Smullin and W. D. Getty: J. appl. Phys. 34(1963) 3421; I. Alexeff and R. V. Neidigh: Phys. Rev. 136(1964)A689.

2) K. Yatsui et al.: J. Phys. Soc. Japan (to be published).

3) A. Hasegawa: ibid. 23(1967)909.

4) A. Hasegawa: ibid. 24(1968)432.

5) G. M. Haas and R. A. Dandl: Phys. of Fluids 10(1967)678.

6) K. Yatsui and Y. Yamamoto: J. Phys. Soc. Japan (to be published).

7) B. S. Akshanov et al.: Sov. Phys.-Tech. Phys. 11(1966)446.

8) K. Yatsui and K. Saeki: J. Phys. Soc. Japan (to be published).

Beam-Plasma Instabilities in Low Density Plasma Regime

by
J.Jančařík, V.Piffl, M.Seidl, J.Ullschmied
INSTITUTE OF PLASMA PHYSICS
Prague 9, Nademlynska Str. 600, Czechoslovakia

The subject of our study was the build-up of a plasma by an electron beam in a uniform mag.field. We paid most attention to the classification of waves excited by beam-plasma interaction and the influence of each type of wave upon the plasma parameters, the plasma electron density n_{pe} and temperature in particular. This work links on to papers [1,2]. This time mainly the region of low plasma densities is discussed.

Our investigation was carried out on ELMAN 2 machine. A parallel flow electron beam /$E_b \leqq$ 7keV, perv.max. 1,7 . 10^{-7}A. $V^{3/2}$, pulse durat.2ms/ a hollow one /r_1= 8mm, r_2 = 11mm/, was injected along a uniform mag.field /B_{max}= 2kG/ into a vacuum chamber of 150mm dia.,filled with Argon gas /p_o=5.10^{-8}Torr, $p_{max} \sim$ 10^{-4}Torr/. The beam produced a plasma column 470mm long.

We divide the procesa of the plasma build-up into three regimes, differing in the n_{pe}regions, types of interaction responsible for the ionization and the highest energy of the accelerated particles [2].

In the first regime the plasma is created only by ionizing collisions of the beam electrons with the neutral gas atoms. No h.f. collective interactions were observed in the 1_{st} regime; on the other hand, with sufficiently strong beam currents /$I_b \geqq I_{in.} \sim E_b$,B/, low-frequency oscillations, corresponding to those described in [3] were recorded. The highest n_{pe}in the 1st regime usually does not exceed that of the beam. The main characteristics of the 1st regime were discussed at large in [2].

When a certain initial value of the n_{pe} has been achieved, a more rapid increase of the density than that corresponding to the rate of the collision ionization by the beam electrons is observed. At the same moment h.f. oscillations of $f_{min} \sim$100 Mcps appear. The necessary initial density is lower with higher I_b /c.f.[4] /. Our measurements in agreement with the theory show that optimally the instability can be excited already at $n_{pe} \sim n_b$= 2-5.10^8cm^{-3}. A dependence of the initial current on B shows that at low densities gradient effects must be taken into account. The state of the plasma from the first excitation of the h.f. oscillations up to the h.f. breakdown we call the second regime. The 2nd regime is illustrated by Fig. 1 /upper tr.: signal~n_{pe}, lower : ampl. of h.f. field a/110Mcps, b/140Mcps; 3kV, 150mA, 900G, 5.10^{-6}Torr; 0,2ms per div./.

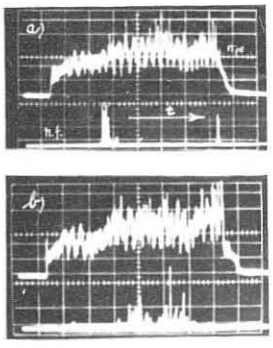

Fig. 1

According to our exp.results, the 2nd regime is characterized by the occurrence of h.f. oscillations of $f \sim f_{pe}$. The freq. spectrum is discreet, it consists of narrow bands 30-40Mcps apart, inaccordance with the longitudinal boundary conditions. The minimum f observed at the very beginning of the 2nd regime depends upon the E_b /is lower at lower energies/. At plasma densities $n_{pe} \leqq 2n_b$ frequencies up to f_{pe} were observed. Waves of higher frequencies had higher amplitude. When $E_b \geqq$ 3keV, the spectrum consists of only two bands /170,210Mcps/; at lower energies the wave amplitude increases and the lower freq. bands become noticeable, too. In the density region defined by relation $3f_{pb} \leqq f_{pe} \leqq f_{ce} \leqq$ 4,2Gcps also oscillations up to f_{pe} were observed, but the highest amplitude had waves of $f \sim f_{pe}/2$. An example of a typical spectrum is in Fig.2 /3keV, 300mA,1000G, 6.10^{-6}Torr./

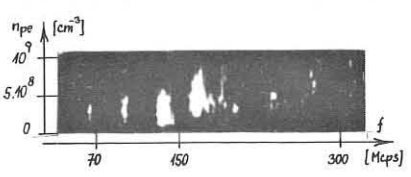

Fig.2

The measuring of phase velocities of excited waves by recording standing wave pattern at the collector end gave values of v_f=0,55 - 0,9v_b; waves of higher f /at higher n_{pe}/had higher phase velocities. Preliminary measurements of the space correlation of h.f. field at $f_p \leqq f_{ce}$in 10cm band confirmed the proximity of $v_f$to the beam velocity. In the whole 2nd regime the freq. spectrum keeps its character and does not depend upon the magnetic field strenth /$f_{max} \cong 0{,}85 f_{ce}$/.

The comparison between the exp. facts and the theory shows that in the 2nd regime only a slow space charge wave interaction takes place /Cherenkov effect/; waves of the highest growth rate have the highest amplitude, as stated also in [5] . At low n_{pe} the influence of the beam density is considerable /$v_f < v_b$/. No h.f.fields of $f \geqq f_{ce}$were observed in the 2nd regime. The excited oscillations occur in very short incidental spikes. The measuring of autocorrelation functions of the plasma oscillations in 2-4Gcps band gave a value of correlation time 3-5ns.

The energy distribution of the electrons leaving the plasma along the mag. field was measured by means of a multigrid electrostatic analyser. Accelerated electrons appear simultaneously with the plasma oscillations, as follows from Fig.3, showing the time correlations between the amplitude of h.f. field /0,4-3Gcps, f_{ce}= 4,2Gcps/ and the analyser current corresponding to the electrons of energies higher than 50eV /upper tr./. Plasma electrons accelerated by the plasma wave interaction contribute to the ionization process and are responsible for the increase in n_{pe}in the 2nd regime. Because the conditions for the resonant damping of the plasma wave in the longitudinal inhomogenity are not satisfied in our case, the stochastic heating mechanism can be assumed. Electrons accelerated along the mag.field can overcome the potential barrier at the surface. The escape of a part of the electrons causes rapid changes in the plasma potential, observable at the signal of a Langmuir probe.

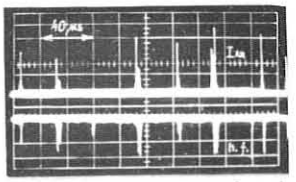

Fig.3

When the average n_{pe} reaches the value of f_p=0,3 -1,0 f_{ce}, the cyclotron /H/ branches of the plasma wave become excited. This brings about an additional increase in the ionization rate and finally a big jump in the plasma density - h.f. break-down. The influence of the H branch is weak at first, its amplitude at the beginning of the intermediate stage is of two orders of magnitude smaller than that of the L branch, as shown in Fig.4 /upper tr.: n_{pe} by 8mm interf., lower: down dir.- ampl. of L branch 1,5-3Gcps, 500mV per.div., up - H branch 3,2-9Gcps, 2mV per div./. The growth rate of the H branches increases gradually with the density and the mode competition manifests itself by strong fluctuations of n_{pe}. The discharge becomes stable as soon as the amplitudes of both waves are comparable. The plasma density fixes itself at the average value so that the conditions for excitations of some of the H branches are satisfied /c.f. also[1] . This stationary condition we call the third regime /c.f.[2,7]/.

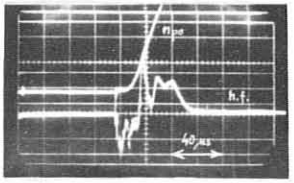

Fig. 4

According to the results presented in this paper, the substantial part of the plasma build-up in our system up to the h.f. break-down is conditioned by the collective interaction of the low branch of the cold plasma wave /c.f. also[8,9]/. Only after a relatively dense plasma has been created, do the interactions with the excited H branches near the cyclotron harmonics take over the decisive role.

References:

[1] M.Seidl, P.Šunka, Nuclear Fusion 7 /1967/ 237
[2] J.Jančařík at all.,Third Conf.Pl.Phys...,Novosibirsk 68 CN-24/L-5
[3] M.V.Nezlin, Novosibirsk 68, CN-24/L-7 (in Russian)
[4] J.E.Simpson, D.A.Dunn, Jour.Appl.Phys.,37 /1966/ 4201
[5] A.K.Berezin at all., At.Ener., 18 /1965/ 5 (in Russian)
[6] V.Kopecký, J.Preinhaelter, IPPCZ-108, July 1968
[7] J.Jančařík at all., Phys.Letters, 28A /1968/ 331
[8] M.T.Vlaardingerbroek, K.R.Weiner, Philips Tech. Tijdschrift 27 /1966/ 273
[9] H.S.Hopman at all., Assot.Euroatom FOM, No 24974, Amster.68

COLLISIONAL QUENCHING OF THE BEAM-PLASMA INSTABILITY
FOR ELECTRON BEAMS WITH LARGE VELOCITY SPREAD

by
H. Böhmer, J. Chang and M. Raether
COORDINATED SCIENCE LABORATORY AND DEPARTMENT OF PHYSICS
University of Illinois, Urbana, Illinois 61801, U.S.A.

The instability of an electron beam interacting with a plasma depends critically on the velocity spread of the beam or, with other words, the beam temperature. For $u/v_o \ll (n_B/n_p)^{1/3}$ the beam is "cold" and the interaction is nonresonant, for $u/v_o \gg (n_B/n_p)^{1/3}$ the beam is "warm" and we have a resonant type interaction. n_B and n_p are the beam and plasma density respectively, v_o the average beam velocity and u the r.m.s. velocity spread for a displaced maxwellian distribution function. Apart from drastic changes is the dispersion relation [1], this difference also manifests itself in the influence of collisions on the growth rate. For a cold beam and the collision frequency ν_c large compared to the growth rate γ, collisions reduce the growth rate to [2]

(1) $$\gamma_c = 1.03\ \gamma_o\ (\alpha^{1/3}/\nu)^{1/2} = \omega_p\ (\alpha/2\nu)^{1/2}$$

where γ_o is the collisionless growth rate $0.69\ (n_B/n_p)^{1/3}\ \omega_p$, $\alpha = n_B/n_p$ and $\nu = \nu_c/\omega_p$. The growth rate stays positive even when $\nu_c > \gamma_o$. For a warm beam the growth rate is reduced to

(2) $$\gamma_c = \gamma_o - \frac{\nu_c}{2}$$

with $$\gamma_o = \tfrac{1}{2}\sqrt{\frac{\pi}{2e}}\ (\omega_B^2/\omega_p)\ (v_o/u)^2$$

It follows that for a warm beam the instability can be quenched for a sufficiently large collision frequency or velocity spread.[3] The criterium for quenching has been given by Singhaus [4] as

$$\nu\tau^2 > 0.66$$

where $\tau = (u/v_o)\ (n_p/n_B)^{1/2}$

We have investigated the instability of electron beams of finite velocity spread, interacting with a Neon afterglow plasma in the density regime where Coulomb collisions are important. No external magnetic field was present. The interaction region was 40 cm long, 4 cm in diameter, the neutral gas pressure was 4×10^{-2} Torr. The velocity spread of the beam was produced by passing the beam through Beryllium foils of approximately 1μ thickness.[5] Values of u/v_o of 1-2% were produced with transmitted beam currents up to 400 ma at energies between 14 and 17 kV, 1-2 μ sec beam duration and 15 Hz repetition frequency. The energy distribution was measured with an electrostatic deflection type analyzer of 0.3% resolution. Measurements were performed at plasma densities of $1.2\times10^{12}/cm^3$ and $1.4\times10^{13}/cm^3$. The instability was detected by measuring the microwave radiation from the unstable plasma waves with receivers of 10 dB noise figure in the X- and K- band and by monitoring the beam distribution function at the end of the interaction-region.

For cold beams ($\tau \ll 1$) the instability shows a spatial growth with a growth rate $\sigma = 2\gamma_c/v_o$. The experimental values of γ agree to within 25% with those calculated from eq. 1. The radiated power increases by 6 - 9 orders of magnitude over the interaction region, depending on beam density. As the velocity spread becomes larger, the growth rate, the radiated power and the velocity spread produced by the interaction decrease. For values of $\nu\tau^2 > 0.66$ (Singhaus limit) radiation is no longer detectable, that is, the radiated power is less than 10^{-14} Watt, which is the sensitivity limit of our receivers. At the same time the change in the distribution function produced by the interaction decreases rapidly and becomes undetectable for values of $\nu\tau^2 \gg 1$.

In Fig. 1 the ratio $(u)_{final}/(u)_{initial}$ which is a convenient relative measure for the growth rate and in many cases more sensitive than the radiated power, is plotted for a variety of cases versus $\nu\tau^2$. We see that this ratio goes to 1 for values of $\nu\tau^2$ close to the Singhaus limit.

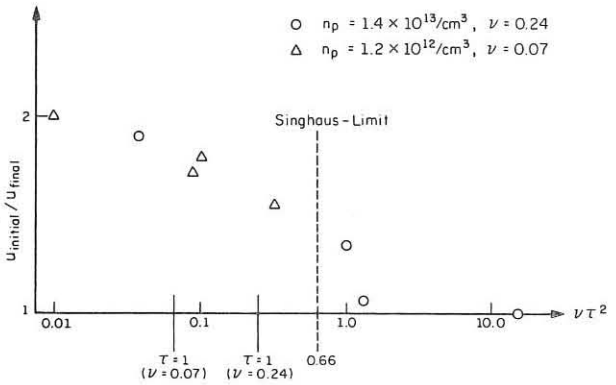

Fig. 1

It should be noted that $\nu\tau^2$ is a good universal parameter only if $u/v_o \gg \alpha^{1/3}$. In the investigated cases for which $\nu\tau^2 > 0.66$ no microwave radiation was detected. These points also satisfy the condition $\tau \gg 1$, although $(u/v_o)\alpha^{-1/3}$ is still not large compared to unity but ranges between 0.3 and 1.0. Nevertheless, the effect of collisions on the instability is already quite dramatic. As a demonstration for this we present one particular example where a cold and a warm beam are compared. The beam and plasma densities and the collision frequency were the same in both cases, only the velocity spread was different.

I_B	V	n_B	$(\frac{u}{v_o})_i$	$(\frac{u}{v_o})_f$	P	τ	$\nu\tau^2$
320 ma	17 kV	$3\times10^8/cm^3$	< 0.2%	0.4%	2×10^{-11} W	0.43	0.042
400 ma	16 kV	$3.1\times10^8/cm^3$	1%	1.3%	$< 10^{-14}$ W	2.1	1.05

The plasma density was $1.4\times10^{13}/cm^3$, radiation was detected at 35 GHz. I_B = beam current, V = beam energy, P = max. radiated power. As a consequence of the velocity spread the μ-wave power radiated by the instability has decreased by more than 3½ orders of magnitude.

We conclude that collisions have a much larger effect on the instability of beams with finite velocity spread than on monoenergetic beams even under conditions where $u/v_o \leq \alpha^{1/3}$. For $u/v_o \approx \alpha^{1/3}$ and $\nu\tau^2 > 0.66$ the instability is effectively suppressed. Although the distribution functions used in these experiments were not displaced maxwellians, the experimental results compare favorably with the theoretical model calculated by Singhaus.

[1] T. M. O'Neil and J. H. Malmberg, Phys. Fluids 11, 1754 (1968)
[2] S. A. Bludman, K. M. Watson and M. N. Rosenbluth, Phys. Fluids 3, 747, 1960
[3] G. Ascoli, Coordinated Science Laboratory Report R-131, Urbana, 1961
[4] H. E. Singhaus, Phys. Fluids 7, 1535, (1964)
[5] J. Chang, H. Böhmer and M. Raether, Rev. Sci. Instr. 39, 1873, (1968)

INTERACTION OF A CYLINDRICAL BEAM WITH A PLASMA: THEORY AND EXPERIMENT

by

S. A. Self

INSTITUTE FOR PLASMA RESEARCH

Stanford University, Stanford, California, U.S.A.

THEORY: The dispersion relation for electrostatic interaction when both beam and plasma are homogeneous, cold and collisionless, and B = 0, may be written,

$$D(\omega,k) \equiv 1 - \frac{\omega_p^2}{\omega^2} - \frac{\omega_b^2}{(\omega - k v_b)^2} G = 0 \quad . \qquad (1)$$

For infinite geometry and $k_\perp = 0$, G = 1. For a cylindrical beam, radius a, in a plasma bounded by a conductor, radius b (> a), and perturbations $\exp i(\omega t - m\theta - kz)$,

$$G = G_m(ka,b/a) \equiv (ka)[I_m'(ka)/I_m(kb)][K_m(ka)I_m(kb) - I_m(ka)K_m(kb)] \quad . \qquad (2)$$

Whereas for infinite geometry (1) represents body waves ($\nabla^2\phi = -\rho/\epsilon_0 \neq 0$), for bounded geometry it represents surface waves ($\nabla^2\phi = \rho = 0$), associated with surface charge at the beam edge.

Solving (1) for ω(k real) we find, for G = 1 an unstable root, which for a weak beam, $\beta^2 \equiv \omega_b^2/\omega_p^2 \ll 1$, has $\omega_{i\,max} = \omega_p(\sqrt{3}/2)(\beta^2/2)^{1/3}$. For the bounded system, for real k, $0 \leq G_m \leq 1/2$, and for $\beta^2 \ll 1$, we find a smaller maximum growth rate $\omega_{i\,max} = \omega_p(\sqrt{3}/2)(\beta^2 G/2)^{1/3}$.

While the roots ω(k real) of (1) for an infinitely long system indicate the presence of instability in some sense, they are of little value for interpreting the behavior of real systems of finite length. Although any spatial dependence can be fourier analyzed into real k components, these are coupled by the boundaries, and do not grow as separate modes. Experimentally, boundary conditions corresponding to a single real k mode cannot be realized. In practice, the beam-plasma instability always grows in space. It may exist in a steady state or may grow in time, as well as space. To answer these questions it is necessary to perform a stability analysis, following Briggs [1].

For the unbounded system, (1) represents a convective instability. The roots $k = [\omega \pm \omega_b(1 - \omega_p^2/\omega^2)^{-1/2}]/v_b$ are waves excited for real ω. The growing wave has $k_i \to \infty$ as $\omega \to \omega_p^-$. The inclusion of collisions or temperature serves to make $k_{i\,max}$ finite.

For the bounded system, and m = 0, a comprehensive stability analysis has been carried out in terms of the mapping of ω into the k plane. It is found that for all values of the parameters $\alpha \equiv (\omega_p a/v_b)$, β^2 and $\gamma \equiv (b/a)$, the system is absolutely unstable. However, the absolute instability is always so weak that the effect of a very small collision frequency is sufficient to quench it, leaving a convective instability. Figure 1 shows for a typical case, the amplifying waves for various values of the collision parameter $\delta \equiv (\nu/2\omega_p)$ large enough to quench the absolute instability. It should be noted that, as for the unbounded case, the relative spatial growth can be large ($k_i/k_r \sim 1$), even for a weak beam, when the relative temporal growth for real k is small ($\omega_i/\omega_r \ll 1$).

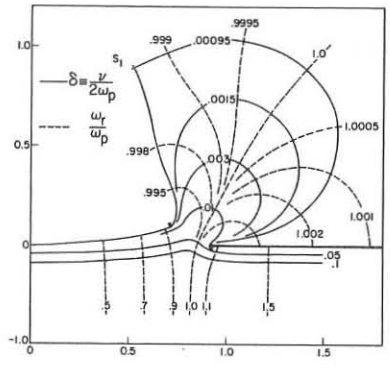

Fig. 1. AMPLIFYING WAVES FOR VARIOUS δ

EXPERIMENT: Apparatus. A beam-generated plasma is used (Fig. 2). The beam ($a = 0.4$ cm, $V_b = 100 \sim 300$ V, $I_b = 0 \sim 10$ mA) penetrates a tube ($b = 1.27$ cm) filled with Hg vapor ($p = 3$ mTorr), producing a plasma with which it interacts. Typically $n_p \sim 10^{10}$ cm^{-3} ($\beta^2 = n_b/n_p \sim 0.01$), $T_e = 0.6 \sim 0.8$ V. The gun may be modulated at UHF and moved axially relative to a radially movable probe. The latter may be used as a Langmuir probe or to sample the radial field E_r.

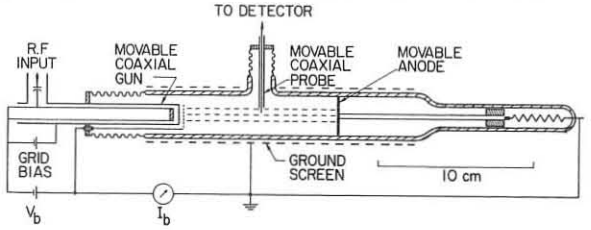

Fig. 2. BEAM-PLASMA TUBE

Growing Wave Measurements. By modulating the beam at f = 500 ~ 1000 MHz, and moving the gun relative to the probe, the amplitude and phase of E_r are measured versus z. Hence k_r and k_i are determined as functions of ω and V_b, I_b. The phase velocity $v_p \equiv \omega/k_r$ lies in the range 0.8 ~ 1.0 v_b. Growth rates as large as 25 dB/cm at 900 MHz are observed ($k_i/k_r \sim 0.3$). Typical results for $k_i(\omega)$ for $V_b = 150$ V, $I_b = 4$ mA, $f_p = 925$ MHz are compared with theory ($\alpha = 3$, $\beta^2 = 0.007$, $\gamma = 3.2$) in Fig. 3. The collision frequency ν is not known accurately but lies in the

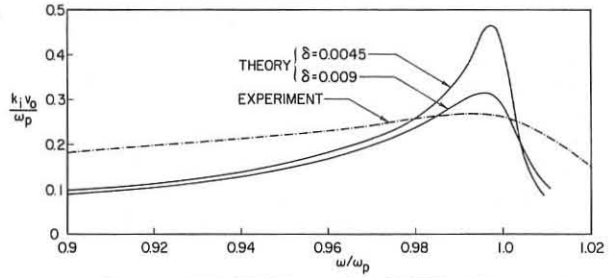

Fig. 3. THEORY AND EXPERIMENT FOR AMPLIFYING WAVES

range $0.5 \sim 1 \times 10^8$ sec^{-1}, and curves are shown for the corresponding values of δ. The agreement is reasonable but the experimental curve shows a lower $k_{i\,max}$ and growth over a wider band. This may be attributed to the effects of temperature and inhomogeneity neglected in the theory. The principal effect is believed to be due to the radial inhomogeneity of the plasma.

Nonlinear Regime. When, with no RF input, I_b is small, the beam is visible as a brighter cylinder extending to the anode and the system is quiet. When I_b exceeds a critical value, dependent on V_b and the interaction length L, the beam breaks up close to the anode, as witnessed by the appearance of a localized brighter region (the meniscus) and no beam is visible beyond it. This is due to the spatial growth of noise components at $f \sim f_p$ on the injected beam, to a nonlinear level where $\phi \sim V_b$. With further increase of I_b, or decrease of V_b, the meniscus moves towards the gun (k_i increases with increasing I_b or decreasing V_b). Reducing L removes the meniscus.

Coincident with the appearance of the meniscus, there is a sudden onset of noise at $f \sim f_p$ and also at low frequencies 0 ~ 100 kHz. The RF spectrum is broad, e.g. 100 MHz wide about $f_p \sim 1000$ MHz, and is detected on the probe or an external antenna. The low-frequency fluctuations of ϕ and n are strongest in the meniscus where $n_1/n_0 \sim 10$-20%, and appear to be a relaxation effect associated with the nonlinear RF interaction. Various mechanisms may be suggested for coupling between RF and LF waves. The meniscus acts as a localized noise generator which launches damped ion acoustic waves along the tube. The RF spectrum corresponds to oscillations at an f_p which is modulated over a band ~ 10% by the low-frequency density fluctuations. Coincident with the appearance of the meniscus there is also a marked increase in T_e from some 0.6 ~ 0.8 V to 2 ~ 3 V.

The meniscus may also be stimulated by applying a sufficiently large signal to the injected beam at $f \sim f_p$. As the signal is increased, the meniscus first appears near the anode and moves towards the gun. As with the meniscus excited from noise, strong low-frequency fluctuations and a marked rise in T_e are observed. However, the RF spectrum is narrow, the injected frequency being amplitude modulated by the low frequencies.

DISCUSSION: The apparatus allows beam-plasma interaction to be studied under particularly simple and well-defined conditions (quiescent steady state, B = 0). By exciting with a single frequency, the spatially growing waves may be checked critically against the roots k(ω real) of the dispersion relation for a bounded system, with reasonable agreement. The nonlinear regime, beam scattering and plasma heating may also be studied under closely controlled conditions. Of particular interest is the nonlinear coupling to ion waves. This work is discussed in greater detail in Refs. 2.

This research was supported by the US AEC.

References

1. R. J. Briggs, Electron-Stream Interaction with Plasmas (MIT Press, 1964).
2. S. A. Self, Stanford University Institute for Plasma Research Reports Nos. 275 and 276 (January 1969).

NON LINEAR STABILITY OF A BEAM PLASMA SYSTEM .

by

A.Samain.

ASSOCIATION EURATOM-CEA
Département de la Physique du Plasma et de la Fusion Contrôlée
Centre d'Etudes Nucléaires
Boite Postale n° 6 - **92 Fontenay-aux-Roses** (France)

I. A special problem arises when a collisionless plasma happens to be in a linearly unstable equilibrium state $\mathcal{E}$ adjoining a marginally unstable equilibrium state $\mathcal{E}_{cr}$. It consists of discriminating between two possibilities which may then occur : The presence of unstable modes in the plasma may reinforce its instability ; in this case, the plasma will reach a strongly turbulent state, independently of the deviation Δ between $\mathcal{E}$ and $\mathcal{E}_{cr}$. On the contrary, the presence of these modes may stabilize the plasma ; a weak turbulence, with a small amplitude, going to o with Δ , will then appear in the plasma. We will study this problem in the case of a beam plasma system, assuming that all phenomena to be considered are periodic along the beam direction oz with a definite period $2\pi/K_o$. We neglect the ion motion and that component of the electron motion which is transverse to oz . We also assume that the marginally unstable mode associated with the state $\mathcal{E}_{cr}$ is described by an electrostatic potential of the form $\exp(iK_o z + i\omega_{cr} t)$ and that the plasma instability is a reactive effect, not a resonant particle effect : the velocities v of the particles verify : $|\omega_{cr} + K_o v| > \Gamma$ where Γ is a finite quantity. We determine which of the two possibilities outlined above effectively occurs, by studying whether a small amplitude electric potential, stationary in time, can exist in the plasma's final state. (the second possibility). Such a potential , if it exists, has grown in the plasma with a small rate, and consists of modes similar to $\exp(iK_o z + i\omega_{cr} t)$ and their harmonics . It can be shown that, without loss of generality for the problem we consider, this potential may be written as :

$$\Psi(z,t) = \sum_{n=-\infty}^{+\infty} \phi_n \exp\left[in(K_o z + \omega t)\right]$$

where n is an integer, ω is a real frequency, and the ϕ_n are small quantities verifying $\phi_n = O(\phi_1^{|n|})$. The calculations which follow show that ω cannot be real. We therefore conclude that our beam plasma system cannot reach a weakly turbulent state, but, on the contrary, reach a state with a finite amplitude turbulence, evidently independent of Δ [1] .

We use a variational method to determine $\Psi(z,t)$. First we study the motion, in the presence of $\Psi(z,t)$, of a particle, (charge e and mass m), having the velocity v before $\Psi(z,t)$ exists. This may be done taking into account that $\Psi(z,t)$ has grown with a small rate and is not resonant with the particle motion, by applying the adiabatic invariant formalism [2]. A function $\mathcal{E}(v)$, depending on the quantities ω , ϕ_n may then be shown to exist with the following property : If $\delta\Psi(z,t)$, $\delta\mathcal{E}(v)$ are the variations of $\Psi(z,t)$, $\mathcal{E}(v)$, when the ϕ_n are varied by $\delta\phi_n$, (ω being kept constant), the mean value of $e\,\delta\Psi(z,t)$ along the particle trajectory, in the presence of $\Psi(z,t)$, is equal to $\delta\mathcal{E}(v)$. At order 5 in ϕ_1 one has :

$$\mathcal{E}(v) = \frac{1}{2} m v^2 + e\left[\alpha|\phi_1|^2 + \frac{5}{4}\alpha^3|\phi_1|^4 + \frac{3}{2}\alpha^2\left(\phi_2\phi_{-1}^2 + \phi_{-2}\phi_1^2\right) + \alpha|\phi_2|^2\right] + O(\phi^6)$$

where $\alpha = K_o^2 e/\left[m(\omega + K_o v)^2\right]$. We finally consider the function $\mathcal{N}$ of ω and the ϕ_n defined by :

$$\mathcal{N} = \frac{K_o^2}{8\pi}\left(\sum_{n=-\infty}^{+\infty} n^2|\phi_n|^2\right) - \int f(v)\,\mathcal{E}(v)\,dv$$

where $f(v)$ is the distribution function of particles, when the plasma is in the equilibrium state $\mathcal{E}$, before $\Psi(z,t)$ exists. It is readily seen that the Poisson equation for $\Psi(z,t)$ is equivalent to the condition that $\mathcal{N}$ is an extremum for all variations of the ϕ_n . Also , the energy density in the plasma in the presence of $\Psi(z,t)$ is given by : $-\mathcal{N} + \omega\,\partial\mathcal{N}/\partial\omega$.

Expressing this variational condition, one finds the non linear dispersion relation giving ω :

$$\mathcal{L}(\omega) + C\,\phi_1^2 + O(\phi_1^4) = 0 \qquad (1)$$

where :

$$\mathcal{L}(\omega) = 1 - \frac{4\pi e^2}{m} I_2 \qquad \text{with :} \quad I_p = \int \frac{f(v)\,dv}{(\omega + K_o v)^p}$$

$$C = -\frac{4\pi e^4 K_o^4}{m^3}\left[\frac{5}{2} I_6 + \frac{18\pi e^2}{m}\,\frac{I_4^2}{3 + \mathcal{L}(\omega)}\right]$$

Note that ω_{cr} is defined by the linear dispersion relation : $\mathcal{L}_{cr}(\omega_{cr}) = 0$, where $\mathcal{L}_{cr}(\omega)$ results from $\mathcal{L}(\omega)$ by changing $f(v)$ into $f_{cr}(v)$, the distribution function associated with $\mathcal{E}_{cr}$. As the plasma in this state is marginally unstable, due to a reactive effect, one has also : $\partial\mathcal{L}_{cr}(\omega_{cr})/\partial\omega = o$. At lowest order in $\omega - \omega_{cr}$, ϕ_1 and $\mathcal{L}(\omega_{cr}) - \mathcal{L}_{cr}(\omega_{cr}) = \mathcal{L}(\omega_{cr})$, (which is small because $\mathcal{E}$ is adjoining $\mathcal{E}_{cr}$), (1) may then be written as :

$$\omega = \omega_{cr} \pm \left(-A - E\,|\phi_1|^2\right)^{1/2}$$

$$E = \frac{K_o^4 e^2}{6 m^2 I_4}\left(5 I_6 + \frac{12\pi e^2}{m} I_4^2\right) ; \quad A = 2\,\mathcal{L}(\omega_{cr})\left[\frac{\partial^2\mathcal{L}(\omega_{cr})}{\partial\omega^2}\right]^{-1}$$

For the plasma in the equilibrium state $\mathcal{E}$ to be linearly unstable, A must be positive. Since , on the other hand, E is positive, the value of ω cannot be real.

II. The problem which has been set above can be solved in the general case by studying whether a small amplitude self consistent electromagnetic field $\mathcal{E}$, stationary in time, can exist in the plasma's final state. If $\mathcal{E}$ is not resonant with the particle motion, it can be proved that such a field can be described without loss of generality by a scalar and vector potential $\Psi(x,y,z,t)$, $\underset{\sim}{A}(x,y,z,t)$ of the form :

$$\Psi(x,y,z,t) = \sum_{n=-\infty}^{+\infty} \phi_n(x,y,z)\exp(in\omega t) ; \cdots$$

where ω is a real frequency adjoining ω_{cr} , the real frequency of the marginally unstable mode which can develop when the plasma is in the state $\mathcal{E}_{cr}$. It is also possible to calculate [3], for each value of ω a functional $\mathcal{N}$ of the functions $\phi_n(x,y,z)$, $\underset{\sim}{A}_n(x,y,z)$ which allows the determination of $\mathcal{E}$ by expressing that $\mathcal{N}$ is extremum for all variations of $\phi_n(x,y,z)$, $\underset{\sim}{A}_n(x,y,z)$. The total energy of the plasma and the field $\mathcal{E}$ is then given by : $-\mathcal{N} + \omega\,\partial\mathcal{N}/\partial\omega$.

Applying this formalism in the general case under study, one finds :

$$\omega = \omega_{cr} \pm \left[A + B\right]^{1/2}$$

where A is a small negative quantity , going to o with Δ , independent of $\Psi(x,y,z,t)$, and B is a real quantity whose principal value is proportional to $|\Psi^2|$. Particularly, the sign of B , which determines obviously the type of evolution of the plasma, can be calculated.

REFERENCES.

[1] V.D.SHAPIRO, V.I. SHEVELENKO, Sov. Phys. JETP, (1967) 25, 92.

[2] A. LENARD, Ann. of Physics (1959) 6 , 261.

[3] A. SAMAIN, Compte rendus à l'Academie des Sciences. (in press).

PARAMETRIC AMPLIFICATION IN A BEAM-PLASMA SYSTEM

by

PHAM-TU-MANH

Institut d'Electronique Fondamentale - Laboratoire associé au CNRS - Bâtiment 220, Faculté des Sciences - 91,ORSAY (France)

We have previously reported experimental results concerning parametric amplification obtained with a beam-plasma system (1, 2) and a former simplified theory has been given (3). A more satisfying theoretical model is analyzed here, where Kino's theory (4) is extended to the case of a cylindrical column including plasma and electron beam of the same diameter, immersed in an infinite magnetic field. In this medium are injected a signal wave (frequency F_S) and a high level pump wave (frequency F_p). A third wave called "idler" is created (frequency $F_i = F_p - F_S$) and the fields of the three waves act on the motion of the electrons and give rise to a varying electron current. The second-order term of this current is a function of the three frequencies and is proportional to the pump field intensity, therefore it can be strong enough to modify the original propagation characteristics of the system at frequencies F_S and F_i. Writing the nonlinear equations and taking second-order quantities into account, we finally obtain the propagation constants of the perturbed system, from which is deduced the spatial growth rate. Let ω_1, ω_2, ω_3 and β_1, β_2, β_3 be the radian frequencies and longitudinal propagation constants of the signal, idler and pump wave respectively. The amplification is maximum when the three waves propagate at the same velocity, i.e. when we have :

$$\omega_1 + \omega_2 = \omega_3$$

$$\beta_1 + \beta_2 = \beta_3 + \delta, \qquad \text{with } \delta = 0$$

where δ expresses the phase difference between the three waves.

We have computed the gain for the theoretical model described above, using quasistatic approximation and considering only the axisymmetric modes (m=0). Moreover we assume that the pump wave is propagated by a beam space-charge mode while signal and idler waves are propagated by a plasma forward mode. Figures 1 to 3 show the dependence of gain on pump, signal and plasma frequencies respectively. The main results are summarized below :

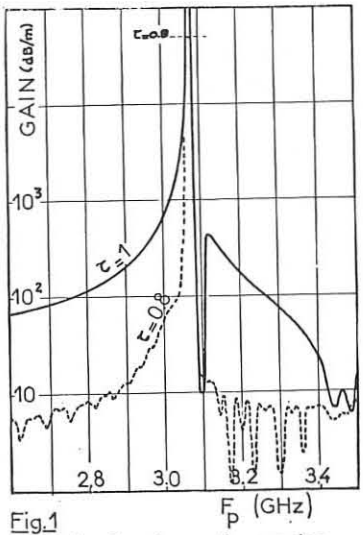

Fig.1

- The beam-plasma system behaves like a travelling wave parametric amplifier and amplification can take place over a wide range of signal and pump frequencies.

- The curves exhibit a strong resonance aspect and the maximum gain occurs at synchronism (δ =0). The gain is highly dependent on the system parameters and consequently parameter fluctuations result in flattening of the curves. Figure 2 shows the influence of a $\pm$ 5% departure of plasma frequency F_o from the synchronism value (dashed curve).

- The calculated gain is extremely high and is several orders of magnitude greater than the experimental one and this is certainly due to the simplifying assumptions we made.

- Up to now we have dealt with pure travelling pump wave. If we assume that, due to its high level, the pump wave is partly reflected at the system ends, we can insert a "reflecting coefficient" τ in the equation :

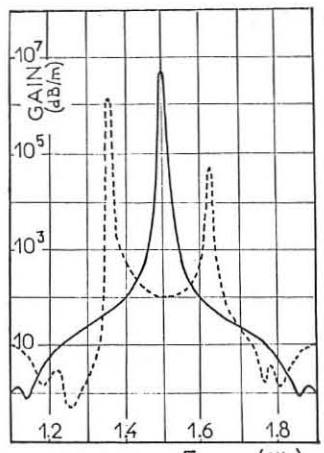

Fig. 2

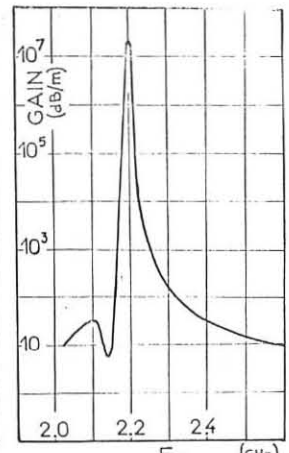

Fig. 3

$$\tau = \frac{\text{forward-wave field amplitude}}{\text{total field amplitude}} ,$$

τ = 1/2 or τ = 1 corresponding to pure stationary or pure travelling-wave respectively. This involves more complicated calculations and the result is illustrated by the dashed curve of figure 1 with τ = 0.8.

In a whole, theoretical results show satisfactory agreement with experimental ones and give a good explanation of the physical mechanism.

References

(1) PHAM-TU-MANH, Sixth Intern. Conf. on MOGA, Cambridge (G.B), Sept. 1966, 485-489.

(2) PHAM-TU-MANH, A. SEPTIER, J. Phys. 29, C3, Apr. 1968, 204-206.

(3) PHAM-TU-MANH, C.R. Ac. Sc. Paris, 268, N4, 27 Jan.1969, 301-304.

(4) G.S. KINO, J.A.P., 31, Aug. 1960, 1449-1458.

HARMONIC GENERATION IN NONLINEAR BEAM-PLASMA SYSTEMS

G. T. Konrad* and J. E. Rowe
Department of Electrical Engineering
The University of Michigan
Ann Arbor, Michigan U.S.A.

When an electron beam is passed through a plasma, amplification of an RF signal propagating through the plasma may take place under certain conditions. In the present analysis a cylindrical system, i.e., a plasma column and a drifting cylindrical electron beam, will be considered. Maximum use will be made of previously developed traveling-wave tube theory, which can be readily adapted to this study.

It is possible to think of the plasma column by itself as a slow-wave "circuit" along which energy can propagate just as along a transmission line. For such a transmission line an equivalent circuit may be found which is made up of distributed elements given in terms of the plasma parameters. This approach restricts the plasma to linear behavior. If the electron displacements and the RF currents in the beam and in the plasma of a beam-plasma system are calculated, it is found that as the device approaches saturation, the beam electrons are driven beyond overtaking, while the displacement of the plasma electrons is very small. Physically speaking, the charge density of a typical electron beam is much smaller than the charge density in the plasma. Since the same field must be supported in both the beam and the plasma, the space-charge restoring forces in the plasma are then much greater than in the beam. This prevents the plasma particles from making large RF excursions. Thus it is justifiable to assume linear behavior for the plasma and to introduce the nonlinearities in the electron beam.

For the present analysis the plasma is assumed to be cold, stationary, uniform and neutral. A static magnetic field is assumed to exist along the axis of the beam-plasma system. The magnetic field is needed to focus the electron beam. Furthermore, nonrelativistic mechanics is used, and a quasi-static analysis is considered to be appropriate.

The equivalent circuit approach to the analysis of a plasma column leads to transmission line equations, which may be combined to form a wave equation or "circuit" equation. In the present analysis a quasi-two-dimensional form of the circuit equation is chosen wherein the electric field is used directly from a one-dimensional model for the plasma column, and the radial variations are taken into account by defining a weighting function which is proportional to the radial variation of the longitudinal electric field. Depending upon the relative magnitudes of the plasma frequency, the electron cyclotron frequency and the signal frequency, the particular electric field variation across the electron beam may be calculated from the field at the plasma edge.

In the present study the static magnetic field is assumed to be finite. As a result the transverse motion of the beam electrons is not neglected. The electron beam is treated in two dimensions, i.e., the "circuit" as well as the space-charge field are assumed to vary in the radial direction but are axisymmetric. The action of the finite axial magnetic focusing field is included by considering electron motion, without bunching, around the axis. This inclusion of the magnetic field does not complicate matters unduly; it merely introduces the angular velocity variable in the equations of motion.

The above model is used to make a Lagrangian (ballistic) analysis in order to calculate the trajectories of the various charge groups into which the electron beam is subdivided. Since overtaking of the various charge groups can be taken into account, this type of analysis lends itself to the study of nonlinearities and large-signal effects. Proper manipulation of the plasma circuit equation, the equations of motion of the beam electrons and the conservation of charge equation leads to a set of differential equations for the fundamental RF frequency and each of the harmonics to be analyzed. The various sets of equations are coupled through the RF charge density. It should be noted that in a practical situation only a finite number of harmonics can be included in the analysis due to the finite number of charge groups distributed over phase that can be tracked through the interaction region.

Due to their complexity the large-signal equations are solved on a digital computer. The differential equations are first written in difference form to be suitable for machine computation. Numerical integration of the equations proceeds in finite steps along the interaction region. Since the wave amplitude at the end of the interaction region is not a priori known for a given input signal, the present analysis is treated as an initial value problem.

The charge group trajectories, the RF currents and the circuit voltages of the fundamental signal and its harmonics generated by the nonlinear operation are calculated. Plasma collision effects as well as collisions due to the beam electrons are included in this study.

A beam-plasma device was found to be considerably more dispersive than, for example, a conventional helix-type traveling-wave amplifier. For this reason the appropriate dispersion equation for a plasma column had to be solved in order to find the phase characteristics before the interaction impedance could be calculated. Even though the phase velocity along the plasma column was appropriate for beam-plasma interaction over a bandwidth of only approximately 20 percent, the interaction impedance remained at a substantial level over a frequency band of several octaves. This suggests that a beam-plasma device should be rich in harmonics, provided they can be coupled out. In the experimental test vehicle plasma uniformities did in fact under certain circumstances enhance the coupling. Thus in some cases the second harmonic was as little as 3 to 6 dB below the fundamental, and harmonics through the fifth could be observed.

Experimentally a xenon plasma column 10.5 cm long was generated by either a hot cathode Penning discharge or by ionization due to the beam electrons passing through the xenon gas. Values of electronic gain as high as 35 dB in the vicinity of 2.0 GHz were obtained by the latter scheme. When collision effects were taken into account in the theoretical calculations, the agreement with experimentally observed values was quite good for the cases that could be compared.

Coupling of RF energy into and out of the experimental beam-plasma device was studied in great detail. Short sections of a slow-wave structure outside of the plasma region were used in the device under test for much of the experimental work. Another coupling scheme used, making use of quasi-optical techniques, was a set of elliptic cavity couplers, which were placed directly around the plasma column. These were found to yield a coupling loss of only 10 to 15 dB per coupler over a frequency range of slightly greater than 20 percent in the low S-band frequency region. This coupling approach is much less lossy than most other methods employed previously. Efforts to use these couplers for RF amplification measurements were unsuccessful due to cathode poisoning at the higher gas pressures required. Since high RF gain per unit length is possible in a beam-plasma interaction, this method of coupling holds great promise to yield net gain in a device similar to the one used for the experimental work of this study.

---

* Presently with M.I.T. Lincoln Laboratory, Lexington, Massachusetts, U.S.A.

NONLINEAR COUPLING OF WAVES IN BEAM-PLASMA SYSTEMS

by
Hans Wilhelmsson
Institute of Physics, Uppsala, Sweden

The purpose of the investigation is to study nonlinear wave interactions in beam-plasma systems including the possibilities of several kinds of species, temperature effects and the presence of a constant magnetic field. The work is of interest not only for microwave beam-plasma techniques but also for the theory of weak turbulence in plasma.

Perfect matching of frequencies and wave-numbers of the interacting waves is assumed. A hydromagnetic description is used and the equations are treated in accordance with coupled mode theory.

The interaction of two transverse waves and one longitudinal wave is treated as well as the coupling between three longitudinal waves. Besides, the case of two longitudinal waves and one perpendicular wave of long wave-length has been studied.

The basic equations used to describe the system are the equation of motion in the hydrodynamic form, the equation of continuity and Maxwell's equations. According to coupled-mode theory [1, 2, 3] linear combinations of the variables entering the problem, such as the fields and the density- and velocity perturbations, are formed. The normal modes are then defined in such a way that the linearized equation for each mode can be written in the simple form $\partial a_n/\partial t - i\omega_n a_n = 0$, where ω_n is a solution of the dispersion relation for the mode n, relating ω_n to the wave-number k. If the nonlinear terms of the basic equations are expressed by means of the same normal modes and if only those terms are kept which fulfil the matching conditions $\omega_0 = \omega_1+\omega_2$ and $k_0 = k_1+k_2$ we obtain a closed system of nonlinear equations of the form

$$\begin{aligned} \partial a_0/\partial t - i\omega_0 a_0 &= c_{12}\, a_1\, a_2 \\ \partial a_1/\partial t - i\omega_1 a_1 &= c_{02}\, a_0\, a_2^* \\ \partial a_2/\partial t - i\omega_2 a_2 &= c_{01}\, a_0\, a_1^* \end{aligned} \qquad (1)$$

In the derivation of these equations the assumption is made that the amplitudes in the nonlinear terms vary slowly in time as compared to the time of oscillations of the waves.

Let us suppose that the interacting waves are *two transverse monochromatic waves* of frequencies ω_0 and ω_1 , wave propagation constants k_0 and k_1 , *and a monochromatic longitudinal wave*, characterized by the corresponding quantities ω_L and k_L. We assume that all waves propagate along the direction of a constant magnetic field present in the plasma, and we allow the different species to have drift velocities $v_{d_\pm}$ and thermal velocities $u_\pm$.

The coupling coefficients for such a case (assuming the two transverse waves to have the same kind of circular polarization, which is necessary for non-vanishing coupling) can then be expressed as:

$$\begin{aligned} c_{1L} &= \left[\frac{\partial}{\partial\omega}(\omega^2\varepsilon_T)\right]^{-1}_{\omega=\omega_1}\left[\frac{\partial}{\partial\omega}(\omega^2\varepsilon_L)\right]^{-1}_{\omega=\omega_L}\cdot F \\ c_{0L} &= -\left[\frac{\partial}{\partial\omega}(\omega^2\varepsilon_T)\right]^{-1}_{\omega=\omega_0}\left[\frac{\partial}{\partial\omega}(\omega^2\varepsilon_L)\right]^{-1}_{\omega=\omega_L}\cdot F \\ c_{01} &= -\frac{1}{2}\left[\frac{\partial}{\partial\omega}(\omega^2\varepsilon_T)\right]^{-1}_{\omega=\omega_0}\left[\frac{\partial}{\partial\omega}(\omega^2\varepsilon_T)\right]^{-1}_{\omega=\omega_1}\cdot F \end{aligned} \qquad (2)$$

where ε_T and ε_L are the dielectric constants for transverse and longitudinal waves, respectively, defined by

$$\varepsilon_T = 1 - \sum_{\pm}(\omega_{p_\pm}^2/\omega^2)(\omega-kv_{d_\pm})/(\omega-kv_{d_\pm}\oplus\pm\omega_{H_\pm})$$

and

$$\varepsilon_L = 1 - \sum_{\pm}\omega_{p_\pm}^2/\left[(\omega-kv_{d_\pm})^2-k^2u_\pm^2\right]$$

where $\varepsilon_T(\omega_{0,1}\,,\, k_{0,1}) = \dfrac{k_{0,1}^2c^2}{\omega_{0,1}^2}$; $\varepsilon_L(\omega_L\,,\, k_L) = 0$

are the dispersion relations for the interacting waves. Furthermore the function F in (2) can be written

$$F = \omega_L\sum_{\pm}\frac{q_\pm}{m_\pm}\cdot\frac{\omega_{p_\pm}^2}{(\omega_L-k_Lv_{d_\pm})^2-k_L^2u_\pm^2}\cdot\left[k_L\oplus\pm\omega_{H_\pm}\left(\frac{k_0}{\omega_0-k_0v_{d_\pm}}-\frac{k_1}{\omega_1-k_1v_{d_\pm}}\right)\right]\cdot$$
$$\cdot\frac{\omega_0-k_0v_{d_\pm}}{\omega_0-k_0v_{d_\pm}\oplus\pm\omega_{H_\pm}}\cdot\frac{\omega_1-k_1v_{d_\pm}}{\omega_1-k_1v_{d_\pm}\oplus\pm\omega_{H_\pm}} \qquad (2a)$$

In these formulae the upper and lower signs of the encircled notations refer to right- and left-handed polarization of the waves, respectively, whereas the other signs refer to the charges of the different particles, and $\omega_{H_\pm}$ to their gyro frequencies.

For the interaction of *three longitudinal waves* we obtain, assuming $\omega_0 = \omega_1+\omega_2$; $k_0 = k_1+k_2$,

$$\begin{aligned} c_{12} &= \left[\frac{\partial}{\partial\omega}(\omega^2\varepsilon_L)\right]^{-1}_{\omega=\omega_1}\left[\frac{\partial}{\partial\omega}(\omega^2\varepsilon_L)\right]^{-1}_{\omega=\omega_2}\cdot G \\ c_{01} &= -\left[\frac{\partial}{\partial\omega}(\omega^2\varepsilon_L)\right]^{-1}_{\omega=\omega_0}\left[\frac{\partial}{\partial\omega}(\omega^2\varepsilon_L)\right]^{-1}_{\omega=\omega_1}\cdot G \\ c_{02} &= -\left[\frac{\partial}{\partial\omega}(\omega^2\varepsilon_L)\right]^{-1}_{\omega=\omega_0}\left[\frac{\partial}{\partial\omega}(\omega^2\varepsilon_L)\right]^{-1}_{\omega=\omega_2}\cdot G \end{aligned} \qquad (3)$$

where

$$G = \omega_0\omega_1\omega_2\sum_{\pm}\frac{q_\pm}{m_\pm}\omega_{p_\pm}^2\left\{\left[(\omega_0-k_0v_{d_\pm})^2-k_0^2u_\pm^2\right]\left[(\omega_1-k_1v_{d_\pm})^2-k_1^2u_\pm^2\right]\cdot\right.$$
$$\left.\cdot\left[(\omega_2-k_2v_{d_\pm})^2-k_2^2u_\pm^2\right]\right\}^{-1}\cdot \qquad (3a)$$
$$\cdot\left[k_0(\omega_1-k_1v_{d_\pm})(\omega_2-k_2v_{d_\pm}) + k_1(\omega_0-k_0v_{d_\pm})(\omega_2-k_2v_{d_\pm})\right.$$
$$\left.+ k_2(\omega_0-k_0v_{d_\pm})(\omega_1-k_1v_{d_\pm}) - u_\pm^2\, k_0k_1k_2\right]$$

The present investigation represents a generalization of the problem of three-wave interaction in a plasma to situations more complex than those of previous works. The work thus demonstrates how the coupled mode theory also for such cases of practical interest leads to formally simple coupled equations for the wave amplitudes, which are useful for analytic studies as well as for simple computer calculations.

It has been shown that the set of equations (1) may lead to so called "explosive instabilities". This may happen if one of the interacting waves has "negative energy" [4]. It has also been found that dissipative effects can stabilize such nonlinear instabilities, which otherwise grow faster than exponentially [5]. Vice versa it seems possible that dissipation may destabilize situations which are otherwise stable.

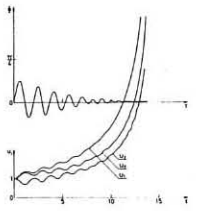

Fig. 1a. Explosively unstable case

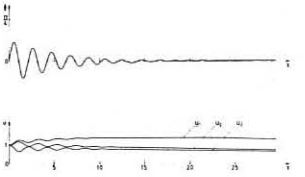

Fig. 1b. Stabilized case. Dissipative effects slightly exceeding the critical limit.

In Figs 1a and 1b u_j and τ are normalized amplitudes (j = 0,1,2) and time, Φ is a linear combination of the phases of the amplitudes of the three interacting waves.

For comparison the set of "random-phase" equations describing wave coupling with dissipation has been solved (also for the n-wave case) and the critical limit for stabilization has been determined [6].

References

1. LOUISELL, W.H. 1960 *Coupled Mode and Parametric Electronics* (John Wiley & Sons, Inc., New York)
2. SJÖLUND, A. & STENFLO, L. 1967 J. Appl. Phys. 38, 2676; Physica 34, 567; Appl. Phys. Lett. 10, 201; Z. Phys. 204, 211
3. WILHELMSSON, H. 1969 J. Plasma Phys. (in press)
4. ENGELMANN, F. & WILHELMSSON, H. 1969 Z. Naturforsch. 24a, 206
5. JARMÉN, A., STENFLO, L., WILHELMSSON, H. & ENGELMANN, F. 1969 Phys. Letters A 28A, 748
6. STENFLO, L. & WILHELMSSON, H. 1969 (to be publ.)

Convective and absolute two stream instabilities for hot plasmas

by

E. Infeld and A. Skorupski

Institute of Nuclear Research, Hoza 69, Warsaw, Poland

Abstract This paper resolves the problem of stability for two streams of hot, charged particles in the resonance model. The instabilities are then classified into absolute and convective.

The subject of this work is the classification of two stream instabilities into absolute and convective in the resonance model. In this model the distribution functions are

$$f_i(v) = N_i u_i^{-1} \pi^{-1} [(v - v_i)^2 + u_i^2]^{-1}, \quad i = 1,2 \qquad (1)$$

where N_i is the number density, and u_i and v_i the thermal and macroscopic velocities of the i'th stream, respectively.

Before giving the classification we will find the stability limit. As far as we know this has previously been done only for $u_1 = u_2$ [1]. To do this generally we write the dispersion relation, corresponding to (1), in the form

$$u_1^2 k^2/\omega_{p1}^2 = F(z) \equiv (z + i)^{-2} + \gamma(z + z_0 + ir)^{-2}, \qquad (2)$$

where $\omega_{p1}^2 = 4\pi N_1 e_1^2/m_1$, $\gamma = \omega_{p2}^2/\omega_{p1}^2$, $z = (\omega/k - v_1)/u_1$, $z_0 = (v_1 - v_2)/u_1$, $r = u_2/u_1$. The parameters r, z_0, γ determine the question of stability; this is a model-independent feature of the two stream instability. The results of the stability analysis performed on (2) are given in Fig.1 for arbitrary z_0, r, and some chosen γ. The figure actually covers $0 \leq r \leq 1$, but is easily extended to other r, since if z_0, r, γ lead to instability so do z_0/r, $1/r$, $1/\gamma$. The part of the stability limit above X is given by F = 0, which leads to

$$r = \gamma^{1/2} z_0 - \gamma \qquad (3)$$

Below X the stability limit corresponds to the Nyquist curve being tangent to the positive real F axis and is described by more complicated equations.

Note that a step function distribution would give one limit for all $\gamma > 0$ at $r = z_0 - 1$, as is seen from Penrose's criterion.

To classify instabilities we use the saddle point method that looks for

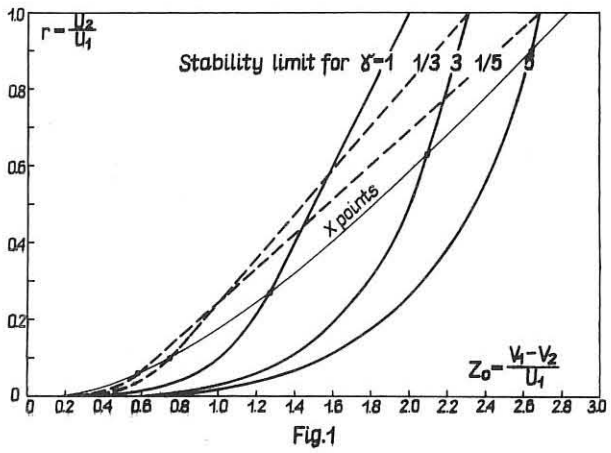

Fig.1

a zero of $d\omega/dk$ between the line $\omega(k)$, k real, and the real ω axis [2]. If we find one at ω_0, k_0 we know that the instability is absolute and its asymptotic growth rate is equal to $\mathrm{Im}(\omega_0)$ [3].

For two streams of equal plasma frequencies ($\gamma = 1$) we have solved (2) in ω (w.l.g. $z_0 > 0$) :

$$\omega/\omega_{p1} = \beta K + i[(1 + 4\xi^2 K^2)^{1/2} - 1 - \xi^2 K^2]^{1/2} \qquad (4)$$

where $K = u_1 k/(2\omega_{p1})$, $\xi = z_0 - i(1 - r)$, $\beta = -z_0 + 2v_1/u_1 - i(1 + r)$. This solution allows us to find the saddle point in question, $\omega_0 = \omega(k_0)$, where

$$(d\omega/dk)_0 = 0 \qquad (5)$$

For $u_1 = u_2 = u_0$ we have recently published the results [4]. A division of data into absolute and convective instabilities and the stable region is given in Fig.2. Lines of equal asymptotic growth rate for absolute instabilities are also indicated. The figure is drawn in the u_0/v_1, $-v_2/v_1$ plane, and $\mathrm{Im}(\omega_0)$ is in units of ω_{p1}.

For $u_1 \neq u_2$ the method is basically the same and the results for r = 2 are given in Fig.3. The broken line indicates parameters for which the peak of the instability becomes stationary as t goes to infinity (on Fig.2 they correspond to $v_2 = -v_1$).

For different plasma frequencies of the streams ($\gamma \neq 1$) the dispersion relation is not easily solved analytically for $\omega(k)$. However, we did succeed in solving analytically the pertinent set of equations:

$$D(\omega,k) \equiv 1 - \omega_{p1}^2(\omega - kv_1 + iku_1)^{-2} - \gamma\omega_{p1}^2(\omega - kv_2 + ikru_1)^{-2} = 0 \qquad (6)$$

$$\partial D(\omega,k)/\partial k = 0 \qquad (7)$$

The trick is to solve (7) first leading to

$$k/\omega = \Phi(\gamma, r, u_1/v_1, v_2/v_1) \qquad (8)$$

When (8) is inserted into (6) one obtaines algebraically ω_0 as a function of the same parameters. The detailes will appear in [5]. We now know the point ω_0, k_0 , and the problem of classification can be solved for any v_1, v_2, u_1, u_2, . Results for $\gamma = 2$, $r = 1$ are given as an example in Fig.4. The authors have solved the problem of classification and asymptotic growth rates numerically for about a score of sets of parameters [5].

Step function distributions which, as we saw above, lead to a common marginal stability line for all γ, have also been investigated by the authors in the context of classification, and found unsatisfactory. The experiment of Looney and Brown [6] has hitherto been explained by using step function distributions [7]. It would seem that when analysing experiments of this type our analysis could give deeper insight into the problem. This is to detract nothing from the pioneer character of [7], without which this analysis would probably not have been attempted.

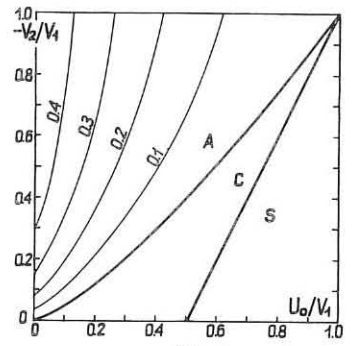

Fig.2

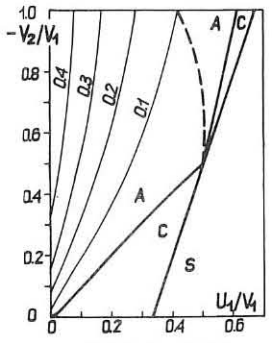

Fig.3: $\gamma=1$, $r=2$

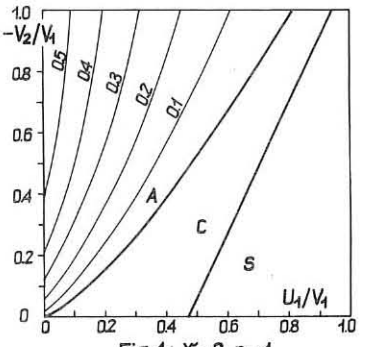

Fig.4: $\gamma=2$, $r=1$

We see that the resonance model gives good qualitative results on the one hand, and leads to simple algebraic expressions on the other. Even slight improvements seem to lead to models that fail to give simple algebraic expressions like those we encountered, and an analysis of this type could easily become cumbersome. This would be true , for example, of the two pole model [8].

References:

[1] P.C. Clemmow, J. of Plasma Phys., 2 , 1 (1968)
[2] Y. Fainberg, V. Kurilko and V. Shupiro, Sov. Phys. Tech. Phys., 6 , 459 (1961)
[3] R. Briggs, Electron stream interaction with plasmas, M.I.T. (1964)
[4] E. Infeld, A. Skorupski, Nuclear Fusion, 9 , 1 (1969)
[5] E. Infeld, A. Skorupski, (in preparation)
[6] D. Looney, S. Brown, Phys. Rev., 93 , 965 (1954)
[7] P.A. Sturrock, Phys. Rev., 117 , 1426 (1960)
[8] B.D. Fried, C.L. Hedrick, J. McCune, Phys. Fluids, 11 , 249 (1968)

TWO-DIMENSIONAL CALCULATIONS ON NON-LINEAR BEAM-PLASMA PROCESSES

By

J.P. Boris* and K. V. Roberts
Culham Laboratory, Abingdon, Berkshire, England.

We report computational studies of the nonlinear stabilization of two-stream instabilities in a two-dimensional doubly-periodic geometry. Since much of our output is obtained in motion-picture form, our results should be viewed as preliminary experimental data taken from a running experiment, the numerical plasma simulation. This work was motivated by the persistent nonuniform structures observed theoretically and computationally in one-dimensional two-stream problems[1,2,3] but not yet experimentally confirmed. Bounded experimental geometries may not support these equilibrium structures, or "holes-in-phase-space", but it is also possible that the 3-D nature of real plasmas differs intrinsically from the 1-D problems usually treated computationally. In a real plasma initial perturbations will contain components with wave-vectors directed at an angle to the relative streaming direction. In the linear growth phase of the instability, some of these nonaligned modes will surely exponentiate at about the same rate as the aligned modes because the linear growth rates, at least in the simplest fluid model, depend only on the component of the wave-vector parallel to the streaming direction. Thus, in the absence of a strong alignment mechanism, one could expect a large fraction of the collective electrostatic energy to reside in nonaligned modes.

The numerical plasma simulations were performed on the Culham KDF9 computer (comparable to the IBM 7090 in size and speed) using the GALAXY programs[4]. To perform maximally efficient simulations, several improvements in technique were devised and incorporated into the GALAXY system. By treating the co-ordinates, velocities, and accelerations as integers, packing both the X and Y components into one word, and by solving the equations of motion in vector form in optimized assembly language, improvement factors of 2 in storage and about 8 in execution speed are obtained. A triple-buffer technique, in conjunction with up to four simultaneous tape transfers, increases the effective core size from 32K words to infinity and a special high-speed graphical output package produces movies of the configuration-space particle motions while increasing total execution time by less than 2%.

The simulation plasmas are composed of 16,384 particles divided into two

Both beams have identical velocity distributions about the mean streaming motion, a Maxwellian with equal temperatures in X and Y. The particles move on the square $0 < X, Y < 64$ with periodic boundary conditions on the potential (64×64 mesh, double fast Fourier transform Poisson solver). Particles leaving this square are considered to be re-entrant in the usual way. The three separate problems reported are Run 1, a positron-positron two-stream where $V_o = 3.0$ and $V_{th} = 0.5$, Run 2, a positron-electron two-stream (the initial-current problem) with $V_o = 3.0$ and $V_{th} = 0.5$, and Run 3, an applied field instability in which a P-E plasma with $V_o = 0.0$, $V_{th} = 2.0$ is subjected to a constant external electric field accelerating the beams in opposite directions.

In 1-D two-stream problems, the electrostatic energy increases at the expected linear growth rate. It then saturates nonlinearly when some of the particles become trapped and decreases rapidly to a value typically one half of the maximum[2]. A more gradual decay then sets in. Our 2-D simulations show qualitatively similar behaviour in the early stages (including correct linear growth rates) because an alignment of the modes with the beam direction takes place during the growth phase of the instability. Figures 2a and 2 b show the fully developed "holes-in-phase-space" for Runs 1 and 2 respectively. Nearly full alignment is signified by the almost complete lack of particles in the holes. Figures 1a and 1b show r, the ratio of electrostatic energy in aligned ($k_y = 0$) modes to the total electrostatic energy, plotted as a function of time for the three problems (here the plasma frequency is unity). Alignment does not seem to persist long past nonlinear saturation ($15 < t < 20$ for Runs 1 and 2, $40 < t < 45$ for Run 3), the extended period of almost complete alignment in Run 3 almost certainly being related to the lag between the growing electrostatic energy and the increase in the kinetic energy arising from the continued action of the electric field. The "shoulders" at $t \sim 6$ in Fig. 1a for Runs 1 and 2 and at $t \sim 26$ in Fig. 1b for Run 3 may be related to a nonlinear mechanisms causing the one-dimensional alignment of the "holes-in-phase-space".

REFERENCES

1. H.L.BERK, C.E.NIELSEN and K.V.ROBERTS, "Phase Space Hydrodynamics of Equivalent Nonlinear Systems: Experimental and Computational Observations", (to be published).
2. R.L.MORSE and C.W.NIELSON, Proceedings of the APS Topical Conference on the Numerical Simulation of Plasma, Los Alamos Report LA-3990(1968), Paper A4.
3. J.M. DAWSON, C.G. HSI, and R. SHANNY, loc at, Paper A.1.
4. J.P.BORIS and K.V.ROBERTS, "The Optimization of Particle Calculations in 2 and 3-Dimensions", (to be published).

*Permanent address: Plasma Physics Laboratory,
Princeton University,
Princeton, N.J., U.S.A.

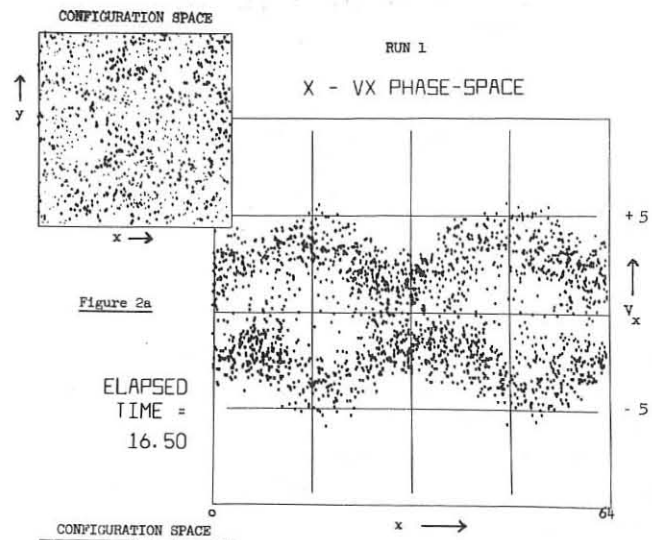

Figure 2a

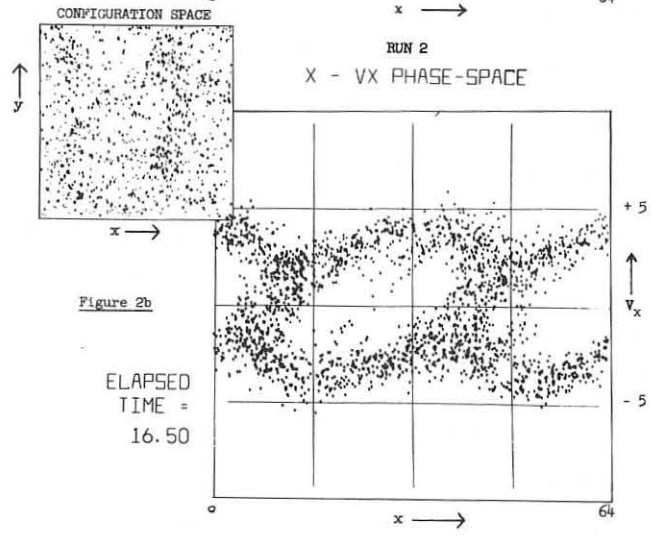

Figure 2b

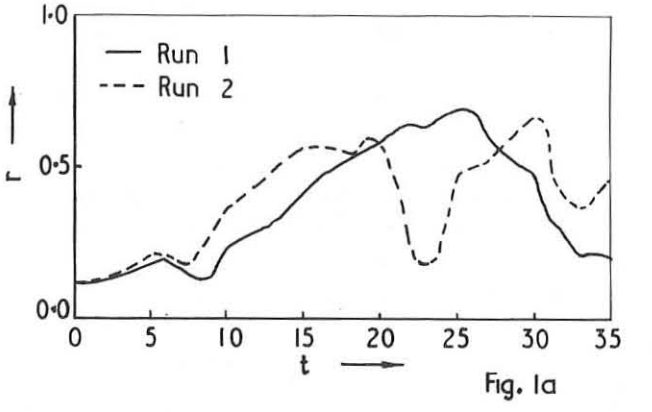

Fig. 1a

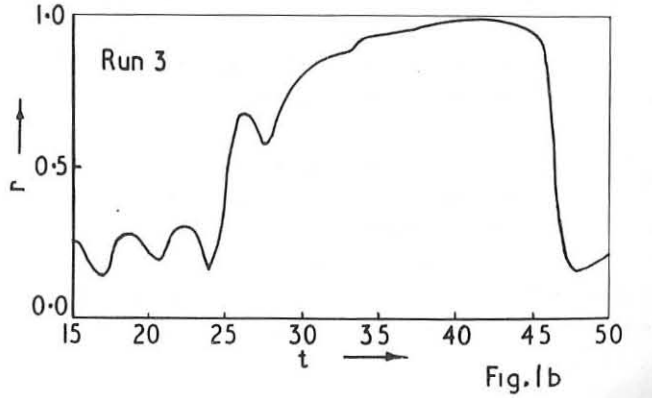

Fig. 1b

NUMERICAL SIMULATION OF BEAM-PLASMA INTERACTIONS USING THE PARTICLE-IN-CELL METHOD*

by

R. L. Morse and C. W. Nielson

University of California
Los Alamos Scientific Laboratory
Los Alamos, New Mexico

The nonlinear behavior of two counter-streaming Maxwellian electron distributions in the presence of a fixed neutralizing ion background has been studied by a variety of analytic and numerical methods. The problem has been treated by quasi-linear theories, [1,2] by numerical simulation using a sheet model for the electrons, [3] and by numerical simulation using a one-dimensional particle-in-cell method. [4] This paper reports the numerical simulation of two-beam problems in one, two, and three dimensions using the particle-in-cell method.

Our simulation method divides the problem region into identical cells, which in one dimension are simply line segments, in two dimensions are squares, and in three dimensions are cubes. Particles are given positions and velocities in the region so as to form a representative sample of the electron distribution to be simulated. Electric fields are computed at cell centers through the numerical solution of Poisson's equation.

As a smoothing procedure, a cell size box is imagined around each particle and weights assigned to neighboring cells in proportion to the overlap of this box with the cells. These weights are used both to interpolate the field at the particle position and to determine the particle's contribution to the charge density in the cells. We refer to this procedure as area weighting because of its geometrical significance in two dimensions. Such smoothing reduces collisional effects so that a relatively small sample of particles adequately simulates collisionless plasma.

The interpolated electric fields are used to advance particle velocities and positions through the equations

$$V_{+\frac{1}{2}} = V_{-\frac{1}{2}} + E\Delta t$$

$$X_1 = X_o + V_{+\frac{1}{2}}\Delta t \ .$$

Periodic boundary conditions are applied, both to the field solution and to the particle motion.

The first group of three simulations, similar except for the dimensionality of the computation, were initialized with two identical Maxwellian beams having opposite streaming velocities of magnitude twice the most probable internal velocity of a beam. The one-dimensional simulation used 64 cells with 20,000 particles, the two-dimensional simulation 64 × 64 cells with 80,000 particles, and the three-dimensional simulation used 32 × 32 × 32 cells with 332,750 particles. In each case, the maximum dimension in one direction was 100 Debye lengths as inferred from the properties of one of the Maxwellians. Times were expressed in plasma periods for the total distribution.

The early behavior is very similar in the three simulations. Field energy builds exponentially at a rate such that $\gamma T_p \approx 1.5$. This energy is concentrated in modes having a period of four in the direction of initial drift, that is, around a wavelength of 25 Debye lengths. These quantities are close to the values predicted by linear theory.

By the time of saturation, the velocity distribution has filled in the region between the bumps, becoming nearly flat in that region. Saturation occurs with a field energy, expressed in terms of the initial kinetic energy of 6%, 3%, and 2% in one, two, and three dimensions respectively. At the time of saturation, Fourier analysis reveals that the field energy is concentrated as would be expected from the linear growth. Moreover, examining plots of the particles in $X\text{-}V_x$ phase space reveals the fact that the potential wells are sufficiently deep to trap a substantial fraction of the particles.

The behavior after saturation is very different in one dimension from that in two and three dimensions. In the one dimensional case, the trapped particle regions persist and the field energy oscillates around a value of approximately 4% of the total energy. In two and three dimensions the field energy falls to less than 10% of its saturation value in five plasma periods. In the one dimensional case, the trapped particle regions eventually coalesce and the field energy falls, but this occurs over tens of plasma periods.

The second set of simulations consider the evolution of a "bump-on-tail" distribution, suggesting a beam in a background plasma. The beam comprises 5% of the particles and has a drift velocity 10 times the most probable velocity of the background. The beam has a thermal spread equal to that of the background. Again the simulations were done in one, two, and three dimensions. Twice as many simulation particles were used in order to adequately represent all parts of the distribution function. Again, early behavior was similar in the three simulations and corresponded closely to linear theory. In this case $\gamma T_p \approx 1.0$ and the wavelength of maximum growth was 80 Debye lengths. Saturation field energy was 17%, 12%, and 11% in one, two, and three dimensions respectively. The mean velocity of the beam at saturation had been reduced to 70% of its initial value, and this value was the same in the three cases to the accuracy of the simulations. At saturation the beam particles were nearly completely trapped in one dimension, whereas trapping was less complete in two and three dimensions. However, in all three cases, field energy at saturation was concentrated in modes having wavelengths in the streaming direction corresponding to that of maximum linear growth.

Behavior after saturation again differed dramatically in the one dimensional simulation from the two and three dimensional cases. In one dimension, the nearly single mode field excitation persisted for many tens of plasma periods, whereas in two and three dimensions the field energy fell to 20% of its saturation value in approximately 25 plasma periods.

Perhaps the most striking conclusion to be drawn from these simulations is the fact that whereas one dimensional simulations differ drastically from two and three dimensional simulations, the properties of the two and three dimensional cases are sufficiently similar that one might feel relatively confident that two dimensional calculations would be sufficient for problems of this type.

REFERENCES

(1) W. E. Drummond and D. Pines, Nuclear Fusion Supple. Pt. 3, 1049 (1962).

(2) I. B. Bernstein and F. Englemann, Physics of Fluids, 9, 937 (1966).

(3) J. M. Dawson and R. Shanny, Physics of Fluids 11, 1506 (1968).

(4) R. L. Morse and C. W. Nielson, Physics of Fluids (to be published).

* Work performed under the auspices of the U. S. Atomic Energy Commission

DEPENDANCE OF THE ELECTRONIC TEMPERATURE OF A SYNTHESIZED PLASMA ON THE PARAMETERS OF THE NEUTRALIZED ION BEAM

by

P. CHENEVIER, J.M. DOLIQUE, J.B. NUGEYRE, C. POMOT, P. SERMET
Université de Grenoble - Laboratoire de Physique des Plasmas
23 rue des Martyrs - 38 . GRENOBLE . France

==

INTRODUCTION

The experience purpose is to realize a synthesized plasma from a fast-ion beam (velocities between 700 and 2000 km/s), by injecting thermal electrons produced by a heater placed inside the beam. The experiments show that, for a given ion-velocity v_+, we get effective neutralization as long as the ion-beam density is smaller than a critical value ; when the density is larger, the beam breaks out [1]. We tried to evidence this effect by a computer simulation.

The principal components of the experimental arrangement are (fig. 1) : an ion H^+ source, S, an ion accelerating grid, O, an emissive grid for the electrons, K (neutralizer) and far from these, a collector.

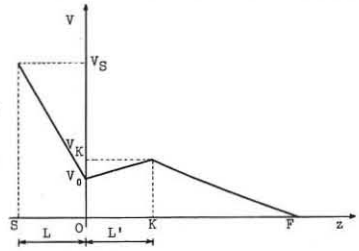

Figure 1 -

SIMULATION MODEL

We use an unidimensional model. We consider a superparticles system propagating along the axis Oz, from the origin. The force law between superparticles is the same that would exist between infinite planes normal to Oz, with an uniform surface density of electrical charge, and mass. The superparticles corresponding to the ions have charge $+|q|$ and a mass m_+, and that ones corresponding to the electrons have a charge $-|q|$ and a mass m_-. The ratios m_i/q_i are the same as the actual ratios for H^+ ions and electrons.

The simulation system geometry is given figure 1. It corresponds to the experimental model (in the unidimensional approximation), without the collector. A potential difference $\phi_1 = V_S - V_0 > 0$ is applied between S and O.

A potential difference $\phi_2 = V_K - V_0 > 0$ is applied between O and K.

L' is chosen as the unit length.

The phenomena occuring for $z < 0$ are considered as outside the system. At $t = 0$, no particle is present for $z > 0$. Potential at infinite is taken as the potential origin.

During the phenomena, the potential will stay zero beyond the beam-front F.

The positive particles, which are monocinetic, enter the system through point O at regularly spaced moments, with an initial velocity v_+ corresponding to the accelerating potential ϕ_1. The current J_+ associated with this injection is connected to ϕ_1 and L by the CHILD-LANGMUIR law.

The negative particles enter the system through K, at regularly spaced moments ; the injection velocity v_- is a random variable, which probability density, related to the cathode temperature θ, is :

$$\Pr(v) = \frac{1}{2} \frac{m_- |v|}{k\theta} \exp\left(-\frac{m_- v^2}{2k\theta}\right)$$

The current J_- associated with this injection is given by the RICHARDSON-DUSHMANN law.

The particles can get out the system by two means :

- every particle, positive or negative, travelling through point O with a negative velocity gets out,
- every negative particle, can be absorbed by the neutralizer K with probability α, at every passage through K.

The problem was solved by a method analogous to that of BUNEMAN [2][3]. The solution gives the position and the velocity of all the system's particles, at every time.

Figure 2 shows one of the $v_-(z)$ curve, at a given moment.

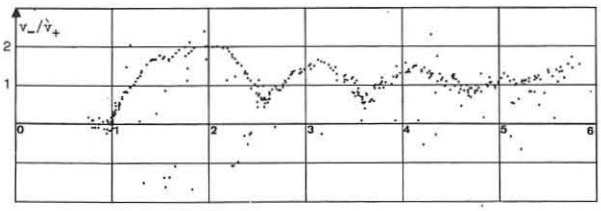

Figure 2 - $n_+ = 10^{13}$ m^{-3} ; $\phi_1 = 5$ kV ; $\phi_2 = 50$ V ; $\theta = 2000$°K.

We observe that, after a rapid growth of their velocities, the electrons experience a damped oscillatory motion about the ion velocity v_+.

This simulation exhibits also the entropy variation, hence the temperature variation, of the electrons and the ions in space and time. The temperatures at point z and time t are defined as the variance of the velocity distribution of the particles.

ELECTRONIC TEMPERATURES CURVES

Figure 3 shows the variation of the electronic temperature T_e, as a function of z, at a given time, for three different ionic densities, and $\phi_1 = 5$ kV, $\phi_2 = 50$ V, $\theta = 2000$°K remaining constant. The density variation is given by the variation of the length L.

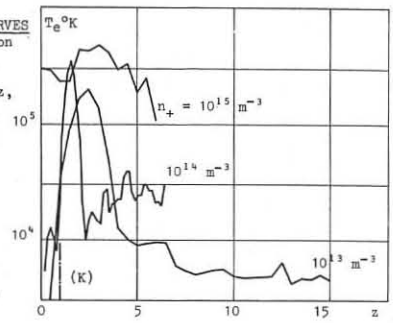

Figure 3 -

The results show an increase of the electronic temperature and of its fluctuations with density.

We must remember, however, that the simulation model is unidimensional, and that, therefore, it cannot account for a possible break up of the beam, due to a large electronic turbulence. In particular, when $n_+ = 10^{15}$ m^{-3}, the simulation gives a temperature for which an actual beam would break up. This in accordance with the experimental results [1].

For high densities ($n_+ = 10^{15}$ m^{-3}), the experience showed that many electrons want back toward the source. Thus, we modified the neutraliser potential ϕ_2 for that density : $\phi_2 = 300$ V. This modification involves only a slight decrease of the electronic temperature. It seems that the electronic temperature depends principally of the beam density, at a given velocity.

EXPERIMENTAL VERIFICATION

We tried to if the temperature measurements in the synthetized plasma were in accordance with the simulation model. These data have been taken with a LANGMUIR probe, although this procedure is critiquable for a beam, specially because of the secondary emission of the probe. However, it is possible to derive from it the variation way of the temperature with the different parameters.

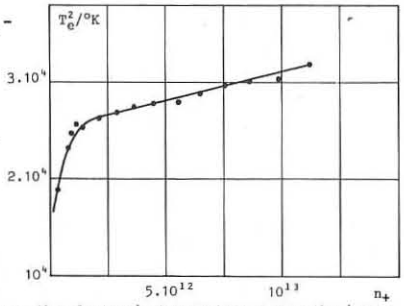

Figure 4 -

Figure 4 gives, for instance, the electronic temperature versus the ion-beam density.

CONCLUSION

The numerical results obtained, on one hand by an unidimensional simulation model, on the other hand by probe measurements in a beam of relatively high energy, are difficult to compare on a quantitative basis.

However, the observed temperature variations are in the same way as the predicted ones. Furthermore, the simulation model, although imperfect, describes the electronic dragging process in a fast ion beam, by occurrence of large amplitude instabilities.

REFERENCES

[1] P. CHENEVIER, J.M. DOLIQUE, J.B. NUGEYRE, C. POMOT, P. SERMET
Neutralization of a fast ion beam by thermal electrons
submitted to Reading Committee of "Physics of Fluids"

[2] O. BUNEMAN, G. KOOYERS
Computer simulation of the electron mixing mechanism in ion propulsion
A.I.A.A. Journal 1 (1963) pp. 2525-2528

[3] R.P. WADHWA, G. KOOYERS
Analysis of electron ion mixing in ion engines
Final Report NASA - C.R.-54033 - 31 march 1964.

°°°

COUNTERSTREAMING ELECTRON BEAMS IN A MAGNETIC FIELD

by

H. Motz and P.T. Rumsby

UNIVERSITY OF OXFORD, DEPARTMENT OF ENGINEERING SCIENCE
Parks Road, Oxford, England.

Theoretical and experimental studies of the instabilities that occur in double counterstreaming cold electron beam systems of finite diameter immersed in a longitudinal magnetic field have shown that for equal beam velocities oscillations arise near half the cyclotron frequency. (1,2). The instability which gives rise to these oscillations is due to the coupling between the two space charge waves on each beam and the fast cyclotron wave on the other. To examine the behaviour of a system of a number of interpenetrating cold electron beams in a magnetic field one uses a dispersion equation based on the quasi-static approximation (3). For two beams only this equation is of 8th order in the frequency ω and 10th in the propagation constant β.

In the present work, as it was intended to examine only the interaction in the neighbourhood of $\omega_{c/2}$, it was found that by making various approximations, the dispersion equation could be reduced to one of third order in both ω and β. In other words one dispenses with all but three of the 8 possible propagating waves.

Using both the cubic equation and the full dispersion equation we have computed the instability growth, frequency and propagation characteristics and found them to be in very close agreement for values of $\omega_c/\omega_p > 2$ and for small diameter beams.

An advantage of having a cubic dispersion equation to describe the behaviour of the instability is that we have been able to apply both Sturrock's (4) and Rolland's (5) instability criteria to the interaction by examination of the descriminant. Application of Sturrock's criterion requires knowledge of when complex ω and β solutions occur. This is immediately obtained for any situation by computing the sign of the descriminant. Rolland's criterion requires a knowledge of where in the complex ω plane the branch points of the dispersion equation $\beta(\omega)$ occur. This is obtained by solving the polynomial obtained by putting the descriminant equal to zero. Both of these analyses show that the instability is always an absolute one under all conditions for which the cubic approximation is valid.

By examination of the full dispersion equation we have found that the oscillations near $\omega_{c/2}$ split into two, one above and one below the original frequency, when the two beam velocities are unequal. The variations of the growth, frequency and propagation characteristics of these two separate instabilities with increasing beam velocity ratio have been computed for two different situations. In one both beam densities remain the same and constant as the velocities are varied while in the other the densities may vary as both beam perveances are assumed to remain constant. Figure 1 shows the growth and frequency characteristics of both upper and lower lines for the two different situations. For the constant density beam case the behaviour of the upper line is regular. For the constant perveance beam case it is irregular in that its growth rate first decreases rapidly for increasing velocity ratio, becomes zero over some region and then increases again very rapidly.

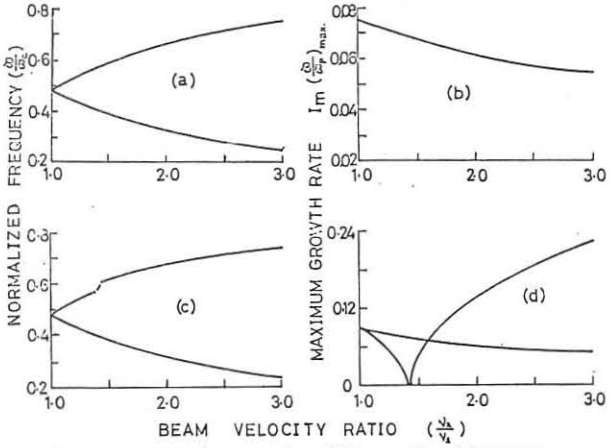

Fig. 1. Non-symmetric system instability growth and frequency characteristics. (a) and (b) constant density beams (c) and (d) constant perveance beams.

An experiment has been performed to try to verify the main points of the analysis. The device used is shown in Figure 2. The two, opposing, pulsed, 3.5KV, 60 mA beams are obtained from Pierce type guns with oxide cathodes arranged to fire into opposite ends of a conducting drift tube 28 cm. long and 5 mm. internal diameter. Between the anode of each gun and the end of the drift tube is a gap by means of which any oscillations occuring may be coupled out. The whole device is situated in a glass envelope and pumped to a pressure better than 10^{-9} torr. A solenoid surrounding the tube provides the longitudinal magnetic field.

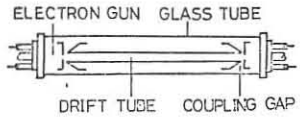

Fig. 2. Schematic of experimental device.

Oscillations of about 1% bandwidth and maximum power level -60 dbm were observed at a frequency of $\omega_{c/2}$ in a symmetric beam system over the range 40 to 1000 MHz, the total range of the receivers available. Harmonics up to the 5th were noted.

Many other series of oscillations were observed in the range covered some varying in frequency with beam velocity and some also with beam current. Strong bands of noise oscillations were also found.

In agreement with previous workers (1,2,) it was noted that at each value of magnetic field, if the beam velocities were reduced the oscillations at $\omega_{c/2}$ weakened and vanished at some critical velocity. The results are shown in Figure 3. It has been suggested that this cut off is due to Landau damping when the wavelength of the oscillations approaches the Debye length. When applied to the cut off results of previous workers this criterion has in our opinion led to unnecessarily high values of beam temperature. An analysis of the system was carried out using a dispersion equation incorporating longitudinal beam temperature. This is due to Lichtenberg (6).

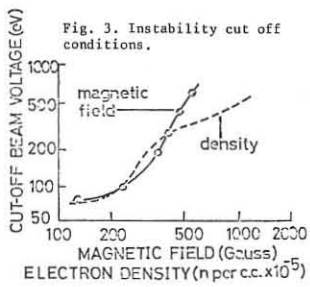

Fig. 3. Instability cut off conditions.

$$\lambda_D^2 \left(\frac{\rho^2}{a^2}\right)_{n\nu} + \beta^2) - S^{(1)}(\omega) = S^{(2)}(\omega)$$

where $S^{(k)} = 1 + \xi_o^{(k)} Z(\xi_o^{(k)}) + \frac{\lambda_D \rho^2_{n\nu} \omega_p}{a^2 2\sqrt{2}\, \beta\, \omega_c} \left[Z(\xi_-^{(k)}) - Z(\xi_+^{(k)}) \right]$

and $\xi_o^{(k)} = (\omega - v\beta)/\beta v_{Th}\sqrt{2}$, $\xi_\pm^{(k)} = (\omega - v\beta \pm \omega_c)/\beta v_{Th}\sqrt{2}$

and $v = +|v|$ for the first beam with $k=1$, $v = -|v|$ for the second beam with $k=2$, v_{Th} the beam thermal velocity, λ_D the Debye length, $Z(\xi)$ the plasma dispersion function, a the radius of the drift tube and $\rho_{n\nu}$ the ν^{th} zero of the n^{th} order Bessel function. This analysis when applied to the cut off results obtained showed that the beam temperature remained constant at about 0.1 eV (the cathode temperature) over a large range of beam velocities and that the postulation of some beam thermalization process in order to explain high beam temperatures is unnecessary. This result also confirms the fact that this type of interaction is reversible in the thermodynamic sense in that there is no increase in entropy, as are all phenomena whose behaviour may be analysed by the Vlasov equation.

The constant perveance non-symmetric beam situation has also been examined experimentally and splitting of the line was observed as expected. It was possible to observe the lower line up to values of velocity ratio of 2.3 before it vanished into noise whereas the upper line vanished at a ratio of about 1.3 as would be expected from the behaviour of the growth rate shown in Figure 1 (d). The strong reappearance of the upper line for higher velocity ratios was not observed however. All the frequencies noted agree within the experimental limit with those predicted and shown in Figure 1 (c).

References

1. E. Etievant and M. Perulli. 6th Int.Conf. on Phenomena in Ionized Gases. Paris 1963.
2. B. Maxum and A.W. Trivelpiece. J.Appl.Phys. 36, 481, (1965).
3. A.W. Trivelpiece and R.W. Gould. J.Appl.Phys. 30, 1784 (1959).
4. P.A. Sturrock. Phys.Rev. 112 1488 (1958).
5. P. Rolland. Phys.Rev. 140, 776 (1965).
6. A.J. Lichtenberg and J.S.Jayson .J.Appl.Phys. 36, 449 (1965).

HIGH-FREQUENCY OSCILLATIONS BEING EXCITED AT A BEAM-PLASMA ELECTRON HEATING

A.N.Karkhov
I.V.Kurchatov Institute for Atomic Energy,
Moscow, USSR

This paper deals with an investigation of the electron heating mechanism at the beam-plasma interaction. The experimental apparatus is the same as in the previously published papers /1/; however the diagnostic equipments is somewhat improved. A radiointerferometer was used to measure plasma density and to switch on the electron beam when the needed density level was obtained. The h.f. probes were mounted in the magnetic field maximum region near an electron gun, at a mirror slope and in the uniform field. The h.f. oscillations were simultaneously registered at four frequencies in the range 0,4–7 GHz. The measurement accuracy of the magnetic field intensity is increased.

It is shown in paper /1/ that the electron heating is detected under the resonante conditions $\omega_{oe} \approx m\,\omega_{He}\,(m=2,3)$, and the electromagnetic oscillations of a whistler mode are being excited. It follows from the simple linear theory /2/ that the oscillations of the whistler mode are characterized by the refraction index:

$$N^2 = 1 + \frac{\omega_{oe}^2}{\omega(\omega_{He}-\omega)},$$

i.e. when $\omega_{oe} > \omega_{He}$ the wave propagation with the frequencies in the band $\omega_{He} < \omega < \alpha\,\omega_{oe}$ $\left(\alpha > 1$ - the coefficient depending on ω_{He} and $\omega_{oe}\right)$ proves forbidden.

In fig. 1 are illustrated the oscillograms of the plasma density, of the X-ray radiation and the oscillations recorded by the probe placed in the uniform field. It is clearly seen that at an increase in the plasma density the oscillations completely disappear at 5 GHz. This behaviour of oscillations of the resonance condition $\omega_{oe} \approx 3\omega_{He}$ allows to clearly identify the case $m = 2$ and $m = 3$, if it is difficult to make with the density measurements (at the additional ionization by the beam).

In fig. 2 are given the oscillation spectra received by the probe placed in the uniform field and obtained under the resonante conditions. The spectra show some typical features: 1. the sharp minima at the cyclotron frequency f^{o}_{He}; 2. according to the oscillograms of the fig. 1. the absence of the oscillations at frequencies more than 4 GHz when $m = 3$; 3. the presence of the minima at the frequencies somewhat lower f^{o}_{He}.

In fig. 3 are given the oscillations spectra received by the probe placed at the mirror slope. These spectra possessing the same features as those in fig. 2 have an additional region of the intensive oscillations with the frequencies $f^{o}_{He} < f < f'_{He}$, where f'_{He} – is the cyclotron frequency corresponding to the local intensity of the magnetic field in the point of the probe placing.

The oscillation spectra received by the probe placed near the electron gun in the maximum of the mirror magnetic field appeared to be quite different from those in figs 2 and 3. The form of these spectra essentially change under the change of the plasma density in the central part of the magnetic trap. In fig. 4 are given, as an example, the spectra obtained for the two values of the average plasma density at m = 2 and m = 3. From the dependence of the oscillation frequency with the maximum intensity on the plasma density one can suppose that the plasma oscillations corresponding to the local plasma frequencies in the probe placing are registered. The plasma density calculated by these frequencies proves to be several times lower than the one measured by the radiointerferometer. The intensity of the oscillations electric field with the spectrum of fig. 4 in the maximum was higher than that with the spectrum of fig. 2 and 3 by approximately an order of magnitude.

It was found out that under the introduction along the radius the probe placed at the mirror slope up to the beam, the intensity of the X-ray radiation slightly changes while the similar probe introduced into the plasma in the region of the uniform field results in a sharp decrease of the X-ray radiation intensity. In fact, hot electrons do not deeply penetrate into the mirror, i.e. under heating it is the transverse energy of electrons that grows.

In papers [3,4,5] theoretically and in experimentally was studied the electron excitation of the electrostatic plasma oscillations by a cold beam, the maximum increment of which is $\gamma \sim (n_1/n_0)^{1/3}\cdot\omega_{oe}$ (n_1, n_0 – beam and plasma densities, respectively). At $n_1 \approx 10^{8}\,cm^{-3}$ and $n_0 \approx 10^{11} \div 10^{12}\,cm^{-3}$ these oscillations spread over several dozens of centimeters that was detected in experiment /5,6/. The electromagnetic oscillations of the whistler mode in the linear approximation are excited by a cold beam with a considerably smaller increment. In case of the hot beam with the directed velocity v_0 and the thermal velocity $v'_T \approx v_0$ the maximum increment oscillations propagating along the magnetic field is

$$\gamma \sim 10^{-2}\,\omega'^{2}_{oe}\cdot\omega^{2}_{oe}\cdot\omega^{-3}_{He}\cdot(v_0/c)^4,$$

where ω'_{oe} – the plasma frequency of the beam, c – the light velocity. For our experimental conditions the typical excitation length of the electromagnetic oscillations is many times higher than the apparatus length. However, the experiment shows that the oscillations of the whistler mode are excited as effectively as plasma oscillations. To interprete this fact it is probably, necessary to use the mechanism of the non-linear transformation of electrostatistic oscillations into the whistler mode. The minimum of the oscillation intensity at the frequency f^{o}_{He} (fig. 2 and 3) obtained experimentally can be explained by the oscillation absorption with cold plasma electrons, and the minimum at the frequency $f < f^{o}_{He}$ by the absorption with hot electrons whose resonance frequency is lower due to the Doppler effect.

In conclusion, the author is grateful to I.N.Golovin for helpful discussions, to A.A.Alekseev and V.F.Nefedov for help in measurements.

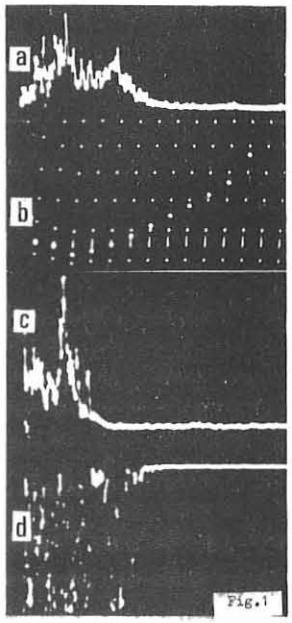

Fig.1

1. Oscillograms X-ray radiation (a), plasma density (b) and oscillations at 5.0 GHz (c) and 2.3 GHz (d); probe placed in uniform field; distance between marks on the density oscillogram 66 μsec.

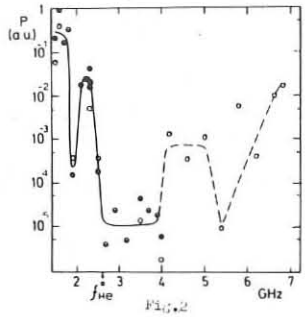

Fig.2

2. Spectra of oscillations accepted by the probe placed in uniform field, O-m=2, ●-m=3, ⊖ - coincident points.

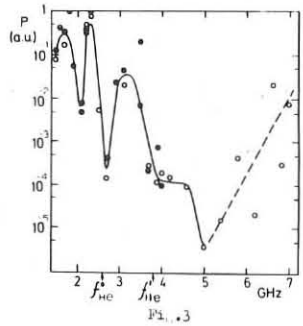

Fig.3

3. As Fig. 2, but probe placed at the mirror slope.

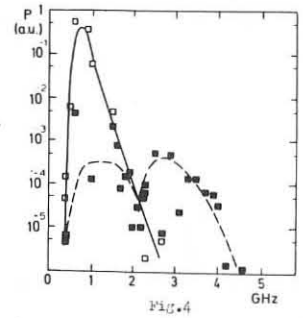

Fig.4

4. Probe placed near the electron gun for two values of the plasma density corresponding approx. to the conditions in the trap centre: □-m=2, ■-m=3.

1. A.N. Karkhov, JETP, 56, 3, 1969 Atomic Energy, 26, 1969.
2. V.D. Shafranov, "Question of Plasma Theory", part 3, 1963.
3. I.F. Kharchenko et al., Nucl. Fusion, Suppl., Part 3, 1101, 1962.
4. M. Seidl, P. Šunka, Inst. of Plasma Phys. Prague, Research Report IPPCZ-81, 1967.
5. I. Cabral et al., Third Conf. on Plasma Phys. and Contr. Fusion. CN26/L-6, Novosibirsk, USSR, 1968.

CYCLOTRON HARMONIC INSTABILITIES IN A BEAM-PLASMA EXPERIMENT

H.J. Hopman, T. Matitti, J.H.A. van Wakeren
Association contract: Euratom-F.O.M.
FOM-Instituut voor Atoom- en Molecuulfysica, Kruislaan 407, Amsterdam, Netherlands.

In our beam-plasma system it is possible to observe the following spectrum: a series of small peaks with frequencies between 0 and ν_{ce} and two large peaks with the frequencies just below and above $2\nu_{ce}$.
The necessary condition to find this spectrum is $\nu_{ce} < \nu_{pe} < 2\nu_{ce}$; ν_{ce} and ν_{pe} are the electron cyclotron frequency and the electron plasma frequency.
In the following we will try to explain some features of this spectrum.

In the experiment, see fig. 1, the plasma ($n_e \approx 9\times10^9$ cm^{-3}), is created by an electron beam (V_b = 1 keV, i_b = 10 - 20 mA, $\phi_b \approx 0{,}2$ cm) in Helium gas, 7×10^{-4} Torr. The plasma is surrounded by a circular wave guide (ϕ = 8 cm) and immersed in an axial magnetic field of $180.\ 10^{-4}$ Wb/m^2; the operation is on a D.C. basis. Estimations for the plasma density are obtained with a microwave cavity working in the TM_{010} mode, placed near the gun. With these experimental conditions we have $\nu_{pe} \approx$ 0.85 GHz, ν_{ce} = 0.5 GHz and $2\nu_{ce}$ = 1.0 GHz. The beam plasma system is in the so-called second regime, where plasma density is mainly determined by hf ionization due to the beam-plasma instabilities.

Typical frequency spectra are shown in fig. 2 and 3 with i_b = 13 and 17 mA respectively; amplitude is on a logarithmic scale. In fig. 3 the amplification is 8 dB less. The spectrum of fig. 2 shows a weak low frequency instability below 0.4 GHz, a strong peak between 0.83 and 0.96 GHz and a third peak between 1.03 and 1.2 GHz. With an increase in beam current the two peaks around 1 GHz hardly move to higher frequencies. They increase in amplitude and merge, becoming one peak extending from 0.8 - 1.2 GHz. With a further increase in i_b the peak narrows because the part below 1 GHz disappears, fig. 3. The peak does not shift to higher frequencies anymore with i_b; it is quite stable at 1.13 GHz and only increases in amplitude. The spectrum depends very little on beam voltage and very strongly on the magnetic field. Both peaks around 1 GHz vary approximately linearly with ν_{ce}.

Explanation of the spectrum is based on the dispersion equation for electrostatic waves in a plasma, with a first order correction for a transverse temperature. Among others, the equation is given by Stix [1, eq. (9-104)] . The equation is simplified by omitting the imaginary part connected with cyclotron or Landau damping. If we use the following definitions:
$\lambda_i = p^2 v_{ti\perp}^2/2\omega_{ci}^2$ (the index i indicates the different plasma constituents);
p and k are the wave numbers respectively perpendicular and parallel to B_o;
the thermal speed $\perp B_o$ is $v_{ti\perp}^2 = 2\kappa T_{i\perp}/m$,
the equation then reads:

$$-\frac{p^2}{k^2} = \frac{1 - \sum_i \{\omega_{pi}^2 (1-\lambda_i)\} / \{(\omega - k v_{bi})^2\}}{1 - \sum_i \frac{\{\omega_{pi}^2 \omega_{ci}^2 (-4+3\lambda_i) + \omega_{pi}^2 (\omega - k v_{bi})^2\}}{\{(\omega - k v_{bi})^2 - \omega_{ci}^2\}\{(\omega - k v_{bi})^2 - 4\omega_{ci}^2\}}} \qquad (1)$$

Confining ourselves to plasma electrons only, we obtain from eq. (1) the high-frequency propagation bands of a plasma, between the resonances and the cut-offs. The resonance frequencies ($k \to \infty$) are $\omega = \pm\omega_{ce}, \pm 2\omega_{ce}, \pm\omega_{pe}\sqrt{1-\lambda}$. The cut-offs ($k \to 0$) are given by $\omega = \pm 0, \pm\frac{1}{2}\sqrt{2}\left[\omega_{pe}^2 + 5\omega_{ce}^2 \pm \sqrt{(\omega_{pe}^2 - 3\omega_{ce}^2)^2 + 12\lambda\omega_{pe}^2\omega_{ce}^2}\right]^{\frac{1}{2}}$. One of these cut-off frequencies is confined between ω_{ce} and $2\omega_{ce}$, another is always greater than $2\omega_{ce}$.

Fig. 4 and 5 represent cut-offs and resonances; along the axes are plotted the wave frequency against the plasma frequency, both are normalized by the cyclotron frequency. The arced bands show where wave propagation is allowed. The cold plasma cut-off $\omega = \sqrt{\omega_{ce}^2 + \omega_{pe}^2}$ is indicated by a dotted line situated between the warm plasma cut-offs.

The complete dispersion diagram for a beam-plasma system, according to Eq.(1), has been published before [2]. In fig. 4 and 5 the heavy horizontal lines represent the frequency ranges of beam-plasma instabilities for fixed values of ω_{pe}. The imaginary part of the frequency ω_i tends to zero at the ends of the lines. The maximum value of ω_{im} is indicated at a cross. The broad unstable intervals are all excited by the beam space-charge wave. The set of narrow intervals in fig. 5 is excited by the slow beam cyclotron wave, their ω_{im} values are not significant. The main difference between fig. 4 and 5 is a factor two in p. The value of this parameter is not precisely known in our experiment but p = 2 is most likely [3]. In accordance to the spectra, described before, we see a cyclotron instability $\omega < \omega_{ce}$, a plasma instability ($\omega_{ce} < \omega < \omega_{pe}$) and a second harmonic cyclotron instability ($\omega > 2\omega_{ce}$). The latter two instabilities merge when ω_{pe} tends to $2\omega_{ce}$. When $\omega_{pe} > 2\omega_{ce}$ there remains only the very strong plasma instability.

References:
[1] T.H. Stix (1962); The theory of plasma waves, McGraw-Hill, New York.
[2] J.A. Cabral, H.J. Hopman, F.G. Insinger, W. Ott (1968); Proceedings IInd Conf. on Plasma Physics and Controlled Nuclear Fusion Research (IAEA, Vienna).
[3] H.J. Hopman, T. Matitti, J. Kistemaker (1968); Plasma Physics 10, 1051.

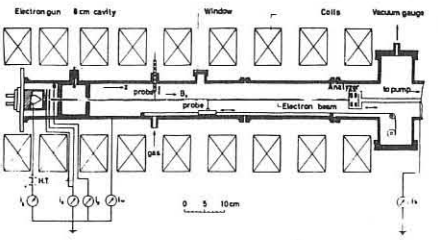

Fig. 1 - Experimental device.

Fig. 2 - Frequency spectrum of beam-plasma instabilities, conditions: i_b = 13 mA, V_b = 1 keV, magnetic field 180×10^{-4} Wb/m^2, gas pressure 7×10^{-4} Torr.
Vertical amplitude scale is given in dB.

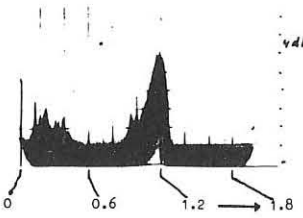

Fig. 3 - As fig. 2, but i_b = 17 mA. The amplification of the spectrum is 8 dB less; the low frequency peak, below 0.4 GHz, has the same amplitude in fig. 2 and 3.

Fig. 4 - Frequency intervals, in which the main beam-plasma instabilities can be observed, as function of the electron plasma frequency ω_{pe}. Both wave frequency and plasma frequency are normalized by the electron cyclotron frequency ω_{ce}. Two vertical lines give the cyclotron resonances $\omega = \omega_{ce}$ and $\omega = 2\omega_{ce}$. The cold plasma resonance is a broken line under 45^o, $\omega = \omega_{pe}$. In a warm plasma the plasma resonance is displaced to a slightly lower value, $\omega = \omega_{pe}\sqrt{1-\lambda}$, $\lambda = p^2\kappa T_\perp/m\omega_{ce}^2$. Also the cut-off frequencies of the plasma are indicated. The dotted line is the cut-off of a cold plasma $\omega = (\omega_{pe}^2 + \omega_{ce}^2)^{\frac{1}{2}}$. The arced areas between cut-offs and resonances give the frequency bands in which a warm plasma allows wave propagation. Heavy horizontal lines represent the frequency intervals in which instabilities are excited on injecting a beam into the plasma. Crosses mark the frequencies with the maximum growthrate ω_{im}. The numerical value of ω_{im} is also given. For $\omega_{pe} = 1.7\,\omega_{ce}$ the plasma instability and the second harmonic cyclotron instability are separated by a minimum in ω_i only. The position of the minimum is indicated by a bar. All instabilities are excited by the slow beam space-charge wave. The diagram has been calculated for T_e = 285 eV. As p = 1 we have λ = 0.062.

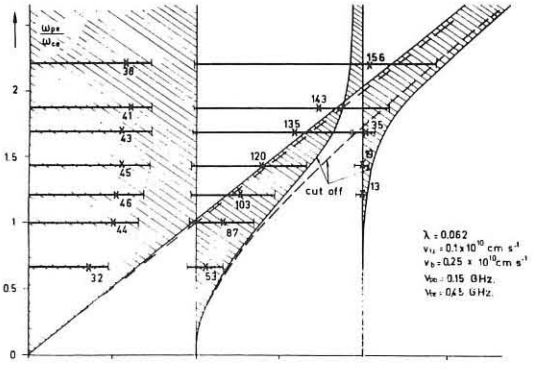

Fig. 4

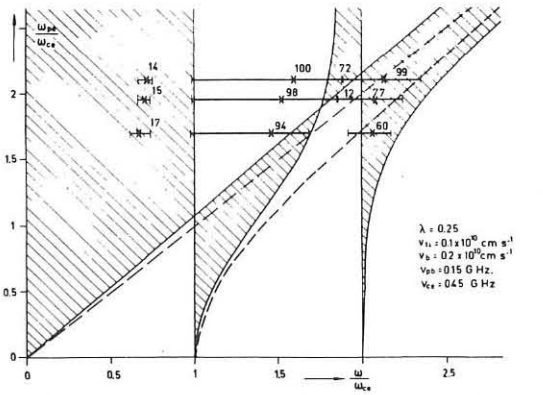

Fig. 5

Fig. 5 - As fig. 4. T_e = 285 eV but p = 2 and thus λ = 0.25. Beam velocity differs slightly from fig. 4, but this has no influence on the frequencies of the beam-plasma instabilities. Only the wave numbers are altered by v_b. For $\omega_{pe} \simeq 2\,\omega_{ce}$ the minimum in ω_{im} between plasma and second harmonic cyclotron instability is indicated.

WAVE GROWTH DUE TO THE INTERACTION OF AN ION BEAM WITH A BOUNDED ELECTRON PLASMA.

G.J. Brakenhoff, A.M. Houtkooper, A. Baan.

Association Euratom-F.O.M.

FOM-Instituut voor Atoom- en Molecuulfysica, Kruislaan 407, Amsterdam, The Netherlands.

Introduction: In this paper we report measurements on the spatial growth of waves due to the interaction of a stream of charged particles with a stationary electron plasma. We have worked with a 20 keV He^+ ion beam and studied the following two cases: I. Interaction with a cold electron plasma column without static magnetic field (beam velocity $v_b >> v_{Te}$, v_{Te} = thermal electron velocity). Wave growth takes place through interaction with the electron plasma surface wave. The growth rate agrees well with the value calculated from simple cold plasma theory. II. Interaction with a warm electron plasma column with magnetic field (B = 885 Gauss, $\omega_{ce} >> \omega_{pe}$, $v_{Te} \simeq v_b$). Wave growth now takes place through interaction with the electron plasma body wave. The growthrate observed is considerably larger than expected from calculations for a warm plasma with a Maxwellian velocity distribution for the electrons. The boundary conditions for a plasma in a partially filled waveguide have been taken into account. These results are at variance with those obtained in electron beam experiments where mostly too low values for the experimental growthrates were observed, with exception of [1].

The 20 keV He^+ ion beam is injected through an entrance tube into the interaction vessel (fig. 1). The slightly diverging beam passes through the plasma, created by the beam itself through collisional ionisation of the gas in the interaction space. The beam density along the axis is measured with the moveable collector. No spontaneous instabilities are observed. Waves are excited in the system by applying an R.F. signal of frequency $\omega/2\pi$ to a probe or a grid. The wave propagating in the plasma is picked up by a movable probe and its amplitude and phase are recorded as a function of axial position in an interferometer set up (fig. 1). With a probe in the interaction vessel we can excite the electron plasma wave. By comparing the dispersion characteristics of the wave propagating in the beam direction and the one propagating in the opposite direction we checked that no important plasma electron drift along the axis occurs. The wave growth in the beam plasma interaction is determined from the amplification, along the axis, of the wave excited on the beam with the grid in front of the entrance tube.

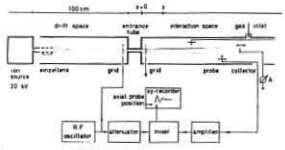

Figure 1.

I. Interaction with the surface wave, B = 0, T_e = 0.

Theory: The dispersion relation for waves on a cold electron plasma column (radius a), without magnetic field in a metal waveguide of radius b, through which a beam of charged particles passes, can be derived from expressions given in [2]. Here we give the relation for the case b/a >> 1, which approximation can be used in our system. Taking the time space dependence as $e^{i(\omega t - kz)}$ and $\vec{v}_b /\!/ k /\!/ \vec{z}$ we get the dispersion relation:

$$1 - \frac{\omega_{pe}^2}{\omega^2} - \frac{\omega_{pb}^2}{(\omega - kv_b)^2} = \frac{I_o(ka)\, K_o'(ka)}{I_o'(ka)\, K_o(ka)} \qquad (1)$$

We have calculated for real from (1) the dispersion with the following parameters:

$\omega_{pe} = 2\pi \cdot 28{,}5$ MHz ($n_e = 1 \cdot 10^7$ cm^{-3})
$\omega_{pb} = 2\pi \cdot 0{,}195$ MHz ($n_b = 2{,}5 \cdot 10^6$ cm^{-3})
$v_b = 10^8$ cm/s (20 keV He^+ ions)
a = 1,1 cm (beam plasma radius),

and we have plotted the results in fig. 2. We see in the lower half of fig. 2 a wave propagating against the beam (ω/k negative), which is the well known surface wave approaching resonance for $\omega \to \omega_{pe}/\sqrt{2}$. Wave propagation in the beam direction (upper half of fig. 2) shows that the beam wave is growing ($\mathrm{Im}(k) = k_i > 0$) for $\omega/\omega_{pe} < 0{,}53$. The surface wave in this quadrant is disturbed near synchronism with the beam waves.

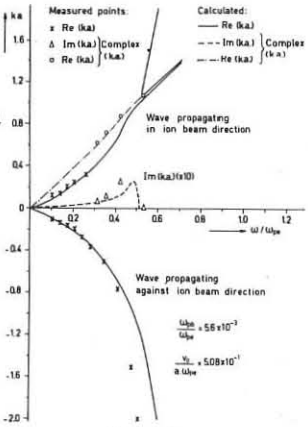

Figure 2.

Experiment: (Gas in the interaction space: Helium p = 1.10^{-4} Torr). In fig. 3 a typical result is given when we follow a wave of frequency $\omega/2\pi$, excited by a probe in the interaction space, propagating in the beam direction. Both the beam and the forward surface wave are excited. The growing beam wave becomes visible after the surface wave has decayed sufficiently. At a certain point "A" the amplitude of the beam wave becomes constant. To understand this we should realize that because of the beam divergence along the axis the beam density, and coupled with it the electron plasma density, diminishes. So the value ω/ω_{pe} increases, until at point "A" it finally becomes larger than $\omega/\omega_{pe} = 0{,}53$ (see fig. 2) and no further wave growth takes place. In the wave propagation opposite to the beam, one observes only the decaying surface wave.

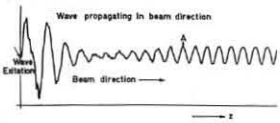

Figure 3.

The dispersion at axial position z_o, measured from traces like fig. 3 of the forward and backward surface wave could be fitted to the theoretical dispersion with a = 1,1 cm, the measured plasma radius at z_o, when $\omega_{pe} = 2\pi \cdot 28{,}5$ MHz, which gives us the plasma density, at z_o. The complex k from the growing beam wave, measured at z_o, is also plotted in fig. 2. We see that the measured growthrates k_i agree with the calculated values. The electron temperature measured with a Langmuir probe is 0,2 eV. It can be shown that the effect of Landau damping by the electrons of the growing beam wave can be neglected for our values of the parameters.

II. Interaction with the electron plasma body wave: B = 885 Gauss, T_e = 4-9 eV.

Theory: With a magnetic field ($\omega_{ce} >> \omega_{pe}$) the interaction with the plasma body wave is important. In this case the thermal electron velocity $v_{Te} \approx v_b$, so the contribution of T_e in the dispersion equation has to be taken into account. For our beam plasma system of radius a we can take the dispersion equation from [2], taking b/a >> 1:

$$\left[1 - \omega_{pb}^2 \Big/ \left((\omega - kv_b)^2 - \omega_{cb}^2\right)\right] \mathrm{Ta}\, J_1(\mathrm{Ta})/J_o(\mathrm{Ta}) = -\, ka\, K_1(ka)/K_o(ka) \qquad (2)$$

$$T^2 = -k^2 \left(1 - \omega_{pe}^2 \int \frac{f(v)}{(\omega - kv)^2}\, dv - \frac{\omega_{pb}^2}{(\omega - kv_b)^2}\right) \Big/ \left(1 - \frac{\omega_{pb}^2}{(\omega - kv_b)^2 - \omega_{cb}^2}\right) \qquad (3)$$

in which we take for f(v) the Maxwellian velocity distribution for the electrons. Likewise as for the beam, interaction with the surface wave, we can derive from (2) and (3) the dispersion of the plasma body wave. The growth for beam waves in the interaction can be calculated with the parameters T_e and n_e obtained by fitting the experimental dispersion of the plasma waves with the theoretical one with a measured beam radius. The values for n_e, measured with the cavity resonance shift method, and for T_e, from Langmuir probe characteristics, agree reasonably with those obtained from the dispersion.

Experiment: Parameters: Gas in the interaction space: N_2, $6.10^{-6} < p < 3 \times 10^{-5}$ Torr, $\omega_{pb} \approx 2\pi \cdot 0{,}4$ MHz, $\omega_{cb} = 2\pi \cdot 0{,}33$ MHz, $a \approx 0{,}8$ cm. By varying the gas pressure in the interaction space one can change the density of the plasma created by the beam. We have obtained two sets of measurements of the growthrate k_i as a function of frequency $\omega/2\pi$ at $\omega_{pe} = 2\pi \cdot 62$ MHz ($n_e = 5{,}5 \cdot 10^7$ cm^{-3}) and at $\omega_{pe} = 2\pi \cdot 130$ MHz ($n_e = 2{,}6 \cdot 10^8$ cm^{-3}) as shown in figure 4 ($T_e = 4$ eV in both cases). We see that the observed growthrates are too high by a factor of about 5 and do not follow too well the calculated dependence on ω. At $\omega_{pe} = 2\pi \cdot 71$ MHz ($n_e = 7 \cdot 10^7$ cm^{-3}), T_e was increased by application of RF power at ω_{ce} by means of a Lisitano coil [3]. This is a structure in which the RF power propagates along a strip line cut out in the surface of a metal cylinder (Ø 4,5 cm), that surrounds the plasma column. We took 3 sets of measurements at $T_e = 4$, 6 and 9 eV with an applied RF power of resp. 0 mW, 30 mW and 200 mW (fig. 5). We find again too high growthrates, but there is agreement with the calculations on the decrease of growthrate with increasing T_e. The day to day reproducibility of the measured growthrates in section II was about 50%. The data for fig. 4 and 5 each were obtained in one day, during which the reproducibility is much better. As yet we have no explanation for the observed high growthrates.

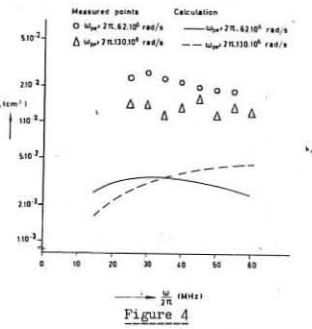

Figure 4

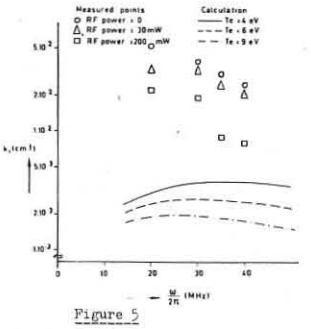

Figure 5

References:

[1] Abraham, E.E. and Crawford, F.W.: Proc.of the VIIth Int.Conf.on Phen. in Ion.Gases (Beograd 1966) Vol. II-377.

[2] Trivelpiece, A.W.: Slow wave propagation in plasma waveguides. San Francisco Press Inc., San Francisco 1967.

[3] Lisitano, G.: Proc. of the VIIth Int.Conf. on Phen. in Ion.Gases (Beograd 1966) Vol.I - 464.

CRITICAL β FOR STELLARATORS*

by
Harold Grad and Harold Weitzner
Courant Institute of Mathematical Sciences
New York University
U.S.A.

Toroidal equilibria with helical windings have been studied using two expansions, low β (Stellarator) [1] and finite β (Scyllac) [2]. A transfer of stability (critical β) found by one expansion is automatically invisible using the other. With each of these expansions, we find new stable regions.

A toroidal configuration with circular axis and a simple periodic helical winding of order ℓ is described by the plasma radius r_o, the coil or conducting wall radius r_1, the helical period $L = 2\pi/k$, the toroidal curvature $\kappa = 1/R$, and the ratio of helical to toroidal field strength at the plasma boundary, ϵ. The equilibrium is described by the six dimensionless parameters, $\rho = (r_1/r_o)^2$, kr_o, κr_o, ϵ, ℓ, and β. For a flat pressure profile (p= const. in the plasma, p = 0 outside), β is unambiguous. For a parabolic profile, β can be taken as a multiplicative factor.

In a previous paper [2], it was discovered that equilibria can be found for a large range of parameters at finite β. We now discuss stability with respect to a certain class of global, approximately m = 1, disturbances. Experimental evidence points to these as the only observable MHD modes.

There are several differences between the Stellarator [1] and Scyllac [2] expansions. We are primarily concerned here with the different choices of $\beta \sim \epsilon^2$ in the former and $\beta \sim 1$ in the latter, and with the fact that the pressure profile is parabolic in the former and flat in the latter.

In both expansions one finds transitions between instability and stability as β crosses a critical value, β_c, other parameters being held fixed. It is evident from the scaling that there is a nonuniform limit when β and ϵ both become small. Any Stellarator value for $\beta_c \sim \epsilon^2$ has shrunk to zero on the Scyllac scale, and any finite Scyllac value for β_c is beyond infinity and invisible on the Stellarator scale. Another manifestation of this nonuniformity is that the limit $\beta \to 0$ with Scyllac scaling is not a vacuum field.

The flat pressure profile has two prime advantages. First, its simplicity frequently yields explicit formulas. Second, it may guarantee existence of an equilibrium configuration where this is impossible for a smoother profile which demands a family of nested flux surfaces.

The primary Stellarator conclusion with a smooth profile is that the system is stable for $\beta < \beta_c$ and unstable otherwise, where β_c is obtained as the lowest eigenvalue of an ordinary differential equation with coefficients depending on the field and pressure profiles [1]. Inspection of this equation shows that $\beta_c = 0$ for $\ell > 2$ and a parabolic profile. Introduction of the flat profile eliminates the singular behavior on the axis and yields nonzero β_c for arbitrary ℓ, in particular, the explicit formula

$$\beta_c = \lambda_\ell^2 a^2/(1-1/\rho)$$

$$\lambda_\ell(x) = -[1-2q + (\ell^2 + x^2)q^2]^2/[1-2(\ell^2+x^2)q + \ell^2 q^2]$$

$$q = I_\ell(x)/I'_\ell(x)\ ,\ x = \ell k r_o,$$

where a is the fractional distortion of the plasma cross-section. The Bessel functions can be approximated; e.g. for small kr_o and $\ell > 1$, $\beta_c \sim 2(\ell-1)a^2$. We can easily obtain $\beta_c \sim 1/2$ or higher, e.g. by taking $a \sim 0.3$ and $\ell = 4$.

Explicit formulas are obtainable for some cases with a parabolic pressure profile, e.g. with small kr_o and $\ell = 2$, $\beta_c \sim 2.88\, a^2$. The frequently quoted value $\beta_c \sim 8.2\%$, obtained by numerical integration for $kr_o = 1/2$, a = 0.194 [1] compares with our value $\beta_c \sim 7.5\%$ for small kr_o and the same value of a.

With a conducting wall surrounding the plasma, the Stellarator value of β_c is increased by a factor $(1-1/\rho)^{-1}$. The plasma can always be stabilized by bringing the wall close enough. But for large β (on the Stellarator scale), the wall must be taken arbitrarily close to the plasma for it to be stabilized.

Turning to the finite β Scyllac scaling, we find an even stronger conclusion as to the ineffectiveness of wall stabilization at low β. With this scaling, there is a finite value β_* (depending on parameters, but not ϵ) such that it is impossible to stabilize the plasma with any position of the wall when $\beta < \beta_*$. On the other hand, if $\beta > \beta_*$, it is possible to stabilize by introducing a conducting wall. This result is, of course, invisible to the Stellarator expansion.

For most parameter values, wall stabilization is impractical and requires small plasma-wall separation. However, for $\ell = 1$ and small kr_o, there is a very significant wall effect. Stability can be achieved with an arbitrary wall separation if kr_o is taken small enough. For large $\rho = (r_1/r_o)^2$, there is a stable region near $\beta \sim 0.738$ when $kr_o < 0.87/\rho$. For $\rho = 16$ (appropriate for Scyllac) taking $kr_o \sim 1/16$ (L ~ 100 cm) gives stability for $\beta \sim 0.83$; $kr_o \sim 1/23$ gives stability for $\beta > 0.44$*. This finite β wall effect is completely invisible in the low β Stellarator expansion, and it is a small effect in the Scyllac expansion except for small kr_o and $\ell = 1$.

Our calculations indicate that MHD stability is favored at low β by large helical order ℓ and large distortion, a, of the plasma cross-section; and stability is favored at high β by $\ell = 1$ and small kr_o. Details are given in References 3 and 4. New, improved expansions are required to extend and bridge the gap between the Stellarator and Scyllac expansions.

*This work was supported by the U. S. Atomic Energy Commission under contract AT(30-1)-1480.

*The earlier definition of β with Stellarator scaling, allowing $0 < \beta < \infty$, should be altered to $\beta/(1+\beta)$ to compare with Scyllac scaling where $0 < \beta < 1$.

References

1. J. Greene, J. Johnson, K. Weimer, Plasma Physics 8, 145 (1966)

2. A. A. Blank, H. Grad, H. Weitzner, 'Toroidal High-β Equilibria,' To appear in Proceedings of IAEA Conference at Novosibirsk, August 1968.

3. H. Grad, H. Weitzner, 'Critical β From Stellarator and Scyllac Expansions,' To appear in Physics of Fluids

4. H. Weitzner, 'Toroidal High-β Equilibria,' To appear in Nuclear Fusion.

ASYMPTOTIC REPRESENTATION OF MAGNETIC FIELD LINES AND OF HYDROMAGNETIC EQUILIBRIA IN A NEIGHBORHOOD OF A CLOSED MAGNETIC LINE

M. Bineau

ASSOCIATION EURATOM-CEA

Département de la Physique du Plasma et de la Fusion Contrôlée
Centre d'Etudes Nucléaires
Boite Postale n° 6 - **92 Fontenay-aux-Roses** (France)

I. INTRODUCTION - An asymptotic definition is given to hydromagnetic equilibria in a neighborhood of a closed magnetic line $\mathcal{L}$ when the "rotation number" on $\mathcal{L}$ is irrational. This property generalizes a similar property of the trajectories of an Hamiltonian system related to the magnetic field. Asymptotic series (in powers of ρ=distance to $\mathcal{L}$) are first written for the components of the magnetic field before deriving an asymptotic representation of the trajectories. This analysis introduces the construction of an asymptotic system as an asymptotic definition of a hydromagnetic equilibrium.

II. REFERENCE COORDINATES. s is the curvilinear abscissa on $\mathcal{L}$ and L the length of $\mathcal{L}$. The function, f(s), satisfies f(s+L)=f(s) when not otherwise stated. A Serret-Frenet trihedral $\vec{t}(s)$, $\vec{n}(s)$, $\vec{b}(s)$ (tangent, normal, binormal), with Darboux vector, $\vec{\delta}(s)=\vec{t}(s)/R(s)+\vec{b}(s)/T(s)$, is used to define position in space and vectors. Coordinates s,x,y are defined by $\vec{X}=\vec{M}(s)+x\vec{n}(s)+y\vec{b}(s)$, $\vec{M}(s)\in\mathcal{L}$, and polar coordinates by $\rho\vec{e}_\rho = x\vec{n}(s)+y\vec{b}(s)$, $\vec{e}_\rho = \vec{n}\cos\theta + \vec{b}\sin\theta$ (the correspondence $\vec{X}\leftrightarrow s,x,y$ is assumed one to one in the domain of $\vec{X}$). With $\vec{e}_\theta = \vec{t}\times\vec{e}_\rho$ the notation, $B_s\vec{t} + B_\rho\vec{e}_\rho + B_\theta\vec{e}_\theta$, represents a vector field $\vec{B}(\vec{X})$. The magnetic field $\vec{B}(\vec{X})$ and the current density $\vec{J}(\vec{X})$ will be constrained to be tangent to $\mathcal{L}$ for $\vec{X}$ on $\mathcal{L}$. To a vector field $\vec{V}(\vec{X})$ with components V_1, V_2, V_3 in a cartesian reference system of coordinates x_1, x_2, x_3 two exterior differential forms are associated by the notations $(V) = \sum_{i=1}^{3} V_i\, dx_i$ and $^*(V) = V_1 dx_2 dx_3 + V_2 dx_3 dx_1 + V_3 dx_1 dx_2$.

III. EXPANSION OF THE MAGNETIC FIELD. One seeks an asymptotic sequence, $\vec{B}_{(n)} = \sum_{0\le m\le n} \rho^m \left(p_m(\theta,s)\vec{t} + \rho q_{m+1}(\theta,s)\vec{e}_\rho + \rho r_{m+1}(\theta,s)\vec{e}_\theta \right)$, related by Maxwell's equation written below (III,1), to $\mathcal{L}$, to a set of data $p_0(\theta,s)=B_0(s)$, $A_m(s)$, $C_m(s)$ and to a current density given by an asymptotic sequence, $\vec{J}_{(n)} = \sum_{0\le m\le n} \rho^m \left((J_s)_m\vec{t} + (J_\rho)_m\vec{e}_\rho + (J_\theta)_m\vec{e}_\theta \right)$ where $(J_s)_o = J_o(s)$. By assumption, $\vec{J}_{(n)}$ satisfies $d\,{}^*(J_{(n)}) = O(\rho^{n+1})$ and the functions of θ and s, $(J_s)_m$, $(J_\theta)_{m-1}$, $(J_\rho)_{m-1}$ have harmonics in θ of orders (m-2p)only with $0 \le p \le m$.

$$d\,{}^*(B_{(n)}) = 0\ ; \qquad d(B_{(n)}) = {}^*(J_{(n-1)}) + O(\rho^n)\,ds\,d\rho + O(\rho^{n+1}) \qquad \text{(III,1)}$$

Lemma 1 - For given $\mathcal{L}$, $B_o(s)$, and for given sequences $A_n(s)$, $C_n(s)$, $\vec{J}_{(n)}$ there is a sequence $\vec{B}_{(n)}$ fulfilling (III,1) and the relations $r_n = \bar{r}_n + A_n(s)\cos(n+1)\theta + C_n(s)\sin(n+1)\theta$; $q_n = \bar{q}_n - C_n(s)\cos(n+1)\theta + A_n(s)\sin(n+1)\theta$, where $\bar{r}_n$ and $\bar{q}_n$ have harmonics in θ of orders (n-1-2p) only with $0\le p\le n-1$; $\bar{r}_n$ and $\bar{q}_n$ are uniquely determined by the data and are independant of A_m and C_m for $m \ge n$.

We observe first that the equations (III,1) are equivalent to the sequence

$$\mathcal{E}_n \begin{cases} \partial_\theta q_n - (n+1)r_n = -(J_s)_{n-1}\ ; \ \partial_\theta R_n + (n+1)Q_n = -(\partial_s - 1/T\,\partial_\theta)p_{n-1} \\ n\,P_n = (\partial_s - 1/T\,\partial_\theta)q_{n-1} - \left[(J_\theta)_{n-1} - \cos\theta/R\,(J_\theta)_{n-2} \right] \end{cases} \qquad \text{(III,2)}$$

with the notations $\partial_\theta = \partial/\partial_\theta$, $\partial_s = \partial/\partial_s$, $P_n = p_n - \cos\theta/R\,p_{n-1}$, $Q_n = q_n - \cos\theta/R\,q_{n-1}$, $R_n = r_n - \cos\theta/R\,r_{n-1}$. $\mathcal{E}_1$ has the solution $r_1 = \frac{J_o}{2} + A_1(s)\cos 2\theta + C(s)\cos 2\theta$; $q_1 = -\frac{B_o'}{2} - C_1\cos 2\theta + A_1\sin 2\theta$; $p_1 = B_o\cos\theta/R$. The lemma is easily proven by recurrence after obtaining the equation (III,3)

$$\partial_{\theta\theta} R_n + (n+1)^2 R_n = -(n+1)/R\left(\cos\theta\, r_{n-1} + \sin\theta\, q_{n-1}\right) + (J_s)_{n-1} - \cos\theta/R\,(J_s)_{n-2} - \partial_\theta\left(\partial_s - 1/T\,\partial_\theta\right)p_{n-1}\ .$$

IV. MAGNETIC TRAJECTORIES. One associates to $\vec{B}(\vec{x})$ a dynamical system by identifying $^*(B)$ with a form dpdq-dHdt. q and t are arbitrarily chosen. For example $^*(B) = d\left(\int_o^\rho \rho B_s\, d\rho\right)d\theta - d\left[\int_o^\rho \left((1-\rho\cos\theta/R)B_\theta - \rho B_\rho/T\right)d\rho\right]$ and also from (III,3), with $\bar{y} = y\sqrt{B_o}$ and $\bar{x} = x\sqrt{B_o} + O(\rho^2)$, $^*(B) = d\bar{x}\,d\bar{y} - d\left\{ \frac{1}{2}\left(\frac{J_o}{B_o} - \frac{1}{T}\right)\left(\bar{x}^2+\bar{y}^2\right) + \frac{A_1}{2B_o}\left(\bar{x}^2-\bar{y}^2\right) + \frac{C_1}{B_o}\bar{x}\,\bar{y} + O(\rho^3)\right\} ds$

The corresponding dynamical system has a limiting degeneracy [1]. The lowest orders of the Hamiltonian are essential for the structure of the trajectories.

Let us note the following observation : a sequence $\Psi_{(n)} = \sum_{m=2}^{n} \rho^m \Psi_m(\theta,s)$ such that $^*(B)d\Psi = 0$, order by order can exist to all orders but diverges in general. The existence of an infinite sequence is neither necessary nor sufficient for the existence of a set of surfaces on which trajectories lie (see in [1] a reference to a result of J. Moser).

Lemma 2 - If the system defined by $^*(B)$ is elliptical, $^*(B)$ can be written $^*(B) = d(F_o - O(\rho))\,d(\rho^2\Psi_2(\theta,s) + O(\rho^3))$; $\alpha(\theta,s)$ and $\sigma(s)$ then exist such that $\alpha(\theta+2\pi,s) = 2\pi + \alpha(\theta,s)$, $\sigma(s+L) = 2\pi + \sigma(s)$, $\sigma'(s) \neq 0$ and $2\pi F_o = -\alpha + \omega\sigma$.

ω is called the rotation number. The coordinates transformation $\theta,s \leftrightarrow \alpha,\sigma$ has the following property : if $f_n(\theta,s)$ has harmonics in θ of orders n-2p only , $0 \le p \le n$, then $g_n(\alpha,\sigma) = \Psi^{-n/2} f_n$ has the same harmonics in α and reciprocally. (Proof of lemma 2 follows from a linear transformation $\bar{x},\bar{y} \to X,Y$ such that $^*(B) = dX\,dY - \omega/2\; d\left(X^2+Y^2+O(\rho^3)\right)ds$)

Lemma 3 - If $\omega, 2\omega, \ldots N\omega \neq$ integer the sequence of equations $^*(B_{(n)})\,d\,(\Psi_{(n+2)}) = O(\rho^{n+3})$ can be solved by recurrence for $n \le N-2$.

Proof of lemma 3 follows from lemma 2 and includes obtaining the solution $\Psi_m(\theta,s)$ which has harmonics in θ of orders m-2p, $0 \le p \le m$. When ω is irrational existence of Ψ_m and its composition in harmonics can be proven separately without using lemma 2.

A set of integrable equations $d\left(\Psi_2^{-n/2} F_n\right) =$ expression in $F_{m-1}, \Psi_{m+1}\ (m \le n)$ associates to the sequence $\Psi_{(n+2)}$ a series of functions F_m (multivalued in θ and s) such that

$^*(B) = dF_{(n)}\,d\Psi_{(n+2)} + dU_n\,d\theta + dV_n\,ds$ where U_n and V_n are $O(\rho^{n+3})$.

The equation of the magnetic lines has the form $d\Psi_{(n+2)}/ds = O(\rho^{n+3})$;

$dF_{(n)}/ds = O(\rho^{n+1}) + O(\rho^{n+3})\,s$.

V. ASYMPTOTIC REPRESENTATION OF HYDROMAGNETIC EQUILIBRIA WITH IRRATIONAL ROTATION NUMBER ω. If ω is irrational there is a unique asymptotic expansion to infinite order solving the equations for a hydromagnetic equilibrium in an asymptotic sense given below, when the data are $\mathcal{L}$, $B_o(s)$, the set $A_n(s)$, $C_n(s)$, $I(\Psi)$ and $p(\Psi)$ ($p(\Psi)$ is the pressure and $p_n(\theta,s)$ a term in the expansion of $\vec{B}$). A complete proof cannot be given because of a delicate discussion of the lowest order. If ω is rational, other solutions appear as soon as the lowest order (one should troncate in θ-harmonics to restore uniqueness for some finite series). The equilibrium equations are written a) $d\,^*(B) = 0$; b) $d(B) = {}^*(J)$; c) $^*(B)d\Psi = 0$; d) $^*(B)\,dG = d\tau$ with $d\tau = \rho(1-\rho\cos\theta/R)d\rho\,d\theta\,ds$; e) $^*(J) = I'(\Psi)\,{}^*(B) + p'(\Psi)\,dG\,d\Psi$.

Equation b) can be split into $d(B)\,ds = {}^*(J)ds$; $d(B)\,(d\theta + ds/T) = {}^*(J)(d\theta + ds/T)$ and $d\,{}^*(J) = 0$; it follows from $d\,{}^*(J) = 0$ that e) is equivalent to 2 equations $^*(J)ds = \ldots$ and $^*(J)(d\theta + ds/T) = \ldots$ The system of equations a) to e) is now replaced by the following asymptotic sequence of equations :

a) $d\,{}^*(B_{(n)}) = 0$

b_1) $d\,(B_{(n)})\,ds = {}^*(J_{(n)})\,ds + O(\rho^{n+2})$

b_2) $d\,(B_{(n+1)})\,(d\theta + ds/T) = {}^*(J_{(n)})(d\theta + ds/T) + O(\rho^{n+1})$

c) $^*(B_{(n)})\,d\Psi_{(n+2)} = O(\rho^{n+4})$

d) $^*(B_{(n)})\,dG_{(n+1)} + \rho^{n+2} P_{n+1}/B_o\; d\rho\,d\theta\,ds = d\tau + O(\rho^{n+3})$

e_1) $^*(J_{(n+1)})\,ds = \left\{ I'(\Psi_{(n)})\,{}^*(B_{(n)}) + \rho^{n+2} I'(o)\,P_{n+1}\,d\rho\,d\theta + p'(\Psi_{(n)})\,dG_{(n+1)}\,d\Psi_{(n+2)} \right\} ds + O(\rho^{n+3})$

e_2) $^*(J_{(n+1)})(d\theta + ds/T) = \left\{ I'(\Psi_{(n)})\,{}^*(B_{(n)}) + p'(\Psi_{(n)})\,dG_{(n)}\,d\Psi_{(n+2)} \right\}(d\theta + ds/T) + O(\rho^{n+2})$

b_3) $d\,{}^*(J_{(n+1)}) = O(\rho^{n+2})$

Note that equations a) b_1) and b_2) make up $\mathcal{E}_n$ (III,2). The written system builds up a recurrent sequence $(\vec{J}_{(n)}, \vec{B}_{(n)}) \to (\vec{J}_{(n+1)}, \vec{B}_{(n+1)})$ provided the equations are soluble. The existence of the solutions follows from two considerations: 1) it is shown by recurrence that the composition in harmonics is as described in section 3 ; 2) the existence of the solutions of c) follows from lemma 3 and a similar procedure allows to solve d).

Fictitions non-uniqueness is removed by taking Ψ equal to the flux in the s-direction.

Reference

[1] V.I. ARNOL'D "Small denominators and problems of stability of motion in classical and celestial mechanics" Russian Mathematical Surveys 18, 6, p. 85 (1963)

Linear and Toroidal Magnetohydrostatic Equilibria

by
Jürgen Nührenberg
Institut für Plasmaphysik
Garching bei München

I. Introduction

A class of linear and toroidal equilibria is investigated which is characterized as follows: β is of order one; the current density is determined so as to satisfy the secondary condition that the longitudinal current through each magnetic surface vanish; the only expansion parameter used in the approximate solution of the equilibrium problem is the quantity

(I.1) $$\frac{\varrho_{max}}{R_0} = \varepsilon$$

where ϱ_{max} is the largest radius of the discharge tube and R_0 the radius of curvature of the magnetic axis, which is constant in lowest order; moreover, the periodicity length L and the torsion in lowest order $\frac{1}{T_0}$ of the magnetic axis obey the relations

(II.2 a,b) $$\frac{2\pi\varrho_{max}}{L} \sim 1 \;,\; \frac{\varrho_{max}}{T_0} \sim 1 \quad (i.e.\ \frac{T_0}{R_0} \sim \varepsilon)$$

Under these conditions the equilibria are of the $\ell = 1$ stellarator type, configurations of the $\ell = 2, 3, \ldots$ types not being included.

II. Description of the equilibrium in a suitable coordinate system and its relationship to the geometry of the configuration

The following independent variables are used: the surfaces of constant pressure (magnetic surfaces) serve as coordinate surfaces on which the magnetic field lines and the current density lines are chosen as coordinate lines. The quantities ρ, φ, s of the Mercier coordinate system [1], which describe the equilibrium geometrically are treated as dependent variables. In the following it is shown briefly what form the equilibrium problem then takes. The magnetic field and current density are written in the form

(II.1) $$\underline{B} = \nabla\chi \times \nabla\psi \;;\; \underline{j} = \nabla K \times \nabla\psi$$

which ensures that they are divergence-free. For convenience the notations

(II.2) $$\underline{a}^1 = \nabla\psi \;,\; \underline{a}^2 = \nabla\chi \;,\; \underline{a}^3 = \nabla K$$

are now introduced for the gradients. It then follows that

(II.3) $$\underline{B} = \underline{a}^2 \times \underline{a}^1 = -\frac{1}{\sqrt{g}}\underline{a}_3 = -\frac{1}{\sqrt{g}} g_{i3}\,\underline{a}^i$$

where

$$\underline{j} = \underline{a}^3 \times \underline{a}^1 = \frac{1}{\sqrt{g}}\underline{a}_2$$

(II.4) $$\sqrt{g} = \underline{a}_1 \cdot (\underline{a}_2 \times \underline{a}_3) \;;\; g_{ik} = \underline{a}_i \cdot \underline{a}_k$$

Because

(II.5) $$\underline{j} \times \underline{B} = -\frac{1}{\sqrt{g}}\underline{a}^1 = \frac{dp}{d\psi}\underline{a}^1 =: p'\underline{a}^1$$

the equilibrium equation is satisfied by

(II.6) $$-\frac{1}{\sqrt{g}} = p'$$

From the equation $\underline{j} = \nabla \times \underline{B}$ the following system of equations is obtained for g_{13}, g_{23}, g_{33} :

(II.7 a-c) $$\frac{\partial g_{33}}{\partial\chi} - \frac{\partial g_{23}}{\partial K} = 0 \;;\; p'\frac{\partial g_{13}}{\partial K} - \frac{\partial}{\partial\psi}(p' g_{33}) = 1$$

$$\frac{\partial}{\partial\psi}(p' g_{23}) - p'\frac{\partial g_{13}}{\partial\chi} = 0$$

If ρ, φ, s are each regarded as a function of ψ, χ, K, the g_{ik} can be represented as follows

(II.8a,b) $$\sqrt{g} = \rho\left(1 - \tfrac{\rho}{R}\cos\varphi\right)\left[\rho_\psi(s_K\varphi_\chi - s_\chi\varphi_K) - \varphi_\psi(\rho_\chi s_K - \rho_K s_\chi) + s_\psi(\rho_\chi\varphi_K - \rho_K\varphi_\chi)\right]$$

$$g_{13} = \rho_\psi\rho_K + \rho^2\varphi_\psi\varphi_K + \left(\left(1 - \tfrac{\rho}{R}\cos\varphi\right)^2 + \tfrac{\rho^2}{T^2}\right)s_\psi s_K - \tfrac{\rho^2}{T}(\varphi_\psi s_K + s_\psi\varphi_K)$$

similar equations being obtained for g_{23}, g_{33}. For φ and s the expressions

(II.9 a,b) $$\varphi = -2\pi\chi + 2\pi\frac{\bar\psi'}{I}K + \tilde\varphi(\psi,\varphi,s)$$

$$s = \frac{L}{I}K + \tilde s(\psi,\varphi,s)$$

are written where $\tilde\varphi, \tilde s$ are doubly periodic functions of φ and s with the periods 2π and L respectively; I is the current-the-short-way per period through the surface described by the normal to the magnetic axis when progressing along this axis, this surface being limited by the surface $\psi = const$; $\bar\psi$ is the analogously defined flux-the-short-way and therefore contains once the flux-the-long-way. The expression (II.9b) ensures that the current-the-long-way vanishes through every magnetic surface. Equations (II.6,7) are a system of equations for the functions (II.10) $\rho, \tilde\varphi, \tilde s, \bar\psi', I'$ which is solved approximately in the next section.

III. Method of expansion

The functions (II.10) are expanded as follows

(III.1) $$\rho = \sum_{\nu\geq 0}\varepsilon^\nu\overset{\nu}{\rho} \;,\; \overset{0}{\rho} = \overset{0}{\rho}(\psi);\quad \tilde\varphi = \sum_{\nu\geq 1}\varepsilon^\nu\overset{\nu}{\varphi} \;;\; \tilde s = \sum_{\nu\geq 1}\varepsilon^\nu\overset{\nu}{s}$$

$$2\pi\frac{\bar\psi'}{I} = 2\pi\frac{\bar\psi_0'}{I_0'}\left(1 + \sum_{\nu\geq 1}\varepsilon^\nu\overset{\nu}{\sigma}\right);\quad \frac{1}{I} = \frac{1}{I_0'}\left(1 + \sum_{\nu\geq 1}\varepsilon^\nu\overset{\nu}{\sigma}\right)$$

Expansion of the equations (II.6,7) yields the following system of equations for the ν-th order: (I.1,2)

$$-2\pi\frac{L}{I_0'}\left(\overset{0}{\rho}\overset{\nu}{\rho}\right)_\psi + 2\pi\left(\frac{L}{I_0'}\right)'\overset{0}{\rho}\overset{\nu}{\rho}_K K + \overset{0}{\rho}\overset{0}{\rho}\left(\frac{L}{I_0'}\overset{\nu}{\varphi}_\chi - \frac{2\pi L\overset{\nu}{\sigma}}{I_0'} - 2\pi\overset{\nu}{s}_K - \frac{L}{T_0 I_0'}\overset{\nu}{s}_\chi\right) = \mathcal{I}_a$$

(III.2 a-e) $$\left[\frac{L}{I_0'}\overset{\nu}{s}_\chi - 2\pi\frac{\overset{0}{\rho}^2}{T_0}\overset{\nu}{s}_K + 2\pi\overset{0}{\rho}^2\overset{\nu}{\varphi}_K\right]_K = \mathcal{I}_b$$

$$p'^2\overset{0}{\rho}'\overset{\nu}{\rho}_{KK} + p'^2\left(\frac{L}{I_0'}\right)'\overset{\nu}{s}_{KK}K - \left(p'^2\frac{L}{I_0'}\overset{\nu}{s}_K\right)_\psi = \mathcal{I}_c^K$$

$$\left(p'^2\frac{L^2}{I_0'^2}\overset{\nu}{\sigma}\right)_\psi = \mathcal{I}_c^\psi \;;\; 2\pi p'\overset{0}{\rho}^2(\overset{\nu}{\sigma} - \overset{\nu}{\tau}) = \mathcal{I}_d^\psi$$

Here the right-hand sides are inhomogeneities which can be calculated with the solutions up to $(\nu-1)$-th order. Equations (III.2 d,e) are ordinary differential equations for determining the functions $\overset{\nu}{\sigma}, \overset{\nu}{\tau}$; equations a, b, c can be reduced to a partial linear elliptic differential equation for $\overset{\nu}{s}$. Once this has been solved, $\overset{\nu}{\varphi}$ and $\overset{\nu}{\psi}$ can be calculated by trivial integration with respect to K. Because of (I.1,2) a zeroth-order solution depending only on ψ is compatible with the system of equations (III.2). Since $\beta \sim 1$, the pressure balance of the linear θ-pinch is then satisfied:

(III.3) $$p + \frac{B^2}{2} = const$$

With this choice of zeroth order the higher orders can be determined in such a way that each contains only a finite number of Fourier components with respect to φ and s. The equation for $\overset{\nu}{s}$ therefore splits into a system of ordinary differential equations for the Fourier components of $\overset{\nu}{s}$. - With the assumptions (I.1,2a) it can be seen that the condition (I.2b) is necessary for solving the system of first order equations.

IV. Solutions up to second order

a) Linear $\ell = 1$ equilibrium. The expressions (III.1) are specialized in the form

(IV.1a) $$\rho = \overset{0}{\rho}(\psi) + \varepsilon\overset{1}{\rho}(\psi)\cos\varphi + \varepsilon^2\left(\overset{2}{\rho}_0(\psi) + \overset{2}{\rho}_2(\psi)\cos 2\varphi\right)$$

(IV.1b,c) $$\varphi = -2\pi\chi + \frac{L}{T I_0'}(1+\varepsilon^2\overset{2}{t})K + \varepsilon\overset{1}{\varphi}(\psi)\sin\varphi + \varepsilon^2\overset{2}{\varphi}(\psi)\sin 2\varphi$$

$$s = \frac{L}{I_0'}(1+\varepsilon^2\overset{2}{\sigma})K + \varepsilon\overset{1}{s}(\psi)\sin\varphi + \varepsilon^2\overset{2}{s}(\psi)\sin 2\varphi$$

to calculate an equilibrium for the case $\beta \approx 0.6$, $\varepsilon = 0.2$ $\varrho_{max} = 1$, $T = 1$, $L \approx 2\pi$, $p(\psi) = 0.6\exp(-2.2\psi - (\psi/0.08)^4)$

Fig.1 shows across section of surfaces with the plane normal to the magnetic axis. Fig.2 shows the vacuum field region. The rotational transform and a stability criterion [1], [2] are represented in Fig.3 in comparison with the pressure ρ.

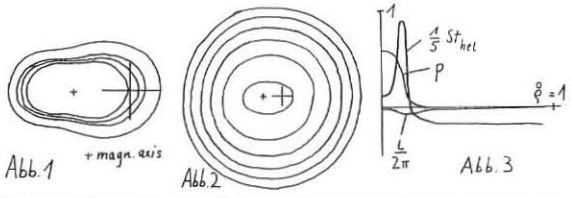

Abb.1 + magn. axis Abb.2 Abb.3

b) Toroidal $\ell = 1$ equilibrium. The toroidal equilibrium corresponding to a) was calculated with the expansions:

$$\rho = \overset{0}{\rho} + \varepsilon\overset{1}{\rho}\cos\varphi + \varepsilon^2\left(\overset{2}{\rho}_{00} + \overset{2}{\rho}_{20}\cos 2\varphi + \overset{2}{\rho}_{11}\cos\varphi\sin m\vartheta + \overset{2}{\rho}_{02}\cos 2m\vartheta\right)$$

(IV.2) $$\varphi = -2\pi\chi + \frac{L}{T_0 I_0'}(1+\varepsilon^2\overset{2}{t})K + \varepsilon\left(\overset{1}{\varphi}_{10}\sin\varphi + \overset{1}{\varphi}_{01}\cos m\vartheta\right)$$
$$+ \varepsilon^2\left(\overset{2}{\varphi}_{20}\sin 2\varphi + \overset{2}{\varphi}_{11}\sin\varphi\sin m\vartheta + \overset{2}{\varphi}_{02}\right)$$

$$s = \frac{L}{I_0'}(1+\varepsilon^2\overset{2}{\sigma})K + \varepsilon\overset{1}{s}\sin\varphi + \varepsilon^2\left(\overset{2}{s}_{20}\sin 2\varphi + \overset{2}{s}_{11}\cos\varphi\cos m\vartheta + \overset{2}{s}_{02}\sin 2m\vartheta\right)$$

where m is the number of periods, $\frac{1}{m} = \varepsilon$.

V. Conclusion

The method described in II allows: 1) equilibria for arbitrary $p(\psi)$ and an integral secondary condition (in this case vanishing current-the-long-way through every magnetic surface) to be calculated; 2) information on stability and the rotational transform in the whole plasma region to be obtained.
Investigations of scaling other than (I.2) are in progress.

The author is grateful to Prof. Dr. A. Schlüter for suggesting the subject and for helpful discussions.

[1] C. Mercier, Nucl. Fus. 4, 1964, 213
[2] J.M. Greene, J.L. Johnson, Phys. Fluids 5, 1962, 510

This work was performed under the terms of the agreement on association between the Institut für Plasmaphysik and EURATOM.

Low Frequency Interchanges

by
Günther Otto Spies
Institut für Plasmaphysik, Garching bei München

This paper deals with the "trapping instability". This is an electrostatic mode conserving the longitudinal invariant of charged particles. Hitherto this mode has been discussed theoretically only for isotropic Maxwellian equilibria (Rosenbluth[1], Kadomtsev and Pogutse[2], Rosinskij et al.[3]), while this paper admits much more general distribution functions.

For simplicity only open ended configurations are considered. The magnetic field is assumed to be a vacuum field having one single minimum on each field line and possessing some symmetry such that $\mathcal{J}=\oint \frac{d\chi}{B}\sqrt{2(K-\mu B(\alpha,\beta,\chi))}$ does not depend on β. The coordinates α,β,χ satisfy $\underline{B}=\nabla\alpha\times\nabla\beta=\nabla\chi$. The equilibrium distribution functions are assumed to be of the form $f_0(\chi,\mathcal{J})=F(\mu,K,\alpha)$, where $\mu=\frac{v_\perp^2}{2B}$, $K=\frac{v^2}{2}$, and to satisfy $F_{IK}<0$, $|F_{I\alpha}\mathcal{J}_{IK}|\gg|F_{IK}\mathcal{J}_{I\alpha}|$, and

$$\sum e\int d\mathcal{K}\sqrt{K}\,F(\lambda K,K,\alpha)=0, \qquad (1)$$

where $\lambda=\mu/K$. Equation (1) is a necessary and sufficient condition for the neutralizing electric field to vanish.

Let $\varphi=\psi(\alpha,\chi)\exp[i(\omega t-k\beta)]$ be the disturbing electrostatic potential. Then the disturbing distribution functions are

$$f_1(\chi,\mathcal{J},t)=\frac{e}{m}F_{IK}\left(\psi-\frac{\omega-kv_C}{\omega-kv_D}\langle\psi\rangle\right)e^{i(\omega t-k\beta)} \qquad (2)$$

where $v_C=(m/e)(F_{I\alpha}/F_{IK})$, $v_D=(m/e)(\mathcal{J}_{I\alpha}/\mathcal{J}_{IK})$, and $\langle\psi\rangle$ is the time average of ψ over the quasi-periodic unperturbed longitudinal guiding centre orbit. The derivation of (2) is done by linearizing and solving the Vlasov equation $g_{It}=\frac{m}{e}(g_{I\alpha}K_{I\beta}-g_{I\beta}K_{I\alpha})$ and then substituting into $f(\chi,\mathcal{J},t)=g(\mu,\mathcal{J},\alpha,\beta,t)=F(\mu,K(\mu,\mathcal{J},\alpha,\beta,t),\alpha)+g_1(\mu,\mathcal{J},\alpha,\beta,t)$, where $\mathcal{J}=\oint\frac{d\chi}{B}\sqrt{2(K-\mu B-\frac{e}{m}\varphi)}$.

The first order charge neutrality now reads

$$\sum\frac{e^2}{m}\int\frac{B\,d\mu\,dK}{\sqrt{K-\mu B}}F_{IK}\left(\psi-\frac{\omega-kv_C}{\omega-kv_D}\langle\psi\rangle\right)=0. \qquad (3)$$

This is a non-symmetric linear integral equation for the χ-dependence of ψ, α being merely a parameter. It serves as a dispersion relation. The stability question is decided by considering the imaginary parts of the eigenvalues ω/k.

In order to obtain a variational principle, we now restrict the frequencies by assuming $|v_D|\ll|\omega/k|\ll|v_C|$, and then expand the denominator. The essential part of eq. (3) is now $\omega^2P\psi=k^2A\psi$, where $P\psi=-\sum\frac{e^2}{m}\int\frac{B\,d\mu\,dK}{\sqrt{K-\mu B}}F_{IK}(\psi-\langle\psi\rangle)$, $A\psi=\sum m\int\frac{B\,d\mu\,dK}{\sqrt{K-\mu B}}F_{I\alpha}\mathcal{J}_{I\alpha}\langle\psi\rangle$.

The large terms of order kv_C/ω appearing in the expansion of eq. (3) have cancelled between ions and electrons. This is proved by using eq. (1). The vanishing of the equilibrium electric field hereby turns out to be necessary in order to arrive at a variational principle for stability. With the inner product $(\psi_1,\psi_2)=\int d\alpha\,d\chi\,\psi_1^*\psi_2/B^2$ the operators P and A are symmetric, while P is positive. Hence the eigenvalues $(\omega/k)^2$ are given by the stationary values of the functional

$$W[\psi]=(\psi,A\psi)/(\psi,P\psi), \qquad (4)$$

and $(\psi,A\psi)>0$ is necessary and sufficient for stability, provided W is bounded from below. The quadratic form $(\psi,A\psi)$ may be computed to be $-\int d\alpha\,d\lambda\,|\langle\psi\rangle|^2\bar{\tau}_B\bar{v}_D\frac{\partial}{\partial\alpha}\sum m\int d\mathcal{K}\,K^{3/2}F(\lambda K,K,\alpha)$, where $\bar{v}_D(\lambda,\alpha)=(1/K)(\mathcal{J}_{I\alpha}/\mathcal{J}_{IK})$, $\bar{\tau}_B(\lambda,\alpha)=\mathcal{J}_{IK}/\sqrt{K}$. Hence

$$\bar{v}_D\frac{\partial}{\partial\alpha}\sum m\int d\mathcal{K}\,K^{3/2}F(\lambda K,K,\alpha)<0 \qquad (5)$$

is sufficient for stability. Taking a trial function ψ, which is highly localized at the mirror points of those particles for which (5) is violated, one shows that this condition is necessary, too, and that the growth rate of the resulting instability is of order $\omega\sim k\sqrt{v_Cv_D}$, consistent with the restriction introduced.

The variational principle may break down only if the numerator of eq. (4) is not positive for all trial functions which make the denominator vanish. Since these trial functions depend only on α, it is easily proved that

$$\int d\lambda\,\bar{\tau}_B\bar{v}_D\frac{\partial}{\partial\alpha}\sum m\int d\mathcal{K}\,K^{3/2}F<0 \qquad (6)$$

is the condition for the criterion (5) to be valid. This condition, obviously less restrictive than (5), is identical with $\sum m\int d\mu\,d\mathcal{J}\,K_{I\alpha}F_{I\alpha}<0$, which specializes a more general criterion first derived by Andreoletti[4] to the present case, and which is sufficient for interchange stability on the faster magnetodynamic time scale (only μ conserved). On the other hand, (5) is less restrictive than

$$\bar{v}_DF_{I\alpha}<0, \qquad (7)$$

which is the appropriate specialization of a criterion recently derived by Rutherford and Frieman[5], and which is sufficient for stability to <u>any</u> electrostatic modes conserving the $\mathcal{J}$-invariant.

The criterion (5) requires that particles drift in the directions given by the gradient of the quantity $\sum m\int d\mathcal{K}\,K^{3/2}F$, which is related to the trace P of the pressure-dyadic by $\int d\chi\,P/B^2=\int d\lambda\,\bar{\tau}_B\sum m\int d\mathcal{K}\,K^{3/2}F$. In the special case of isotropic distribution functions, i.e. for $F_{I\mu}=0$, it is the pressure itself. In this case the criterion (5) requires that all particles belonging to the same species drift in the same direction. This requirement, which severely restricts the magnetic field, is relaxed by allowing for anisotropy.

The more complex cases of closed-line or toroidal configurations with shear in which several types of both trapped and untrapped particles are present will be treated in an extended version of this paper.[6]

This work was performed under the terms of the agreement on association between the Institut für Plasmaphysik and Euratom.

1) M.N. Rosenbluth, Phys. Fluids 11, 869 (1968).

2) B. Kadomtsev and O. Pogutse, Zh. Eksp. Teor. Fiz. 51, 1734 (1966) [Sov. Phys. - JETP 24, 1172 (1967)].

3) S.E. Rosinskij, V.G. Rukhlin and A.A. Rukhadze, III. Conf. on Plasma Physics and Controlled Nuclear Fusion Research, Novosibirsk 1968, CN 24/F - 3

4) J. Andreoletti, C.R. Acad. Sc. Paris 257, 1033 (1963)

5) P.H. Rutherford and E.A. Frieman, Phys. Fluids 11, 252 (1968).

6) G.O. Spies, to be published.

EFFECTS OF FINITE β ON THE STABILITY OF A CONFINED PLASMA

P.H.Rebut and A.Samain

ASSOCIATION EURATOM-CEA
Département de la Physique du Plasma et de la Fusion Contrôlée
Centre d'Etudes Nucléaires
Boîte Postale n° 6 - **92 Fontenay-aux-Roses** (France)

I. The study of the stability of a low β confined plasma, using microscopic equations, has been extensively developed. [1-6]. Our objective in this paper is to contribute to this study by considering the case where β is finite, ($\beta \leq 0,1$), and gravitational forces and magnetic shear are present. We assume that the plasma is uniform along directions OY, OZ and is confined along OX by a magnetic field B parallel to the plane OY, OZ. $\left(d\log(n)/dx = L_p^{-1} ;\ d\,tg^{-1}\left(B_z/B_y\right)/dx = L_s^{-1}\right)$. We assume that the static electric field is 0, and that the guiding centres of ions (i) and electrons (e) have drift velocities v_D along $\underset{\sim}{B} \times \underset{\sim}{OX}$ verifying : $v_{Di} = -v_{De}$. We specify the equilibrium state of the plasma by the distribution functions $F(a, v_{//}, x_c)$ of ions and electrons in the space $a^2, v_{//}, x_c$, where a, $v_{//}$, x_c are the Larmor radius, the velocity along $\underset{\sim}{B}$ and the guiding center abscissa of a particle, respectively. We chose F to be proportional to $\exp(-x_c/L_p - U/T)$ where $U = \frac{1}{2} m (\omega_c^2 a^2 + v_{//}^2)$. ($\omega_c = -qB/m$, q is the charge and m the mass of the particle). We assume that the temperatures T_i, T_e are uniform and that $T_i = T_e$. The diamagnetic velocity of each particle assembly is then $V = T/(m\omega_c L_p)$. ($V_i = -V_e$) . We will study the marginally unstable modes in this plasma, with a frequency ω much less than ω_{ci} . Such modes result from coupling between usual electrostatic waves and Alfven torsion waves. It may be shown that their wave numbers $K_{//}, K_\perp$ parallel and transverse to $\underset{\sim}{B}$ verify : $K_{//} \ll K_\perp$. Also, they can be described by a scalar potential and a vector potential parallel to $\underset{\sim}{B}$. These potentials may be written as : $\phi(x)\exp(i\theta)$, $A_{//}(x)\exp(i\theta)$ where $\theta = \omega t + K_y y + K_z z$. We use the formalism given in ref. [7] to obtain the functional equations which determine $\phi(x), A_{//}(x)$. This formalism allows to calculate, as a functional of $\phi(x), A_{//}(x)$, the quantity $\mathcal{L} = \int dx \left[\frac{1}{4\pi}\left(|\underset{\sim}{E}|^2 - |\underset{\sim}{H}|^2\right) + I_{//} A_{//}^* - \rho\,\phi^*\right]$, where $\underset{\sim}{E}$, $\underset{\sim}{H}$ are the electric and magnetic perturbation and $\rho, I_{//}$ are the charge and current densities induced in the plasma, in the presence of the considered mode :

$$\mathcal{L} \equiv -\frac{1}{4\pi}\int |\nabla A_{//}|^2\, dx + \sum_{i,e}\iiint \frac{q^2 n}{T}|\phi^2|\, dx - \sum_{i,e}\iiint \left(\omega + K_c V\right)\frac{q^2 f(a, v_{//}, x)}{T}\,\frac{|J_o(Y)\cdot(\phi + v_{//}A_{//})|^2}{\omega + K_y v_y + K_c v_D}\, da\, dv_{//}\, dx$$

where $K_{//}$ and K_c are the components of the wave vector : $K_y \underset{\sim}{e_y} + K_z \underset{\sim}{e_z}$ parallel and transverse to the magnetic field, respectively, and Y is the operator $a\left(K_c^2 - d^2/dx^2\right)^{1/2}$ J_o is the usual Bessel function. The equations which determine $\phi(x)$ and $A_{//}(x)$ can be obtained by expressing that $\mathcal{L}$ is extremum for all variations of $[\phi(x)]^*$, $[A_{//}(x)]^*$. This implies that $\mathcal{L}$ is 0, which determines ω if one knows the functions $\phi(x)$, $A_{//}(x)$. We restrict ourselves to the case where $\bar{a}_i \frac{d\cdot}{dx} \ll 1$ or $\frac{d\cdot}{dx} \ll K_c$. ($a_i = \frac{v_i}{\omega_{ci}}$; $2T = m_i w_i^2 = m_e w_e^2$) Also, the finite Larmor radius effects of electrons will be neglected. Expressing $\mathcal{L}$ in terms of the function $A_{//}(x)$ and $\Psi(x) = \phi(x) + \frac{\omega + K_c V_i}{K_{//}} A_{//}(x)$, and using the variational principle outlined above, one obtains the following equations governing $\Psi(x)$, $A_{//}(x)$:

$$R_{em}\left(A_{//}\right) = -\frac{1}{W_i}\, S(\Psi) \ ; \ R_{es}\left(\Psi\right) = -W_i\, S(A_{//}). \qquad (1)$$

where R_{em}, R_{es}, S are the following operators :

$$R_{em} = -\frac{y^2}{\beta} - (\omega + K_c V_i)(\omega + K_c v_{Di})\frac{1}{2}\left[\frac{1}{K_{//}^2 W_i^2}\left(1-\Gamma\right) + \left(1-\Gamma\right)\frac{1}{K_{//}^2 W_i^2}\right] + 2\,\frac{K_c^2 v_{Di}(V_i + v_{Di})}{K_{//}^2 W_i^2} - 4\,\frac{(\omega + K_c V_e)(K_c v_{Di})^2}{K_{//}^3 W_i^2 W_e}\,\mathcal{K}(X_e)$$

$$R_{es} = +2 - (\omega + K_c V_i)\frac{1}{2}\left[\frac{\mathcal{K}(X_i)}{K_{//} W_i}\Gamma + \Gamma\,\frac{\mathcal{K}(X_i)}{K_{//} W_i}\right] - \frac{(\omega + K_c V_e)\,\mathcal{K}(X_e)}{K_{//} W_e}$$

$$S = -(\omega + K_c V_i)\frac{1}{2}\left[\frac{1}{K_{//} W_i}\left(1-\Gamma\right) + \left(1-\Gamma\right)\frac{1}{K_{//} W_i}\right] - 2\,\frac{K_c v_{Di}}{K_{//} W_i} + 2\,\frac{(\omega + K_c V_e) K_c v_{Di}\,\mathcal{K}(X_e)}{K_{//}^2 W_e W_i}$$

and $\Gamma = I_o\left(\frac{y^2}{2}\right)\exp\left(-\frac{y^2}{2}\right)$; $\mathcal{K}(X) = \exp(-X^2)\left[2\int_o^X \exp(t^2)\,dt - i\sqrt{\pi}\right]$

$X = (\omega + K_y v_D)\cdot(K_{//} W)^{-1}$

II. Using these equations, we now discuss whether marginally unstable modes may appear in the plasma. Note that the frequency ω of such modes must be in the interval ($-K_c V_i$, $K_c V_i$). (This results from the equation : $\mathrm{Im}\,\mathcal{L} = 0$). We first study whether marginally unstable modes may exist with ω in the interval $-K_c V_i$, $-K_c v_{Di}$. Discarding the small interval where $X_e \geq 1$, such modes may be seen to verify : $\mathcal{R}e\left[R_{em}(A_{//})\right] = \varepsilon$, where ε is a positive quantity. This equation, which is very similar to the Suydam equation which determines the radial profile of low frequency modes in MHD approximation, can be shown to have no eigensolution if :

$$\beta < \frac{1}{2}\,\frac{L_p^2}{L_s^2}\cdot\frac{V_i}{v_{Di}} \qquad (2)$$

This stability criterium is twice more severe than the Suydam criterium.

We then study whether marginally unstable modes may exist with ω in the interval ($-K_c v_{Di}, K_c V_i$). We restrict ourselves to the case $V_i v_{Di} > 0$, when unstable flutes may exist in the MHD approximation. We shall apply the WKB technique to study the actual structure of the modes. This may be done as usual by calculating with the help of equations (1), where ω is kept constant, $K_\perp^2 = -\frac{\partial^2}{\partial x^2} + K_c^2$ as a function of $K_{//} \approx K_c \frac{x}{L_s}$. We begin with the case $v_{Di} = 0$. The modes are then found to be amplified along OX by electron Landau effect for small values of $K_{//}$ and heavily damped by ion Landau effect for greater values of $K_{//}$. $K_\perp$ calculated as explained above is an increasing function of $K_{//}$ up to these values. This situation, which is similar to the situation of the electrostatic modes present when $\beta = 0$, means that the modes cannot be reflected before they reach the region where they are damped. The stability criteria given in the case $\beta = 0$ (2) for such convectively unstable modes do not change significantly when $\beta < 0,1$. Also, it may be calculated that the presence of a finite β reduces the domain in the plane $(K_\perp, K_{//})$ which corresponds to unstable modes.

The problem is more complex when $V_i\, v_{Di} > 0$. The figure 1 shows in this case the structure of the curve giving $K_\perp$ as a function of $K_{//}$ for given ω . Part (1) of this curve corresponds to electrostatic modes verifying $R_{es}(\Psi) = 0$, and part (2) to Alfven torsion modes verifying $R_{em}(A_{//})$. The arc $\propto M/\beta$ corresponds typically to unstable modes. Again the arc $M\propto$, where $K_\perp$ is an increasing function of $K_{//}$, corresponds to modes which can be convectively unstable only. What has been said about the modes present when $v_{Di} = 0$, apply as well to these modes. On the contrary the arc $M\beta$ corresponds to modes which may be absolutely unstable. A sufficient condition for stability may be obtained, in presence of shear, by expressing that for all these modes, one has : $\frac{K_\perp K_{//}}{K_c} < \frac{1}{L_s}$

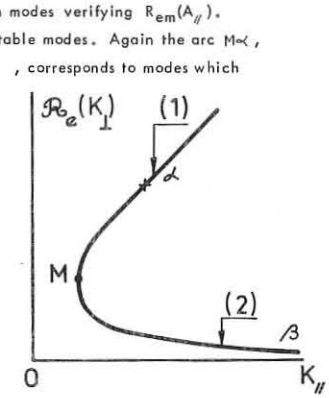

Fig. 1

Numerical calculations have been made for $v_{Di}/V_i = 0,1$.

The criterium which has been obtained is approximately twice more severe than the criterium (2).

REFERENCES

[1] N.A.KRALL, M.N.ROSENBLUTH
Phys.Fluids (1965) vol.8, p.1488

[2] B.COPPI, G.LAVAL, R.PELLAT, M.N.ROSENBLUTH
Nuclear Fusion (1966) vol.6, p.261

[3] P.H.REBUT
Plasma Physics (1967) vol.9, p.671

[4] L.B.MIKHAILOVSKAYA, A.B.MIKHAILOVSKII
Nuclear Fusion (1963) vol.3, p.113

[5] A.A.GALEEV
Sov.Physics JETP (1963) vol.17, p.1292

[6] Kazuo KATAO - Report MPI-PAE/PL 3/67 -
Max-Planck Institut für Physik und Astrophysik, München.

[7] P.H.REBUT, A.SAMAIN
Comptes Rendus Acad.Sci.(Fr.) - in press -

THE INFLUENCE OF NON-ELECTROSTATIC EFFECTS UPON A HYBRID INSTABILITY

by

F.A. Haas

U.K.A.E.A., Culham Laboratory, Abingdon, Berkshire, England.

1. Introduction. There now exist a number of papers discussing the MHD stability of high-β machines, particularly for cusp and the linear theta-pinch[1-4]. Little is known however about the effect of non-MHD instabilities on these machines. Recently, Ashby and Paton[5] considered the stability of a collision-free low-β plasma sheath whose thickness is of the order of an ion Larmor radius. To simulate the directed motion of the ions in the sheath, they use a homogeneous model in which ions move in straight lines perpendicular to a magnetic field (see Fig.1). Assuming electrostatic perturbations Ashby and Paton obtain a dispersion equation of the two-stream type (see eqn.(3.2), and show the existence of a hybrid instability. In this paper we examine the influence of non-electrostatic effects upon their instability.

2. The Model. The work is based on the two-fluid equations, which in c.g.s. units take the form

$$\frac{d\underline{v}_i}{dt} = \frac{e}{M}\left(\underline{E} + \frac{\underline{v}_i \times \underline{B}}{c}\right)$$

for the ions, and

$$\frac{d\underline{v}_e}{dt} = -\frac{e}{m}\left(\underline{E} + \frac{\underline{v}_e \times \underline{B}}{c}\right)$$

for the electrons, all symbols having their usual meaning. Collisions are neglected and both the ions and electrons are taken to be cold. The continuity equations for both species are

$$\frac{\partial n_{i,e}}{\partial t} + \nabla.(n_{i,e}\,\underline{v}_{i,e}) = 0.$$

We also require Maxwell's equations, namely,

$$\nabla\times\underline{E} = -\frac{1}{c}\frac{\partial \underline{B}}{\partial t}, \quad \nabla\times\underline{B} = \frac{4\pi \underline{j}}{c} + \frac{1}{c}\frac{\partial \underline{E}}{\partial t}$$

and $\nabla.\underline{E} = 4\pi e\,(n_i - n_e)$ where $\underline{j} = e(n_i\underline{v}_i - n_e\underline{v}_e)$.

For our equilibrium we consider a beam of ions with uniform velocity V to be streaming in straight lines perpendicular to a magnetic field (see Fig.1). Charge neutrality is provided by a background of electrons. The magnetic field and density are related by

$$\frac{dB}{dx} = -4\pi e n_i \frac{V}{c}.$$

The assumption of straight-line motion for the ions is valid for frequencies very large compared to the ion gyro-frequency. The above equations are linearised and perturbed quantities assumed to have the form $\exp[i(k_x x + k_y y + k_z z + \omega t)]$. The taking of normal modes is valid provided $\lambda_x \ll L$, the plasma scale length. We consider stability under the following set of conditions:

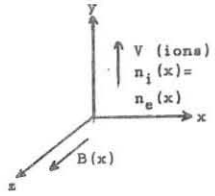

Fig.1

$$k_z \sim k_y \left(\frac{m}{M}\right)^{\frac{1}{2}}, \quad \omega \sim k_y V \sim \omega + k_y V, \quad \frac{\omega_{pe}}{k_y c} \sim 1,$$

$$\frac{\omega}{k_y c} \ll 1, \quad \frac{\omega_{pi}}{k_y c} \ll 1, \quad \Omega_i \ll \omega_{pi},$$

where ω_{pi} & ω_{pe} denote the ion and electron plasma frequencies respectively, and Ω_i & Ω_e denote the ion and electron gyro-frequencies respectively. It is also assumed that the wavelength $\lambda_y \ll a_i$, the ion Larmor radius, which is of order V/Ω_i.

3. The Dispersion Equation. After considerable algebra the above set of equations leads to the following dispersion equation:

$$D(\omega) = \frac{1}{\omega^2} + \frac{2\alpha}{(\omega + k_y V)^2} - \frac{2\gamma}{\omega} = Q, \qquad (3.1)$$

where

$$2\alpha = \frac{m}{M}\frac{k_y^2}{k_z^2}\left(1 + \frac{\omega_{pe}^2}{k_y^2 c^2}\right), \quad 2\gamma = \frac{1}{\Omega_e}\frac{k_y}{k_z^2}\left[\frac{1}{n}\frac{dn}{dx} - \frac{1}{B}\frac{dB}{dx}\right]$$

and

$$Q = 2\alpha\left(\frac{1}{\omega_o^2} + \frac{1}{\Omega_e\Omega_i}\frac{\omega_{pe}^2}{k_y^2 c^2}\right),$$

the lower hybrid frequency ω_o being defined by

$$\frac{1}{\omega_o^2} = \frac{1}{\omega_{pe}^2} + \frac{1}{\Omega_i\Omega_e}.$$

In obtaining this result it has been assumed that $k_x^2 \ll k_y^2$.

In the low-β situation (electrostatic modes) eqn.(3.1) becomes

$$\frac{1}{\omega^2} + \frac{\frac{m}{M}\frac{k_y^2}{k_z^2}}{(\omega + k_y V)^2} = \frac{m}{M}\frac{k_y^2}{k_z^2}\frac{1}{\omega_o^2}. \qquad (3.2)$$

This dispersion equation has been discussed by Ashby and Paton[5]. It is straightforward to show that all wavelengths $\lambda_y > \lambda_o$ are unstable, where λ_o is a critical wavelength $\lambda_o = 2\pi V\omega_o^{-1}\, s^{\frac{1}{4}}(1 + s^{\frac{1}{2}})^{-3/2}$, s being defined to be $mM^{-1}\,k_y^2\,k_z^{-2}$.

We now return to eqn.(3.1). Taking $k_y > 0$, since $\frac{dB}{dx} < 0$, it is clear that $\gamma > 0$, and the dispersion equation may be easily sketched (see Fig.2).

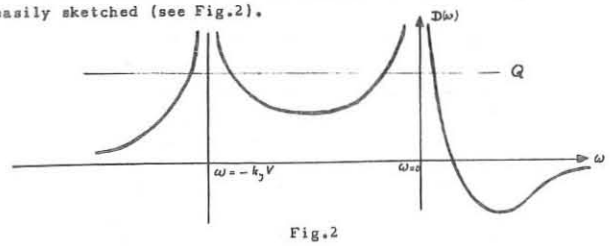

Fig.2

It can be shown that a sufficient condition for stability is

$$V^2 > \frac{\frac{2}{s}(1 + (\frac{s}{2})^{\frac{1}{2}})^3\, V_A^2}{1 - \frac{s}{16}\frac{V_A^2}{\Omega_i^2}\left(\frac{1}{n}\frac{dn}{dx} - \frac{1}{B}\frac{dB}{dx}\right)^2}, \qquad (3.3)$$

where the denominator must be positive. A necessary condition for stability is given by:

$$V^2 > \frac{1}{4}V_A^2 \frac{1}{1 + \frac{\Omega_i\Omega_e}{\omega_{pi}^2}\cdot\frac{1}{s}}(1 + s^{\frac{1}{2}})^3. \qquad (3.4)$$

V_A denotes the Alfvén speed and is given by $V_A^2 = \frac{c^2}{\omega_{pe}^2}\Omega_i\Omega_e$. It is straightforward to show that the R.H.S. of (3.4) is smaller than the R.H.S. of (3.3) - as it should be.

4. Conclusion. A simple model for the sheath region of a high-β plasma has been set up. Under low-β conditions an instability at the lower-hybrid frequency can always occur. Under high-β conditions however, given that the appropriate conditions are satisfied, then this instability can be stabilised.

References

1. BERKOWITZ, J., GRAD, H. and RUBIN, E., in Proc. Second International Conference on Peaceful Uses of Atomic Energy (U.N.), Geneva, 31, p.177 (1958).
2. HAAS, F.A. and WESSON, J.A., Phys. of Fluids, 9, p.2472 (1966).
3. HAAS, F.A. and WESSON, J.A., Phys. of Fluids, 10, p.2245 (1967).
4. WOBIG, H., Institute for Plasmaphysik (Garching) Report IPP6/53, (1966).
5. ASHBY, D.E.T.F. and PATON, A., Plasma Physics, Vol.9, p.359 (1967).

DISSIPATIVE TRAPPED PARTICLE INSTABILITY IN A DENSE PLASMA

B.B.Kadomtsev, O.P.Pogutse,

I.V.KURCHATOV INSTITUTE OF ATOMIC ENERGY,
Moscow, USSR

A B S T R A C T

It has already been shown by the authors that the trapped particle instability can be very dangerous for confinement of a rarefied plasma in magnetic traps. As the collision frequency grows the effect of trasformation from trapped particles into the transit ones (and the reverse process) begins to acuire a new importance, and the instability assumes the dissipative character. For the instability considered earlier to develop the presence of trapped ions was rather important. The present paper shows that when the frequency of electron collisions is sufficiently high a new trapped particle dissipative instability may develop for which it is not important if there were any or no trapped ions. For this reason this instability should be called the trapped electron instability. As the collision frequency increases this instability takes the form of the resistive drift instability.

An avaluation is made of the turbulent diffision coefficients and thermal conductivity. It is shown that due to the instability under consideration the coefficients of the electron thermal conductivity are appreciably larger than those known earlier. The theoretical results are compared with the experiment.

OVERSTABLE MODES DUE TO RESISTIVITY GRADIENTS

by
F. Herrnegger
INSTITUTE FOR THEORETICAL PHYSICS
Innsbruck University, A-6020 Innsbruck, Austria

1. Introduction

In a sheet pinch in a plasma of variable electrical resistivity the following types of instabilities occur
a) the tearing instability in which the sheet breaks up under the action of the magnetic field into filaments parallel to the direction of the current
b) the rippling instability in which the locally variable electrical resistivity changes the current density. A coupling occurs between the transverse variation of resistivity and the steady current associated with the main magnetic field. Several authors discussed these problems (e.g. [1]-[5]). Furth et al. [1] have investigated the stability of such a sheet and have shown that the linearized MGD equations for incompressible inhomogeneous plasmas do not possess overstable solutions but aperiodically growing instabilities.

The purpose of this paper is to study these problems, especially the effect of resistivity gradients perpendicular to the main magnetic field on the generation of overstable modes in a current-carrying inhomogeneous plasma sheet in the presence of a magnetic shear field and of a constant gravitational field $\underline{g}$. It is shown that overstable modes may exist. These solutions are connected with the second derivative of the mean resistivity ($\bar{\eta}''$) i.e. they depend on whether the course of $\bar{\eta}(x_2)$ in the plasma sheet is convex or concave. Furthermore it is shown that the region of neutral stability depends essentially on the resistivity gradient and on $\bar{\eta}''$ except in the case of homogeneous plasmas.

2. Stability equation

We consider a current-carrying plasma sheet supported by a gravitational field. The following assumptions are made:
a) the main magnetic field depends on x_2:
$\underline{B}(x_2) = [B_1(x_2), 0, B_3(x_2)]$
b) neglecting the thermal conductivity along the magnetic field lines, the perturbation in electrical resistivity results only from convection: $\partial\eta/\partial t + \underline{v}.\nabla\eta = 0$, (1)
($\underline{v}$ flow velocity)
c) no zero-order diffusion velocity exists. The Boussinesq-approximation is assumed to be valid.

Starting from the linearized MGD basis equations [1]

$$\bar{\rho}\frac{d\underline{v}^*}{dt} = -\nabla p^* + \rho^*\underline{g} + \frac{1}{\mu}\{(\nabla\times\underline{\bar{B}})\times\underline{B}^* + (\nabla\times\underline{B}^*)\times\underline{\bar{B}}\} \quad (2)$$

$$\frac{\partial\underline{B}^*}{\partial t} = \nabla\times\{(\underline{v}^*\times\underline{\bar{B}}) - \frac{1}{\mu}[\bar{\eta}(\nabla\times\underline{B}^*) + \eta^*(\nabla\times\underline{\bar{B}})]\} \quad (3)$$

$$\nabla\cdot\underline{v}^* = 0, \qquad \nabla\cdot\underline{B}^* = 0 \quad (4)$$

and looking for solutions of the form
$f^*(\underline{x},t) = f^*(x_2)\exp[i(\underline{a}\cdot\underline{x} - \beta t)]$ (p pressure, ρ density, $\underline{a} = (a_1, 0, a_3)$ wave vector, the equilibrium quantities are denoted by bar, the perturbations by asterisk) we find a fourth-order differential equation for B_2 (asterisk is dropped)

$$B_2^{(4)} + a_3 B_2^{(3)} + a_2 B_2'' + a_1 B_2' + a_0 B_2 = 0 \quad (5)$$

where the coefficients are given by

$$a_0 = -a^2\Big[-N'' + 2\frac{N'^2}{N^2} - a^2 + \frac{\gamma\bar{\rho}''i}{\bar{\rho}\beta^2} + \frac{a^2 g_2\bar{\rho}'}{\beta^2\bar{\rho}} - \frac{\gamma\bar{\rho}'i}{\bar{\rho}\beta^2}\Big(\frac{N'}{N} - \frac{\bar{\eta}'}{\bar{\eta}}\Big) +$$

$$- 2\frac{\bar{\eta}'N'}{\bar{\eta}N} + \frac{\bar{\eta}''}{\bar{\eta}} - \frac{\beta\mu}{i\bar{\eta}} + \frac{sN}{i\bar{\rho}\beta^2\mu\bar{\eta}}\Big] - \frac{\mu N}{i\bar{\eta}}\Big(\frac{1}{N}\Big)'' - \frac{\mu}{i\bar{\rho}\bar{\eta}}\Big(\frac{i\gamma\bar{\rho}''}{\beta} + \frac{a^2}{\beta}g_2\bar{\rho}'\Big) +$$

$$+ \frac{\mu\bar{\rho}'N'\gamma}{\beta\bar{\rho}\bar{\eta}N} - \frac{Ns''}{i\bar{\rho}\beta^2\mu\bar{\eta}}$$

$$a_1 = -a^2\Big(-2\frac{N'}{N} + \frac{\gamma\bar{\rho}'i}{\bar{\rho}\beta^2} + 2\frac{\bar{\eta}'}{\bar{\eta}}\Big) + \frac{2\beta\mu N'}{i\eta N} - \frac{\mu\gamma\bar{\rho}'}{\bar{\eta}\beta\bar{\rho}}$$

$$a_2 = -2a^2 - N'' + 2\frac{N'^2}{N^2} + \frac{\gamma\bar{\rho}''i}{\bar{\rho}\beta} + \frac{a^2 g_2\bar{\rho}'}{\beta^2\bar{\rho}} - \frac{\gamma\bar{\rho}'i}{\bar{\rho}\beta^2}\Big(\frac{N'}{N} - \frac{\bar{\eta}'}{\bar{\eta}}\Big) +$$

$$- 2\frac{\bar{\eta}'N'}{\bar{\eta}N} + \frac{\bar{\eta}''}{\bar{\eta}} - \frac{\beta\mu}{i\bar{\eta}} + \frac{sN}{i\bar{\rho}\beta^2\mu\bar{\eta}}$$

$$a_3 = -2\frac{N'}{N} + \frac{\gamma\bar{\rho}'i}{\bar{\rho}\beta^2} + 2\frac{\bar{\eta}'}{\bar{\eta}}, \qquad N = \beta\mu s - i\bar{\eta}'s', \qquad \gamma = (\underline{a}\cdot\underline{g}).$$

In the case of neutral stability ($\beta = 0$) Eq. (5) reduces to

$$B_2''\Big(1 - \frac{i\mu\bar{\rho}'\gamma}{ss'}\Big) - B_2\Big(\frac{s''}{s} + a^2 + a^2\gamma\bar{\rho}'\frac{i\mu}{ss'}\Big) + \frac{i\bar{\eta}\mu}{s}\{(-\gamma\bar{\rho}'' +$$

$$+ ia^2 g_2\bar{\rho}')\frac{b}{\bar{\eta}'s'} - \gamma\bar{\rho}'\Big[\frac{b}{\bar{\eta}'s'}\Big]'\} = 0, \text{ where } b = B_2'' - a^2 B_2. \quad (6)$$

This equation shows that the region of neutral stability depends on the resistivity gradient $\bar{\eta}'$ and on the curvature of $\bar{\eta}$ (according to $\bar{\eta}''$). These resistivity-curvature instabilities are coupled with the gravitational-force component in the plane of the magnetic field. The region of neutral stability of a homogeneous sheet does not depend on $\bar{\eta}'$.

3. Overstable solutions

Treating a homogeneous sheet in a magnetic field of constant shear, Eq. (5) can be reduced to a selfadjoint differential equation of second order for b (b defined in (6))

$$(\bar{\eta}^2 b')' + b[-a^2\eta^2 + \eta\eta'' + i\beta\mu\eta + (s^2\eta/i\beta)] = 0. \quad (7)$$

Multiplying (7) by the complex conjugate of b, integrating across the plasma slab, and assuming homogeneous boundary conditions we get from (7) a quadratic equation for $\bar{\beta}$ ($\bar{\beta} = i\beta$) which has complex solutions if the condition

$$\left|\frac{\int\bar{\eta}^2|b'|^2dx_2}{\int\bar{\eta}^2|b|^2\,dx_2} + a^2 - \frac{\int\bar{\eta}\bar{\eta}''|b|^2dx_2}{\int\bar{\eta}^2\,|b|^2dx_2}\right| < 2\sqrt{\frac{\mu}{\bar{\rho}}}\,|s|\left|\frac{\int\bar{\eta}|b|^2dx_2}{\int\bar{\eta}^2|b|^2dx_2}\right| \quad (8)$$

is fulfilled. Therefore oscillatory increasing or decreasing modes exist. This condition shows that overstable modes are associated with the second derivative of the resistivity and consequently depend on whether the curve $\bar{\eta}(x_2)$ has a positive or negative curvature. Therefore we see that, since the left-hand-side of (8) is positive semi-definite, overstable modes occur where s is different from zero. So it might be pointed out that the absence of overstable modes found by other authors (e.g. [1]) is due to the fact that making an expansion of the solution about the point where $s = 0$ [1] and breaking off after the first or second term, results in losing the effect of resistivity curvature. Defining local mean quantities (denoted by $\langle\ \rangle$) similar to Pridmore-Brown [3] the condition for overstability derived from (8) reads in a local sense

$$\left|\left\langle\frac{|b'|^2}{|b|^2}\right\rangle + a^2 - \left\langle\frac{\bar{\eta}''}{\bar{\eta}}\right\rangle\right| < 2\sqrt{\frac{\mu}{\bar{\rho}}}\left\langle\frac{s}{\bar{\eta}}\right\rangle. \quad (8')$$

The inequality (8') contains the unknown function b. In order to make quantitative conclusions we have to solve (7). An approximate solution of (7) valid also in the case of high resistivity gradients, provided the wave number a is sufficiently high, reads

$$b(x_2) = \frac{1}{\bar{\eta}q^{1/4}}\Big[c_1\exp\Big\{1\int_{\bar{x}_2}^{x_2}(1 + \varepsilon/2)\sqrt{q}\,d\xi\Big\} +$$

$$+ c_2\exp\Big\{-1\int_{\bar{x}_2}^{x_2}(1 + \varepsilon/2)\sqrt{q}\,d\xi\Big\}\Big] \quad (9)$$

with $q(x_2) = -a^2 + \frac{\beta\mu}{i\bar{\eta}} + \frac{s^2}{i\beta\bar{\rho}\bar{\eta}}$ and $\varepsilon = q^{-3/4}\frac{d^2}{dx_2^2}(q^{-1/4})$.

This approximate solution holds in a region where $q \neq 0$ fulfills certain conditions (c_1, c_2 constants of integration).

A general criterion for overstability due to resistivity gradients (curvature) and an approximate solution of the stability equation were derived.

The author wishes to thank Professor F. Cap for many discussions. This work has been sponsored in part by the United States Government under Contract No. F61052-67-C-0014.

[1] H.P.Furth, J.Killeen, M.N.Rosenbluth, Phys.Fluids 6, 459 (1963)
[2] B.B.Kadomtsev, Nucl.Fusion 1, 286 (1961)
[3] D.C.Pridmore-Brown, Phys.Fluids 11, 1789 (1968)
[4] R.J.Hosking, Phys.Fluids 10, 1654 (1967)
[5] D.A.McPherson, D.C.Pridmore-Brown, Phys.Rev.Let. 19, 1279 (1967)

DIAMAGNETIC DISTORTION OF THE CONFINING MAGNETIC FIELDS

N.A.Khizhnjak

Physical Thechnical Institute of the Academy of Science Ukr.S.S.R., Kharkov, U.S.S.R.

The forming of plasma in the external magnetic field $\vec{H}_0(\vec{r})$ disturbed this field and created some real field $\vec{H}(\vec{r})$ wich did not concied with the $\vec{H}_0$. The discrepancy between the fields $\vec{H}$ and $\vec{H}_0$ can arise due to induction processes and also due to the plasma diamagnetism. It is easy to see that the discrepancy between $\vec{H}$ and $\vec{H}_0$ after the damping of the induction currents was mainly due to the thermal diamagnetism of plasma and had the value of order of $\beta = \frac{8\pi nkT}{H^2}$. The determination of the field $\vec{H}$ depending upon the plasma parameters and geometry is the very complicated and actual problem for both $\beta \ll 1$ and $\beta \sim 1$ cases. Here we consider the problem of distortion of the confining field by the diamagnetic currents in plasma.

Magnetic moment of the volume unite collisionless magnetized plasma is equal to

$$\vec{\mathcal{M}} = \frac{nmv_\perp^2}{2H^2}\vec{H} = \frac{nkT}{H^2}\vec{H},$$

and

$$\vec{B} = \left(1 + \frac{4\pi nkT}{H^2}\right)\vec{H},$$

where $\vec{H}$ - the distorted magnetic field in plasma. To find $\vec{H}$ one can use integral equation

$$\vec{H}(\vec{r}) = \vec{H}_0(\vec{r}) + \frac{1}{8\pi}\,\mathrm{grad}\,\mathrm{div}\int_V \beta(\vec{r}')\vec{H}(\vec{r}')\frac{d\vec{r}'}{|\vec{r}-\vec{r}'|}, \qquad (I)$$

where V - plasma volume.

It is easy to see that $\mathrm{rot}\,\vec{H}=0$, $\mathrm{div}\,\vec{B}=0$ at $\vec{r}\in V$, $\mathrm{rot}\,\vec{H}=0$, $\mathrm{div}\,\vec{H}=0$ at $\vec{r}\ni V$.

From (I) one can see, that real distortion of the field had the value of order β, but the important role played the plasma geometry. The solution of the integral equation at $\beta \ll 1$, can be found by the iteration method. The first approximation on β gives

$$\vec{H}(\vec{r}) = \vec{H}_0(\vec{r}) + \frac{1}{8\pi}\,\mathrm{grad}\,\mathrm{div}\int_V \beta(\vec{r}')\vec{H}_0(\vec{r}')\frac{d\vec{r}'}{|\vec{r}-\vec{r}'|}. \qquad (2)$$

When $\beta \sim 1$, one need to look for the new method of solving the equation (I).

I. The uniform ellipsoidal plasma β = const at $r \in V$. The components of external unperturbed magnetic field in the plasma occupied region are the power function of cartesian coordinates:

$$H_{oi} = \sum a_{oi}^{(p,q,r)} x^p y^q z^r, \qquad (3)$$

$$\max\,(p+q+r) = n.$$

In this case the $\vec{H}$ field has components at $r \in V$:

$$H_i = \sum a_i^{(p,q,r)} x^p y^q z^r, \qquad (4)$$

$$\max\,(p+q+r) = n.$$

Really the volume potential has the form

$$\int_V \frac{x'^p y'^q z'^r\, dr'}{|\vec{r}-\vec{r}'|} = P_{n+2}(x,y,z), \qquad (5)$$

where p+q+r=n, for internal points of ellipsoid, and also is the power function of the cartesian coordinates in power n+2. After substitution of (3) and (4) in (I) one can see that in accordance with (5) the polinom power increases by integral on two units and second order differential operator decreases this power also on two units. Comparing coefficients at the equal power terms, we obtain the system of the linear algebraic equations for coefficients $a_i^{(p,q,r)}$.

As example we consider the distortion of the uniform field by the uniform ellipsoidal plasma. In this case from (I) it follows

$$H_i = \frac{H_{oi}}{1 + \frac{3V}{2}\cdot\frac{n_0kT}{H^2}\cdot I_i}, \qquad (6)$$

where $V = \frac{4\pi}{3}abc$ - the ellipsoid volume, I_i - Dirichlet coefficients for the uniform ellipsoid potential

$$P_2(x,y,z) = I_0 - \pi abc\left(I_1 x^2 + I_2 y^2 + I_3 z^2\right).$$

In the simple case of the plasma sphere $I_1 = I_2 = I_3 = \frac{2}{3a^3}$, from (6) it follows

$$H = \frac{H_0}{2}\left(1 + \sqrt{1 - \frac{16\pi}{3}\cdot\frac{n_0kT}{H_0^2}}\right).$$

The maximal density of confined plasma is

$$\frac{8\pi n_0kT}{H_0^2} = \frac{3}{2},$$

the total magnetic moment of plasma with maximal density wich depended upon the thermal particle motion is

$$\vec{\mathcal{M}} = \frac{3V}{4\pi}\vec{H}_0.$$

The self magnetic field of diamagnetic currents decreased the initial magnetic field on the value

$$H' = -\frac{1}{2}H_0.$$

When the plasma geometry is spheroidal with $I_2 = I_3$, $I_1 + I_2 = 2I_0$, $I_1 - I_2 = 2\delta$, $\delta \ll I_0$, $H = \frac{1}{2}H_0\left\{1 + \left[1 - 6I_0V\frac{n_0kT}{H_0^2} + 6\delta V\frac{n_0kT}{H_0^2}\cdot\frac{H_{0x}^2 - H_{0z}^2}{H_0^2}\right]^{1/2}\right\}$,

where $H_{0z}^2 = H_{0y}^2 + H_{0z}^2$, and

$$\vec{\mathcal{M}} = \frac{\vec{H}_0}{3\left[I_0 - \delta\frac{H_{0x}^2 - H_{0z}^2}{H_0^2}\right]}.$$

2. Now consider the uniform ellipsoidal plasma in mirror magnetic field $0 < z < L$,

$H_{z0} = H_0 + (H_m - H_0)I_0(\kappa z)\cos\kappa z$, $H_{z0} = (H_m - H_0)I_1(\kappa z)\sin\kappa z$, where $\kappa = \frac{\pi}{L}$, H_m - mirror field, H_0 - field in the centre between the mirrors. Plasma was situated in the region with $|\kappa(\frac{L}{2} - x)| \ll 1$, $\kappa z \ll 1$, so

$$H_{x0} = \frac{\pi}{2L}(H_m - H_0)x, \quad H_{y0} = \frac{\pi}{2L}(H_m - H_0)y,$$

$$H_{z0} = H_0 - \frac{\pi}{L}(H_m - H_0)z.$$

Internal magnetic field in plasma with definite β equals to

$$H_x = \alpha^{(1,0,0)}x, \quad H_y = \alpha^{(0,1,0)}y,$$

$$H_z = \frac{H_0}{1 + \frac{abc\beta}{4\pi}I_3} + \alpha^{(0,0,1)}z; \quad \alpha^{(1,0,0)} = \alpha^{(0,1,0)}$$

So inside the plasma the magnetic field has the structure the same as in mirror machine without plasma, but the mirror rotio $\frac{H_m - H_0}{H_m}$ becames

$$\left(\frac{H_m - H_0}{H_0}\right)_p = \frac{H_m - H_0}{H_0}\cdot\frac{1 + \beta F_1}{1 - \beta F_2},$$

where F_1, F_2 - are the functions of the ellipsoid semiaxis.

substituted paper

ENERGY CRITERION FOR STABILITY OF EQUILIBRIUM PLASMA AND ITS APPLICATIONS

by

J. Lacina

INSTITUTE OF PLASMA PHYSICS, Czech. Academy of Sciences

Nademlýnská 600, Prague 9 - Czechoslovakia

Exact criteria for stability of plasma (given by a stationary distribution function) in an external non-uniform magnetic field are derived using the variational method rigorously. The discussion concerns any kind of low-β collisionless plasma; no other restriction with respect to plasma parameters occures in this formulation. It is also important to note that the criteria derived in this paper recpect non-linear motion of particles in perturbed fields so that they are more general than those derived from linearized equations (e.g. from linearized Vlasov equation).

The motion of charged particles in an external non-uniform magnetic field is given by a Hamiltonian

$$\mathcal{H}_0 = E_0(P_k) \quad , \quad P_i(q_i, p_i) = \text{const.} \quad ; \tag{1}$$

and the stationary distribution function $f = F(P_k)$, where F is an arbitrary function. Perturbations in the stationary distribution give rise to perturbations in electromagnetic field. We discuss here such perturbations for which two time-independent integrals of motion exist:

$$\varphi_1(P_k) = \text{const.} \quad , \quad \varphi_2(P_k) = \text{const.} \tag{2}$$

We use now new canonical variables J_k, w_k, where $J_1 = \varphi_1$, $J_2 = \varphi_2$.

The perturbed (non-stationary) distribution functions to a stationary state $F(J_k)$ are given by the perturbed integrals of motion in the following way:

$$f = F(J_1, J_2, J_3 + \Psi) \quad , \quad J_1 = \text{const.} \quad , \quad J_2 = \text{const.} \quad , \quad J_3 + \Psi(J_k, w_3; t) = \text{const.} \tag{3}$$

The problem is now formulated as follows (see also [3]): Stability is determined by the variation of the total kinetic energy of all particles in the stationary state

$$\delta W_K = \int E_0(J_k)\left[F(J_1, J_2, J_3 + \delta\Psi) - F(J_k)\right] d^3J_k\, d^3w_k \tag{4}$$

under the following accessory condition

$$S = \int G\left[F(J_1, J_2, J_3 + \delta\Psi), J_1, J_2\right] d^3J_k\, d^3w_k = \text{const.} \tag{5}$$

where G is an arbitrary function of the distribution and of the constants of motion J_1, J_2.

This formulation gives us the following stability criterion: The necessary and sufficient condition for the stationary distribution $F(J_k)$ in the given external field represented by the kinetic energy $E_0(J_k)$ to be stable against a perturbation of motion $\delta\Psi$ is

$$\int \frac{\partial E_0}{\partial J_3} \cdot \frac{\partial F}{\partial J_3} \cdot (\delta\Psi)^2 d^3J_k\, d^3w_k < 0 \quad ; \tag{6}$$

if in this inequality the opposite sign holds for a certain perturbation then the given distribution is unstable with respect to this perturbation.

We get the following sufficient conditions for stability from the criterion (6):

1) The distribution $F(J_k)$ is stable in the field represented by $E_0(J_k)$ if for all values J_k it holds

$$\frac{\partial E_0}{\partial J_3} \cdot \frac{\partial F}{\partial J_3} < 0 \quad ; \tag{7}$$

the distribution is unstable if the opposite sign holds in this inequality for all values J_k.

2) In case the perturbed motion $\delta\Psi$ does not depend on constants J_1, J_2 then the sufficient condition for stability has the following integral form:

$$\int \frac{\partial E_0}{\partial J_3} \cdot \frac{\partial F}{\partial J_3}\, dJ_1\, dJ_2\, dw_1\, dw_2 < 0 \quad ; \tag{8}$$

the distribution is unstable if the opposite sign holds in this inequality for all values J_3.

The most simple application of this approach is in the case of electrostatic perturbations propagating in homogeneous plasma without external field. If perturbing potential propagates in x-direction then $p_y = \text{const.}$, $p_z = \text{const.}$. Using the criterion (8) we get the following condition for plasma stability:

$$\frac{df_0}{dp_x} \cdot p_x < 0 \quad , \text{ where } f_0(p_x) = \int F(p_x, p_y, p_z)\, dp_y\, dp_z \quad .$$

This result is in full agreement with the Landau damping and gives a physical explanation of it (or of growing of waves) from the energy point of view.

Further we shall deal with stability of plasma against interchanges. First, we shall deal with axisymmetric mirrors. For the motion of particles and stationary distributions in this case see [1,2]. As far as the field of perturbations is concerned, we make here the usual assumption (see [5,7]): the Larmor radius and periods of cyclotron and longitudinal oscillations are small compared to wave lengths and periods of a perturbation. Thus the Larmor magnetic flux p_1 and the longitudinal invariant J_3 are adiabatic constants of motion:

$$p_1 \approx \frac{mc}{eB}\frac{\partial \mathcal{H}_\perp}{\partial B} \approx \text{const.} \quad , \quad J_3 = \oint \sqrt{2m(E_0 - \mathcal{H}_\perp)}\, h_3\, dq_3 \approx \text{const.}$$

while the guiding center magnetic flux p_2 changes due to a perturbation.

Using (7) we get: a configuration $F(p_1, p_2, J_3)$ is stable if

$$\frac{\partial E_0}{\partial p_2} \cdot \frac{\partial F}{\partial p_2} < 0 \tag{9}$$

for all p_1, p_2, J_3 ; here $E_0(p_1, p_2, J_3)$ is the unperturbed Hamiltonian. Note that expression $\partial E_0 / \partial p_2$ is the average drift frequency. On the usual assumption that the perturbation field changes the position of the guiding center p_2 in the transverse direction independently of the constants p_1, J_3 we get the following integral criterion from (8)

$$\int \frac{\partial E_0}{\partial p_2} \cdot \frac{\partial F}{\partial p_2} \cdot dp_1\, dJ_3 < 0 \tag{10a}$$

or

$$\iint \left[\frac{\partial F}{\partial p_2} + \frac{\partial F}{\partial E_0} \cdot \frac{q_2(T_3)}{T_3}\right] \cdot q_2(T_3)\, dp_1\, dE_0 < 0 \tag{10b}$$

where $q_2(T_3)$ = the drift angle during the longitudinal period T_3 ; the distribution F, $q_2(T_3)$ and T_3 being functions of E_0, p_1, p_2.

A stable configuration is formed by particles whose drift angle $q_2(T_3)$ is positive. A negative curvature of field lines must predominate for a positive drift angle. A magnetic field geometry with predominant negative curvarure is easy to realize by combining a homogeneous field with the field of a narrow current coil that produces a magnetic field in the opposite direction. We have shown the existence of stable configurations against interchanges in such fields in [4]. However, any axisymmetric configuration of mirror type stable against interchanges is formed by contrastreaming beams in the longitudinal direction so that the interchange instability is replaced by beam instability, as it follows generally from the criterion (10b).

We shall consider now a general magnetic field in which particle drift orbits are closed. Ioffe stabilized mirror fields and some toroidal fields are of this type. Two adiabatic constants of motion in perturbed fields exist here on the same assumption as previously: the magnetic moment $\mu \approx \text{const.}$, longitudinal invariant $J_3 \approx \text{const.}$. The perturbation potential changes the drift surfaces (guiding center orbits) $\phi(\alpha, \beta)$. We get a sufficient condition for stability from (7) as follows

$$\frac{\partial E_0}{\partial \phi} \cdot \frac{\partial F}{\partial \phi} < 0 \tag{11}$$

where $F(\mu, \phi, J_3)$ is a stationary distribution, $E_0(\mu, \phi, J_3)$ = the unperturbed Hamiltonian. An equivalent condition

$$\frac{\partial F}{\partial E_0} < 0 \quad , \qquad \text{where } F(E_0, \mu, J_3) \tag{12}$$

follows from the Eq. (11). The condition (12) has been first derived by Taylor [7] by means of an intuitive approach.

As we see, the supplementary condition of Rutherford and Frieman [6], stating that $dF/dE_0 < 0$ is also required, is unnecessary (superfluous).

Using (8) we get the following integral criterion for stability

$$\int \frac{\partial E_0}{\partial \phi} \cdot \frac{\partial F}{\partial \phi}\, d\mu\, d\phi\, dJ_3 < 0$$

which must be satisfied for all ϕ. This integral criterion replaces the integral criteria derived by Taylor [7] (considered as necessary and sufficient conditions by him); from the point of view of our theory Taylor's integral criteria are incorrect.

REFERENCES

[1] Lacina J., Nuclear Fusion 6, 268 (1966).

[2] Lacina J., Nuclear Fusion 6, 276 (1966).

[3] Lacina J., IPPCZ - 113 (1968).

[4] Lacina J., IPPCZ - 115 (1968).

[5] Rosenbluth M.N., Longmire C.L., Ann. Phys. (N.Y.) 1, 120 (1957).

[6] Rutherford P.H., Frieman E.A., Phys. Fluids 11, 252 (1968).

[7] Taylor J.B., Phys. Fluids 7, 767 (1964).

Exact Treatment for the Instability of a Class of Inhomogeneous Equilibrium Plasmas

by

R. Croci and R. Saison

Institut für Plasmaphysik, 8046 Garching bei München, Germany

An infinite equilibrium plasma homogeneous in the y and z directions and contained in the x direction by a magnetic field $B = \hat{i}_z B_z(x)$ is studied. We consider the following class of equilibrium distribution functions:

1) $f_0 = g(v_\perp^2, v_{//}^2) \exp\left\{-\alpha \left| v_y + \int_0^x \frac{e}{m} B_z(x')dx' \right|\right\}$, $\alpha > 0$

$B_z = B_0 - b(x)$ with $\int_{-\infty}^{+\infty} b(x)\,dx < \infty$ which leads to density profiles everywhere infinitely differentiable. The stability of such a configuration against electrostatic perturbations is studied.

Let us assume a quantity $F(x,t)$ to have a Laplace transform, i.e. there exists a finite γ such that $F(x,t)\,e^{\gamma t}$ is integrable.

A necessary and sufficient condition for $F(x,t)$ to grow indefinitely in time is that the transform $\hat{F}(x,\omega) = \int_0^\infty e^{i\omega t} F(x,t)$ have a singularity (not necessarily a pole) in the half-plane $\mathrm{Im}\,\omega \geq 0$. The same condition is true for the Fourier transform: $\hat{F}(\underline{K},\omega) = \int d^3r\, e^{i\underline{K}\cdot\underline{r}} \hat{F}(x,\omega)$ of $\hat{F}(x,\omega)$ with K real.

We therefore deduce an equation for the Laplace-Fourier transform of the electric potential and look for the singularities of this potential without explicitly solving the equation.

A necessary and sufficient condition is obtained for the existence of singularities in the form:

(2) $$\mathbb{D}(\omega, \underline{K}) = 0$$

where $\mathbb{D}$ is a functional of the distribution f_0 and is independent of the initial conditions.

If the linearized Vlasov equation is solved with the method of characteristics and the result substituted in the Poisson equation, the following integral equation is obtained for the electric potential :

(3) $$K^2 \phi(\omega,\underline{K}) = \phi^e(\omega,\underline{K}) + \int_{-\infty}^{+\infty} dK'_x\, \mathbb{K}(\omega,\underline{K}|\underline{K}')\,\phi(\omega,\underline{K}')$$

where $\underline{K} = (K_x, K_y, K_z)$, $\underline{K}' = (K'_x, K_y, K_z)$

$$\phi^e(\omega,\underline{K}) = \sum_{j=e,i} 4\pi e_j \int d^3r \int_0^\infty dt\, e^{i\omega t}\, e^{i\underline{K}\cdot\underline{r}} \int d^3v\, f_{0j}(\underline{r},\underline{v},t'=0)$$

f_{0j} = initial perturbation for species j

$$\mathbb{K}(\omega,\underline{K}|\underline{K}') = -\frac{i}{4\pi} \sum_{j=e,i} \frac{4\pi e_j^2}{m_j} \int_{-\infty}^{+\infty} dx \int d^3v \int_0^\infty du\, e^{i\omega u}\, e^{i(K_x - K'_x)x}\, e^{i\underline{K}'\cdot(\underline{r}-\underline{R})}\, \underline{K}'\cdot\nabla_v f_{0j}(X,V)$$

X, V describe the unperturbed orbits (position and velocity respectively) of the particles between initial time $t' = 0$ and time $t' = x$. Let $\mathbb{K}$ be written as:

$$\mathbb{K} = \mathbb{K}^- - \mathbb{K}^+$$

where $\mathbb{K}^\mp = +\frac{i}{4\pi} \sum_{j=e,i} \frac{4\pi e_j^2}{m_j} \int_{x_c}^{\mp\infty} dx \int d^3v \int_0^\infty du \cdots$ with $x_c = x_c(v_y, B_z)$ and such that $v_y + \int_0^{x_c} \frac{e}{m} B_z(x')dx' = 0$

If B_z were constant ($B_z = B_0$) and only f_0 depended on x (which is an approximation valid when $\beta \ll 1$), $(\underline{r} - \underline{R})$ would be independent of x. Then

$$\mathbb{K}^\mp = \frac{C^\mp(\underline{K}', \underline{K}, \omega)}{K'_x - (K_x \mp i\alpha)} \quad , \quad \alpha = \alpha \left|\frac{e}{m}\right|$$

where the $C^\mp$ are entire functions if, as we assume in the following $\lim_{v_\perp \to \infty} g(v_\perp^2, v_{//}^2) \exp\{\beta v_\perp\} = 0$, $\beta = \text{const.} > 0$

when B_z depends on x, then: $\mathbb{K}^\mp = \frac{C^\mp}{K'_x - (K_x \mp i\alpha)} + G^\mp$

$$G^\mp = -\frac{i}{4\pi} \sum_{j=e,i} \frac{4\pi e_j^2}{m_j} \int d^3v \int_{x_c}^{\mp\infty} dx \int_0^{+\infty} du\, e^{i\omega u}\, e^{-i(K'_x - K_x)x} \left[e^{\frac{i\underline{K}'\cdot(\underline{r}-\underline{R})}{\underline{K}'\cdot\nabla_v}} \underline{K}'\cdot\nabla_v f_{0j}(X,V) - \lim_{|x|\to\infty} e^{\frac{i\underline{K}'\cdot(\underline{r}-\underline{R})}{\underline{K}'\cdot\nabla_v}} \underline{K}'\cdot\nabla_v f_{0j} \right]$$

Further analysis of $G^\mp$ requires knowledge of the form of $b(x)$

We shall consider two classes of $G^\mp$ corresponding to the following classes of $b(x)$ (always with the assumption $\int_{-\infty}^{+\infty} b(x)dx < \infty$)

1) $b(x)$ goes to zero more rapidly than $e^{-c|x|}$ when $|x| \to \infty$ for all positive c. Here $G^\mp$ is an entire function.

2) $b(x)$ goes to zero more slowly than $e^{-\varepsilon|x|}$, when $|x| \to \infty$ for an arbitrary small $\varepsilon > 0$. Then $G^\mp$ has a branch point at $K'_x = K_x \mp i\alpha$ with: $\lim_{K'_x = K_x \mp i\alpha} (K'_x - K_x \pm i\alpha)\, G^\mp = 0$

The problem would be more complicated with other classes of $b(x)$, but the mean line of the method would remain the same

It can be shown that, when has a singularity at $K_x = K_0(\omega)$ ($\mathrm{Im}\,K_0 = c$), it is also singular at $K_x = K_0 \pm in\alpha$, $(n = 1, 2, \ldots)$

The necessary and sufficient condition for the existence of a singularity at $K_x = K_0(\omega)$ is:

$$\mathbb{D}\left(\frac{K_0}{i\alpha}\right) = 0 \text{ where:}$$

$$\mathbb{D}(\sigma) \equiv \int_{iv_{1_1}-\infty}^{iv_{1_1}+\infty} dv\, \frac{H_+(v)\, e^{-i\sigma v}}{e^{-iv} - 1} + \int_{iv_{1_2}-\infty}^{iv_{1_2}+\infty} dv\, \frac{H_-(v)\, e^{-i\sigma v}}{e^{-iv} - 1}$$

$$H_+(v) = \frac{1}{i\alpha} \int_0^{+i\infty} h(K_0)\, e^{iK_0 v/\alpha}\, dK_0 \,, \quad H_-(v) = \frac{1}{i\alpha} \int_{-i\infty}^{c} h(K_0)\, e^{iK_0 v/\alpha}\, dK_0$$

$$h(K_0) = \log\left[\frac{c^- e^{K_x^2 \rho^2}}{K^2}\right]_{\substack{K'_x = K_0 \\ K_x = K_0 + i\alpha}} - \log\left[\frac{c^+ e^{K_x^2 \rho^2}}{K^2}\right]_{\substack{K'_x = K_0 \\ K_x = K_0 - i\alpha}}$$

$$\rho^2 = v_\perp^2 / \Omega^2 \quad , \quad \Omega = \left|\frac{e}{m} B_0\right|$$

In the quasi-neutrality approximation, the left hand side in (3) drops out. Consequently, the whole set of singularities $K_0 \pm in\alpha$ appears no more with the singularity $K_0(\omega)$ and the dispersion relation degenerates into the form:

$$C^\mp(K'_x = K_x \mp i\alpha\,,\, K;\omega) = 0$$

This work was performed under the terms of the agreement on association between the Institut für Plasmaphysik and EURATOM.

MICROWAVE INTERFEROMETRIC STUDIES OF A PLASMA BOUNDARY

by
N.I. Vinogradov* and E. Tennfors
Royal Institute of Technology, 100 44 Stockholm, Sweden

1. Introduction

Microwaves of a frequency lower than the plasma frequency are reflected at the boundary of a plasma. The phase shift of the reflected beam depends on the position of the boundary and on the electron density distribution in the boundary region. Lehnert (1,2) has earlier suggested the use of microwave interferometry for the measurement of the displacement of a plasma boundary due to centrifugal or thermal pressure. The aim of this work is to investigate the behaviour of the boundary and its expansion due to the centrifugal force of a rotating plasma.

During the final period of a decaying plasma the density is low and the microwaves pass through the plasma. When the waves are reflected by a metal wall after having passed the plasma, the phase shift becomes an integrated effect along the whole plasma region.

2. Experimental arrangement

The rotating plasma device F I used in the present experiments has been described earlier (3). The average magnetic field in the equatorial plane $\bar{B}_o$ is varied from 0.32 Vsec Vsec/m^2 to 0.57 Vsec/m^2. The discharges are run with hydrogen at initial gas pressures p_o from 24×10^{-3} mm Hg to 53×10^{-3} mm Hg. The plasma confinement region consists of the volume situated between the field lines which touch the anode rings and the cathode plate. In the equatorial plane the calculated vacuum field gives the inner and the outer boundary radii r_{o1}= 0.185 m and r_{o2}= 0.260 m respectively. The microwave beam enters the discharge chamber radially through a quartz window in the equatorial plane. When the density is low the beam is reflected by the stainless steel box containing the main coil at the centre of the device.

3. Microwave interferometer

The block diagram of the interferometer is shown in Fig. 1. The horn is placed in front of the window. The amplitude of the wave reaching the crystal depends on the difference in phase shift between the two paths. A change in the detector output signal between consecutive maxima corresponds to a change in phase shift of 2π.

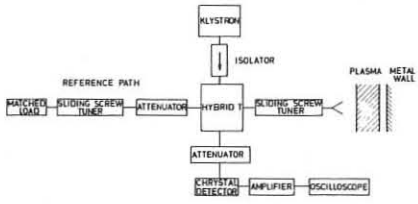

Block diagram of 8mm microwave interferometer.

Fig. 1

For 8 mm waves the critical density which makes the plasma frequency equal to the wave frequency is $n_{cr}= 1.75\times10^{19}$ m^{-3}. The waves are strongly absorbed in a plasma with density close to the critical value. When $n_{max}>n_{cr}$ the beam is reflected by the plasma. When n_{max} approaches n_{cr} the region of high absorption increases in thickness and the fringe amplitude decreases. When n_{max} passes n_{cr} and becomes lower we suddenly get a second mode of operation with transmission through the plasma. Further decrease in density increases the fringe amplitude. This change in amplitude is illustrated in Fig. 2 where the minimum separates the two modes of operation.

The boundary changes direction of motion during the discharge. There are three ways to determine the direction from the detector output signal:

a) The beam is diverging and the reflecting surface is convex. This gives a decreasing amplitude with increasing distance from the horn to the plasma boundary.

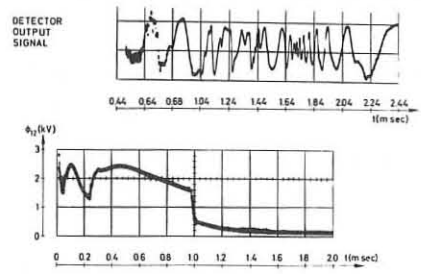

Fig. 2 $\bar{B}_o$= 0.43 Vsec/m^2

b) Usually the detector output signal does not appear at a maximum or minimum at the moment when the motion changes direction.

c) Multiple reflections distort the fringes and make the fringe chape depend on both the position and the direction of motion of the boundary. The distorted fringe shape gives a means of relating interferograms from separate discharges.

4. Experiments

The well-defined phase shift during the main part of the discharge indicates that the boundary is at least macroscopically stable.

The measured centrifugal expansion is larger than expected from theory and measured by probes (3). The discrepancy may be explained by the fact that the probes were sensitive only to densities much higher than n_{cr}. The expansion measured by microwaves then includes the change in width of the boundary layer. The measured expansion is delayed with respect to the voltage change by 0.1 to 0.2 msec. This indicates that the weakly ionized plasma where the waves are reflected does not instantly follow the motion of the magnetic field lines.

When the velocity of rotation is slowly decreased a level is reached below which the plasma suddenly changes state (4,5). Fig. 3 shows that the boundary becomes irregular somewhat before this is taking place. After the voltage step at $t\approx1.9$ msec the fringes get clear and show that the waves pass through the plasma. This means that the density is everywhere less than $n_{cr}= 1.75\times10^{19}$ m^{-3}.

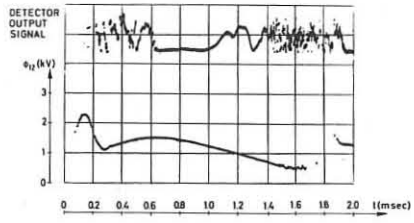

Fig. 3 $\bar{B}_o$= 0.43 Vsec/m^2

The total number of fringes after $n_{max}= n_{cr}$ is a measure of the plasma dimension along the microwave path at the time when $n_{max}= n_{cr}$. The decay time of the average density can then be estimated from an assumed density distribution assuming constant dimensions.

Simultaneous measurements at shorter wave-lengths are being planned. They are expected to give more accurate measurements both of the boundary behaviour and of the plasma decay.

5. References

(1) B. Lehnert, Plasma Phys. 10 (1968) 281.
(2) B. Lehnert, Electron- and Plasma Physics, Royal Institute of Technology, Rep. 67-26 (1967).
(3) J. Bergström, S. Holmberg, B. Lehnert, Plasma Physics and Controlled Nuclear Fusion Research, Vol. I, p. 341, I.A.E.A., Vienna (1966).
(4) B. Lehnert, Arkiv f. Fysik 38 (1968) 499.
(5) B. Lehnert, J. Bergström, S. Holmberg, see paper of these proceedings.

* Guest Professor from the A.F. Ioffe Physico-Technical Institute, Leningrad, U.S.S.R. during October-December 1968.

MINIMUM TEMPERATURE AND POWER INPUT OF A FULLY IONIZED DENSE PLASMA

by

B. Lehnert, J. Bergström and S. Holmberg

ROYAL INSTITUTE OF TECHNOLOGY
100 44 Stockholm 70, Sweden

1. Introduction

Experimental studies of fully ionized high-density plasmas are important to fusion research at least for two reasons. Firstly, such plasmas are likely to be used in future reactors. Secondly, the plasma does not necessarily have to be surrounded by ultra-high vacuum, but can be embedded in a neutral gas blanket which is prevented from interaction with the hot plasma core (1). In such a system there are small power losses due to neutral gas interaction as compared to the power generated by a thermonuclear plasma. Still the same losses become important to the heat balance in experiments where only limited power resources are available.

2. Theoretical Considerations

In a stationary state the particle losses from a fully ionized plasma have to be balanced by a back-flux of ions and electrons which are re-ionized in the surrounding partially ionized boundary regions. Since the ionization rate drops with the temperature there exists a minimum value of the latter, and a corresponding minimum power input, below which a fully ionized stationary plasma cannot be sustained (2).

Fig. 1 gives an example under conditions roughly corresponding to the rotating plasma devices F I and F II (3, 4) at a mean density $n = 10^{21}$ m^{-3} of hydrogen. P and Λ are the power input, mainly by viscous heating, and the losses, and T_o and v_o the maximum temperature and velocity of rotation. A plasma balance becomes only possible when $T_o > 3\times10^4$ °K, $v_o > 4.6\times10^4$ m/sec, and P exceeds about 0.9 MW.

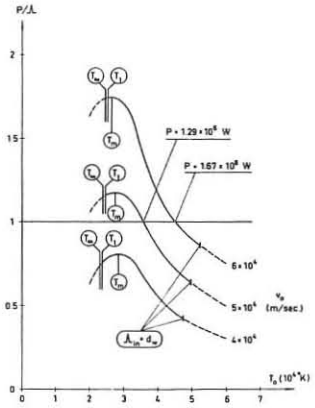

Fig. 1

Fig. 2 demonstrates high-frequency heating of a static plasma by an azimuthal current J_φ in a ring-current device similar to F II. Here κ_w is the fraction of the magnetic field lines which hit the supports of the central coil system. As an example, when κ_w = 0.1 the plasma can only be sustained at $T_o > 2\times10^4$ °K, $J_\varphi > 900$ A, and P>0.25 MW.

3. Experiments with a Rotating Plasma

The existence of a minimum power level has been verified in device F II. In Fig. 3 the upper trace represents the discharge current J and the lower the voltage ϕ_{12} between the electrodes. At times $t < t_c = t(\phi_{12\,min})$ can be shown that a short-circuit yields large reversed current pulses which reveal a fully ionized state. No such pulses are detected at $t > t_c$. The plasma density drops steeply within a short time-interval around t_c. This has also been verified by microwave measurements (5). Thus, the voltage $\phi_{12}(t_c)$ corresponds roughly to the minimum power level. It agrees with theoretical calculations, within the limits of experimental error. The measured minimum power is about 0.35 MW, i.e. somewhat less than that predicted by theory. The discrepancy can be explained by the uncertainty in the numerical values of the coefficients used in the heat balance equations.

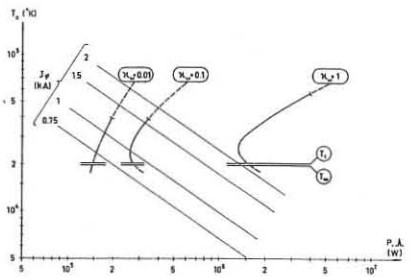

Fig. 2

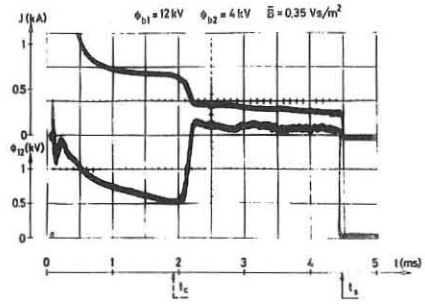

Fig. 3

4. High-frequency Heating of a Static Plasma

High-frequency heating by azimuthal currents is being planned for a static plasma in a ring-current device with magnetically screened supports. A strong absorption of energy has been observed at the magneto-acoustic resonance at about 1 MHz, but the minimum power limit of Fig. 2 has not yet been passed.

5. References

(1) B. Lehnert, Nuclear Fusion 8 (1968) 173.

(2) B. Lehnert, Arkiv f. Fysik 38 (1968) 499.

(3) J. Bergström, S. Holmberg, B. Lehnert, Plasma Physics and Controlled Nuclear Fusion Research, Vol. I, p. 341, I.A.E.A., Vienna (1966).

(4) B. Lehnert, J. Bergström, S. Holmberg, Nuclear Fusion 6 (1966) 231.

(5) N. Vinogradov, E. Tennfors, see paper of these proceedings.

This work has been supported by the Swedish Atomic Research Council.

ENERGY BALANCE AND TEMPERATURE PROFILES OF A CYLINDRICAL HYDROGEN PLASMA COLUMN SURROUNDED BY COLD GAS

by
G.K. Verboom
Association Euratom-FOM
FOM-Instituut voor Plasma-Fysica
Rijnhuizen, Jutphaas, The Netherlands

The temperature profile, the pressure profile, and the voltage-current characteristic are calculated for an arc discharge in hydrogen, surrounded by a rotating cold-gas blanket.

The arc is assumed to be stationary, cylindrically symmetric, and infinitely long. The dissociation and the ionization can be handled separately if the influence of electrons and ions on the momentum and energy transport of the molecules is neglected. If the mean free paths are sufficiently small, the usual equations of gas dynamics can be used to describe the macroscopic properties. Except for the azimuthal velocity, all mean velocities are assumed to be much smaller than the thermal velocities, because the arc rotates like a solid body as in the rotating-wall arc. The externally applied magnetic field, which has a component, B_z, in the z-direction only, is weakened by a diamagnetic effect due to the azimuthal current, j_ϕ. The field B_ϕ due to the axial heating current, j_z, is much smaller than B_z. Rationalized M.K.S.A. units are used.

The equations describing the energy balance and the pressure balance have to be solved for the entire cross section of the discharge vessel, since the gas blanket is an integral part of the arc discharge.

Assuming local thermal equilibrium and quasi-neutrality, and neglecting radiation losses, the total energy balance becomes:

$$\frac{1}{r}\frac{d}{dr}\left[r\left\{q_{e_r} + q_{i_r} + q_{o2_r} + \sum_s \left(h_s + \frac{1}{2}\rho_s \bar{v}_{s_\phi}^2\right)\bar{v}_{s_r}\right\}\right] = E_z j_z, \qquad (1)$$

where the indices e, i, o, and 2 refer to ions, electrons, atoms, and molecules, respectively, while s may indicate either species, h is the enthalpy, $\bar{v}$ is the mean velocity, ρ is the mass density, q is the heat flux, E is the electric field strength, and r, ϕ, and z are cylindrical coordinates.

Since the rotation energy, $\frac{1}{2}\rho_s \bar{v}_{s_\phi}^2$, is at most some tenths of an eV, while the enthalpy contains the ionization and the dissociation energy, we can neglect $\sum_s \frac{1}{2}\rho_s \bar{v}_{s_\phi}^2 \bar{v}_{s_r}$ against $\sum_s h_s \bar{v}_{s_r}$.

If the electron cyclotron frequency is much larger than the rotation frequency and if the azimuthal velocity of the neutrals equals the centre of mass velocity in the azimuthal direction, V_ϕ, then the radial component of the mean velocity can be written as:

$$\bar{v}_{s_r} = f(p, T, B_z, r, V_\phi)\frac{dT}{dr}, \qquad (2)$$

where p is the scalar pressure.

The pressure gradient is given by:

$$\frac{dp}{dr} = j_\phi B_z + \frac{\rho V_\phi^2}{r} = g(p, T, B_z)\frac{dT}{dr} + \frac{\rho V_\phi^2}{r}, \qquad (3)$$

where ρ is the total mass density and f and g are complicated functions of the indicated variables.

With equations (2) and (3) the energy balance reduces to

$$\frac{1}{r}\frac{d}{dr}\left\{r\,\kappa\,\frac{dT}{dr}\right\} = -E_z j_z. \qquad (4)$$

This is the well-known Elenbaas-Heller differential equation. However, the coefficient of thermal conductivity, κ, is now modified by transport of energy due to dissociation and ionization.

The radial pressure gradient, equation (3), is established by the rotation and by the diamagnetic current, j_ϕ. For a low temperature this current is caused by the ambipolar diffusion of electrons and ion across the magnetic field lines[8]. For a higher temperature the current is the result of the Nernst-Ettinghausen effect[1, 5].

For one set of parameters the resulting temperature and pressure profiles are given in figs. 1 and 2. The voltage-current characteristic is given in fig. 3. The influence of the rotation on the pressure profile is negligibly small, because of the large temperature gradient near the wall. If gas is blown in and out of the vessel the situation may change completely, because of the large amount of heat that would be transported in this way.

Since local thermal equilibrium was assumed, the Saha equation was used to describe the ionization equilibrium. The partition function in this equation had to be calculated up to the last bound state of the atom. If the Debye-Hückel theory is used to calculate the lowering of the ionization potential, which is needed to find this last bound state, then the density of the atoms is still 1‰ of that of the electrons for a temperature of one million degrees Kelvin. Since these atoms freely cross the magnetic field lines, and since there is no average radial mass velocity, a radial velocity of the charged particles is caused. In combination with the axial magnetic field this radial velocity of the charged particles can disturb the Nernst equilibrium characterized by n^4T = constant, where n is the number density of either charged particles. This equilibrium is reached under the assumption that there is no radial velocity, which implies no atoms, and that the product of the electron-cyclotron frequency and the electron-ion collision time is much larger than one. Using the formula for the lowering of the ionization potential (other theories arrive at the same result for an electron number density of $10^{21} - 10^{22}$ m^{-3}), it can be shown that the number density of the atoms can only become larger if the assumption of local thermal equilibrium is dropped.

One point of the calculated voltage-current characteristic can be compared with an experimental value obtained by Mahn et al.[7]. With the appropriate transformation formulae[3] their result is represented by the cross and error bar in fig. 3. Although their experiment was done at a pressure of 7 Torr, it can be seen in fig. 3 that the pressure dependence of the electric field strength is rather small. Since they measured an axial temperature of 1.10^5 K the agreement can be said to be satisfactory.

This work was performed under the association agreement of Euratom and FOM with financial support from ZWO and Euratom.

References:

1) S.J. Braginskii, Soviet Phys. JETP 6 (1958) 358.
2) W. Feneberg, VIième Conf. intern. sur les Phénomènes d'Ionisation dans les Gaz, Paris (1963).
3) U. Heidrich, Z. Naturforschung 20a (1965) 475.
4) E.H. Kennard, Kinetic Theory of Gases, McGraw-Hill, New York (1938).
5) O. Klüber, Z. Naturforschung 22a (1967) 1599.
6) H. Maecker, Handbuch der Physik, Bd. XXII, Springer-Verlag, Berlin (1956).
7) C. Mahn, IPP 3/44, Institut für Plasma Physik, Garching (1966).
8) R. Wienecke, Z. Naturforschung 18a (1963) 1151.

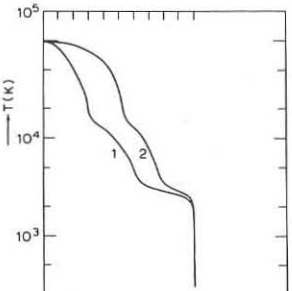

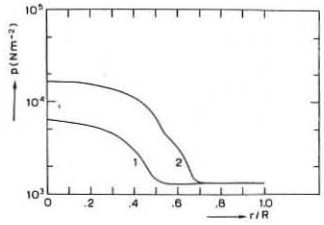

Fig. 2 Pressure profile: T(r=0) = 10^5 K, B_z = 1 T, p(r=R) = 10 Torr.
1 without the Nernst effect,
2 with the Nernst effect.

Fig. 1 Temperature profile: p(r=R) = 10 Torr, B_z = 1 T, R = 5.10^{-2} m, the radius of the discharge vessel.
1 without the Nernst effect: p(r=0) = 49 Torr, E_z = 113 V/m, I_z = 2430 A,
2 with the Nernst effect: p(r=0) = 128 Torr, E_z = 81 V/m, I_z = 6010 A.

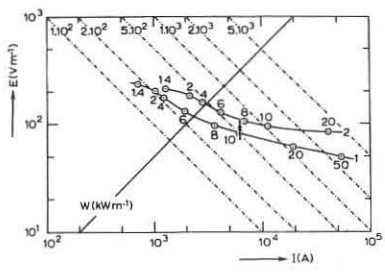

Fig. 3 Voltage-current characteristic: o = axial temperature in 10^4 K, B_z = 1 T, R = 5.10^{-2} m. 1 p(r=R) = 10 Torr, 2 p(r=R) = 100 Torr.

DIFFUSION EXPERIMENTS WITH LOW-PRESSURE LOW-CURRENT ARGON DISCHARGES IN AXIAL MAGNETIC FIELDS

by L. Rothhardt and G. Popov [1]
Institute of Magnetohydrodynamics, Jena, G.D.R.
([1] Guest from Institute of Electronics, Sofia, Bulgaria)

1. The discrepancies between the results and interpretations of various plasma diffusion experiments under the influence of magnetic fields arise from uncertainties in boundary conditions and from lack of knowledge of gas discharge behaviour. Therefore, we tried to study homogeniously magnetized discharges in all their parts and to measure local quantities. Fig.1 shows typical discharge tube examples. We decided to use argon because of its high ionic mass and its Ramsauer collision cross section in order to distinguish easily between electron and ion effects and between primary and secondary electrons. Glas tubes were used because of their insolating properties and in order to allow for optical observations. Typical parameters (see fig. 1a): Electrode spacings about 60 cm, tube diameters 4-6 cm, filling pressure about 0.5 torr, discharge currents 2-20 ma, magnetic field intensities 0-0.2 tesla. Cold tantalum disc cathodes with a diameter of 3 cm as well as hot tungsten filament cathodes with a diameter of about 1 cm were applied.

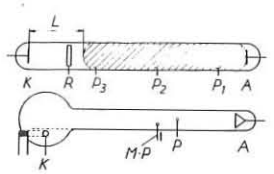

fig.1

The magnetized low-pressure low-current argon discharge may be described phenomenologically as follows:

a) The cathode fall region is not influenced by the magnetic field.

b) Magnetic reduction of diffusion losses causes an increase of plasma particle density in the negative glow and an expansion of Faraday's dark space.

c) There is a sharply localized thin boundary between Faraday's dark space and positive column; it is shifted by variation of magnetic field intensity. /1/

d) Both Faraday's dark space and positive column are two types of magnetized, collision dominated plasma columns. The first of them ('type 1') shows no volume production of charged particles and very weak axial E-field. The second one ('type 2') shows E-field values of the same order of magnitude as the unmagnetized positive column; volume production of charged particles is significant and electron temperature is about three times higher than in type 1.

e) Cold cathode and hot cathode discharges behave very similar. There is no intrinsic difference in characteristical features given in this section.

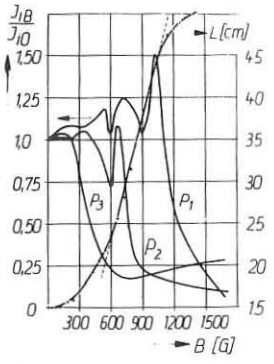

fig.2

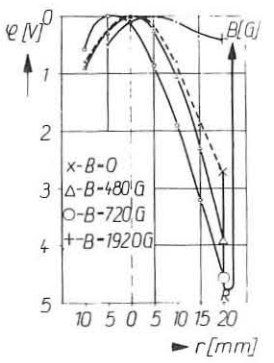

fig.3

2. Some experimental results are summed up in this section in more detail.

a) Ion flux into cylindrical probe at the tube wall (see fig.1a) is a function of B. As long as type 2 column stays in front of a probe, ion flux is high. As soon as type 1 column is arriving at probe position by an increase of B, ion flux is strongly reduced. Optical investigations by means of photodiodes show the same tendancy of boundary movement (see fig.2).

b) An increase of discharge current and a decrease of filling pressure give similar movement of the boundary between the two types of plasma columns as an increase in B field intensity does. Electrostatic potential at the ring electrode R in fig. 1a deviating from floating value also shifts that boundary; positive deviations yield elongation of type 1 column and vice versa!

c) Langmuir probe measurements in type 1 column are very much complicated, because the probe shaft acts as a recombination surface.and thereby the boundary between the two types of columns is shifted in the direction of the cathode. Any large recombination surface in contact with the plasma column suppresses type 1. Therefore a discharge in a tube as shown in fig.1b has only a plasma column of type 2. The results of probe measurements of the radial distribution of potential in this plasma column are shown in fig.3. They are in principle consistent with the theoretical work of ECKER /2/. The discharge is non-isothermal and electron mobility across the magnetic field still dominates over ion mobility at low values of B. Therefore, the interpretation of ECKER's special case $\epsilon = 0$ is valid and the wall potential becomes more negative. At higher values of B the relation between the diffusion coefficients is inverted, and the well known case of ambipolar diffusion in a strong magnetic field is present; the wall potential becomes less negative with increasing B field intensity.

d) In order to get information on the azimutal Hall drift current /3/ in type 2 column (type 1 suppressed by biassing ring electrode R) we inserted a special Hall probe (see insert fig. 4) . By compensating the difference of potential U_H between the two discs (surfaces perpendicular to drift vector), we got a qualitative measure of that drift current. At low B values (low $\omega\tau$) a linear dependence on B is found. At higher values saturation occurs. Furhter increase of B causes effects arising from collective phenomena like current-convective instability /4,5/ as can be seen in the dissimilar behaviour of the two curves with B parallel to $I_{disch.}$ and B antiparallel to $I_{disch.}$.

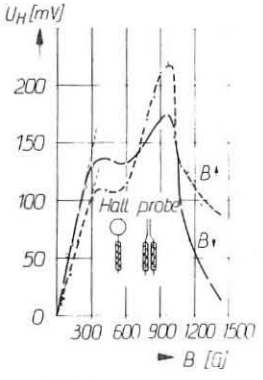

fig.4

3. In this section we try to comment on earlier results of various authors. We suppose that our results are transferable to helium work, too, because we only discussed basic features of gas discharges in magnetic fields.

a) All measurements of E_z using probes at large distance or tube voltage get values dependant on the distribution of type 1 and type 2 columns over the measuring distance . Therefore, the measured dependence on B is weakened by this averaging process. /4,5,6/

b) Axial inhomogeneities of the magnetic field or axial variation of tube cross section disturb the discharge strongly because of the action of electrostatic phenomena and/or additional recombination surfaces. /4,5,6/

c) The inclination effect of NEDOSPASOV and SOBOLEV /7/ may be interpreted as suppression of type 1 column by contact with an additional recombination surface.

4. REFERENCES

/1/ POPOW,G.; ROTHHARDT,L.: Mber.Dt.Akad.Wiss. 11 (1969) 182
/2/ ECKER,G.: Physics Fluids 4 (1961) 127
/3/ ALFVEN,H.;FÄLTHAMMAR,C.-G.: Cosmical Electrodynamics. 1963
/4/ BOESCHOTEN,F.: Plasma Physics 6 (1964) 339
/5/ GRANOVSKI,V.L.: Radiotekhn. i Electron. 11 (1966) 371
/6/ ADATI,K. et al.: Physics Fluids 9 (1966) 1464
/7/ NEDOSPASOV,A.V.; SOBOLEV,S.S.: Sh.Tekhn.Fis. 36 (1966)1758 and Belgrade Conf. Proc. II (1966) 633

Contributions to the

"THIRD EUROPEAN CONFERENCE ON CONTROLLED FUSION AND PLASMA PHYSICS"

and the

"SYMPOSIUM ON BEAM-PLASMA INTERACTIONS"

Utrecht, The Netherlands, 23-27 June 1969

S U P P L E M E N T

DISSIPATIVE TRAPPED PARTICLE INSTABILITY IN DENSE PLASMAS

B.B.Kadomtsev, O.P.Pogutse

I.V.Kurchatov Institute of Atomic Energy, Moscow, USSR

As has been previously shown /1,2,3/ the trapped particle instability may be very dangerous for toroidal plasma confinement. In a collisionless case this instability develops in the form of the flute-type perturbations with the trapped particles of both kinds, i.e. electrons and ions. In the case of a dense plasma the trapped particle instabylity leads to the development of the drift waves due to dissipation associated with collision conversion of the trapped particles into the transit particles. This instability may be called the trapped electron instability.

For the sake of simplicity we shall consider an axisymmetric toroidal device of the Tokamak-type.

To derive a dispersion equation for a small oscillation frequency it is necessary to obtain an experssion for the electron and ion density perturbations n_e' and n_i' and then to equalize them. The ion density perturbation n_i' is well known:

$$n_i' = \frac{\omega_*}{\omega} \frac{e n_0}{T_e} \varphi \qquad (1)$$

where ω is the frequency, $\omega_* = -\kappa_y \frac{c T_e}{e B n_0} \frac{d n_0}{d r}$ the drift frequency, k_y is the component of the wave vector $\vec{k}$ transverse to $\vec{B}$ and $\vec{r}$, r - the radius of a magnetic surface, m_i the mass of ions, n_0 the unperturbed density, T_e the electron temperature.

The electron density perturbation consists of two components $n_e' = \frac{e n_0}{T_e}\varphi + n_t'$ where the first is the Boltzmann distribution of the main part of the electrons and n_t' is the trapped electron perturbation. To get n_t' we may use the formalism developed in the paper of Ref.2. Thus we obtain

$$n_e' = \frac{e n_0}{T_e}\varphi - \sqrt{\varepsilon} \left\langle \frac{\omega - \omega_{*e}}{\omega + i\nu_{ef}} \right\rangle \frac{e n_0}{T_e} \hat{K} \varphi \qquad (2)$$

where $\sqrt{\varepsilon}$ is the fraction of the trapped electrons ($\varepsilon = r/R$ is the ratio between the minor and major radii), the brackets show the averaging over the Maxwellian function, $\omega_{*e} = -\frac{\kappa_y c T_e}{e B n_0} \frac{d n_0}{d r}\left[1 + \eta\left(\frac{m_e v^2}{2T_e} - \frac{3}{2}\right)\right]$ is the electron drift frequency, $\eta = d\ln T_e / d\ln n_0$, $\hat{K}$ is the integral operator with respect to the angle ϑ. It may be replaced by unity /1/ in the case of smooth perturbations whose maximum is at the external surface of the torus. The effective collision frequency $\nu_{ef} = \nu_e v_{th}^3 / \varepsilon v^3$ takes into account the differential character of the Coulomb collision term.

By equalizing Eqs.(1) and (2) we obtain the dispersion equation for ω. It follows that the frequency of unstable oscillations is $\omega \approx \omega_*$ and the maximum growth rate $\gamma \sim \sqrt{\varepsilon}\,\omega_*$ can be reached at $\omega_* \sim \nu_e/\varepsilon$. When $\nu_e \gg \varepsilon\,\omega_*$

$$\gamma \cong \varepsilon^{3/2} \frac{\omega_*^2}{\nu_e} \eta . \qquad (3)$$

The growth rate sharply increases with κ_y, therefore the instability causes turbulence. The estimates show that for developed turbulent motions the effective diffusion coefficient appears to be three times smaller than the coefficient of thermal conductivity. At a higher collision frequency this instability becomes the drift-dissipative instability. At a low collision frequency it becomesthe trapped ion instability /2/.

The effect of electron trapping may appear in the finite amplitude drift waves due to particle oscillationsin the electric potential wells /3/. Since the number of such particles is proportional to the square root of the amplitude their fraction may be quite appreciable even for small amplitude waves.

We have shown that the E-trapped electrons similar to B-trapped electrons may cause generation of the drift waves. Such an instability takes place only for standing waves along the Z axis when the collision frequency is of the order of the drift frequency and the temperature gradient is opposite to the density gradient, i.e. $\eta < 0$. The corresponding growth rate is of the order of $\gamma_{non\,lin} \sim \left(\frac{e\varphi}{T_e}\right)^{1/2} \omega_*$ for $\nu_e \sim \frac{e\varphi}{T_e}\omega_*$ where φ is the amplitude of the electric potential. This growth rate is greater than the linear one $\gamma \sim \omega_*^2/\kappa_\parallel v_{th\,e}$ for $\frac{e\varphi}{T_e} \lesssim \left(\frac{\omega_*}{\kappa_\parallel v_{th\,e}}\right)^2 \sim \frac{m_e}{m_i}$ i.e. for small amplitudes. Although the conditions $\eta < 0$, $\nu_e \sim \omega_* e\varphi/T_e$ considered here are rather specific the fact of nonlinear excitation of waves is very interesting in itself and is exciting apprehension.

We have also considered the nonlinear convection of a toroidal plasma for simultaneous E and B trapping of electrons in the case of $\eta > 0$. In this case the E-trapping plays a stabilizing part and restricts the amplitude of oscillations by the value of $\varphi \sim \varepsilon \frac{T_e}{e}$. This restriction is of a very simple physical meaning-there are no B-trapped electron for greater amplitudes of φ.

An estimate of the heat flux by thermal convection is also given.

References:

1. B.B.Kadomtsev, JETP Letters, 4, 15 (1966) In Russian.
2. B.B.Kadomtsev, O.P.Pogutse, JETP, 51, 1734 (1966).
3. H.G.Furth, M.N.Rosenbluth, 3-rd Conf. on Plasma Physics and Controlled Nucl. Fusion Research, Novosibirsk (1968).

HELICAL RADIO-FREQUENCY FIELD INTERACTION WITH MAGNETOACTIVE PLASMA IN TORUS

R.A.Demirkhanov, A.G.Kirov, V.N.Zharikov

Physical-Technical Institute of State Commettee on Utilization of Atomic Energy, Sukhumi, USSR.

On using radio-frequency (r.f.) multipole magnetic fields of the mcps frequency range of E-wave type in combination with a strong quasistationary magnetic field for plasma confinement in toroidal systems, along with the problem of the plasma column equilibrium over the major radius, its stability, etc. /1, 2, 3/, there arises an important problem on the character of the r.f. field propagation in a plasma.

If intense collective processes develope in a skin-layer then high frequency of collisions related to the turbulence (ν_{eff}) can result in the rapid "parasitic" overheating of electrons and can essentially decrease the Q-factor of the system as a whole. Effective heating of the plasma by the current as a result of small-scale instability development is theoretically and experimentally shown in /2-5/. The electron movement under the influence of the r.f. electrical field with the oscillatory velocity which considerably varies at the skin-layer depth, can result in the onset of short wavelength oscillations of various types from ion-sound to Langmuir ones. However, from the stability point of view /1/ the system with the combined fields must operate at $\beta = \frac{nT}{H^2/16\pi} \geq 1$, i.e., as it is readily shown, always $v_{\sim ave} < v_{Te}$ and at not very small T_e $v_\sim > C_s$ (C_s is the ion sound velocity). The condition $T_e > T_i$ is natural for such r.f. discharges. Therefore the principal type of oscillations in a skin-layer must be ion-sound one. In paper /4/ it is shown that on accelerating electrons in an electrical field during the sufficiently long time, the electron drift velocity becomes frozen at the level C_s. Hence it follows that the skin-layer turbulent depth is of the order of $\delta_T \simeq \frac{c}{\omega_{pi}}$ at $\beta \simeq 1$ and the maximum of the skin must take place in a plasma with heavy ions.

The present paper represent the first experiments in the toroidal device "R-QM", described in /2/, concerning the measurements of the r.f. rotating quadrupole magnetic field propagation depth into a magnetoactive plasma against the ion masses and the plasma density. The r.f. field has the frequency of the order of 0,5 mcps, the pulse duration of 500 μsec and the strength of 500g. The plasma operating densites are sufficiently high $n \geq 10^{14}$ cm^{-3} (the operating gas initial pressures were $2 \cdot 10^{-3} \div 7 \cdot 10^{-2}$ torr), and so $\omega_{pe} >> \omega_{He}$ always (the quasistationary magnetic field strength being 4,2 Kg). H_2, He, Ar, Xe served as operating gases. The r.f. field distribution in a plasma has been measured by means of magnetic probes and the plasma energy density nT - by diamagnetic probes. The plasma density has been estimated from the microwave signal passage with $\lambda = 2$ mm.

The experimental results are represented in Table; they are obtained with the quasistationary magnetic field strength of the order of 4.2 Kg when the plasma dragging effects due to the r.f. field rotation are small.

P_{torr} / m_i	δ_{cm}				
	$2 \cdot 10^{-3}$	$5 \cdot 10^{-3}$	$7 \cdot 10^{-3}$	$2 \cdot 10^{-2}$	$7 \cdot 10^{-2}$
1^{H_2}	–	0,7	–	0,6	1,3
4^{He}	–	–	0,6	0,7	0,8
40^{Ar}	0,6	–	–	1,0	1,1
131^{Xe}	0,7	–	–	0,9	–

From the table it is seen that in all gases the parameter δ_{exp} is decreased with the drop of the initial pressure and there is no essential broadening of the skin-layer depth with the increase of the ion masses. The plasma diamagnetism measurement together with the microwave measurements indicates that on decreasing the initial pressure, the plasma temperature grows (up to 10÷20 ev) and the corresponding decrease of δ_{exp} can be explained by Coulombain collision processes. However, the absolute value δ_{exp} is more than calculated one which corresponds to the temperature determined by diamagnetic measurements. If for Ar and Xe this effect can be explained by the multicharge ion formation, for hydrogen it is evidently related to the turbulent phenomena development. At the same time, for all gases the fact of the electron drift oscillatory velocity freezing absence in the C_s region is common, especially for heavy gases, where $v_\sim \gg C_s$. This shows that at least for heavy gases the turbulent effective frequency of collisions is not high. In this earlier paper /2/ similar phenomena have been observed: in the case of hydrogen discharge we observed a considerable anomalous resistance as in /5/, which is well explained by the ion-sound instability theory /4/; however, in the case of Ar, Ohmic resistance essentially decreased (nearly by an order of magnitude).

The experimental data in their entirety allow us to suppose that though the short wavelength ion-sound instability causing the high effective frequency of collisions and the corresponding turbulent heating is the theoretically and experimentally established fact the effective frequency of collisions essentially decrease on growing the ion masses.

The estimations made by us show that Coulombian collisions electron-ion, ion-neutral, charge exchange and the ion-sound oscillation dampings at the chamber wall (in accordance with /4/) can not essentially affect the ion-sound instability onset under our conditions. A possible explanation of the skin-layer broadening absence in heavy gases is given by the theory /6/, which calculates the ion-sound instability onset considering the nonlinear damping of waves on electrons and shows that $\nu_{eff} \simeq 2\frac{m_e}{m_i}\left(1 - \frac{C_s}{v_\sim}\right)^2$ i.e., ν_{eff} decreases with the rise of ion masses and under our conditions (for Ar and Xe) can be less than ν_{ei}. Another possibility is the suppression of the ion-sound instability as a result of electrical field alternation and the disturbance of the quasistationary condition which, in accordance with the theory from /7/ appears to be more rigid than $\omega \ll \gamma_s$ (γ_s - is the ion-sound instability increment, ω - is the r.f. field frequency) $\omega \ll \frac{v_\sim}{v_{Te}} \cdot \frac{m_e}{m_i} \omega_{pe}$. The more detailed experimental studies of the above effects are the aim of the authors' further work.

REFERENCES

1. Р.А.Демирханов. Труды II Международного симпозиума по взаимодействию ВЧ полей с плазмой. Париж. 2, 809-900 (1968).
2. Р.А.Демирханов и др. Труды II Международной конференции по управляемому синтезу и физике плазмы. Вена. т.II, 1966.
3. Р.А.Демирханов, А.Г.Киров, М.А.Стотланд, Н.И.Малых. Plasma Physics, 10, 4 (1968).
4. Л.И.Рудаков, Л.В.Кораблев. ЖЭТФ, 50, 220 (1966).
5. С.Д.Фанченко, Б.А.Демидов, Н.И.Елагин, Д.Д.Рютов. ЖЭТФ, 46, 497 (1964).
6. К.Н.Степанов, В.Л.Сизоненко. Письма в ЖЭТФ. 9, в.10 (1969) (в печати).
7. Ф.М.Некрасов. Ядерный синтез, 1969 (в печати).

EFFECT OF HIGH-FREQUENCY ELECTROMAGNETIC FIELD ON THE STABILITY OF A SLIGHTLY NONHOMOGENEOUS MAGNETIZED PLASMA

R.A.Demirkhanov, T.I.Gutkin, S.N.Lozovsky, F.M.Nekrasov, V.P.Sidorov

Physical-Technical Institute of State Committee on Utilization of Atomic Energy, Sukhumi, USSR.

The present paper gives the results of investigations of the E-wave (i.e. the wave with the electric vector $\vec{E}$ paralled to the constant magnetic field $\vec{H}_0$) high-freguency field effect on the stability of some types of oscillations in a slightly inhomogeneous collisionless magnetoactive plasma.

On assuming the conditions $\omega, k_z v_{Te}, \frac{k_z e\tilde{E}}{m_e\Omega_e} \ll \Omega$; $k_\perp v_{Te} \ll \omega_{He}, \omega_{pe}$; $\omega \ll \omega_{Hi}$, the dispersion relation for low-frequency oscillations can be approximately solved; over the range $k_z v_{Ti} < \omega < k_z v_{Te}$ it has two branches (as in case when the h.f. field is absent) which can be called drift and ion-sound branches. The drift branch has been investigated in /1/. For the increment of the ion-sound branch we obtain the following expression:

$$\gamma = -\sqrt{\frac{\pi}{2}}\frac{\omega_e^{*2}}{|k_z|v_{Te}}\left(\frac{k_z^2 T_e}{m_i\omega_e^{*2}}\right)^2 \frac{1-\xi-\frac{\tau_e}{2}}{(1+F)^2} \qquad (1)$$

(denotations are the same as in /1/).

This expression shows that the instability of the ion-sound branch occurs at $\xi > 1-\frac{\tau_e}{2}$, while the condition for exciting of the drift type oscillations found in /1/ is $\xi < -F-\frac{\tau_e}{2}$. Comparing these two conditions we see that the plasma is stable only over the range $-F-\frac{\tau_e}{2} < \xi < 1-\frac{\tau_e}{2}$. For existing of such a range we must have $F > -1$; otherwise, an instability occurs at small values of the parameter ξ.

In the case when $\tau_i \gg 1$ (large ion temperature gradient) we have obtained the following dispersion equation which in absence of the h.f. field is reduced to that for drift-temperature oscillations:

$$x^3-(1+F)x^2-\beta x(1+F)-\tau\beta(1+\tau_i)(1+F)=0 \qquad (2)$$

where we denote: $x=\frac{\omega}{\omega_e^*}$, $\tau=\frac{T_i}{T_e}$, $\beta=\frac{k_z^2 T_e}{m_i\omega_e^{*2}}$ (it is assumed that $\tau\beta(1+\tau_i)\sim 1$).

Under the condition $(1+F)>|1+\tau_i|$ Eq. (2) is reduced to $x^2=-\tau\beta(1+\tau_i)$.; consequently, in the case $\tau_i<0$ an instability occurs, i.e. we can say that in this case the drift-temperature instability can be stabilized by the h.f. field.

In the experiments with sufficiently hot ions there may occur the drift-cyclotron instability, its characteristic frequencies lying near the ion-cyclotron frequency or that of its harmonics; the transverse wavelength is $\lambda_\perp \approx \frac{\rho_i^2}{L}$, where ρ_i is the ion Larmor radius, L - the plasma inhomogeneity dimension. The effect of inhomogeneous h.f. field on the drift-cyclotron instability has been considered in /2/. Let us consider the h.f. field influence on the drift-cyclotron oscillations with $k_z \neq 0$. The dispersion equation describing these oscillations has the form:

$$1+\frac{1}{k^2\lambda_{Di}^2}+\frac{\omega_{pe}^2}{\omega_{He}^2}-\frac{\hat{\omega}_{pe}^2}{(\omega-\omega_g^* B)^2}-\frac{\omega_i^*}{k^2\lambda_{Di}^2(\omega-\omega_g^* B)}=\frac{1}{k^2\lambda_{Di}^2\sqrt{2\pi}z_i}\sum_{n=-\infty}^{\infty}\frac{\omega-\omega_i^*}{\omega-n\omega_{Hi}}$$

where $\omega_i^*=\frac{k_y c T_i}{e H_0}\frac{d\ln n_0}{dx}$, $z_i=\frac{k_\perp^2 v_{Ti}^2}{\omega_{Hi}^2}$, $\hat{\omega}_{pe}^2=\frac{k_z^2}{k^2}\omega_{pe}^2$, $\hat{\omega}_{He}^2=\frac{k_z^2}{k_\perp^2}\omega_{He}^2$, $\omega_g^*=\frac{k_y}{2\omega_{He}}\frac{\tilde{v}_{e0}^2}{}^{(3)}\frac{d\ln\tilde{E}_0}{dx}$,

$\tilde{v}_{e0}=\frac{e\tilde{E}_0}{m_e\Omega}$, $\lambda_{Di}^2=\frac{v_{Ti}^2}{\omega_{pi}^2}$, $B=1+\frac{P\hat{\omega}_{pe}^2}{\Omega^2}$, $P=1-\frac{\hat{\omega}_{pe}^2}{\Omega^2}\left(1-\frac{\Omega^2}{\hat{\omega}_{He}^2}\right)$, $Q=-\frac{\omega_i^*}{\Omega k^2\lambda_{Di}^2}$

To obtain the Eq.(3) it was assumed that the inequality $\Omega^2 \gg |\omega_{Hi}\omega_{He}|$ is satisfied, that enables us to neglect the ion contribution in the waves with combination frequencies $\omega \pm s\Omega$, Far from harmonics of the ion-cyclotron frequency Eq.(3) can be written as follows:

$$(\omega-n\omega_{Hi})(\omega-\omega_0^{(+)})(\omega-\omega_0^{(-)})=(\omega-\omega_g^* B)\frac{\omega-\omega_i^*}{\sqrt{2\pi}z_i}\zeta \qquad (4)$$

where $\omega_0^{(\pm)}=\omega_g^* B+\frac{\zeta}{2}\left[\omega_i^* \pm \left(\omega_i^{*2}+4k_z^2 T_i/m_e\zeta\right)^{1/2}\right]$, $\zeta=1-k_\perp^2\rho_i^2\frac{m_e}{m_i}$.

According to /3/ the instability occurs at intersection of the $\omega_0^{(+)}$ and $n\omega_{Hi}$ branches. In the presence of the h.f. field we have the following relation for critical value of k_z at the stability boundary:

$$k_{zc}=k^2\omega_{Hi}^2\frac{m_e}{T_i}\left(1-\frac{\omega_g^* B}{\omega_i^*}\right)\left\{\left(1-\frac{\omega_g^* B}{\omega_i^*}\right)k^2\lambda_{Di}^2\left(1+\frac{\omega_{pe}^2}{\omega_{He}^2}\right)-\frac{\omega_g^* B}{\omega_i^*}\right\} \qquad (5)$$

From (5) it follows that in real situations when $\frac{d\ln\tilde{E}_0}{d\ln n}<0$ the stabilization criterion has the form:

$$\frac{\hat{\omega}_{pe}^2}{\Omega^2} \lesssim 1+\frac{k_\perp^2}{k^2}\frac{\omega_{pe}^2}{\omega_{He}^2}-\frac{\omega_i^{*2}}{\Omega^2 k^4\lambda_{Di}^4\left(1+k_\perp^2\omega_{pe}^2/k^2\omega_{He}^2\right)} \qquad (6)$$

Otherwise the destabilization will occur.

The h.f. field imposing on the plasma can result in exciting instabilities, as it was originally shown in the works of V.P.Silin et al. /4/. The maximum increments are obtained for the oscillations the eigenfrequencies ω of which are connected with the h.f. field frequency by means of relation

$$\omega=\frac{n\Omega}{2} \qquad (n=1,2,\ldots)$$

In these works were considered the instabilities arising in a plasma on imposing the h.f. field with frequencies $\Omega \gg \omega_{pi}$. We have investigated the plasma behaviour in the region of lower frequencies. We considered the problem of exciting the parametric ion-sound instability in a magnetized plasma by oscillating currents. In the hydrodinamical approach the equation for plasma density perturbations in the h.f. field $\tilde{E}_z=\tilde{E}_0\sin\Omega t$ has the form of Mathieu equation

$$\frac{d^2\delta n}{dt^2}+\omega_s^2\left[1-\frac{\tilde{v}_0^2}{2v_T^2}(1+\cos 2\Omega t)\right]\delta n=0;\ \omega_s^2=\frac{k_z^2(T_e+T_i)}{m_e+m_i},\ v_T^2=\frac{T_e+T_i}{m_e} \qquad (7)$$

At $\tilde{v}_0^2/v_T^2 \ll 1$ the parametric instability increment is $\gamma=\omega_s\frac{\tilde{v}_0^2}{v_T^2}$. The instability zone width is defined by the expression

$$\frac{1}{4}\frac{\tilde{v}_0^2}{v_T^2}<\frac{\omega_s-\Omega}{\Omega}<\frac{3}{4}\frac{\tilde{v}_0^2}{v_T^2} \qquad (8)$$

In the region $\omega_s \approx 2\Omega$ the increment and zone width are of order $\left(\frac{\tilde{v}_0}{v_T}\right)^4$. The consideration of instability in the kinetic approach gives practically the same results for the increment and the instability zone width. However, here arises one fundamental difference, connected with the kinetic damping of the ion-sound oscillations due to electrons. The damping results in arising the threshold value $\tilde{v}_0^* = v_{Te}\left(\frac{m_e}{m_i}\right)^{1/4}$. The instability occurs only at $\tilde{v}_0 > \tilde{v}_0^*$. It is interesting to note that the velocity threshold value is much higher than in the case of excitation by the direct current. When it is equal to several v_{Ti}.

References

/1/ Р.А.Демирханов, Т.И.Гуткин, С.Н.Лозовский. ЖЭТФ. 55, 2195, 1968.

/2/ V.Kopecky, Plasma Physics 10, 609, 1968.

/3/ А.Б.Михайловский. Nuclear Fusion 5, 125, 1965.

/4/ V.P.Silin. The paper, presented on the 8th International Conference on the Ionization Phenomena in Gases. Vienna, 1968.

(3) substituted paper

ABSORPTION OF HIGH-FREQUENCY WAVES IN PLASMA

V.N.Budnikov, B.V.Galaktionov, V.E.Golant,
A.A.Obuchov, A.D.Pilija and O.N.Shcherbinin

A.F.Ioffe Physico-Technical Institute,
Leningrad, USSR

Collisionless absorption of electromagnetic waves by plasma in the frequency range between electron cyclotron and upper hybrid as well as at the frequency somewhat lower than electron cyclotron was obtained in previous experiments [1-4]. An analysis of the experimental data has shown that the absorption observed is due to the effect of transformation of the incident wave into shortlength plasma wave followed by damping [4].

Theoretical consideration in the one-dimensional linear approuch of wave transformation in an inhomogeneous plasma leads to the conclusion of the existence of two high-frequency transformation ranges (at $\omega > \omega_i$):

$$\omega_e < \omega < \omega_1 \qquad (1)$$

$$\omega_i < \omega < \omega_2 \qquad (2)$$

where

$$\omega_1^2 = \frac{\omega_e^2 + \omega_{pmax}^2}{2} + \left[\left(\frac{\omega_e^2 + \omega_{pmax}^2}{2}\right)^2 - \omega_e^2 \omega_{pmax}^2 \cos^2\alpha\right]^{\frac{1}{2}}, \qquad (3)$$

$$\omega_2^2 = \frac{\omega_e^2 + \omega_{pmax}^2}{2} - \left[\left(\frac{\omega_e^2 + \omega_{pmax}^2}{2}\right)^2 - \omega_e^2 \omega_{pmax}^2 \cos^2\alpha\right]^{\frac{1}{2}} \qquad (4)$$

at $\cos^2\alpha >> \frac{m_e}{m_i}$,

$$\omega_2^2 = \frac{\omega_e \omega_i \omega_{pmax}^2}{\omega_{pmax}^2 + \omega_e^2}\left(1 + \frac{m_i}{m_e}\cos^2\alpha\right) = \omega_{Lmax}^2\left(1 + \frac{m_i}{m_e}\cos^2\alpha\right) \qquad (5)$$

at $\cos^2\alpha << 1 \qquad \omega_{pmax}^2 >> \omega_e \omega_i$;

ω_e - electron-cyclotron frequency, ω_i - ion-cyclotron frequency, ω_{pmax} - plasma frequency, corresponding to the maximum electron density, ω_{Lmax} - low hybrid frequency, α - the angle between the density gradient and the magnetic field. It should be noted that the boundaries of the transformation ranges are determined by the density gradient rather than the direction of the incident wave.

The experiments described were aimed at studying the collisionless absorption in the second transformation range (2) - between electron cyclotron and low hybrid frequency.

The data on microwave absorption were obtained from measurments of plasma existence region in magnetic field by microwave power. The experiments were carried out under stationary conditions with the uniform magnetic field. Plasma was obtained in a quarz tube, 70cm long and 2,5cm in diameter filled with argon. Stationary microwave power in 10-cm band was delivered by the waveguide to the one end of the disxharge tube, and to the other from an impulse generator of 3-cm band. Electron density was measured by an 8-mm interferometer. Plasma was created by 3-cm power in the electron-cyclotron conditions. After the impulse of the 3-cm power the plasma kept existing due to absorption of the stationary 10-cm power if the plasma density was high enough. In this case the operating frequency was 3 times less than cyclotron. It was possible to determine the boundaries of plasma existence region corresponding to absorption range by changing the magnetic field strength and the applied microwave power (i.e. the plasma density).

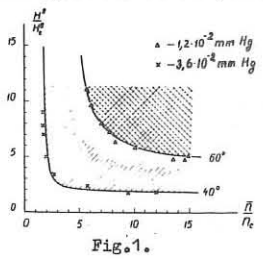

Fig.1.

Fig.1 shows the experimental data obtained at two different pressures. The data are in agreement with theoretical transformation boundaries calculated from (4) for angles α of 40° and 60° (solid curves). The increase of the angle between the density gradient and magnetic field at lower pressure might be caused by the increase of the longitudinal diffusion coefficient.

Also, experiments on wave absorption in plasma were conducted near low hybrid frequency. In this experiments plasma was obtained in a glass tube 1m long and 5cm diameter. The magnetic field was directed parallel to the tube axis. 3-cm microwave generator was used for plasma production. Operating pressure of hydrogen was 5.10^{-4} - 10^{-2} mm Hg, electron density was 5.10^{11} - 10^{12} cm^{-3}. Low power at frequencies 120-140 Mhz was delivered to the single turn coil placed in the central part of the tube. The broad absorption maximum was observed at the magnetic field strength, for which low hybrid frequency was near to the applied frequency. The change of excitation conditions (the coil length, the angle between the coil and tube axis) did not couse any change of absorption frequency. At the same time the maximum absorption frequency did rise with the increase of neutral gas pressure. This is shown in fig.2 where the ratio of this frequency to low hybrid is plotted. The results obtained are keeping with the assumption that the absorption is connected with the linear wave transformation. The increase of the maximum absorption frequency at higher pressures can be accounted for by the deflection of the angle between the density gradient and magnetic field from 90°. The high frequency boundary of the transformation range increases essentially even at a small deflection. The effect is confirmed by longitudinal gradient measurements.

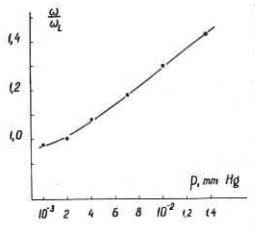

Fig.2.

In conclusion, the data on wave absorption regions in plasma are presented. Fig.3 shows the experimental results of this report and those of the paper [1,2] and the theoretical transformation boundaries calculated from (3-5) for several α -angles. The agreement of the experimental data and the theoretical curves confirmes the idea that the absorption observed is connected with the wave transformation. The collisionless character of the absorption permits to use it for plasma heating up to high temperature.

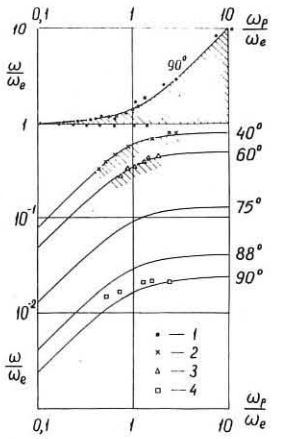

Fig.3.

LITERATURE

1. A.I.Anisimov, N.I.Vinogradov, V.E.Golant, L.P.Pachomov, ZTP*, 37, 680, (1967).
2. V.N.Budnikov, N.I.Vinogradov, V.E.Golant, A.A.Obuchov, ZTP, 37, 861 (1967); 38, 28 (1968).
3. V.N.Budnikov, V.E.Golant, A.A.Obuchov, ZTP, 38, 576 (1968).
4. A.I.Anisimov, V.N.Budnikov, N.I.Vinogradov, V.E.Golant, C.I.Nanobashvili, A.A.Obuchov, L.P.Pachomov, A.D.Pilia, V.I.Fedorov. Report CN-24/J-3 on III International conference on plasma physics and controlled thermonuclear reactions, Novosibirsk, 1968.
5. A.D.Pilia, V.I.Fedorov. Preprints Phys.-Techn.Inst. Academy of Sciences of the USSR N 104,144, Leningrad, 1968.

* ZTP - Zhurn. Tekhn. Phys.

STABILIZATION OF MICROINSTABILITIES BY MEANS OF H.F. FIELDS

by
J. Teichmann
Institute of Plasma Physics, Czechoslovak Academy of Sciences
Prague 9, Nademlýnská 600, Czechoslovakia

There has recently been considerable interest in the effect of applied time dependent electromagnetic fields on plasma instability. Those fields may be used for stabilization of the plasma-vacuum boundary, for preventing the escape of particles along the magnetostatic field lines in open-ended systems [1] (and thus for suppression the loss-cone modes) or for stabilizing the most dangereous microinstabilities.

The effect of H.F. longitudinal electric fields upon drift waves has been studied previously [2]. It has been found, that the effective increase of the electron temperature results in the narrowing down of the instability region with respect to the parameter $\eta = d\ln T/d\ln n$. An other study [3] of the possibility of stabilizing dynamically drift modes by modulating the electron temperature showed, that in the case of low frequency modulation $\Omega < \omega_e^*$ (Ω being the modulating frequency, ω_e^* - drift frequency of electrons), the stabilizing effect takes place only in the collisionless regime and only if one of the beat frequencies $\omega_e^* \pm \Omega$ is absorbed by resonant ions.

A new method for suppression of several electrostatic instabilities with small k_z, $k_z \ll k$, in a collisionless plasmas has been described recently [4,5]. The H.F. azimuthal magnetic field $H_\varphi = H_1 \cos\Omega t$ $H_1 \ll H_0$ superimposed to the longitudinal magnetostatic field H_0 changes periodically the instantaneous direction of magnetic field lines. This allows to particles to travel across the flute-shaped perturbations and to short out the electric field of perturbations. This mechanism takes place, when the inequality

(1) $$k_z v_{therm} H_1 > \Omega H_0$$

is satisfied.

In such H.F. fields, the perturbation e.g. of the electron distribution function is described for $\omega < \Omega \ll \omega_{cc}$ by the expression

(2) $$f_{k\omega} \simeq \phi_{k\omega} \left\{ -\frac{e}{m_e} \frac{1}{\omega_0} \frac{\partial f_0}{\partial v_0} + \left[\frac{e}{H_0} k_\varphi \frac{\partial f_0}{\partial r} - \frac{e}{m_e} \frac{\omega}{\omega_0^2} \frac{\partial f_0}{\partial v_0} \right] \frac{1}{k_z v_z - \omega} J_0^2\left(k_\varphi \frac{v_\varphi}{\Omega} \frac{H_1}{H_0} \right) \right\}$$

which is an average over the time interval $\sim \Omega^{-1}$. Let us note, that for low frequency modes the perturbation of the distribution function of ions is important. The presence of the multiplier J_0^2 reduces substantially for large arguments (1) of the Bessel functions the "unstable" term in (2). We observe [5], that under the influence of the H.F. magnetic field, the dispersion properties of plasma undergo a substantial change due to the circumstance, that particles are free to move across the magnetostatic field lines. Thus instabilities, based on the Hermitian part of the dieletric tensor, (such as loss-cone $\nabla n = 0$ and cyclotron modes) vanish completely. On the other hand, for instabilities, caused by resonant electrons or ions (such as drift-temperature or universal modes), the H.F. field reduces only their growth rate γ by the factor proportional to $\left[\int_{-\infty}^{+\infty} dv_z f_0 J_0^2\left(k_\varphi \frac{H_1}{\Omega} v_\varphi \right) \right]^2$ with respect to the value γ_0 in absence of the H.F. field. The γ of such instabilities may be further reduced by applying the multiperiodic H.F. field: $H_\varphi = \sum_n H_n \cos(\Omega_n t + \psi_n)$, $\Omega_n \ll \omega_c$. When the beat frequencies $|\Omega_p - \Omega_r|$ are larger than the characteristic frequency of the instability, the effect of the H.F. field raises nearly $\left[\int_{-\infty}^{+\infty} dv_z \left(J_0 \prod_n J_0^2\left(k_\varphi \frac{H_n}{\Omega_n} v_\varphi \right) \right) \right]^{-2}$ times. Even those instabilities, that fail to vanish in such a H.F. field, have growth rates practically equal to zero. The influence of the multiperiodic H.F. field has a more general physical meaning as it has been shown on the case of a simple two-stream instability [6]. It may be shown, that a similar stabilizing effect have standing and propagating electromagnetic waves polarised perpendicularly to the magnetic field e.g. the helicon wave.

For the purpose of experimental verification of the influence of the H.F. transversal magnetic field, the theory of the stabilizing of instabilities occuring in the presence of particle-particle collisions has been developed [7] by taking into account the influence of the longitudinal electric component $E_z = E_1 \sin\Omega t$. The dispersion equation for the drift dissipative instability ($\varphi_{Li} \ll d\ln n/dx$, $\nu_{ei} \ll \omega_{ce}$, $\nu_{ii} \ll \omega_{ci}$, $\nu_{ei} \gg \omega$, $T_e \sim T_i$, $\nabla T = 0$, ω being the frequency of instability) takes the following form:

(3) $$\omega^2 \left[2 - A - I_0(\mu) e^{-\mu} \right] + \omega \left[\omega^* A - \omega^* I_0(\mu) e^{-\mu} + 2 i K^2 D_e - i K^2 D_e I_0(\mu) e^{-\mu} - \right.$$
$$\left. - \delta_e k_z E_1 A' \right] - i \omega^* K^2 D_e I_0(\mu) e^{-\mu} = 0$$

where $D_e = T/m_e \nu_{ei}$, $\mu = k_z^2 \rho_{Li}^2$, $\omega^* = -k_y c T/e H_0 \cdot \partial \ln n/\partial x$, $K^2 = k_z^2 + \frac{1}{2} k_y^2 H_1^2/H_0^2$

The influence of the H.F. field is manifested in the functions A and A', defined for $k_z E_1 e/\Omega m_e \nu_{ei} \ll 1$ as:

$$A = \sum_{r,s} I_r(\eta) I_r(\delta) I_s(\eta) I_s(\delta) \qquad \eta = \frac{1}{4\Omega} D_e k_y^2 \frac{H_1^2}{H_0^2}$$
$$A' = \sum_{r,s} I_r(\eta) I_r(\delta) I_s'(\eta) I_s(\delta) \qquad \delta = 2 k_z k_y \frac{1}{\Omega} \frac{H_1}{H_0}$$

For a laboratory plasma $\mu \ll 1$ and the growth rate of instability in the absence of the H.F. field ($E_1 = H_1 \equiv 0$) is of the order of $\gamma_0 \simeq k_z^2 D_e/\mu$ when $\omega \simeq \omega^* \simeq \gamma_0$. For sufficiently large amplitude H_1, $\delta \gtrsim 1$, $\eta < 1$ and thus $A' \ll 1$, $A \gg 1$. The growth rate γ is now $\gamma \simeq k_z^2 D_e/A$ which is μ/A times smaller than γ_0. For an other interesting case, when $\eta \gg 1$, $\gamma \simeq \omega^{*2}/\Omega \eta^{3/2}$. Again a rather strong stabilizing effect takes place. Other microinstabilities occuring in experimental devices are screw-type instabilities of the inhomogeneous plasma, driven by a longitudinal current of the discharge. Let us demonstrate here only one particular case, when relaxation times for electrons and ions are large enough, $\omega_{ce}\tau_e \gg 1$, $\omega_{ci}\tau_i \gg 1$. Thus the instability may be studied in one-fluid approximation. The equations for perturbations of electron density and conductivity σ yield for the frequency of instability:

(4) $$\omega = -i K^2 D_A + i \frac{c}{H_0} \frac{k_y k_z}{K^2} E_1 \frac{d\ln\sigma}{dx} I_0^2(\delta) I_1^2(\chi), \quad \delta = 2 k_y k_z \frac{D_A}{\Omega} \frac{H_1}{H_0}, \quad \chi = k_y^2 \frac{D_A}{4\Omega} \frac{H_1^2}{H_0^2}$$

D_A means the coefficient of ambipolar diffusion. With the growing amplitude H_1, the value of K increases magnifying the first "stable" term. In the same time the second term decreases provided $I_0^2(\delta) \simeq 1$. Large amplitudes H_1 cause exponential growth of the second term and thus lead to instability. Other screw-type modes are suppressed without this restriction. The stabilizing mechanism is now due rather to the influence of the longitudinal H.F. electric field which affects the current of the discharge. Results of several experiments performed recently on helium discharge [8], on potassium Q machine [9] and on a large PIG discharge [10], are in a good agreement with the theory. The azimuthal H.F. field has been generated by the longitudinal H.F. current, conducted along the axis of the plasma by an insulated wire [8,9] or directly through the plasma column [10]. The amplitude H_1 was small, $H_1/H_0 \sim 0{,}05 - 0{,}1$ [8,9]. According to theory, the decrease of amplitudes of resistive instabilities has been observed, beginning for modes with highest k_z and ω. A qualitative decrease of the radial diffusion has been measured. The temperature of electrons remained without large changes and no new instabilities have been generated by the H.F. field.

Recently, low frequency microinstabilities have been analysed in a time periodic magnetic field [11]. Another study [12] for the field $H_\varphi(\vec{r},t) = \vec{e}_\varphi H_\varphi(\vec{r}) (1 + \alpha \cos\Omega t)$, $\alpha \ll 1$ showed, that the influence of particle drifts generated by the magnetic and electric induced fields, results in a relatively weak stabilizing effect in the frequency range $\omega^* \leq \Omega$.

References:

1 Teichmann J., Nuclear Fusion 5 (1965), 107.
2 Fainberg Ya.B., Shapiro V.D., Zh. Exp. Teor. Fiz. 52 (1967) 293.
3 Dobrowolny M., Engelmann F., Levine A.M., Report LGI 68/28 (1968).
4 Ivanov A.A., Rudakov L.I., Teichmann J., Zh. Exp. Teor. Fiz. 52 (1967) 1832.
5 Ivanov A.A., Rudakov L.I., Teichmann J., Zh. Exp. Teor. Fiz. 54 (1968) 1380.
6 Teichmann J., Physics Letters 26A (1968) 328.
7 Ivanov A.A., Teichmann J., Report IPPCZ - 111 (1968).
8 Artsimovich L.L., Ivanov A.A., Rusanov V.D., Sobolev S.S., Teichmann J., Physics Letters 27A (1968) 573.
9 Ivanov A.A., Kazakov Yu.B., Lukianchuk V.P., Rusanov V.P., Sobolev S.S., Teichmann J., Pisma Zh. Exp. Teor. Fiz. to be published.
10 Dubovoi L.V., Djatlov V.D., Proc. 3rd. Conf. Peacef. Uses of At. Energy and Therm. Reactions. Novosibirsk (1968).
11 Cotsaftis M., Physics Letters 27A (1968) 662.
12 Teichmann J., Physics Letters, to be published.

ON POSSIBILITIES OF ELIMINATING THE LOSS CONE BY MEANS OF A HIGH-FREQUENCY FIELD

by

R. Klíma

Institute of Plasma Physics, Czechoslovak Academy of Sciences

Prague 9, Nademlýnská 600, Czechoslovakia

The containment of plasma by means of a magnetostatic and a superimposed high-frequency (h.f.) field has been analysed in many previous papers, see e.g. [1] and [2]. In the present paper, we estimate some possibilities which the mirror magnetostatic field yields in comparison with the simple radiation pressure (homogeneous magnetostatic field)[3]. We consider the stationary state of a collisionless plasma with "cold" ions, $T_i \ll T_e$. A circularly polarised wave with frequency $\omega \gg \omega_{ci}$ $(= e B_0/m_i c)$ falls on the plasma in the direction of the magnetostatic field $\vec{B}_0$, which is perpendicular to the plasma-vacuum boundary. The direction of the field rotation coincides with the electron cyclotron rotation. If $-\omega \neq \omega_{ce}$ $(= -e B_0/m_e c)$ and the thermal velocities of electrons are sufficiently small, the potential U [4], [5] of the time-averaged motion exists:

$$U(s) = \frac{e^2 \varkappa(s)}{2 m_e \omega^2} E(s) E^*(s), \quad \varkappa(s) = \left(1 + \frac{\omega_{ce}(s)}{\omega}\right)^{-1}, \quad \omega_{ce} < 0,$$

s is the length measured along the line of force of $\vec{B}_0$, $E(s)$ is the amplitude of the h.f. field. An appropriate barrier of the potential U eliminates the loss cone of the velocities distribution. The distribution function of electrons is zero for particles the trajectories of which reach over the boundary of plasma ($s = s_1$). The quality of plasma containment is characterised by the relative height of the barrier $U(s_1)/T_e = q$; we suppose $q \gtrsim 3$. The wave propagation in plasma can be solved by means of the corresponding formula for concentration $n(s)$ [6], Eq. (2.15), which is a modified "barometric formula". We present the results of selfconsistent analytical solutions of some typical cases.

1. Homogeneous $\vec{B}_0$, total reflection of the wave: $\omega \neq \omega_{ce}$, $\varkappa > 1$, $n(s_2) T_e = E_J E_J^*/(2\pi)$, $n(s_2)$ is the concentration in the region of homogeneous plasma, E_J is the amplitude of the incident wave; $q = 2 e^2 E_J E_J^* \varkappa/(m_e \omega^2 T_e)$; $\omega_0^2(s_2)/\omega^2 = q/\varkappa$, $\omega_0^2 = 4\pi n e^2/m_e$. The condition of existence of the potential U is formulated by means of the small parameter δ [5], which implies the following restrictions (C.G.S. - units): $T_e \lesssim m_e c^2/[2q(q-1)(12\pi\varkappa)^2]$ and thus $T_e \lesssim 3 \times 10^{-11}$ erg; $\omega m_e c \gtrsim 10^2 e (E_J E_J^*)^{1/2}$, $E_J E_J^* \gtrsim 3 \times 10^2 \times m_e^{1/2} T_e^{3/2} \omega^2/(e^2 c)$.

2. Homogeneous $\vec{B}_0$, partial reflection of the wave in the boundary layer of plasma, the wave propagates in the region of homogeneous plasma: The pressure F_{12} acts on the boundary layer in the direction of (- grad n):

$$F_{12} = E_J E_J^* (1+N_2)^2 \frac{R - R_s}{8\pi N_2}, \quad N_2 = \left[1 - \frac{\omega_0^2(s_2)}{\omega^2}\varkappa\right]^{1/2}, \quad R < R_s = \left(\frac{1-N_2}{1+N_2}\right)^2,$$

R is the reflection coefficient. There is no containment of plasma in this case and, strictly speaking, no stationary state in the collisionless approximation.

3. Inhomogeneous $\vec{B}_0$, generally: We define the characteristic lengths $L_E \approx |d \lg E E^*/ds|^{-1}$ and $L_\varkappa \approx |d \lg \varkappa/ds|^{-1}$. If it is $L_E \ll L_\varkappa$, the barrier $U(s)$ is approximately the same as in the case of homogeneous $\vec{B}_0$. We note that the hydrodynamic condition of equilibrium is

$$\frac{d}{ds}(E E^* + H H^*) + 8\pi T_e \frac{dn}{ds} + E E^* \frac{\omega_0^2(s)}{\omega^2}\frac{d\varkappa}{ds},$$

another case see [7]. Let us consider a volume which is bounded by the lines of force of the field $\vec{B}_0$; the cross-section of the volume is $\mathcal{S}(s_2)$ in the region of homogeneous plasma. The incident wave power necessary for the containment of plasma in the considered volume is P_J. We shall compare the power P_J with the incident wave power P_{Jk} $(= c\, n(s_2)\, T_e\, \mathcal{S}(s_2)/2)$ which is required for containment of plasma with the same value of $\mathcal{S}(s_2) n(s_2) T_e$ in the case of homogeneous $\vec{B}_0$.

4. Inhomogeneous $\vec{B}_0$, total reflection of the wave: We assume that $\varkappa(s)$ changes substantially only in the interval $s_1 < s < s_m$, $(s_m - s_1)$ is much less than the skin depth $c(\omega_0^2 \varkappa - \omega^2)^{-1/2}$; $\varkappa(s_1) \gg q\, \varkappa(s_m)$. It is then $P_{Jk}/P_J = q^{-1}[\varkappa(s_1) - 1]/[\varkappa(s_m) - 1]$; q is chosen according to the definition mentioned above, with $E(s_1) = 2E_J/(1+N_m)$, $N_m = i\left[\varkappa(s_m)\omega_0^2(s_m)/\omega^2 - 1\right]^{1/2}$. The allowable temperature is relatively low. E.g., for $\omega_0^2(s_m)\varkappa(s_m) = 2\omega^2$, $\varkappa(s_1) = 15$, $q = 5/2$, it must be $T_e \lesssim 10^{-12}$ erg.

5. Inhomogeneous $\vec{B}_0$, no reflection of the wave: We suppose $\omega_0^2 \varkappa < \omega^2$, the W.K.B. approximation is valid. A transcendent (but not differential!) equation for the concentration $n(s)$ has been derived [3], which must be solved numerically. The main results, however, can be formulated analytically:

$$\frac{P_{Jk}}{P_J} = \frac{\omega_0^2(s_1)\,\varkappa(s_1)}{4 q \omega^2}\,\frac{\varkappa(s_1)-1}{\varkappa(s_2)-1}, \quad E(s_1) = E_J, \quad T_e \lesssim \frac{m_e c^2}{q[\varkappa(s_1)]^2},$$

s_2 is in the region of homogeneous plasma.

6. Inhomogeneous $\vec{B}_0$, partial reflection of the wave on the boundary of plasma ($s = s_1$): The W.K.B. approximation is now assumed to be valid for $s > s_1$. The temperature T_e is limited approximately as in the previous case and

$$\frac{P_{Jk}}{P_J} = \frac{\omega_0^2(s_2)\,\varkappa(s_2)}{q\omega^2(1+N_1)^2}\,\frac{\varkappa(s_1)-1}{\varkappa(s_2)-1}, \quad N_1 = \left[1 - \frac{\omega_0^2(s_1)}{\omega^2}\varkappa(s_1)\right]^{1/2}, \quad E(s_1) = \frac{2E_J}{1+N_1}$$

The space distribution of concentration and other quantities has been found numerically [3].

We conclude that the mirror magnetic field yields some advantages in comparison with the homogeneous field, when the plasma and field parameters are chosen carefully. The required incident wave power can be less and (in the cases 5. and 6.) the allowable temperature of electrons can be higher. If the temperature of ions is not negligible, $T_i \gtrsim T_e$, the limits for T_e are unchanged; T_e is replaced by $T_e + T_i$ in the remaining equations. Further results and references can be found in the preprint [3].

The author is indebted to the participants of the seminar held at the Institute on 10 December 1968 for the review of the results presented here.

References

[1] Teichmann J., Beitr. Plasmaphys. 5 (1965) 13.

[2] Motz H. und Watson C.J.H., Adv. E. E. Phys. 23 (1967) 153.

[3] Klíma R., Preprint IPPCZ - 121, Prague 1968.

[4] Miller M.A., Radiofizika (USSR) 1 (1958) 110.

[5] Klíma R., J. E. T. P. (USSR) 50 (1966) 807.

[6] Klíma R., Czech. J. Phys. B 17 (1967) 996.

[7] Watson C.J.H., Preprint CLM - P164 Culham 1968.

ON THE STABILITY OF A MAGNETIZED PLASMA CONFINED WITH H.F. FIELDS

by

H.J.L. Hagebeuk

Association Euratom-FOM

FOM-Instituut voor Plasma-Fysica,

Rijnhuizen, Jutphaas, The Netherlands

A magnetized plasma can be confined in a cylindrical cavity excited in the TM_{011} mode. The leakage of particles along the magnetic lines of force is suppressed by the z-component of the time average h.f. force[1)]

$$F_z = -e\frac{\partial\psi}{\partial z} = -\frac{e^2}{4m\omega^2}\frac{\partial}{\partial z}\left(E_{//}^2 + \frac{\omega^2}{\omega^2-\Omega^2}E_\perp^2\right). \qquad (1)$$

There is no h.f. confinement in the perpendicular plane, because there is no azimuthal gradient of the h.f. field. Radially, the collisional diffusion of electrons and ions across the magnetic field will determine the electron density distribution. In addition to axial confinement, the h.f. field supplies energy to the plasma. In the steady state, balances must exist between production and loss of particles, and between gain and loss of energy.

According to the perturbation formula[2)]

$$\frac{\delta\omega}{\omega} = \frac{\int \frac{e^2 n_e(r,z)}{m\omega^2}\left(E_{//}^2 + \frac{\omega^2}{\omega^2-\Omega^2}E_\perp^2\right)dVol}{2\int \varepsilon_o E^2 dVol} \qquad (2)$$

the resonance frequency of the cavity is shifted by the presence of a plasma. Without the magnetostatic field the frequency shift is positive and proportional to the electron density. The addition of a magnetostatic field above cyclotron resonance makes it possible to have a plasma in the cavity without the cavity being detuned, as the volume integrals over $E_{//}^2$ and $E_\perp^2$ can compensate[3)]. Numerical calculations yield an approximation

$$n_e(r,z) \approx n_o J_o\left(2.4\frac{r}{R}\right)\left(\sin\frac{\pi z}{L}\right)^{5.08 + 0.56\, e\psi_m/kT}, \qquad (3)$$

where ψ_m is the height of the h.f. barrier on the axis of the cavity. It is seen that the frequency shift is zero if

$$\frac{\omega^2}{\omega^2-\Omega^2} = -\frac{\int n_e(r,z)E_{//}^2 dVol}{\int n_e(r,z)E_\perp^2 dVol} = -\frac{1}{3.04 + 0.28\frac{e\psi_m}{kT}}\left(\frac{2.4\,L}{\pi R}\right)^2. \qquad (4)$$

Schematically, we have for the steady state

$$\psi_m \rightarrow \boxed{\begin{matrix}\text{energy balance}\\ \text{part. balance}\end{matrix}} \rightarrow \left.\begin{matrix} kT, \frac{n_o}{n_n} \\ \Omega, n_n \end{matrix}\right\} \rightarrow \boxed{\text{pert. form. (2)}} \rightarrow \left.\begin{matrix} \omega_{res} \\ \omega, P, Q \end{matrix}\right\} \rightarrow \boxed{\text{res. curve}} \rightarrow \psi_m$$

Here, ω_{res} is the resonance frequency of the cavity with plasma, ω and P are the frequency and power of the h.f. source, Q is the quality factor of the cavity, and the resonance curve of the cavity is given by

$$\psi_m = \frac{\psi_o(P,Q)}{1+4Q^2\delta^2} \quad \text{with} \quad \delta = \frac{\omega_{res}-\omega}{\omega_{res}}. \qquad (5)$$

The independent variables are Ω, n_n, ω, P, and Q, whereas the dependent variables are kT, n_o/n_n, ω_{res}, and ψ_m.

Electron-electron collisions cause diffusion in velocity space and thus escape of the most energetic electrons over the h.f. barrier

$$F_{esc} = \nu_{e\text{-}e} n_e \varepsilon^{-e\psi_m/kT}. \qquad (6)$$

This flux of particles must be produced by ionization and if one neglects diffusion losses the particle balance for electrons becomes on the axis

$$\int_0^L n_e n_n \langle\sigma_{ion}v\rangle\, dz = \int_0^L \nu_{e\text{-}e} n_e \varepsilon^{-e\psi_m/kT}\, dz. \qquad (7)$$

As the electrons move adiabatically in the h.f. field we take the ionization rate $\langle\sigma_{ion}v\rangle$ to be independent of ψ. Also, $\langle\sigma_{ion}v\rangle$ must be calculated for a truncated Maxwellian velocity distribution. The quantity kT is only the parameter in the distribution function and the average energy, $\langle E\rangle$, can deviate strongly from $\frac{3}{2}$ kT.

The h.f. electric field supplies energy to the plasma. On the axis, this energy gain through collisions is:

$$P_{e.m.} = \int_0^L (\nu_{e\text{-}n}+\nu_{e\text{-}i})\frac{n_e e^2 E_{//}^2}{2m\omega^2}\, dz. \qquad (8)$$

The electrons lose their energy in ionizing and exciting collisions:

$$P_{ion+exc} = \int_0^L n_e n_n \langle\sigma_{ion}v\rangle\, 2.2\,eV_{ion}\, dz. \qquad (9)$$

Escaping electrons cause an energy loss:

$$P_{esc} = \int_0^L \nu_{e\text{-}e} n_e \varepsilon^{-e\psi_m/kT}\, 3\, e\psi_m dz \qquad (10)$$

Equating (8), (9), and (10) gives the energy balance for electrons. The solution of the balance equations is shown in Figs. 1 and 2.

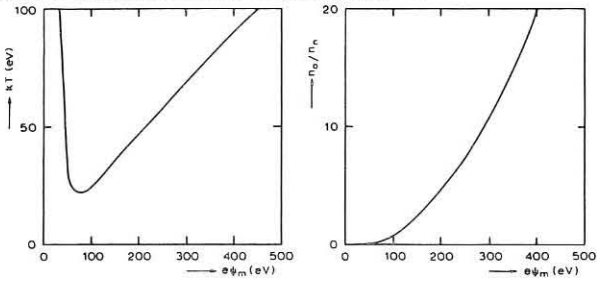

From Fig. 1 it is seen that there are two regimes, separated at $\psi_m \sim 75$ V. For $\psi_m < 75$ V, the electron velocity distribution deviates strongly from the Maxwellian, $kT \sim e\psi$, and $\langle E\rangle \ll \frac{3}{2}$ kT, whereas for $\psi_m > 75$ V, the electron velocity distribution is almost Maxwellian, $kT \approx 0.23\, e\psi$, and $\langle E\rangle \approx \frac{3}{2}$ kT.

Now we consider the stability of the cavity with plasma against perturbations of ψ, caused by small perturbations of P, on two different time scales: 1) connected with the pressure balance ($\tau \sim Q/\omega$), where n_o and kT are constant, and 2) connected with the energy balance ($\tau \sim$ collision times), where n_o and kT can vary.

Suppose that the cavity with plasma is excited at a frequency ω near its resonance frequency ω_{res} and a steady state is reached. Consider a fast perturbation of P on a time scale where n_o and kT are constant. Then, combining the effects of variation of (2) and (5), we obtain ($A = e\psi_m/kT$):

$$\frac{\partial\psi_o}{\partial P}\delta P = \left\{1+4Q^2\delta^2 - 0.0024A\left[1-36.4\frac{\Gamma(3.04+0.28A)}{\Gamma(4.54+0.28A)}\frac{\omega^2}{\omega^2-\Omega^2}\right]\frac{\omega_{po}^2}{\omega^2}8Q^2\delta\right\}\delta\psi_m. \qquad (11)$$

Thus small perturbations of P give rise to large perturbations of ψ_m if there exists a value of δ such that the coefficient of $\delta\psi_m$ is zero. There are no such values of δ if

$$-1 < 0.0048A\left[1-36.4\frac{\Gamma(3.04+0.28A)}{\Gamma(4.54+0.28A)}\frac{\omega^2}{\omega^2-\Omega^2}\right]\frac{\omega_{po}^2}{\omega^2}Q < 1. \qquad (12)$$

Correspondingly, on a slow time scale where n_o and kT can vary we find by variation of the particle and energy balances, (2), and (5)

$$\frac{\partial\psi_o}{\partial P}\delta P = \left\{1+4Q^2\delta^2 + 0.33\frac{\Gamma(3.04+0.28A)}{\Gamma(4.54+0.28A)}\left[1+(5.82+0.54A)\frac{\omega^2}{\omega^2-\Omega^2}\right]\frac{\omega_{po}^2}{\omega^2}8Q^2\delta\right\}\delta\psi_m. \qquad (13)$$

The system is again stable if there are no such values of δ that the coefficient of $\delta\psi_m$ is zero:

$$-1 < 0.66\frac{\Gamma(3.04+0.28A)}{\Gamma(4.54+0.28A)}\left[1+(5.82+0.54A)\frac{\omega^2}{\omega^2-\Omega^2}\right]\frac{\omega_{po}^2}{\omega^2}Q < 1. \qquad (14)$$

In Figs. 3 and 4 the stable regions (unshaded) are shown for A = 4.3 on both sides of the resonance curve.

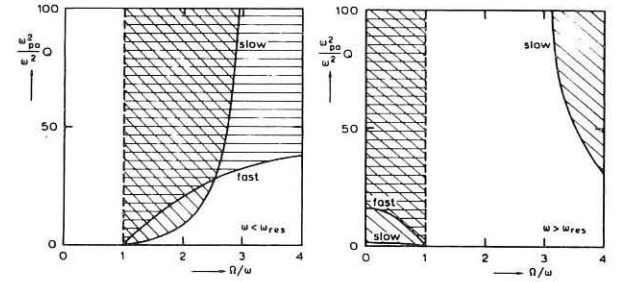

In the experiment the cavity is excited in the TM_{011} mode with a magnetron (2 kW CW, 2450 MHz, $\psi_m = 40$ V); it is filled with hydrogen at a pressure between 10^{-6} and 10^{-4} Torr. The electron density is obtained from the shift of the resonance frequency of the TM_{020} mode, excited simultaneously. On the high-frequency side ($\omega > \omega_{res}$) of the resonance curve of the cavity a stable plasma is present for $1.2 < \Omega/\omega < 3$ (compare Fig. 4). The electron density is proportional to the neutral hydrogen density ($n_o/n_n \approx 10^{-3}$) and independent of the strength of the magnetic field (compare Eq. (7)). The low-frequency side ($\omega < \omega_{res}$) of the resonance curve is unstable for $\Omega/\omega < 2.3$.

The author is grateful to Prof. C.M. Braams and to L.Th.M. Ornstein and M.P.H. Weenink for suggestions and helpful criticism, to H. Lemmen and C.A.J. van der Geer for able assistance, and to Mrs. H. Toft-Betke for the composition of the manuscript.

This work was performed under the association agreement of Euratom and FOM with financial support from ZWO and Euratom.

References:

1) A.V. Gaponov, and M.A. Miller, Zh. Eksperim. i. Teor. Fiz., 34 (1958) 242.

2) S.J. Buchsbaum, L. Mower, and S.C. Brown, Phys.Fluids, 3 (1960) 806.

3) H.J.L. Hagebeuk, Rijnhuizen Report 68-46 (thesis 1968).

NONLINEAR EFFECTS IN ELECTRON CYCLOTRON HEATING

M. BRAMBILLA

CENTRE d'ETUDES NUCLEAIRES DE SACLAY

Service d'Ionique Générale

Département de Physique du Plasma et de la Fusion Contrôlée
B. P. n°2 - 91-Gif-sur-Yvette (France)

This paper is an extension of the work of Stix [1] on the absorption of a circularly polarized electromagnetic wave at the cyclotron resonance in a cold nonuniformly magnetized plasma. Our purpose is to apply the modified theory to experiments on electron cyclotron heating with high R. F. power, such as those made in Saclay [2]. In these experiments nonlinear phenomena (accceleration along the magnetic lines by the $\vec{\mu}\cdot\vec{\nabla}B$ force, relativistic shift of the resonance condition) may be very important in the motion of the electrons in the resonance zone [3]. We wish to take these effects into account in evaluating the efficiency of power absorption by the plasma.

Outside the resonance zone the usual cold plasma, small signal approximation can be used, implying that the field equation is

$$\frac{d^2E_\perp}{dz^2} + \left(1 - \frac{A}{z}\right)E_\perp = 0$$

Here $A = (\omega_p^2/\omega^2\delta)$, with $\delta = \left[B_0^{-1}(\partial B_0/\partial z)\right]_{z=0}$; units are such that $\omega = c = 1$, and the complex notation $E_\perp = E_x + iE_y$ is used. The solution of Eq. (1) satisfying the appropriate conditions at infinity is

$$E_\perp(z) = \begin{cases} \alpha M_{\frac{iA}{2},\frac{1}{2}}(2iz) + \beta W_{\frac{iA}{2},\frac{1}{2}}(2iz) & \text{for } z > 0 \\ \beta' W_{\frac{iA}{2},\frac{1}{2}}(2iz) & \text{for } z < 0 \end{cases}$$

where M and W are Whittaker's functions [5]. If the resonance zone is thin, we can describe it as a current sheet of intensity $J_\perp^* = \sigma^* E_\perp(z=0)$. Then the conditions which determine the ratios of the coefficients in Eq. (2) are the continuity of the electric field and the jump of the magnetic field of the wave at the resonance plane due to this current sheet. This model was first proposed by A. F. Kuckes [4] for the linear case.

These conditions lead to the following expressions for the coefficients of reflection R, transmission T and absorption η:

$$R = e^{-\pi A}\,Sh^2\left(\frac{\pi A}{2}\right)(\gamma-1)^2/|\Delta|^2 ; \quad T = e^{-\pi A}/|\Delta|^2 ; \quad \eta = 2\gamma e^{-\frac{\pi A}{2}}\,Sh\left(\frac{\pi A}{2}\right)/|\Delta|^2 \quad (3)$$

where $\Delta = 1 + (\gamma-1)e^{-\pi A/2}\,Sh\left(\frac{\pi A}{2}\right)$ and $\gamma = 4\sigma^*/A$.

We are concerned with a plasma in which thermal effects are small, so that the mechanism responsible for the absorption is the coherent acceleration of the electrons at the resonance [2]. Then the quantity σ^* can be evaluated using the nonlinear theory of the electron orbits developed by E. Canobbio [3]. Since outside the resonance the refractive index is hermitean, we can write

$$\sigma^* |E_\perp(0)|^2 = Re\left\{\int_{-\infty}^{+\infty} \sigma(z)\,|E_\perp(z)|^2\,dz\right\}$$

This integral represents the power dissipated per unit area in the resonance plane; it is therefore equal to the kinetic energy K gained by each particle, multiplied by the flux of particles. K is given for different physical situations in Ref. [3].

If the equations of motion can be linearized inside the resonance zone ($v_\parallel^2 >> \left|\int \vec{\mu}\cdot\vec{\nabla}B\,dz\right|$) one finds $K = 2\pi q_p^2 (\delta v_\parallel/c)^{-1}$, where $q_p = |E_\perp(z=0)|/B_0$ is proportional to the electric field at the resonance. Thus $\gamma = 1$, and expressions (3) reduce to those obtained by Stix :

$$R = 0 ; \quad T = e^{-\pi A} ; \quad \eta = 1 - e^{-\pi A} \quad (4)$$

Stix derives these results using the "Ansatz" that the solution for $z < 0$ be the analytic continuation of the solution for $z > 0$. Our method, based on a detailed energy balance, shows that this Ansatz is justified in this particular case.

As an example of the application of the more general equation (3), let us consider the case in which the energy gained by each electron in the resonance is limited by relativistic and Doppler effects, a case frequently encountered in experiments [2]. Then $K = \left[q_p/|1 - N_r(N_r - iN_i)|\right]^{2/3}$ ([3], [6]) where

$$N \equiv N_r + iN_i = i\,E_\perp^{-1}(dE_\perp/dz)_{z=z_R} = -1 + iA\left[\ln 2z_R + i\frac{\pi}{2} + \psi\left(1 - \frac{iA}{2}\right)\right] \quad (5)$$

ψ being the logarithmic derivative of the Γ-function. z_R is the width of the resonance region which depends in turn on N and q_p. However, for sufficiently large A we have $N \approx iA\ln(Az_R) + O(A^{-2})$, so that it is easily seen that the factor containing N in the expression for K can be replaced by unity. To make our calculation self-consistent, we must express q_p in terms of q_0, the value of $E_\perp(0)/B_0$ in the absence of the plasma. This leads to

$$\gamma = \frac{2}{\pi}\delta\frac{v_\parallel}{c}\frac{1}{q_0^{4/3}}\left(\frac{\pi A}{1-e^{-\pi A}}\right)^{2/3}|\Delta(\gamma)|^{4/3} \quad (6)$$

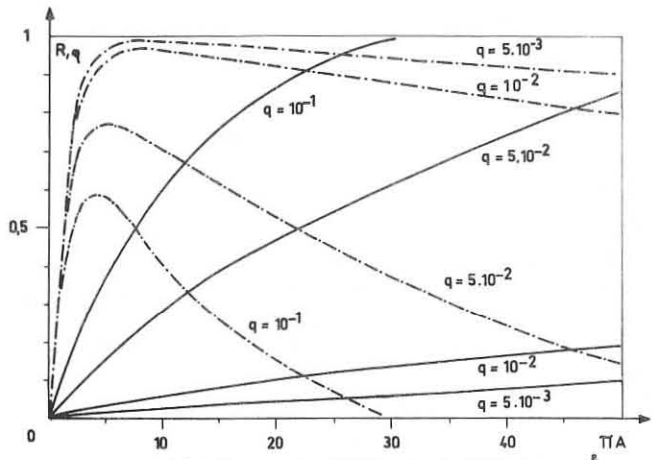

Fig. 1 - R (dotted lines) and η (full lines) as functions of $A = \frac{\omega_p^2}{\omega^2\delta}$.

Solving this equation for γ and substituting into Eq. (3) completely solves the problem. The results are shown in Fig. (1) for different values of $q = \frac{2}{\pi}\delta\frac{v_\parallel}{c}q_0^{-4/3}$.

From Eq. (6) we see that γ is small compared to unity, as long as

$$A \ll q_0^{-2}(\pi c/2\delta v_\parallel)^{3/2} \quad (7)$$

When this condition is satisfied, the wave is strongly reflected from the resonance zone, as soon as A is larger than unity. Thus, if the R. F. power is high and the velocity with which the particles are injected is low, efficient coupling can be reached only if the plasma density is sufficiently high. In fact, as the density increases, the electric field at the resonance decreases. Eventually, when condition (7) is violated, q_p is so small that nonlinear effects become negligible, γ approaches unity, and R, η, T approach the values given in Eq. (4).

It should be noted that we are justified in considering the resonance region as being thin only if $|z_R(dE_\perp/dz)_{z_R}| \ll |E_\perp(0)|$, i. e. if

$$Az_R \ll 1 \quad (8)$$

A closer consideration of the results of Ref. [3] shows that condition (8) can be satisfied at densities such that the linear regime is attained only if the axial motion of the electrons is strongly coupled to the motion of the ions through the space-charge electric field [7]. If the electrons move freely along the lines of force, condition (8) is usually more severe than contition (7). In this case it is more difficult to follow the transition to the linear regime.

In the preceding analysis we have neglected the effects of the electron temperature. These effects can be strong, since it has been shown [4] that if the linear theory applies and if $(\omega_p^2/\omega^2) \gtrsim \delta(\delta c/v_{therm.})$ absorption by Landau damping before the resonance becomes dominant. A study of the nonlinear effects when the temperature is significant has not yet been done.

Finally it can be shown that due to the spatial dependence of the magnetic field the transverse wave described by Eq. (1) couples with an electrostatic wave outside a region of radius $r \approx 2z_R\left|1 - \frac{\omega^2}{\omega_p^2}\right|$ near the resonance plane. Thus, at densities such that $\omega_p^2 \gtrsim \omega^2$ the electron acceleration can be strongly influenced by the existence of a non negligible component of the electric field along the magnetic lines.

1 T. H. STIX, The theory of plasma waves, Ch. 10, Mc Graw Hill 1962

2 T. CONSOLI, 3d Int. Conf. on Plasma Physics and Controlled Nuclear Fusion Research, Novosibirsk, 1968, Paper CN-24/J1

3 E. CANOBBIO, Nuclear Fusion 9, , 1969

4 A. F. KUCKES, Plasma Physics 10, 366, 1968

5 E. T. WHITTAKER, G. N. WATSON, A course of modern analysis, Ch. 16, Cambridge Univ. Press , 1963

6 C. S. ROBERTS, S. J. BUCHSBAUM, Phys. Rev. 135, A 381, 1964

7 E. CANOBBIO, U. FINZI, 2ème Colloque International sur les interactions entre les champs oscillants et le plasma, Saclay 1968, p. 605.

ELECTRON CYCLOTRON RESONANCE EXPERIMENTS IN ICARE IN THE PRESENCE OF A SYMMETRIC MAGNETIC FIELD

J. BOSSAERT, P. BRIAND, T. CONSOLI, P. GRELOT, F. PARLANGE
W. J. SCHRADER*, L. SLAMA et P. VIAL

CENTRE d'ETUDES NUCLEAIRES DE SACLAY
Service d'Ionique Générale
Département de Physique du Plasma et de la Fusion Contrôlée
B. P. n°2 - 91 - Gif-sur-Yvette (France)

INTRODUCTION : In the machine ICARE (cf. fig. 1) plasma interacts with a high-powered linearly polarised e.m. wave propagating in a cylindrical guide parallel to the magnetic field, with up to 1 MW at 1,25 GHz during 100 μs. The plasma is formed by laser impact on a solid target, and the background pressure is $\leqslant 10^{-6}$ torr. In previous experiments /1/ microwave acceleration of plasma was studied with one mirror suppressed. Up to 1 A of 20 keV deuterons was obtained at resonance. Results at higher magnetic fields (up to $2B_{res.}$) were similar. In the present work we shall consider the accumulation of plasma in the presence of two mirrors.

EXPERIMENTS AND RESULTS ON ACCUMULATION : The R.F. power is fed in symmetrically from both ends and the initial plasma is formed by laser impact on an Al_2O_3 target. The resulting characteristics are very similar to those of the D_2 plasma used before. The electron density was measured with a 4mm interferometer, the total plasma energy with a magnetic flux coil around the plasma on the inside of the guide wall, and the hot electron energy by means of the X-ray from a metallic target at the edge of the plasma. Although accumulation of a hot electron plasma could be obtained for a wide range of the magnetic field, measurements were made for $0,4 < B_0/B_{res} < 1,1$, where B_0 is the magnetic field in the center of the bottle. The optimum results were obtained for B_0/B_{res} around 0,75. The target was located at $1,5\ B_{res}$, well behind the resonance zone. Fig. 2 gives the magnetic flux change as a function of laser energy.

The interaction typically shows two distinct phases which are characterized respectively by strong and weak absorption. The strong absorption regime follows immediately after the formation of the plasma and lasts on the average of 10 μs. After this period, one enters into the weak absorption regime where the plasma appears to be quiet. The transition to the afterglow is not particularly marked. This evolution of the plasma is illustrated experimentally in fig. 3, which shows the temporal behaviour of plasma energy and density for two different laser energies. It is seen that the cold electron plasma decays much faster than the hot plasma (0,5 and 1,5ms. respectively). The time of 1,5ms is also found from the X-ray intensity. Without R.F. the 10^{11} to 10^{13} eV/cm^3 laser plasma decays in about 20 μs. The X-ray spectrum showed a temperature of about 20keV.

The density profile of the hot electrons has been determined from perturbations of the flux of the magnetic coil resulting from the presence of a radial probe as shown in fig. 4. Fig. 5 gives finally the variation of the plasma energy with R.F. power. It is indicated that work on ion energy is in progress, but at present, the data is not conclusive.

DISCUSSION : Assuming that the distribution over the cross section of fig. 4 leads to a plasma pressure of approximately 3×10^{14} eV/cm^3 the corresponding value of $\beta (= 8\pi nkT/B^2)$ will be slightly over 0,1. The actual values may be even higher since no account has been taken of the lines of force that close on themselves in the interior of the magnetic loop. This value of β is not very different from the limit set by the pressure anisotropy mirror instability, which in our case is $\beta \simeq 0,25$ by following the work of Ard and al. /2/.

If one assumes that the cold electrons are distributed uniformly in space and that the hot electrons have a temperature of 20 keV, a ratio of cold to hot electron density of about 6 is found initially. This value will clearly be smaller in the afterglow due to the difference in decay times. Obviously at the beginning and probably later, the quiet behaviour must be attributed to the presence of a sufficient number /3/ of cold electrons which effectively short-circuit the electric field. This electric field could arise from macro-instabilities. The decay of the hot electrons agrees well with scattering into the loss-cone on the background gas.

The variation of plasma energy with R.F. power indicates the existence of two regimes of power transfer, which is in agreement with the theory of acceleration of Brambilla /4/. In the low power regime the absorption is total, while in the high power regime Doppler and relativistic effects are important, leading to a non-negligible reflection of the e.m. wave and less than proportional growth of plasma energy with power. The agreement of both β in the region where the bend in the curve occurs (0,2 theoretical and 0,1 experimental) and the slope in the high-power part of the curve (1/3 theoretical and experimental) supports the theoretical model.

CONCLUSION : It has been shown that a relatively short period of R.F. heating - 100 μs, of which approximately 10 correspond to strong absorption - highly improves the confinement of a laser-produced plasma in a simple mirror machine ; the decay time rises from 20 to 1500 μs. Since the value of β that was obtained is close to the limiting value of this magnetic field configuration, the machine has probably yielded optimum results. A better performance would require a stronger magnetic field and a minimum B configuration.

REFERENCES

/1/ T. CONSOLI - NOVOSIBIRSK, Conference 1968, paper CN24 - J1
/2/ W. B. ARD, R. A. DANDL, and R. F. STETSON, Phys. Fluids 9, 1498, 1966.
/3/ W. B. KUNKEL and J. U. GUILLORY, Proc. Conf. on Phen. in Ionized Gases, II p.702, Belgrad 1965.
/4/ M. BRAMBILLA, Proc. Conf. on Phen. in Ionized Gases, Belgrad 1965.

* Association Euratom - FOM Instituut voor Plasmafysica Jutphaas - The Netherlands.

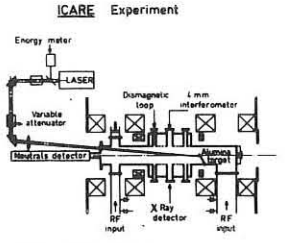

Fig 1. Diagram of the experiment

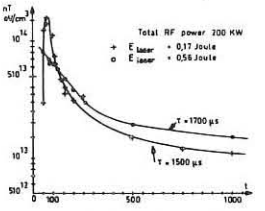

Fig 3. Behaviour of diamagnetic loop signal in time

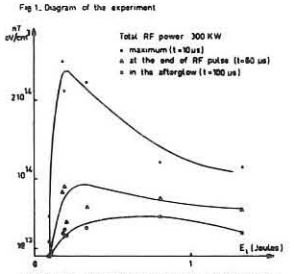

Fig 2. Variation of diamagnetic loop signal with laser energy

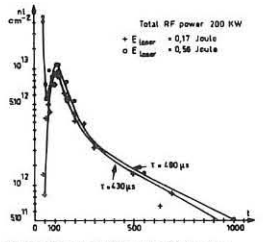

Fig 3bis. Behaviour of interferometer signal in time

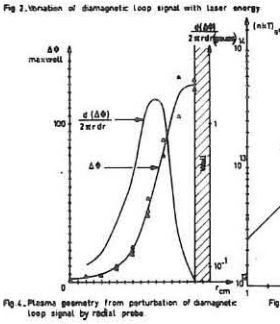

Fig 4. Plasma geometry from perturbation of diamagnetic loop signal by radial probe

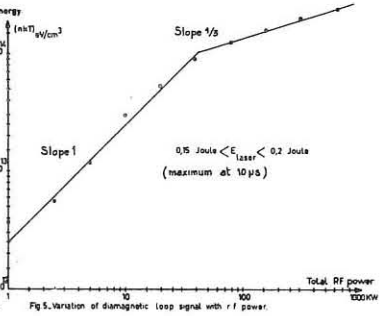

Fig 5. Variation of diamagnetic loop signal with r f power

ENERGETIC PARTICLE ACCUMULATION IN THE PLEIADE MIRROR DEVICE

R. GELLER, B. JACQUOT, C. JACQUOT
CENTRE d'ETUDES NUCLEAIRES DE SACLAY
Service d'Ionique Générale
Département de Physique du Plasma et de la Fusion Contrôlée
B. P. n°2 - 91- Gif-sur-Yvette (France)

I - a) THE PRINCIPLE OF ACCELERATION : On the left side of the device (fig. 1) the preionization is created in a capillary tube ϕ = 8mm, $p=10^{-3}$ torr) by the RF leakage field of a cavity. The energetic electrons are generated in the resonance $\omega_c^- = \omega_{RF}$ obtained with a continuous standing wave (3000 MHz, P_{RF}=500 W) inside the RF cavity (Mode TE_{111} $p\leq 10^{-5}$ torr) located in the steady state gradient of a magnetic mirror. As a result of this gradient, the spiraling electrons are driven towards the decreasing magnetic field, and ions are accelerated in the same direction by an ambipolar space charge field + $E_{//}$ along the axis. The electron energy ($W_\perp^- \sim W_{//}^+ \sim W$) is given by $W_\perp^- = mc^2/2\,(1-\delta z)\,g^{2B}$; $\delta = 1/B_0 \cdot \Delta B/\Delta z \cdot c/\omega$; $g = eE_{RF}/m\omega$. The ion energy $W_{//}^+$ equals a potential ϕ, which is roughly determined by $W_{//}^+ \propto (Q\,P_{RF})^{1/3}$ $(Q_0/Q_0-Q)^3 \propto P_{RF}^2/n_0^3$ where Q_0 and Q represent the unloaded and loaded cavity n_0 being the density of the preionized cold plasma. In the present case $W \sim 1$ KeV is expected.

b) THE PRINCIPLE OF REFLECTION AND ACCUMULATION : On the right side of the device a pulsed magnetic field is established either by a rectangular current pulse, the duration of which can vary between 70 μs and 600 μs, or by a 50 p/s sinusoidal current. This mirror reflects the energetic electrons ($W_\perp^-/W_{//}^- \gg 1$) and their reflection creates a symmetrical space charge field $-E_{//}$ for the ions which in turn are also reflected. In this manner, during the existence of the mirror, spiraling electrons and axially accelerated ions are reflected and accumulated inside the magnetic bottle. Hence the velocity space is no longer characterized by the loss cone of the usual mirror configuration. The loss cone is substituted by loss hyperboloïds. A one sheet hyperboloïd for the electrons and a two sheet hyperboloïd for the ions. Between these two sheets ions with almost isotropic velocity distribution can by confined. This situation can be achieved, provided that the RF field is able to prevent the electrons from diffusing through their one sheet loss hyperboloïd over a large number of electron oscillations between the mirror points (fig. 2). At high RF field amplitudes, when the wave particle phase difference φ in the resonance region is controlled by the relativistic variation of mass, it is found that at each axial oscillation $\langle W_\perp^- \rangle_\varphi$ increases. In this manner, we have in addition to an RF plug a supplementary heating.

II - EXPERIMENTAL RESULTS : Optical diagnoctics measure the continuum (mainly generated by H^2 dissociation and therefore proportional to the density of energetic electrons with $W^- > 20$ eV and H_β line (cold plasma). X ray intensity and spectrun provide information of electron energy, velocity distribution and density without the mirror and during the accumulation. Fast neutrals coming out from both sides of the bottle give the same indications for the energetic hydrogen ions (fig. 5). Pyrometric probes, ES probes and RF probes measure the energy flux, particle densities and RF noise in the plasma. Without the pulsed mirror up to 10% of the RF power is coupled to the plasma beam. $W_{//}^+ \sim W_\perp^- \sim 1$ KeV ; $n^+ \simeq 3\,10^8\,cm^{-3}$; $I^+ \simeq 2$ mA/cm^2 At the end of the mirror pulse $T_B = 200\,\mu s$: $I^+ \propto 200$ mA/cm^2; $n^+ \simeq 3\,10^{10}\,cm^{-3}$ and ionic energy increases slightly (additional acceleration) (fig. 3). As long as the signal $N_0^{\rightarrow}$ of the fast neutrals increases, the injected ions are alive. At $2\,10^{-5}$ torr the life time is of the order of 200 μs, which is compatible with charge exchange losses. No severe instabilitiesare present. Even with a pulsed mirror of T_B=600 μs the signal shows a saturation which can be explained by charge exchange (life time $\sim$ 300 μs at 10^{-5} torr). Under these conditions a better vacuum may still improve the performance (fig. 4 a). With a 50 p/s sinusoïdal current in the mirror coil, accumulation is also possible. However since the rise time of the magnetic field is longer than the life time of the ions, only rough evaluations on the accumulation are available (fig. 5 a). It was shown that with a strong mirror cold plasma is also trapped (fig. 5 c) and when the H_β line is detected no accumulation is possible. Instabilities or a short circuit of the $E_{//}$ field by the cold plasma might occur. The creation of a potential ϕ_2 in the mirror region was experimentally ascertained. Floating potentials of hundreds of volts (+V) are detected in the mirror during the time the reflections occur. The existence of ϕ_2 is always related to stable accumulation signals. When for a given reason ϕ_2 collapses, the accumulation is perturbed (either by instabilities or by the presence of a cold plasma) (fig. 4b et 5b).

III - CONDITIONS FOR STABLE ACCUMULATION : In order to obtain a stable behaviour, some conditions have to be fulfilled . a) When the pulse mirror field is zero, the continuously accelerated plasma beam must be trapped behind the mirror zone and recombined on a target. This condition is necessary in order to avoid that beam electrons return towards the cavity after retrodiffusion on the end wall of the device. Such particles after colliding with a wall have lost their anisotropy and perturb badly the ion accumulation mechanism. In order to achieve a good recombination of the beam particles, beyond the mirror and far away from the axis, the beam is deflected by a magnet, towards a floating recombination target. b) Close to the regions where electric fields are created and where ϕ potentials are developed, grounded walls should by eliminated. Destruction of the accumulation mechanism for the ions and emission of RF noise with a peak at ω_c^+ are observed whenever the wall near the reflection region is connected to the ground, whereas floating quartz or spray coated walls give correct results(fig. 6 et 7)(This situation might also be true in other types of mirror devices). c)As previously mentioned, cold plasma destroys the space charge fields and a good vacuum is therefore indispensable ($p < 5.\,10^{-5}$ torr). A strong mirror ratio trapping the cold plasma plays the same role than high neutral pressure.

Bibliographie
2ème Colloque International sur les Interactions entre les Champs Oscillants et les Plasmas - Saclay, Janvier 1968 - Vol. II, p. 541 - 70

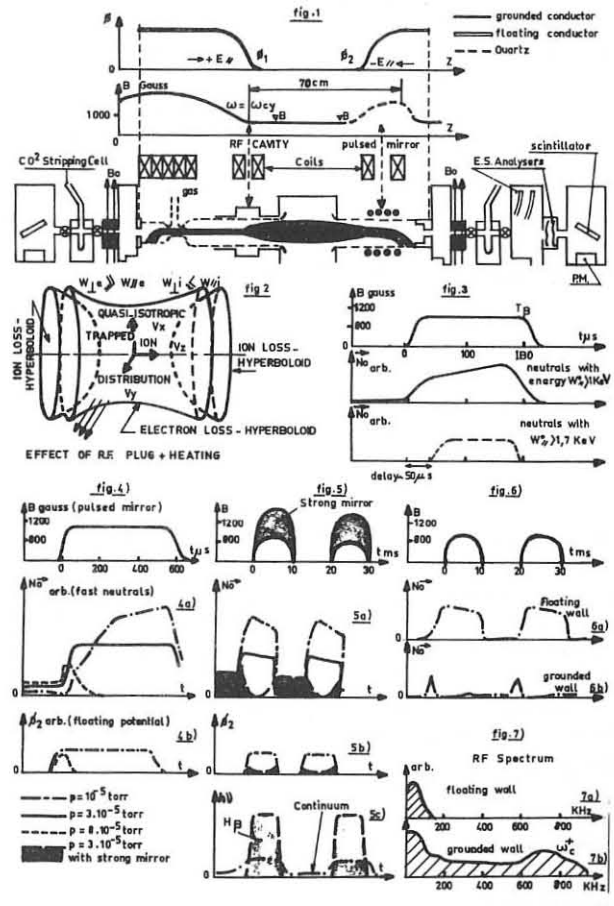

ION HEATING AND TRAPPING IN HOT ELECTRON MIRROR MACHINES

E. Canobbio *, O. De Barbieri, U. Finzi, S. Giuffré *

R. Bardet, L. Dupas, C. Gormezano

CENTRE d'ETUDES NUCLEAIRES DE SACLAY

Service d'Ionique Générale
Département de Physique du Plasma et de la Fusion Contrôlée
B. P. n°2 - 91 - Gif-sur-Yvette (France)

In this paper some aspects of ion coherent acceleration, turbulent heating of ions and electrons and electrostatic ion confinement are considered in a mirror machine where the plasma electrons are heated at the cyclotron resonance. Effects due to non-linearities in the motion of resonant particles and in HF wave propagation have been considered in/1-2/. Here we shall examine other factors which limit the power transfer.

The collisions limit the electron HF heating efficiency when

$$\int_0^{\tau_R} \nu_{eff}(\tau)\,d\tau > 1 ,$$

τ_R being the resonance time. By following Ref. /1/ and by using the Spitzer τ_D time, we find a limit due to Coulomb collisions when

$$A_1 \equiv 10^8\, n\, \ln\Lambda\, (\omega_{HF} v_{\parallel}^2 g)^{-1} > 1 , \quad [n(cm^{-3}), v_{\parallel}(cm/s)]$$

where $v_{\parallel}$ is the electron injection velocity and $g = E_{HF}/300 B_0$(Volt/cm Gauss). In this case the relative axial velocity v_d of the electrons with respect to the ions is less than the ion sound speed c_s. With the parameters of our machines /3/ : Circe (10 GHz, 2.5 KW), Circe-Pleiade (3 GHz, 700 W) and Icare (1.25 GHz, 1 MW) we find : $10^{-3} < g < 10^{-2}$; $10^{-1} < (\omega_{pe}/\omega_{HF})^2 < 10^2$; $10^6 < v_{\parallel} < 5\cdot 10^6$. This shows that A_1 is just below the limit given above. Even if the turbulence level is negligible, a considerable non-collisional spread in energy and in the pitch angles of the trapped electrons may occur in this case. This is the result of phase effects between $\vec{v}$ and $\vec{E}$ after repeated crossings of the resonance region /3/ and might explain the temperature observed in the accumulation regime.

When v_d exceeds c_s, anomalous particle scattering by unstable waves must be considered /4/. A build up of low frequency waves is possible if the effective electric field is less than the Dreicer critical field, giving rise to moderate turbulence (emission in the range 0.1÷10MHz is observed in our experiments). In the opposite case, when v_d exceeds the electron parallel thermal speed $\overline{v_e}$ in the resonance region, the number of electrons which escape axially increases exponentially, and the anomalous resistivity approaches the large limiting value $\eta = 2(m_e/m_i)^{1/3}\omega_{pe}^{-1}$ predicted by Buneman for two-stream unstable plasmas. From Ref./1/ we find that a limitation due to turbulence occurs when v_d becomes larger than $\overline{v_e}$ at a time $\bar{\tau} < \tau_R$, (i. e. when $\overline{v_e}/c < \epsilon\delta$) such that $\tau_R - \bar{\tau} > \nu_{eff}^{-1}$, i. e.:

$$A_2 \equiv 4(m_e/m_i)^{1/3}(\omega_{pe}/\omega_{HF}\, g^{2/3})\left[1 - (3\overline{v_e}/4c\epsilon\delta)^{1/3}\right] > 1 ,$$

where $\delta = (c/\omega_{HF})|\nabla_{\parallel} \ln B_0|$; $\epsilon = 1$ if $\lambda_D^* \equiv (\overline{v_e}\omega_{HF}/c\omega_{pe}) > z_R \equiv 0.1\delta \cdot g^{-2/3}$ (which is the case in our experiments) and $\epsilon = O(m_e/m_i)$ in the opposite case. Here the parameters are evaluated at the point of injection. In the accumulation experiments it is found that $T_e \simeq 5 \div 20$KeV corresponding to a value of A_2 slightly above the turbulence threshold value. Moreover the plasma potential structure was found to change radically when A_2 is slightly above or below 1 (see: A. Buffa et al. Saclay Report 530(1967)). In the acceleration experiments, at low HF power ($g \lesssim 10^{-3}$), where $A_2 \lesssim 1$, no large electron temperature is observed.

Consider now the ion acceleration by the space charge field which is driven by the electrons. Coherent ion acceleration, in a $\nabla B_0 \neq 0$ region, can only be achieved in the low turbulence regime, $c_s \lesssim v_d \lesssim \overline{v_e}$. In this case the ions follow adiabatically the electron guiding centers without any considerable spread of their distribution function. The optimum energy transfer to the ions takes place if the critical condition $v_d \simeq c_s$ holds in the entire $\nabla B_0 \neq 0$ region. This implies

$$0 \lesssim eE_{eff} - (dp_i/dt)_{coll} \simeq m_e c_s/\tau_D \quad \text{where} \quad -eE_{eff} \equiv -\mu\nabla_{\parallel}B_0 - e\mathcal{E}_{\parallel} \approx -\epsilon\mu\nabla_{\parallel}B_0 .$$

Here $\epsilon = O(m_i/m_e)$ when $\overline{v_e}/\omega_{pe} \ll \delta c/\omega_{HF}$ and $\epsilon \simeq 1$ in the inverse case. Using the Spitzer diffusion coefficients, we find

$$A_3 \equiv 10^8 (c/v_{te})^2 \left[n c_s \ln\Lambda/\epsilon\delta B_0 c\right]^{2/5} \lesssim 1 .$$

Outside this narrow parameter range beam temperature effects become important. When $v_d > \overline{v_e}$ the turbulent heating efficiency is expected to increase with B_0 field strength /4/. In accumulation regimes $A_3 \approx 10^{-2}$, whereas $A_3 \approx 0.2$ in low HF power acceleration regimes. An almost monoenergetic ion population has been observed in the latter case only /3/.

The importance of temperature can be estimated by finding the limits of validity of a nonlinear cold plasma calculation /3/. In the case of a monotonously decreasing B_0 field, we get the following condition on the injection parameters in order to have $|v_d| < v_{\parallel}$

$$A_4 \equiv (\delta g^2 c/v_{\parallel})(\omega_{HF}/\omega_{pe})^3 (3m_i/m_e)^{1/2} < 1 .$$

In our acceleration experiments this condition is fullfilled. In the case of beam reflection from a magnetic mirror, the corresponding condition is

$$A_5 \equiv \left(\delta g^{2/3} c\omega_{HF}/v_{\parallel}\omega_{pe}\right)^2 (m_i/gm_e) < 1 ,$$

where $v_{\parallel}$ and ω_{pe} are now evaluated at the center of the machine and δ at the reflection point. In Circe-Pleiade and in Circe machines we have $A_5 \approx 2.5$ and in Icare, $A_5 \approx 2.5\cdot 10^3$. The condition on A_5 is usually more strigent than that on A_4 except when $\delta \simeq 0$. If one at least of these conditions is violated, the structure of the Langmuir oscillations becomes shock-like giving rise to turbulence. In that case the monoenergetic model is no longer realistic.

We are thus led to consider the electrostatic ion confinement taking particle energy and pitch angle spread into account. Since, in the presence of an electric field, the ion loss cone is replaced by a two sheet hyperboloid /5/, the trapping of a nearly isotropic ion distribution is in principle possible with a mean energy $kT_i \approx eV_0 \ll kT_e$, V_0 being the overall potential drop in the machine. T_i, or V_0, is determined by the condition that the ion and electron losses are balanced $\tau_{e_i f_e}^{(ion)} = \tau_{e_i f_e}^{(el.)}$. In a stable situation in the absence of neutral gas $\tau_{e_i f_e}^{(ion)}$ is essentially the energy relaxation time for a thermal plasma /6/. In the presence of an HF field we simply write

$$T_i \approx 10^{-4}\left(n\tau_{eff}^{(el.)} \ln\Lambda/2\right)^{2/3} \quad [T_i(eV)]$$

since no expression for $\tau_{e_i f_e}^{(el.)}(H.F.)$ is available. Only when the particle beams remain monoenergetic, the overall potential drop is uniquely determined by their characteristics and by the mirror ratio /3/. V_0 is greater in this case than when thermalization is present. We use the following trapped particle distributions

$$f_i(\mathcal{E},\mu) = K_i \exp\left\{-\mathcal{E}/kT_i\right\}\left[\mu^m (1-\eta\beta/\mu)\Theta(eV_0-\mathcal{E}) + \right.$$
$$\left. + (\mu - (\mathcal{E}-eV_0)/B(z_0))^m (1-\eta\beta/(\mu-(\mathcal{E}-eV_0)/B(z_0)))\Theta(\mathcal{E}-eV_0)\right]$$

$$f_e(\mathcal{E},\mu) = K_e \exp\left\{-\mathcal{E}/kT_e\right\}(\mathcal{E}-\mu B(o))^n \left(\mu B(z_0) - \mathcal{E} - eV_0\right)^n \quad ; V(o) = 0$$

where K_e, K_i, β are normalization constants, Θ is the step function, $\eta = 0$ or 1, $\pm z_0$ are the points at which $V = V_0$, (z is the distance along a $\vec{B}$-line of force, from the center of the machine). $f_e(v_{\parallel}, z)$, $f_i(v_{\parallel}, z)$ are double humped functions of $v_{\parallel}$ if $\eta = 1$ and single humped if $\eta = 0$. The parameters $n, m > -\frac{1}{2}$ control the degree of anisotropy of the distributions. The normalized potential $\phi_{iN} \equiv V_N(z)/V_0$ which corresponds to exact charge neutrality, is

$$\phi_{iN} = 1 - 2G\left/\left(1+\sqrt{1-8\eta G\left|\delta(2m+3)\right|}\right)\right. ; \quad G = \left[\frac{n_e(o)}{n_i(o)}\,\delta^{m-n}\left\{1+2\eta(n+1)\frac{\delta_0}{\delta}\frac{\delta-1}{\delta_0-1}\right\}\right]^{\frac{2}{2m+3}}\left(\frac{\delta_0-\delta}{\delta_0-1}\right)^{\frac{2n+1}{2m+3}}$$

where $\delta = \delta(z) \equiv B(z)/B(o)$, $\delta_0 = \delta(z_0)$. This expression is a solution of Poisson's equation to lowest order in the parameters $T_i/T_e \ll 1$, $(\lambda_{D_i}/L_B)^2 \ll 1$, $(L_B^{-1} = |\nabla_{\parallel}\ln B|$, $\lambda_{D_i}^2 = 4\pi e^2 n_i(o)/kT_i)$. Since $E_{\parallel} = -V_0\left(d\phi_N/d\delta\right)\left(d\delta/dz\right)$, the net charge in the system is zero if $\left(d\delta/dz\right)_{z=\pm z_0} = 0$. This condition holds for all trapped particle distributions dependent on $\mathcal{E}$ and μ provided that $\left(d\phi_N/d\delta\right)_{z=\pm z_0} \neq \infty$. The net charge density along z has quadrupolar structure (+ - - +) with an inhomogeneity length $L_B \gg \lambda_D$. This structure has been confirmed by axial measurements of the plasma potential and is clearly the basis of the different electrostatic phenomena observed in our machines, when isolating or conducting grounded walls are near the plasma column.

References

* EURATOM-CEA Association

/1/ E. Canobbio, Nuclear Fusion, 9, 27, (1969)

/2/ M. Brambilla, These Proceedings, (1969).

/3/ T. Consoli, Proceedings of the Novosibirsk Conference, (1969).

/4/ B. B. Kadomtsev and O. P. Pogutse, Soviet Phys. JETP, 26, 1146(1969) S. M. Hamberger and M. Friedman, Phys. Rev. Letters, 21, 674, (1968); see also : L. A. Artsimovich et al. and P. Ya. Burchenko et al., Proceedings of the Novosibirsk Conference, (1969).

/5/ H. Persson, Physics of Fluids, 9, 1090, (1966).

/6/ D. J. Ben Daniel, J. Nuclear Energy Part C, 3, 235, (1961).

ELECTRON CYCLOTRON HEATED PLASMAS IN MINIMUM-B CONFIGURATION*

W. J. Herrmann,** N. H. Lazar

Oak Ridge National Laboratory, Oak Ridge, Tennessee, U.S.A.

Electron cyclotron heated plasmas (ECH-plasmas) are being studied as target plasmas for injection and trapping of energetic atomic beams. The concept of the target plasma has been described elsewhere.[1] The early results of ECH-plasmas in minimum-B configuration were presented at the Novosibirsk Conference.[2] The apparent advantage of the minimum-B configuration is that at low neutral gas pressures ($\sim 5 \times 10^{-7}$ Torr, limited only by the base pressure of 3×10^{-8} Torr) energetic and dense electron plasmas (20 - 100 keV, 10^{11} - 10^{12} cm^{-3}) can be produced, which are not subject to low frequency instabilities which periodically destroy the plasma. However, at nearly all but the very lowest microwave power levels high frequency instabilities which occur in pulses with irregular, but power dependent repetition frequency, are present. During these pulses a small amount of the stored energy, normally less than 5%, is dissipated.

At the lowest power levels at least three different modes of oscillation could be observed. Figure 1 shows the spectrum at a set of parameters, where all three modes occur. This spectrum was obtained by mixing a sweeping local oscillator (frequency: 8.2 - 12.4 GHz) with the signals from the plasma passed through an X-band waveguide. The 30 MHz beat frequencies are amplified and recorded. At the heating frequency f_h = 10.6 GHz, the two sideband signals are indicated. Mode 1 has frequencies above the heating frequency. Mode 2 fills a broader band below the heating frequency with a peak value not far from it. Within that broad band, and occasionally at even lower frequencies, high-amplitude, narrow-band oscillations are detected. These are grouped together as mode 3. At very low neutral pressures a fourth mode exists which occurs in a broad band at frequencies corresponding to the cyclotron frequency near the bottom of the well.

Mode 1 is present only at pressures above 2.5×10^{-6} Torr. Its frequency increases with power (Figure 2), which at these low levels probably determines the density. We conclude that this mode can be excited only if a sufficiently dense, cold plasma is present. The frequency of mode 1 appears to be the upper hybrid frequency $\omega = \sqrt{\omega_c^2 + \omega_{pe}^2}$. Because close to threshold, the instabilities always appear with frequencies close to the heating frequency, it seems to be excited at a place close to the heating surface. If Δf is the observed shift from the heating frequency f_{ch} with Δf = 200 MHz, we find $\omega_{pe}/\omega_{ch} \sim 1/5$ or a cold plasma density of about 6×10^{10} cm^{-3}. This is a reasonable estimate for the cold density at the edge of the plasma.

An experiment using a movable skimmer was performed in order to localize the instabilities. Figure 3 shows the geometry involved. The heating surfaces and the flux lines are shown for different coil currents. The minimum of the field in this quadrupole-mirror geometry lies on axis in the midplane. The hot electrons are assumed to be mostly confined within the heating surface although the cold plasma may be found all along those flux lines intersecting the heating surface. At each value of central field there exist small regions where the flux lines are nearly tangential to the heating surface. In these regions we observe a sharp edge in the radial profile of the cold plasma density. The skimmer could be moved in such a way, that it just crossed these edges.

It was found in the experiment, that the frequencies above f_{ch} disappeare when the tip of the skimmer scraped off the edges of the plasma. This shows that the mode 1 instabilities are localized in a small region surrounding the plasma. They may be cured either by operating at lower neutral densities or by a careful design of the cavity (skimmer), which avoids plasma buildup in these outer regions.

Mode 2 is related to instabilities in approximately the same regions, extending with increasing power more toward the axis. The entire broad band of instabilities disappears upon moving the skimmer in to just intersect the surface as described above. The shape of the field near the plasma edges provides a very small mirror ratio for particles confined in the heating zone and therefore a high degree of anisotropy. Although different anisotropy driven modes might be possible, mode 2 is most easily identified with unstable whistler modes. It grows fastest at frequencies just below $\omega_s = \omega_c\left(1 - \frac{\langle E_\parallel \rangle}{\langle E_\perp \rangle}\right)$. In the region indicated $\frac{\langle E_\parallel \rangle}{\langle E_\perp \rangle}$ is very small and ω_c is close to the heating frequency. Mode 2 is not seen at very low pressures and at high pressures only with the larger volume plasmas.

Characteristically the third mode appears in short pulses with high amplitude, in narrow bands at particular frequencies below ω_{ch}. These microwave pulses are accompanied by current pulses of hot and cold electrons leaving the plasma axially along flux lines from the more central part of the plasma. Upon moving the skimmer in radially, the higher frequencies disappear first. The mode occurs for higher powers at all pressures and seems to be serious, because no way is seen to avoid it.

Mode 4 may not be different from mode 3. It occurs at the lowest pressures we could achieve and the band of frequencies connected with it is always just below the cyclotron frequency, corresponding to the minimum magnetic field of the well.

Our thanks go to W. B. Ard, J. L. Dunlap, and H. O. Eason for valuable advice and to O. D. Matlock and C. W. Blue for helpful assistance. One of the authors (W.J.H.) also wishes to express his sincere thanks to A. H. Snell and H. Postma for their courtesy during his stay at Oak Ridge National Laboratory.

References

Dandl, Guest, and Lazar, ORNL-4080, April 1967.

Dandl, et al., Conference on Plasma Physics and Controlled Nuclear Fusion Research, Novosibirsk, USSR, 1968; Paper No. CN-24/J-6.

Fig. 1

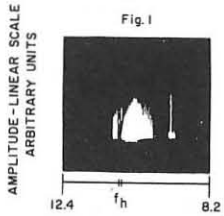

Fig. 2

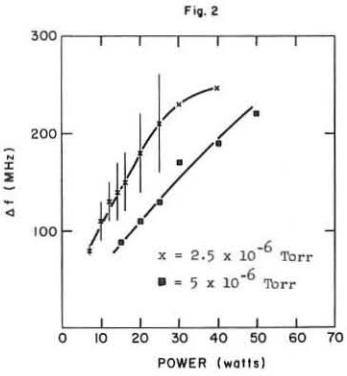

Fig. 3

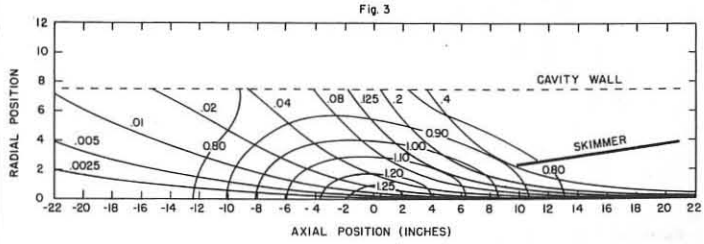

The eliptical lines, labeled 0.80, 0.90,...1.25 are cross sections through the heating surfaces for different coil currents. The other lines are the flux lines. The numbers give their radial distance from axis in inches where they intersect the wall in the mirror throat.

*Research sponsored by the U. S. Atomic Energy Commission under contract with the Union Carbide Corporation.

**On leave of absence from the Institut für Plasmaphysik, Garching, Germany.

THE ENERGY GAIN OF PARTICLES PULLED THROUGH CYCLOTRON RESONANCE

by
D.C. Schram, W. Strijland and L.Th.M. Ornstein
Association Euratom-FOM
FOM-Instituut voor Plasma-Fysica
Rijnhuizen, Jutphaas, The Netherlands

Charged particles in a TEM wave which propagates along a static magnetic field $\underline{B}_o$ would gain an infinite amount of energy if the resonance condition $r(t) = \{\omega - kv_z - \Omega(t)\}/\omega = 0$ were sustained for an infinitely long time. Here, $\Omega(t) = eB/m(t)$ is the cyclotron frequency related to the apparent mass, ω is the frequency of the wave, $k = \omega/v_p$ is the wave number, v_p is the phase velocity, and v_z is the axial velocity component of the particle. In uniform e.m. and static magnetic fields, our "undisturbed" case, the resonance function r(t) will be a periodic function because of the relativistic variations of the mass and of the axial velocity[1,2]. Therefore, the energy will oscillate with a limited amplitude. However, if by an external effect an additional variation is imposed on r, a net energy increase occurs. Such a variation may be imposed on r by making Ω or ω time-dependent or by the application of an electrostatic field. In an inhomogeneous B_o-field the situation is similar but somewhat more complicated.

The solution of the undisturbed case depends on the index of refraction, c/v_p, and generally yields an oscillation in time ($\tau_{os} \equiv \omega t_{os}$) of the energy (Fig.1, curve labelled 0)[2]. In free space, $v_p = c$, the time variations in r of $\Omega(t)$ and kv_z cancel[1]. An unrestricted resonance occurs for $r(0) = 0$ as follows from a non-relativistic theory. In a fast wave the relativistic mass variation is dominant and the resonance is limited and shifted towards higher values of the magnetic field. For a slow wave the variation of v_z dominates and the shift is reversed. In terms of a parameter $\beta \equiv \{\Omega(0)/\omega - 1 + v_{zo}/v_p\}/\{1 - v_{zo}/v_p\}$, the magnitude of the shift is equal to $\beta_c \approx 1.5(2G)^{1/3}$. Here, G is the parameter of the electric field strength of the wave: $G = \frac{g^2(1-c^2/v_p^2)}{\gamma_o^2(1-v_{zo}/v_p)^2}$, where $g = eE/m\omega c$, $\gamma_o = \mathcal{E}(0)_{total}/mc^2$, $\mathcal{E}_{total}$ is the total energy of the particle, and m is the rest mass.

The influence of an externally imposed variation of r(t) may be understood by assuming β as time-dependent in the undisturbed case. We may estimate the relative importance of the external effect by comparing $\tau_{ext} \equiv \omega t_{ext}$, the characteristic time associated with the external effect, with τ_{os} of the undisturbed case. By definition t_{ext} is the time in which the external effect changes the value of r from zero to $-\beta_c$. We suppose that $t_{ext} > 2\pi/\omega$. We find three regimes:

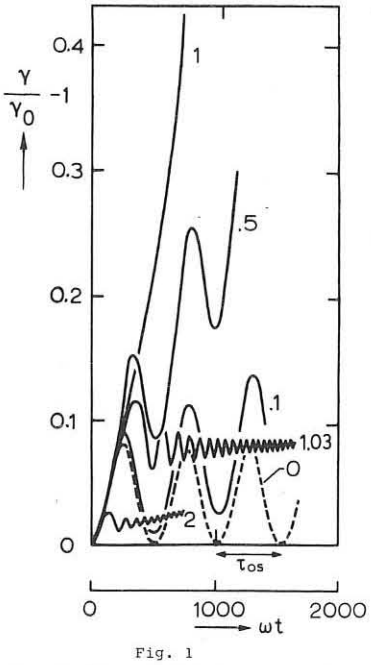

Fig. 1
Numerically calculated energy gain as a function of time in the case of an e.s.field; $c^2/v_p^2 = 1.25$, $g = 2.10^{-3}$, $\gamma_o = 1$, $\beta = 0$, $a_{sync} = -1.2\times10^{-4}$. The quantity a/a_{sync} is curve parameter.

I. $\tau_{ext} < \frac{1}{2}\tau_{os}$, the external effect is strong, the method of solution is by a nonrelativistic approximation, and the result is a stepwise energy increase followed by a decaying energy oscillation (Fig. 1, curves labelled 1.03 and 2).

II. $\tau_{ext} \approx \frac{1}{2}\tau_{os}$, the synchronous external effect. An exact numerical treatment results in a steady increase of the energy (Fig. 1, curve labelled 1).

III. $\tau_{ext} > \frac{1}{2}\tau_{os}$, the case of weak external effect, for which a numerical solution has been applied. The result is a net increase of the energy superimposed on the oscillation (Fig. 1, curve labelled 0.1). The rate of energy gain depends on $2\tau_{ext}/\tau_{os}$.

A. Uniform axial electrostatic field. The axial velocity increases due to electrostatic acceleration: $\Delta r = -\Delta v_z/v_p = -a\tau$, where $a \equiv -eE_o/m\omega v_p$, and E_o is the electrostatic field strength. Thus:

$$a\tau_{ext} = \beta_c, \text{ or } \tau_{ext} = 1.5\, a^{-1}(2G)^{1/3}.$$

For a strong external effect the average energy gain of a population with an isotropic transverse velocity distribution is[3]:

$$\frac{\mathcal{E}_\perp - \mathcal{E}_\perp(0)}{mc^2} \approx \frac{\pi g^2(1+\beta)^2}{|a|}.$$

With τ_{os} from ref. 2: $a_{sync} \approx G^{2/3}.G/|G|$ (ref. 3). For free space interaction $a_{sync} = 0$, so for nonzero E_o we always find regime I. For small electrostatic field a substantial gain in energy can only occur if the interaction takes place during a long period of time (Fig. 1, curve labelled 0.1).

B. Frequency modulation. Frequency modulation of ω causes a periodic variation of r. Suppose $\omega = \omega_o + \Delta\omega.\sin\mu t$. Now a repeated stepwise energy gain occurs if the condition for regime I is fulfilled: $\tau_{ext} < \frac{1}{2}\tau_{os}$, yielding $\mu/\omega_o > 2\tau_{os}^{-1}.\arcsin(\beta_c\omega_o/\Delta\omega)$, with $\tau_{ext} = -\omega_o/\mu.\arcsin(\beta_c\omega_o/\Delta\omega)$. Obviously, a supplementary condition is that the modulation depth $\Delta\omega/\omega_o$ is larger than the resonance width β_c (Fig. 2). Thus, with τ_{os} from ref. 2, $\mu/\omega_o > G^{2/3}\,\omega_o/\Delta\omega$. The average energy increase for an isotropic transverse velocity distribution is analogous to the electrostatic case:

$$\frac{\mathcal{E}_\perp - \mathcal{E}_\perp(0)}{mc^2} \approx \frac{\pi g^2(1+\beta)^2}{\mu\Delta\omega/\omega_o^2}.$$

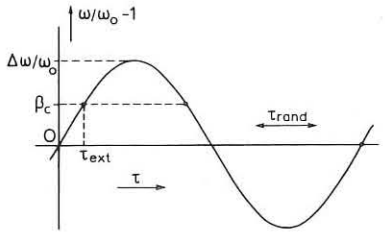

Fig. 2
Comparison between two sets of characteristic quantities for frequency modulation: $\tau_{rand} - \tau_{ext}$, and $\Delta\omega/\omega_o - \beta_c$.

The condition for irreversible heating is the occurrence of a randomizing effect between successive accelerations. This yields the condition $\tau_{ext} < \tau_{rand} < \omega_o/\mu$. A synchronous acceleration may occur as long as the increase of ω is linear: $\omega - \omega_o = \Delta\omega\sin\mu t \approx \Delta\omega\mu t$ for small μt. The condition $\tau_{ext} = \frac{1}{2}\tau_{os}$ yields: $(\Delta\omega/\omega_o \times \mu/\omega_o)_{sync} = -G^{2/3}.G/|G|$.

C. Magnetic pumping. Time variation of the magnetic field ($\Omega = \Omega(t)$) yields the same results as variation of ω.

D. Inhomogeneous magnetic field. Particles which cross a resonance zone in an inhomogeneous static magnetic field experience a variation in Ω. If the gradient is steep enough, $\tau_{ext} < \frac{1}{2}\tau_{os}$, (regime I). Observe, that the gradient is supposed to be small enough in order to ignore $\underline{B}_\perp \times \underline{v}_z$, where $\underline{B}_\perp$ is the transverse component of the magnetic field. If, moreover, the axial velocity is nonzero and can be regarded as a constant while the particle passes through the resonance zone, the average energy gain for an isotropic distribution of the transverse velocity is:

$$\frac{\mathcal{E}_\perp - \mathcal{E}_\perp(0)}{mc^2} = \frac{m\pi g^2\omega^2}{v_{zo}e\ \text{grad}\ B_z}.$$

In a second order approximation, involving a constant axial acceleration by $\underline{v}_\perp \times \underline{B}_{1o}$, v_{zo} can be replaced by the average axial velocity. Except for small v_{zo} the inclusion of the second order term is found to be negligible. The first order result yields an estimate of the average increase in energy per encounter in the experimental situation described in ref. 4. A more elaborate treatment of the resonance phenomena in an inhomogeneous magnetic field is given in refs. 5 and 6.

This work was performed under the association agreement of Euratom and FOM with financial support from ZWO and Euratom.

References:

1) V.Ya. Davydovskii, Soviet Phys. JETP 16 (1963) 629.
2) D.C. Schram, Physica 37 (1967) 617, Physica 40 (1968) 422.
3) D.C. Schram and G.P. Beukema, Physica 42 (1969) 247.
4) W. Strijland and H. de Kluiver, paper to this conference.
5) E. Canobbio, Nuclear Fusion 9 (1969) 27.
6) H. Grawe, Plasma Physics 11 (1969) 151.

MAGNETIC MIRROR EFFECTS ON A COLLISIONLESS RADIO FREQUENCY PLASMA

by

P.Caldirola[+], S.Bernabei[+], M.Fontanesi[+], G.Lisitano[++], and E.Sindoni[+]

\+ Institute of Physics - University of Milan - Italy

++ Institut fur Plasmaphysik - Garching - D.B.R.

A collisionless rf plasma produced in a magnetic mirror shows a marked effect of nkT energy concentration inside the magnetic bottle. As shown schematically in Fig.1 the plasma is generated and heated at one end of a magnetic bottle (mirror ratio 2.7) in condition of electron gyromagnetic resonance using a "L-coil" (1)(2) fed with a microwave 100 watt cw, 2.4 Ghz. Due to the little volume surrounded by the "L-coil" the plasma is heated on high levels of r-f power densities (15KW/liter). The plasma column is 1 m long with a diameter of 1.5 cm. The high nkT content of the plasma permits the use of pyrometric diagnostics.

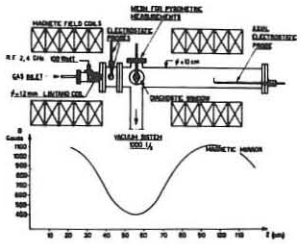

Fig.1 - Experimental equipment

In Fig.2 the radiated power from an incandescent mesh of tungsten wires (transparence 90%, 0.1 mm diameter) is plotted in function of the axial distance from the coil. We can see that the radiated power has a maximum at the centre of the magnetic bottle. In correspondence with the point symmetrical to the one where the plasma is heated at E.C.R. (antiresonant point) we note a rapid drop of the radiated power. This effect may be understood as due to the magnetic reflection of the particles reaching the right end of the magnetic bottle. The presence of a marked maximum in the centre of the mirror indicates that the energy transferred to the electrons in the E.C.R. region is mainly transversal. This is confirmed by the measurements shown in Fig.3a, where the electron temperature at the axis of the plasma column is plotted against the distance from the L-coil. The temperature has been measured at an input r-f power to the coil lower than the one employed for the pyrometric measurements of Fig.2. This was necessary in order to avoid electron emission current from the incandescent tip of the probe. Qualitatively the temperature profile along the beam axis shown in Fig.3 indicates a minimum at the centre of the bottle in correspondence with the maximum value of the radiated power. This fact may be explained as due to the transformation of transversal energy gained in the E.C.R. region to directed energy in regions of lower magnetic field. The temperature increase outside the magnetic bottle may be due to the termalization recovered by the plasma. Note that the dip in the temperature profile is lower at higher neutral gas pressures, in accordance with the damping of the energy transformation rate due to the presence of neutrals. Fig. 3c shows the electrons density profile along the axis of the plasma column. One may observe the accumulation of particles in the middle of the magnetic bottle. Measurements of plasma density and of electron temperature profiles taken through cross sections at different points along the plasma column show that this method of plasma production generates a ring of hot electrons surrounding the plasma column, for a neutral gas filling pressure ranging from 10^{-4} to 5×10^{-6} mmHg.

Fig.2 - Radiated power from a mesh.

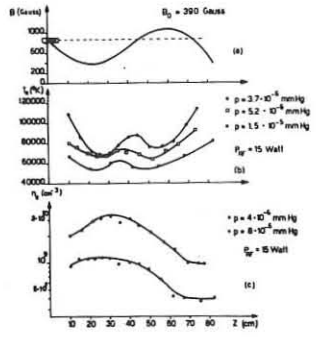

Fig.3 - 3a.Profile of the magnetic field - 3b. Electron temperatures along the axis - 3c. Electron density along the axis.

This ring of hot electrons can be filled up with electrons of more uniform distribution temperature by increasing the applied r-f power or by decreasing the neutral pressure. Fig.4 shows the electron temperature versus the neutral filling pressure. Fig.4A is the temperature measured at the centre of the plasma beam and Fig.4B is the temperature measured at the hot electron ring. We see that by lowering the neutral pressure the region of highest electron temperature is shifted toward the central region of the plasma beam and that the plasma confinement is better. The essential feature of this experiment was the indication of a strong mirroring effect upon the most energetic particles of the plasma beam.

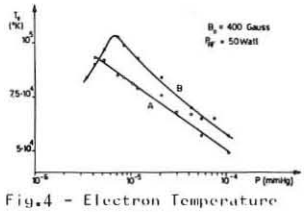

Fig.4 - Electron Temperature versus pressure. A at the plasma beam center, B into the electron ring.

REFERENCES

(1) G.Lisitano: Proceedings of the 7th ICPIG Beograd, 1 (1966) 464.

(2) G.Lisitano, P.Caldirola, N.Barassi, M.Fontanesi, E.Sindoni: 3rd Conference on Plasma Physics and Controlled Nuclear Fusion Research. CN-24/J-4 Novosibirsk 1968.

End Losses of a Quiescent Collisionless Plasma in a Magnetic Mirror.

G. Lisitano and B. Green
Institut für Plasmaphysik GmbH, 8046 Garching b. München
West Germany

Collisionless, steady state plasmas showing a remarkably low level of density fluctuation ($\Delta n/n < 5\%$) have been generated in a mirror geometry magnetic field, by applying 50 W, Cw, 2,4 Gc/s to a coupling structure of new design.[1), 2)]. The plasma has electron temperatures 5 to 30 eV, ion temperatures around 5 eV, electron densities of 10^{10} to 5 x 10^{11} cm^{-3}, and can be produced in various gases at pressures as low as 10^{-5} torr. for a wide range of magnetic field strengths ($\Delta B/B < 80\%$). This quiescent plasma, with electron temperatures two orders of magnitude greater than thermal alkali plasma ("Q"machines) is particularly suitable for basic plasma physics studies. Also the long mean free path for ions and electrons makes study of this plasma relevant to problems in space physics and controlled thermonuclear research.
We have investigated experimentally,

a) the density fluctuation level

b) the temperature and density profiles at different positions along the plasma column

c) the variation of density and temperature with magnetic field strength, applied r.f. power and neutral gas pressure.

From these measurements we have studied end losses (the dominant loss mechanism) and have obtained verification of the following simple model for plasma losses in a magnetic mirror. We consider a steadystate plasma,volume V, density n and particle energy kT produced by applying r.f. power $P_{R.F.}$ with coupling efficiency η . Then the containment time τ is given by the relation

$$n\,(V\,kT/\eta P_{R.F.}) = \tau \qquad (1)$$

For constant V, T, and $P_{R.F.}$ we have from (1), $n \propto \tau$. Following Spitzer,[3)] we employ a particle reflection coefficient R, where $R = 1-B_{ce}/B_m$, (B_{ce} is the magnetic field strength corresponding to electron cyclotron resonance, and B_m is the maximum field strength in the mirror) and obtain from the consideration of mass conservation

$$-(1/n)(dn/dt) \propto (1-R) \qquad (2)$$

From (1) and (2) we have $n \propto \tau \propto (1-R) = B_m/B_{ce}$. Further, we must take account of the fact that in a collisionless plasma, no particle build-up is possible in the absence of mirror confinement; i.e. n = 0 for $B_m/B_{ce} = 1$, and n > 0 for $B_m/B_{ce} > 1$. Hence we have,

$$n \propto (B_m - B_{ce}) \qquad (3)$$

The experimental arrangement is shown in Fig. 1. The r.f. power is fed to an "L" coil[1), 2)] of 3 cm internal diameter. As the vacuum wavelength of the applied r.f. power (=12.5 cm) is much greater than the cut-off wavelength of the "L" coil, no r.f. power will be radiated out of the coil. Plasma is generated whenever the magnetic field strength equals the value B_{ce} for electron cyclotron resonance (ECR) with the exciting frequency. Because the "L" coil extends over a large region of non uniform magnetic field, plasma is produced for a variation of nearly 80% of the minimum value of B_m (for which plasma generation takes place).

From the measurements a), b),and c) we conclude that for magnetic field strengths in the range $1,2 < B_m < 2$ kG, the production of plasma in the ECR region is unaffected by the position of B_{ce}. The neutral gas pressure was 6 x 10^{-5} torr. for all the reported measurements. With 40 W of applied r.f. power the measured electron temperature was 10 eV and little deviation from this value (< 10%) has been detected on the temperature profiles at various positions along the plasma column. The characterisation of this plasma as collisionless appears well justified from the relevant time and length scales derived from the plasma parameters at the given neutral gas pressure.[2)]

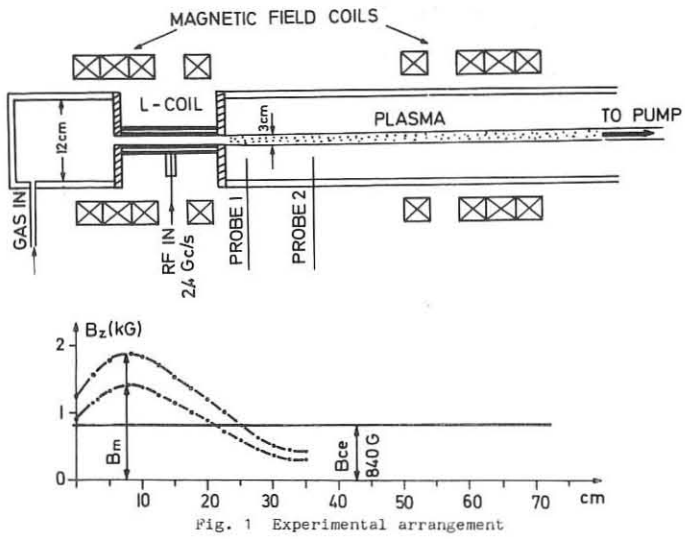

Fig. 1 Experimental arrangement

the mirror. The different sets of data, each for a given r.f. power level, clearly define a common value of magnetic field strength corresponding to the electron cyclotron resonance B_{ce}. With the same neutral gas pressure and the same range of power levels, the zero value of density has been verified with a homogeneous magnetic field $B = B_{ce}$. Clearly the relation (3) is experimentally well verified. Fig. 2b shows plasma density measured at the middle of the mirror plotted against applied power $P_{R.F.}$ for different magnetic field strengths. For const. B_m we have $n \propto P_{R.F.}$ in agreement with (1).

In Fig. 2a the plasma density measured at the centre of the mirror (position of probe 2) is plotted against B_m, the maximum value of the magnetic field strength at the end of

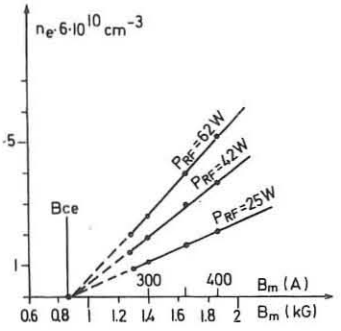

Fig. 2a Plasma density as a function of B_m for different values of applied r.f. power $P_{R.F.}$

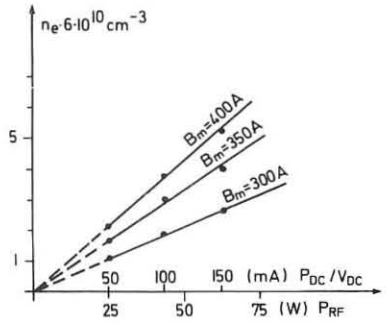

Fig. 2b Plasma density as a function of $P_{R.F.}$ for different values of magnetic field strength B_m.

We have described a particularly versatile plasma source and used it to carry out a study of plasma losses in a magnetic mirror. Experimental results agree well with the description given by a simple model involving the single particle reflection coefficient in a magnetic mirror.

This work was performed under the terms of the agreement on association between the Institut für Plasmaphysik and Euratom.

1) G. Lisitano, Proceeding Seventh International Conference on Ionization Phenomena in Gases (Gradevinska Knjiga Publishing House, Beograd 1966) Vol. 1 pp. 464-467.

2) G. Lisitano, R.A. Ellis, W.M. Hooke, T.H. Stix, MATT-539, Rev. Sci. Instr. 39, 3, 1968

3) L. Spitzer, Jr. "Physics of Fully Ionized Gases", (Interscience, 1962) p. 14-15.

THE EARLY STAGES OF A THETA PINCH

by

H.A.B. Bodin, J. McCartan, G.H. Wolf*

U.K.A.E.A. Culham Laboratory, Abingdon, Berks., England

* On attachment from Garching

1. Introduction

The anomalous diffusion in the early stages of low density theta pinches, which leads to a diffuse radial density distribution and average values of $\beta < 1$, has been explained[1] by an anomalous resistivity due to a microinstability which is excited by electron-ion streaming when the electron-ion drift velocity, v_D, exceeds the sound speed, $v_s = \sqrt{k(T_e + T_i)/m_i}$. It has been shown using an analytical model, which assumes a steady state distribution in which $v_D = v_s$, that the current sheath thickness is characterised by an e-folding length of a few ion collisionless skin depths, and when the line density was less than a critical value, N_c, the current sheath extends to the axis. This model also predicts that for $N \gg N_c$ the radial density distributions has a square form with $\beta \sim 1$, while for $N \lesssim N_c$ there is a diffuse distribution with $\beta < 1$, as is observed experimentally.

Such streaming instabilities are also expected to modify the heating processes during the initial implosion. In this paper it is shown that at low filling pressures (~ 5 mtorr) corresponding to $N \approx N_c$, the anomalous resistivity leads to rapid field penetration and laminar radial flow, i.e. no strong shock is formed. Thus at these pressures the principal heating mechanism is expected to be resistive; experimentally in such conditions the measured electron temperature is considerably higher than that computed with classical resistivity, and the ratio T_i/T_e has the opposite dependence on pressure to that predicted by classical theory. In both cases theoretical computations using the anomalous resistivity give satisfactory agreement.

2. Experimental Details and Results

The coil is 771 cm long and of 11 cm bore encircling a quartz tube of I.D. 8.3 cms. The magnetic field rises to a peak of 25 kG in 5.5 μsec. The deuterium gas, at a filling pressure of 5-30 mtorr, was preionized to more than 50% by an axial current. Densities of $1 \sim 4 \times 10^{16}$/cc and electron temperatures in the range 400-160 eV were obtained. Detailed measurements could not be made in the early stages and the following new experimental results have been obtained later in the discharge, ($t \gtrsim 1$ μsec):
(1) v_D/v_s is of order unity for times subsequent to the implosion; (2) no measureable anomalous broadening of the density profile occurs after 1 μsec; (3) the density profile has a thickness of a few ion-collision skin depths; (4) at low filling pressures the ratio $T_e/T_i > 1$.

3. Theoretical Model

It follows from 2.(1)(2) that the anomalous resistivity only occurs during the first microsecond of the discharge, and its absence later in the discharge when $v_D/v_s \lesssim 1$ suggests that the anomalous resistivity only occurs when $v_D/v_s > 1$. Two examples of instabilities which fulfil this onset criterion are as follows: firstly, the ion acoustic instability[2] which requires $v_D/v_s > 1$, $T_e/T_i \gg 1$, $\omega_{pe} \gg \omega_{ce}$; and secondly an oblique electrostatic instability[3] which is possible for all values of T_e/T_i if $v_D \gtrsim v_s$ and is characterised by a growth rate $\approx \sqrt{\omega_{ce}\,\omega_{ci}}$. The resulting anomalous resistivity η^* has been estimated by Sagdeev[4] and Babykin[3], and is given by:

$$\eta_1^* = \frac{m}{ne^2}\,\omega_{pi}\,\frac{T_e}{T_i}\,\frac{v_D}{v_s}\,\frac{1}{100} \quad \text{(ion acoustic)} \qquad \eta_2^* = \frac{m}{ne^2}\,\frac{\omega_{ce}}{60}\,\frac{v_D}{v_s} \quad \text{(oblique)}$$

The diffusion rates corresponding to η_1^* and η_2^* are of the order of the Bohm values for parameters typical of most theta pinches.

The results of computations using the M.H.D. code modifed to include the anomalous resistivity[1] are insensitive to the choice of η^*. It is found that at pressures above about 10 mtorr, a discontinuity occurs in the radial density and velocity profiles, during the implosion, indicating that the anomalous resistivity is insufficient to maintain laminar flow. As the filling pressure is reduced this discontinuity occurs closer to the tube axis and below 10 mtorr it disappears (Fig.1). These results are similar to those derived by Chodura[5]. The inclusion of an artificial shock term[6], which simulates an ion viscosity, allows the computation of the ion heating and it was found that the influence of the viscous term was small below 10 mtorr.

The predicted ratio of T_i/T_e at peak field for both classical and anomalous resistivities (η_1^*) as a function of filling pressure are shown, with the experimental values in Fig.2. At high pressure the short electron-ion energy equipartition time ensures $T_e/T_i \approx 1$, while at low pressures the theory including η_1^* predicts $T_e > T_i$, as observed; classical resistivity gives $T_e < T_i$. Thus at low pressures the dominant heating process is resistive. The code with η_1^* also predicts the shape of the density distribution, the pressure dependence of β, and classical behaviour after the implosion when $v_D \lesssim v_s$, all in agreement with observation.

A dimensional analysis shows that for a resistivity with a Bohm dependence i.e. $\eta^* = \frac{m_e}{ne^2}\,\frac{\omega_{ce}}{16}$, the ratio of the field diffusion time to the snowplough implosion time τ_I scales as: $\tau_D/\tau_I \propto [N/N_o]^{\frac{1}{2}}$ where $N_o = \frac{5\pi\, m_i}{2\mu_o e^2} \gtrsim N_c$. This ratio only depends weakly on line density and is independent of $\dot{B}$.

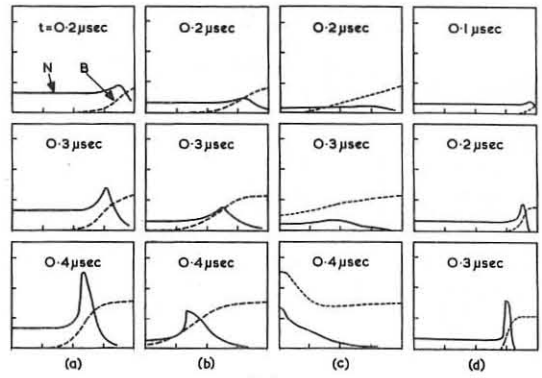

Fig.1 Computed density and field distributions during implosion for different filling pressures.
(a) 20 mtorr, $\eta = \eta_1^*$; (b) 10 mtorr, $\eta = \eta_1^*$; (c) 5 mtorr, $\eta = \eta_1^*$
(d) 10 mtorr, $\eta = \eta_{classical}$
Scale: 1 cm, 0.2×10^{16}/cc, 2 kG per division

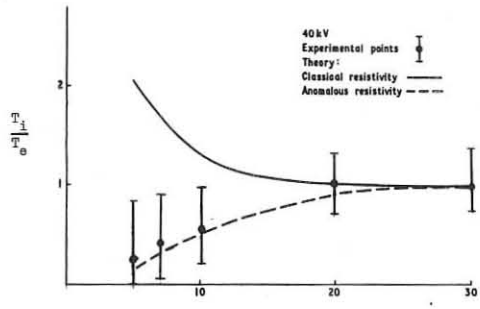

Fig.2 Ratio T_i/T_e as a function of filling pressure.

Conclusions

It is concluded that during the early stages when $v_D > v_s$ a two-stream instability leading to an anomalous resistivity occurs; this broadens the current sheath and heats the electrons; these two effects tend to reduce the ratio v_D/v_s and the instability cuts itself off when $v_D \lesssim v_s$. Two possible instabilities were discussed. It is shown that for line densities less than $N_o (\approx 1 \times 10^{16})$ cm there is little shock heating and the principal heating mechanism is resistive, while for $N > N_o$ ion shocks are possible if there is a collisionless ion viscosity. Scaling laws suggest that these results are insensitive to $\dot{B}$.

References

1. Bodin, H.A.B. et al. Novosibirsk Conference Paper CN-24/K-1 (1968).
2. Stringer, T.E. Plasma Physics (J. Nucl. Energy Part C) 6, 267 (1964).
3. Babykin, M.V. et al. J.E.T.P. 46, 511 (1964).
4. Sagdeev, R.Z. et al. "Lectures on the non-linear theory of plasma" (1966) IC/66/69.
5. Chodura, R. Phys. Fluids 11, 400 (1968).
6. Richtmeyer, R.D. "Difference Methods for Initial-Value Problems". Interscience Publishers Inc. New York. (1957).

THE FORMATION OF AN AXISYMMETRIC BULGED REGION IN A LONG UNIFORM PLASMA COLUMN

by

H.A.B. Bodin, E.B. Butt, J. McCartan, G.H. Wolf*

U.K.A.E.A., Culham Laboratory, Abingdon, Berks., England.

* On attachment from Garching

1. Introduction

The study of bulged theta pinch plasmas is currently of interest in relation to the stability of bumpy M & S type configurations.[1] Here we report an experimental and theoretical study of the growth of a bulge in a collisional plasma column. The axial and temporal variation of the radial density distribution were obtained with image converter cameras; values of the mean beta and plasma radius were deduced for comparison with the predictions of an analytic model, and with the results of a time dependent one dimensional M.H.D. computation.[2]

2. Experimental Details

The coil is 771 cm long and of 11 cm bore. For the experiments reported here the bank voltage was 32 kV giving a peak field of 20 kG rising in 5.5 μsec and decaying with a time constant of 180 μsec. The quartz tube of bore 8.3 cm was filled with deuterium gas at an initial pressure of 20 mtorr and was preionized to more than 50%. The plasma properties on the axis at peak field were $n_e = 3 \pm .5 \times 10^{16}$/cc, $T_e = T_i = 120 \pm 15$ eV, $\beta = 0.7 \pm .2$.

3. Generation of the Bulge

The method of generating the bulge is shown schematically in Fig.1. The coil section surrounding the region where the bulge was to be formed, known as the field shaping coil, was short circuited at a time, t_1, earlier than the rest of the coil, which was short circuited at field maximum ($t = t_2$). The length of the field shaping coil is 25 cm and determines the length, L, of the bulged region. The magnetic fields were measured at the inner surface of the midplane of the field shaping coil, and at the inner surface of the neighbouring coil and are denoted by B_2, B_1 respectively. The ratio B_2/B_1 could be varied continuously between 0.5 and 1 by altering the time interval between short circuiting the shaped and unshaped regions of the coil.

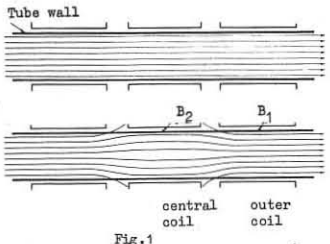

Fig.1
The generation of the unstable bulge

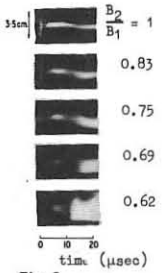

Fig.2
Streak photographs at midplane of bulge for different B_2/B_1.

4. Experimental Results

Fig.2 shows a series of streak photographs taken at the centre of the bulge for various values of B_2/B_1.

Fig.3 shows radial electron density distributions at 9.8 μsec for a discharge with no field shaping and with $B_2/B_1 = 0.75$. Without field shaping there is the Gaussian-like distribution observed previously and typical of most low density theta pinches. In contrast, for the bulged plasma the distribution is no longer og Gaussian form but tends to be more square shaped.

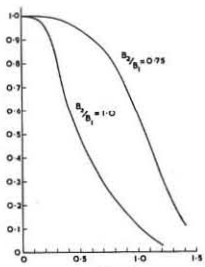

Fig.3
Normalised density profiles in midplane for field ratio of $B_2/B_1 = 0.75$ and of $B_2/B_1 = 10$.

To compare the results with a one-dimensional axial theory a square density distribution is assumed. Thus, when the profile is diffuse, an effective plasm radius r_p is introduced. Since the observed temperature distribution is uniform this quantity may be defined by replacing the diffuse density distribution by a square one, of equal temperature, which has the same line density and diamagnetism. The strength of the bulge is defined by $\delta = \frac{1}{2}(r_{p2} - r_{p1})/r_{p1}$ where r_{p2} is the average radius of the plasma in the midplane of the bulge and r_{p1} its radius in the unperturbed region. The observed value of δ is plotted as a function of time in Fig.4, which shows that the bulges grow almost linearly with time over a wide range of B_2/B_1. Only when $B_2/B_1 > 0.75$ does δ tend to a constant value before the m = 1 instability prevents further measurement of δ.

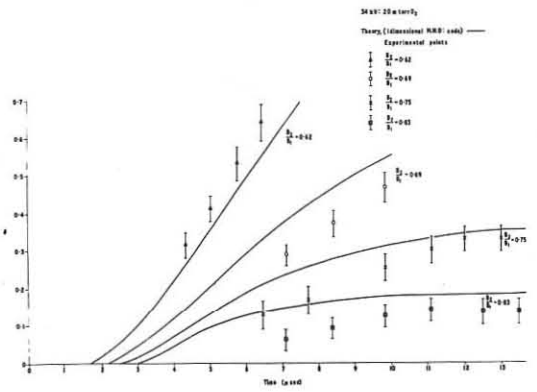

Fig.4
Temporal development of bulge

5. Analytic Model - Comparison with Experiment

We define B_i and B_e as the internal and external field strengths; suffixes 1 and 2 refer to the unshaped region and the midplane of the shaped region, respectively. The vacuum value of B_e is assumed and curvature terms are neglected. These assumptions lead to the following expressions for δ and β_2

$$\delta = \tfrac{1}{2}\left\{\left[\left(\frac{B_{e1}}{B_{e2}}\right)^2 \frac{[1-\beta_1]}{[1-\beta_1(\frac{B_{e1}}{B_{e2}})^2]}\right]^{\frac{1}{4}} - 1\right\} \qquad \ldots (1)$$

$$\beta_2 = \beta_1 \left(\frac{B_{e1}}{B_{e2}}\right)^2 \qquad \ldots (2)$$

It can be seen that $\delta \to \infty$ and $\beta_2 \to 1$ as $B_{e2}/B_{e1} \to \sqrt{\beta_1}$ i.e. no simple equilibrium is possible for

$$\frac{B_{e2}}{B_{e1}} \leqslant \sqrt{\beta_1} \quad . \qquad \ldots (3)$$

Fig.5 shows δ as a function of β_1, and the experimental values. Comparison with theory could only be made for $B_{e1}/B_{e1} < 0.75$, as only in these cases has the bulge reached a steady state. The best fit was found with $\beta_1 = 0.5$ in reasonable agreement with the measured value of 0.7 ± 2. The critical value of B_{e2}/B_{e1} for the bulge to grow continuously, given by equation (3), is $\frac{B_{e2}}{B_{e1}} = 0.7$ for $\beta_1 = 0.5$; the value is consistent with that at which a lack of equilibrium is experimentally observed (cf. Fig.4). The experimentally measured value of β of almost unity and a square density profile for $B_2/B_1 = 0.75$ are also in agreement with equation (2).

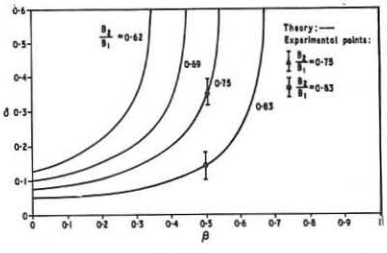

Fig.5
Strength of bulge as function of β for different B_2/B_1

M.H.D. Code Calculations

In order to calculate the temporal history of the bulge shape the one-dimensional M.H.D. equations were solved using the measured axial and temporal variation of the external field together with the initial plasma properties, at the onset of field shaping, as input data. It is found that the computed bulge growth rate is strongly dependent on the ratio of B_2/B_1 and is in reasonable agreement with experimental observations (cf. Fig.4). For strong bulges (i.e. $B_2/B_1 < \sqrt{\beta_1}$) no equilibrium is attained and a strong m = 0 neck occurs at the end of the bulge as plasma flows continuously into the bulged region and an area wave propagates away from it. For weak bulges an equilibrium is reached and an m = 0 wave travels axially away from the bulge.

Conclusion

It is shown that the growth of a bulged region in a long plasma column is a sensitive function of field shaping ratio, B_{e2}/B_{e1}, and β, and that for $B_{e2}/B_{e1} \lesssim \sqrt{\beta}$ no simple equilibrium is possible.

References

1. H.A.B. Bodin et al. Novosibirsk Conference Paper CN-24/K-1 (1968)
2. F. Meyer and H.U. Schmidt. Z. Naturforsch. 13a, 1005 (1958).

DYNAMIC STABILISATION OF AN m = 1 INSTABILITY

by

H.A.B. Bodin, E.P. Butt, J. McCartan, G.H. Wolf*

U.K.A.E.A. Culham Laboratory, Abingdon, Berks., England.

* On attachment from Garching

Experiments on the 8 metre theta pinch at Culham have shown[1] that the plasma at the midplane is stable during the transit time of an Alfven wave from the ends. Other experiments on this apparatus have also shown[2] that an m = 1 instability can be deliberately induced during this period by forming an axisymmetric bulge at the midplane. The growth rate of the induced instability is found to agree with ideal M.H.D. theory and can be varied by adjusting the amplitude of the bulge. This paper describes a third series of experiments in which this controlled m = 1 instability was dynamically stabilised by means of a high frequency oscillating axial magnetic field.

Methods of stabilising an infinite periodic theta pinch (equivalent to a linear M & S system) have been proposed using either, a travelling wave system[3], or, an oscillating axial current[4]. Both these systems have disadvantages and are not strictly relevant to the single bulge configuration used in previous experiments. These considerations led to the choice of a standing wave oscillatory system superimposed on the static bulge, as shown in Fig.1. This system has the additional merit of experimental simplicity. Theoretical work[5] has shown that this system may be stabilising for the modes $m \geq 1$ if the normalised amplitude of the high frequency component ε is of the same order as that of the bulge, 2δ. Instantaneously the oscillating bulge is always M.H.D. unstable. The oscillator frequency must also be greater than the growth rate of the instabilities due to the static bulge. With these conditions satisfied there still exists the danger of exciting new modes by parametric resonance. No evidence of this has been found in our new experiments.

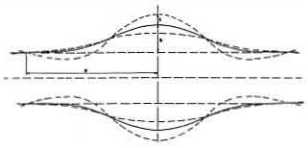

Fig.1 Standing wave configuration ($a = L/2$); $b = 2\delta r_1$; $c = \varepsilon r_2$; $r_2 = (1 \pm 2\delta)$)

A cross section of the experimental arrangement is shown in Fig.2. The high frequency field is generated by a coil which forms part of an oscillatory circuit ($Q \approx 60$). Two high voltage capacitor banks (~ 50 kV) are mounted above and below the coil and connected to it by transmission lines. The oscillator is switched on by means of a metal to metal switch developed for this experiment. Before this instant a large electric field is generated by the 50 kV potential between the two halves of the coil. The plasma is shielded from this field by an electrostatic screen close to the surface of the quartz tube. The oscillating field produced is about 3 kG at 2 MHz. The coil (ℓ = 100 mm) is placed in a 120 mm gap at the centre of the normal 'shaping' section of the main coil[6], itself 240 mm long. Two shields on the outside of the system adjust the flux leakage at the gap in order to avoid a lack of plasma equilibrium observed in preliminary experiments with this arrangement.

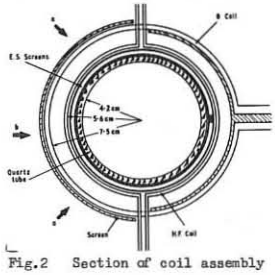

Fig.2 Section of coil assembly

Measurements of the magnetic field were made at the centre and end of the bulge and an image converter streak camera was used to observe plasma motion from two positions simultaneously either at the centre of the coil to give a 'stereo' view or horizontally at the end and centre of the bulge.

The main capacitor bank was operated at reduced voltage (30 kV) in order to maximise the ratio of the oscillating field to the main field. In preliminary experiments with a filling pressure of 20 mtorr D_2 it was found that the m = 0 mode due to lack of equilibrium of the bulge was dominant owing to the relatively high value of β ($\beta \approx 0.7 \pm 0.2$ from earlier work). The dependence of this mode on β is discussed elsewhere[6]. However, it was found that a strong m = 1 instability could be induced at a filling pressure of 10 mtorr D_2 without generating an excessive m = 0 expansion and all subsequent work was done at these conditions. The plasma parameters on the axis, at 30 kV, 10 mtorr, are approximately: $n_e = 2.0 \pm 5.10^{16}$; T_e = 100 eV; $\beta = 0.5 \pm 0.2$.

Typical stero-view streak pictures are shown in Fig.3. Picture 1 shows the results without the oscillating field. An m = 1 motion (lower trace) starts at about 6 μsec (see arrow) and leads to a strong interaction with the wall at about 10 μsec. In Picture 2 the oscillating field is switched on at about 6 μsec and no interaction with the walls occurs. However, there is a displacement of the upper trace starting 2-3 μsec after the high frequency field is switched on and the plasma appears to move just out of the field of view (about half the tube diameter) by the end of the trace (20 μsec). Recent work[7] has suggested that an oscillating field can also produce an equilibrium so that this displacement may be due to a change in the equilibrium position of the plasma.

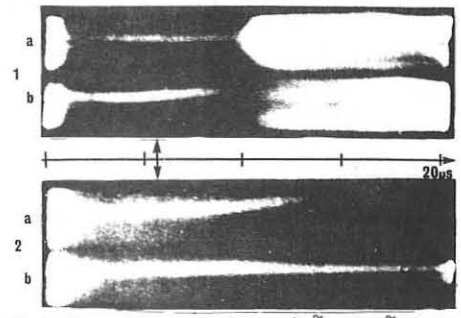

Fig.3 Stereo view streak pictures ($1.\tilde{B} = 0$; $2.\tilde{B} \approx 0.1\ B_2$)

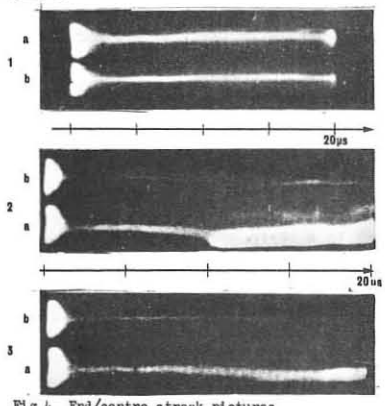

Fig.4 End/centre streak pictures ($1.B_1/B_2$ - no small; $2.\tilde{B} = 0$; $3.\tilde{B} \approx 0.1\ B_2$)

Simultaneous streak pictures taken at the centre (a), and end (b), of the bulge are shown in Fig.4. Picture 1 shows the result obtained when the field ratio, $B_1/B_2 = 1.1$, was insufficient to produce a strong m = 1 mode. In Picture 2 this ratio was increased to 1.2 and this gave an m = 1 instability (with some expansion of the bulge) resulting in a strong interaction with the wall at about 10 μsec. In Picture 3 the oscillator is switched on at 6 μsec; other conditions remain the same. The onset of the instability is delayed and there is no wall interaction.

An analysis of the vertical displacement in Pictures 2 and 3, Fig.4 is given in Fig.5. In the unstabilised case the measured growth rate is about 4.10^5, the same as in Fig.3. With the stabilising field the onset of the instability is delayed by about 6 μsec and it then grows at the same rate as before. During this period the ratio of the oscillating field to the main field remains about the same (≈12%) because the low frequency oscillations of the crowbar circuit (≈ 50 KHz) cause the fields to decay at the same rates.

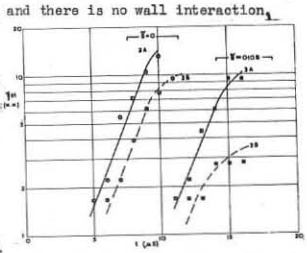

Fig.5 Analysis of Fig.4 (same legend)

The radius of the plasma at the end of the bulge is about 10 mm, $C_s \sim 1.4 \times 10^5$ msec^{-1} from earlier work, and the frequency of the oscillator, $\omega_D \sim 1.4 \times 10^7$ so that the product $(\omega_D\ r_1/C_s)$ is about equal to unity. The estimated average value of δ, during the period when dynamic stabilisation is effective, is 0.13 and the estimated value of ε, neglecting second order effects, is 0.07 so that Berge's criterion[5], $\varepsilon \gtrsim (2\delta)/4$, is met to within experimental error. The value of δ increases after this period, to about 0.2 and hence the growth rate of the instability, taking L = 200 mm, is expected to be 2.5×10^5 which is consistent with the observed value of 4.10^5, allowing for the uncertainty in L. In the unstabilised shot the average value of δ after 6 μsec is about 0.2 ± 0.05 so that the predicted growth rate is again consistent with the observed value, allowing for the experimental uncertainties.

The measured damping of the oscillator by the plasma corresponds to a dissipation which is small compared with the local plasma energy.

Conclusion - The instability of a single axisymmetric bulge in the 8 m theta pinch can be stabilised by a high frequency standing wave. Estimates of the amplitudes of the high frequency and static bulges are consistent with the requirements of theory. No new instabilities were observed to be excited by the oscillating field.

References: 1. Bodin, H.A.B. et al. Novosibirsk Paper CN-24/K-1 (1968).
2. Bodin, H.A.B. et al. To be published Phys. of Fluids.
3. Haas, F.A. and Wesson, J.A. Phys. Rev. Letters 19, 833 (1967).
4. Ribe, F.L. and Riesenfeld, W.B. Phys. Fluids 11, 2035 (1968).
5. Berge, G. presented at this conference.
6. Bodin, H.A.B. et al. presented at this conference.
7. Berge, G. and Wolf, G.H. Culham Report CLM-P 200.

DYNAMIC STABILISATION OF THE m=1 INSTABILITY IN A BUMPY THETA PINCH

by
G. Berge
University of Bergen, Norway and
Culham Laboratory, Abingdon, Berkshire, England.

1. Introduction. The stability of a linear (as opposed to a toroidal) high β bumpy theta pinch has been investigated both theoretically[1,2] and experimentally[3]. The results reveal that such systems always are unstable. It is therefore of great interest to see whether there exist any means by which they can be made stable. One possibility is dynamic stabilisation[4-8]. Apart from being of interest in itself, the main interest in straight systems of this kind is because of the relevance they have to large aspect ratio toroidal systems. In this connection the M and S systems[9-13] are of special significance. An expansion of a toroidal system in the reciprocal aspect ratio results in a linear system in leading order. In addition to this of course a linear system is much easier to handle mathematically than the corresponding toroidal system.

In the proceeding analysis we first outline the model being studied. The m=1 instability of this model is then investigated. Finally the obtained results are discussed.

2. The Model. (a) Equilibrium. We shall study a high β axisymmetric system where the plasma is confined to the region around the axis by a mainly axial magnetic field ($B_z \gg B_r$). The axis is taken to be straight and the plasma is assumed to be separated from the vacuum region by a sharp boundary carrying a sheet current. The equilibrium is the same as that investigated by Haas and Wesson[2]. We shall also make use of their stability calculations, neglecting the stabilising effect of finite infinitely conducting boundaries in the vacuum region. The stabilising effect from a wall is small unless the wall is very close to the plasma vacuum interface. For obvious reasons this situation is not realised for highly compressed theta pinch plasmas. Cylindrical coordinates and the usual notation is used.

(b) The oscillatory state. It is assumed that by controlling the external magnetic field, an oscillatory motion is set up around the equilibrium state just described. Although this has to be done experimentally by oscillating currents in external circuits, we assume that by doing this properly we are able to give the interface between plasma and vacuum a prescribed motion. This interface is assumed to be given by

$$F(r,z,t) \equiv r - R(z,t) = 0 \qquad (2.1)$$

where

$$R(z,t) = \bar{R}(z)\left\{1 + \varepsilon \sin \omega_s t \cos \alpha z\right\} = \bar{R}(z) + \tilde{R}(z,t). \qquad (2.2)$$

We assume that $\varepsilon \ll 1$, and ω_s is the frequency of the oscillations, $\alpha = 2\pi/L$ where L is the wavelength in the axial direction. The magnetic field is assumed to remain tangential to the plasma-vacuum interface during the course of motion. The following solutions are obtained for the oscillatory motion:

$$\tilde{\underline{v}} = \varepsilon\left\{\omega_s \bar{R} S \cos \alpha z,\ 0,\ C_s^2 \alpha A Q \omega_s^{-1} \sin \alpha z\right\} \cos \omega_s t + O(\varepsilon^2), \qquad (2.3)$$

$$\tilde{\rho} = -\varepsilon \bar{\rho} A Q \cos \alpha z \sin \omega_s t + O(\varepsilon^2), \quad \tilde{p} = C_s^2 \tilde{\rho} + O(\varepsilon^2), \qquad (2.4)$$

$$\tilde{\underline{B}} = -\varepsilon \bar{B}_{izo}\left\{\alpha \bar{R} S \sin \alpha z,\ 0,\ Q \cos \alpha z\right\} \sin \omega_s t + O(\varepsilon^2). \qquad (2.5)$$

The symbols are defined as follows: $Q = x_o J_o(x)/J_1(x_o)$, $S = J_1(x)/J_1(x_o)$, J_o and J_1 are the zero and first order Bessel functions, $A = (1-a^2)^{-1}$, $a = \alpha C_s \omega_s^{-1}$, $x_o = k\bar{R}$, $x = kr$, $k = \frac{\omega_s}{C_s}\left[\frac{1-ba^2}{A+b}\right]^{\frac{1}{2}}$, $b = \frac{2}{\gamma}\frac{1-\beta_o}{\beta_o}$, $\beta_o = \frac{2\bar{p}}{\bar{B}^2_{vzo}}$, $C_s^2 = \frac{\gamma \bar{p}}{\bar{\rho}}$ and the barred quantities refer to the equilibrium. Subscripts i and v refer to the internal plasma region and the vacuum region respectively.

3. Stability. The stability analysis of this model is to be based on results derived elsewhere[7,8]. The notation of ref.8 is used and the problem is to investigate the sign of

$$\delta\bar{W} = \delta\bar{W}_O + \delta\bar{W}_D + \delta\bar{W}_E, \qquad (3.1)$$

where

$$\delta\bar{W}_O = -\omega_s^{-2}\int \underline{\xi}_o^* \cdot (\varepsilon^{-2}\underline{F}_e + \tilde{F}_2)(\underline{\xi}_o)\,d\underline{r}, \quad \delta W_D = \int \rho_o^{-1} |F_1'(\underline{\xi}_o)|^2 d\underline{r}. \qquad (3.2)$$

According to the results obtained in ref.8 Appendix H, sec.b $\delta W_E \geq 0$, and we can obtain sufficient conditions for stability with this term omitted. Analysis shows that for the case m=1 (and $\partial/\partial r = 0$ for the perturbations) δW_D minimizes to zero for $\xi_z = 0$. Moreover the most unstable modes are those for which $\nabla \cdot \underline{\xi}_o = 0$ and $\partial \xi_r/\partial z$ is small of order ε ($\underline{\xi}_o = \{\xi_r, \xi_\theta, \xi_z\}$). After a considerable amount of algebra involving expansions in small parameters, we arrive at the following expression

$$\delta\bar{W} \geq 2\pi \int \left\{a\left|\frac{d\xi_r}{dz} + \frac{b}{a}\xi_r\right|^2 + \left(c - \frac{b^2}{a}\right)|\xi_r|^2\right\} B_{vzo}^{-2}\, dz, \qquad (3.3)$$

where

$$a = (2-\beta_o)\bar{R}^2, \quad b = 2(1-\beta_o)\,\bar{R}\frac{d\bar{R}}{dz}$$

$$c = 2(1-2\beta_o)(1-\beta_o)\left(\frac{d\bar{R}}{dz}\right)^2 + \left(\frac{\partial\tilde{R}}{\partial z} + \varepsilon \bar{R}\,\bar{B}_{vzo}^{-1}\frac{\partial}{\partial z}\tilde{B}_{vz1}\right)^2 + \varepsilon\, 2\bar{R}\,\bar{B}_{vzo}^{-1}\tilde{B}_{vz1}\frac{\partial^2\tilde{R}}{\partial z^2}. \qquad (3.4)$$

From eq.(3.3) we now obtain the following sufficient condition for MHD stability ($\langle\rangle$ averaging over z, $\bar{}$ averaging over t):

$$\langle\bar{c}\rangle - \langle\overline{\frac{b^2}{a}}\rangle > 0. \qquad (3.5)$$

From the pressure balance condition we obtain in leading order

$$\tilde{B}_{vz1} = -\bar{B}_{vzo}\, Y \cos \alpha z \sin \omega_s t, \quad Y = Q\left[1-\beta_o + \frac{\gamma\beta_o}{2}A\right]. \qquad (3.6)$$

Let $I = \left[-\frac{\pi}{\alpha}, \frac{\pi}{\alpha}\right]$ be an interval on the z-axis. We define

$$\bar{R} = R_o\left[1 + \delta(1 + \cos \alpha z)\right],\ z \in I \text{ and } \bar{R} = R_o,\ z \notin I. \qquad (3.7)$$

This gives us a single bulge with amplitude $2\delta R_o$. By averaging condition (3.5) over the bulged region we obtain from condition (3.5)

$$\frac{\varepsilon^2}{4}\left[Y^2+1\right] - \left[(2\beta_o - 1)(1-\beta_o) + \frac{2(1-\beta_o)^2}{2-\beta_o}\right]\delta^2 > 0, \qquad (3.8)$$

which is the stability criterion.

4. Discussion. Using parameter values relevant to the experimental results obtained by Bodin et al.[14] ($Y \approx 2$, $\beta_o \approx 0.5$) condition (3.8) becomes $\varepsilon > 0.5\delta$. This can explain the observed effect.

By considering a periodic structure rather than a single bulge one obtains the same condition (3.8). One would think that this case had some relevance to large aspect ratio M and S systems. Realistic values of Y are of the order 2-3, and one can easily estimate the amount of dynamic stabilisation required to stabilise a given δ[11].

The present scheme may also be used to produce "dynamic equilibrium" where no equilibrium would otherwise exist[15].

In the context of a fusion reactor the application of dynamic stabilisation will become an economic problem. This has not yet been properly considered. Dynamic stabilisation may, however, also prove useful in cases where one has to pass through an unstable stituation in order to build up a configuration which finally is stable.

References

[1] HAAS, F.A. and WESSON, J.A. Phys. Fluids 9, 2472 (1966).
[2] HAAS, F.A. and WESSON, J.A. Phys. Fluids 10, 2245 (1967).
[3] BODIN, H.A.B., McCARTAN, J., NEWTON, A.A. and WOLF, G.H. Novosibirsk Conference Paper CN-24/L-1 (1958), and BODIN, H.A.B., NEWTON, A.A., WOLF, G.H. and WESSON, J.A., Subm. to Phys. Fluids (1968).
[4] WEIBEL, E.S. Phys. Fluids 3 946 (1960).
[5] HAAS, F.A. and WESSON, J.A. Phys. Rev. Lett. 19, 833 (1967) and Culham Report CLM-P 188 (1968)
[6] TROYON, F. Phys. Rev. Lett. 19 1963 (1967)
[7] BERGE, G. Novosibirsk Conference Paper CN-24/J-11 (1968).
[8] BERGE, G. Culham Report CLM-R97 (1969).
[9] MEYER, F. and SCHMIDT, H.V. Z. Naturf. 13a, 1005 (1958).
[10] PFIRSCH, D. and WOBIG, H. Proc. Culham Conference paper CN-24/55, IAEA. Vienna (1966).
[11] JOHNSON, J.L., MORSE, R.L. and RISENFELD, W.B. Plasma Phys. 10, 543 (1968).
[12] LOTZ, W., REMY, E. and WOLF, G.H. Nucl. Fusion 4, 335 (1964).
[13] WOLF, G.H. Culham Translation CTO/458 (1968), in press Z. Naturf. 24a, (1969).
[14] BODIN, H.A.B., BUTT, E.P., McCARTAN, J. and WOLF, G.H. (this conference).
[15] WOLF, G.H. and BERGE, G. Culham Report CLM-P200, (to be published in Phys. Rev. Lett.).

FINITE LARMOR RADIUS EQUATIONS IN A FINITE β COLLISIONLESS PLASMA AND THEIR APPLICATION TO A θ PINCH

by

E. Bowers and M.G. Haines

Physics Dept., Imperial College, London, England.

Introduction

In Section I a set of equations is derived for a general magnetic configuration using the "finite larmor radius approximation". This approximation - which is similar to that used by Rosenbluth and Simon[1], Kennel and Greene[2] and Bowers and Haines[3] - consists of ordering all quantities appearing in the Vlasov equation in terms of ϵ (assumed < 1) the ratio of the ion larmor radius to a characteristic length perpendicular to the magnetic field. The equations are used in Section II to study the stability of axisymmetric plasmas. In Section III results using a computer programme are presented for a θ pinch. They demonstrate the effects of density profile, boundary conditions, finite plasma pressure, finite ion larmor radius and axial wavelengths.

I. Derivation of Equations.

Following Hastie et. al.[4] the coordinate system is defined by three orthogonal unit vectors, $\underline{e}_x$, $\underline{e}_y$ and $\underline{e}_\ell$, where $\underline{e}_\ell = \underline{B}/B$ and $\underline{e}_x$, $\underline{e}_y$ define the plane perpendicular to $\underline{B}$. Since $\underline{B}$ is the equilibrium field the unit vectors will be independent of time. In these coordinates we may write

$$\underline{\nabla} = \underline{e}_x \frac{\partial}{\partial x} + \underline{e}_y \frac{\partial}{\partial y} + \underline{e}_\ell \frac{\partial}{\partial \ell}$$

where $\frac{\partial}{\partial x} = \underline{e}_x . \underline{\nabla}$ etc. The kinetic velocity may be expressed as $\underline{v} = v\cos\varphi\, \underline{e}_x + v\sin\varphi\, \underline{e}_y + v_\ell \underline{e}_\ell$ and the Vlasov equation is then expressed in terms of these velocity variables. The ordering scheme that follows is then used to solve for the distribution function f.

$$\frac{1}{\tau} \sim \epsilon^2\Omega^i, \quad \frac{L_\perp}{L_\parallel} \sim \epsilon, \quad E_x \sim E_y \sim \epsilon \frac{v_i B_\ell}{c}, \quad E_\ell \sim \epsilon E_x, \quad B_x \sim B_y \sim \epsilon B_\ell$$

$$\kappa_x \sim \kappa_y \sim \tau_x \sim \tau_y \sim \tau_\ell \sim \frac{\epsilon}{L_\perp}, \quad \sigma_\ell \sim \kappa_\ell \sim \frac{\epsilon^2}{L_\perp}, \quad \sigma_x \sim \sigma_y \sim \frac{1}{L_\perp}$$

In the above σ, κ and τ are components of curvature and torsion of the coordinate system, Ω is the gyrofrequency $\frac{eB_\ell}{Mc}$ and B_x, B_y will allow bending of the lines of force when stability is studied. This ordering gives a self consistent set of equations and ensures that the current produced by finite ion larmor radius (F.L.R.) is comparable with that caused by effects such as curvature. Solving the Vlasov equation order by order and then taking moments gives the traceless stress tensor appearing in the equation of motion, ignoring $O(\frac{M^e}{M^i})$, in the form

$$\frac{\pi_{xx} - \pi_{yy}}{2} = \frac{-P_\perp}{2\Omega}\left[\left(\frac{\partial}{\partial x} - \sigma_y\right)u_y + \left(\frac{\partial}{\partial y} + \sigma_x\right)u_x\right] - \frac{1}{4\Omega}\left[\left(\frac{\partial}{\partial x} - \sigma_y\right)q^\perp_y + \left(\frac{\partial}{\partial y} + \sigma_x\right)q^\perp_x\right]$$
$$- \frac{B_y}{2B_\ell}\pi_{\ell y} + \frac{B_x}{2B_\ell}\pi_{\ell x} + (\tau_x - \tau_y)\frac{1}{2\Omega}\left(q^\perp_\ell + u_\ell P_\perp\right).$$

$$\pi_{xy} = \frac{P_\perp}{2\Omega}\left[\left(\frac{\partial}{\partial x} - \sigma_y\right)u_x - \left(\frac{\partial}{\partial y} + \sigma_x\right)u_y\right] + \frac{1}{4\Omega}\left[\left(\frac{\partial}{\partial x} - \sigma_y\right)q^\perp_x - \left(\frac{\partial}{\partial y} + \sigma_x\right)q^\perp_y\right]$$
$$+ \frac{B_y}{2B_\ell}\pi_{\ell x} + \frac{B_x}{2B_\ell}\pi_{\ell y} + (\kappa_x - \kappa_y)\frac{1}{2\Omega}\left(q^\perp_\ell + u_\ell P_\perp\right).$$

$$\pi_{\ell x} = -\frac{P_\perp}{\Omega}\frac{\partial u_\ell}{\partial y} - \frac{1}{\Omega}\frac{\partial q^\perp_\ell}{\partial y} + \frac{B_x}{B_\ell}\left(\Sigma P_{\ell\ell} - \Sigma P_\perp\right).$$

$$\pi_{\ell y} = \frac{P_\perp}{\Omega}\frac{\partial u_\ell}{\partial x} + \frac{1}{\Omega}\frac{\partial q^\perp_\ell}{\partial x} + \frac{B_y}{B_\ell}\left(\Sigma P_{\ell\ell} - \Sigma P_\perp\right).$$

Here $\underline{u}$ is the lowest order centre of mass velocity, $P_\perp$ and $P_{\ell\ell}$ are zero order pressures perpendicular and parallel to the equilibrium field, while $\underline{q}^\perp$ is part of the heat flux tensor defined by

$$\underline{q}^\perp = \frac{M}{2}\int f (\underline{v}_\perp - \underline{u}_\perp)^2 (\underline{v} - \underline{u})\, d^3v$$

II. Stability of Axisymmetric plasmas

In this case we find that the zero order equilibrium distribution function must be of the form $f(\psi, \mu, \xi)$ where $\mu = \frac{1}{2}\frac{Mv^2}{B}$, $\xi = \frac{1}{2}M(v^2 + v^2_\ell) + e\phi$ and the equilibrium field $\underline{B} = \nabla\psi \times \nabla\theta$. When perturbations of the form $A'(\psi, \ell)e^{i(\omega t + m\theta)}$ are assumed it is found that the linearised equation for f' yields either a dispersion relation for ω describing a microscopic instability or an adiabatic incompressible perturbation. We consider the latter case and then find that the linearised equation of motion gives

$$B\frac{\partial}{\partial\psi}\left(r^3 P_\perp S + rB\frac{\partial}{\partial\psi}\left(\frac{u'_\psi}{\omega_i}\right)\right) + \left((1-m^2)\rho_\ell S + Br^2\frac{\partial\rho_\ell}{\partial\psi}\omega^2 - \kappa_\ell m^2 rB\frac{\partial}{\partial\psi}\left(\Sigma P_{\ell\ell} + \Sigma P_\perp\right)\right)\frac{u'_\psi}{\omega_i} = 0$$

$$S = \omega_i^2 - \frac{m\omega_i}{\rho}B\frac{\partial}{\partial\psi}\left(\frac{P_\perp}{r\Omega}\right) + \frac{m^2}{2\rho r\Omega}\frac{dB}{d\psi}q^\perp_\theta, \quad \omega_i = \omega + m v_{\theta 0}.$$

In the above we are just considering the flute perturbation, i.e. $B'_\psi = B'_\theta = 0$. If, for the case of no curvature in equilibrium, we take the disturbance $A'(r)\, e^{i(\omega t + m\theta + kz)}$ we obtain the above equation with $\frac{\partial}{\partial r}$ replacing $rB\frac{\partial}{\partial\psi}$, $S + \frac{k^2}{\rho}(\Sigma P_{\ell\ell} - \Sigma P_\perp - B^2/\mu_\pi)$ replacing S and rk^2 replacing $-\kappa_\ell m^2$.

III. Results for a θ Pinch

Neglecting surface currents on the plasma the boundary condition (b.c.) to be satisfied at the plasma-vacuum interface is

$$\left(C^{2m} - 1\right)\frac{\partial}{\partial r}\left(\frac{ru'_r}{\omega_i}\right) + m\left(C^{2m} + 1\right)\frac{u'_r}{\omega_i} = 0$$

where a wall of infinite conductivity lies at $r = Cr_0$. Figs. 1 and 2 show that $C \to \infty$ is the most unstable b.c. while figs. 2 and 3 show that a steep density gradient enhances F.L.R. stabilisation. Fig. 4 shows the stabilising effect of finite plasma pressure while Fig. 5 demonstrates that θ pinches should be stable against axial wavelengths shorter than ~ 1 metre. We note also that F.L.R. can stabilise the m = 1 mode.

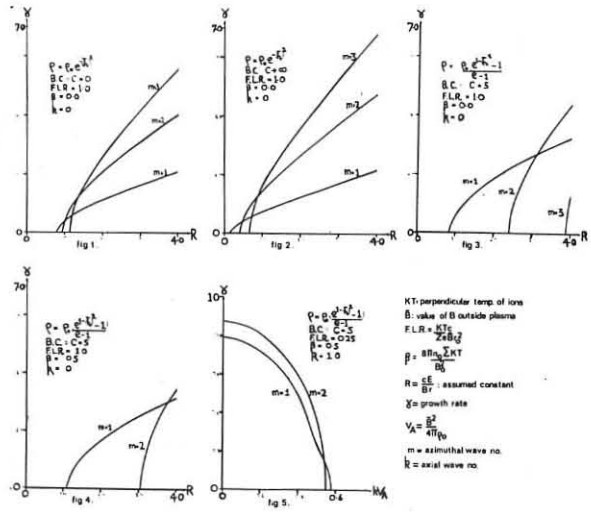

Acknowledgements

The authors would like to thank B. McNamara of Culham Laboratory for the use of his computer program, and one of us (E.B.) the Science Research Council for providing a Research Studentship.

References

[1] M.N. Rosenbluth and A. Simon. Phys. Fluids, 8, P.1300, (1965).

[2] C.F. Kennel and J. Greene. Ann. Phys. 38, P.63, (1966)

[3] E. Bowers and M.G. Haines. Phys. Fluids, 11, P.2695, (1968).

[4] R.J. Hastie, J.B. Taylor and F.A. Haas. Ann. Phys. 41, P.302, (1967).

DYNAMIC-STABILIZATION AND TURBULENCE EXPERIMENTS ON θ-PINCH PLASMAS*

R. F. Gribble, E. M. Little, W. E. Quinn, F. L. Ribe, G. A. Sawyer, K. S. Thomas, and D. M. Weldon

Los Alamos Scientific Laboratory, University of California, Los Alamos, New Mexico 87544 USA

I. INTRODUCTION. All of the configurations presently under consideration for the Scyllac high-β toroidal θ pinch [1] (the screw pinch, the Grad-Weitzner Stellarator [2] and the M and S torus [3]) exhibit dominant m = 1 unstable modes which can theoretically be stabilized by means of an oscillating longitudinal current I_z. This is related to dynamically stabilizing the helical m = 1 Kruskal-Shafranov modes (of wave number k) on a straight plasma column of radius a in a constant longitudinal field B_o, where the magnetic lines have pitch wave number $\mu = 2I_z/a^2B_o$. With $\mu = \mu_o$ consat the condition [4] for stabilization (assuming μa, ka ≪ 1) is that k not exceed the value

$$k_s = \frac{\mu_o}{2-\beta}\left\{\left[1+\frac{\omega^2}{\gamma^2}\right]^{\frac{1}{2}} - 1\right\}, \qquad (1)$$

where $\gamma = \mu_o v_A/(2-\beta)^{\frac{1}{2}}$ is the maximum MHD growth rate with ω = 0; $v_A = \left[B_o^2/4\pi\rho\right]^{\frac{1}{2}}$ is an Alfvén speed, and ρ is the plasma density.

We report experiments on dynamic stabilization of the K-S mode and measurements of turbulence from the oscillating current in high-β linear θ pinches. Preliminary results were given in Refs. [1,5,6]. See Ref. [7] for earlier related work.

II. PLASMA PARAMETERS. Two θ pinches were used, each having a compression coil length ℓ of one meter and an inner diameter of 10.5 cm. Scylla IV [1] produced hot, collisionless plasma with $kT_i \approx 2000$ eV, $kT_e = 300$ eV at $B_o \approx 90$ kG. The radius of the toe of the density distribution was approximately 1.0 cm, inside of which the average density and beta were 1.0×10^{16} cm^{-3} and 0.3. Scylla III [5] produced colder, collision-dominated plasma with $kT_i \approx kT_e \approx 150$ eV, $\beta_{av} \approx 0.5$, a = 1.8 cm, and $v_A \approx 0.43 \times 10^8$ cm/sec. B_o had a period of 6.8 μsec and a maximum value of 25 kG. In Scylla IV [1] K-S modes with quasi-steady I_z were previously identified and found to occur with a wave length twice the plasma length.

III. DYNAMIC-STABILIZATION EXPERIMENTS ON SCYLLA III. The apparatus is shown in Fig. 1. The capacitor bank consisted of six 60-kV, 0.17-μF capacitors and a metal-contact dielectric switch, producing a secondary current I_s (= I_z) of 33 kA at a frequency of 0.8 MHz. With minor modifications a quasi-steady current of 1.5-μsec rise time and 39 kA was produced. Results

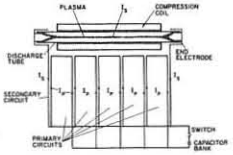

Fig. 1. Dynamic stabilization circuit.

are shown in the streak pictures of Fig. 2, taken at the coil midplane and at 25-cm on either side (the upper streak picture is inverted in each case). Fig. 2B (I_z = 0) shows only a slight drift toward the coil feed slot, owing to the end-electrode feed plates. With quasi-steady I_z initiated after B_o (Fig. 2C) the plasma is unstable and contacts the discharge tube wall. With oscillating I_z(~) [Fig. 2D] no instability occurs, even though I_z is sufficient under quasi-steady conditions to excite the K-S mode. Evaluating Eq. (1), we find $k_s = 0.06$ cm^{-1}, compared to $k = \pi/\ell = 0.03$ cm^{-1}. Thus the observed stabilization of the K-S mode is also theoretically possible. Measurements similar to those for Scylla IV (below) showed that I_z(~) was indeed carried at r ≈ a.

IV. TURBULENCE EXPERIMENTS ON SCYLLA IV. Oscillating I_z was driven by a 0.17-μF capacitor in the circuit of Fig. 3A where L_s is an adjustable, calibrated coaxial inductance. The inductances L_1 and L_2 due to cables and connections were determined using a copper tube (1.9-cm diam) along the compression-coil axis. Then the radius a of the current channel on the plasma was determined from its inductance L_L. In the preionized plasma (Fig. 3B, lower) a = 3.4 cm. With full magnetic compression (Fig. 3B, upper) a = 1.0 ± 0.2 cm, corresponding to the tail of the measured density distribution [1,6]. The current-carrying plasma has a density lying between 10^{14} and 10^{15}/cm^3.

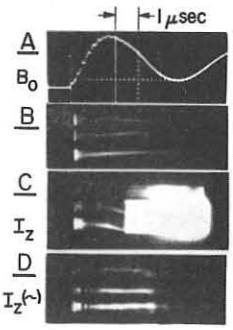

Fig. 2. Scylla III dynamic-stabilization measurements.

The Q values of the circuit with L_L open, with the copper tube, with the compressed plasma, and with preionized plasma gave a compressed-plasma resistance of 100 mΩ [1,6].

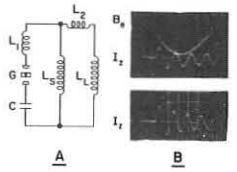

Fig. 3. Circuit and waveforms for oscillating I_z on Scylla IV.

V. INTERPRETATION OF THE PLASMA RESISTANCE. In order to calculate the resistance of the plasma the skin depth s was first derived on the basis of a phenomenological collision time τ [from turbulence or from binary (i-e)collisions] for which the conductivity is $\sigma = (ne^2\tau/m_e)(1+i\omega t)(1+\omega^2\tau^2)^{-1}$. The calculated plasma resistance R is plotted vs τ in Fig. 4 for various values of n. The experimental value of R (hatched line) corresponds to $\tau \approx 10^{-11}$ sec, corresponding to s ≈ 0.2 cm. The average electron drift velocity is calculated to be about 2×10^9 cm/sec for the present values of I_z(15 kA) and is well below the electron thermal velocity $v_e \approx 1.0 \times 10^9$ cm/sec. It is however greater than the ion thermal speed of 4×10^7 cm/sec and the ion sound speed $[kT_e/m_i]^{\frac{1}{2}} = 1.2 \times 10^7$ cm/sec. On the average, ion sound would be unstable provided $kT_e/kT_i > 1$ which, however, is not the case in the absence of I_z. The inverse ion plasma frequency ω_{pi}^{-1} is about 10^{-10} sec and is much less than the experimental value of τ, which in turn is greater than $\tau_{ie} = 3 \times 10^{-6}$ sec.

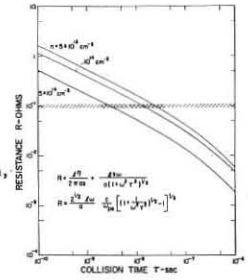

Fig. 4. Calculated and observed plasma resistances (ℓ = 90 cm, a = 1 cm) vs collision time τ.

We conclude that the present experiment exhibits weak turbulence. The diffusion coefficient $D = r_e^2/2\tau$ is about 10^{-3} of the Bohm value (r_e is the electron Larmor radius).

* Work performed under the auspices of the U. S. Atomic Energy Commission.

REFERENCES.

[1]. E. M. Little, A. A. Newton, W. E. Quinn, and F. L. Ribe, Third Conference on Plasma Physics and Controlled Nuclear Fusion Research, Novosibirsk, USSR, August 1-7, 1968 (IAEA, Vienna, 1969). Paper CN-24/H2.

[2]. A. A. Blank, H. Grad, and H. Weitzner, Op. Cit., Paper CN-24/K6. Also these proceedings.

[3]. R. L. Morse, W. B. Riesenfield, and J. L. Johnson, Plasma Phys. 10, 543 (1968).

[4]. N. A. Bobyrev and O. I. Fedyanin, Zh. Tekhn. Fiz. 33, 1187 (1963). [Sov. Phys. - Tech. Phys. 8, 887 (1964)].

[5]. K. S. Thomas, G. A. Sawyer, and D. M. Weldon, Bull. Am. Phys. Soc. Series II, 13, 1489 (1968).

[6]. W. E. Quinn, E. M. Little, and F. L. Ribe, Bull. Am. Phys. Soc. Series II, 13, 1566 (1968).

[7]. V. P. Gordienko, L. V. Dubovoi, and I. M. Roife, Plasma Phys. 10, 499 (1968).

m = 0 INSTABILITIES IN A HIGH - ENERGY THETA PINCH[+)]

by

M. Kaufmann, J. Neuhauser, H. Röhr
INSTITUT FÜR PLASMAPHYSIK
Garching bei München, Germany

1) The velocity distribution of the ions in a high energy theta pinch is in general anisotropic. In the fast compression phase all the ions are accelerated towards the axis. In the adiabatic compression phase that follows only the temperature $T_\perp$ perpendicular to the axis is increased, provided that relaxation can still be neglected.
The relaxation of this strongly anisotropic plasma is due to collisions [1] and instabilities. The relaxation due to Coulomb collisions is usually of the order of the confinement time of the plasma, allowance having to be made for ion-electron collisions. In addition, however, a major contribution to relaxation is to be expected from instabilities.
Low frequency instabilities which already occur at relatively low degrees of anisotropy are the familiar mirror type [2,3]. For large anisotropy, instabilities have the frequency of the ion cylotron frequency and its harmonics. In high temperature theta pinches the criterion for the onset of mirror instabilities in the adiabatic phase may sometimes be exceeded. In a homogeneous plasma with superposed magnetic field these instabilities should occur when the ratio $\eta = \frac{p_\perp}{p_\parallel}$ exceeds a critical value $\eta_k = \frac{4}{\beta}$ [2]. The influence of wall stabilization should be negligible under theta pinch conditions [4]. The instabilities should be of the m = 0 type.

2) The experimental detection of these mirror instabilities in the Isar I high energy theta pinch is reported in this paper. The essential parameters of this device are:
E_{max} = 2.6 MJ, B_{max} = 146 kG, $\tau/4$ = 11 µsec, coil length 1.5m, vessel diameter = 9 cm. The energy was varied between 0.5 and 2.6 MJ, the filling pressure between 6 and 90 micron. As a result the collision times of the adiabatic phase varied over a wide range (Fig. 1, hatched region) and were both larger and smaller than the heating time.

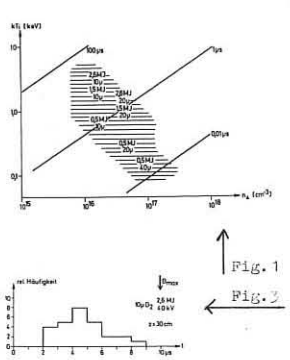

Fig. 1

Fig. 3

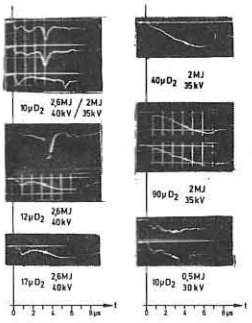

Fig. 2

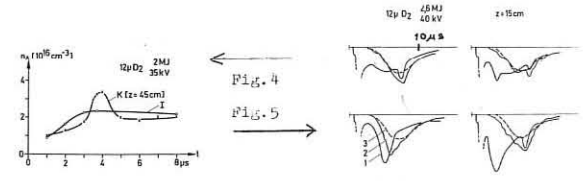

Fig. 4

Fig. 5

Fig. 4: Electron density on the axis end-on (I) and side-on (K)
Fig. 5: Continuum signal (1), neutron signal side-on (2) and neutron signal integrated over the coil (3)

Mirror instabilities were observed in discharges with collision times greater than about 1 µsec. Observation was made by:
1) Side-on measurement of the continuum radiation
2) 90° laser scattering
3) Measurement of the magnetic field between the vessel and coil
4) Measurement of the local neutron rate.
All measurements showed correlated disturbances of the plasma column in time and space.

Time developments of the side-on continuum radiation are represented in Fig. 2. Under discharge conditions leading to large collision times (left-hand side) there are distinct spikes in the time development. The frequency distribution of these irreproducible spikes (Fig. 3) shows that they only occur during the rise of the field and hence of the temperature. The electron density was determined from the side-on measurement of the continuum radiation. The time development of the electron density on the axis showed distinct, irreproducible deviations from interferometric end-on measurements (Fig. 4).
Laser scattering measurements of the electron density exhibited equally pronounced fluctuations of the local density which were correlated with the simultaneously measured continuum. Spikes correlated with the continuum were also observed in side-on measurements of the fusion neutrons (Fig. 5). Measurement of the magnetic field between the coil and vessel revealed that the spikes were accompanied by a field rise of up 1 %. It should be noted here that the field rise near the plasma must have been much larger since the disturbance extended only a few centimetres in the axial direction.

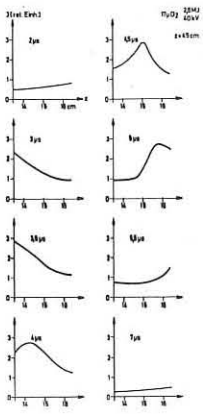

Fig. 6

Fig. 7

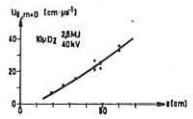

The extension of the disturbation in the axial direction was measured by means of the continuum radiation. The intensity over a 3 cm section of the axis is plotted in Fig. 6. A disturbance is observed to pass through in the time from 3 to 5.5 µsec. The velocity of the disturbances in the z-direction $u_\parallel$ increased almost linearly with the distance from the midplane and corresponded to the outflow velocity (Fig. 7, t = 5.5 µs).

3) Calculations from the bounce model [3] for β = 1 yield values of the rise time for m = 0 instabilities at anisotropic pressure that are about five times as high as the transit time of the ions across the colums (η = 2). For T_i = 2 keV this would yield a value of 0.2 µsec. The rise time lapses several times before the adiabatic phase starts. The further development of the instabilities is governed by the development of η. As empiric condition for instabilities to occur with certainty it was found from the observations that the collision relaxation time has to be about 5 µsec, this being approximately the heating time.

For β = 1 and η = 2 the calculations in [3] would yield wavelengths with maximum growth rate that are of the order of the diameter. This agrees with the observation.

In this investigation the β-value could not be varied independently of the collision times. With rising collision time there was a decrease of β. At full bank energy and filling pressure 6 µ the value attained by β on the axis was 0.1. This should explain the fact that it is not at the lowest pressures that the instabilities are most frequent and pronounced.

The instabilities resulted in increased relaxation and increased end losses. This was clearly demonstrated by a premature increase of velocity $u_\parallel$ of the disturbances themselves. After the relaxation was increased by instabilities, the development of the discharge was highly irreproducible.

[1] C. Andelfinger, et al.; IPP-Report 1/67 (1967)

[2] A.A. Vedenov, R.Z. Sagdeev; Plasma Phys. Probl. Contr. Therm. React. 3, 332 (1958)

[3] R.L. Morse; Phys. Fluids, 10, 1017, (1967)

[4] S. Chandrasekhar, et al.; Proc. Roy.Soc. 245A, 435, (1958)

[+)] This work was performed as part of the joint research program of the Institut für Plasmaphysik, Garching, and Euratom.

MULTICHANNEL ENERGY ANALYSIS OF THE ION FLUX+) FROM A THETA PINCH

by

G. Becker
INSTITUT FÜR PLASMAPHYSIK
Garching bei München, Germany

Conventional diagnostic methods for ion energies in hot theta pinch plasmas use the neutron flux or the laser light scattered in the forward direction. None of these gives the detailed energy distribution of the ions. Determination of the spectrum from the axial end losses has already been reported by [1].

The new 10-channel energy spectrometer used here measures the time resolved energy distribution in the flux ∥ to the axis from each discharge (E = 1 - 10 keV). Preliminary diagnostic investigations and the measurements were made on the Isar III theta pinch [2] with the standard parameters 10 mTorr D_2, B_{max} = 75 kG, and 30 cm long straight coil. The experimental set-up is shown in Fig. 1.

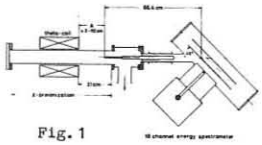

Fig. 1

The particle beam of small divergence passes through a metal collimator and is energy dispersed in the field of a planar capacitor. Behind each of the 10 exit slits there is a fast detector system. The energy resolution is found to be dependend only on the slit assembly and not on space charges in the capacitor.

Figure 2 shows the deuteron flux for 1 - 7 keV from one discharge (channel width 200 eV). In addition, the neutron flux and the pinch field are displayed as a time reference.

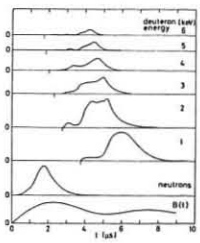

Fig. 2

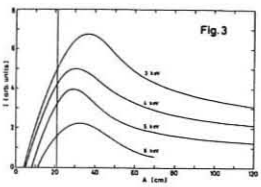

The distance A (Fig. 1) was varied originally to investigate the influence of the coil field on the distribution. This, however, proved to be unimportant. Figure 3 shows the maximum ion currents versus A. Although the solid angle Ω_o, in which particles can be detected, decreases with growing A, the measured flux increases. This is inconsistent with the existing conception of direct measurement of deuterons as well as the fact that the decrease for large A does not go faster than $\propto \Omega_o$. Behind the long path through neutral gas the measured flux can only exist if equilibrium between D atoms (90 %) and deuterons (10 %) builds up as a result of charge exchange cycles in D_2. The deuteron flux diverges at the limit of the coil field (B_{lim}) in the aperture, and so the capacitor is bypassed. Additional experiments confirmed that the measured flux increases with the neutral gas length in front of B_{lim}. Deuterons can only be detected, if they pass B_{lim} as D atoms without being deflected, and if they are reionized by one more charge exchange in the field-free region. Changes of energy and direction due to charge exchange cycles can be neglected here. $I = I(A,E)$ in Fig. 3 can be calculated from the change of deuteron flux at the coil end ($I_o(E)$) due to charge exchange and electron-impact ionization. The reduction of I_o depends only slightly on E in the range 4 - 10 keV, but is much greater for low E (1 keV).

In Fig. 4 measured flux spectra $\frac{dn}{dE}(E)$ are plotted at several times of one discharge. They are similar to the averaged results of [1]. The dip in $\frac{dn}{dE}$ at low energies, interpreted as a lack of slow ions in [1], is now explained in terms of the above processes. For $E > 3$ keV $\frac{dn}{dE} \propto \exp\left\{-\frac{E}{\bar{E}}\right\}$. $\bar{E}$ is compared with kT from the neutron flux in the case of a 3-dim. Maxwellian.

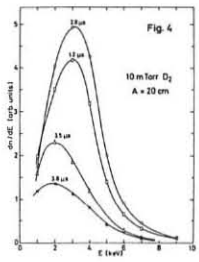

10 mTorr	$\bar{E} \approx$ 1-1.3	keV	kT ≈	1 keV
20 mTorr	$\bar{E} \approx$ 900	eV	kT ≈	0.9-1 keV
30 mTorr	$\bar{E} \approx$ 600	eV	kT ≈	500-600 eV

The first pulse 300 nsec after the beginning of the main discharge (t = 0) is ascribed to the separation of the divergent plasma ends (Fig. 2). The onset of the main signal at $t = t_1 \simeq 1$ µsec is unexpectedly steep. Mach-Zehnder measurements of the end losses into 2π show that about 30 % of the plasma has already been lost up to $t = t_1$, when $\frac{v_\perp}{v_\parallel}$ is large (anisotropic outflow, $l_p/v_\parallel < t_c$ ion relaxation time; l_p plasma length). The starting point and t_1 can be determined independently by means of the 10-channel energy spectrometer. l_p is found to equal the coil length fairly well. t_1 shows an n and m-dependence contrary to that of t_c given by the theory. The sudden onset of losses into Ω_o observed in all channels at $t = t_1$ suggests anomalously fast relaxation, which may be caused by mirror instability. Relaxation must take place within a few 100 nsec because the outflow is isotropic for $t > t_1$. This follows from a comparison of the total particle flux into 2π with the end loss into Ω_o, calculated from the absolute E-integrated flux spectrum. At t = 1.6 µsec one measures, for example:

Total end loss into 2π	:	≈ 2.5 kA
E-integrated loss into $\Omega_o = 2 \cdot 10^{-6}$ rad^2	:	≈ 1 mA
Loss into Ω_o for E = 7 ± 0.1 keV	:	max. ≈ 2 µA.

The extremely high spectrometer detection efficiency allows analysis of late end losses despite the fact that Ω_o is only $2 \cdot 10^{-6}$ rad^2 and the channel width only 200 eV. The end loss into 2π corresponds to about 1 kA at the detection limit of interferometry for $l_p \approx 30$ cm. Ion analysis is possible, however, down to $I_o \approx 10^{-7}$ A.

After the instability at t_1 relatively few energetic ions are seen in Ω_o. Thus, there is no fast relaxation for these ions. A late anomaly (possibly a loss-cone instability) affects particularly E ≥ 7 keV ions (2nd main signal), but is also to be seen in the decay of the signals of low energy ions that have already become rare at this time. The increase of the fraction of energetic ions in the flux with time corresponds to a longer confinement of these ions. The discussed results with straight coil are obtained with a mirror ratio R = 1.6 as well.

[1] R.L. Bingham, L.M. Goldman, R.W. Kilb; Plasma Phys. and Contr. Nucl. Fus.Res., I.A.E.A., I., 301 (1966)

[2] A. Heiss, H. Herold, E. Unsöld, Proc. APS Top. Conf., Los Alamos (1967), LA-3770, p.D7-1.

+) This work was performed as part of the joint research program of the Institut für Plasmaphysik, Garching, and Euratom.

PLASMA PRODUCTION AND HEATING IN SUPERPOSED FIELDS THETA PINCH

R.Bono, S.Costa, P.L.Mondino, G.Rostagni

UNIVERSITA' DEGLI STUDI DI PADOVA
Istituto di Elettrotecnica
Gruppo Gas Ionizzati del CNR

Abstract

In a previous paper(x) we have shown the possibility of studying the long time confinement in theta pinches without limits imposed from the discharge duration (a problem of interest for the new toroidal devices).

A "sustained field" theta pinch was realized by means of two independent coaxial coils. The first produced a fast varying pulsed field, the second a constant or nearly contant field of opposite direction and slightly smaller maximum amplitude.

The present paper presents systematic measurements and a more detailed analysis of the breakdown and heating mechanism in the sustained field configuration. The influence of a fast ionising axial discharge on trapped field and plasma behaviour at different pressures is also shown.

(x) - R.Bono, I.Faccini, P.L.Mondino, G.Rostagni
"Breakdown and Compression in superposed fields theta-pinch"
presented at the 2nd European Conference on Controlled Fusion and Plasma Physics, Stockholm 1967.

Experimental and Theoretical Progress on the Polytron

by

A.E. Dangor, M.G. Haines, J. Kilkenny, G.J. Parkinson,

D.E. Potter, M.J. Watkins.

Physics Dept., Imperial College, London, England.

Introduction

Since our report in the Third IAEA Conference on Plasma Physics and Controlled Fusion Research (1968) (1) the torus bore was increased from 46 mms to 71 mms. With this modification a twofold increase in the cusp radial magnetic field at the quartz wall is obtained using the same magnetic field coils. It was hoped that this increase together with the larger bore would increase the time before the leakage through the ring cusps became important. Measurements of the containment time show that the expected improvement was not obtained for reasons to be given. However, much progress in studying the Hall acceleration process has been made.

The computational work referred to in the abstract will be included in the oral presentation.

Containment time measurements

Fig. 1 shows typical oscillograms of the total current in the z-direction (cylindrical coordinates are used, in which the z-axis is taken to be in the toroidal direction) for the two different discharge regimes: the left trace is the regime in which the ions are the dominant current carriers and the right trace is the regime in which an electron current begins to grow at the time of the change in slope. At this time for both conditions the AIV λ2809 Å radiation, shows an intensity peak and also it coincides approximately with the time at which the signal from a Faraday probe, at the wall, biased to collect ions, reaches half its maximum value. This time is therefore taken to be a measure of the containment time, i.e. the time at which cusp losses become evident. The value obtained is found to decrease with increasing applied electric field. This is probably due to a larger increase in the thermal speed of the particles through Ohmic heating outweighing any increase in axial directed motion. The containment time is also found to decrease weakly with increasing cusp magnetic field. Langmuir probe and microwave investigations of the interaction of the rising cusp magnetic fields with the decaying preionizer plasma show that the plasma is compressed into the region between cusp coils. The electron density in this region is found to be approximately four times larger than in absence of the cusp field. Ion probe measurements indicate that the size of each plasma leakage ring is approximately 3 mms in length, it decreases with increasing radial cusp field B_r and is of the order of the ion Larmor radius. Thus at the time when the main accelerating electric field is applied a very non-homogeneous plasma distribution obtains. The measured containment times is determined partly by this unfavourable distribution and this explains the similarity in the containment times found in the large and small bore vessels.

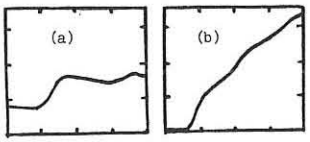

Fig. 1: I_z oscillograms for (a) E = 6.3 kv/m (b) E = 12.6 kv/m: B cusp = 4 kgauss, pressure 4 microns argon, 5 ka/div, time base: 1 μsec/div.

Acceleration Process

Some further measurements concerning the acceleration process are obtained at times earlier than the containment time. In particular the magnetic field generated by the azimuthal Hall currents (due to $j_z \times B_r$) is found using diamagnetic loops placed internally in the region where B_r is a maximum. These show a maximum in their variation with cusp magnetic field showing the expected linear dependence for small B_r and inverse variation for large B_r. Figs. 2-4 show the variation of the initial dI_z/dt with applied electric field E_z, applied cusp magnetic field, and initial gas pressure in argon. These graphs are consistent with a model in which the electrons are trapped by the cusp field and the ions along are accelerated by the applied electric field. Then the ion inertia enters the plasma toroidal circuit equations as an inductance in addition to geometrical inductance per unit length L. We write

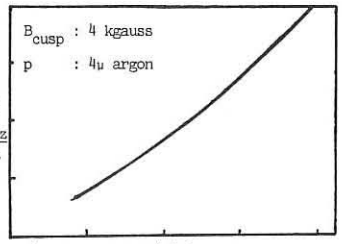

Fig. 2 3.15 kv/m/div. E_z →

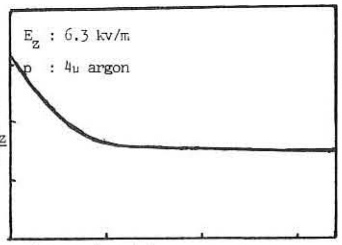

Fig. 3 4 kg/div B_r →

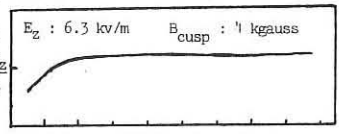

Fig. 4 1 micron/div p →

Fig. 2 - 4 : 1 vertical division : 5 ka/μs.

$$\left[L + \frac{m_i}{N_i e^2 z^2}\right]\frac{dI_z}{dt} + \left[R - \frac{m_i}{z^2 e^2 N_i^2}\cdot\frac{dN_i}{dt}\right] I_z = E_z$$

where N_i is the ion line density, R is the resistance per unit length, and ze is the mean ionic charge. For n_i small, the ion inertia dominates the equation when $I_z = 0$. This is in agreement with Fig. 4 where dI_z/dt is proportional to p at small pressure and is independent at large p. The variation of initial dI_z/dt with E_z (Fig. 2), is approximately linear for large E_z. Thus numerically

$$\left.\frac{dI_z}{dt}\right|_{t=0} = \frac{E_z \quad 10^6}{[0.5 + 4.5/z^2]}$$

in MKS units. Experimentally $\frac{dI_z}{dt} = 1.2 \cdot 10^6 E_z$ A sec^{-1}, which indicates a value of z for argon between 3 and 4 in agreement with measurements of line intensities from various ionization states.

The variation of dI_z/dt with B_{cusp} is in agreement with the MHD calculations made by Dunnett (2) in which the magnetic field of the Hall current is included. In these calculations a critical applied electric field is derived, above which the electrons do not remain trapped. Approximately the condition for no axial current is

$$\frac{\mu_o n_e e E_z}{k \bar{B}_r^2} < 1$$

where $\bar{B}_r$ is an averaged value of the cusp radial field and π/k is the cusp seperation. At low values of the cusp magnetic field this condition will be violated, and the electron trapping model with ion inertia in the circuit equation no longer holds. The initial dI_z/dt will be larger and determined by only the geometric inductance as found in Fig. 3.

References

1. Dangor, A.E. et. al. 1969. "Plasma Physics and Controlled Nuclear Fusion Research" Vol.1, pp.255-262 (I.A.E.A.: Vienna).

2. Dunnett, R.M., Nuclear Fusion 8, 4 (1968).

RECENT MEASUREMENTS ON A ROTATING MAGNETIC FIELD PINCH

by

A. Berney, A. Heym, F. Hofmann, and I.R. Jones

(Centre de Recherches en Physique des Plasmas,

Lausanne - Switzerland)

ABSTRACT

Measurements made on a rotating magnetic field pinch are presented. These measurements include streak and framing photography, transfer of energy from the R.F. generators to the discharge tube, magnetic field profiles and the variation with time of ion and electron temperatures.

1. INTRODUCTION

The name "rotating magnetic field pinch" is given to a configuration in which a high - β cylindrical plasma column is surrounded by a confining field which has a longitudinal (B_z) and an azimuthal (B_θ) component. Both components oscillate at the same fixed frequency but are dephased by 90°. At any given point on the plasma surface, the magnetic field vector rotates in a tangent plane. Theoretical studies by Weibel[1] and Troyon[2] show that such a plasma column is stable against all surface deformations.

A rotating field pinch can be obtained by the superposition of an alternating Z-pinch and an alternating θ-pinch. An apparatus constructed to generate such a pinch was described at the Second European Conference at Stockholm. Details of this apparatus can be found in Ref. 3. The basis parameters are as follows:

Discharge tube radius	= 2.45 cm
Distance between Z-electrodes	= 48.8 cm
Maximum amplitude of rotating field at inner wall of discharge tube	= 2.2 kGauss
Frequency of rotation	= 3.1 MHz
Duration of discharge	= 2.6 μsec (7 periods)

This paper presents detailed measurements made on a modified version of this apparatus. The modifications were mainly concerned with reducing the impurity content of the discharge.

The experimental results which follow refer uniquely to discharges in helium at an initial filling pressure of 60 mTorr.

2. MEASUREMENTS

2.1 Streak and framing photography

Fig. 1b shows an axial streak photograph of the rotating field pinch. A comparison of this photograph with the ones published in Ref. 3 shows that the wall light which appears towards the end of the implosion stage and which was previously so prominent, is much reduced. The origin of the time scale below the photograph corresponds to the start of the rotating field discharge. Above the streak picture is shown a row of framing camera pictures. These show that cylindrical symmetry is maintained by the plasma throughout its lifetime.

The light intensity in these streak/framing photographs is about ten times less than in the photographs published in Ref. 3. The collapse time for the pinch is also shorter in the present experiments. Both these effects are attributed to a reduced impurity concentration in the modified version of the apparatus.

2.2 Electrical measurements

Simultaneous measurements were made of the voltage between the Z-electrodes and the axial current (I_z). Analysis of these signals gave the power flow between the R.F. Z-generator and the discharge tube as a function of time. This result is shown in Fig. 1c. Power input reaches a peak value of 116 megawatts. Fig. 1d shows how the total energy deposited in the discharge tube increases with time. At the end of the discharge, 45 joules have been transferred from the Z-generator to the discharge tube. Since initially 70 joules were stored in the generator, this implies a transfer efficiency of 65%.

The Z-component of the electric field at the inner wall of the discharge tube reaches a peak value of 150 V/cm at 1.13 μsec.

Analysis of the energy transfer from the θ-generator to the discharge tube has not yet been completed.

2.3 T_i

The broadening and shift of the N II 4447 Å line of ionized nitrogen (which exists in the plasma as an impurity) was measured by means of a multi-channel Fabry-Perot interferometer/4,5. It was thus possible to deduce the ion temperature of N^+ and also the gross motion of these ions in the plasma volume under observation (Figs. 1e and 1f). The measurements shown in these diagrams represent the average of six shots and were made with the interferometer adjusted in such a manner that only ion temperatures in the range 5 - 25 × 10^4 K were measured with a good precision. Between 1.5 and 2 μsec, the measured temperatures lie outside this range and are consequently known with less certainty. After 2 μsec the uncertainty in the value of T_i increases yet again due to a decrease in light intensity. The horizontal line shown in Fig. 1e indicates the maximum ion temperature attained during the preionization stage of the discharge.

These measurements were made using an optical system which was sighted axially along the discharge tube and which had a small depth of focus. The slab of plasma observed was situated about 10 cm from the centre plane of the discharge tube and the movement of the plasma as deduced from spectral line shift is towards the end of the tube.

2.4 T_e

The ratio of the total line and continuum intensities (in 100 Å band centred at the line) for the ionized helium line He II 4686 Å was measured as a function of time. The variation of the electron temperature, as deduced from this ratio, is shown in Fig. 1g. Care must be taken in the interpretation of these measurements. For the case of a plasma which is undergoing rapid ionization, the population of the level may depart considerably from its Saha value. In addition there may be some uncertainty involved in the experimental measurement of the continuum intensity.

2.5 Magnetic field profiles

Typical profiles of B_θ are shown in Fig. 2. Each point in the diagram represents the average of three shots. In the interior of the plasma ($r < 1.1$ cm), the B_z component is less than 2% of the surface field.

2.6 Electron line density

Measurements of the electron line density as a function of radius and time are currently being made using a Mach-Zehnder interferometer[6]. These results will be reported at the Conference.

ACKNOWLEDGEMENTS

The authors gratefully acknowledge the assistance of Dr. A. Lietti and J.-M. Aeschlimann, P. Hafner, J.-P. Perotti, and H. Ripper in the construction, maintenance and use of the experimental apparatus. They thank Drs. E.S. Weibel and F.S. Troyon for many fruitful discussions.

This work was financed by the "Fonds National Suisse de la Recherche Scientifique".

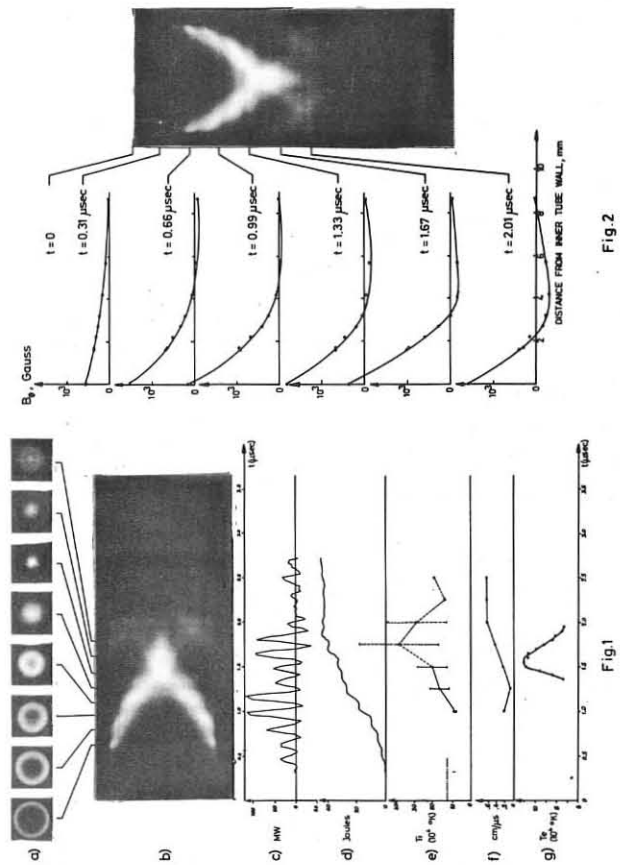

Fig.1

Fig.2

1. WEIBEL, E.S., Phys. Fluids 3 (1960) 946.

2. TROYON, F.S., Phys. Fluids 10 (1967) 2660.

3. JONES, I.R., LIETTI, A., and PEIRY J.-M., Plasma Phys. 10 (1968) 213.

4. BERNEY, A.P., ZAMP 18 (1967) 588.

5. BERNEY, A.P., Plasma Physics Laboratory, Lausanne Report LRP 39/68 (1968).

6. HEYM, A., Plasma Phys. 10 (1968) 1069.

post-deadline paper

TOROIDAL CONFINEMENT OF A HIGH BETA PLASMA IN A HELICAL HARDCORE THETA PINCH

by

P. Noll and J. Schlüter

Institut für Plasmaphysik der Kernforschungsanlage Jülich GmbH.
ASSOCIATION EURATOM-KFA

Germany

Introduction:

In theta pinches with sustained reverse bias field, a plasma annulus surrounded by closed fieldlines can be produced. In an attempt to achieve improved stabilization of this plasma torus against positional and kink instabilities, Kolb /1/ and Yoshikawa /2/ proposed to place an insulated rod carrying a high current along the axis of the pinch tube. Experimentally however the containment time was not significantly increased. The limitation was ascribed to instabilities which were induced by plasma rotation starting at the ends of the coil /3/.

Such a rotation is driven by a volume force in theta direction (theta pinch notation throughout)

$$f_\theta = j_z B_r - j_r B_z \qquad (1)$$

This force vanishes, if either $\vec{j}$ and $\vec{B}$ are parallel in the r-z-plane or if j_z and j_r are zero. It seems difficult to fulfil the first condition experimentally at the end of the dynamic phase where the cross-section of the plasma torus is not circular. Therefore the rotation of the plasma can only be avoided if the toroidal field B_θ is a vacuum field. In this case only the poloidal fields B_z, B_r can contribute to the confinement. In the center-plane of the coils these conditions read

$$B_z^2 / 2\mu_0 + p = \text{const} \qquad (2)$$

$$j_z = 0 \qquad (3)$$

A confinement of the plasma by poloidal fields only is not possible if a straight hardcore and a reverse bias field is used. The bias field is compressed only in the plasma region whereas the vacuum field inside the plasma annulus is nearly unchanged. However, a B_z-field of arbitrary amount in the internal vacuum region can be generated using the external field of a theta coil placed within the plasma annulus (anti-theta pinch). The hardcore in the experiment TESI /4/ has therefore helical conductors.

The field distribution

The equilibrium field distribution and the plasma boundary have been calculated for the case $\beta = 1$ /5/. Experimentally, a stable $\beta \approx 1$ configuration could not be obtained. We tried to satisfy eqs. 2 and 3 by allowing the toroidal field to diffuse into the plasma. Consider the simplified model in Fig. 1, where the plasma is represented by a rigid hollow cylinder between the radii r_0 and r_1. R_0 and R_1 are the radii of the hardcore and of the theta coil. At $t = 0$, the β is assumed to be unity. In the vacuum B_θ has a 1/r dependence and the B_z-fields inside and outside are antiparallel to each other. For $t > 0$, B_θ and B_z approach their vacuum distributions with the characteristic times

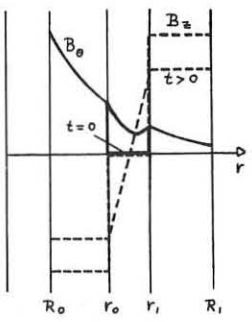

Fig. 1: Diffusion of the magnetic field in a conducting hollow cylinder

$$\tau_\theta = \frac{\mu\sigma d^2}{\pi^2} \qquad (4)$$

and

$$\tau_z = \frac{\mu\sigma \bar{r} d}{2}\left(1 - \frac{\bar{r}^2}{R_1^2}\right) \qquad (5)$$

($d = r_1 - r_0 \ll r_1$, $\bar{r} = (r_0 + r_1)/2$). Using the experimental values $\bar{r} = 7$ cm, $d = 1.7$ cm, $R_1 = 10$ cm, $T_e \approx 20$ eV we obtain $\tau_\theta \approx 3$ /usec and $\tau_z \approx 30$ /usec. Thus, the diamagnetic dip of the B_θ-field disappears before the B_z-fields change considerably.

The equilibrium will only be maintained, if the B_z-fields outside and inside the plasma torus are equal in magnitude and decrease at the same rate. Therefore, also the fluxes should be equal in these two regions:

$$B_z(r_0)\pi r_0^2 = B_z(r_1)\pi(R_1^2 - r_1^2) \qquad (6)$$

which imposes

$$\bar{r} \approx R_1/\sqrt{2} \qquad (7)$$

At higher temperatures a vacuum distribution of B_θ cannot be rapidly established by field diffusion. In this case we propose to fill up the diamagnetic dip in the main B_θ-field by using a "parallel" B_θ-bias field.

Experiment:

Along the axis of a standard theta pinch coil (20 cm diameter, 30 cm length), connected to a 40 kV - 15 kJ bank, a hardcore is placed, consisting of 16 insulated current conductors in parallel, distributed over the surface of a tube of 4.5 cm diameter (Fig. 2). In the region of the theta coil these conductors have a pitch angle of 45°. Four conductors outside the theta coil provide the return connection to a 60 kV - 15 kJ bank. By clamping the coils at peak current with metal-to-metal crowbar switches /6/ the currents decrease with an e-folding time of 1.5 msec. The filling gas, deuterium, is contained in a hollow cylindrical vessel formed by two coaxial quartz-tubes. It is ionized and preheated by a predischarge.

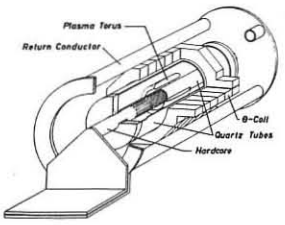

Fig. 2: Apparatus

Results:

Observations by streak cameras and image converters and measurements of the B_z-field showed that equilibrium in radial direction could be obtained if the eqs. 2, 3 and 7 were fulfilled. It is remarkable, that the (reverse) B_z-field between the inner quartz-tube and the hardcore does not change its sign nor decrease considerably as long as the plasma does not touch the walls. Observations of the occurrence in time of several carbon and oxygen lines give the estimation $T_e \approx 20$ eV. When the equilibrium conditions are exactly satisfied a macroscopically stable plasma is observed for about 30 /usec. The β is estimated to be 15% on the magnetic axis.

The establishment of the equilibrium in axial direction depends sensitively on the length l_V of the quartz vessel. When l_V is longer than the length l_C of the theta coil, the closing of the field lines takes place far away from the ends of the coils because the preheated plasma has a high conductivity even beyond the coil ends. In this case one plasmoid is emitted from each coil end. The axial compression of the remaining plasma in the central region is slow. Presumably the two plasmoids and the central plasma are still surrounded by some common fieldlines. On the other hand, when l_V is shorter than l_C, a strong axial compression with a velocity comparable to that of the radial compression is observed. In this case the whole of the plasma is confined in one region. The contours of this volume are roughly those calculated in /5/.

The observed containment time is of the order of the estimated diffusion time τ_z. However, if the plasma length l_p becomes too short, the Kruskal-Shafranov condition $B_z/B_\theta < l_p/(\pi\bar{r})$ may be violated.
The energy containment time is restricted by radiation losses and is estimated to be 10 /usec. This energy loss may be balanced to a certain amount by resistive heating.

References:

/1/ A.C. Kolb, M.P. Young and E.A. McLean, LASL Report LA-3770, p. G 5-1 (1967)

/2/ S. Yoshikawa, LASL Report LA-3770, p. G 6-1 (1967)

/3/ D. Düchs, R.H. Dixon, R.C. Elton and A.C. Kolb, Bull. Am. Phys. Soc., Series II, Vol. 13, p. 1551 (1968)

/4/ L. Janicke, P. Noll and J. Schlüter, Bull. Am. Phys. Soc., Series II, Vol. 13, p. 1551 (1968)

/5/ L. Janicke, Proc. of this Conf.

/6/ P. Dokopoulos, Rev. Sci. Instr., Vol. 39, p. 697 (1968)

TOROIDAL MAGNETO-HYDRODYNAMIC EQUILIBRIUM CONFIGURATIONS FOR PLASMAS WITH ß = 1 AND ARBITRARY ASPECT RATIO

by

L. Janicke

Institut für Plasmaphysik der Kernforschungsanlage Jülich GmbH

ASSOCIATION EURATOM-KFA

Germany

In the calculation of equilibrium configurations of plasma in coil systems like the hardcore thetapinch, two difficulties occur. Firstly, the confining field is not only determined by the total currents flowing through the coils. Since the currents are pulsed, with the duration of the current pulse being usually smaller than the penetration time of the magnetic field into the coil, the field is determined by a boundary value problem with the normal field component being approximately zero at all conducting boundaries. Secondly, configurations occur with rather large aspect ratio, i.e. the extension of the plasma parallel to the axis of rotation (only systems with axial symmetry will be considered) is of the same order of magnitude as the diameter of the plasma torus. Hence, an expansion of the field distribution in powers of the aspect ratio, which is usually employed for small aspect ratio, is not possible, and one has to use numerical procedures. The problem can be simplified considerably by the restriction to the case $\beta = \frac{8\pi nkT}{B_{ext}^2} = 1$, i.e. the plasma is assumed to be a perfect conductor, and hence can be treated in the computation of the magnetic field as part of the coil system. Therefore computation methods for the magnetic field of coil systems in vacuum can be applied. The procedure which upon modification has been used for the present calculation, is described in detail in Ref. 1.

For the computation of the equilibrium configuration, we start with an estimated shape of the plasma equilibrium boundary. Having computed the magnetic field for the given boundaries, we consider the variation of the magnetic pressure along the plasma surface. This variation is an immediate measure of the accuracy of the approximation. Then the plasma boundary is displaced by an amount which is proportional to the difference between the magnetic and the thermal pressure. In the final state, the thermal pressure must be balanced by the magnetic pressure.

In order to carry out the displacement numerically, the plasma boundary is represented by a set of points Q_i (i = 1, 2,..., N), and each point is shifted separately. The actual boundary curve is then redefined as a curve passing through these points and with coordinates, which are cubic spline functions of the distance along the boundary. The shifting procedure consists of the repeated application of a cycle of three steps. The first step deals with the smoothing of short wavelength perturbations of the magnetic pressure. This can be done, for example, by applying a kind of surface tension. In the second step, each point Q_i is shifted perpendicular to the boundary by a displacement δl_i which is proportional to the difference between the thermal pressure $p^{(th)}$ and the magnetic pressure $p_i^{(m)}$ at this point,

$$\delta l_i = \lambda (p^{(th)} - p_i^{(m)}).$$

The stepsize λ has a relatively small fixed value. In the third step, the result of the second step is extrapolated linearly for larger λ, and that value of λ is chosen which minimizes the average quadratic deviation of the magnetic pressure from the thermal pressure.

Computations are made for the Jülich hardcore theta-pinch TESI. The coil system (s. Fig. 1) consists of a theta-pinch coil and a hardcore with many helical windings in parallel. The pitch angle is 45°. The windings are very close together, so that the perturbation of the axial symmetry can be neglected. Since the hardcore can be penetrated by field lines (s. Fig. 2), it is not treated as a compact conductor, but rather the magnetic field generated by the Θ-component of the hardcore current is determined from a fixed surface current. One equilibrium configuration

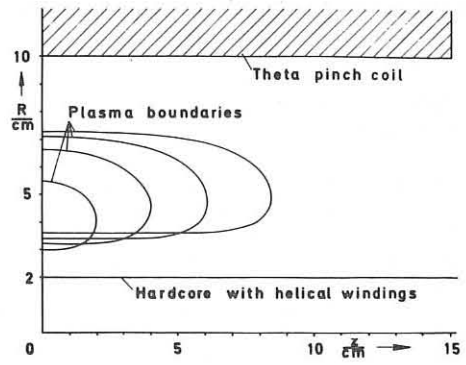

Fig. 1: Some equilibrium configurations for a plasma with ß = 1 in the TESI coil system. The ratio of the total currents in the theta-pinch coil and the hardcore (Θ-component) is 1.8, the pitch angle of the hardcore is 45°.

is plotted in Fig. 2, together with the surrounding field lines. It can be seen that the shape of the magnetic field is everywhere tangential to the boundaries of the conductors. Actually, there exists with fixed total currents in the coil system an infinite number of equilibrium configurations. They can be labelled by their different volumes, which in turn depend on the temperature and the particle density. Fig. 1 shows equilibrium configurations for four different volumes. The rate of convergence of the described procedure is demonstrated in Fig. 3. It shows the decreasing pressure variation for the configuration drawn in Fig. 2. The dots are the values after the completion of one computation cycle. The procedure as described above is not restricted to the particular coil system of the TESI experiment. It is applicable to a more general class of

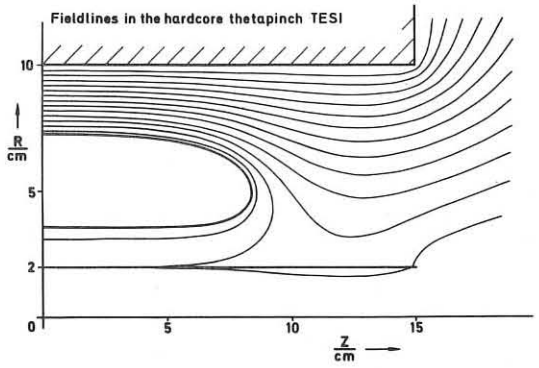

Fig. 2: Equilibrium configuration and field lines in TESI.

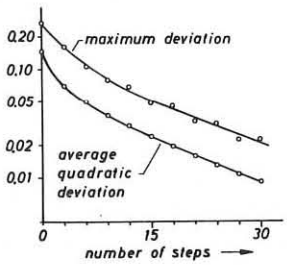

Fig. 3: Approach to the equilibrium: Relative deviation of the magnetic pressure from the thermal pressure.

configurations, and has been tested in several other cases. For a comparison between numerical results and the experimental observations, we refer to the paper by P. Noll and J. Schlüter of these Proceedings.

Reference

1. L. Janicke, J. Krüger
Berechnung eines gepulsten zweidimensionalen Magnetfeldes bei vorgegebener Spulengeometrie.
KFA-Bericht JÜL-513-PP (1968)

CURRENTS IN THE REGION OUTSIDE TOROIDAL AND LINEAR PINCHES

by
P.C.T. van der Laan
Association Euratom-FOM
FOM-Instituut voor Plasma-Fysica
Rijnhuizen, Jutphaas, The Netherlands

A pinched plasma is surrounded by a dilute plasma whose density is two or three orders of magnitude less than that of the central column[1]. The existence of this low-density plasma was already noted in 1958 in pinch experiments at Livermore[2] and was taken into account in MHD computer programs written in 1960[3]. At that time it was realized that this pressureless plasma often carries considerable currents parallel to the field. These force-free currents are not induced in the pure θ-pinch; in that case the low-density plasma can be ignored. However, since toroidal versions of the θ-pinch require an additional field component to provide equilibrium, the presence of the low-density plasma is again important.

The role of the pressureless plasma is most easily discussed in the limiting case that the plasma is frozen to the field lines. In practice an interdiffusion of field and plasma occurs due to the resistivity and the electron inertia; this effect is small if the electron temperature and density in the outside region exceed certain limits[4]. Anomalous resistivity caused by streaming instabilities may cause a faster diffusion; whether these instabilities are excited depends on the magnitude of the electron drift velocity. In general the interdiffusion of field and plasma starts locally and does not affect the overall character of the field distribution before more time has elapsed. Ohmic heating of the low-density plasma may reduce the resistivity and consequently the diffusion rate.

In a plasma frozen to the field the magnetic flux enclosed by a loop moving with the plasma is constant. From this one can prove that the pitch of a helical field line in a long cylindrical system remains constant during its radial motion[2,4]. A crucial condition for this is that a contour lying in the r-z plane must remain in that plane, i.e. differential rotation around the axis is not allowed. The plausible assumption $\partial/\partial z = 0$ made in many computer programs[3] automatically leads to pitch conservation in the case of negligible resistivity. In a torus the symmetry around the axis of revolution gives rise to an analogous conservation property: the rotational transform angle of a given helical field line embedded in the low-density plasma outside the pinch remains constant.

The field distribution in the pressureless plasma outside an infinitely long cylindrical pinch follows from the conservation of pitch, the equation of motion and the time history of the fields at the wall. In most cases the configuration formed will be different from a vacuum field, which means that a current j//B must flow. Such currents can flow in an infinitely long system and in a torus.

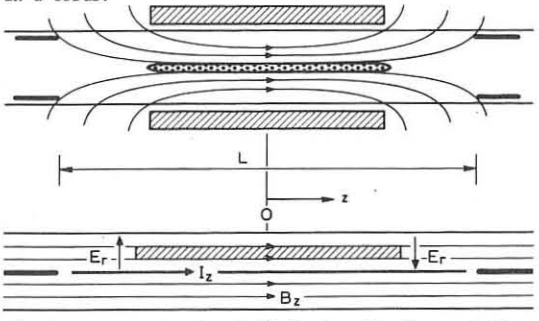

In linear experiments of finite length, the condition $\partial/\partial z = 0$ does not necessarily apply and the flow of currents may be impossible. Let us consider a combined pinch system, used in several laboratories, as sketched in the upper half of the figure. If the voltage between the ring-shaped electrodes is applied after the θ-pinch has been formed, the z-current starts to flow along the few field lines that intersect the electrodes. The rising B_θ-field induces E-fields in the region outside the current channel. The E-fields parallel to B are shorted out by the electrons of the low-density plasma. The remaining perpendicular E-fields are calculated for the simplified geometry of the lower half of the figure where the lines of force are straightened and where the electrodes have shrunk to pins in the middle of the non-conducting end plates. The changing B_θ-flux in the shaded rectangle gives rise to E_r-fields $E_r = z\dot{B}_\theta$. The plasma then starts to rotate with an azimuthal velocity $v_\theta = z\dot{B}_\theta/B_z$. This is precisely the velocity with which the originally straight field lines are being wound up into helices. In a symmetrical system the field lines half way the coil do not rotate, therefore the direction of rotation is different at the two ends of the machine. The configuration thus formed is that of two oppositely rotating Ixions, driven by the induced E-field. Since no currents flow in the outside region a vacuum field is formed. Problems arise however, if the acceleration of the low-density plasma is large. The polarization current $j_r = \rho\dot{E}_r/B_z^2$ can be expressed in terms of the central I_z-current: $j_r = (\mu_o\rho/B_z^2)(z/2\pi r)\,\ddot{I}_z$. This radial current turns into a z-current at the edge of the outside plasma, either where the mass density ρ falls off, or where the rotation is stopped. An integration of the polarization current flowing in one half of the system ($0 < z < 1/2\ L$) yields the z-current near the wall at $z = 0$ as $\ddot{I}_z L^2/8v_A^2$, where v_A^2 is the Alfvên velocity in the outside region. To retain the vacuum field this current must be much smaller than I_z. This imposes a condition on the frequency ω with which I_z changes, namely, $\omega^2 \ll 8v_A^2/L^2$. The high frequencies contained in the initial rise of I_z violate this condition. A second problem is that, as in all rotating plasma devices, breakdown may occur along the insulator where the field lines leave the system. A total breakdown would cause I_z to flow along the tube wall, as in a toroidal system. A partial breakdown would close current loops in which the currents would tend to stop the rotation of field and plasma.

A different situation arises if in the sketched apparatus the θ-pinch coil is energized after the z-pinch has been formed. Azimuthal currents flowing along the closed B_θ-field lines oppose the penetration of the B_z-field. The pressure exerted by the B_z-field pushes the circular field lines inward allowing tightly wound helical field lines to enter the tube. The helical field lines are not closed, therefore they form a vacuum field. Also here, polarization currents and wall breakdown may complicate the situation.

In conclusion it is difficult to predict what field distribution will be formed in a linear combined pinch. It is therefore dangerous to base the design of toroidal pinches on the results obtained in more complicated linear systems.

In some experiments the plasma volume comprises both toroidal and linear regions or rather regions of closed and open field lines. In the hard-core θ-pinch and in a pulsed high-β stellarator a separatrix separates the closed field lines at the inside from the open field lines at the outside. The closed field lines will conserve their pitch, whereas the behaviour of the open field lines cannot be easily predicted.

For several reasons the arguments given here do not apply to a Tokamak. In a Tokamak the plasma is formed in a quasi-static B_z-field, no implosion takes place, the field lines outside the column intersect a diaphragm and the density is much less than in a pinch. Consequently, the field outside the column is a vacuum field. The field distribution in an analogous pinched system would be greatly influenced by the unavoidable currents in the outside region.

The author thanks Prof. C.M. Braams, Dr. C. Bobeldijk, and Dr. R.J.J. van Heijningen for helpful discussions.

This work was performed under the association agreement of Euratom and FOM with financial support from ZWO and Euratom.

References

1) C. Bobeldijk et al., Proc. 3rd Conf. on Plasma Physics and Contr. Nucl. Fusion Res., Novosibirsk (1968) Vol. 1 287.

2) S.A. Colgate et al., Proc. 2nd UN Int.Conf.PUAE 32 (1958) 140.

3) K. Hain et al., Z. Naturforschg. 15a (1960) 1039.

4) P.C.T. van der Laan, Proc. Coll. Interaction of Electromagn. Fields with a Plasma, Saclay - France (1968) Vol. 4 1095.

OPTIMAL LONGITUDINAL CURRENTS FOR THE TOROIDAL SCREW PINCH

by
R.F. de Vries, R.J.J. van Heijningen, C. Bobeldijk,
J.P. Goedbloed, P.C.T. van der Laan, and W. Schuurman
Association Euratom-FOM
FOM-Instituut voor Plasma-Fysica
Rijnhuizen, Jutphaas, The Netherlands

The screw pinch is produced and confined by a helical magnetic field. The pitch of this magnetic field is observed to be constant in space and time as a result of force-free currents induced in the low-density plasma outside the main column[1]. The experimentally observed stable behaviour of this discharge has been explained by means of an MHD normal mode stability analysis[2]. For a homogeneous infinitely long plasma column of radius r_o surrounded by a force-free magnetic field the analysis yields the following general dispersion relation:

$$(1-\beta)\ f_{m,k}(\omega,r_o) = \frac{r_o^2}{k^2 r_o^2 + m^2}\left\{k^2 + r_o k_{//}^2 \left(\frac{v_r'}{v_r}\right)\right\}_{r_o}$$

where k, m, and ω are the wavenumbers and the growth rate of the perturbation, v_r is the radial velocity, and β is the ratio of plasma pressure to external magnetic pressure. The distribution of the confining field enters into the equation through the term v_r'/v_r. The behaviour of perturbations parallel to the confining field (i.e. $k_{//} = 0$) is not influenced by the distribution of the magnetic field in the outside region. One can try to find a force-free field distribution which gives the optimal stabilization for modes with $k_{//} \neq 0$, leaving the parallel mode as the most dangerous one. If all fields with a constant ratio α between current and magnetic field and having the same pitch at r_o are compared, a range of values of α is found for which the stability is better than for a vacuum field (α = 0). The field distribution corresponding to the value of α giving optimal stability is close to the constant-pitch field, at least for not too small values of the pitch.

The toroidal geometry allows only discrete modes with wavelengths $\lambda_n = 2\pi R/n$, where n is an integer and R is the major radius of the torus. The criteria for stability of a pinch surrounded by a constant-pitch field are then greatly relaxed[3]. If β rises above a critical value an m = 1 mode develops. This critical β is comparatively small if the pitch of the magnetic field lines fits the circumference of the torus, that is at the Kruskal-Shafranov current and its harmonics. Between these harmonics higher values of β are allowed.

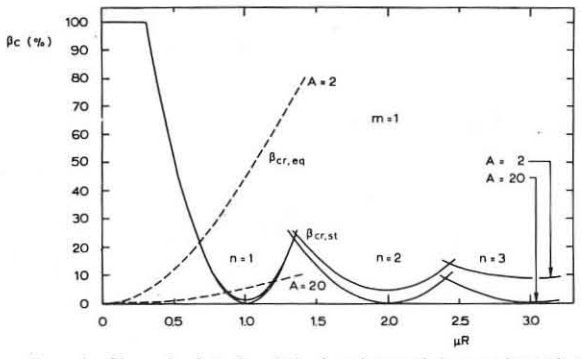

Numerically calculated critical values of β are plotted in the graph for the parameters $r_o = 0.01$ m, tube radius $r_1 = 0.04$ m, and R = 0.08 m or R = 0.8 m. The horizontal dimensionless coordinate is μR, i.e. the ratio of the longitudinal current to the Kruskal-Shafranov current. The quantity $2\pi/\mu$ is equal to the pitch of the field lines.

Calculations show that the optimal values of μR (1.3, 2.4, etc.) are not sensitive to the choice of the parameters r_o, r_1, and $A = R/r_1$. The graph illustrates this for a variation of the aspect ratio A from 2 to 20.

According to the stability theory, experiments should be done with currents 1.3 or 2.4 times the Kruskal-Shafranov limit or below this limit. Whether confinement at low currents is feasible depends on equilibrium considerations. For small $\mu^2 r^2$ the displacement Δ of the plasma ring[4] is roughly proportional to $\beta/\mu^2 R$. For a fixed value of μR, Δ is proportional to R and therefore a small R is preferable. This is illustrated in the graph where the dotted curves give the values of β at which the plasma would be at 1 cm distance from the wall. Although the linear theory gives only an estimate at large displacements, the dependence on the aspect ratio is significant.

Experiments have been carried out around 2.4 and 1.3 times the Kruskal-Shafranov current. Up till now in these experiments the value of β was too high to give stability. The wavelength of the observed m = 1 instability was measured; in agreement with the theory λ was found to be 2πR/3 (i.e. n = 3) for μR > 2.4, πR (i.e. n = 2) for 2.4 > μR > 1.3, and 2πR (i.e. n = 1) if μR < 1.3. Estimates of the growth rate around μR = 2.4 were in agreement with the theory[3].

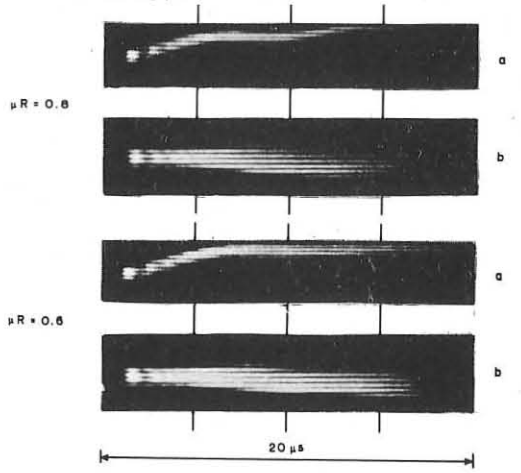

The streak pictures show screw pinches in 40 mTorr helium, produced in our new device at μR-values of 0.8 and 0.6. The pictures a and b are taken from two mutually perpendicular directions; picture a shows the motion towards the eccentric equilibrium position. At this filling pressure β is apparently too high to provide stability; however, in agreement with the theory the m = 1 instability is observed to grow more slowly at the lowest μR-value. Similar measurements at 80 mTorr filling pressure showed a stable discharge even at μR = 0.8. In this case the confinement time was limited to about 20 μsec because of an excessive dip in the clamped current.

Future experiments will aim at the production of pinches below or at 1.3 times the Kruskal-Shafranov current. To achieve this, β should be lowered. To allow the production of high-β pinches at rather low longitudinal currents the design of a short fat torus (A ≳ 2) with a thin insulating coating at the inside is being studied. Field errors, especially those at the outside wall, are to be minimized.

The authors thank Prof. C.M. Braams for stimulating discussions and Messrs. P.J. Bouman, C.T. van Driel, A.C. Griffioen, W. Kooyman, and D.J. Maris for their invaluable assistance.

This work was performed under the association agreement of Euratom and FOM with financial support from ZWO and Euratom.

References

1) C. Bobeldijk, R.J.J. van Heijningen, P.C.T. van der Laan, L.Th.M. Ornstein, W. Schuurman, and R.F. de Vries, Proc. Third Conf. on Plasma Physics and Contr. Nucl. Fusion Research Novosibirsk (1968), Vol. 1, 287.

2) W. Schuurman, C. Bobeldijk, and R.F. de Vries, to be published in Plasma Physics (1969).

3) R.F. de Vries, Rijnhuizen Report 69-52 (Thesis, Utrecht 1969).

4) C. Bobeldijk, Rijnhuizen Report 68-45 (Thesis, Utrecht 1968).

SINGULARITIES OF MAGNETIC FLUX IN "HARMONICA DEUX" .

P.Ginot , M. Kuus, P. Plinate.

ASSOCIATION EURATOM-CEA
Département de la Physique du Plasma et de la Fusion Contrôlée
Centre d'Etudes Nucléaires
Boite Postale n° 6 - **92 Fontenay-aux-Roses** (France)

ABSTRACT.

"Harmonica Deux" is a torus in which the rotational transform is due to a longitudinal current induced into the gaz, as in Tokamak. The longitudinal axis of the machine is planar with a variable curvature and has the shape of a guitar. A M.H.D. theory from Mercier predicts singularities in the equilibrium for discrete values of the rotational transform linked to the variations of curvature of the axis.

The experiment shows that singularities occur in the magnetic flux around the plasma for a given value of the rotational transform whose relationship with the theory is not clear. This phenomena is discussed.

INTRODUCTION.

The machine "Harmonica Deux" is shown on figure 1. A longitudinal current I_δ is induced along the axis of intrinsic equation :

$$\frac{1}{R(\delta)} = \frac{1}{R_o}\left(1+2\cos 4\pi \frac{\delta}{L}\right)$$

δ : curviline abscissa
$R(\delta)$: radius of curvature
R_o: mean radius of curvature = 43 cm.
L : length of the axis = 270cm

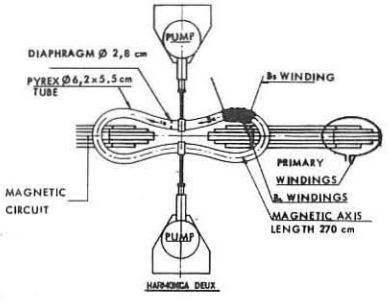

Fig. 1.

A theory from Mercier [1] predicts that a lack of equilibrium or changes of topology should occur whenever :

$$\iota/2\pi\,(r) = \frac{B_\theta\,(r)}{B_\delta\,(r)} \cdot \frac{r}{R_o} = 2$$

where $B_\delta(r)$, $B_\theta(r)$ are the longitudinal and azimuthal components of the magnetic field and $\iota/2\pi(r)$ is the rotational transform at the point of little radius r. This phenomena is similar to the well known lack of equilibrium in a circular torus when $\iota/2\pi = 0$.

The experiment has been designed to verify this prediction.

THE MACHINE.

The gaz is contained in a pyrex tube of internal diameter 5.5 cm . Several versions of the machine have been used successively. Flux singularities have been observed in the first one (1966-67) with few diagnostic possibilities. A second version (1967-68), fitted with flux loops, has given a better description of the phenomena [2]. Those measurements have been extended to the full range of working conditions and completed by internal flux measurement . There is no copper shell in those first two versions.

A net of wires surrounding the pyrex tube can be energised to give a transverse field on the axis.

Up to now the working conditions have been :

$-6KA < I_s < +6KA$ $\quad -16KG < B_s < +16KG$ $\quad 4\times10^{-3} < p_o < 3\times10^{-2}$ mm Hg, H_2

THE DIAGNOSTICS.

Flux loops have been wrapped arround the pyrex tube according to Fig.2 in order to make an harmonic analysis of the flux leaving the enveloppe with the modes :

$$m\left(\theta-\theta_o\right) + 2k\pi \frac{\delta}{L}$$

A line of 32 coils, whose axis are alternatively parallele and perpendicular to the line, can be inserted along a vertical or horizontal diameter into the plasma. It is protected by a quartz tube whose external diameter is 2,7 mm.

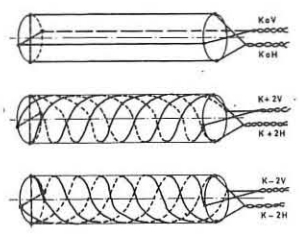

Fig. 2.

THE RESULTS.

Fig.3 shows the appearence of the flux singularities observed on the flux loops

$k = +2$, $m = 1$, $\theta_o = 0$
$k = +2$, $m = 1$ $\theta_o = \frac{\pi}{2}$

The beginning and the end of the singularities in a given discharge are reported on Fig.4 in a I_δ , B_δ plan. The value of $\iota/2\pi$ quoted on the straight line has been deduced from the internal magnetic probes.

The same points drawn in a (I_δ , p_o) or (I_δ^2 , p_o) plan do not show any clear correlation.

One concludes to the existence of a deformation linked with $\iota/2\pi \geq 1$. Nothing has been observed, using this method, around $\iota/2\pi = 2$.

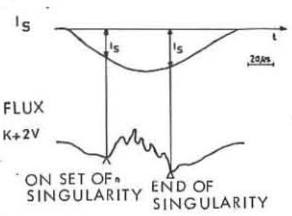

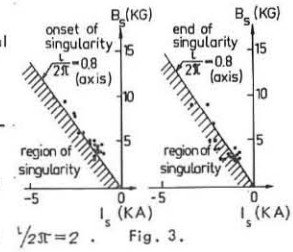

Fig. 3.

DISCUSSION.

Qualitatively the mode (k=2 , m=1) has been isolated in the flux perturbation and the occuring of such a phenomena is in agreement with the theory. Quantitatively there is a disagreement on the value of the rotational transform. Moreover (k=2 , m=1) is not the only mode present. k=1 is also observed. Several arguments for this can be invoqued :

- The stability of such a discharge for the kink modes is not yet known theoritically. The observed singularity could be the Kruskal - Shafranov limit. A full mode analysis should bring some light on this subject.

- Even if the theory predicts kink stability , this would require the presence of a copper shell which was absent in the reported experiment.

- There is many evidence of strong interactions with the wall which could veilled the $\iota/2\pi=2$ predicted phenomena. This may be related to the poor temperature (5 eV) attained, from what rapid convective resistive motions can be expected.

- The predictions of the theory depend on the internal distribution of the current. The difference between "no equilibrium" and "equilibrium" is clear only when this distribution is flat. From the magnetic probes a bell shaped distribution is observed for which there could be no equilibrium at all, regardless the value of $\iota/2\pi$.

- The diagnostic used is unable to record internal rearrangement of the current. This rearrangement can be a good method of detecting the $\iota/2\pi=2$ phenomena when the interactions with the walls is large.

A new version of the machine has been completed. A copper shell has been added. The B_δ field is increased to 30 KG in order to rise the temperature. The internal coils signal are now digitalised and automatically recorded. The net of flux loops has been extended for an extensive harmonic analysis with :

$k = -2\ , -1\ , 0\ , +1\ , +2\ , +3\ , +4$
$m = 1 \quad \left(\theta_o = 0\ ,\ \theta_o = \frac{\pi}{2}\right)$, $m = 2 \left(\theta_o = 0,\ \theta_o = \frac{\pi}{4}\right)$

REFERENCES.

[1] MERCIER C, Nuclear Fusion 1964 , 4 , Second Conference on plasma physics and Controlled Fusion, Culham 1965 CN 21/73.

[2] E.P. BUTT, P. GINOT, W.M. JONES, H.KUSS, P. PLINATE, Journal de Physique , Colloque C 3 - Suppt.au N° 4 - Tome 29, avril 1968 p : 173.

ELECTRON HEATING DUE TO THE PLASMA INSTABILITY

V.T.Astrelin, N.S.Buchelnikova, A.M.Kudryavtsev

Institute of Nuclear Physics, Novosibirsk, USSR

The experiments have been performed on a Q-machine. Plasma column diameter is 4 cm, and its length is 80 cm, $n \sim 10^9 - 10^{10}$ cm^{-3}, $H \sim 800$ G. Electron beam with the diameter 1 cm is injected along the axis of the column. The energy of the beam is 10-600ev, the current ~ 10 ma.

The experiments have been carried out in the electron sheath regime. High frequency oscillations have been registrated by a single probe covered with glass. The energy distribution of plasma electrons has been investigated with the help of two-grids electrostatic analysers.

The nature of instability. When the electron beam passes through the plasma, the excitation of high-frequency oscillations of potential with wide spectrum (10-1000 MHz) is observed. The frequencies are lower then the electron plasma frequency f_{oe} ($f \lesssim f_{oe}$). The maximum frequency increases with the density increasing. The oscillations are longitudinal waves. The longitudinal phase velocity V_{ph} (measured by the aid of a correlometer) is equal to the beam velocity V_o. The amplitude of oscillations is maximal on the axis and falls off in the radial direction. There is threshold beam energy U_c, so that oscillations are excited only in the case $U_o < U_c$. The value of U_c is proportional to the plasma density.

The observed oscillations and their excitation conditions can be described by the theory of beam-limited plasma interaction [1,2]. As a matter of fact it was found in [1,2] that the beam excites the plasma instability with oscillations spectrum $f \sim k_z/k \cdot f_{oe} \lesssim f_{oe}$. The type of the waves is $A(r,\varphi,z,t) = A_o J_m(\lambda_p r/a)\exp(-i\omega t + im\varphi + ik_z z)$ (λ_p - the root of bessel function J_m, a - beam radius). The excitation mechanism is Cherenkov's effect ($V_{ph} \sim V_o$). The excitation condition is

$$V_o < V_c = \frac{a\omega_{oe}}{\lambda_p}\left[1 + \frac{3}{2}\left(\frac{\Omega_{oe}}{\omega_{oe}}\right)^{2/3}\right]$$

(Ω_{oe} - Langmuir frequency of the beam). So one can state that the observed instability is plasma instability [1,2]. The turbulent plasma state in the case of developed instability was investigated. It was found that the oscillations are random. The experimental autocorrelation function can be described by the formula $\rho(\tau) = e^{-\tau/\tau_o}\cos 2\pi f_m$. The middle frequency f_m coincides with the maximal spectrum ferquency, correlation time τ_o changes from ~1 to ~3 periods of f_m. Correlation length ℓ_c changes from ~1 to ~3 longitudinal wave lengths.

The heating of plasma electrons. The electrons temperature in the quiescent plasma (in the absence of the beam) is ~0.2eV. While passing the beam through the plasma column the longitudinal acceleration of plasma electrons is observed. The accelerated electrons appear simultaneously with the oscillations excitation and disappear when $V_o > V_c$. As a rule the plasma electrons distribution function $f(V_\parallel)$ is Maxwellian one and can be characterysed by the longitudinal temperature $T_\parallel$. Thus the heating of plasma electrons due to the plasma instability takes place.

The dependence of the temperature $T_\parallel$ on different oscillations parameters was investigated. It was found that $T_\parallel$ increases with oscillations amplitude increasing and decreases with middle frequency and correlation time increasing. The mechanism of the heating can be described by the theory of stochastic heating [3,4]. It was found in [3] that $T_\parallel$ is described by the formula

$$\frac{dT_\parallel}{dt} = \frac{e^2}{m}\sum_\kappa \frac{\overline{E_\kappa^2}\,\tau_\kappa}{1+\omega_\kappa^2\tau_\kappa^2}$$

Before comparing it with the experimental results let us take into account that $\overline{E_\kappa^2} \simeq \kappa^2\overline{\varphi^2}$, $\omega_\kappa/\kappa = V_{ph} \simeq V_o$, $\omega_\kappa^2\tau_\kappa^2 \gg 1$, so that $\frac{dT_\parallel}{dt} \simeq \frac{e^2}{m}\frac{\overline{\varphi^2}}{V_o^2\tau_o}$, where $\overline{\varphi^2}$ - average square of the oscillations' amplitude measured in experiment. We can find the temperature $T_\parallel$ taking into account that the energy flux carrying out to the edges of plasma column by the heated electrons is $\sim \frac{nV_\parallel}{4} T_\parallel S$. For the stationary state

$$T_\parallel \simeq \left(\sqrt{\frac{\pi}{2}}\,\frac{e^2 L}{\sqrt{m}}\,\frac{\overline{\varphi^2}}{V_o^2\tau_o}\right)^{2/3}$$

(L is the length of the plasma column). The dependence of $T_\parallel$ on the parameter $\frac{\overline{\varphi^2}}{V_o^2\tau_o}$ is shown on Fig.1. The unbroken line is the calculated curve, the points - experimental values. It is seen that the dependence $T_\parallel$ on $\frac{\overline{\varphi^2}}{V_o^2\tau_o}$ is in a good agreement with culculation. The values of experimental and calculated $T_\parallel$ are also in a rather satisfactory agreement. So one can state that the electron heating due to the plasma instability is stochastic heating [3,4].

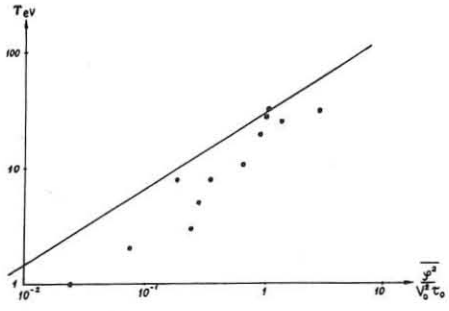

REFERENCES :

1 Gorbatenko, M.F., ZH.Tekn. Fiz. (USSR) 9 1070, 1963.

2 Briggs, R., Electron-Stream Interaction with Plasmas. The M.I.T. Press, Cambrige, 1964.

3 Bass, F.G., Fainberg, Ya.B., Shapiro, V.D., Zh.Eksp.Teor.Fiz. (USSR) 49, 329, 1965.

4 Puri, S., Phys.Fluids 9, 2043, 1966.

ON THE RADIATION FIELD ACCOMPANYING SURFACE WAVES ON PLASMA COLUMNS

B.A.Aničin and D.Ilić

Boris Kidrič Institute of Nuclear Sciences, Belgrade, Yugoslavia

1. Introduction

A surface wave launched on a plasma-dielectric inteface is always associated with radiation and evanescent fields due to the fact that the surface wave alone cannot match the boundary conditions at the launcher. The problem has two practical aspects: a. the radiation field is adverse to surface wave plasma diagnostics and b. the radiation field itself can be used as a diagnostic tool.

In this paper we present experimental evidence of the presence of radiation fields in standing surface wave patterns and derive launching efficiency and radiation diagrams from a theory assuming an infinite slot antenna.

2. Experiments

An axially symmetric TM type of surface wave is launched on a mercury vapour positive column maintained in a pyrex tube having $\varepsilon_{glass}=4.8$, 12.2 mm ID and 15.2 mm OD . At 200 MHz signal frequency and 50 mA arc current the surface wave wavelength λ_s is 11.5 $\pm$ 0.3 cm. Various launchers, including wire loops and circular slot antennae have been tried. The detection was invariably via a radial wire probe coupled to a 1N21B crystal. The resulting standing wave patterns (figure 1.)contain cos $4\pi x/\lambda_s$ and cos $2\pi x/\lambda_s$ terms. The presence of the latter is not to be expected in a single mode experiment. To explain the waveforms in figure 1. we have to postulate the existence, near the guide, of some electromagnetic mode other than the TM surface wave. None of the higher surface wave modes can be excited in our experiment. we therefore assume that the mode causing λ_s periodicity is the radiation field and/or evanescent modes. Rayleigh range considerations and subsequent analysis show that apart from the first few cenimetres from the launcher the radiation field is the dominant factor. The wavelength of the radiation field(1.5 m) is 13 times larger than the wavelength of the surface wave (11.5 cm). We can therefore assume that the phase and amplitude of the radiation field do not change much within one surface wave wavelength, and write for the signal:

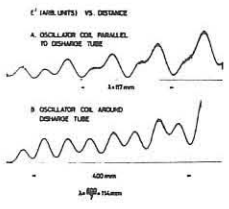

Figure 1. Standing surface wave patterns for two launcher coil orientations.

$$\left| C_0 + C_1 \exp/-(\alpha + j\beta)x/ + C_2 \exp/(\alpha + j\beta)x/ \right|^2 , \quad /1/$$

where α is the attenuation constant and $\beta = 2\pi/\lambda_s$ the phase constant. This expression obviously contains both $\lambda_s/2$ and λ_s variation.

The harmonic content of a standing wave pattern depends on the ratios C_1/C_0 and C_2/C_0. When the wire probe is displaced radially away from the discharge tube the surface wave field decreases as $K_0(\beta r)$ and one would expect the cos $2\beta x$ term to disappear more quickly from the waveform than cosβx. Such behaviour was in fact observed experimentally.

Another strong indication that the λ_s periodicity in figure 1 is caused by the radiation field is the fact that the λ_s periodic term is more pronounced when the exciting wire loop is parallel to the discharge tube axis (upper curve) and less pronounced with the loop around the discharge tube (lower curve). This is consistent with the radiation characteristics of a loop antenna or its equivalent dipole.

3. Theory

The aim of this section is to derive basic quantities related to surface wave excitation on plasmas.We adopt as a model the planar plasma - free space interface with a voltage fed slot antenna at a height h above the plasma and apply Cullen's method[1,2] to this model. This consists essentially in forming a general integral representation of the electromagnetic field from inhomogeneous waves generated by a distribution of surface magnetic current at the height of the slot and deriving the relevant fields near the guide, and at arbitrary elevation, from this solution. Referring to the inset in figure 4 for notation, the integral representation for H_z is

$$H_z = \frac{-j\omega\varepsilon_0 V}{2\pi} \int_{-\infty}^{\infty} \left(e^{uy} + \frac{u+g}{u-g} e^{-uy} \right) \frac{e^{-uh}}{u} e^{-j\beta x} \, d\beta , \quad /2/$$

$$u = (\beta^2 - k^2)^{1/2} , \quad g = -\frac{\varepsilon_0}{\varepsilon_p} (\beta^2 - k_p^2)^{1/2} , \quad /3/$$

with V the voltage applied to the slot, $k^2 = \omega^2 \varepsilon_0 / u_0$ and $k_p^2 = \omega^2 \varepsilon_p / u_0$. This holds for $y < h$, for $y > h$ y and h should be interchanged in /2/. This integral is evaluated for large x but finite y using a contour in the complex β plane. The residus at the pole defined by $u = g$ gives the surface wave amplitude expressed by the exciting voltage and the branch cut starting at $\beta = k$ gives the radiation field near the guide. A second branch cut at $\beta = k_p$ gives rise to an evanescent field. To compute launching efficiency the radiation field at arbitrary θ is derived from /2/ by the method of stationary phase, and the total radiated power obtained by integration over θ. Figure 2 is a plot of launching efficiency vs. plasma relative dielectric constant. Radiation patterns are presented in figures 3 and 4; although the angular variation is smooth the extraction of ε_p from such data seems feasible.

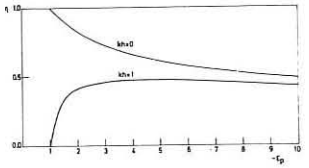

Figure 2. Launching efficiency vs. plasma dielectric constant for kh = 0 and kh = 1

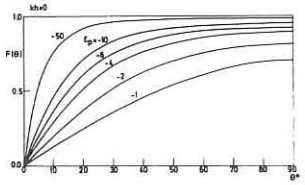

Figure 3. Radiation patterns for kh = 0

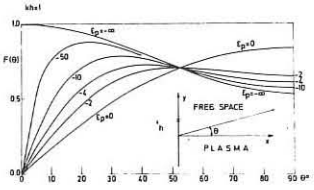

Figure 4. Radiation patterns for kh = 1

The parameter is plasma permittivity

-.-

It is possible in principle to minimize the radiation field near the guide by launcher design; the relevant condition is $kh\,(1 - \varepsilon_p)^{1/2} = -\varepsilon_p$ or, for large $-\varepsilon_p$, $kh \cong \omega_p/\omega$. In our experiment $kh \ll \omega_p/\omega$, and it was not possible to change h , ω_p and ω sufficiently to verify this relationship experimentally.

References

1. A.L.Cullen, The excitation of plane surface waves, Proc. I.E.E., 101, part IV, pp 225 - 34, August 1954.

2. H.M. Barlow and J.Brown, Radio Surface Waves,Clarendon Press, Oxford, p.93, 1962.

THE USE OF ELECTROACOUSTIC AND ELECTRON PLASMA WAVES FOR PLASMA DIAGNOSTICS

by

H. G. Jones and J. W. Sturgess

Department of Physics, Loughborough University of Technology, Loughborough, Leicestershire, England

In previous experiments, electroacoustic waves in a positive column have been excited using external exciter coils (1), (2), (3) or grids (4), (5). Using external coils, the highest frequency which can be propagated is limited to waves whose wavelength is approximately that of the physical length of the coil - usually about 50 kHz. Waves have not been reported for grid excitation above about 100 kHz except for Sessler (5) who found waves up to 800 kHz with f_{pi} = 1.3 MHz.

In the work reported here, the waves were generated in mercury in a pressure range 1.6×10^{-4} to 1.5×10^{-2} Torr at frequencies up to 3 MHz. No magnetic field was used. Waves have been observed at frequencies up to 1.5 f_{pi}. The waves were generated by means of a short cylindrical probe mounted across the axis of the discharge tube. They were detected by a second probe which could be moved axially along the column by a synchronous motor on both sides of the exciter probe. The radial position of the detector probe could also be altered. The signal from the receiver was fed to a phase sensitive detector the output of which was plotted on a chart recorder driven in synchronism with the probe.

It was found that electro-acoustic waves could be detected both on the anode and cathode side of the exciter probe. A typical normalised dispersion curve is shown in Fig. 1. The waves appear to be propagated in the (0,1) mode which is the strongest in a cylindrical discharge (6). The theoretical curve for this mode is shown in Fig. 1 plotted for the value of $\gamma = 5/3$ to give the best fit. The value of electron temperature obtained agreed closely with that determined from probe measurements.

The waves in the cathode direction have a higher velocity than those in the anode direction because of the Doppler shift introduced by the ion drift velocity which can therefore be determined as a function of plasma parameters. By using a Penema trap between the cathode and anode (7) high current discharges have been produced in a range of gases and ion drift velocities measured over a wide range of plasma conditions. This work will be reported later elsewhere.

Wave traces were taken at fixed frequency and signal amplitude with the detector probe at various radial positions. From these traces, wave fronts can be constructed by joining points of equal phase (Fig. 2). This gives both the radial and axial wave velocities. From the assymmetry of the wave fronts the radial ion drift velocity can be determined. This is considerably larger than the axial ion drift velocity. Typically the radial drift velocity is 2×10^4 cm.sec^{-1} at 300 kHz which is about four times the axial ion drift velocity. This method of wave front reconstruction is being extended to cover the reflection of waves from surfaces and sheaths.

Similar experiments have been performed in the same positive column in which waves have been propagated in a range of frequencies around the electron plasma frequency (Fig. 3). Again it may be seen that the waves travel both in the anode and cathode direction, the Doppler shift being due to the electron drift velocity. Using the theory of Franklin (8) the electron plasma frequency may be determined. Because $\omega_{pe} = (ne^2/\epsilon_o m_e)^{\frac{1}{2}}$ this allows a determination of the plasma density to an accuracy of about 5% which is considerably more accurate than that determined from probe characteristics taken at the same time. The calculation of the plasma density allows the ion plasma frequency to be determined with correspondingly increased accuracy.

The authors wish to thank Professor J. F. Raffle for his encouragement and the Plasma Wave Group at U.K.A.E.A. Culham Laboratory for many stimulating discussions.

References:

1. Little, P. F. 1961, Proc. 5th Int. Conf. on Phenomena in Ionized Gases, Munich (p.1440)
2. Crawford, F. W. and Self, S. A. 1963, Proc. 6th Int. Conf. on Phenomena in Ionized Gases, Paris (p.129)
3. Barrett, P. J. and Little, P. F. 1965, Phys. Rev. Letters 14, 356
4. Hatta, W. and Sato, N. 1961, Proc. 5th Int. Conf. on Phenomena in Ionized Gases, Munich (p.478)
5. Sessler, G. M. 1965, Proc. 7th Int. Conf. on Phenomena in Ionized Gases, Belgrade (p.322)
6. Woods, L. C. 1965, Culham Laboratory Report P.73
   Davies, D. R. 1962, D. Phil. Thesis, Oxford University
7. Allen, J. E. and Mastrelli, F. 1962, Nature, 194, 1167
8. Barrett, P. J., Jones, H. G. and Franklin, R. N. 1968, Plasma Physics, 10, 911

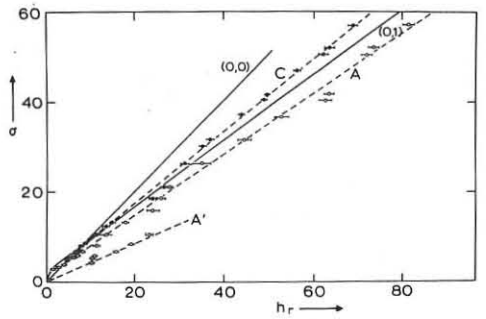

Fig 1

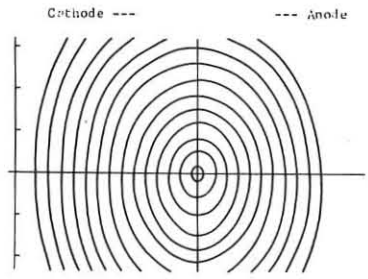

Fig 2

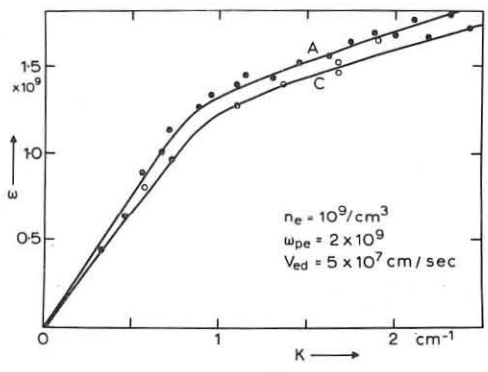

Fig 3

INFLUENCE OF ION-SOUND WAVE WITH FINITE AMPLITUDE ON ELECTRICAL CONDUCTIVITY OF NONISOTHERMAL PLASMA.

Barkhudarov E.M., Baimbetov F., Kervalishvili N.A., Kortkhonjia V.P., Tsintsadze N.L.
Institute of Physics, Academy of Sciences of the Georgian SSR, Tbilissi, USSR

In this work the influence of a monochromatic wave with finite amplitude on electrical conductivity of both completely and partially ionized plasma is studied.

Two cases should be distinguished:

1) a strong wave ($\gamma \ll \frac{\varphi_0}{T_e}$) 2) a weak wave ($\gamma \gg \frac{\varphi_0}{T_e}$) where $\gamma = \nu_{ef} \frac{1}{KV}$ (the frequency ν_{ef} is of the order of frequency of collisions between electrons and ions in a completely ionized plasma while it is of the order of collisions of electrons with neutral particles for partially ionized plasma), K is the wave number, $V = \sqrt{\frac{T_e}{m_e}}$ is the thermal velocity of electrons, φ_0 - is the wave amplitude.

In case of weak waves a linear theory may be applied. As to strong waves, the solution by the method of expansion over the power of a small parameter of the kinetic equation with the collision term of the Focker-Planck type for uncaptured ($\frac{m_e V^2}{2} > \varphi_0$) and captured ($\frac{m_e V^2}{2} < \varphi_0$) particles leads to the following expression for electrical conductivity of completely ionized plasma:

$$\sigma = \sigma_0 \left(1 - \gamma \sqrt{\frac{\varphi_0}{T_e}}\right), \quad \sigma_0 = \frac{e^2 n_e}{m_e \nu_{ef}} \qquad (1)$$

It is seen from this expression that the existence of a monochromatic wave with a finite amplitude leads to a considerable decrease of plasma electrical conductivity.

Only uncaptured electrons contribute to electrical conductivity of plasma (that reminds the situation existing in metals).

The captured particles are transported by the wave. The transport velocity is different for electrons and ions. Let us also note that the appearance of relative motion of ions and electrons may in principle lead to an excitation of an acoustic wave with the phase velocity lower than the relative velocity of electrons and ions.

In a similar way the calculations of electrical conductivity of weakly ionized plasma were made. At the assumption $\gamma = \frac{\nu_{ef}}{KV} \ll 1$ and $\frac{\varphi_0}{T_e} \gg \frac{m_e}{M}$ the following expression is obtained for σ:

$$\sigma = \sigma_0 \left[1 - \left(\frac{\varphi_0}{T_e}\right)^{\frac{3}{2}}\right] \qquad (2)$$

Comparison of formulae (2) and (1) shows that the influence of a monochromatic wave of the finite amplitude on electrical conductivity of weakly ionized plasma is less than in the case of completely ionized plasma.

Later the results of the experiments on the influence of a monochromatic ion-sound wave on electrical conductivity of weakly ionized nonisothermal plasma are given.

Experiments were made with the arrangement shown schematically in Fig.1.

The diameter of a discharge tube is 5 cm, the length is 20 cm, the cathode made of tungsten is of direct heating.

Movable grids and Langmuir probe were placed between the anode and cathode. The grid was of an asterisk type. The operating gas was argon at the pressure of $p \simeq 10^{-3}$ mm Hg. The discharge current and voltage were varied in the range $J = 0.1 \div 0.4$ A and $U = 30 \div 50$ v. respectively. The tube was placed in a

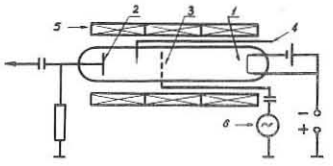

Fig.I. Scheme of the arrangement: I - cathode, 2- anode, 3-grid, 4- Langmuire probe, 5-solenoid, 6-generator of sinusoidal oscillations.

longitudinal magnetic field with the strength $H = 0 \div 50$ oe. The temperature of electrons was $T_e = 4$ eV, the concentration $n_e \simeq 10^{10}$ cm $^{-3}$.

Low frequency oscillations were excited spontaneously when the current flowed through the plasma. They corresponded to the main mode of the standing ion-sound wave between the grid and the anode. The frequency did not depend on the value of the discharge current, changed inversely proportional to the distance between the grid and the anode and coincided well with the value determined from the expression $f = \frac{1}{2L}\sqrt{\frac{T_e}{M}}$, where M is the mass of an ion, L - is the distance between the grid and the anode.

When a sinusoidal signal of the certain value was applied to the grid, situated under the floating potential, a considerable amplification of the oscillation at its natural frequency took place (Fig.2a).

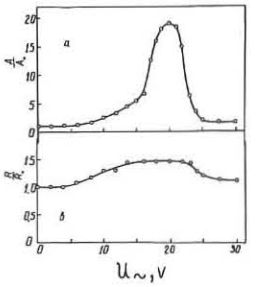

Fig.2. Dependence of the amplitude of natural oscillations (a) and of resistance (b) on the value of the external signal. J =0.25 A, U = 42 v, H = 40 oe, f = 22 kc, f = 44 kc , L = 7 cm.

The frequency and the amplitude of the external signal changed correspondingly in the range f =10 ÷ 200 kc and U = 0 ÷ 30v.

Amplification of natural oscillations leads to an increase of resistance of the discharge gap (Fig.2b).

The direct connection between these phenomena is indicated by the fact that, at sufficiently large amplitude of the external signal, when there is no amplification of natural frequences, the resistance of the discharge gap practically does not differ from its initial value.

For a detailed comparison of the experimental data and the theory the contribution made by the layers at the electrodes to the total resistance of the discharge gap should be eliminated and the oscillations of the electric potential measured.

INVESTIGATION OF THE INTERACTION BETWEEN A GRID AND A Q-MACHINE PLASMA

by
S.A. Andersen, V.O. Jensen and P. Nielsen
AEC RESEARCH ESTABLISHMENT RISØ
Roskilde, Denmark.

I. Experimental Set-up

A "single-ended" Q device as shown schematically in Fig. 1 was used for this experiment[1]. With the cold plate, either grounded or left electrically floating, we had a continuous plasma flow from the hot to the cold plate. Different grids were placed in the flow, and the change in the upstream plasma was studied as function of grid voltage by a shielded twin probe. The twin probe consists of two 0.2 mm diameter stainless steel wires, 4 cm long. The shield consists of two stainless steel tubes 1.5 mm diameter cut in half along their axes and welded together. In Fig. 1 a cross section of the twin probe can be seen. In use the shield was left electrically floating. When biased to collect ions (V_{probe} ~-20 V) the front probe is assumed to measure a signal proportional to $\int_0^\infty f(v_{\parallel}) \cdot v_{\parallel} \, dv_{\parallel}$ where $f(v_{\parallel})$ is the distribution over velocities parallel to the magnetic field. Similarly the backprobe measures a signal proportional to $\int_{-\infty}^0 f(v_{\parallel}) \cdot v_{\parallel} \, dv_{\parallel}$.

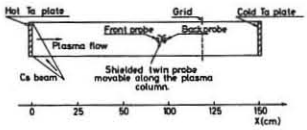

Fig. 1. Experimental set-up.

All the experiments were performed in Cs-plasmas.

II. Ion-reflection on Grid

a) DC-Measurements

When the grid is left electrically floating the ion saturation current to the front probe is 10 to 100 times larger than that measured by the back probe. This shows that the plasma is drifting from the hot to the cold plate. When the grid voltage, V_g, is decreased below floating potential the changes in the two signals are typically as shown in Fig. 2 a. For all densities in the region $10^9 < n < 10^{11}\,cm^{-3}$ the measurements show the following features. At floating grid potential no reflection takes place. When the potential, V_g, is decreased the back current, I_{back}, increases and reaches a maximum at V_{gmax}, while leaving the front probe signal relatively unchanged. For further decreasing grid voltages I_{back} decreases and approaches asymptotically zero for very negative values of V_g.

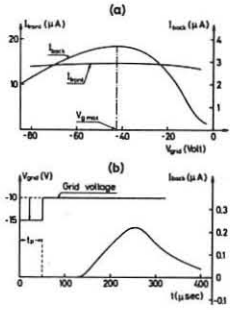

Fig. 2(a) DC-characteristics $n \simeq 1.5 \times 10^{10}\,cm^{-3}$, spacing between grid wires 2 mm. (b) Reflected pulse. Grid-probe distance = 30 cm.

b) Pulsed Grid

In order to find the velocity distribution of the reflected particles we have pulsed the grid voltage and measured the time dependence of the back probe signal. Assuming the reflected ions move as freely streaming particles, the time dependence of this signal gives the velocity distribution. To get an easy determination of the velocity distribution the grid pulse was kept short as compared with the pulse received on the probe. Fig. 2b shows a redrawing of a typical oscilloscope picture. The upper beam shows the grid voltage. From -10V a 50μsec negative square pulse is applied to the grid. The redrawing of the lower beam shows the ac-signal received on the back probe.

c) Discussion of Reflection

It was observed in the experiments that a negatively biased grid reflects ions. This cannot be explained by the sheath reflection which may be observed for a positively biased grid or plate. If we write down the balance equations[1,2] for the electrons it can be seen that a potential barrier arises between the two plasma regions separated by the grid, when the grid is biased negatively. The height of the potential barrier is increasing with decreasing grid voltage. This explains the observation of Fig. 2a for grid voltages between floating and V_{gmax}. The decrease in I_{back} for more negative grid voltages is easily understood because the grid must at very low voltages absorb all the incoming ions.

Curves as the one on the lower beam in Fig. 2b were taken with the twin probe placed in different distances from the grid. In the density region $n < 10^{11}\,cm^{-3}$ no discrepancy from similarity between such curves could be detected. (The width of the received pulse was proportional to the distance from the grid and the height inversely proportional to the distance). This indicates that the reflected ions move as freely streaming particles.

The distributions over parallel velocities deduced from pictures like Fig. 2b fit drifting Maxwellian distributions with temperatures close to the plate temperature. It is observed that the drift velocity increases with decreasing grid voltage. This is in agreement with the idea of the ions being reflected from a potential barrier. The drift velocities deduced are about the ion thermal velocity at grid voltages close to floating potential and increases to about two times this velocity near V_{gmax}.

In conclusion we may state that a biased grid in a plasma of a single-ended Q-machine can produce a velocity distribution function essentially consisting of two Maxwellians drifting either way. The relative drift velocities and the densities can be varied within certain limits.

III. Upstream Waves

In this part we describe measurements which show that we can excite upstream waves with phase velocity and damping that cannot be explained by the normally considered "natural mode" of the Landau dispersion relation but rather by "phase mixing" of freely streaming particles of the initial perturbation. The waves were excited by applying a small sinusoidal voltage to a negatively biased grid. The phase velocity and damping of the waves were studied by means of the back probe. The signal was analysed by a PAR lock-in amplifier. The phase velocity was found to vary from approximately 10^5 to 2×10^5 cm/sec, when the bias of the grid was increased from floating to V_{gmax}. The damping although not strictly exponential was found to give values of the damping distance over wavelength, δ/λ, of at least 0.5. Fig. 3 shows the measured amplitude and phase as function of distance for a 10 kc/sec wave. The calculations of the solid curves are based on a model of freely streaming particles. The velocities of the reflected ions are assumed to follow a Maxwellian distribution. The drift velocity used in this case is equal to the ion thermal velocity.

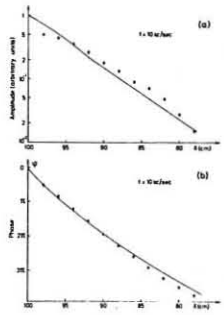

Fig. 3. + phase and amplitude of upstream wave. Solid curve calculated from a model with freely streaming particles.

Measurements as the ones shown in Fig. 3 were taken for several frequencies and grid biases. For all measurements it has been possible to get agreement with calculations based on freely streaming particles.

IV. Conclusion

We have shown that in a single-ended Q-machine a biased grid can produce a distribution function consisting of two Maxwellians drifting through each other. In this plasma we can excite waves with dispersion properties that cannot be explained by the "natural mode" in Landau's dispersion relation.

It should be emphasized that our measurements done in a single-ended Q-device need not be in contradiction with earlier wave experiments in double-ended machines neglecting the "initial" perturbation. We think, however, that a more detailed knowledge of the interaction between grid and plasma and a more thorough investigation of the influence of the "initial" perturbation on ion-acoustic waves would be appropriate.

---

1. S.A. Andersen, V.O. Jensen and P. Nielsen, to be published.
2. S. v.Goeler, Phys. of Fluids 7, 463 (1964).

INTERPRETATION OF ION WAVE DECAY MEASUREMENTS*

by
J. L. Hirshfield and J. H. Jacob
Yale University, Department of Engineering and Applied Science
New Haven, Connecticut, USA.

INTRODUCTION. Advances in experimental technique and in theoretical development have led to recent low frequency wave-plasma observations such as ion-wave echoes[1] and non-linear Landau damping of ion-acoustic waves.[2] Full interpretation of these (and other) non-linear interactions clearly must rest on a solid bed of understanding in the linear problem. It is the purpose of this paper to explore the connections between experimental observations of grid-excited linear spatial disturbances in collisionless plasmas, and the customary theoretical interpretation in terms of spatial Landau and collisional damping. Our conclusions are that, while the physical mechanism responsible for wave damping in the Landau problem clearly is at hand in the experiments, the spatial response may be dominated by interference (near-field) effects due to finite source geometry. Space limitation prevents any extensive review of the extant literature except by reference.[3]

EXPERIMENTAL. Our requirements for a steady-state plasma in which to study ion-acoustic wave propagation include: low background gas pressure (<10 mTorr) to minimize ion-atom collisions; low electron and ion densities ($<10^{10}$ cm^{-3}) to minimize electron-ion and ion-ion collisions, and to provide a large Debye length; significant ratio T_e/T_i(>3) so as to avoid strong wave damping due to the ions; reasonable spatial homogeneity (<5%) over the plasma volume (10^3 cm^3) in which the waves propagate; and low noise fluctuation (<1% r.m.s. variation in ion saturation current to a small Langmuir probe) so as to allow detection of weak signals.

These requirements were met by employing a cylindrical pyrex discharge-tube with diameter 20 cm and height 33 cm. Copper straps 1 cm wide encircled the bottle at symmetrical positions 13 cm apart. These straps were connected via sliding taps to the coil in a tank circuit of a 10 watt 90 MHz oscillator. The data to be presented were all taken with Argon as the filling gas at a pressure of 4 mTorr. A movable cylindrical Langmuir probe (diameter 7.5 x 10^{-2} cm, length 0.5 cm) was used to measure electron density and temperature. All data to be presented are for a measured electron density of 5 x 10^8 cm^{-3}, corresponding to an ion plasma frequency of 740 KHz, and for an electron temperature of 0.80 eV. The ion temperature was not measured.

Under these conditions the Debye shielding length λ_D is 3 x 10^{-2} cm. A wave transducer was used constructed of three parallel fine mesh circular grids of diameter 4.5 cm with an intergrid spacing of 7.5 x 10^{-2} cm. The grid mesh spacing was 2.5 x 10^{-2} cm. The two outer grids were connected together and, with the supporting structure, provided the dc reference potential for the plasma. The inner grid was connected to the external rf generator by coaxial transmission line. The plasma floating potential was about 6 volts positive with respect to ground so that plasma electrons were virtually all turned around in a retarding sheath external to the structure. Ions, on the other hand, were accelerated in this sheath and traveled through the grid structure nearly parallel to the axis. The ion space charge in the intergrid spaces perturbed the constant vacuum electric field by a negligible amount since the Debye length in the intergrid spaces was increased to about 0.3 cm due to the ion acceleration.

This 3-grid transducer was positioned axially in the discharge tube, and served as the wave transmitter. The wave receiver was constructed as a grid-shielded ion collector. The grid (at ground potential) reflected electrons, while the ions were accelerated to the collector. The receiver diameter was 0.20 cm, and could be moved axially in the discharge over an excursion of 5 cm. As long as the distance between transmitter and receiver exceeded 0.5 cm, motion of the receiver did not significantly alter the plasma properties.

For the wave transmitter it could be estimated that, since transit angles were small, a thermal ion received a peak energy perturbation of about 0.025 Vf eV, where V is the applied rf voltage and f the frequency in MHz. Since V < 1 volt, the perturbations were considered weak enough to allow linearized considerations.

Figure 1 shows results of measurements of received ion current versus axial displacement of the receiver, for various values of ω/ω_{pi}. Fig. 2 shows the resulting inferred phase velocity, and Fig. 3 the inferred ratio of imaginary-to-real part of the wavenumber k_i/k_r. This latter reduction of the data is clearly suspect since it is clear from Fig. 1 that the decays are not exponential, not even monotonic, and (at the higher ω/ω_{pi}) not at all expressible as simple damped sinusoids.

THEORETICAL. In Fig. 3 are also shown theoretical curves of k_i/k_r for spatial damping due both to ion-atom collisions, and to Landau damping. Both are computed from a conventional one-dimensional theory[4] modified to take into account only perturbations of the ions at the source. The Landau damping theory is shown for several ion temperatures corresponding to room temperature and multiples thereof. Although the agreement between the data and the theory is acceptable, we shall now show that this agreement may be fortuitous since there is reason to doubt the applicability of the theory to experiments such as these.

Due to space limitations we shall limit the discussion to frequencies $\omega < \omega_{pi}$. Thus, since $T_e/T_i \gg 1$, the spatial response is governed by the dominant root $k_0(\omega)$ of the dispersion relation $D(\underline{k}, \omega) = 0$. The net charge density at an axial displaced receiving probe of radius R_2 can then be shown to be[5]

$$\rho(t,z) = \frac{i}{4\pi^2\lambda_D^2 R_1^2}\left(\frac{\omega_{pi}^2}{\omega^2} - 1\right) \frac{\partial}{\partial z} E_0 L^2 \int_0^{R_2} d\rho' \rho' \int_0^{R_1} d\rho'' \rho'' \int_0^{2\pi} d\phi \left(\frac{z}{h}\right) e^{-i(k_0 h - \omega t)} \quad (1)$$

where $h^2 = z^2 + \rho'^2 + \rho''^2 - 2\rho'\rho'' \cos\phi$ is the ray path from a point on the source to a point on the receiver. The applied field in the transmitter is E_0, the transmitting intergrid spacing is L, and the transmitting grid radius is R_1. For convenience we have taken Im k_0 to be given only by the collisional component in computing the curves in Fig. 4. Eqn. 1 shows two important features: a) For a three-dimensional solution the source function may be highly anisotropic. b) Whatever the source function, the resulting signal at a given field point results from phase interference of many elementary contributions coming from the source and propagating over different path lengths $h(\phi, \rho', \rho'')$. Thus, as a corollary to point (b), unless the damping is fairly strong, the three-dimensional solution (even for a one-dimensional source) is quite different from the one-dimensional solution $e^{-ik_0 z}$. The phase interference effect is analogous to familiar near-field Fresnel zone effects in acoustics and optics, except that damping is important in the ion-wave case.

REFERENCES
* This work was supported in part by the National Science Foundation.
1. D.R. Baker, N.R. Ahern, and A.Y. Wong, Phys. Rev. Letters 20, 318 (1968).
2. N. Sato, H. Ikezi, Y. Yamashita, and N. Takahashi, Phys. Letters 26A 437 (1968).
3. G.M. Sessler and G.A. Pearson, Phys. Rev. 162, 108 (1967).
4. R.W. Gould, Phys. Rev. 136, A991 (1964).
5. J. H. Jacob and J. L. Hirshfield, to be published.

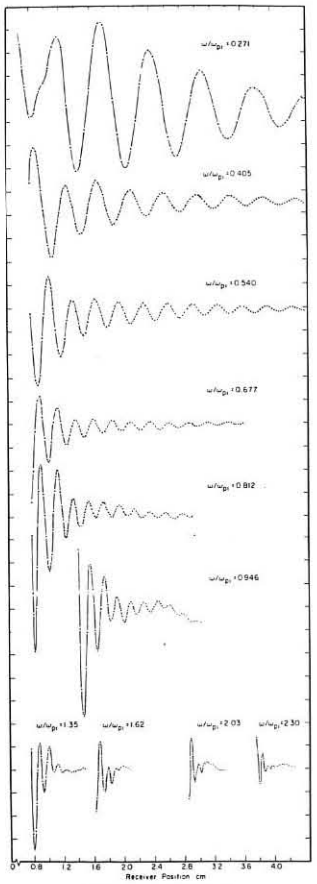

Fig. 1 Raw Data

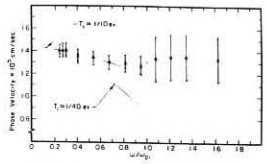

Fig. 2 Phase Velocity

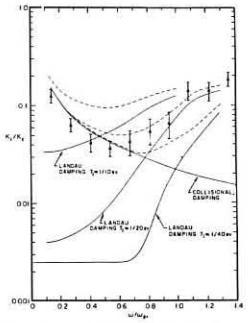

Fig. 3 "The ratio" k_i/k_r

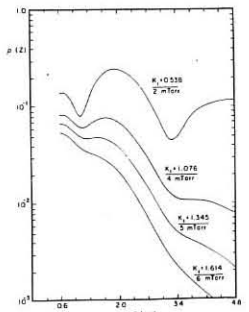

Fig. 4 Theoretical Spatial Decay

NEW ION-ELECTRON RESONANCES IN BOUNDED MAGNETIZED PLASMAS AND COUPLING TO THE EXTERNAL ELECTROMAGNETIC FIELD.

P.E.VANDENPLAS, A.M.MESSIAEN*, J-L.MONFORT*, J.J.PAPIER.
Laboratoire de Physique des Plasmas
Ecole Royale Militaire,
Bruxelles 4.

Around 1961 [1][2] and since then, ion oscillations and ion waves have been the subject of considerable experimental and theoretical investigations. This work is summarized elsewhere [3]. Recently, many laboratories have been concerned for thermonuclear purposes with the heating of ions at the lower hybrid frequency. Recent results on the obtention of plasma densities high above critical density have again shown the importance of considering the boundedness of actual plasmas [7]. We now investigate in general a bounded plasma and show in I and II that there exist essential differences between the behaviour of an infinite plasma and that of a bounded hot magnetized plasma; this leads to new ion thermal resonances and to heretofore unknown main resonances.

The hot electron-ion plasma ($T_e \neq 0$, $T_i \neq 0$) is uniform and immersed in an uniform magnetic induction $\bar{B}_o$. The $e^{-i\omega t}$ perturbed quantities are described by the linearized hydrodynamic equations and by Maxwell's equations. We adopt the notations of ref.[4a]. If the quasi-static approximation ($\bar{E}=-\nabla\phi$) is made, elimination leads to

$$(\nabla_\perp^2+k_1^2)(\nabla_\perp^2+k_2^2)\nabla^2\phi=0 \qquad (1)$$

where $\bar{B}_o=B_o\,\bar{1}_Z$, $\partial/\partial Z\equiv 0$ and $\perp$ means perpendicular to $\bar{B}_o$. The dispersion relation for purely longitudinal waves of the infinite plasma is given by $(k_1^2-k_1^2)(k_1^2-k_2^2)=0$ [5]. Three regions (I,II and III) appear in fig.1 and play an important role in the behaviour of a bounded plasma.

I. NEW ION THERMAL RESONANCES.

We now examine a plasma cylinder with $\bar{B}_o$ and incoming wave ($\bar{E}_{inc}$, $\bar{k}_o$) as indicated on fig.2a. A resonance is defined as a value of the variables involved for which the scattered field, and thus the field inside the plasma, becomes infinite when there is no damping. The known electron thermal resonances [4b] of region I ($k_1^2>o$) are practically unaffected by the ions. The ion thermal resonances are characterized by $\omega_{pe}^2 \gg \omega^2$ and $k_2^2>o$ (region II). A first set of dipolar resonances $e^{\mp i\theta}$ is sketched on fig.2b.when $T_e/T_i=200$. These resonances are well approximated by $k_2 a=x_N$ (a:radius of the column) where x_N is the $(N+1)$-th zero of $J_1'(k_2 a)$, i.e.the boundary conditions select a set of eigenvalues.With no magnetic field ($B_o=o$), $N=7$ is the first value for which we obtain (at the operating frequency) a positive ω_{pi}^2.The set is limited at the other end by a maximum value of N.The effect of a sufficiently high magnetic field is thus to affect the existing resonances and to render the first six resonances possible by bringing them within the domain of positive ω_{pi}^2.The latter "magnetic" ion thermal resonances form a bunch for which ω_{pi}^2/ω^2 can become very high;the $N=1$ resonance lies very close to the lower hybrid but to the left of it.

Another set of resonances is shown on fig.2c in the same conditions except that $T_e/T_i=1$.There exist much fewer resonances than when $T_e \gg T_i$ and the resonances lie at lower density. Although $\bar{k}$ is $\perp$ to $\bar{B}_o$ their Landau damping should be investigated since there is very strong Landau damping of ion oscillations when $T_e=T_i$ and $B_o=o$ [2].

II. NEW MAIN RESONANCES.

Since $k_1^2<o$ in region II of fig 1, we expect main resonances to occur because the plasma can behave as a self inductance ($k_1^2<o$) and resonate with the capacitance constituted by the outer vacuum.We indeed obtain two main resonances which are given in the cold plasma limit ($T_e=T_i=o$) by

$$\Omega_e^2=\omega_{pe}^2/\omega^2=2\left(1\pm\frac{\omega_{ce}}{\omega}\right)\left(1\mp\frac{\omega_{ci}}{\omega}\right) \qquad (2)$$

In the electron wave domain (ω_{ce} and $\omega_{pe}\gg\omega$), $\omega_{ci}/\omega<<1$ and we have the well known splitting of the main cold plasma resonance [4c].The $(1+\omega_{ce}/\omega)(1-\omega_{ci}/\omega)$-resonance leads to very high values of Ω_e^2 when $\omega_{ce}/\omega \overset{\sim}{=} 1/2\; m_i/m_e$ but when $T_e \neq o$, Ω_e^2 decreases strongly as T_e increases.

We now concentrate on the two entirely new main resonances which should, according to our philosophy,occur in region III of fig 1 since $k_2^2<o$.The computed resonance values show that T_i affects the resonances in a non-negligible but nevertheless secondary way. The essence of the phenomenon can thus be obtained by setting $T_i=o$.The plasma is then governed by $(\nabla_\perp^2+k_{T_i=o}^2)\nabla_\perp^2\phi=o$ instead of eq (1).In most of the domain of interest $\omega^2<<\omega_{pe}^2<<\omega_{ce}^2$ and we then have $k_{T_i=o}^2 \overset{\sim}{=} -e^2B_o^2/\gamma_e KT_e m_e$.The main dipolar resonances ($n=\pm 1$) are then given by

$$\Omega_i^2=\omega_{pi,n}^2/\omega^2=2\left(1-n\,\frac{\omega_{ci}}{\omega}\right)\left(\sqrt{\frac{\gamma_e KT}{a^2\omega^2 m_e}e}-n\right)\Big/\left(\sqrt{\frac{\gamma_e KT}{a^2\omega^2 m_e}e}-\frac{\omega}{\omega_{ci}}\right) \qquad ;\; n=\pm 1 \qquad (3)$$

*Chercheur agréé de l'Institut Interuniversitaire des Sciences Nucléaires.

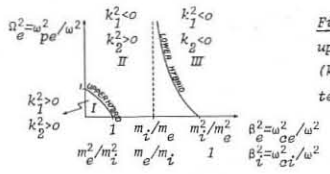

Fig.1. $\Omega_e^2=\omega_{pe}^2/\omega^2$ *versus* β_i^2 *or* β_e^2. *The upper hybrid* ($k_1=o$) *and lower hybrid* ($k_2=o$) *determine three regions of interest for the hot magnetized plasma.*

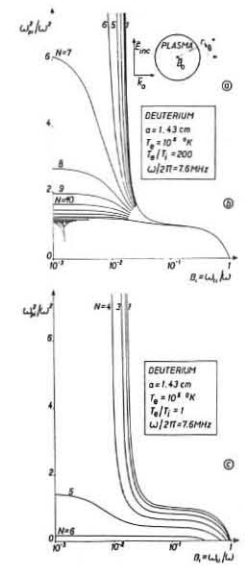

Fig.2.(a) Plasma cylinder with $\bar{B}_o$ *and incoming wave* ($\bar{E},\bar{k}_o$). *(b) Normalized density of ion thermal resonances (each characterized by a given N) versus* β_i *with* $T_e/T_i=200$. *(c) Same with* $T_e/T_i=1$.

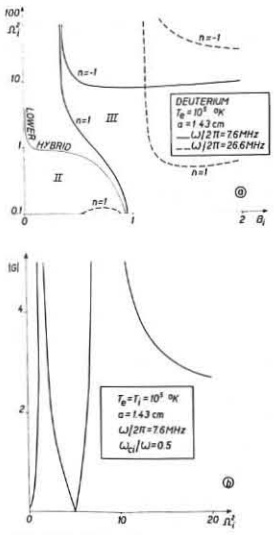

Fig.3.(a) The two main resonances in III represented by the solid curves when $T_e > a^2\omega^2 m_e/\gamma_e K$ *together with the two main resonances in III and the main resonance in II represented by dashed curves when* $T_e < a^2\omega^2 m_e/\gamma_e K$. *(b) Normalized amplitude* $|G|$ *of scattered field as a function of* Ω_i^2 *showing the two new resonances of region III.*

If $T_e > a^2\omega^2 m_e/\gamma_e K$, we have two resonances lying in region III and given by the solid curves of fig 3a.If $T_e < a^2\omega^2 m_e/\gamma_e K$, we have, besides the two resonances in region III, another $n=1$ resonance in region II which is precisely that given by eq (2) in the $T_e=o$ limit; see the three dashed curves of fig 3a. The importance of the resonance peaks of region III as a function of Ω_i^2 for given β_i (fig 3b) clearly shows that the external field is strongly coupled [4d] to the plasma at resonance.

Besides their relevance to basic plasma physics,the two new main resonances resulting from a proper combination of B_o and T_e can also be of interest for the transfer of hf energy to the plasma. For hot dense deuterium,we have typical values like $\langle N\rangle=10^{13}$ cm^{-3}, $T_e=10^7$ °K, $\omega/2\pi=50$ MHz, $a=10$cm, $B_o=100$kG or $\langle N\rangle=10^{13}$ cm^{-3}, $T_e=10^8$ °K, $\omega/2\pi=100$MHz, $a=10$cm, and $B_o=150$kG. We must underline,however,that if the quasi-static approximation is usually warranted when $a^2<<k_o^{-2}$[4e],this approximation will be reexamined in region III,for a given a,by carrying out the full electromagnetic treatment.Anyhow, since a real plasma is nonuniform,this approximation is certainly satisfactory in the outer region of the plasma.

This study clearly shows that strong resonances exist in a HOT BOUNDED magnetized plasma which are only indirectly connected to the upper and lower hybrid frequencies characterizing a COLD UNBOUNDED plasma.These results have been summarized elsewhere [6] and complete details will be given in a full-length paper.

REFERENCES.

1. I.ALEXEFF and R.V.NEIDIGH,Oak Ridge Nat.Lab.Rep ORNL-CF-61-2-57;Phys.Rev. Letters 7 (1961) 223;F.W.CRAWFORD,Phys.Rev.Letters 6 (1961) 663;R.GELLER and M.LUCARAIN,C.R.Acad.Sc.Paris 253 (1961) 1542.
2. I.B.BERNSTEIN, S.K.TREHAN,Nucl.Fusion 1 (1960) 3;B.D.FRIED and R.W.GOULD, Phys.Fluids 4 (1961) 139.
3. H.MOTZ,Reports on Progress in Phys.vol XXIX,Part II (1966) 623;Wm.DENVER JONES,Oak Ridge Nat.Lab.Rep. ORNL 4089 UC-20-Controlled Thermonuclear Processes (1967).
4. P.E.VANDENPLAS"*Electron waves and resonances in bounded plasmas*" John Wiley (Interscience),London-New York-Sydney (1968);(a) p 4-5;(b) Sections 2-1,5-1 and 5-2 a,b,c;(c)p99-103;d)p149-152;(e)p8-10 and 134.
5. J.F.DENISSE and J.L.DELCROIX,"*Théorie des Ondes dans les plasmas*"Dunod (61)
6. P.VANDENPLAS,A.MESSIAEN,J.MONFORT,J.PAPIER,subm.for publ.(1969).
7. P.VANDENPLAS,A.MESSIAEN,Physics Letters 28a (1968) 159.

NONLINEAR BEHAVIOUR OF PLASMA UNDER THE INFLUENCE OF LARGE-AMPLITUDE WAVES.

I. Fidone.

ASSOCIATION EURATOM-CEA
Département de la Physique du Plasma et de la Fusion Contrôlée
Centre d'Etudes Nucléaires
Boite Postale n° 6 - **92 Fontenay-aux-Roses** (France)

ABSTRACT.

In this paper we consider examples of wave-wave coupling in plasma. Three typical situations are discussed, i.e., coupling between longitudinal waves, longitudinal-transverse and transverse waves. The conditions for wave parametric amplification and wave conversion are found.

INTRODUCTION.

When large-amplitude waves are present in a plasma the study of wave propagation may be extended beyond the small-signal theory by consideration of nonlinear wave-wave coupling. Moreover, in a number of cases, as for instance the problem of plasma turbulence, nonlinear effects play a dominant role. In spite of the large number of papers on turbulence theory a satisfactory treatment of this important problem is still lacking [1]. On the other hand in those cases in which a small number of interacting waves is considered a detailed solution can be given, thus, offering material for experimental check. In this case the phase of the waves will not be considered random and systematic use can be made of the method of nonlinear optics [2].

In this paper we refer to this class of problems and by discussing a selected number of examples we hope to give a glance at some problems encountered in the literature on the subject.

We shall treat stable waves but very often the methods will apply to internally generated unstable waves as well. The plan of the paper is as follows. In section I the general theory of three waves interaction as obtained by a perturbation solution of the Maxwell-Vlasov equations is presented. In section II we consider the case of three waves propagating across the confining magnetic field. The interactions of two high frequency electromagnetic waves with Bernstein modes is considered and results are obtained for energy conversion and wave parametric amplification. Futhermore, the interaction of three electromagnetic waves is treated and a possible application to diagnostics is mentioned. In section III we discuss the interaction of electron waves propagating along a strong magnetic field. This examples is of particular interest because it is well adapted for providing an experimental verification of the Manley-Rowe cycle. In section IV we give a short survey of the literature on nonlinear effects.

I. GENERAL THEORY OF THREE WAVES INTERACTION.

We describe the plasma by the following equations

$$\nabla\wedge\vec{B} = \frac{1}{c}\frac{\partial\vec{E}}{\partial t} + \frac{4\pi}{c}\vec{J} \qquad \nabla\wedge\vec{E} = -\frac{1}{c}\frac{\partial\vec{B}}{\partial t} \qquad (1)$$

$$\frac{\partial F}{\partial t} + \vec{v}\cdot\frac{\partial F}{\partial\vec{r}} + \frac{q}{m}\left(\frac{\vec{v}}{c}\wedge\vec{B}_0 + \vec{E} + \frac{\vec{v}}{c}\wedge\vec{B}\right)\cdot\frac{\partial F}{\partial\vec{v}} = 0 \qquad (2)$$

where F is the electron distribution and $\vec{B}_0 = B_0\vec{\iota}_z$ the constant confining field. We consider high frequency oscillations and neglect the ion motion. We seek solutions of eqs. (1) of the form [3] $\vec{E} = \sum_{k\omega}\vec{a}_\omega E_\omega\left(\frac{\vec{k}\cdot\vec{r}}{k}\right) e^{i\vec{k}\cdot\vec{r}-i\omega t}$ etc.., etc... where $\vec{a}_\omega$ is the polarization vector defined in such a way that $\vec{a}_\omega\cdot\vec{a}_\omega^{*}=1$. The amplitude E_ω is supposed to be a slowly varying function of $\vec{r}\left(k \gg \frac{1}{E}\frac{\partial E}{\partial r}\right)$, therefore the treatment will be valid for weak nonlinearity. Maxwell equations take the form

$$\left(\vec{k}\vec{k} - \left(k^2 - \frac{\omega^2}{c^2}\right)\bar{\bar{1}}\right)\cdot\vec{a}_\omega E_\omega - 2i\vec{k}\wedge\left(\nabla E_\omega\wedge\vec{a}_\omega\right) = -i\frac{4\pi\omega}{c^2}\vec{J}_{k\omega} \qquad (3)$$

neglecting terms of the order $\left(\frac{1}{kE}\frac{\partial E}{\partial r}\right)^2$. To calculate the Fourier component of the current we assume that in absence of waves $F = n_0 f_m = n_0\left(\frac{m}{2\pi T}\right)^{\frac{3}{2}} e^{-mV^2/2T}$ In presence of waves we write $F = n_0 f_m + f$ where

$$\frac{\partial f}{\partial t} + \vec{v}\cdot\frac{\partial f}{\partial\vec{r}} + \omega_c\vec{v}\wedge\vec{\iota}_z\cdot\frac{\partial f}{\partial\vec{v}} = -n_0\frac{q}{m}\vec{E}\cdot\frac{\partial f_m}{\partial\vec{v}} - \frac{q}{m}\left(\vec{E} + \frac{\vec{v}}{c}\wedge\vec{B}\right)\cdot\frac{\partial f}{\partial\vec{v}}\ , \qquad \omega_c = \frac{qB_0}{mc} \qquad (4)$$

The linear solution of eq. (4) is given by

$$f^{(1)}_{k\omega} = -n_0\frac{q}{m}\int_{-\infty}^{0} dt\, e^{i\vec{k}\cdot\left(\vec{r}'-\vec{r}\right)-i\omega t} E_\omega(\vec{r}')\vec{a}_\omega\cdot\frac{\partial f_m}{\partial\vec{v}'} \qquad (5)$$

where $\vec{r}' = \vec{r}'(t)$ and $\vec{v}' = \vec{v}'(t)$ are the solution of the equation $\frac{d\vec{V}}{dt} = \omega_c\vec{V}\wedge\vec{\iota}_z$. Developing $E(\vec{r}')$ we have

$$f^{(1)}_{k\omega} = -n_0\frac{q}{m}\left\{E_\omega\int_{-\infty}^{0} dt\, e^{i\vec{k}\cdot(r'-r)-i\omega t}\frac{\partial f_m}{\partial\vec{v}'}\vec{a}_\omega - i\frac{\vec{k}}{k^2}\cdot\frac{\partial E_\omega}{\partial\vec{r}}\left(\vec{k}\cdot\frac{\partial}{\partial\vec{k}}\int_{-\infty}^{0} dt\, e^{i\vec{k}\cdot\left(\vec{r}'-\vec{r}\right)-i\omega t}\frac{\partial f_m}{\partial\vec{v}'}\right)\vec{a}_\omega\right\}$$

from which

$$\vec{J}^{(1)}_{k\omega} = \bar{\bar{\sigma}}_{k\omega}\vec{a}_\omega E_\omega - i\frac{\vec{k}}{k^2}\frac{\partial E_\omega}{\partial\vec{r}}\left(\vec{r}\cdot\frac{\partial}{\partial\vec{k}}\bar{\bar{\sigma}}_{k\omega}\right)\cdot\vec{a}_\omega\ , \qquad \bar{\bar{\sigma}}_{k\omega} = -n_0\frac{q^2}{m}\int d\vec{v}\vec{v}\int_{-\infty}^{0} dt\, e^{i\vec{k}\cdot\left(\vec{r}'-\vec{r}\right)-i\omega t}\frac{\partial f_m}{\partial\vec{v}'} \qquad (6)$$

Eq. (3) with eq. (6) becomes :

$$\left(\vec{k}\vec{k} - k^2\bar{\bar{1}} + \frac{\omega^2}{c^2}\bar{\bar{\varepsilon}}_{k\omega}\right)\cdot\vec{a}_\omega E_\omega - 2i\left(\vec{k}\vec{k} - k^2\bar{\bar{1}}\right)\cdot\vec{a}_\omega\frac{\vec{k}}{k^2}\cdot\frac{\partial E_\omega}{\partial\vec{r}} - i\frac{\omega^2}{c^2}\left(\vec{k}\cdot\frac{\partial}{\partial\vec{k}}\bar{\bar{\varepsilon}}_{k\omega}\right)\cdot\vec{a}_\omega\frac{\vec{k}}{k^2}\cdot\frac{\partial E_\omega}{\partial\vec{r}} = -i\frac{4\pi(\omega)}{c^2}\vec{J}^{(2)}_{k\omega} \qquad (7)$$

where $\bar{\bar{\varepsilon}}_{k\omega} = \bar{\bar{1}} + \frac{4\pi i}{\omega}\bar{\bar{\sigma}}_{k\omega}$ and $\vec{J}^{(2)}_{k\omega}$ is the second order current obtained from the nonlinear correction $f^{(2)}_{k\omega}$. From eq. (4) with $f = f^{(1)} + f^{(2)}$ we have

$$f^{(2)}_{k\omega} = -\frac{q}{m}\sum_{k'\omega'}\int_{-\infty}^{0} dt\, e^{i\vec{k}\cdot\left(\vec{r}'-\vec{r}\right)-i\omega t}\left(\vec{E}_{k'\omega'} + \frac{\vec{v}'}{c}\wedge\vec{B}_{k'\omega'}\right)\cdot\frac{\partial}{\partial\vec{v}'}f^{(1)}_{k''\omega''} \qquad (8)$$

with $\omega'' = \omega - \omega'$, $\vec{k}'' = \vec{k} - \vec{k}'$. For slowly damped (or growing) waves the vector $\vec{k}$ has a small imaginary part, $\vec{k} = \vec{k} + i\vec{k}_i\ (k_i \ll k)$. Let us now assume that in first approximation the linear dispersion relation is fulfilled and that $\vec{k}_i = k_i\frac{\vec{k}}{k}$ (homogeneous waves), then

$$\left(\vec{k}\vec{k} - k^2\bar{\bar{1}} + \frac{\omega^2}{c^2}\bar{\bar{\varepsilon}}_{k\omega}\right)\cdot\vec{a}_\omega = 0 \qquad (9)$$

$$\left(\bar{\bar{\varepsilon}}_{k\omega} - \frac{1}{2}\vec{k}\cdot\frac{\partial}{\partial\vec{k}}\bar{\bar{\varepsilon}}_{k\omega}\right)\cdot\vec{a}_\omega\frac{\vec{k}}{k^2}\cdot\frac{\partial E_\omega}{\partial\vec{r}} = \frac{k_i}{k}\left(\bar{\bar{\varepsilon}}_{k\omega} - \frac{1}{2}\vec{k}\cdot\frac{\partial}{\partial\vec{k}}\bar{\bar{\varepsilon}}_{k\omega}\right)\cdot\vec{a}_\omega E_\omega - \frac{2\pi}{\omega}\vec{J}^{(2)}_{k\omega} \qquad (10)$$

Eq. (10) is the basic equation for studying nonlinear interactions of waves. When expressing $\vec{J}^{(2)}_{k\omega}$ in terms of the electric field we find that E_ω could interact with all the waves existing in the system. We limit ourselves to the investigation of the interaction of three waves $E_\omega, E_{\omega'}, E_{\omega''}$, assuming that the synchronism condition $\vec{k} = \vec{k}' + \vec{k}''$ is exactly satisfied. Moreover we shall consider situations for which the temperature dependence of the dielectric tensor is given by a term that is a quadratic form of $\vec{k}$. Then, $\bar{\bar{\varepsilon}}_{k\omega} - \frac{1}{2}\vec{k}\cdot\frac{\partial}{\partial\vec{k}}\bar{\bar{\varepsilon}}_{k\omega} = \bar{\bar{\varepsilon}}_0(\omega) = \lim_{k\to 0}\bar{\bar{\varepsilon}}_{k\omega} = \lim_{T\to 0}\bar{\bar{\varepsilon}}_{k\omega}$ In this case eq. (10) reads

$$\bar{\bar{\varepsilon}}_0(\omega)\cdot\vec{a}_\omega\frac{\vec{k}}{k^2}\cdot\frac{\partial E_\omega}{\partial\vec{r}} = \frac{k_i}{k}\bar{\bar{\varepsilon}}_0(\omega)\cdot\vec{a}_\omega E_\omega - \frac{2\pi}{\omega}\vec{J}^{(2)}_{k\omega}\ . \qquad (11)$$

Up to now the amplitude and direction of the propagation vectors of the three waves have been left arbitrary. For sake of simplicity in this paper, we consider only two limiting situations : waves propagating across $\vec{B}_0$ and parallel to it. Moreover we assume that the ratio of the electron Larmor radius to the wavelength is much smaller than one.

II. WAVES PROPAGATING ACROSS $\vec{B}_0$.

Assuming $k_\perp v_\perp/|\omega_c| \ll 1$ and neglecting relativistic effects $\bar{\bar{\varepsilon}}_{k\omega}$ takes the form [4]

$$\varepsilon_{xx} = \varepsilon + \gamma^2 k_y^2 \qquad \varepsilon = 1 - \frac{\omega_p^2}{\omega^2-\omega_c^2}\left(1 + \frac{T}{m}\frac{3k^2}{\omega^2-4\omega_c^2}\right)$$

$$\varepsilon_{yy} = \varepsilon + \gamma^2 k_x^2 \qquad g = -\frac{\omega_c}{\omega}\frac{\omega_p^2}{\omega^2-\omega_c^2}\left(1 + \frac{T}{m}\frac{6k^2}{\omega^2-4\omega_c^2}\right)$$

$$\varepsilon_{xy} = ig - k_x k_y\gamma^2 \qquad \eta = 1 - \frac{\omega_p^2}{\omega^2}\left(1 + \frac{T}{m}\frac{k^2}{\omega^2-\omega_c^2}\right)$$

$$\varepsilon_{yx} = -ig - k_x k_y\gamma^2 \qquad \gamma^2 = 2\frac{T}{m}\frac{\omega_p^2/\omega^2}{\omega^2-\omega_c^2}$$

$$\varepsilon_{zz} = \eta\ ,\ \varepsilon_{xz} = \varepsilon_{zx} = \varepsilon_{yz} = \varepsilon_{zy} = 0$$

From eq. (9) we deduce that there exist two kinds of non-potential waves

ordinary waves $\frac{c^2k^2}{\omega^2}=\eta$ $\quad a_\omega=\vec{\iota}_z$ (12)

and extraordinary waves $\left(1-\frac{\omega^2}{c^2}\gamma^2\right)\frac{c^2k^2}{\omega^2}=\frac{\varepsilon^2-g^2}{\varepsilon}$ (13)

$$\vec{a}_\omega=\frac{1}{\lambda_\omega}\left\{\vec{\iota}_x-\frac{\frac{\omega^2}{c^2}\varepsilon-\left(1-\frac{\omega^2}{c^2}\gamma^2\right)k_y^2}{\left(1-\frac{\omega^2}{c^2}\gamma^2\right)k_xk_y+i\frac{\omega^2}{c^2}}\vec{\iota}_y\right\},\lambda_\omega^2=1+\frac{\frac{\omega^2}{c^2}\varepsilon-\left(1-\frac{\omega^2}{c^2}\gamma^2\right)k_y^2}{\frac{\omega^2}{c^2}\varepsilon-\left(1-\frac{\omega^2}{c^2}\gamma^2\right)k_x^2}$$

The branch of potential waves is obtained from eq.(9) with $\vec{a}_\omega=\frac{\vec{k}}{k}$. The dispersion relation is

$$\varepsilon=\frac{\vec{k}\cdot\vec{\vec{\varepsilon}}_{k\omega'}\vec{k}}{k^2}=0 \quad \text{(Bernstein modes).} \qquad (14)$$

We now discuss two examples of nonlinear interaction between these three waves. More specifically, in the system of waves two are non-potential of the ordinary type (eq. (12)) with frequencies ω', ω'' much greater than ω_p and $|\omega_c|$. Therefore, their indexes of refraction are close to one and $k'\simeq\frac{\omega'}{c}, k''\simeq\frac{\omega''}{c}$. The third wave of frequency ω will be either extraordinary (eq. (13)) or longitudinal (eq. (14)). It is clear that the processes of interest are those for which $\omega=\omega'-\omega''\ll\omega', \omega''$ and $\vec{k}=\vec{k}'-\vec{k}''$. In Fig.1 we give the diagram of the system of waves considered.

Let us first awell on the implication of the relation $\vec{k}=\vec{k}'-\vec{k}''$. By squaring

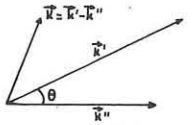

-fig.1-

$$k'^2+k''^2-2k'k''\cos\theta=k^2=n^2(\omega)\frac{\omega^2}{c^2} \quad \text{or}$$

$$n^2(\omega)=1+2\frac{\omega'\omega''}{\omega^2}(1-\cos\theta)=1+R, \quad 0\ll\theta\leq\pi, \quad \omega'>\omega''>0 \qquad (15)$$

The two forms of $n(\omega)$ considered in this section are

$$n^2(\omega)=1-\frac{\omega_p^2}{\omega^2}\frac{\omega^2-\omega_p^2}{\omega^2-\omega_c^2-\omega_p^2} \qquad \text{(low temperature plasma)} \qquad (13')$$

$$n^2(\omega)=\frac{1}{3\beta^2\omega^2\omega_p^2}(\omega^2-\omega_c^2-\omega_p^2)(\omega^2-4\omega_c^2) \qquad \beta^2=T/mc^2 \qquad (14')$$

With $a=\frac{\omega_p^2}{\omega^2}, b=\frac{\omega_c^2}{\omega^2}$, eqs. (13') and (15) give

$$b=1-\frac{a^2-a(1-R)}{R} \qquad (16)$$

The non propagation band is defined by the resonances and cut-off

$n^2=\infty$ for $b=1-a$

$n^2=0$ for $b=(1-a)^2$

and $n^2>0$ for $b<(1-a)^2$ or $b>1-a$.

In Fig.2 we represent grafically ep.(16) for a given value of $R>0$. The maximum value of b is $b_m=1+\frac{(1-R)^2}{4R}$. For $a<1$ we get $b>1-a$, i.e., the secondary wave can propagate. Repeating the same analysis on eq. (14') we have

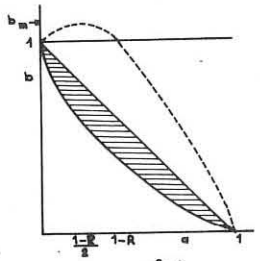

-fig.2-

$n^2=0$ for $b=\frac{1}{4}$, $b=1-a$

$n^2>0$ for $b<1-a$, $b<\frac{1}{4}$ o $b>1-a$, $b>\frac{1}{4}$.

In Fig.3 we show the propagation bands (shaded regions) as defined by the previous relations. The lines b_1 and b_2 are obtained from the following consideration. The assumption $k_\perp v_\perp/\omega_c\ll 1$ leads to $n^2<\frac{b}{\beta^2}$, then $(1-a-b)(1-4b)<3ab$ or $(b-b_1)(b-b_2)<0$ with $b_1=1, b_2=\frac{1}{4}(1-a)$.

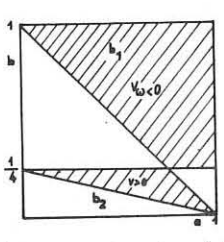

The conclusion to be drawn is that for given values of R and a the value of b must lie inside the shaded bands (fig.3) otherwise the process is forbidden. It is worthwhile to note that the $\vec{k}$ component of the group velocity has opposite sign in the two bands.

$$\frac{\vec{k}}{k}\cdot\frac{d\omega}{d\vec{k}}=V_\omega=\frac{2}{k(\partial\varepsilon/\partial\omega)}\frac{1-a-b}{1-b}, 0<\frac{\partial\varepsilon}{\partial\omega}=\frac{2\omega}{\omega^2-\omega_c^2}\left(1+\frac{\omega^2-\omega_c^2-\omega_p^2}{\omega^2-4\omega_c^2}\right).$$

a) INTERACTION OF ELECTROMAGNETIC WAVES WITH BERNSTEIN MODES.

The second order current is obtained from eq. (8). For ω', ω'' very large

$$f^{(1)}_{k''\omega''}\simeq -i\frac{q}{m}n_0\frac{\partial f_m}{\partial v_z} \quad , \quad \vec{J}^{(2)}_{k\omega\perp}=i\frac{q}{m}\frac{E_{\omega'}E_{\omega''}}{\omega'\omega''}\vec{\vec{\sigma}}_{k\omega}\cdot\vec{k}$$

To calculate $\vec{\iota}_z\cdot\vec{J}^{(2)}_{k'\omega'}$ and $\vec{\iota}_z\cdot\vec{J}^{(2)}_{k''\omega''}$ we make use of the symmetry relations of the coupling coefficients (7).

The final results are

$$\vec{\iota}_z\cdot\vec{J}^{(2)}_{k'\omega'}=-\frac{q}{m}\frac{1}{4\pi}k\frac{E_\omega E_{\omega''}}{\omega''}, \quad \vec{\iota}_z\cdot\vec{J}^{(2)}_{k''\omega''}=-\frac{q}{m}\frac{1}{4\pi}k\frac{E_\omega E_{\omega'}}{\omega'}, \omega\ll\omega',\omega''.$$

Let $q=-e$, $\vec{r}=\hat{n}\delta$ and using eq.(11) with $k_i=0$ the system of the three waves takes the form

$$\left(\frac{\partial\omega\varepsilon}{\partial\omega}\right)\frac{V_\omega}{\hat{k}\cdot\hat{n}}\frac{dE^*_\omega}{ds}=2\left(\frac{ek}{2m}\right)\frac{\omega}{\omega'\omega''}E^*_{\omega'}E_{\omega''}$$

$$\frac{c}{\hat{k}'\cdot\hat{n}}\frac{dE_{\omega'}}{d\delta}=-\left(\frac{ek}{2m}\right)\frac{1}{\omega''}E_\omega E_{\omega''} \qquad \hat{k}=\frac{\vec{k}}{k} \text{ etc...}$$

$$\frac{c}{\hat{k}''\cdot\hat{n}}\frac{dE^*_{\omega''}}{d\delta}=+\left(\frac{ek}{2m}\right)\frac{1}{\omega'}E_\omega E^*_{\omega'}$$

Defining the real amplitude $\mathcal{E}_\omega$ by the relation $E_\omega=\mathcal{E}_\omega e^{i\psi_\omega}$ we have

$$\frac{\partial\omega\varepsilon}{\partial\omega}\frac{V_\omega}{\hat{k}\cdot\hat{n}}\frac{d\psi_\omega}{d\delta}=-2\left(\frac{ek}{2m}\right)\frac{\omega}{\omega'\omega''}\mathcal{E}_{\omega'}\mathcal{E}_{\omega''}\cos\theta$$

$$\frac{c}{\hat{k}'\cdot\hat{n}}\frac{d\mathcal{E}_{\omega'}}{d\delta}=\left(\frac{ek}{2m}\right)\frac{1}{\omega''}\mathcal{E}_\omega\mathcal{E}_{\omega''}\cos\theta \qquad (17)$$

$$\frac{c}{\hat{k}''\cdot\hat{n}}\frac{d\mathcal{E}_{\omega''}}{d\delta}=-\left(\frac{ek}{2m}\right)\frac{1}{\omega'}\mathcal{E}_\omega\mathcal{E}_{\omega'}\cos\theta$$

with $\sin\theta(\delta)\mathcal{E}_\omega(\delta)\mathcal{E}_{\omega'}(\delta)\mathcal{E}_{\omega''}(\delta)=\text{const.}$ $\theta=\psi_{\omega'}-\psi_{\omega''}-\psi_\omega$.

As we expect

$$\frac{V_\omega}{\hat{k}\cdot\hat{n}}W_\omega+\frac{c}{\hat{k}'\cdot\hat{n}}W_{\omega'}+\frac{c}{\hat{k}''\cdot\hat{n}}W_{\omega''}=\text{const} \quad \text{(conservation of flux),}$$

where $W_\omega=\frac{1}{16\pi}\left(\frac{\partial\omega\varepsilon}{\partial\omega}\right)\mathcal{E}^2_\omega$, $W_{\omega'}=\frac{1}{8\pi}\mathcal{E}^2_{\omega'}$, $W_{\omega''}=\frac{1}{8\pi}\mathcal{E}^2_{\omega''}$.

As may be seen from eqs.(17) parametric excitation of Bernstein modes under the effect of a strong electromagnetic wave $\mathcal{E}_\omega\gg\mathcal{E}_{\omega''}$ will take place if $\frac{+(\hat{k}\cdot\hat{n})(\hat{k}''\cdot\hat{n})}{V_\omega}>0$. Let $V_\omega=+|V_\omega|$ $\quad(\hat{k}\cdot\hat{n}),(\hat{k}'\cdot\hat{n}),(\hat{k}''\cdot\hat{n})>0$, $W_\omega(0)=0$ $\quad W_{\omega^{(0)}}\ll W_{\omega'^{(0)}}$, the characteristic length for total conversion of energy is

$$z_0\simeq\frac{1}{2H\sqrt{W_{\omega'}(0)}}\ln\frac{W_{\omega'}(0)}{W_{\omega''}(0)} \qquad (18)$$

with $H=\left(\frac{ek}{mc}\right)\frac{1}{\omega'\omega''}\sqrt{4\pi\left(\frac{\partial\omega\varepsilon}{\partial\omega}\right)^{-1}\frac{c}{|V_\omega|}\omega\omega''(\hat{k}\cdot\hat{n})(\hat{k}''\cdot\hat{n})}$ (see next section).

Another situation of interest is the conversion of two electromagnetic waves of comparable amplitudes $\mathcal{E}_{\omega'}\simeq\mathcal{E}_{\omega''}$ into a longitudinal one. Let $\omega_\omega(0)=0$ $W_{\omega'}(0)=W_{\omega''}(0)$ and $\omega'\simeq\omega''$ $\hat{k}'\cdot\hat{n}\simeq\hat{k}''\cdot\hat{n}\simeq 1$ we get from eqs. (17) the following solutions

$$W_{\omega'}=W_{\omega'}(0)\,sn^2\left[\sqrt{2W_{\omega'}(0)}\,H(z-z_0)\frac{1}{\sqrt{2}}\right]$$

$$W_\omega=\frac{\omega}{\omega''}\frac{\hat{k}\cdot\hat{n}}{\hat{k}'\cdot\hat{n}}\frac{c}{|V_\omega|}W_{\omega'}(0)\left(1-sn^2\left[\sqrt{2W_{\omega'}(0)}\,H(z-z_0)\frac{1}{\sqrt{2}}\right]\right) \qquad (19)$$

$$W_{\omega''}=W_{\omega''}(0)+\frac{\omega'}{\omega''}\frac{\hat{k}''\cdot\hat{n}}{\hat{k}'\cdot\hat{n}}W_{\omega'}(0)\left(1-sn^2\left[\sqrt{2W_{\omega'}(0)}\,H(z-z_0)\frac{1}{\sqrt{2}}\right]\right)$$

where

$$z_0 = \frac{1}{\sqrt{2}} \frac{1}{H\sqrt{\omega_{\omega'}(0)}} \frac{1}{4\sqrt{\pi}} \left[\Gamma\left(\frac{1}{4}\right)\right]^2 \simeq 4 \frac{0.82}{\sqrt{2\pi}} \frac{1}{H\sqrt{\omega_{\omega'}(0)}} \simeq 1.3 \frac{1}{H\sqrt{\omega_{\omega'}(0)}}$$

In fig. 4 we show graphically the behaviour of eqs. (19).

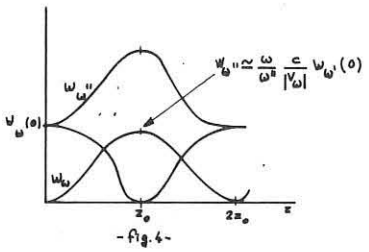

- fig. 4 -

b) INTERACTION OF THREE ELECTROMAGNETIC WAVES.

It may be seen that in this case the third wave must be extraordinary. The second order current can be calculated as before and with $\vec{k} = k\vec{i}_z$ the three wave system becomes

$$\begin{aligned} \vec{a}^*_\omega \cdot \bar{\bar{\varepsilon}}_0(\omega) \cdot \vec{a}_\omega \quad & \frac{\vec{k}}{k} \cdot \frac{\partial E^*_\omega}{\partial \vec{r}} = \left(\frac{e}{2m}\right) \frac{E^*_{\omega'} E_{\omega''}}{\omega' \omega''} \frac{k^2}{\lambda_\omega} \\ & \frac{\vec{k}'}{k'} \cdot \frac{\partial E_{\omega'}}{\partial \vec{r}} = -\left(\frac{e}{2m}\right) \frac{E_\omega E_{\omega''}}{\omega'^2} \frac{k k'}{\lambda_\omega} \\ & \frac{\hat{k}''}{k''} \cdot \frac{\partial E^*_{\omega''}}{\partial \vec{r}} = +\left(\frac{e}{2m}\right) \frac{E_\omega E^*_{\omega'}}{\omega''^2} \frac{k k''}{\lambda_\omega} \end{aligned} \qquad (20)$$

For small interaction region and low temperature the secondary wave E_ω has the amplitude [5]

$$\frac{\mathcal{E}_\omega}{l} \simeq \left(\frac{e}{2mc^2}\right) \mathcal{E}_{\omega'}(0)\, \mathcal{E}_{\omega''}(0)\, \frac{\omega^2}{\omega'\omega''} \left(\frac{g_0}{\mathcal{E}_0}\right) \sqrt{1 + \left(\frac{g_0}{\mathcal{E}_0}\right)^2} \quad , \hat{k}\cdot\hat{n} = 1 \qquad (21)$$

$$= \left(\frac{e}{2mc^2}\right) \mathcal{E}_{\omega'}(0)\, \mathcal{E}_{\omega''}(0)\, \frac{\omega|\omega_c|}{\omega'\omega''} \frac{\omega_p^2}{(\omega^2 - \omega_c^2 - \omega_p^2)^2} \sqrt{\omega_p^4 \frac{\omega_c^2}{\omega^2} + (\omega^2 - \omega_c^2 - \omega_p^2)^2}$$

Conversion of high frequency waves into an extraordinary one may suggest a scheme to provide a method for mesuring the local electron density of a rarefied plasma confined by a strong magnetic field. If the magnetic field at a given point $\vec{r}_0$ is known eq. (16) can be used to deduce ω_p. Moreover in a magnetic field varying in direction and amplitude with $\vec{r}$ the signal generated at $\vec{r}_0$ can still escape the plasma provided that the representative point $[a(\vec{r}_0), b(\vec{r}_0)]$ be outside the region defined by the curves $b = (1-a)^2$ and $b = \frac{1-a}{1-a\cos^2\alpha_m}$, where α_m is the minimum angle between $\vec{k}$ and the direction of $\vec{B}_0$ at the periphery of the plasma.

III. INTERACTION OF ELECTRON WAVES IN A STRONG MAGNETIC FIELD.

We now consider the case of three longitudinal waves propagating along the direction of $\vec{B}_0$ [6]. With B_0 very large

$$\bar{\bar{\varepsilon}}_{k\omega} = \bar{\bar{1}} - \vec{i}_z \vec{i}_z \frac{\omega_p^2}{\omega^2} \left(1 + \frac{3T}{m} \frac{k_z^2}{\omega^2}\right) \qquad (22)$$

and

$$\vec{J}_{k\omega} = -\frac{q}{m} \frac{\omega_p^2}{4\pi} \frac{k'_z k''_z}{k' k''} \frac{E_{\omega'} E_{\omega''}}{\omega' \omega''} \left(\frac{k_z}{\omega} + \frac{k'_z}{\omega'} + \frac{k''_z}{\omega''}\right) \vec{i}_z \qquad \omega = \omega' + \omega'', \; k_z = k'_z + k''_z \qquad (23)$$

The system of the three waves in this case is

$$\begin{aligned} V_\omega \frac{\partial E_\omega}{\partial z} &= k_i V_\omega \frac{k_z}{k} E_\omega + V \frac{E_{\omega'} E_{\omega''}}{\omega' \omega''} \\ V_{\omega'} \frac{\partial E^*_{\omega'}}{\partial z} &= k'_i V_{\omega'} \frac{k'_z}{k'} E^*_{\omega'} - V \frac{E^*_\omega E_{\omega''}}{\omega \omega''} \\ V_{\omega''} \frac{\partial E^*_{\omega''}}{\partial z} &= k''_i V_{\omega''} \frac{k''_z}{k''} E^*_{\omega''} - V \frac{E^*_\omega E_{\omega'}}{\omega \omega'} \end{aligned} \qquad (24)$$

where $V_\omega = \frac{\omega}{k_z} \frac{k_i^2}{k_z^2}$ and $V = \frac{e}{2m} \omega_p^2 \frac{k_z k'_z k''_z}{k k' k''} \left(\frac{k_z}{\omega} + \frac{k'_z}{\omega'} + \frac{k''_z}{\omega''}\right)$. We remark that the value of V is the same for the three equations. This is hardly surprising as we know from the symmetry relations of the coupling coefficients [7]. The dispersion relation is given by

$$D \simeq 1 - \frac{\omega_p^2}{\omega^2} \frac{k_z^2}{k^2} \quad ; \omega^2 = \omega_p^2 \frac{k_z^2}{k^2} . \qquad (25)$$

By introducing the real amplitude $\mathcal{E}_\omega$ etc... we may verify that the condition for parametric excitation of the waves $\mathcal{E}_{\omega'}$, $\mathcal{E}_{\omega''}$ in the presence of a strong amplitude wave $\mathcal{E}_\omega$ is given by

$$\frac{V^2 \mathcal{E}_\omega^2(0)}{V_{\omega'} V_{\omega''} \omega^2 \omega' \omega''} > |k'_i k''_i| \frac{k'_z k''_z}{k' k''} \qquad k'_i, k''_i < 0 \qquad (26)$$

For $\mathcal{E}_\omega$ much greater than the threshold value given by eq. (28) the system of eqs. (24) can be simplified by letting $k_i = k'_i = k''_i = 0$. By introducing the energy density $w_\omega = \frac{1}{16\pi} \frac{\partial \omega D}{\partial \omega} \mathcal{E}_\omega^2 = \frac{1}{8\pi} \mathcal{E}_\omega^2$ we have

$$\frac{dW_\omega}{dz} = 2\mathcal{K} \sqrt{\omega_\omega \left(\frac{c_1}{\omega' V_\omega} - W_\omega\right)\left(\frac{c_2}{\omega'' V_\omega} - \omega_\omega\right)} \; , \quad \mathcal{K} = \sqrt{8\pi} \sqrt{\frac{V^2}{V_{\omega'} V_{\omega''} \omega^2 \omega' \omega''}} \qquad (27)$$

with

$$\omega' V_\omega W_\omega(z) + \omega V_{\omega'} W_{\omega'}(z) = C_1 = \omega' V_\omega W_\omega(0) + \omega V_{\omega'} W_{\omega'}(0)$$

$$\omega'' V_\omega W_\omega(z) + \omega V_{\omega''} W_{\omega''}(z) = C_2 = \omega'' V_\omega W_\omega(0) + \omega V_{\omega''} W_{\omega''}(0)$$

The solution of eq. (27) is well-known [2]. Let $W_{\omega''}(0) = 0$ $\quad W_{\omega'}(0) < W_\omega(0)$ we have

$$\begin{aligned} W_\omega &= W_\omega(0)\, Sn^2\left[\sqrt{\alpha}\, H(z - z_0), k_0\right] \\ W_{\omega'} &= W_{\omega'}(0) + \frac{\omega' V_\omega}{\omega V_{\omega'}} W_\omega(0) \left(1 - Sn^2\left[\sqrt{\alpha}\, H(z - z_0), k_0\right]\right) \\ W''_\omega &= \frac{\omega'' V_\omega}{\omega V_{\omega''}} W_\omega(0) \left(1 - Sn^2\left[\sqrt{\alpha}\, H(z - z_0), k_0\right]\right) \end{aligned} \qquad (28)$$

where $k_0^2 = \frac{W_\omega(0)}{W_\omega(0) + \frac{\omega V_{\omega'}}{\omega' V_\omega} W_{\omega'}(0)}$, $\alpha = W_\omega(0) + \frac{\omega V_{\omega'}}{\omega' V_\omega} W_{\omega'}(0)$

and

$$z_0 \simeq \frac{1}{2H\sqrt{\alpha}} \ln \frac{W_\omega(0)}{W_{\omega'}(0)} . \qquad (29)$$

IV. CONCLUDING REMARKS.

In the literature there exists extensive theoretical and experimental work on wave-wave interactions [8-14]. We have tried in this paper to give a few typical examples. Due to the fact that the plasma system, especially if the motion of ions is taken into account, may allow a large number of different waves, one could discuss many more coupling processes. In particular, we should mention the possibility of negative energy waves which coupled with positive energy waves, may give rise to nonlinear instability [16, 17].

The nonlinear effects discussed in this paper are not the only important ones. We have ignored, for instance, plasma wave echoes [18] and wave-

particle interactions (nonlinear Landau damping[1]).

Finally, we want to mention an important application of wave-wave coupling to the scattering of electromagnetic waves by the intemal pulsations of an unstable plasma [19,20]. Of course, for practical applications it is often necessary to take into account finite geometry effects which have been entirely neglected in this paper.

I wish to thank G. Granata for reading the manuscript of this paper.

REFERENCES.

[1] B.B. KADOMTSEV, Plasma Turbulence (Academic Press, New York 1965).

[2] J.A. ARMSTRONG, N. BLOEMBERGEN, J. DUSUINGO and P.S. PERSHAN Phys. Rev. , 127 , 1919 (1962).

[3] I.S. DANILKIN , Zh. Tekh. Fiz., 35, 667 (1965) Sov. Phys. Tech. Phys., 10 , 524 (1965).

[4] M.A. HEALD and C.B. WHARTON, Plasma Diagnostics with Microwaves, John Wiley and Sons Inc., New York (1965).

[5] C. ETIEVANT, S. OSSAKOW, E. OZIZMIR, C.H.SU and I.FIDONE, Phys. of Fluids, 11 , 1778 (1968).

[6] C. CANO, C. ETIEVANT, I. FIDONE , G. LAVAL, J.OLIVAIN, R. PELLAT, M. PERULLI, B. ZANFAGNA, International Conference on Thermonuclear Fusion and Plasma Physics, CN-24/E - 9 , NOVOSSIBIRSK(1968).

[7] L.M. AL'TSHUL and V.I. KARPMAN, Sov. Phys. - JETP, 20 , 1043 (1964).

[8] V.M. TSYTOVICH, Nonlinear Effects in Plasma, Ed . "Nanka", Moscow, (1967).

[9] V.N.TSYTOVICH , Sov. Phys. Tech. Phys., 10 , 605 (1965).

[10] L.M. KOVRIZHNYKH, Sov. Phys. Tech. Phys. , 11 , 1183 (1967).

[11] N.M. KROLL, A. RON, and N. ROSTOKER, Phys. Rev. Lett., 13 , 83 (1964).

[12] M.V. GOLDMAN and D.F. DUBOIS, Phys. of Fluids, 8, 1404 (1965).

[13] R.A. STERN and N. TZOAR Phys. Rev. Lett. 17 , 903 (1966).

[14] A.Y. WONG, M.V. GOLDMAN, F.HAI, and R. ROWBERG, Phys. Rev. Lett. , 21 , 518 , (1968) .

[15] T.J.M. BOYD , Phys. of Fluids, 7, 59, (1964).

[16] B. COPPI, M. ROSENBLUTH, and R. SUDAN, presented at the Sherwood Theor. Meeting, New York University, May , 1967.

[17] V.DIKASOV , L.RUDAKOV , and D. RYUTOV, Sov. Phys., JETP, 21, 608 , (1965).

[18] R.W. GOULD, Phys. Letters, 25 A , 559 (1967) ; R.W. GOULD, T.M. O'NEIL and T.H. MALMBERG, Phys. Rev. Lett. 19 , 219 (1967).

[19] D.M. SAKHOKIYA and V.N. TSYTOVICH, Nuclear Fusion, 8 , 241 , (1968).

[20] V. ARUNASALAM and S. C. BROWN, Phys. Rev. 140 , A.471, 1965.

Non-linear Quasi-neutral Electrostatic Plasma Waves and Shock Waves[*)]

Henri Tasso

Institut für Plasmaphysik GmbH, Garching b. München, W. Germany

The non-linear electrostatic Vlasov equation has been studied in the stationary one-dimensional case by Bernstein, Green and Kruskal[1] using the Poisson equation. The solutions were obtained in two different ways: 1) The full distribution function was given, the density of the ions and electrons was then calculated as a function of the electrostatic potential, and the Poisson equation allowed the potential to be determined. 2) The potential and the distribution functions for all ions (trapped and free) and free electrons were given; an integral equation then allowed the distribution function for the trapped electrons to be calculated. For each solution of 2) it was necessary to verify that this latter calculated function was positive.

This work will show that, by the second method, a wide class of solutions is obtained, namely the quasi-neutral solutions, for which the positiveness condition is automatically satisfied in a potential interval. The existence of such solutions is based on the non-monotony of the distribution functions with respect to the total energy of a particle. Furthermore, quasi-neutrality imposes a maximum on the relative amplitude of the potential.

The basic equations for stationary quasi-neutral waves are:

$$(1)\qquad v\frac{\partial f_\pm(x,v)}{\partial x} \mp \frac{e}{m_\pm}\frac{\partial \varphi}{\partial x}\frac{\partial f_\pm(x,v)}{\partial v} = 0$$

$$(2)\qquad \int_{-\infty}^{+\infty} f_+\,dv = \int_{-\infty}^{+\infty} f_-\,dv \qquad \text{(Quasi-neutrality)}$$

f is the original distribution in v_x, v_y, v_z space integrated over v_y and v_z ; the subscript of v_x has been dropped. The general solution of eq. (1) is:

$$(3)\qquad f_\pm = f_\pm\left(E_\pm\right)$$

where $\quad E_\pm = \frac{1}{2}m_\pm v^2 \pm e\phi$.

Substituting eq. (3) in eq. (2) and denoting "trapped" and "untrapped" by the subscripts t and u, one gets:

$$(4)\qquad \int_{-e\phi}^{-e\phi_{min}} dE\, f_{-t}(E)\left[2m_-(E+e\phi)\right]^{-\frac{1}{2}} = g(e\phi)$$

$$(5)\ \text{where}\quad g(e\phi) = \int_{e\phi}^{\infty} dE\, f_+(E)\left[2m_+(E-e\phi)\right]^{-\frac{1}{2}} - \int_{-e\phi_{min}}^{\infty} dE\, f_{-u}(E)\left[2m_-(E+e\phi)\right]^{-\frac{1}{2}}$$

According to eq. (4) $g(e\phi_{min}) = 0$. When $f_+(E)$ and $f_{-u}(E)$ are given, eq. (4) is an integral equation of the convolution type and following B.G.K[1] the solution is obtained by way of a Laplace transform:

$$(6)\qquad f_{-t}(E) = \frac{(2m_-)^{\frac{1}{2}}}{\pi}\int_{e\phi_{min}}^{-E} dV\,\frac{dg(V)}{dV}\left[-(E+V)\right]^{-\frac{1}{2}}$$

The derivative of $g(e\phi)$, $\frac{dg}{d(e\phi)} \to +\infty$, when $e\phi \to e\phi_{min}$ This is readily seen from eq. (5) if integration over E is replaced by integration over v .

Equation (5) could then be written

$$(7)\qquad g(e\phi) = \int_{-\infty}^{+\infty} f_+\,dv - \int_{\sqrt{\frac{2}{m_-}e(\phi-\phi_{min})}}^{\infty} f_{-u}(\sigma>0)\,dv - \int_{-\infty}^{-\sqrt{\frac{2}{m_-}e(\phi-\phi_{min})}} f_{-u}(\sigma<0)\,dv$$

where σ = sign v

$$(8)\qquad \frac{dg}{d(e\phi)} = \int_{-\infty}^{+\infty}\frac{\partial f_+}{\partial(e\phi)}\,dv - \int_{\sqrt{\frac{2}{m_-}e(\phi-\phi_{min})}}^{\infty}\frac{\partial f_{-u}(\sigma>0)}{\partial(e\phi)}\,dv - \int_{-\infty}^{-\sqrt{\frac{2}{m_-}e(\phi-\phi_{min})}}\frac{\partial f_{-u}(\sigma<0)}{\partial(e\phi)}\,dv +$$

$$+\frac{1}{\sqrt{2m_-}}\cdot\frac{1}{\sqrt{e(\phi-\phi_{min})}}\, f_{-u}\left(v = \pm\sqrt{\frac{2e}{m_-}(\phi-\phi_{min})}\right)$$

Let us assume v integrability for $\frac{\partial f_+}{\partial(e\phi)}$ and $\frac{\partial f_{-u}}{\partial(e\phi)}$

and that $f_{-u}(\sigma>0) = f_{-u}(\sigma<0)$ for $e\phi = e\phi_{min}$

(The latter assumption was not made in a recent work of Montgomery and Joyce[2]).

The first three terms of eq. (8) are then finite for $e\phi \to e\phi_{min}$. The last term goes to $+\infty$ when $e\phi \to e\phi_{min}$, and makes the main contribution to eq. (6) when $E \to -e\phi_{min}$. Calculating this contribution one gets $f_{-t}(E) \to f_{-u}(E)$ when $E \to -e\phi_{min}$. This means that there must be at least a finite interval where $f_{-t} > 0$.

Finally, according to eq. (5), $g(e\phi)$ becomes negative if $e\phi$ is above a certain $e\phi_{max}$; because of eq. (4) f_{-t} is no longer positive anywhere.

CONCLUSION

The use of quasi-neutrality instead of the Poisson equation for non-linear electrostatic waves allows one to prove the positiveness of the trapped particle distribution in a finite interval $\left[e\phi_{max}, e\phi_{min}\right]$. It is possible to give explicitly a class of solutions with a potential which depends arbitrarily on the position, but which has to be limited, and, in order that quasi-neutrality be a good approximation, must have an inhomogeneity length much bigger than the Debye length. The correction on $g(e\phi)$ which comes from $\frac{d^2\phi}{dx^2}$ if the Poisson equation is used makes a small contribution to f_{-t} . If f_{-t} was sufficiently positive the addition of the Poisson term does not change the property. In this way, one can study static electrostatic equilibria, oscillating waves, and shock waves: The density depends on the potential in a simple way.

ACKNOWLEDGEMENT

The author is indebted to Dr. D. Pfirsch for his interest and critical reading of the manuscript.

[*)] This work was performed under the terms of the agreement on association between the Institut für Plasmaphysik and Euratom.

[1] I.B. Bernstein, J.M. Green, M.D. Kruskal. Physical Review, vol. 108, no. 3, 1957, p. 546

[2] D. Montgomery and G. Joyce. University of Iowa 68-24.

ON COLLISIONLESS ION ACOUSTIC SHOCK WAVES

by

D. Biskamp, K. Lackner, D. Parkinson

European Space Research Institute (ESRIN)
of the European Space Research Organisation (ESRO)
Frascati, Italy

ABSTRACT

The well known fluid model for ion acoustic waves [1] ($T_i = 0$, $n_e \sim e^{e\phi/T_e}$) is investigated in further detail with application to the formation and structure of electrostatic shock waves. In particular the following problems are treated:

a) For low Mach numbers ($M<1.6$) stationary shock like solutions exists, where the downstream state consists of a periodic ion acoustic wave[1]. A periodic ion wave is however known to be unstable with respect to long wave length perturbations for sufficiently high amplitudes[2]. This instability is investigated in further detail. It is first shown that this type of instability is a special property of the ion acoustic waves, being absent in similar hydrodynamic systems. Then the development of the instability is studied by means of a computer.

b) Since for higher Mach numbers ($M>1.6$) no stationary, shock like solutions exists, the time evolution of various initial pulses is studied numerically to recover the qualitatively different behaviour of low and high Mach number shocks. Special attention is devoted to the question of overturning of the ions (breaking of the wave).

c) The nonlinear instability due to two interpenetrating ion streams, which might occur in the front of an overturning shock wave, is examined, Growth rates are caldulated (for the case that one stream is very tenuous) and numerical computations are carried through to follow the non-linear evolution.

REFERENCES

1. Moiseev, S.S. and R.Z. Sagdeev, Plasma Phys. 5, 43 (1963)

2. Petviashvili, V.I., Sov. Phys.-Tech. Phys., 13, 149 (1968)

OBSERVATION OF COLLISIONLESS PLASMA HEATING BY STRONG SHOCK WAVES +)

by
R. Chodura, M. Keilhacker, M. Kornherr,
H. Niedermeyer, K.-H. Steuer
INSTITUT FÜR PLASMAPHYSIK
Garching bei München, Germany

Strong shock waves (Mach number between 2 and 4) are produced in a tube of 14 cm inner diameter by the fast rising magnetic field (rise to 12 kG in 0.5 µsec) of a theta pinch discharge (coil length 60 cm). The shock waves propagate into an almost homogeneous, 50 percent ionized hydrogen or deuterium plasma formed by a fast theta pinch preionization. The initial density ranges from 2 to 5 x 10^{14} cm^{-3}, the electron temperature from 3 to 10 eV (both quantities determined by 90° laser scattering) and the ion temperature (from Doppler-broadening of the H_α or D_α-line) from 15 to 30 eV (H_2) or 25 to 50 eV (D_2). The radial distribution of the magnetic field B_o trapped in the initial plasma is measured with six magnetic probes. By slightly varying the filling pressure or the voltage of the preionization theta pinch conditions can be found where the radial variation of B_o is less than 10 %. The amplitude of B_o can be varied between 300 and 1000 G, thereby changing the local β of the initial plasma (β_o = 0.2 - 4) and the Mach number of the shock waves $M = u/\sqrt{V_{Ao}^2+V_{So}^2}$ (u = shock velocity, V_{Ao} = Alfven velocity, V_{So} = sound velocity).

In a previous paper [1] we reported that under the above conditions almost stationary shock waves can be observed with a clear separation between shock front and piston. From a comparison of the measured shock width with the mean free path for Coulomb collisions it was concluded that the shock waves were collision-free. To check this inference and to get insight into the heating mechanism a local measurement of density and electron temperature in the shock wave was carried out using the Thomson scattering of laser light (600 MWatt, 12 nsec laser pulse; spatial resolution 3 mm; spectral resolution by narrow band width interference filters).

Fig. 1 shows a typical example of the measured variation of magnetic field B, density n and electron temperature T_e in a shock wave propagating with M = 2.5 into a preionized deuterium plasma (filling pressure 10 mtorr, B_o = + 900 G, β_o = 0.7). Profiles measured at two radial positions, at r = 3.5 cm (solid lines) and at r = 2.3 cm (dotted lines), demonstrate that in this region the shock front is almost stationary. The first rise in B, n and T_e corresponds to the shock front whose width is about 1 cm, corresponding to 0.6 c/Ω_p (Ω_p = ion plasma frequency).

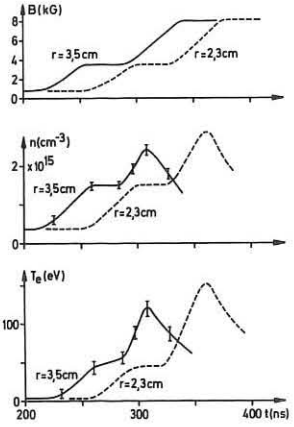

Fig. 1

The jumps in density and magnetic field across the shock front are 3 to 4 and the electron temperature increases from 3 eV in the initial plasma to 45 eV behind the shock. The second rise in temperature to 120 - 150 eV occurs in the piston of the shock wave and is probably due to turbulent heating caused by the high current densities in the piston region. More examples of measured shock profiles are published in ref. [2].

We now check whether the rise in electron temperature measured in the shock front can be ascribed to adiabatic compression and Ohmic heating. The energy equation for the electrons in a plane, stationary shock front moving in x-direction is

$$\frac{3}{2} n k u_x \frac{dT_e}{dx} = -nkT_e \frac{du_x}{dx} + \eta j^2 \qquad (1)$$

The current density j and the velocity u_x can be calculated from measured magnetic field and density profiles, using Ampere's law and continuity equation, respectively. Inserting Spitzer's resistivity ($\eta \sim T_e^{-3/2}$), integration of (1) leads to a temperature profile given by the dotted line in Fig. 2. Comparison with the measured profile shows that only 20 % of the observed electron heating can be accounted for by collisional resistive and adiabatic heating, indicating that appreciable collisionless electron heating takes place. The measured profile can be gained from (1) inserting $\eta = \eta_{turb} = m_e \nu_{eff}/ne^2$ assuming a constant collision frequency ν_{eff} almost two orders of magnitude higher than the classical value and roughly equal to the ion plasma frequency Ω_p.

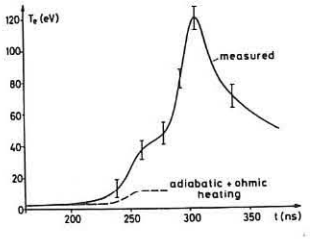

Fig. 2

From the steady state conservation relations the total shock heating $(T_e + T_i)_2$ can be derived. As T_{e2} is known from the laser scattering measurements, the ion temperature T_{i2} behind the shock can be estimated. For the example of Fig. 1 we get $T_{i2} \approx$ 110 eV, which in the main can be explained by adiabatic ion heating. For shock waves with higher Mach numbers however the calculated ion temperatures exceed those one would expect for a merely adiabatic heating.

The time dependent complete profiles of magnetic field, density, electron and ion temperature were calculated using a two fluid model [3]. The classical electron-ion collision frequency $\nu_{Spitzer}$ was increased by an effective collision frequency $\nu_{eff} \sim \sqrt{n}$ ($\nu_{eff} \approx \Omega_p \gg \nu_{Spitzer}$). Ion heating was assumed to be adiabatic.

[1] R. Chodura, M. Keilhacker, M. Kornherr, H. Niedermeyer; Proc. of III^rd Conf. on Plasma Physics and Controlled Nuclear Fusion, Novosibirsk 1968, paper CN - 24/A - 3

[2] M. Keilhacker, M. Kornherr, K.-H. Steuer; Z.f. Physik (in press 1969)

[3] R. Chodura; Phys. Fluids, 11 (1968), 400

+) This work was performed as part of the joint research program of the Institut für Plasmaphysik, Garching, and Euratom.

ON THE MECHANISM OF PLASMA HEATING BY COLLISIONLESS SHOCKS

V.G.Eselevich, A.G.Eskov, R.Kh.Kurtmullaev, A.I.Malutin

Institute of Nuclear Physics
Siberian Department of the USSR Academy of Sciences
Novosibirsk, USSR

Oscillatory structure of oblique shocks was predicted theoretically/1,3/ and confirmed experimentally/2,4,5,7/. However at Mach number $M > M_c$ ($M=u/v_A$, u - wave velocity, v_A - Alfvén speed, M_c - critical Mach number) destruction of front oscillatory structure is possible/4,6/.

In the present experiment oblique shocks were excited in cylindrical plasma volume 16 cm in diameter (initial hydrogen plasma density $n_0 \sim 5.10^{13} \div 10^{15}$ cm^{-3}, initial magnetic field 100÷1000 gauss) with a magnetic piston produced by shock loop/5/. Local values of the components of magnetic and electric fields were measured with probes placed in the (r,z) plane. Investigation of plasma dissipative nature was carried out by study of macroscopic distribution of main parameters within the front as well as by measurement of electric field microfluctuations.

Connection between various parameters within shock front, assuming shock is stationary, may be obtained from the force-balance equation including ion inertia, magnetic and electric pressure. In shock reference frame

$$p_e - p_0 = n_0 m_i u^2 \left(1 - \frac{V_n}{u}\right) - \left(\frac{H^2}{8\pi} - \frac{H_0^2}{8\pi}\right) \qquad (1)$$

where p_0 and p_e - electron pressure before and within front, m_i - ion mass,

$$V_n = \left[1 - \frac{2e}{m_i u^2}\left(\int_0^x E_n(x')dx' + \frac{u \sin 2\theta}{2M^2 c}\int_0^x H_\varphi(x')dx'\right)\right]^{\frac{1}{2}} \qquad (2)$$

E_n - normal component of electric field,
H_φ - azimuthal component of magnetic field,
θ - angle between the shock front and magnetic field.

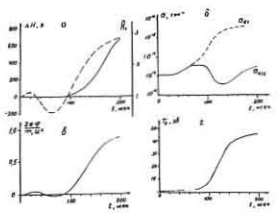

Fig 1.

In Fig.1(a,δ,ε) we show the experimental time-dependence of H, $n=n_0 u/v_A$, $\varphi = \int_0^x E_n(x')dx'$ and $T_e = p_e/n$ in the oblique shock. A lag of density profile from magnetic profile (previously established by interferometric method/4/) testifies that plasma electric conductivity within front is low. Fig.1(ε) shows that electrons are heated essentially in the region of H jump. The measured value of T_e in wavetrain is very small under our conditions and may be explained by collisional dissipation. Conductivity variation within front may be determined from the following relation

$$\frac{d}{dt}\frac{p_e}{n(\gamma-1)} = \frac{j^2}{\sigma n} - p_e \frac{d}{dt}\frac{1}{n} \qquad (3)$$

where current $\vec{j} = (c/4\pi)\,rot\vec{H}$.
Conductivity growth in wavetrain is proportional to $T^{3/2}$ whereas in the region of main jump sharp fall of conductivity up to anomalous low value $\sigma_{ef} = 10^{-3}\sigma_{ei}$ is observed. It was established that this fall is connected with realization of conditions: $T_e \gg T_i$ and $v_d \gg c_s$ where v_d - electron drift velocity, c_s - ion-sound velocity.

With diamagnetic probes the dependence of electron pressure behind shock front on relative amplitude $h = \frac{H_{t2}}{H_{t1}}$ (H_{t1} and H_{t2} are tangential components of magnetic field before and behind shock front, respectively) was measured [8].

Since the experimental results are close to calculated Hugoniot curve (Fig.2, solid line) one may state that at $h < h_c$ ($M < M_c$, respectively) preferential heating of plasma electrons and predominance of resistive dissipation takes place. It may be supposed that ion pressure is increased sharply at $M > M_c$ in order to explain the variation of nT_e dependence.

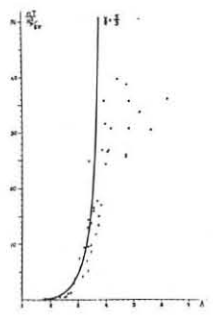

Fig 2.

It is very important that overturning of an oblique shock observed in other experiments/6/ also takes place at $M=M_c$. The M_c dependence on θ was discovered (for instance, $M_c \simeq 3$ at $\theta = 0^0$; $M_c = 4.5 \div 5.5$ at $\theta \simeq 30^0$). The dependence of front width Δ on θ for Mach numbers $M \sim 2 \div 3$ was also investigated. Fig.3 shows that at $\theta < 14^0$ the Δ value is constant and coincides with a width of dissipative front of perpendicular shock being equal to $10\frac{c}{\omega_0}$ (ω_0 - plasma electron frequency. Therefore for these angles resistive dissipation is constant ($\nu_{ef} \sim 10 M\omega_r$ where ω_r - hybrid Larmor frequency $\omega = \frac{eH_0}{c\sqrt{m_i m_e}}$) and skin-depth is larger than dispersion length $\frac{c}{\Omega_0}\theta$ (Ω_0 - plasma ion frequency).

If one assumes that effective collision frequency is weakly dependent on θ at $\theta > 14^0$ and is equal to $10M\omega_r$ than corresponding skin-depth is smaller than dispersion length and oblique shock keeps oscillatory structure under turbulent dissipation conditions. Observed front width increases proportionally to θ^2 and agrees with estimation

$$\Delta \sim B \frac{u}{v_{ef}} \frac{m_i}{m_e} \theta^2 \qquad (4)$$

(B - amplitude-dependent coefficient being equal to 1/3 at $M \sim 2 \div 3$).

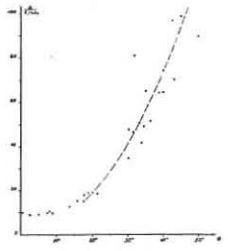

Fig 3.

In order to estimate relative effect of pair collisions on dissipation and to find limits of collisionless approach the dependence of shock front width on initial plasma density was investigated (Fig.4). It is seen that front width is constant up to 10^{15} cm^{-3} hence collisionless dissipation is dominant (Fig.4a, $\theta \sim 0^0 \div 14^0$, $\Delta \simeq 10\frac{c}{\omega_0}$). The increase of Δ at $n_0 > 2.10^{15}$ cm^{-3} is connected with a rise of pair-collision influence. ($\nu_{ef} \sim 10^6 \theta$ sec^{-1}, temperature behind front $T_e \simeq 5$ eV, plasma density $n \simeq 5.10^{15}$ cm^{-3}). Transition to aperiodic profile at larger θ (Fig.4b, $\theta \sim 20^0$) takes place at a larger n_0 values which is connected with a growth of characteristic dispersion length $\frac{c}{\Omega_0}\theta$.

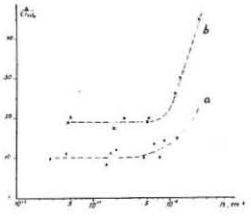

Fig 4.

Microfluctuations were measured with double electric probe/6/ in argon plasma at $n_0 \sim 10^{12}$ cm^{-3} and $M < M_c$. Electrostatic oscillations with frequencies close to Ω_0 were detected in oblique shock front when condition $v_d > c_s$ was fulfilled.

Combination of the described experimental results indicates that there exists anomalous resistive dissipation in the oblique shock at $M < M_c$ which seems to be explained by ion-sound instability. At $M > M_c$ the resistive dissipation is of no more importance.

The authors are indebted to R.Z.Sagdeev for stimulating discussions.

REFERENCES

1. R.Z.Sagdeev, Review of Plasma Theory, Vol.4, 20, Atomizdat, Moscow, 1964
2. A.M.Iskoldsky et al, Zhur.Eks.Teor.Fiz., 47, 774 (1964)
3. K.W.Morton, Phys. Fluids, 7, 1800 (1964)
4. V.G.Eselevich et al, Report on Second Euro. Plasma Conf. Stockholm, 1967
5. V.G.Eselevich et al, ZETF Pis'ma, 7, 65 (1968)
6. S.G.Alikhanov et al, Report CN-24/A-1, IAEA Plasma Conf. Novosibirsk, 1968
7. A.E.Robson et al, Report CN-24/A-6, IAEA Plasma Conf. Novosibirsk, 1968
8. R.Kh.Kurtmullaev et al, Preprint 228, Novosibirsk, 1968

QUASI-LINEAR THEORY OF THE ION WAVE INSTABILITY

by

D. Montgomery and G. Vahala

The University of Iowa, Iowa City, Iowa 52240, U.S.A.

Quasi-linear theory[1,2,3] treats, under certain assumptions, the evolution of unstably growing electron plasma oscillations produced by a tenuous stream of high-velocity electrons. We treat here an attempted generalization to the ion wave instability. The positive ions are considered mobile, and the electrons initially stream through them. Since it is still far from clear what the domain of validity of quasi-linear theory is,[4] it is of interest to see what results similar assumptions give in other situations.

The problem is made one-dimensional by assuming a strong magnetic field parallel to the streaming direction. The quasi-linear approximations lead to a diffusion-like equation for the time development of $f_j(v,t)$, the velocity distribution of the jth species of particle (charge e_j, mass m_j, plasma frequency ω_{pj}):

$$\frac{\partial f_j}{\partial t} = \left(\frac{e_j}{m_j}\right)^2 \frac{\partial}{\partial v}\left(\mathcal{D}\frac{\partial f_j}{\partial v}\right) \qquad (1)$$

where $\mathcal{D}$ is given by

$$\mathcal{D}(v,t) = \lim_{L\to\infty} \int_{-\infty}^{\infty} \frac{dk(2\pi/L)\,|E(k,t)|^2}{i(kv - \omega(k))} \qquad (2a)$$

$$\tilde{=} \; 2\pi\,|v - v_g|^{-1}\,\mathcal{E}(v,t)\,. \qquad (2b)$$

$E(k,t)$ is the kth Fourier component of the electric field, and the spectral density is $\mathcal{E}(v,t) = \lim_{L\to\infty}(2\pi/L)\,|E(\omega_r(v)/v,t)|^2$. L is the length of the plasma. $E(k,t)$ varies temporally as $\exp(-i\omega(k)t)$, where the slowly-varying (complex) frequency $\omega(k) = -\omega^*(-k)$ has its real and imaginary parts instantaneously determined by the solution of ($\omega_i(k) \ll \omega_r(k)$):

$$1 = \Sigma_j \frac{\omega_{pj}^2}{k^2} P\int \frac{\partial f_j(v,t)/\partial v}{v - \omega_r(k)/k}\,dv\,, \qquad (3a)$$

and

$$\omega_i(k) = \frac{-\pi\,|k|\,\Sigma_j\,\omega_{pj}^2\,\partial f_j(\omega_r(k)/k,t)/\partial v}{\Sigma_j\,\omega_{pj}^2\,P\int \frac{\partial^2 f_j(v,t)}{\partial v^2}\,\frac{dv}{v - \omega_r(k)/k}}\,. \qquad (3b)$$

$\omega_r(v)$ means the solution of $\omega_r(k) = kv$ for fixed v, and in Eq. (2b), v_g is the group velocity of a wave with phase velocity v. If $v_g \ll v$, Eq. (2b) reduces to the usual result[1,2,3] for the single species case. $\partial\mathcal{E}/\partial t = 2\,\omega_i\,\mathcal{E}$, as usual.

If we include (as usual) only non-negative $\omega_i(k)$, $\mathcal{D}$ is ≥ 0. Therefore each f_j obeys separately an "H-like" theorem,[3] and in that interval of velocity where $\mathcal{E}(v,\infty) \neq 0$, it develops a flat "plateau". The height of each plateau is uniquely determined by conservation of particles ("equal area rule"). The equal area rule also applies to any linear combination of the f_j. The end points $(v_1,v_2$, say) of the interval are the same for each f_j.

To determine v_1 and v_2, we need to consider the details of the formation of the plateau more carefully than is necessary in the immobile ion case, where v_1 and v_2 are uniquely determined simply by applying the equal area rule to $f_e(v,0)$. We assume the $f_j(v,t)$ remain continuous in v. The region of non-zero $\mathcal{E}(v,t)$ broadens with increasing t until one reaches such values of v that the immediately adjacent values lie on portions of the curve $\Sigma_j\,\omega_{pj}^2\,\partial f_j(v,t)/\partial v$ for which Eq. (3b) predicts no growth. This implies that the equal area rule must be applied to the function $\Sigma_j\,\omega_{pj}^2\,f_j(v,0)$. This makes v_1 and v_2 unique, and fully determines the $t\to\infty$ state.

This is shown in Fig. 1a, which applies to an electron-proton plasma with enough initial relative drift to make the ion acoustic branch of the dispersion relation weakly unstable. Figures 1b and 1c show f_e and f_i separately. Note that only minor modifications have occurred for f_e, but that considerable ion heating has occurred: f_i has been broadened significantly [Figs. 1b and 1c are on different scales, but v_1 and v_2 are the same for all three curves]. In this example, initially Maxwellian

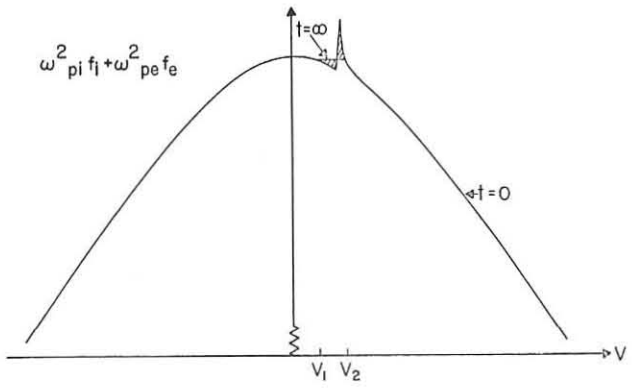

FIG. 1a

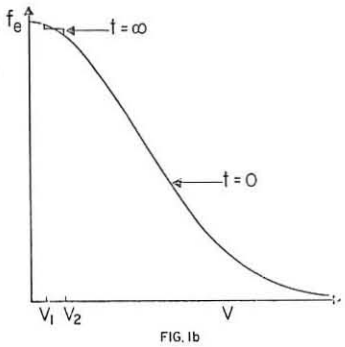

FIG. 1b

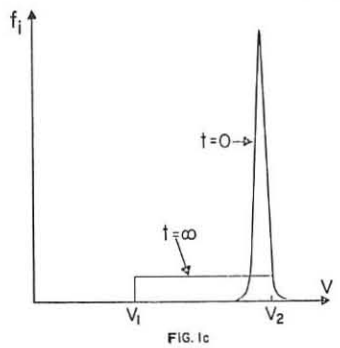

FIG. 1c

electrons and protons drift with relative velocity $V_d \tilde{=} 0.25\sqrt{kT_e/m_e}$, $T_e/T_i = 20$, and so have maximum $\omega_i/\omega_r \tilde{=} 0.12$; the ratio of final to initial ion temperature is about 60; there is no comparable turbulent heating in the electron plasma case. Note that momentum conservation is severely violated.[5]

This work was supported by NASA Grant NGR-16-001-043 at The University of Iowa.

FOOTNOTES

[1] A. Vedenov, E. Velikhov and R. Sagdeev, Nucl. Fusion, 1962 Suppl., p. 465.

[2] W. E. Drummond and D. Pines, ibid., p. 1049.

[3] I. B. Bernstein and F. Englemann, Phys. Fluids 9, 937 (1966).

[4] See, e.g., T. P. Armstrong and D. Montgomery, Univ. of Iowa Report 69-10 (1969)

[5] The form Eq. (2a) for $\mathcal{D}(v,t)$ leads to conservation of momentum and energy, but Eq. (2b) does not. Indeed, it is clear that the "equal area rule" can never apply to the unapproximated form (2a), either here or in the usual theory,[1,2,3] since the "equal area rule" manifestly violates conservation of momentum. It is at the present time an open question as to what the $t\to\infty$ solution of the quasi-linear equations is when the unapproximated expression (2a) is used for $\mathcal{D}$, even in the case treated in References 1-3.

COMPUTATIONS OF THE NONLINEAR GROWTH OF THE ION SOUND INSTABILITY IN TWO DIMENSIONS

by

I. Cook, B. McNamara, A. Sykes, J. Boris

U.K.A.E.A., Culham Laboratory, Abingdon, Berks., England.

Introduction. The nonlinear theory of the ion sound instability and its role in collisionless shocks is investigated and reported in reviews by Sagdeev[1,2], Galeev[2], Kadomtsev[3] and others. Strong ion sound oscillations are observed in, for example, the collisionless shock experiment TARANTULA[4] and the turbulent heating experiment TWIST[5] but the agreement between theory and experiment is only qualitative. The ion sound seen experimentally is driven by magnetic field and density gradients in a plasma carrying a turbulent spectrum of Langmuir oscillations. The theory has been done mostly for ion sound in an unmagnetised, quiescent, uniform plasma.

The present investigation aims to relate theoretical studies to a numerical experiment to justify the many simplifying assumptions required.

Nonlinear Theory. Following Kadomtsev[3] one can derive equations for the coupling between ion-sound waves, Langmuir waves, and the particle distribution functions. The nonlinear processes which arise in leading order are: Landau damping of ion sound on beats between waves propagating at an angle to each other; The quasi-linear distortion of the electron distribution function f_e by scattering from ion sound; Decay of Langmuir waves into ion sound; Diffusion of energy in the Langmuir waves to longer wavelengths.

The spectral density I_K is defined to be the ensemble average of the Fourier transform of the electrostatic potential,

$$\langle \phi^*_{K'\omega'}\, \phi_{K\omega} \rangle \equiv \left[I^{\ell}_K\, \delta(\omega-\omega_K) + I^{s}_K\, \delta(\omega-\Omega_K) \right] \delta(K-K')\, \delta(\omega-\omega').$$

The superscripts denote Langmuir and sound wave densities. The wave kinetic equation for ion sound can be written as

$$\frac{1}{2}\frac{\partial I^s_K}{\partial t} = \gamma^s_K I^s_K + \frac{\Omega_o^2 T_i}{2M^2\Omega_K^3 k^2 n}\, I^s_K \int (K.K')^2\,(K\times K')^2\,\delta'(|K-K'|\sqrt{\frac{T_e}{M}})\, I^s_{K'}\, dK'$$

$$+ I^s_K \frac{\omega^3}{2\Omega_o^2}\left[\mathrm{Im}\int \frac{v_{s\ell}\, v_{\ell s}}{\varepsilon(K-K',\omega_{K'})}\, I^{\ell}_{K'}\, dK' - \frac{4\pi e^4}{3k^5}\int \frac{(K.K')^2}{\omega_{K'}}\frac{\partial^4 f_e}{\partial V^4}\right.$$

$$\left. \delta(\Omega_K-K.V)\, I^{\ell}_{K'}\, dV\, dK' \right] + \frac{\pi}{8}\frac{\Omega_K^6}{\Omega_o^4}\int |v_{s\ell}|^2\, \delta(\Omega_K-\omega_{K'}$$

$$-\omega_{K-K'})\, I^{\ell}_{K'}\, I^{\ell}_{K-K'}\, dK' \qquad (1)$$

where the matrix elements are given by

$$v_{s\ell} = \frac{4\pi e^3}{k^2M^2}\int \frac{dV}{(\Omega_K-K.V)^2}\,\frac{1}{\omega^2_{K'}}\left[(K.K'')(K'.V)K' + (K.K')(K''.V)K''\right].\frac{\partial f_e}{\partial V}$$

$$v_{\ell s} = \frac{4\pi e^3}{k^2m^2}\int \frac{K'.(K-K')}{\omega^2_{K'}(\Omega_K-K.V)}\, K.\frac{\partial f_e}{\partial V}\, dV$$

γ_K is the growth rate of the K^{th} mode and ε is the usual linearised dielectric constant

$$\varepsilon(K,\omega) = 1 + \sum_j \frac{4\pi e^2}{m_j k^2}\int \frac{K.}{(\omega-K.V)}\frac{\partial f_j}{\partial V}\, dV.$$

A similar equation to (1) describes the intensity of Langmuir waves. The quasilinear equation for the electron distribution function to be used in this dielectric constant is

$$\frac{\partial f_e}{\partial t} = \left(\frac{e}{m}\right)^2 \int dK\, K.\frac{\partial}{\partial V}\left(\frac{\gamma^s_K}{(\Omega_K-K.V)^2+\gamma^{s2}_K}\, K.\frac{\partial f_e}{\partial V}\right) I^s_K$$

The principal assumptions used in the derivation of these equations are that $\gamma_K \ll \omega_K$, $\omega_K \simeq (4\pi ne^2/m)^{\frac{1}{2}} \gg \Omega_K \simeq k(T_e/M)^{\frac{1}{2}}$, $\Omega_o^2 = 4\pi ne^2/M$, $k\lambda_D \equiv k(T_e/4\pi ne^2)^{\frac{1}{2}} \ll 1$, $\delta = m/M \ll 1$, $\theta = T_e/T_i \gg 1$ and only the leading term of every possible expansion is retained.

Characteristic Times. The linear theory of the ion sound instability is given by Fried and Gould[6]. In its simplest form this theory shows that a relative drift velocity of the ions and electrons greater than $V_o = \sqrt{T_i/m}$ will drive the ion sound instability with a small growth rate of order $k\lambda_D(\delta/\theta)^{\frac{1}{2}}$. The plasma also supports Langmuir oscillations which must be taken into account in numerical calculations.

A crude estimate of the nonlinear Landau damping rate γ_L in units of the plasma period for fully developed ion sound gives

$$\frac{\gamma_L}{\omega_o} \sim \frac{kV_o}{\omega_o}\frac{\delta^{\frac{1}{2}}}{14}\quad n\,\frac{1}{k\lambda_D}.$$

Similar estimates of the rate of decay into ion sound γ_I and diffusion rate γ_D of Langmuir waves of wave number k_o and amplitude ϕ give

$$\frac{\gamma_I}{\omega_o} \sim \frac{k_o\lambda_D}{2}\,\delta^{\frac{1}{4}}\,\left(\frac{\phi}{T_e}\right), \qquad \frac{\gamma_D}{\omega_o} \sim (k_o\lambda_D)^5\,(\phi/T)^2.$$

Numerical Experiments. The equations of motion of a 'plasma' of 8192 electrons and 8192 ions moving in a square region in the X-Y plane are integrated using periodic boundary conditions in both directions. The equations are

$$\frac{dX_j}{dt} = V_j \qquad \frac{dV_j^+}{dt} = -\,\delta/p(J/64)^2\nabla\phi \qquad \frac{dV_j^-}{dt} = +\,(J/64)^2\nabla\phi$$

and

$$\nabla^2\phi = (n_e-n_i)$$

where J^2 is the number of Debye squares in the region, p is the average number of electrons in each of 64×64 cells in the region and n_e, n_i are the number of electrons and ions in each cell. Poisson's equation is solved by a fast Fourier transform method. Acceptable running times for the computer program are given by $\delta = 1/16$, $T_e/T_i = 4$ and $J = 16$ when the nonlinear effects can be observed in about 100 electron plasma periods. The particle positions and velocities and the Fourier coefficients of the potential are recorded on magnetic tape for subsequent analysis. Movies have been made of the plasma behaviour in phase space and spectral density in K-space.

Runs with the relative streaming velocity of ions and electrons just below the two-stream threshold show the growth of a wide spectrum of oscillations which levels off at about 50 plasma periods. The growth rate compares well with the growth rate of ion sound. A distinct enhancement of the growth is produced by an initial electron distribution function corresponding to a nonlinear Langmuir wave as given by Bernstein et al.[9]. This includes a distribution of trapped electrons which have not been taken into account in the wave-kinetic theory and it remains to discover how important this effect is.

References

(1) SAGDEEV, R.Z., Reviews of Plasma Physics, 4, Consultants Bureau, New York, (1967).

(2) SAGDEEV, R.Z. and GALEEV, A.A., International Centre for Theoretical Physics, Trieste. IC/66/64.

(3) KADOMTSEV, B.B., Plasma Turbulence, Academic Press, 1965.

(4) PAUL, J.W.M., Private Communication.

(5) HAMBERGER, S.M. et al., 3rd European Conference on Plasma Physics, Utrecht (1969).

(6) FRIED, B.D., GOULD, R.W., Phys. Fluids 4, 1, 139 (1961).

(7) BERNSTEIN, I.B., GREEN, J.M. and KRUSKAL, M.D., Phys. Rev. 108, 3, 546, (1957).

PLASMA HEATING BY MAGNETOSONIC RESONANCE METHOD

I.A.Kovan, V.D.Rusanov, A.M.Spektor, D.A.Frank-Kamenetskii

I.V.Kurchatov Institute of Atomic Energy, Moscow, USSR

The phenomenon of magnetosonic resonance, predicted theoretically /1/ was observed experimentally in 1958 /2/ . The effect of amplification of magnetosonic (ms) waves under the condition of resonance has been described in /3,4/. The possibility of applying the ms resonance for plasma heating was proved in /5,6/ . The present work is concerned with a study of the physical nature of ms resonant heating.

Plasma was prepared and heated in a magnetic field under the action of hf waves produced by a 300 kw generator with a frequency of 20 mhz (fig.1). The maximal temperature has been attained at a concentration of hydrogen plasma 10^{13} cm^{-3} and static magnetic field strength 2 koe, which corresponds to the ms resonance condition for a plasma column 6 cm in diameter /5,6/ .

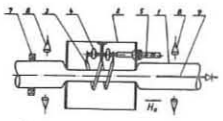

Fig. 1.
Experimental arrangement. 1-diamagnetic gange, 2-uhf interferometer, 3-6hf inductor, 7-vacuum chamber, 8-magnetic probe.

For the study of hf magnetic field configuration magnetic probes have been employed. The radial distribution of H_z in central cross-section beneath the hf inductor is shown by the curol 1 in fig. 2, where the vacuum field on the axis is taken as unity. The radial H_z dependence is represented by the expression

$$H_z(z,0) \approx i\,\frac{4\pi}{c} I\left[A\,2J_0(\mu_0 \tfrac{z}{z_0}) - i\,\tfrac{2z}{z_0} J_1(\mu_0 \tfrac{z}{z_0})\right], \qquad (1)$$

which comprises a superposition of a proper oscillation (curve 2) and a sagged field of the inductor (curve 3). Herein A is a coefficient depending on the geometry of the inductor and on dissipative properties of the plasma, $\mu_0 = 2{,}4$, $z_0 = 3$ cm is the radius of the plasma column, I - surface current density in the inductor.

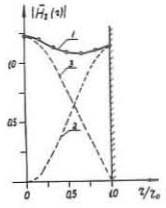

Fig. 2.
Radial H_z distribution in central plane.

Outside the inductor the radial wave field distribution, shown in fig.3, approximates the proper function $J_0(\mu_0 \frac{z}{z_0})$.

The axial H_z distribution is shown in fig. 4. Outside the inductor a progressive wave is propagated with a wave-number k and the amplitude decreasing as exp (-kz), whence:

$$K = \frac{\omega_{Hi}\,\mu_0}{\omega \cdot z_0}\,\frac{1}{\sqrt{2Q}} \qquad (2)$$

Here ω_{Hi} is the ion cyclotron frequency, Q - the quality of the plasma, ω - wave frequency

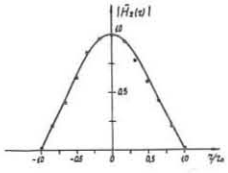

Fig. 3.
Radial H_z distribution outside the inductor (32 cm out the central plane).

Experimental value of k deduced either from the amplitude decline or from the ratio H_r/H_z is 0,05 cm^{-1}, whence by the formula (2), Q = 4. The quality Q can also be estimated from the spatial field amplification η in the central plane. According to the theory

$$\eta = 2\sqrt{Q}\,\frac{\omega_{Hi}\,\ell}{\omega \cdot z_0} \qquad (3)$$

Substation of numerical values (ℓ = 9 cm, r_0 = 3 cm, $\frac{\omega_{Hi}}{\omega} = \frac{1}{7}$) leach for the measured value η = 1,2 to Q = 2. The quality defined as a ratio of reactive power the measured loss power has the value between 1.5 and 2.

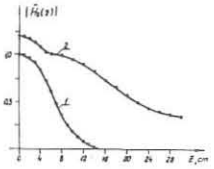

Fig. 4.
Axial H_z distribution.
1 - in vacuum;
2 - in plasma.

The attenuation observed is 2-3 orders of magnitude more than the dissipation due to binary collisions or to the Cherenkov mechanism. The anomalous dissipation is, according to /7/ , connected with the instability of the azimuthal current of the ms wave bading to the excitation of short-wave potential oscillations of the frequency $(\omega_{Hi} \cdot \omega_{He})^{1/2}$.

The theoretical Q-value is then given by the expression:

$$Q = \sqrt{\frac{\omega_{Hi} \cdot \omega_{He}}{\omega}} \qquad (4)$$

This gives for a hydrogen discharge Q = 7. The discrepancy between Q-values calculated by various methods may be explained by the non-linear nature of damping. The instability of the type considered leads to an effective ion heating, the ion temperature tending according to the theory /7/ to the value:

$$T_i = \frac{M\omega_{Hi} \cdot z_0 \cdot U}{4} \qquad (5)$$

where U is the directed azimuthal electron velocity. For our experiments with hydrogen discharge U = 3.10^7 cm/sec and the formula (5) gives T_i = 450 eV.

Our experiments in an uniform magnetic field /5,6/ give the dependence of T_i on the ion mass and the velocity U (fig.5) in good agreement with the formula (5) but the absolute value of T_i, measured by means of an external diamagnetic gange outside the inductor, was only about 100 eV. In a magnetic mirror trap the ion temperature, measured in the same manner, approached the theoretical value 300 - 400eV. It follows that the low temperature, measured in the uniform magnetic field, is due to the cooling of the plasma streaming out from the inductor. This explanation is confirmed by direct measurements of nT by means of a miniature diamagnetic gange (fig. 6).

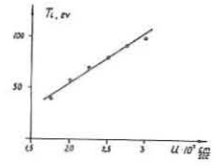

Fig. 5.
Dependence of T_i on U.

The results obtained permit us to conclude that the possibilities of plasma heating in magnetic traps by the method considered here are quite promising.

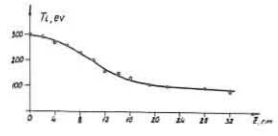

Fig. 6.
Axial T_i distribution.

REFERENCES

1. D.A.Frank-Kamenetskii. Journ.Tech.Phys.,30,899(1960).
2. A.P.Akhmatov et al. JETP, 39,536(1960).
3. I.A.Kovan, B.I.Patrushev, V.D.Rusanov, G.N.Tilinin, D.A.Frank-Kamenetskii, JETP, 43, 16 (1962).
4. V.D.Rusanov, V.P.Smirnov, D.A.Frank-Kamenetskii, Nucl.Fusion, 3, 38 (1963).
5. I.A.Kovan, A.M.Spektor, JETP, 53, 116 (1967).
6. I.A.Kovan, L.L.Kozorovitskii, I.M.Podgorny, V.D.Rusanov, V.P.Smirnov, A.M.Spektor, D.A.Frank-Kamenetskii, Atomic Energy, 25, 503 (1968).
7. V.I.Arefyev, I.A.Kovan, L.I.Rudakov, JETP, Letters, 7, 286 (1968).

substituted paper

PLASMA TURBULENT HEATING IN THE TOR WITH A CURRENT

O.A.Zinoviev, G.D.Milnikov, V.D.Rusanov,
A.V.Titov.
I.V.KURCHATOV INSTITUTE OF ATOMIC ENERGY,
Moscow, USSR

Turbulent heating of plasma in a toroidal system with a current has been investigated experimentally [1]. Impulse of a vortex e.m.f. about 0,3 μsec-long which generated instability in a plasma was produced by a discharge of a condenser 19 μF onto the conductivity casing enclosing the ceramic vacuum chamber (Fig.1). Initial plasma was prepared by a quasi-stationary current discharge (I_o=I-3 kA) in a magnetic field (H_o=4-6 kgs). The current column diameter was confined by a 4cm diaphragm. The hydrogen pressure was $p=4.10^{-4}$ - $1,5.10^{-3}$ torr, the electron concentration was within the range of 2.10^{13} - 10^{14} cm^{-3}, the electron temperature was of order of 5 ev.

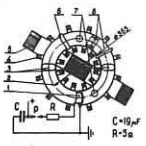

Fig.1. The shheme set-up.
1-ceramic chamber; 2-copper casing; 3-pump out; 4-toroidal solenoid; 5-transformer; 6-diamagnetic coil; 7-microwave interferometer (λ=4mm); 8-Rogowski coils.

The shape of short impulse of the voltage induced in the plasma is shown in Fig.3. There were two ways to apply the e.m.f. to the quasi-stationary current: cophased or antiphased. The sequence of processes in the set-up is shown in Fig.2. If e.m.f. is applied along the direction of the quasi-stationary current, the summary current strongly will increase during the time of order of 0,3 μsec up to the value which is four times larger than the initial level. The total e.m.f. after short-time rising from 0,5 v/cm up to 40v/cm will fall down to a value close to zero. The drop must correspond to a sharp increase of the plasma conductivity. The current having increased to the maximum keeps constant.

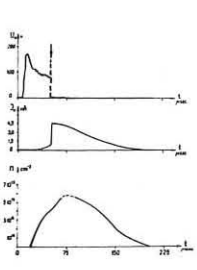

Fig.2. Behaviour of the main processes.

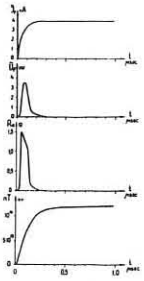

Fig.3. The heating phase.

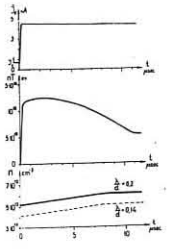

Fig.4. Behaviour of $\tilde{I}_p$, nT and n against the Time.

Behaviour of the plasma pressure and the plasma effective resistance R_a during the heating process are shown on Fig.3. It is seen that the resistance goes up to 1,5 Ω for the time $\tau \sim 0,1$ μsec. At this moment there is a break in the curve $R_a(t)$. The point of break may be compared with the current value in the plasma $\tilde{I}_p$=1,8 kA.

As nT increases, the resistance R_a falls and when nT reaches the value of $1,5.10^{16}$ $ev.cm^{-3}$ ($\tau \sim 0,3$ μsec) which corresponds to the plasma column diameter of 3 cm, the resistance decreases by a factor of ten, the value of the initial concentration being practically invariable. The temperature estimated from the value of the diamagnetic signal is $T_e + T_i$ = 300-500 ev.

Diamagnetism of plasma decreases less than by a factor ≤ 2 for the time of 14 μsec, current amplitude in plasma does not vary practically, and the concentration increases by 50-60 % for the time about 5 μsec. The latter process is connected with an additional ionization of a residual gas and probably with the resorbtion of gas from the walls and diaphragm (see Fig.4).

High values of nT (> 10^{16} $ev.cm^{-3}$) correspond to plasma overheating for the longitudinal current I_{max}=5,5 kA, what is expected to induce the drop of nT [2].

It should be noted that rising of the anomalous resistance of plasma occurs at a certain value of current and is accompanied by an intensive increase of nT. In the contrary, at a current maximum of order of 4kA, the resistance falls sharply ($nT=9.10^{15}$ $ev.cm^{-3}$). Hence we have two trhreshold values for the current and for the directed electron velocity.

The first threshold takes place at T_{eI}=40 ev and $\tilde{I}_{pI}$ = =1,8 kA, the second- at T_{eII}=200 ev and $\tilde{I}_{pII}$=4 kA. The comparison of these results for the plasma diameter of order of 3cm gives $U_I=3.10^7$ $cm.sec^{-1}$, $(T_e/M)^{1/2}=6.10^6$ cm/sec and $U_{II}=6.10^7$ cm/sec, $(T_e/M)^{1/2}=1,2.10^7$ cm/sec.

For the heating regime (cophased) the radiation was not observed practically near ω_o. The radiation appears to be present for antiphased switching on when the initial current is destroyed.

Thus the possibility of the intensive plasma turbulent heating and the assimilating of nT at cophased e.m.f. is shown. The qualitation between heating and the excitation of ion acoustic instability is established.

This method is perspective for a toroidal current system of the "Tokamak" type. Unfortunely, the thikness of heating layer and the plasma column diameter are not understood yet for the case $c/\omega_{oi} \ll a$.

References

1. E.K.Zavoiski et al. Report CN- 24/L-I, Novosibirsk, USSR (1968).
V.Ya.Balakhanov, V.K.Zivotom, O.A.Zinoviev, G.D.Milnikov, V.D.Rusanov, A.V.Titov, JETP, 56, 439 (1969).

2. V.D.Shafranov. Atomnaya energiya, 13, 521 (1962).

substituted paper

COLLECTIVE INTERACTIONS AND PLASMA HEATING IN A HIGH-CURRENT GAS DISCHARGE

V.L.Sizonenko, K.N.Stepanov, V.A.Souprunenko, E.A.Sukhomlin, and V.T.Tolok.

Physical-Technical Institute of Academy of Sciences of Ukr.SSR, Kharkov, USSR.

As well known, the electron drift relative to ions in a highly non-isothermal plasma ($T_e \gg T_i$) being in a low electric field, which is lower than some critical value ($E < E_{cr}$), causes the growth of ion-sound instability [1]. In this case the drift velocity U will be lower than the electron thermal velocity $V_{th.e.}$ and much higher than the ion velocity $V_{th.i.}$.

Electron scattering upon the turbulent ion-sound pulsations results in electron hampering and heating [2]. Turbulent pulsation electron hampering indicates the appearance of an additional ("anomalous") electric resistance of plasma. In the case of a low-frequency Coulomb collision plasma, the resistance of a plasma caused by the existence of turbulent ion-sound oscillations may be much higher than the resistance due to collisions.

The main mechanism limiting the growth of unstable ion-sound oscillations is the non-linear scattering of these oscillations on electrons [3]. Making use of the kinetic equation for waves and electrons, one may get the following approximated equation for plasma electroconductivity at turbulent ion-sound pulsations:

$$\sigma(E) = \frac{e n_0}{2E(\nu_c+\nu_{\infty})}\left\{\nu_{\infty}(U_b+U_1)+\frac{eE}{m_e}\pm\left[\left(\nu_{\infty}(U_b+U_1)+\frac{eE}{m_e}\right)^2-4(\nu_c+\nu_{\infty})\nu_{\infty}U_1U_b\right]^{1/2}\right\} \quad \ldots\ldots(1)$$

Here n_0 is the plasma density, U_b is the cut-off value of drift velocity, above which the ion sound is excited, and it is evaluated by linear theory formulae and depends upon T_e/T_i and m_e/m_i parameters, normally $U_b \sim 3V_{th.i.}$. The value of U_1 is somewhat less than the velocity of sound $V_s=(T_e/m_i)^{1/2}$, ν_c is the binary collision frequency, and ν_{∞} is the frequency defining the turbulent pulsation electron scattering at $U \gg V_s$. In this region at $\nu_c \ll \nu_{\infty}$ the plasma conductivity doesn't depend upon E value (the plateau area), i.e. $\sigma = \sigma_{\infty}$, where

$$\sigma_{\infty} = \frac{\omega_p^2}{4\pi\nu_{\infty}} = \frac{\omega_p m_i}{8\pi m_e \alpha} \quad (\alpha \sim 1) \quad \ldots\ldots(2)$$

In Fig.1 the solid line shows $\sigma(E)$-dependence according to eq.(1).

The energy-balance equation (neglecting the ion heating term) has the following form at $U > V_s$ and $\nu_c < \nu_{\infty}$:

$$\frac{dT}{dt} = \frac{T}{\tau_{heat}} - \frac{T}{\tau_{loss}} - \nu_i\left(\varepsilon_i + \frac{3}{2}kT\right) \quad \ldots\ldots\ldots(3)$$

where $\tau_{heat} = \frac{V_{th.e.}^2}{U^2}\frac{1}{\nu_{\infty}}$ is the time of heating in the absence of losses, τ_{loss} is the time of energy loss due to particles leaving the trap (in our experiments $\tau_{loss} = 0.3\,(\mu sec)$), the last term in eq.(3) which defines the ionization loss is negligible in our case.

The experiments were made in hydrogen plasma of high-current gas discharge ("GROM-1" 4 and "GROM-3"[5]). At $n_0 = 7 \times 10^{14}$ cm^{-3}, $U = 1.7 \times 10^8$ cm/sec one gets from eq.(3) $T_e = 4$ keV. The electron temperature measured on the absorption analysis in aluminium foils of soft x-ray radiation, resulting from thermal electron hitting in a solid target, being placed directly in the discharge [6], was of the order of 3 keV [7].

Plasma conductivity was measured by means of local magnetic probes which made possible taking measurements at any discharge point [4]. The measurements were taken both at low ($E \ll E_{cr}$) and high ($E \gtrsim E_{cr}$) fields (see Fig.1). The critical field value defined from $U = V_{th.e.}$ condition will give for hydrogen:

$$E_{cr} = E_{Dr} = m_e\nu_c V_{th.e}/e \sim 10^{-12} n_0/T_e \quad (\nu_c > \nu_{\infty}) \quad \ldots\ldots(4)$$

$$E_{cr} = m_e\nu_{\infty}V_{th.e}/e \approx 2\cdot 10^{-6}\alpha\sqrt{n_0 T_e} \quad (\nu_c < \nu_{\infty}) \quad \ldots\ldots(5)$$

It should be noted that when $\nu_c \ll \nu_{\infty}$, the critical field of eq.(5) is well in excess of Dreicer critical field. At $U > V_{th.e.}$ the ion-sound instability will transform into the electron-ion instability by Pierce-Budker-Buneman.

The experimentally measured dependence $\sigma(E)$ at low fields 4 is in fair agreement with eq.(1) ($\alpha = 1.6$; $U_b \approx 0.3 \cdot V_s \approx U_1$). With the electrical field growth the condition $T_e \gg T_i$ is violated due to ion heating, and with E = 30 v/cm the ion-sound instability is suppressed and in E = 30÷80 v/cm region σ is defined by binary collisions. At gaining E = 80 v/cm value which approximates the critical field value of eq.(4), the electron-ion instability will be excited in plasma followed by an intense electron heating.

As electrons are heated, the condition $U > V_{th.e.}$ is violated because the discharge current is limited by an external source. In this case the conditions for exciting the ion-sound instability ($T_e \gg T_i$ and $V_{th.i.} \ll U \ll V_{th.e.}$) continue to be held in the discharge. Therefore, with $E > E_{Dr}$ (but in this case $E_{Dr} \ll E_{cr}$ as now $\nu_c \ll \nu_{\infty}$) the conductivity of plasma and heating will be defined by the electron scattering on turbulent pulsations.

Within $E < E_{Dr}$ fields the electron heating wasn't observed (in spite of the ion-sound instability) because of great ionization loss at low $T_e \sim 10$ eV values. Only at $E > E_{Dr}$ the fast electron heating due to the electron-ion instability up to $T_e \gg \varepsilon_i$ values will eliminate the ionization process effect and provide for further heating due to the ion-sound instability. It should be emphasized that according to eq.(5), at $E \sim E_{cr} \sim 2$ kv/cm the conditions of the given experiment the electron-ion instability should appear over again.

Thus the performed experiments on dense current-carrying plasma heating are explained fairly well by the anomalous resistance and plasma heating theory with the ion-sound pulsation existence [3]. Utilization of this heating mechanism would allow, in accordance with eq.(3), to gain much greater T_e values with E increasing and the decrease of loss.

REFERENCES

1. G.V.Gordeev, Zh.Exp.i Teoret.Fiz., 27 (1954) 19.
2. L.I.Rudakov, L.V.Korablyov, Zh.Exp.i Teoret.Fiz., 50 (1966) 220.
3. V.L.Sizonenko, K.N.Stepanov, Zh.Exp.i Teoret.Fiz., Letters to Editor, 9 (1966), No.7.
4. V.A.Souprunenko et al., Zh.Tekhn.Fiz., 31 (1961) 1057.
5. V.A. Souprunenko et al., Atomnaya Energia, 17 (1964) 85.
6. V.F.Alexin et al., Zh.Tekhn.Fiz., 36 (1966) 620.
7. E.A.Sukhomlin et al., Zh.Exp.i Teoret.Fiz., Letters to Editor, 1 (1965) 45.

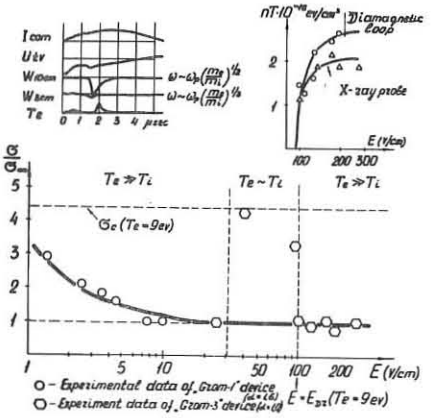

Fig.1

FLUCTUATION SPECTRUM DURING TURBULENT HEATING OF A TOROIDAL PLASMA

S.M. Hamberger, J. Jancarik, L.E. Sharp & P.C.V. Richold
U.K.A.E.A., Culham Laboratory, Abingdon, Berkshire, England

We have been examining the fluctuation spectrum present during the turbulent heating of a toroidal plasma column of density 10^{12}-10^{13} cm^{-3}. The heating current pulse, which lasts ~300 nsec, is produced by electromagnetically inducing a large axial electric field (~300 V/cm) in the plasma parallel to a magnetic field ≈3 kG. As already described[1,2,3] the plasma column exhibits an anomalously high resistivity, which depends on the plasma density n_e and ion mass M[2].

Figures 1 and 2 show both the time scale of the current pulse, and the time at which the turbulence is strongest, indicated by the strong microwave emission. The observations have been made both in hydrogen plasma of density ~10^{12} cm^{-3}, for which the discharge is highly resistive (current almost in phase with the electric field), and which reaches a maximum temperature ~10 keV, and in argon at a higher density (5×10^{12} cm^{-3}) for which the plasma resistance is smaller (current out of phase) and the maximum electron temperature lower (several hundred eV).

Probe Measurements

The principal diagnostic used is a small, double electric probe consisting of two platinum electrodes 0.1mm diameter, 0.5mm long, and 0.35mm separation, at one end of a balanced transmission line, with a 1,000Ω resistor in series with and close to each electrode. The probe is oriented to respond to potential fluctuations parallel to the current flow. The difference signal is fed via a matching transformer and 50Ω coaxial line to oscilloscopes, either directly, or via a set of bandpass filters and crystal detectors. The oscilloscope used for direct recording has a bandwidth >300 MHz. The oscillograms are converted to digital form and the Fourier transform of the autocorrelation function, i.e., the power spectrum P(f), calculated by computer.

Some typical results are shown in the diagrams. Fig. 1 shows, for a hydrogen plasma at $n_e \approx 10^{12} cm^{-3}$ the peak power received (per unit bandwidth) at several frequencies up to 3GHz, corrected approximately for frequency sensitivity. The spectrum appears to be broad, and shows no obvious variation in spectral distribution with time.

Since the frequencies and growth rates are higher for hydrogen, direct measurements are difficult and so far have been performed mainly in argon. Figures 2 and 3 show the computed power spectra for argon discharges. Figure 2 shows the analysis of a single trace in two parts, each lasting 105 nsec, for early and late times during the turbulent phase. No correction has been made for sensitivity, which in fact falls with increasing frequency. Both show distinct maxima at ~50 MHz and ~75MHz. If we tenatively ascribe the first to an ion-acoustic wave whose half-wavelength corresponds to the probe separation d ($k_s = \pi/d \approx 90$ cm^{-1}) then the corresponding phase velocity $c_s = \omega_s/k_s = \sqrt{kT_e/M} \approx 3.10^6$ cm sec^{-1}, or $T_e \approx 300$ eV. The higher frequency corresponds to the ion plasma frequency ω_{pi} for the measured density $5\times10^{12} cm^{-3}$.

A more detailed examination of the early part of the discharge shows the presence of frequencies $>\omega_{pi}$, which seem to arise from a form of the two-stream instability. The spectra are shown in Figure 3. The peak occurs near the frequency at which fastest growth would be expected ~0.5 $(M/m)^{1/6}$ $\omega_{pi} \approx 230$MHz. The growth rate (from inspection of the oscillogram, not reproduced here) is ~10^8 sec^{-1}, which is slower than the hydrodynamic growth rate ($\gamma \sim (m/M)^{1/3}$ $\omega_{pe} \approx 2\times10^9$ sec^{-1}), but in reasonable agreement with that for the kinetic instability $\gamma \sim (v/\Delta v)^2 (m/M) \omega_{pe}$: where v, Δv refer to the drift velocity and its spread, if $v/\Delta v \approx 7$. The lower characteristic frequency of the ion sound fluctuations which fill the spectrum below ω_{pi} (75 MHz) appear in the latter part of the trace (Figure 3b). These may be directly generated by the ion-sound instability or arise from non-linear interactions of the original beam-type instability.

Microwave scattering

Density fluctuations perpendicular to the current are studied by the scattering of a 2 mm wavelength microwave beam transmitted radially to the plasma by a horn antenna outside the silica wall. The scattered signal is accepted by a second antenna and fed to a crystal mixer whose local oscillator is the same microwave generator which supplies the probing beam. In this way the fluctuation wavelength is defined by the angle between incident and received signal, and the corresponding frequency shifts by the mixer output. A preliminary measurement was performed with a scattering angle of 45° ($k_s \sim 20$ cm^{-1}) under the same conditions as that used to obtain the results in Figure 2. The mixer output showed strong signals around 10 MHz, which is in good agreement with the expected sound speed deduced from the probe observation ($c_s \approx 3 \times 10^6$ cm sec^{-1}). Much higher frequencies (> 100 MHz) were also seen early in the current pulse, but which could not be resolved. Similar observations have been reported by Demidov et al[4] using longer wavelength microwaves.

References

1. S.M. Hamberger, A. Malein, J.H. Adlam and M. Friedman, Phys. Rev. Lett. 19, 350 (1967).
2. S.M. Hamberger and M. Friedman, Phys.Rev.Lett.21,674 (1968)
3. J.H. Adlam et al, Proc. 3rd Conf. on Plasma Physics and Controlled Nuclear Fusion, CN-24/D-8.
4. B. Demidov et al, Kurchatov Inst. Preprint IAE-1651.

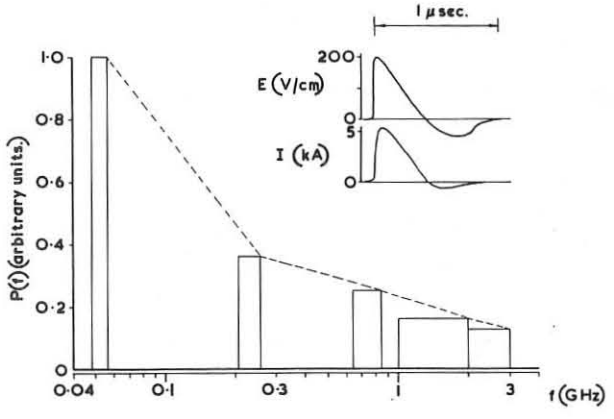

Figure 1

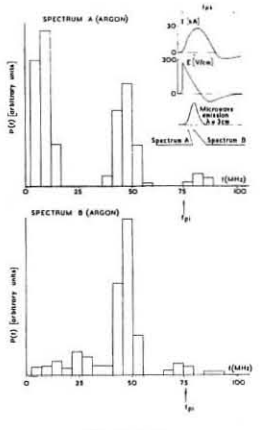

Figure 2

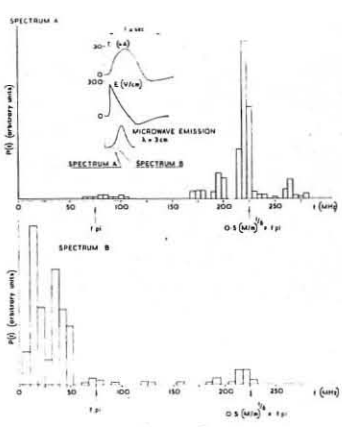

Figure 3

TURBULENT HEATING EXPERIMENTS WITH PLASMA
PRODUCED BY A HOLLOW CATHODE ARC

by
H. de Kluiver and W. Strijland
Association Euratom-FOM
FOM-Instituut voor Plasma-Fysica
Rijnhuizen, Jutphaas, The Netherlands

Introduction

A hollow cathode arc plasma can be produced with a high degree of ionization, with densities of 10^{18} to 10^{20} m^{-3}, and with little contamination. The shape of the plasma column is controlled by the external magnetic field. The topics of study have been the formation of the arc, the dc properties, the determination of the threshold field for turbulent heating, the heating efficiency, and the repartition of the energy between electrons and ions.

The apparatus

In a linear geometry the arc is run between a tantalum hollow cathode and a copper anode, which are mounted on brass tubes of 5 cm diameter. The tubes are provided with connections for the gas flow and for the water cooling. The dimensions of the cathode are a diameter of 3 or 10 mm, and a length of 5 cm. The arc length is approximately 1 m. The vacuum system consists of a 10 cm diameter pyrex tube that may be evacuated to a few times 10^{-6} Torr. The arc is struck by means of a third ring electrode in an E × B configuration. About 70% of the energy of the auxiliary discharge is deposited by the ions on the cathode. When the cathode is heated sufficiently, the main discharge takes over.

The magnetic configuration is a magnetic bottle with a mirror ratio 4 and a 0.8 T peak induction, while the electrodes are situated just outside the mirrors.

The electron density near the midplane is determined with a 2 mm microwave interferometer bridge. The density is proportional to $B^{1/2}$ for a wide range of currents. As a function of the arc current the density reaches a saturation value. The neutral density outside the column depends on the balance between pumping speed and gas feed. Inside the arc the neutral density mainly depends on the pressure balance. The electron temperature has been determined spectroscopically as 1.5 eV. From this we conclude that ionization may be neglected, but that heating of the neutrals by collisions is considerable. This is consistent with the fact that the emission lines of neutral argon are weak compared with A II lines. Therefore, in A the ionization degree may be near 100%, whereas in helium the ionization is less (near 60%).

Turbulent heating of the arc plasma

Heating by turbulence is observed when the capacitor voltage exceeds a critical value depending on the plasma density[1, 2]. Measurements have been performed with argon and helium with densities between 2×10^{19} and 9×10^{19} el/m^3. The oscillograms a ... e show phenomena typical for a turbulent plasma. Here a helium arc of 5×10^{19} el/m^3 has been excited by the discharge of the capacitor at 35 kV. Extra damping resistance was 1 Ohm.

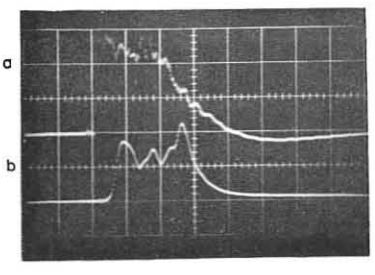

Fig. a. The voltage across the arc vs time. Vertical scale 12.5 kV/div. Horizontal scale 1 μs/div. Plasma density in the helium arc 5×10^{19} $ions/m^3$. Gas pressure is 3×10^{-3} Torr. B-field near the mirrors 0.4 Tesla. Capacitor: 1.9 μF.

Fig. b. 3 cm radiation signal vs time obtained with a superheterodyne method; 1 μs/div.

Fig. a is the voltage measured across the arc. Fig. b shows the electromagnetic radiation picked up by a 3 cm horn antenna. Fig. c represents the plasma diamagnetism obtained by integration of a loop signal. Figs. d and e show the X-ray emission of the plasma transmitted through a mica window and through a 0.2 mm Cu-foil, respectively. The measurements have been made with a scintillator and photomultiplier perpendicularly to the axis. Further diagnostics have been current measurements and the determination of the X-ray energy by the absorption method.

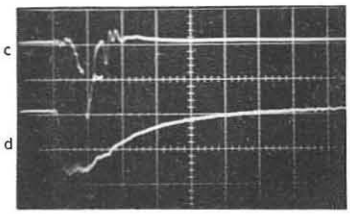

Fig. c. The diamagnetic loop signal vs time; 2 μs/div.

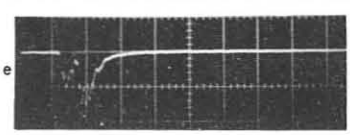

Fig. d. X-rays emission measured through a mica window; 2 μs/div.

Fig. e. X-ray emission through a 0.2 mm Cu-foil; the reduction to a more energetic X-ray signal; 2 μs/div.

The turbulent state is characterized by a high resistivity and strong electromagnetic radiation. From the averaged initial slope of the voltage decrease in Fig. a an equivalent resistance of 15(± 5) Ohm can be derived. After 2.3 microseconds the noisy regime ends, followed by a faster decay determined by the external impedance only. The current, not shown here, is extremely hashy and changes to a smooth nearly aperiodic decay in the same way as the voltage does. From Fig. c the perpendicular energy gain of the plasma can be derived. The increase is approximately 60 Joules, which is 7% of the capacitor energy. Only during turbulence a significant part of the X-ray emission has an energy above 50 keV as is concluded from foil absorption measurements. The maximum intensity of this radiation component often appears near the time when the diamagnetic signal is diminishing or zero. With a mica window, which is transparent down to approximately 1 keV, e-folding times between 2 and 3 microseconds have been found for the afterglow. If one assumes mirror losses by electron-ion collions, an electron temperature of 1 keV can be calculated.

The results obtained thus far can be summarized as follows. Turbulent heating can be induced with similar effects in helium and argon for densities between 2×10^{19} and 9×10^{19} el/m^3. With increase of the initial plasma density a higher critical electric field is needed to reach a turbulent state which is characterized by a high effective resistance. At a density of 5×10^{19} ion/m^3 for helium an apparent minimum field strength of 17 kV/m has been measured. Above the critical field strength the plasma resistivity is essentially constant.

It is suggested that the heating efficiency is presently limited by the tube diameter and by the small magnetic field used, as is also found in the literature[2]. When the perpendicular energy of electrons and ions increases the particles will hit the wall in a few microseconds. The plasma dissipation at the wall is accompanied by a rapid decrease of plasma pressure and an enhanced X-ray emission at higher energies. Turbulence ceases because the field strength at that moment will be too low. Typically, 60 Joules are dissipated in the plasma; related to the volume of the discharge tube this amounts to at least 4×10^{22} eV/m^3.

Many thanks are due to Messrs. K.L. Buisman, B. de Groot, A.M.J. Paans, and P.J. Blaas for their enthusiastic help during the measurements.

This work was performed under the association agreement of Euratom and FOM with financial support from ZWO and Euratom.

References

1) M.V. Babykin et al., Soviet Physics JETP, Vol. 25 (1967) 421.
2) E.K. Zavoiskiĭ et al., Turbulent heating of plasma by a current, Proc. Third Conf. on Plasma Physics and Contr. Nucl. Fusion Research, Novosibirsk (1968), CN-24/L-1, pp 1-24.

Anomalous Scattering of Laser Light by a Steady State Plasma

H. Ringler and R.A. Nodwell[+]
Institut für Plasmaphysik
8046 Garching bei München, Germany

The theory of electromagnetic scattering by a plasma developed by Salpeter [1] satisfactorily accounts for the backscatter profile of a radar from the ionosphere reported by Bowles [2]. Following the development of this theory several laboratory experiments were performed [3-7] in which the observed profiles were consistent with the theory. In this paper we report on measurements of the scattering of the plasma in a magnetically stabilized arc which show large and significant departure from the theory.

In the Salpeter theory it is shown that the shape of the profile of the scattered light is determined by the parameter α, defined by $\alpha \equiv \frac{\lambda_i}{4\pi \sin \theta/2 \, \lambda_o}$ (λ_i = wavelength of the incident hight, λ_o = Debye length, θ = the scattering angle). When α is much smaller than one the correlation of the electron motion is small and a Doppler profile is predicted, when α is larger than one the correlation is large and a very narrow central peak with two symmetric satellites displaced by approximately the plasma frequency is expected. For α intermediate between the two extremes the theory predicts a sharp central peak with smooth wings extending out beyond the plasma frequency; a broad maximum occurs at approximately the plasma frequency but well defined peaks are not predicted.

In the experiment reported here a plasma is formed in a magnetically stabilized electric arc. A magnetic field of 10.8 kG is imposed parallel to the axis of a high current arc discharge. The arc is operated at an initial pressure of 10 Torr of hydrogen, the arc current being 1800 A. Temperatures of 10 eV and electron densities of up to 10^{16} cm^{-3} have been measured and reported elsewhere [8].

Light from a Q-spoiled ruby laser is focussed at a point in the plasma. The scattered light is detected by a 7265 RCA photomultiplier after passing through a rotatable interference filter (band pass 7.5 Å). The incident beam is horizontally polarized and is perpendicular to the axis of the arc. The scattered beam is perpendicular to both the incident beam and the arc axis. Thus the direction of the scattering electron density fluctuation is perpendicular to the applied magnetic field. The dimensionsof the scattering volume defined by the intersection of the incident beam and the field stop of the detecting system are approximately 1.2 mm.

In Fig. 1 the results for scattering from the centre of the discharge are shown. The most remarkable feature of this profile is the presence of satellites at 7.5 Å, 15 Å, 30 Å and possibly 45 Å. We know that for this plasma the α is about 0.4 and hence, by the Salpeter theory, no satellites should appear. To confirm that these satellites were not a result of perturbation due to the laser we repeated the experiment with higher incident power (25 MW in the first case, 60 MW in the second) and these results are also shown in Fig. 1. The position and the relative magnitudes of the satellites are apparently independent of the laser power. Although the ratio of the incident power in the two cases is 2.4, and the ratio of the Rayleigh signal from nitrogen is also 2.4, it is surprising to find that the ratio of the scattered signals is only 1.4. We therefore conclude that we cannot reliably predict the electron density of the plasma from the Salpeter theory. Note

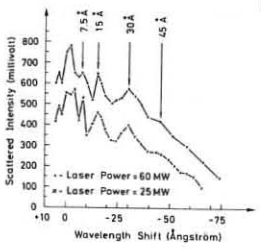

Fig. 1

that the profile near the central frequency is apparently asymmetric.

A plasma with electron density of 1 x 10^{16} cm^{-3} has a plasma frequency of 8.9 x 10^{11} cps and if a satellite were due to the plasma frequency we would expect to find a satellite at 15 Å. This agrees remarkably well with one of the observed peaks, and the other peaks would then appear to be harmonics[+]. To check that the satellite position is dependent on the local electron density we repeated the experiment at a point 8 mm from the centre of the discharge where the electron density and temperature are smaller. The results of this experiment are shown in Fig. 2. Peaks are again observed but this time at 12.5 Å and 25 Å. A shift of 12.5 Å corresponds to an electron density of 7.4 x 10^{15} cm^{-3}.

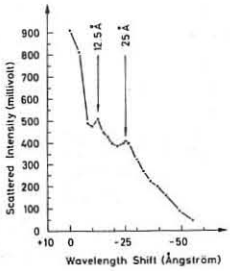

Fig. 2

The satellite peaks remind one of Tonks-Dattner resonances in which one observes enhanced scattering at approximately $\omega_p/\sqrt{2}$, $n\omega_p (n = 1,2...)$ [10]. However, Tonks-Dattner resonances require that the plasma density be non-uniform on a scale comparable to the wave length of the scattering vector. Since the scattering vector in our experiment is 4900 Å we require small inhomogeneities in the plasma to account for the observed satellites. One is led to wonder if small scale turbulence is present. We have noted that the scattering cross section is sensitively dependent on initial external parameters such as initial pressure. More work is being done both on the scattering profile and on spectroscopic measurements in order to clarify this.

This work has been undertaken as part of the joint research programme between the Institut für Plasmaphysik and Euratom.

References

1 Salpeter, E.E., Phys. Rev. 120 (1960) 1528

2 Bowles, K.L., Phys. Rev. Letters 1 (1958) 454

3 DeSilva, A.W., Evans, D.E. and Forrest, M.J., Nature 203 (1964) 1321

4 Ramsden, S.A. and Davies, W.E.R., Phys. Rev. Letters 13 (1964) 227

5 Chan, P.W. and Nodwell, R.A., Phys. Rev. Letters 16 (1966) 122

6 Kronast, B., Roehr, H., Fuenfer, E., Glock, E. and Zwicker, H., Phys. Rev. Letters 16 (1966) 1082

7 Gerry, E.T. and Rose, D.J., J. Appl. Phys. 37 (1966) 2715

8 Mahn, C., Ringler, H. and Zankl, G., Z. Naturforschg. 23a (1968) 867

9 Neufeld, C.R., Institute for Plasma Physics, Garching (private communication)

10 Parker, J.V., Nickel, J.C. and Gould, R.W., Phys. Fluids 7 (1964) 1489

+) On leave from the University of British Columbia, Vancouver, Canada.

+) C.R. Neufeld has found a similar satellite in an "Eieruhr" plasma and has noted that it coincides with his predicted plasma frequency [9].

PRODUCTION OF ENERGETIC IONS IN A PENNING DISCHARGE

M.Fumelli, R.Dei-Cas, J.P.Girard, F.P.G.Valckx

ASSOCIATION EURATOM-CEA
Département de la Physique du Plasma et de la Fusion Contrôlée
Centre d'Etudes Nucléaires
Boîte Postale n° 6 - **92 Fontenay-aux-Roses** (France)

I. INTRODUCTION

Ion heating has been observed, under particular experimental conditions, by several authors [1] in the magnetically confined plasma column of low pressure gas discharges. Different theoretical models have been proposed to explain the ion heating [2]. We report here the experimental investigation of a hot lithium plasma produced with a Penning discharge in a magnetic mirror geometry.

II. DESCRIPTION OF THE EXPERIMENT

The confining magnetic field has a mirror ratio R=2,2 and a distance of 50cm between the mirrors (fig.1). The field strength during most experiments was 9,25 kG at the centre. The heated cylindrical anode, where the Li-vapor is supplied, is 20cm long and has a 2cm bore. The cylindrical tungsten cathode, 0,5cm in diameter, which enters in the anode, is heated by the discharge current. The anode and the Li oven are placed in a water cooled chamber with a diaphragm, a 3cm hole, to reduce the neutral gas flow into the main chamber. The reflector is placed beyond the other mirror. The Li-vapor flow was $\approx 10^{19}$ atoms/s. Two very different kinds of discharges have been observed depending on the applied electrical power P:

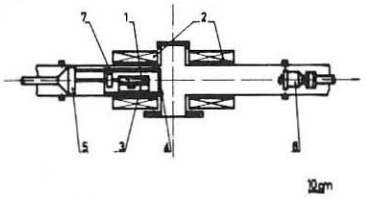

Fig.1 : Experimental apparatus : 1-anode, 2-coils, 3-oven, 4-diaphragm 5-cathode 1, 6-cathode 2, 7-water cooled chamber.

Regime I : $P \leq 2kW$. This is an ordinary gas discharge mode.

Regime II: $P \geq 2kW$. Energetic ions are produced. The arc voltage is about 500V and the current between 4 to 7A. The current on the reflector drops practically to zero. The plasma column expands radially. The transition to regime II is due to the rise in temperature of the cathode under the plasma ions bombardment; the estimated thermoemission at the transition is about 1,5A. The transition from regime II to regime I is observed when the neutral lithium flow is increased.

III. PLASMA PROPERTIES

In regime I the plasma density is roughly proportional to the applied power. The electron temperature is about 3eV (Langmuir probe measurements). The transition to regime II is accompanied by a drop in plasma density and an increase of the electron temperature ($T_e \approx 40eV$), (fig.2). The quantity $N_e = \int n(r)dr$ has been deduced from absorption measurements of a thermal beam of potassium atoms, crossing the plasma column in the median plane; some points were obtained with different diagnostics (Langmuir probes, microwaves 8mm). To study the hot plasma the following diagnostics also have been used :

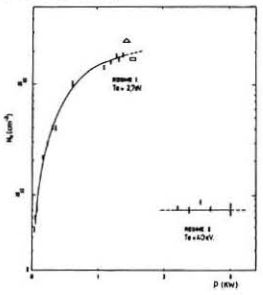

Fig.2 - Line density versus the electrical power of the discharge.

a) three secondary emission detectors measuring the axial distribution of the charge exchange fast neutrals. b) A little Faraday cup, which can be introduced radially in the plasma, measuring hot ions flux. c) An electrostatic analyser placed on the median plane, to record the energy spectrum of the perpendicular flux of fast neutrals. d) Electric probes to detect plasma oscillations. The density profiles measured with the neutrals detectors and the Faraday cup show that the hot plasma is confined in the center of the magnetic configuration in a volume of 250cm^3. The ion temperature is highly anisotropic $\frac{T_{//}}{T_{\perp}} \approx 2.10^{-2}$. The maximum density, at the center is about 10^{11}cm^{-3} for ions of some 100eV energy, the density of more energetic ions (of order of keV) is an order of magnitude lower. The energy spectra measured for three values of the magnetic field are given in fig.3. The highest ion perpendicular energy detected is 30keV. In the low energy regions of the spectra extrapolated values of charge exchange and ionisation cross sections were used. The temperature of the more energetic ions seems to increase with the square of the magnetic field strength. The decay of the hot ion plasma, after cut-off of the discharge, is very irregular with a e-folding time varying from 10 µs to 100 µs. This time is much shorter than the charge-exchange time.

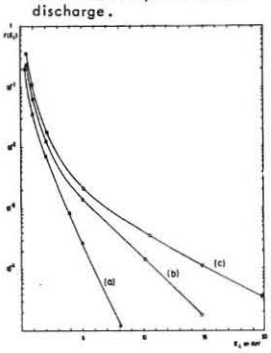

Fig.3 - Distribution function of the perpendicular energy of ions: a)6,15 kG b)9,25 kG c)12,3 kG

IV. PLASMA OSCILLATIONS IN REGIME II.

a) Low frequency oscillations : $\omega \ll \omega_{ci}$ (ion cyclotron frequency) - Strong periodic fluctuations at a frequency of 20kHz have been detected. These fluctuations are due to a m=2 (sometimes m=1 and m=3) mode having a rotational frequency of 10kHz. The ion flux measured near the walls at each passage of the plasma "tongues" is of order of 2.10^{15}cm^{-2}s^{-1}. Low frequency large amplitude fluctuations (~ 100V) with irregular periods of the order of 20µs have been observed on the cathodes.

b) Oscillations near ω_{ci}. Large amplitude fluctuations appear in the neighbourhood of ω_{ci} (fig.4) Azimuthal phase correlations of the signals detected by three probes placed near the diaphragm at 1,5cm from the axis show that these oscillations don't possess an azimuthal mode.

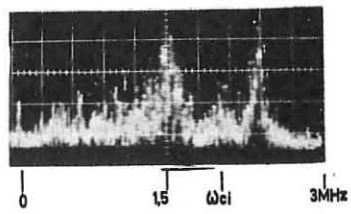

Fig.4 - Spectrum of the plasma oscillations near the ion cyclotron frequency

c) High frequency oscillations $\omega \gg \omega_{ci}$. Oscillations in the range 30 to 90 MHz and 150 to 250 MHz are observed.

V. DISCUSSION OF RESULTS

Our observations are consistent with the hypothesis that ion heating is due to the cyclotron resonance of ions with the observed oscillations near ω_{ci}. These oscillations can be attributed to an acoustic ion wave. Self excited acoustic waves and resonance effects have been observed by [3] in a similar experimental apparatus. The parallel wave length is estimated to be about 2,5 cm. From the resonance condition : $\omega - n\omega_{ci} - k_z V_z = 0$ we deduce that ions with an energy of some eV can be in resonance in the central region of the mirror. These ions, gaining energy from the perpendicular component of the wave's electric field, can be captured between the mirrors and further heated. Due to a strong radial diffusion, a longitudinal plasma density gradient exists in the column and a negative space charge is created [4] at the surface of the reflector where the electrons emitted by the cathode arrive with practically zero energy. This fact can explain the large amplitude fluctuations observed at the cathodes.

The short containment time of the hot ions can be explained by the strong flute-like instability observed.

[1] V.NEIDIGH and C.H.WEAVER
Proc.2nd U.N.Int.Conf.on the Peaceful Uses of Atomic Energy, Geneva 1958, vol.31, p.315.

M.V.NEZLIN and A.M.SOLNTSEV
Sov.Phys.JETP, vol.45, p.840 (1963)

H.W.DRAWIN and M.FUMELLI
Zs.Naturf. vol.20a, p.445 (1965)

[2] G.GUEST and A.SIMON
Phys.Fluids, vol.5, p.503 (1962)

A.B.MIKHAILOVSKII
Atomnaia Energya, vol.20, p.103 (1966)

M.V.NEZLIN
Sov.Phys.JETP, vol.26, p.693 (1968)

[3] I.ALEXEFF and R.V.NEIDIGH
Phys.Rev., vol.129, p.516 (1963)

[4] I.LANGMUIR
Phys.Rev., vol.33, p.954 (1929)

Experimental Investigation of Plasma Production by Irradiating Solid Hydrogen Foils with an Intense Pulse Laser

R. Sigel, P. Mulser and S. Witkowski
Institut für Plasmaphysik
8046 Garching bei München, Germany

It is already known [1,2,3] that interaction between intense laser light and solid hydrogen in a one-dimensional model yields three regions (0,1,2) with different states of matter (Fig. 1a): In a strongly absorbing deflagration front F a hot, transparent plasma of moderate density is produced and streams towards the laser with high velocity (Region 2, $v \approx 10^7$ cm/sec). F may be regarded as a piston almost impervious to matter that generates an intense shock wave in the solid because of the reaction of the escaping plasma. The compressed matter (Region 1, $v \approx 10^6$ cm/sec) streaming away from the laser with F is separated from the undisturbed solid with density ϱ_0 (Region 0) by the shock front S. Most of the laser energy is transferred to Region 2.

The effect of a focused laser beam on a plane target can be described by a piston model based on the one-dimensional model. The

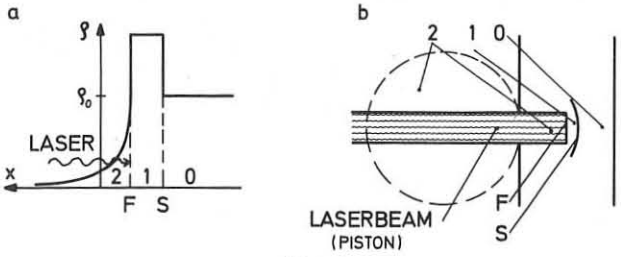

Fig. 1
a) Schematic density profile for a solid hydrogen target irradiated with an intense laser beam (one-dimensional model).
b) Piston model describing the penetration of a solid hydrogen target (foil) by a focused laser beam.

focused beam is represented in Fig. 1b as a parallel beam of finite cross section, the numbers denoting the regions 0 - 2 as in the one-dimensional model. The beam penetrates the target like a piston, the face of the piston being formed by F. The shock wave generated by the piston resembles a bow shock. The matter caught up by the shock front S is pushed aside owing to the high pressure between S and F [2] and thus transfers the reaction of the plasma to the matter surrounding the piston. The plasma produced in F is ejected towards the laser and expands in the front half-space. The ions and electrons are expected to expand at the same velocity. Since the plasma cools during expansion, its energy can be found far from the target as directed kinetic energy of the ions.

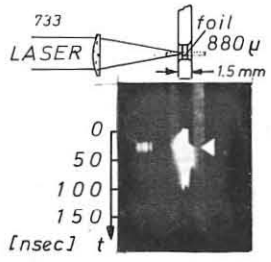

Fig. 2
Streak picture of a laser-irradiated solid hydrogen foil (time mark ◀ corresponds to the moment, when the foil becomes transparent to the laser light).

In the experiment a ruby laser was focused on solid hydrogen foils [4] in high vacuum. The intensity in the focus was about 10^{12} W/cm^2 over an area of diameter 0.1 mm. The model was verified in the following respects: 1) Absorption measurements [5] revealed the existence of the strongly absorbing deflagration front F, which moves with a velocity of 3×10^6 cm/sec. 2) Streak pictures (Fig. 2) taken tangentially to the surface of the foil show luminous phenomena caused by the penetrating piston on the front of the foil at the start of the laser pulse. The back of the foil is not affected until the piston appears there a few nanoseconds before the foil becomes transparent. 3) The plasma produced by the laser was observed at various times after the maximum of the laser pulse by

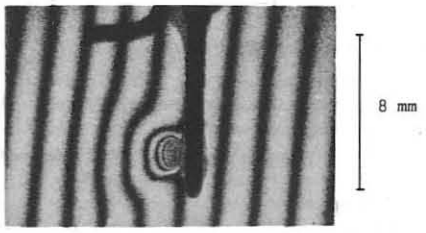

Fig. 3
Interferogram (reconstructed from a hologram) of the plasma produced by a laser from a solid hydrogen foil (18 nsec after maximum of laser pulse). The foil (thickness 1.5 mm) is not pierced by the laser, therefore no plasma is observed on the back of the foil.

means of holographic interferometry [6] (Fig. 3). In the case of thick foils that are not pierced by the laser the number of free electrons in the plasma attains the final value of 4×10^{16} after 30 nsec. 4) Two charge separating probes each consisting of an earthed perforated plate and a collector at negative potential were mounted 20 cm in front of and behind the target at an angle of 45° to the laser axis for making time resolved measurements of the number of impinging ions. As in the interferometric measurements, it was found in agreement with the model that with thin foils as well the bulk of the plasma was ejected into the front half-space. Integration over the whole solid angle with the data of [7] yielded 4×10^{16} ions in the case of thick foils. This number agrees well with the value determined interferometrically for electrons. The mean kinetic energy of the ions was 200 eV. Thus 45 % of the laser energy was recovered as kinetic energy of the ions. Considering that part of the laser energy is transferred to the dense matter as work done by the plasma at the interface between the piston and dense matter and that ionization energy has to be provided and radiation losses covered, this result appears satisfactory and confirms the described model like the other results.

This work was performed as part of the joint research programme between the Institut für Plasmaphysik and Euratom.

References

1 Yu.V. AFANASIEV, O.N. KROKHIN and G.V. SKLIZKOV, IEEE J. Q. El., QE-2 (1966) 483.

2 A. CARUSO and R. GRATTON, Int. Rep. L.G.I. 68/2 (1968).

3 P. MULSER and S. WITKOWSKI, Phys. Lett. 28A (1968) 151.

4 R. SIGEL, H. KRAUSE and S. WITKOWSKI, J. Sci. Instr., Ser. 2, Vol. 2 (1969) 187.

5 R. SIGEL, K. BUECHL, P. MULSER and S. WITKOWSKI, Phys. Lett. 26A (1968) 498.

6 J.M. BURCH, J.W. GATES, R.G.N. HALL and L.H. TANNER, Nature 212 (1966) 1347.

7 H. OPOWER and W. PRESS, Z. Naturforschg. 21A (1966) 344.

INVESTIGATION OF INSTABILITIES AND COLLISIONLESS DAMPING MECHANISMS IN THE FRONT OF A LASER PRODUCED PLASMA INTERACTING WITH A MAGNETIC FIELD

F. Schwirzke
Naval Postgraduate School, Monterey, California 93940, USA

The two problems of creating and confining a high temperature plasma in a magnetic field configuration are usually closely linked together and a laser produced plasma is no exception. Theoretical calculations[1-3] and experimental results[4-8] show that energy from a giant laser pulse can be absorbed by a small target within a few nanoseconds thus creating a high temperature plasma. Obviously the next step is then to investigate the interaction of the expanding plasma with a magnetic field. This interaction is of special importance in the CTR program where the purpose is to confine a thermalized hot plasma in a stable magnetic field configuration. A laser produced plasma which expands across a magnetic field also uncovers new extensive possibilities for the investigation of instabilities and collisionless damping mechanisms in the wave front. If a low density (collisionless) background plasma is present, then the "exploding" laser plasma acts as a very fast piston and collisionless shockwaves can be studied.

In the initial expansion phase of the $\beta \gg 1$ plasma the temperature decreases rapidly $T_r = T_o(r_o/r)^2$, where T_o and r_o are the temperature and radius of the plasma when it ceases to absorb laser energy. Most of the energy content of the plasma shows up as kinetic expansion energy. Mainly surface currents in the wavefront provide the possibility to thermalize the expansion energy again by resistive effects. If the electron Coulomb-collision frequency ν_e becomes smaller than the growth rate, instabilities may develop in the front and contribute effectively to the energy dissipating process. ν_e remains constant in the expanding plasma if resistive heating can be neglected. According to Spitzer[9] $\nu_e = n_r Z^4 \ell n\, \Lambda / 0.266\, T_r^{3/2}$, where T is in ^oK. Z is the ionic charge. For a spherically expanding plasma with a homogenous distribution of N electrons $n_r = 3N/4\pi r^3$. Introducing n_r and T_r and assuming $Z = 1$ and $\ell n\, \Lambda \approx 10$ we obtain a r-independent expression for $\nu_e \approx 9N/(T_o r_o)^{3/2}$. However, taking into account the resistivity, T_r increases again after the initial sharp drop which is due to the adiabatic expansion over the first few mm, and hence, ν_e decreases with further expansion. The two-stream instability has a large growth rate $\gamma \approx \omega_{pe}(m/M_i)^{1/3}$ and has a chance to develop if $\nu_e < \gamma$. ω_{pe} is the plasma frequency, m and M_i are the electron and ion mass. Furthermore, the criterion for instability requires that the current associated ordered velocity of the electrons in the wavefront becomes larger than their mean thermal velocity. The growth time of the two-stream instability $\frac{1}{\gamma}$ is rather small in comparison with the propagation time of the wavefront which is in the order of $\tau \approx 10\ (c/\omega_{pe} V_A)$, where V_A is the Alfven velocity and $d \approx 10\ c/\omega_{pe}$ is of the order of the characteristic width of the front when the resistivity of the plasma is determined by the turbulence caused by the instability. If $\gamma\tau \gg 1$ a steady state will exist within the wave front and the onset of the instability can be studied locally. Considering a stationary wavefront which is common to shock theory, propagating in r-direction across the magnetic field, the electric current is perpendicular to B and r in the θ direction and is given by Maxwell's equation $j = -enV_{e\theta} = -(c/4\pi)dB/dr$. Substituting $\omega_{pe}^2 = 4ne^2/m$ and $K = \left|(1/B)dB/dr\right|$ where $K = \pi/d$, the instability criterion $V_{e\theta}^2 > T_e/m$ becomes $d < (\pi c/\omega_{pe})\ (2/\beta)^{\frac{1}{2}}$ where $\beta = (8\pi n T_e/B^2)$. This condition will be satisfied at a certain radius since n decreases rapidly during the expansion of the laser produced plasma. If we want to compare the instability criterion with the measured width, d, of the front of the expanding plasma we have to introduce the ω_{pe} and β values which exist within the wavefront where $V_{e\theta}$ has a maximum, i.e. where the pressure gradient has a maximum, $d^2p/dr^2 = 0$. We can assume that at the turning point $\omega_{pc}^2 \approx (1/2)\omega_{per}^2$ and $\beta \approx (1/2)\beta_r$ where ω_{per}, β_r are the quantities at the edge of the plasma which can be determined rather easily in the experiment at a given radius. Thus, $d < 2\pi(2/\beta_r)^{\frac{1}{2}}(c/\omega_{per})$. (1)

The plasma was produced by a 150 MW, 20 nsec Nd-laser pulse which was focused on the tip of a pyrex fiber of 30 μdiam. About 1 joule was absorbed by $N = 10^{16}$ target atoms. The velocity of the expanding plasma (10^7-10^8 cm/sec) depends on the absorbed laser energy. The observed velocities are comparable with the ones obtained in θ-pinches which have been used so far exclusively to study collisionless mechanisms in laboratory plasmas. A 1 mm diam moveable magnetic probe was used to measure the expansion velocity and the width of the wavefront. Fig. 1 shows an oscilloscope trace of the magnetic signal. An increase of B is observed before the diamagnetic signal is recorded in positive, upwards direction, i.e., the expanding plasma compresses B like a piston and thus produces an increase of the magnetic field. A steep front exists as indicated in the sudden increase of the diamagnetic signal. Assuming a homogeneous distribution of $N = 10^{16}$ electrons and an ionization level of Z = 1 over a sphere of r = 1.5 cm, the density would be $n_r = 7 \times 10^{14}$ cm^{-3}. In reality a density profile exists and a reasonable estimate gives $n_r \sim 3 \times 10^{14}$ cm^{-3} and $\omega_{per} \approx 10^{12}$. Introducing these values into criterion (1) we find that the two-stream instability should occur if d < 0.46 cm. From the measured expansion velocity $V = 10^7$ cm/sec and the rise time of the diamagnetic signal in Fig. 1 we observe a width of d = 0.4 cm = 13.3 c/ω_{per}, i.e. the criterion for instability is fulfilled. Furthermore, from the observed magnetic probe signal $\beta_r = 8\pi n_r T/B^2 = 0.33$ with $n_r \approx 3 \times 10^{14}$ cm^{-3} follows a temperature of $T_{obs} \approx 31$ eV. From this value we calculate $\nu_e = 5.3 \times 10^7$. The mean ion mass in the considered plasma is $M_i = 20 \times 1.67 \times 10^{-23}$ g. Thus, the growth rate of the two-stream instability is of the order $\gamma \approx 3 \times 10^{10}$. Hence, the condition $\nu_e \ll \gamma$ is fulfilled too.

That a collisionless mechanism is contributing to the energy dissipation process in the wave front is also indicated by the discrepancy in the determination of T from the magnetic probe signal and from the effective conductivity which can be estimated from the measured width of the front. The distance for which B penetrates into the plasma is given by the magnetic Reynolds number $R_M = 4\pi V\sigma d/c^2 = 1$. Hence, σ can be determined from the measured V and d, $\sigma_{eff} = c^2/4\pi Vd = 1.8 \times 10^{13}$ esu. We can compare this value with Spitzer's formula which is based on the Coulomb collision frequency only, $\sigma = 2(2T)^{3/2}/\pi^{3/2} m^{\frac{1}{2}} Ze^2 c^2\, \ell n\, \Lambda$. Assuming $\ell n\, \Lambda \approx 10$ the measured conductivity σ_{eff} appears to correspond to an effective temperature of $T_{eff} \approx 1$ eV only. In conclusion, the observed conductivity is about 170 times smaller than the "collisional" one based on the temperature of $T \approx 31$ eV, $(\sigma_{eff}/\sigma_{cou}) = (T_{eff}/T_{obs})^{3/2} \approx 1/170$. This result indicates that the two-stream instability enhances the resistivity in the wave front by more than two orders of magnitude and thus the width of the front. The steep front disappears between r = 1.5 and 2 cm, where the thickness of the front is now of the same order as the radius, and the compressed magnetic field signal is reduced considerably. Obviously, the energy which was stored in the compressed B is suddenly released into the plasma and the plasma temperature increases. A fast diffusion of B back into the plasma is possible only when the conductivity of the plasma has been reduced. This is the typical effect associated with the occurence of instabilities. The increase of the thermal energy of the plasma is related to the emission of a second light hump seen in Fig 2. In Fig. 2a the signal which indicates field compression is missing. Correspondingly the second light hump is also missing. In agreement with this interpretation Fig. 2b shows that compressed magnetic field signal starts to decrease at the time when the second light pulse begins to build up.

This research is partially supported by the Air Force Office of Scientific Research.

Fig. 1. Total light photomultiplier and magnetic probe signals at r = 1.5 cm. B = 1500 Gauss.

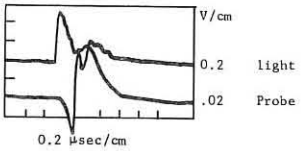

Fig. 2. Correlation between the structure of the wavefront and the light emitted from the plasma probe at r = 3 cm.

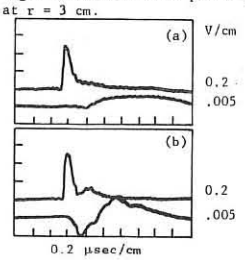

REFERENCES

1. Basov, N. G. and Krokhin, O. N. (1963) Proceedings of the Conference on Quantum Electronics, Paris, Vol. 2, p. 1373.
2. Dawson, J. M. (1964) Phys. Fluids 7, 981.
3. Hora, H. (1964) Institut für Plasmaphsik, Garching bei München, IPP/6/23.
4. Ascoli-Bartoli, U., et al. (1965) Plasma Physics and Controlled Nuclear Fusion Research, Vol II, p. 941.
5. Haught, H. F. and Polk, D. H. (1966) Phys. Fluids 9, 2047.
6. Lubin, M. (1968) Bull. Am. Phys. Soc. 13, 320.
7. Sigel, R., Büchl, K., Mulser, P. and Witkowski, S. (1968) Phys. Letters, 26A, 498.
8. Tuckfield, R. G., Schwirzke, F. (1969), Plasma Phys. 11, 11.
9. Spitzer, L. Jr.,"Physics of Fully Ionized Gases", 2nd Ed., Interscience Publisher Inc., New York, 1962.

FOCUSING OF HIGH Z PLASMA ON A DEUTERIUM JET

M. Haegi and J.G. Linhart

Laboratori Gas Ionizzati (Associazione EURATOM-CNEN),
C.P. 65, 00044 Frascati, Rome, Italy.

INTRODUCTION

The basic idea of this experiment is to transform the energy stored in a condenser bank in the kinetic energy of a high atomic number plasma imploding towards an axis or a point. This kinetic energy is then in turn partially transformed into thermal energy of a deuterium plasma or into an energy of a compressed magnetic field.

It is well known that deuterium itself is inadequate as a vehicle for directed kinetic energy in fast dynamic pinches whereas high atomic number gases can form an accelerated plasma liner (by which one means of well defined slab or layer of plasma) radiating intensely. In this case the internal energy of the liner and consequently its temperature and internal kinetic

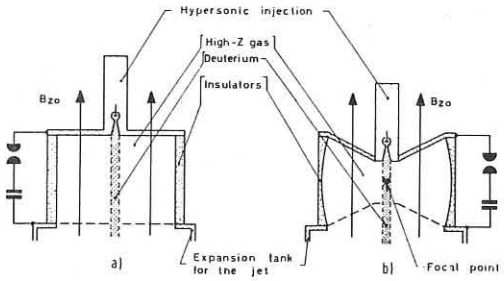

Fig. 1

pressure remains at a relatively low level, so that the "snow-plough" thickness including the shock front is relatively small [1].

Such a cylindrical or spherical imploding plasma shell could then both compress and heat the central deuterium core and later impede its expansion and delay the onset of the deuterium core instabilities. The thermal and particles insulation between the cold liner and the hot core would be obtained by means of a trapped magnetic field. If the two successive energy transfers are not too inefficient and if the high temperature confinement time reaches about 1 μsec [4], a zero energy reactor working on such a principle would be feasible with stored energies that have already been obtained in other laboratories (a few Megajoules)

EXPERIMENTAL SET UP

Figure 1b) is a sketch of a device [1],[2] which resembles a linear Z-pinch which provides (thanks to the curved shape of the initial plasma [3]) a nearly spherical mass concentration.

The neutral deuterium plasma is injected axially by means of a hypersonic jet [2]. Apart from experiment reported in [1] all measurements reported here have been so far performed in cylindrical geometry (Figure 1a). The Z-pinch has an initial diameter of 32 cm, a length of 20 cm and is operated between 10÷0.01 torr in rare gases using a 40 kV, 25 kJ condenser bank allowing

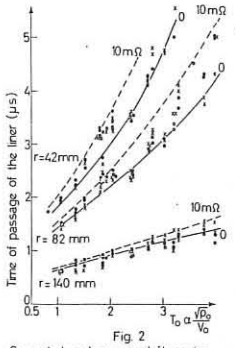

Fig. 2
Computed and measured dynamics for argon.

current up to $1{,}2.10^6$ A. The B_{zo} magnetic field is produced by external Helmholtz coils providing a reasonably constant field of 100 to 2500 gauss in the experimental chamber. The general dynamics and the internal structure of the liner are measured by means of both, small B_θ magnetic probes and the light-probes located on the generatrix passing through the B_θ probe.

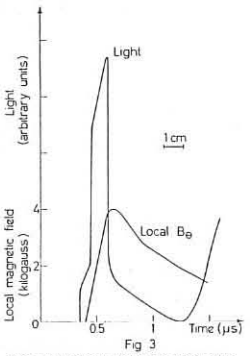

Fig 3
Light and magnetic field at r=40 mm for 125 μ of neon.

Spectroscopical measurements of the light burst generated by the final collapse have been made.

Time resolved mass density measurements in the axial region are in course using x-ray absorption.

The maximum value of the compressed magnetic field is a representative parameter of the compression efficiency of the liner. Therefore, in spite of the measurement difficulties due to the destructive effect of the high field, an extensive effort has been made, essentially by means of magnetic probes, microfuses and by the Paschen-Back effect.

THEORETICAL AND EXPERIMENAL RESULTS

The results of the numerical calculation made on the simple "snow-plough" model with various series-resistances are confronted with the dynamics given by the magnetic B_θ probes and the light probes for the different rare gases. Figure 2 represents such a confrontation for argon. The ordinates, expresses the time of passage of the magnetic signal (•) and light signal(x) at three different radii. The abscissa represents the reduced voltage $\tilde{V}_o$. There is an excellent first order agreement between theoretical and experimental points if we assume that the resistance is somewhere between 0 and 10 $m\Omega$. However small systematic deviations suggest second order effects.

The liner is shown within the range of our parameters to have thicknesses varying between 3 and 15 mm., increasing with initial density. No shock front is visible. Thinnest liners are observed in neon (Figure 3).

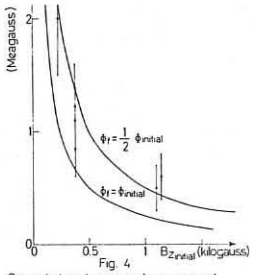

Fig. 4
Computed and measured compressed magnetic field.

On the basis of the numerical computation of the liner dynamics we can calculate the maximum magnetic field that can be obtained for a certain stored energy. Figure 4 represents the computed results in the case of total and half flux conservation during compression. The experimental points refer to measurements obtained from both the B_z probe and microfuse technique. The relatively large error band is essentially due to the uncertainties in measurement techniques. Even here the agreement is fairly good, showing that a megagauss field, i.e. considerable pressure, can be obtained from decelerated plasma liners. The density in the liner can then be taken from the relation [5]: $\rho v^2 \sim \frac{B^2}{8\pi}$ which gives for 10^6 gauss, a density of neon of about 10^{20} ions/cm^3.

REFERENCES

(1) - J.G. Linhart et al., LGI 67/26 (1967).
(2) - M. Haegi, Thèse N° 1474, Université de Genève, Suisse (1968).
(3) - B. Robouch, LGI 68/9 (1968).
(4) - J.G. Linhart, Neue Technik, B6, p. 237 (1967).
(5) - J.P. Somon, LGI 66/11 (1966).

COMPARISON OF A TWO-DIMENSIONAL MAGNETOHYDRODYNAMIC NUMERICAL MODEL WITH THE DENSE PLASMA FOCUS EXPERIMENT

by

P.D. MORGAN*, N.J. PEACOCK† and D.E. POTTER‡

*Royal Holloway College, Englefield Green, Surrey, England.
†The Culham Laboratory, Abingdon, Berkshire, England.
‡Imperial College, London, S.W.7, England.

ABSTRACT

A two-dimensional numerical fluid model of the implosion phase of the dense Plasma Focus [1,2] is compared with experiment. The plasma parameters are determined from radiation measurements, while the plasma dynamics are established by image converter and pulsed laser Schlieren photography. The theoretical model assumes a fully ionized two fluid plasma. Transport processes include electron and ion heat conduction, ion viscosity, resistive and Hall electric fields. Variable coefficients are used to describe both collisionless and collision-dominated regimes.

Such a thermal fluid model is shown to describe the dynamical formation and high kinetic energy densities of the plasma focus. A magnetic trap on the anode acts as a plasma source for flow through the pinch. Short wavelength instabilities are stabilised by ion viscosity. Non-linear effects repinch long wavelength $m = 0$ type instabilities (growth rate $\sim$ 40 nsec) and a double pinch effect (double neutron peak, voltage spike) results. A total sustainment time of $\sim$ 150 nsec is demonstrated.

EXPERIMENTAL RESULTS

The Plasma Focus device and its operating conditions relevant to this paper are described in [3]. Values of electron temperature and density have been obtained from the shape of the emission spectrum and from the absolute radiation flux in the soft X-ray region. At an initial gas pressure of 1·1 torr (D_2 + 3% A) $T_e \sim 1{\cdot}8 \pm 0{\cdot}6$ keV and $n_e \sim 1{\cdot}5 \times 10^{19}$ cm^{-3}. The ion confinement time is $\sim$ 40 nsec [3].

Image converter photographs of the focus show that the compression is sustained for $\sim$ 70 nsec by the radial collapse of the axially-travelling current sheath [3]. The pinch diameter from X-ray pinhole photographs is $\sim$ 0·7 mm at peak compression, and the total volume of hot ($\sim$ 2 keV) plasma varies between 10^{-3} and 10^{-2} cm^{-3} [3]. The spatial definition of the plasma boundary in the image converter photographs is limited by the 10 nsec exposure.

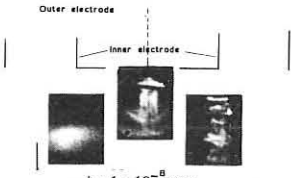

Fig.1 Pulsed laser Schlieren photographs of Focus

Shorter exposures were obtained by using a cryptocyanine dye cell to mode-lock a ruby laser pulse and using the train of irregularly spaced light pulses of $\sim$ 1 nsec duration as a source for Schlieren photography. Fig.1 shows a Schlieren time sequence of the focus using a spherical Schlieren obstacle and an initial gas filling of 2·5 torr (D_2 + 5% A). Frame 1 shows an ionization front 90 nsec before peak density is attained, frame 2 shows the detailed structure of the pinch and frame 3 shows its subsequent break up. The characteristic length ($\sim$ 0·1 mm) of the density gradients is smaller than the plasma radius measured from X-ray photographs. Also the prominent flutes in frame 2 Fig.1 are absent in the image converter photographs.

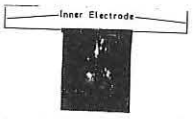

Fig.2 Dense pinch region

If a sufficiently large Schlieren obstacle is used, only the denser pinch regions are recorded, Fig.2. Assuming an electron density distribution of the form $n_e = \hat{n}_e \left(1 - \frac{x^2}{r^2}\right)$, r is the pinch radius, enables a minimum density value of 3·8 × 10^{19} cm^{-3} to be derived from Fig.2. Increasing the obstacle size until all the refracted light is just eliminated yields a maximum density value of 8 × 10^{19} cm^{-3}. The above values are several times the maximum obtained from X-ray measurements. These however give the mean value throughout the plasma volume.

A laser operating in the pulsed transmission mode is at present being used to obtain $\sim$ 6 nsec exposure Schlieren photographs.

TWO-DIMENSIONAL MHD MODEL

A two fluid electron-ion fully ionized plasma is assumed. The equations are written in conservation form, in cylindrical co-ordinates assuming azimuthal symmetry, with the magnetic field restricted to the θ-direction. The set of six dependent variables satisfies the equations of continuity, conservation of axial and radial momentum, Faraday's law (with the generalised Ohm's law), conservation of electron pressure and total energy [4]. The equations are integrated in time using the two-step Lax-Wendroff method [5] on an Eulerian mesh, and are coupled with an external L-C circuit.

Results are given for an anode length of 10 cm, initial filling pressure of 1 torr D_2 and an initial capacitor voltage of 40 kV.

In the collapse to the axis, Fig.3, momentum flow parallel to the current sheet removes 90% of the plasma initially at the end of the centre electrode. Adiabatic compression is thus permitted to raise the remaining plasma to thermonuclear temperatures.

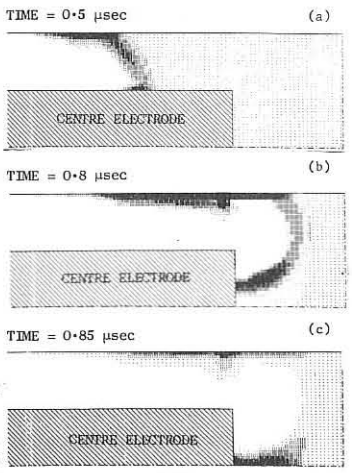

Fig.3 Distribution of plasma density $\rho = \rho(r,z)$. (a) Run down phase. (b) Collapse phase. (c) Dense pinch phase. (The scale in (c) is a factor 10 greater than in (a,b)).

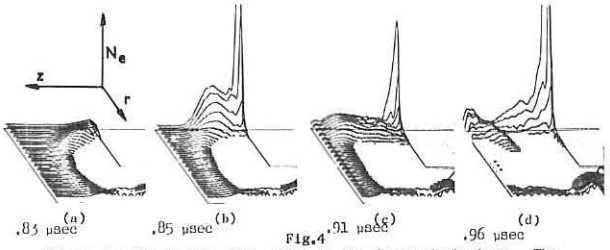

Fig.4 Plasma density in the R-Z plane in the dense pinch phase. The series shows the collapse, (a) to the axis, the dense pinch (b), partial break up (c), and repinch (d).

A near equilibrium magnetic trap is established on the anode, by the removal of thermal energy through electron heat conduction and the resultant resistive diffusion of field. The trap sustains the pinch by axial flow ($V_z \sim 4 \times 10^7$ cm sec^{-1}) Short wavelength fast hydromagnetic instabilities are damped by the large ion viscosity. The break-up of the pinch through a long wavelength ($m = 0$) mode is observed in Fig.4, with a growth rate of 40 nsec. Fig.4d shows a non-linear effect on the instability causing a 're-pinch'. This double pinch effect manifests itself in the interruption of the characteristic drop in the 'focus-shot' current curve, Fig.5.

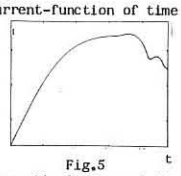

Fig.5 Theoretical curve of the current (peak value - 800 kA) against time.

Typical values for the plasma parameters in the pinch are $T_i \sim 2$ keV, $T_e \sim 1$ keV, $n_e \sim 4 \times 10^{18}$ cm^{-3}. Although these values are in qualitative agreement with experiment more accurate values are obtained on a fine scale mesh (switched in at the focus stage) in which the pinch relaxes to a radius $\sim$ 0·6 mm and electron densities $n_e \sim 10^{19}$ cm^{-3} are obtained.

DISCUSSION

Qualitative agreement with experiment for the dense pinch phase (pinch radius, electron density, electron temperature, sustainment time) demonstrates that the essential features of the plasma focus can be described in terms of a thermal fluid model.

The duration of the pinch is enhanced by two effects: ion viscous stabilisation of short wavelength hydromagnetic instabilities and the non-linear repinch of the slower modes; and a sustainment of the pinch through axial flow.

REFERENCES

[1]. FILIPPOV, N.V., FILIPPOVA, T.I. and VINOGRADOV, V.P. Nucl. Fusion Suppl. Pt.2, pp.577-587, (1962).

[2]. BOTTOMS, P.J., CARPENTER, J.P., MATHER, J.W., WARE, K.D. and WILLIAMS, A.H. Paper CN-24/G-5. IAEA Third Conference on Plasma Physics and Controlled Nuclear Fusion Research, Novosibirsk, Aug.1968.

[3]. PEACOCK, N.J., WILCOCK, P.D., SPEER, R.J. and MORGAN, P.D. Paper CN-24/G-4. IAEA Third Conference on Plasma Physics and Controlled Nuclear Fusion Research, Novosibirsk, Aug.1968.

[4]. POTTER, D.E. and ROBERTS, K.V. Methods of Computational Physics, vol.9, Academic Press (To be published).

[5]. RICHTMEYER and MORTON. Difference Methods for Initial Volume Problems, Interscience, (1967).

OBSERVATION OF COAXIAL M.H.D. PLASMA FLOW

by

A.A. Newton*, John Marshall+ and R.L. Morse+

* U.K.A.E.A. Culham Laboratory, Abingdon, Berks., United Kingdom.

+ University of California, Los Alamos Scientific Laboratory, Los Alamos, New Mexico 87544, U.S.A.

In experiments at LASL the current sheet in a coaxial gun was deliberately broadened to occupy about half the length of the interelectrode cavity. New phenomena[1] were observed and these are described and interpreted in this paper.

An enlarged Marshall gun, having a 17 cm diameter anode and an inner cathode 6.3 cm dia., each 100 cm long, was positioned in a large evacuated tank. About 2.5×10^{21} deuterium molecules were admitted under 30 kG cm^{-2} pressure by a fast valve through an annular port in the cathode 40 cm from the gun exit. Gas was still flowing in 500 μsec after the valve opened when 2880 μF at 10 kV was switched on. The current rose to a peak of 400 kA and fell through zero 100 μsec later. From observations made with image converter cameras and magnetic probes we diagnosed the following behaviour.

Initially electrical breakdown occurs at the inlet port where the neutral density is a maximum. A snowplough front moves down-stream from this position reaching the exit at 20 μsec and ejects a plasma from the gun at 12 cm μsec^{-1}. The usual 'focus' is observed in front of the gun[2]. Upstream from the inlet ionization spreads at ~ 8 cm μsec^{-1} into the gas which is simultaneously being magnetised by the cathode currents. The low-β plasma formed in this way expands to fill the space behind the snowplough front.

The 'focus' does not disperse, as in other gun studies or in the dense plasma focus type of device, but in a few μsec expands to about half the cathode diameter and extends away from the cathode for 50-60 cm with increasing diameter. This columnar structure persists for ≲ 100 μsec and is grossly stable. If the time lag between admitting gas and firing the bank is reduced or the amount of gas admitted is reduced then turbulence is seen which moves along the column away from the gun at 14-20 cm μsec^{-1}. Thus the column persists for ~ 20 characteristic times for the flow of plasma along its length. (Substantial reduction of the gas supply shortens the life of the column which then breaks up in m = 0, 1 instabilities.)

The long lived flow pattern produced resembles a pinch and we call this phenomenon the 'continuous flow pinch'. The column is maintained by the axial and radial inward flow of the low-β plasma from the interelectrode space.

Electron densities, n_e, were measured by an interferometric technique using holographic recording[3]. An example of a reconstructed fringe pattern taken 54 μsec after firing the bank is shown in Fig.1. The field diameter was 25 cm with electrodes shown schematically to the left. The continuous flow pinch seen in front of the gun has peak $n_e \sim 10^{17}$ cm^{-3}; also seen is plasma emerging from the interelectrode space. Pressure balance calculations using magnetic fields measured just outside the column indicate a total "transverse temperature" of 100-150 eV and spectroscopic investigations suggest a low level of impurities.

When interpreting the phenomena we recall that the snowplough and focus are well understood[2] and we concentrate on the magnetised plasma. The magnetic Reynolds number is large so we assume perfect conductivity. Then plasma in a flux tube is isomagnetic, i.e. $B_\theta/\rho r$ = constant, where B_θ is the azimuthal field, r the peak tube major radius and ρ the plasma density. Plasma motion in the radial direction is given by

$$\rho \frac{dV_r}{dr} = \frac{\partial}{\partial r}\left(P + \frac{B_\theta^2}{8\pi}\right) + \frac{B_\theta^2}{4\pi r}$$

The last term describes the "tension" which always collapses the flux tube for low-β and can result in heating up to $kT \sim B_{\theta o}^2 m_i(\gamma - 1)/4\pi\rho_o\gamma$ (subscript zero for the initial state). By contrast axial motion has no restraining "tension" and the trapped field can drive an expansion to an ultimate velocity $\sim\sqrt{2}\, v_{ao} = B_{\theta o}/\sqrt{2\pi\rho_o}$.

The motion has been traced by a 2D P.I.C. (particle in cell) computation[4]. Initially the interelectrode cavity is filled with cold isomagnetic plasma ($B_o \propto r^{-1}$, $\rho_o \propto r^{-2}$) which is released at time zero. In Fig.2 each tube of fixed mass and flux is represented by a point (ρ ∝ point density x r^{-1}). The expansion of the plasma into vacuum can be seen after t = 1.4 units (t in r_o/v_{ao}) and by t = 6.4 a steady flow pattern has been reached. In detail the computation shows heating and axial velocities in qualitative agreement with the above considerations. Heating in the pinched region is accomplished by a stationary shock.

The absence of m = 0 instabilities of wavelength larger than a few cell lengths from the computer prediction may be due to perturbations being swept across the absorbing boundary before they grow to significant amplitude. (Axisymmetry precludes the representation of m = 1.) However, the experiental results which show that m = 0, 1 occur when the gas supply is restricted, suggest that the spatial distribution of plasma causes a substantial reduction in growth rate. It has been shown that for slow, steady, isomagnetic, adiabatic flow (i.e. no stationary shocks) a particular pressure distribution is required which has neutral stability to m = 0[5].

The model shows that the continuous flow pinch resembles a wake shock in the expansive flow of plasma past a cylindrical obstruction i.e. the center electrode. It appears that the pinch could be maintained indefinitely given a continuous supply of low-β plasma and electric current. With suitable changes in geometry one might expect compressive flows with substantial density increases and heating.

This work was performed under the auspices of the U.S. Atomic Energy Commission and supported in part by the United Kingdom Atomic Energy Authority. The first author is grateful for the hospitality of LASL. It is a pleasure to acknowledge our colleagues I. Hennins, F.C. Jahoda, W. Riesenfeld and B.R. Suydam.

References

1. A.A. Newton, I. Hennins and J. Marshall. A.P.S. Plasma Division Meeting, Miami, (1968).
2. T.D. Butler et al. LASL Report LA-DC-9003 (1968).
3. F.C. Jahoda LASL Report LA-3968 (1968).
4. T.D. Butler et al. LASL Report LA-3990 Paper C6 (1968).
5. J. Marshall and A.A. Newton. LA-4075-MS p.28 (1969).

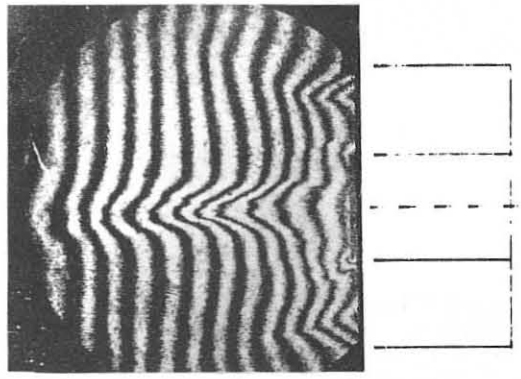

Fig.1 Reconstructed interferogram of continuous flow pinch

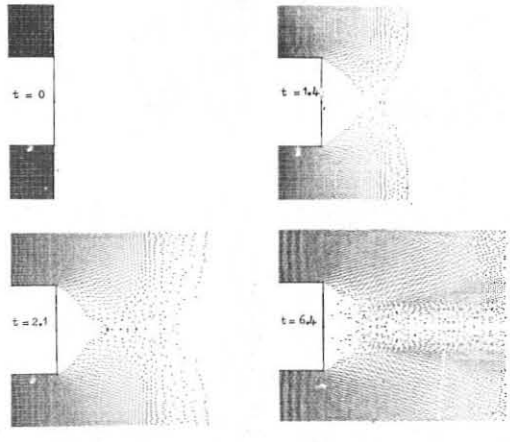

Fig.2 Particle plots showing the plasma configuration at different times during the calculation

NEUTRON PRODUCTION BY VORTEX ANNIHILATION IN THE PLASMA FOCUS

by

W. H. Bostick, L. Grunberger, and W. Prior

Stevens Institute of Technology

Physics Department

Hoboken, New Jersey 07030, USA

Filamentary plasma vortices are observed (1) to be produced in pairs in deuterium gas in plasma coaxial accelerators operated in the pressure range of 1 to 10 torr. There is some evidence (1) to indicate that these pairs of vortex filaments have right-handed and left-handed magnetic field configurations and mass flow configurations. Figures 1, 2, and 3 are 5-nanosecond, axial, image-converter photographs of the filamentary vortices.

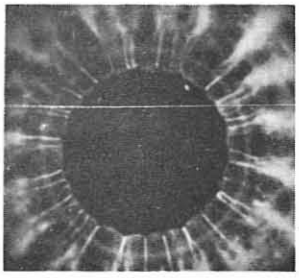

Fig. 1. t = - 250 ± 20 nsec
Current sheath is already crossing face of center conductor. Note vortex pair combining at 5 o'clock.

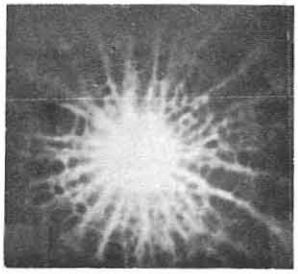

Fig. 2. t = 20 ± 20 nsec
"Plasma focus" has occured.

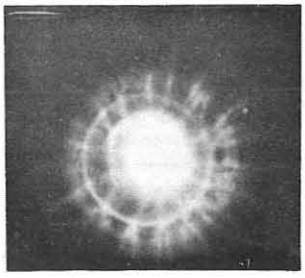

Fig. 3. t = 230 ± 20 nsec

Fig. 4. t= - 250 ± 20 nsec

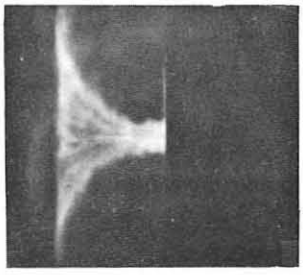

Fig. 5. t = 0 ± 20 nsec

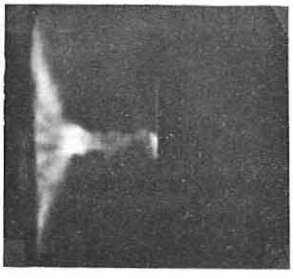

Fig. 6. t = 50 ± 20 nsec

The authors have examined the spectrum of the light coming from these filaments and from the plasma focus with space-and time-resolved (5-nanosecond) spectroscopy. The Hβ line is prominent in emission and fairly sharp in the background and where the filaments fuzz out. However, in the core of the filaments and in the "plasma focus" the Hβ emission line has broadened to the extent that it is indistinguishable from the continuum which makes up the light. In absorption Hβ is prominent and fairly sharp here. The degree of broadening of the Hβ in the filaments places the electron density there > $10^{18}/cm^3$. The scalloping of the current sheath observed in figures 1 and 4 is an indication that even at this early time before the moment of the "plasma focus" (t = o) those filaments are carrying a fairly large fraction of the total current carried by the current sheath in which they are imbedded. When the spacing between the vortex filaments is small enough, they annihilate in pairs (see figures 1 and 3), and at the plasma focus near the axis a general region of annihilation (enhanced illumination) starts at the end of the center conductor and moves away from the center conductor along the axis at a speed of 1.5×10^7 cm/sec. This moving annihilation region can be seen in the profile views in figure 5 and 6. The plasma coaxial accelerator has inner and outer conductor diameters of 3.4 and 10 cm, and an inner conductor length of 13.6 cm. It is driven by a 45 μf capacitor bank capable of 25 kv, and is usually operated at 11 to 14 kv with deuterium at 8 torr. At 13 kv the energy storage is 3.5 kj, and the peak current 500 ka. The half cycle time is 2 μ sec.

Two main neutron pulses occur; the first during the vortex annihilation along the axis while the bright region moves from the center conductor to the crown of the "umbrella" (figures 5 and 6). The second main neutron pulse is associated in time with the vortex annihilation occurring in the crown of the umbrella as the vortices "burn" pair by pair as a shock wave moves radially outward in the crown (figure 3). This observed vortex annihilation, in figures 1, 2, 3, 5 and 6 is, the authors believe, the laboratory scale version of the solar flare phenomenon. With this relatively small scale apparatus the neutron yield per pulse is about 5×10^8 neutrons. This yield is much less than that obtained by other experimenters[2,3] who use much higher energy storage. Magnetic probe measurements of B_θ show that the major portion of the current sheath during collapse is approximately the thickness of the illuminated ring seen in figure 4 where the current sheath intersects the face of the center conductor, that is about 1 mm, which is approximately the diameter of the filaments. Probe measurements of B_r and B_z show the stochastic fluctuations to be expected from the fields of the vortex filaments.

References

1. W. H. Bostick, W. Prior, L. Grunberger, and G. Emmert, Phys. Fluids 9, 2079 (1966).
2. N. J. Peacock, Third Conference on Plasma Physics and Controlled Nuclear Fusion Research, Novosibirsk, USSR, August 1968 CN-24/G-4.
3. P. J. Bottoms, J. W. Mather and A. H. Williams, ibid G-5.

Credits

Research sponsored by the Air Force Office of Scientific Research, Office of Aerospace Research, United States Air Force, under AFOSR Grant No. AF-AFOSR-465-67.

THE GENERATION AND ACCELERATION OF PLASMA BY A HIGH AMPLITUDE RF TRAVELING WAVE TRAIN

A. Stampa[+], W. Bieger, K.H. Finken, H. Tuczek

Institut für Plasmaphysik der Kernforschungsanlage Jülich GmbH, 517 Jülich, Postfach 365, BRD

[+]Deutsche Versuchsanstalt für Luft- und Raumfahrt e.V.

Assoziation EURATOM - KFA

The interaction of a high amplitude traveling RF wave with a plasma is investigated with respect to plasma heating and plasma acceleration. The principle of the experimental setup is shown in fig. 1. A high frequency oscillator feeds its energy into a delay line, producing a magnetic field of picket-fence configuration with several cusps propagating along the line. The gas inside the coils of the transmission line will be ionized at proper values of the initial gas pressure. When the conductivity is sufficiently high the plasma will also be accelerated. We are concerned in the acceleration modes of this device in order to produce a plasma beam with an electron density 10^{13} - 10^{14} cm^{-3} and a velocity 10^6 - 10^7 cm/s, which is homogenous and stationary for some milliseconds [1]. Such a plasma may be of importance for certain injection experiments or for fundamental investigations. On the other hand the observation of modes with dominant heating may be of interest for fusion experiments using a similar field configuration for plasma confinement [2], [4].

The mechanism of the discharge may be rather complex because of the coupling of ionization and acceleration. Simple models show, that effective acceleration is only expected, when plasma density and conductivity are kept in certain limits [3]. Therefore the question arises, whether sufficiently fast ionization and heating will be possible, when the plasma generation is done by the accelerating wave itself. In order to get an answer a pulsed experiment was performed with a maximum duration of 6 µs. A special condenser bank discharge produced a sinosoidal pulse of variable length with a frequency 1 MHz and a maximum magnetic field of 800 Gauss.

The discharge vessel was initially filled with a stationary pressure of hydrogen. Plasma generation was observed at filling pressures between $2 \cdot 10^{-3}$ and 2 Torr. The lower limit is shifted to smaller pressures, when a wavetrain of longer duration is applied. The plasma was investigated with microwave diagnostics, magnetic probes and a piezoelectric pressure probe of high sensitivity.

The measurements showed, that there are certain regions of initial conditions with effective plasma acceleration, others with effective heating. Especially two different modes of acceleration could be observed. At initial gas pressures smaller than 10^{-2} Torr and working with only 4 halfecycles of the wave a single plasmoid is observed traveling along the axis of the discharge tube with the phase velocity of the wave. Fig. 2 shows the stagnation pressure measured with the pressure probe at different axial positions. The plasma density increases along the accelerationline with a maximum value of 10^{12} cm^{-3} at the end of the tube. For this particle density the magnetic pressure of the wave exceeds the kinetic pressure of the plasma, i.e. The heating rate is sufficiently fast to prevent the magnetic field from penetration into the plasma after 2 µs. The acceleration mechanism can be described by a piston model.

At an initial pressure near 0,5 Torr the heating of the gas is slow enough to admit penetration of the magnetic field through the plasma. Here also acceleration is observed resulting in a final plasma velocity smaller than the phase velocity of the wave. The acceleration process can be described by a mechanism with slip between plasma and magnetic field. This process allows to accelerate a plasma of higher density than the critical density n_c corresponding to pressure balance.

At intermediate filling pressures ($10^{-2} < p < 5 \cdot 10^{-2}$ Torr) no macroscopic velocity is measured. In this domain an abnormal high energy transfer to the plasma is observed, which results in a very fast heating. As much as 60 Joule may be consumed from a total available amount of 120 Joule. This phenomenon occurs, when the electron density exceeds n_c and the plasma can no longer be confined in axial direction. 1 or 2 microseconds after the start of the wave the degree of ionisation reaches 100 % and the ion temperature rises to some 10 eV. This heating phase is accompanied by an axial current with a preference direction parallel to the velocity of the traveling wave. The explanation of the axial current will be different from that observed in toroidal systems with similar field configuration [4] because of the open ended geometry in our experiment.

[1] W. Bieger et. al.
Z. f. Naturforschung 23, 263, (1968)

[2] S.M. Osovets
Plasma Physics and the Problem of Controlled Thermonuclear Reactions IV (1960)

[3] W. Bieger
Thesis Aachen 1968

[4] N.A. Borzunow et.al.
Sov. Phys. Dokl. 8, 914, (1964)

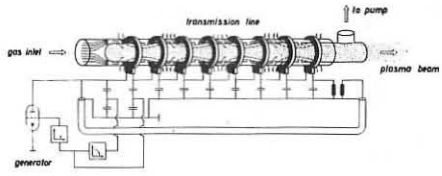

Fig. 1
Experimental setup of the pulsed plasma accelerator.

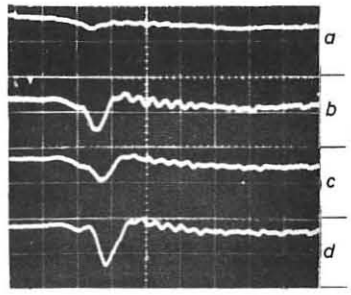

Fig. 2
Ramming pressure of the accelerated plasma at different points along the acceleration line
a) at the beginning b) at the end.

A HIGH CURRENT HALL ACCELERATOR

by H. C. Cole
U.K.A.E.A., Culham Laboratory,
Culham, Nr. Abingdon, Berkshire,
England

A high current, two stage d.c. Hall accelerator is investigated in order to determine its possible application in controlled thermonuclear fusion work. The accelerator is similar to that described by Morozov et. al. [1] but has less than half the linear dimensions. It consists essentially of two radial magnetic field sections in an annular channel, the fields being generated by a solenoidal winding on the inner iron core, see Fig. 1.

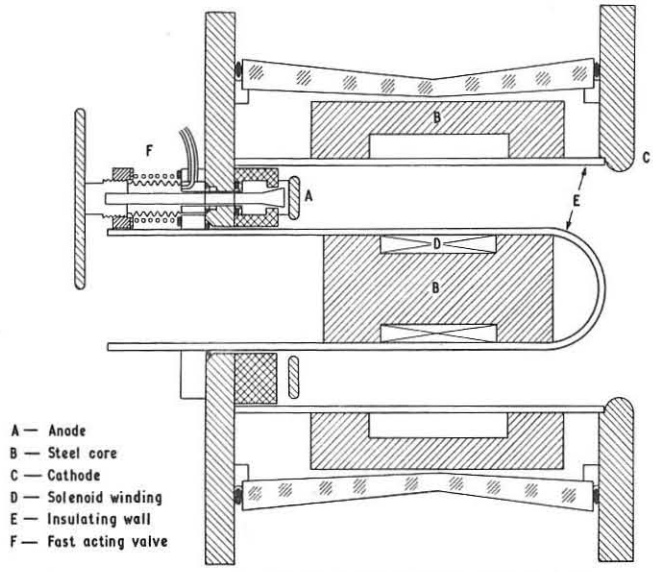

An axial electric field is set up in the annulus such that the Larmor radius of the ions is greater than a stage length while that of the electrons is smaller. A unidirectional current pulse is supplied by a 10kV 45kJ capacitor bank. Hydrogen gas is fed into the device from a fast gas valve situated behind the anode ring.

The essential processes occurring during operation of the device are as follows: the ions can move relatively unimpeded through the system, while the electrons, which are prevented from moving directly towards the anode by the radial magnetic field move in an azimuthal direction as a result of the crossed electric and magnetic fields. This drift of electrons constitutes a Hall current which interacts with the radial magnetic field to produce a magnetomotive force acting on the ions in the same direction as the initial electric field. The plasma should also be effectively collisionless, i.e. $\omega_e \tau_e > 1$ where ω_e and τ_e are the electron gyro frequency and collision time respectively. The accelerated ions collect electrons as they pass the cathode.

Experimental Observations & Discussion

The breakdown characteristics of the device are examined. It is shown that the minimum breakdown potential is 5kV coupled with a pressure of several mtorr at the cathode. Hence a delay of ≥ 500 μsec is required between triggering the fast gas valve and the main condenser bank ignitron.

A detailed investigation of the electrical characteristics of the device was undertaken. The volt-ampere curve shows a negative slope. This must be due to heating effects. The impedance of the device increases directly with the magnitude of the radial magnetic field Br. An increase in the latter reduces the electron back leakage and hence a larger proportion of the current must be carried by the ions. This is confirmed by measurements of the variation of output with Br which show the same form as the impedance - Br characteristic. As the impedance increases so does the P.D. across the device. This in turn leads to an increase in energy of the ions in the ejected plasma.

A multigrid probe was used for measuring both the magnitude of the output and its ion energy distribution. The latter shows two maxima at ~ 350 eV and 700 eV for typical operating conditions. These maxima are considered to be related to the two stages in the accelerator.

It is calculated that the maximum divergence of the plasma output for typical operating conditions is 20° (½ angle). Measurements of the change in density with distance from the device are reasonably consistent with the above divergence. The density of the output beam is increased by a factor of five or six with a simple guide field. This could probably be further improved by proper matching of the guide field with the accelerator.

The presence of a large rotating cathode spot is shown by means of high speed framing and streak photographs. The rotation of this spot is in the same direction as the E/B drift, but its velocity is only about 1/20th of the drift velocity in the annulus. This is consistent with the fact that the ions do not achieve the full drift velocity because their Larmor radius is larger than a stage length.

The effect of the electron Hall current was determined by inserting a set of three radial quartz baffles in the annulus. Under these circumstances a continuous Hall current no longer flows and an azimuthal electric field builds up. This field crossed with the radial magnetic field drives the electrons towards the anode. As a result the impedance of the system decreased to ~ 1/3rd of its normal value and the output from the device fell to less than 1% of its normal value. This is strong evidence that most of the current is carried by the electrons under these circumstances.

The electrical efficiency was determined calorimetrically the maximum value obtained being ~ 15%. This means that the maximum output is ~ 420 amp equivalent for the following conditions. Average value of Br 500 gauss, PD across device ~ 1000v, Gas current 2800 amp, total pulse length 5ms with current constant at max. value for ~ 1.5ms. The total number of ions produced is then ~ 5×10^{18}. If operated continuously at its maximum current it would deliver ~ 3×10^{21} ions/sec. This is only about 1/20th of the requirement for providing the "start up" plasma for a reactor providing that it could be effectively injected into the system.

It is considered that the output from the device could be increased simply by scaling up its dimensions. The energy of the accelerated plasma could also be increased by increasing Br. In addition the overall efficiency of the device could be improved by ionising the gas mainly near the anode. Under these conditions the output would be more nearly monoenergetic, the wall interaction should be reduced and the collimation improved.

The author is indebted to Mr. M.J. Terry for his invaluable help with the experimental work.

REFERENCES

(1) A.I. Morozov et.al. CTO 516.

INDEX OF AUTHORS